

7338

# **NASA Contractor Report 171931**

(NASA-CR-171931) NASA/AMERICAN SOCIETY FOR  
ENGINEERING EDUCATION (ASEE) SUMMER FACULTY  
FELLOWSHIP PROGRAM, 1985 (NASA) 733 p

CSSL 05I

N86-31409  
THRU  
N86-31436  
Unclas  
G3/80 43197

NASA/AMERICAN SOCIETY FOR ENGINEERING  
EDUCATION (ASEE) SUMMER FACULTY  
FELLOWSHIP PROGRAM - 1985

Robert G. Chilton (Editor)

Texas A&M University  
College Station, Texas

Clarence E. Williams (Editor)

Office of University Affairs  
Johnson Space Center  
Houston, Texas

Grant NGT-44-001-800  
July 1986



National Aeronautics and  
Space Administration

Lyndon B. Johnson Space Center  
Houston, Texas

## PREFACE

The 1985 JSC NASA/ASEE Summer Faculty Fellowship Research Program was conducted by Texas A&M University and the Johnson Space Center. The ten week program was operated under the auspices of the American Society for Engineering Education (ASEE). The program at JSC, as well as those at other NASA Centers, was funded by the Office of University Affairs, NASA Headquarters, Washington, D.C. The objectives of the programs, which began in 1965 at JSC and in 1964 nationally, are:

- a. To further the professional knowledge of qualified engineering and science faculty members;
- b. To stimulate an exchange of ideas between participants and NASA;
- c. To enrich and refresh the research and teaching activities of participants' institutions; and,
- d. To contribute to the research objectives of the NASA Centers.

The faculty fellows spent ten weeks at JSC engaged in a research project commensurate with their interests and background and worked in collaboration with a NASA/JSC Colleague. This document is a compilation of the final reports on their research during the summer of 1985. Texas A&M Research Foundation Report No. 4194-85 is the Co-Directors' report on the administrative operations of the Summer Faculty Fellowship Program.



## CONTENTS

1. Agresti, David G.: "Mossbauer Spectroscopy of Extraterrestrial Materials"
2. Allen, Robert: "Design Criteria for Expert Systems"
3. Bard, Jonathan F.: "Evaluating Space Station Applications of Automation and Robotics Technologies from a Human Productivity Point of View"
4. Bourgeois, Brian A.: "Distributed Synthetic Aperture Radar Simulation"
5. Chow, L. C.: "Condensation Heat Transfer Under a Microgravity Environment"
6. Dasch, E. Julius: "Chronology and Isotopic Geochemistry of Apollo 14 Basalts and Skaergard Gabbro, Eastern Greenland"
7. Davis, Bruce E.: "Application of Computer Image Enhancement Techniques to Shuttle Hand-Held Photography"
8. DeAcetis, Louis A.: "Investigation of Local Area Networks for an Orbiting Space Station"
9. Emanuel, Ervin M.: "An IBM PC-Based Math Model for Space Station Solar Array Simulation"
10. Fenton, Donald L.: "Fire Control Method and Analytical Model for Large Liquid Hydrocarbon Pool Fires"
11. Greenisen, Michael C.: Paper Unavailable
12. Hommel, Mark J.: "Development of a Numerical Procedure to Map a General 3-D Body onto a Near-Circle"
13. Ito, Takeru: "Effects of Lunar Soil, Zagami Meteorite, and Ocean Ridge Basalt on the Excretion of Itoic Acid, a Siderophore, and Coproporphyrin by Bacillus subtilis"
14. Janik, Daniel S.: "Defining Reclaimed Water Potability Requirements"
15. Johnson, Richard E.: "Review and Analysis of High Temperature Chemical Reactions and the Effect of Non-Equilibrium Conditions"
16. Kauffman, David: "An Analysis of Ullage Heat Transfer in the Orbital Refueling System"
17. Lacovara, Robert C.: "Engineering Graphics Data Entry for Space Station Data Base"

18. Lessard, Charles S.: "Analysis of Nystagmus Response to Pseudorandom Velocity Input"
19. Liebert, Bruce E.: "Materials Considerations in the Design of a Metal-Hydride Heat Pump for an Advanced Extravehicular Mobility Unit"
20. Meehan, Richard T.: "Flow Cytometry Analysis of Hormone Receptors on Human Peripheral Blood Mononuclear Cells to Identify Stress-Induced Neuroendocrine Effects"
21. Minn, Howard S.: "Automation of Review/Approval Cycle of MCAUTO CAD/CAM Generated Drawings and Documents"
22. Morehouse, Jeffrey H.: "Thermally Regenerative Hydrogen/Oxygen Fuel Cell Power Cycles"
23. Prichard, Howard M.: "Cytogenic Analysis of Peripheral Lymphocytes Subjected to Simulated Solar Flare Radiation"
24. St. Clair, Daniel C.: "Integration of an Expert System into a User Interface Language Demonstration"
25. Torres, Joseph: "In Vitro Cytogenic Studies of Organic Chemicals Found as Contaminants in Spacecraft Cabin Atmospheres"
26. Uhde-Lacovara, Jo A.: "CSTAR Star Catalogue Development"
27. Wierum, Frederic A.: "Laser Techniques for Arc Jet Plasma Diagnostics: Continuation of a Feasibility and Design Study"
28. Wolinsky, Ira: "Selection of an Appropriate Animal Model for Study of Bone Loss in Weightlessness"

12875

## MOSSBAUER SPECTROSCOPY OF EXTRATERRESTRIAL MATERIALS

David G. Agresti, Ph. D.  
Associate Professor of Physics  
University of Alabama at Birmingham  
Birmingham, AL 35294

18812

## ABSTRACT

Mossbauer Spectroscopy (MS) has recently been added to the tools used by Dr. Richard Morris of the Experimental Planetology Branch of the Solar System Exploration Division at Johnson Space Flight Center in his research on synthetic and natural analogues of lunar and Martian soils. During this summer's stay at JSC I have adapted for use on an IBM-PC microcomputer a least-squares fitting program for MS data written originally for an IBM 360 mainframe computer. The adapted program has been applied to the analysis of MS spectra obtained from several samples of Antarctic soil under investigation at JSC as analogs to soil of the Martian regolith. Preliminary conclusions have been drawn from the MS data about the composition of the Antarctic samples. Inferences from optical spectra obtained for these same samples have been compared with the MS results. The principal achievement for this summer's effort is the establishment of the basis for continued collaboration between myself and Dr. Morris when I return to UAB.

---

NASA Colleague: Richard V. Morris, Ph. D., SN4, X5874

## INTRODUCTION

Mossbauer Spectroscopy (MS) is a research tool in which  $\gamma$ -rays from a source containing a particular radionuclide are allowed to pass through an absorber containing like nuclides. By moving the source with respect to the absorber, the  $\gamma$ -ray energy (usually expressed in velocity units, mm/s) is varied over a small range, and one obtains an absorption spectrum that is characteristic of the material in the absorber. The spectral data are typically collected as  $\gamma$ -ray counts into several hundred channels in a multi-channel analyzer, each of which corresponds to a particular  $\gamma$ -ray energy. Reduction in counts with respect to a certain "background level" [Fig. 1] is evidence of resonant absorption and provides information about the nature of the material in the absorber.

The particular radionuclide used in this study is Co-57, which decays to the stable Fe-57, which has a natural abundance of approx. 2%. Martian soil is approx. 18% iron by weight [Clark et al., 1982], and this isotope yields reasonably well-resolved spectra, uniquely characteristic of the sample studied. Because of the penetrating radiation involved (14.4 keV for Co-57), MS probes the interior of samples under study, and thus serves as a good complement to the more frequently used technique of optical spectroscopy, which is sensitive to surface and near-surface atoms.

As mentioned above, each spectrum consists of several hundred values (512 for the present work) representing  $\gamma$ -ray transmission versus velocity. The typical theoretical model for a Mossbauer spectrum consists of a sum of Lorentzian-shaped curves oriented downward from the background level, with a group of six of these forming the spectrum of a pure magnetic material and a pair forming the spectrum of a pure non-magnetic material [Fig. 1] -- magnetic hyperfine sextet and electric quadrupole doublet, resp. (See, for example, Greenwood and Gibb, 1971, for further discussion.) The spectra of many natural samples are more complex than these simple models and usually consist of a superposition of quadrupole pairs and magnetic sextets.

In analyzing the data obtained from such natural samples, one typically is forced to resort to a computing procedure by which the parameters of an a priori theoretical model are adjusted by some particular convergence criterion to provide the best match of the theoretical with the observed spectrum. I have co-authored and subsequently modified one such fitting procedure, which employs the method of linearized least squares by Taylor's approximation [Agresti et al., 1969; Bent et al., 1969; Agresti et al., 1974]. This program was originally written in Fortran IV for the CalTech IBM 360 and later adapted for the University of Alabama in Birmingham PRIME 750, both "mainframe" computers. My principal assignment this summer was to adapt the program for a microcomputer environment, namely the IBM-PC in use in the laboratory of my NASA colleague, Dr. Richard V. Morris.

As a consequence of my stay at NASA-JSC, I have begun a collaboration with Dr. Morris in the investigation of samples obtained from the Dry Valleys of Antarctica, a cold desert region whose weathering processes and soil development are believed to be analogous to those of the Martian regolith [Gibson et al., 1983]. MS spectra have been obtained for three samples to date [Fig. 2], WV485 from Wright Valley, and DJ208 and DJ-Castle Rock from Don Juan Pond [labeling, Gibson, private communication]. The spectra are non-magnetic and are assumed to consist of a superposition of quadrupole pairs, representing the several component minerals present in the sample.

The least-squares fitting procedure, as modified for the IBM-PC, has been employed in a preliminary analysis of the MS spectra of the three Antarctic samples. The parameters obtained have been compared with those of MS spectra of standard pure minerals to give a preliminary indication of the nature of the iron-containing phases in the samples. For two of the samples the conclusions drawn are generally supported by optical spectra (350-2200nm) obtained with a Cary-14 on these same materials. The other sample is uniformly dark and no comparison could be made.

## RESULTS AND DISCUSSION

Mossbauer spectra were obtained and analyzed for three Antarctic soils [Fig. 2] and three reference minerals that may be present in the soils [Fig.1]. Unlike the spectra of the reference minerals, the spectra of the Antarctic soils are poorly resolved, and, while the relative magnitudes vary, all show three rather broad peaks, one at zero, one around 0.7 mm/s, and one around 2 mm/s. In order to find the theoretical model for the spectra most indicative of the composition of such non-magnetic samples of mixed mineralogy, one generally assumes a superposition of quadrupole pairs, one for each nonequivalent atomic site. The results of a fit with just two atomic sites are shown in Table 1, which displays best estimates from the fit for

Sample	QS	CIS	fraction (%)
San Carlos olivine	2.998 (1)	1.147 (1)	
Bamle enstatite	2.135 (1)	1.156 (1)	
Hull diopside	1.928 (2)	1.183 (1)	
DJ-208	2.127 (4) 0.99 (3)	1.165 (2) 0.32 (1)	82 (1) 18 (1)
DJ-Castle Rock	2.046 (6) 0.90 (3)	1.052 (6) 0.35 (2)	78 (2) 22 (2)
WV-485	2.233 (2) 0.812 (2)	1.122 (1) 0.197 (1)	37 (2) 63 (2)

Table 1. Fitted Mossbauer spectral parameters. Symbols are explained in the text. Fitted statistical errors in last displayed digit are shown in parentheses.

the values of three parameters: quadrupole splitting (QS); chemical isomer shift (CIS); and for the Antarctic samples, the fraction of the spectrum in each quadrupole pair, which is proportional to the relative amount of the corresponding mineral in the sample. QS is the distance between the two peaks of a pair in mm/s, while CIS, also in mm/s, is the position midway between the two peaks. Both parameters are characteristic of a particular mineral and are related to the local crystalline asymmetry at the Mossbauer atom and its chemical charge state (for iron, 2+ or 3+) [Greenwood and Gibb, 1971].

Although the features of the spectra are too broad to be properly fit with just two atomic sites, we may nevertheless draw some preliminary conclusions from the results presented in the Table 1. The spectra of each Antarctic sample contains a component, in varying proportions, with nearly the same QS and CIS as the Bamble enstatite, an orthopyroxene, or the Hull diopside, a clinopyroxene. Although this is not sufficient to state with certainty that these samples are largely pyroxene, it is unlikely that any of the samples contains olivine in any significant amount. The values of QS and CIS are in the range indicative of iron in the 2+ valence state, while the other component has QS and CIS in the proper range for 3+ valence. Thus it is likely that the spectral fractions listed in Table 1 also represent valence fractions; that is, iron is roughly 80% divalent and 20% trivalent in the samples from Don Juan Pond, while for the Wright Valley sample, iron is only 37% divalent and roughly 63% trivalent.



In addition to the two-site fit of Table 1, a large number of additional fits were tried with more sites and a variety of parameter constraints in an attempt to find a more suitable basis for determining the composition of these samples. None was successful. The difficulty lies in the nature of the spectra. Reasonable choices for component quadrupole doublets will either put one peak around zero velocity and the other around 2mm/s (2+ valence) or put one around zero and the other at 0.7 (3+ valence). Thus the peak at zero is the sum of a number of overlapping peaks, and the parameters associated with the component site strengths, widths, as well as each QS and CIS are so strongly coupled that the fit does not converge to a minimum.

The difficulty faced in analyzing the samples of this study is likely to be present in future Antarctic soil studies and must be dealt with. In an analysis of shifts induced in NMR spectra of macromolecules by trivalent lanthanide ions [Agresti et al., 1977], I faced a similar problem, where the parameters defining the position of the paramagnetic ion and its magnetic susceptibility tensor were so strongly coupled that a linearized least-squares fitting procedure such as that used in this study [Bent et al., 1969] did not converge to a minimum. The solution was to use a Marquardt search technique [Marquardt, 1963], which combines a steepest descent routine with a first-order Taylor's approximation. This method provides convergence even for arbitrary initial parameter estimates (steepest descent feature) as well as error estimates for the parameter values obtained at the best fit convergence (Taylor's approximation). I propose to add this feature to the fitting program used in this study.

## REFERENCES

1. Agresti, D. G., M. F. Bent, and B. I. Persson, "A Versatile Computer Program for Analysis of Mossbauer Spectra," Nucl. Instr. and Methods, Vol. 72, pp. 235-236, 1969.
2. Agresti, D. G., and M. L. Belton, "A Randomization Procedure with Applications to Mossbauer Spectroscopy," Nucl. Instr. and Methods, Vol. 121, pp. 407-410, 1974.
3. Agresti, D. G., R. E. Lenkinski, and J. D. Glickson, "Lanthanide Induced NMR Perturbations of HEW Lysozyme: Evidence for Nonaxial Symmetry," Biochem. Biophys. Res. Commun., Vol. 76, pp. 711-719, 1977.
4. Bent, M. F., B. I. Persson, and D. G. Agresti, "Versatile Program for Analysis of Mossbauer Spectra," Computer Physics Communications, Vol. 1, pp. 67-87, 1969.
5. Clark, B. C., A. K. Baird, R. J. Weldon, D. M. Tsusaki, L. Schnabel, and M. P. Candelaria, "Chemical Composition of Martian Fines," J. Geophys. Res., Vol. 87, pp. 10059-10067, 1982.
6. Gibson, E. K., S. J. Wentworth, and D. S. McKay, "Chemical Weathering and Diagenesis of a Cold Desert Soil from Wright Valley, Antarctica: An Analog of Martian Weathering Processes," J. Geophys. Res., Vol. 88, pp. A912-A928, 1983.
7. Greenwood, N. N., and T. C. Gibb, Mossbauer Spectroscopy, Chapman and Hall, London, 1971.
8. Marquardt, D. W., "J. Soc. Indust. Appl. Math., Vol. 11, pp. 431-441, 1963."

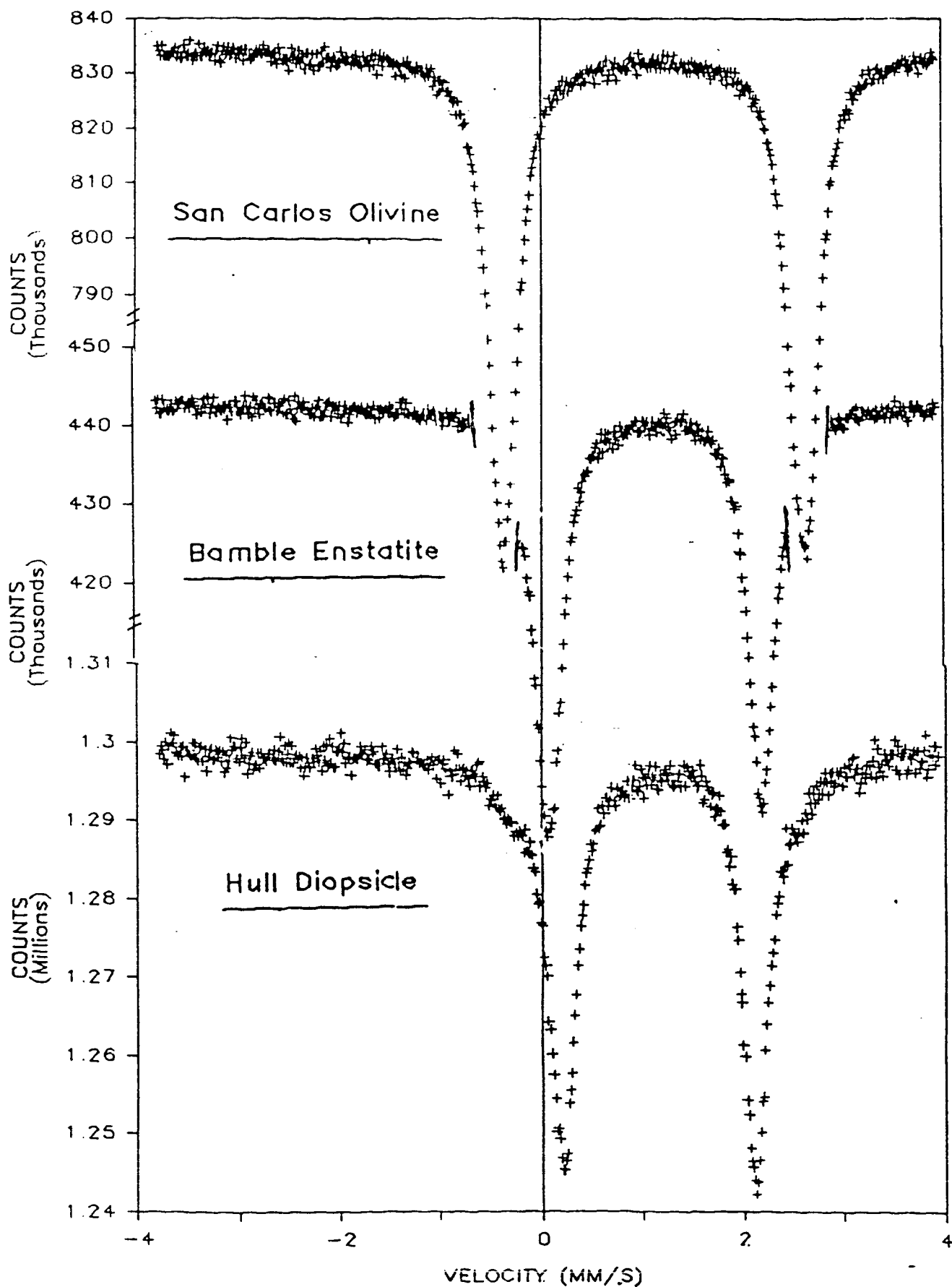


Figure 1. Mossbauer spectra of three reference minerals.

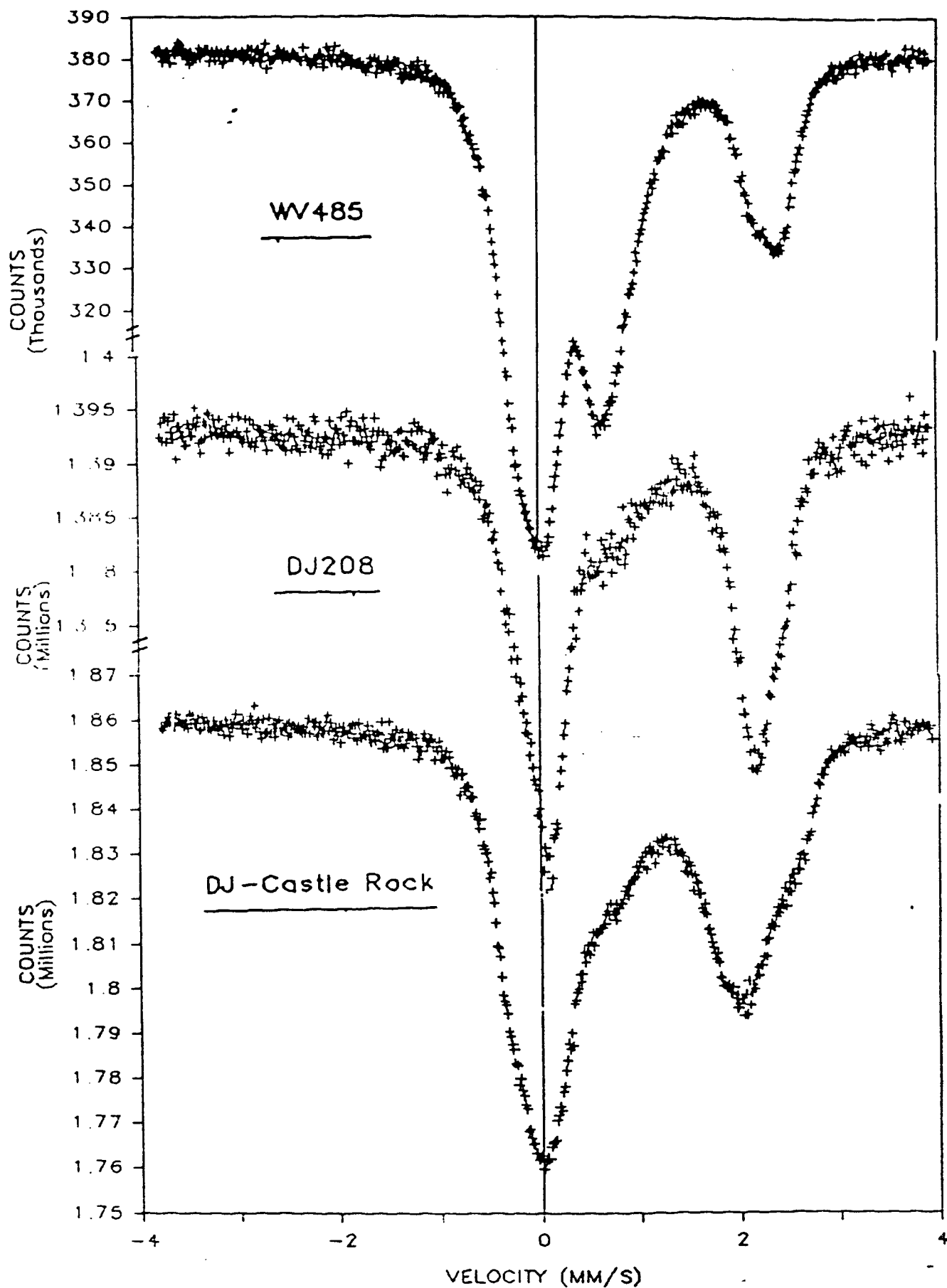


Figure 2. Mossbauer spectra of three Antarctic soils.

**Design Criteria for Expert Systems**

by

Robert Allen, P.E.

Assistant Professor of Mechanical Engineering

University of Houston - University Park

Houston, Texas

18813

Knowledge based expert systems are applicable to a wide range of engineering problems ranging from formation to derivation. At the formation end of the spectrum, design, planning and prediction have been identified as generic tasks with similar issues that are dealt with by experts, and need to be formalized for successful expert system implementation. At the derivation end, diagnosis, interpretation and monitoring have been identified as generic tasks with similar subproblems with which experts must cope. At the implementation level, four levels of programming have been identified: logic programming, production system programming, object oriented programming and hybrid programming. The following tentative guidelines are offered to aid an expert system architect in developing a system as efficiently and effectively as possible:

- Define the expert domain and the eventual environment of the implementation.
- Ensure that the domain is well defined and there is a wealth of information and, more importantly, expertise.
- Start at the highest programming level possible.
- For derivation type problems, rule based systems (or hybrid rule based systems) offer a number of advantages.
- For diagnosis, the EMYCIN model is adaptable.
- For formation problems, object oriented code (or hybrid object-oriented systems) offer some distinct advantages.
- Production systems offer a number of advantages to both formation and derivation problems including modularity and portability.

## Introduction

Knowledge based expert systems<sup>1</sup> (KBES) are a new technology stemming out of artificial intelligence (AI) that have received phenomenal notoriety for computer-aided problem solving. In science and engineering alone, expert systems have been used for such generic tasks as design, diagnosis, interpretation, monitoring, planning and prediction in well over 100 applications [Sriram84]. In addition to this, the expert systems development market has burgeoned with both specialized hardware (e.g., Symbolics and Lambda computers) and software (e.g., OPS5, KEE, and ART). As a result, there currently exist numerous methods for achieving expert system design and implementation. This report attempts to identify certain aspects of the problem and an implementation methodology that will make expert system development less time consuming and more cost effective than it has been in the past. Specifically, this report addresses the following two issues:

- What are some domain characteristics that uniquely define it in terms of expert system formalization?
- What are some of the key characteristics of AI software that make such implementation tools desirable?

This report is by no means complete. As the expert systems development tools improve, the types of problems to be tackled by expert systems will become broader and more complex. Nevertheless, problems need to be solved and heuristics for expert system design and implementation should make that task less time consuming and more cost effective.

---

<sup>1</sup>The phrase "knowledge based expert system" or "expert system" has numerous definitions. A working definition for this paper claims that KBES are interactive, problem solving computer programs incorporating judgment, experience, rules of thumb and other expertise to provide knowledgeable advice about a variety of tasks. They must have a separated knowledge base and reasoning mechanism (usually called the inference engine) in their implementation. The phrase could easily be "reason based expert system." However, it is virtually assured that all experts are knowledgeable; not all are reasonable!

## Characterization of Expert Tasks

The type of expert tasks that are applicable to KBES implementation include design, diagnosis, interpretation, monitoring, planning, and prediction. Design, planning and prediction are at the *formation* end of the problem classification spectrum; these problems create higher level objects from integrating lower level classes of objects. Diagnosis, interpretation and monitoring are *derivation* type problems; they reason about and interpret data to draw conclusions and suggest possible solutions. Each of these problem domains is partially decomposed in an attempt to isolate its particular characteristics, i.e., to help understand expert reasoning in a specific domain.

### Diagnosis

Diagnosis is the process of fault-finding in a system. The most noted example is MYCIN, a backward chaining expert system that, given symptoms and patient history, is able to diagnose over 100 infectious diseases, [Shortliffe76]. Engineering examples include such fault finding systems as FIXER, a monitoring and diagnostic tool for a life support system [Malin85], and as DELTA, a diagnostic aid for maintenance engineers working on diesel electrical locomotives [Bonissone83]. The common expertise for these systems include finding consistent, correct and *incorrect* interpretations of the data and understanding the interactions between subsystems. The key issues with diagnostic systems are:

- Data may be partial, contradictory or unreliable.
- Multiple faults may mask or create symptoms not usually considered by experts.
- Equipment may be faulty, test results may be incorrect, etc.
- Some data about a system may be inaccessible or hazardous to retrieve.

## Design

Design is the creation of a system or object satisfying given specifications. One prominent expert system in design is XCON (originally named R1) [McDermott82], a system that configures computers using a partial solution scheme. XCON is one of the few commercially successful expert systems. Requirements for designing systems include goal satisfaction without resource consumption or constraint violation. Priorities need to be established for conflicting goals. Designers also need to be flexible as requirements may change with time and unforeseen changes during the design process are inevitable. Some key issues with designing expert systems that design are:

- The overall consequences of design decisions cannot be predicted until the design has progressed considerably.
- Creating a hierarchy of sub-problems is often a necessity.
- Design constraints come from a host of sources.
- Redesign is inevitable and the impact of design changes can only be seen from a broad perspective.
- Spatial relationships are a necessary parameter for designers; they are not easily approximated symbolically or qualitatively.



## **Interpretation**

Interpretation is the analysis of data to determine their meaning. A noted expert system of the interpretive type is DENDRAL [Buchanan78], a system capable of mimicking chemists' expertise. The requirements for interpretation are the same as for diagnosis, i.e., the skill is in finding consistent, correct interpretations of the data and without discarding possible candidates until there is enough evidence to rule them out. Issues associated with interpretation are the same as diagnosis with one addition. Typically the pattern recognition schemes associated with interpretation are longer and more complicated than those associated with diagnosis.

## **Monitoring**

Monitoring means to continuously or intermittently interpret signals and to set off alarms when intervention is required (usually in a real time environment). One recent system is AAMS [Haran85], an intermittent acoustic monitor to flag defective railroad wheels *in situ*. Another monitoring system is NAVEX, a flight controller's assistant for flagging unusual conditions during ascent and descent of NASA's shuttle missions [Culbert85]. In addition to interpretation and partial diagnosis, a monitoring system must cope with variable alarm situations and be able to spot false alarms. The principal issue with monitoring systems is that an alarm condition is often context dependent and, for this reason, monitoring systems need to vary signal expectations with time and situation.

## **Planning**

Planning is the creation of a program of actions to achieve a set of goals. The first planning expert system was MOLGEN [Stefik81], a system to plan experiments in molecular genetics. More recent examples include EXEPS [Heath85], a system that schedules electrical power system activity blocks for NASA spacecraft, and ESFAS [Culbert85], a system to aid in NASA's flight design. The requirements and issues for planning are similar to those for design, with the addition that planning problems may have a scheduling requirement.

## **Prediction**

Prediction is the forecasting of the future from a model of the past and present. Prediction requires reasoning about time and event sequences.

The issues facing prediction systems are:

- Predictive theory is often contingent on events in the future.
- Diverse sources of information abound.
- Multiple futures are always possible; they should be priority listed.

Several characteristics appear repeatedly across this small spectrum of applicable expert tasks. At the formation end, large solution spaces and tentative reasoning are important organizational parameters. In planning and design, for example, the number of possible solutions is astronomical compared with the number of reasonable solutions. At the derivation end, tentative reasoning, time varying data and noisy data are principal parameters. Re-analyzing the effect of either unwarranted assumptions or infeasible plans or designs is an important requirement for any successful expert system.

## Characterization of Software Tools

The purposes of this section are to identify the categories of languages that are applicable to expert system development<sup>2</sup> and to discuss some of the advantages and disadvantages of these implementation tools.

The keys for development of any expert system are representation *and* control of knowledge. Artificial intelligence researchers have provided a number of usable tools with which to accomplish this goal. The major categories (with some specific languages) are:

- Logic programming (LISP<sup>3</sup>, PROLOG, DUCK),
- Production system programming (OPSS, EXPERT),
- Object oriented programming (SMALLTALK, FLAVORS), and
- Hybrid language programming (ART, KEE, LOOPS).

Logic programming languages are the oldest of the language types (LISP was developed in the late 1950's) and form the basis of higher level AI languages (OPSS is written in LISP and BLISS). While excellent for nonprocedural, symbolic processing, logic programming languages are the lowest level of AI languages and require the most development time for implementation because desirable characteristics such as the user interface, inheritance and method of reasoning need to be coded. Nevertheless it appears that LISP, in the United States, and PROLOG, in Europe and Japan, will remain the stepping stones for higher level languages (PROLOG

---

<sup>2</sup> Expert systems can be built in virtually any programming language. In fact, a successful production system named EXPERT [Weiss79], developed at Rutgers University, has been implemented in FORTRAN. However, expert systems require symbolic manipulation and context dependent control. Using a sequential language for that purpose is limited in that extensions or modifications to a system would be difficult, at best, to perform. A reasonable comparison to expert system development in FORTRAN is algorithmic programming in ASSEMBLY: better tools exist to do the job.

<sup>3</sup> In a strict sense, LISP is a procedural language rather than a logic programming language. Its great flexibility, however, allows it to be compared with logic programming languages such as PROLOG.

will be the implementation language of Japan's fifth generation computer project). As a result, knowledge of these languages is extremely useful in attempting to make use of the more powerful programming languages.

One of the main distinctions between production rule systems and procedural or applicative languages is that a rule, or a "chunk" of knowledge, in a production system is a *data sensitive and unordered* unit of computation rather than a sequenced instruction [Brownston85]. Knowledge engineers often extract information from experts in terms of situation-action pairs. Hence, production-rule systems, that provide a natural accumulation of symbolic IF-THEN statements, are especially applicable for encoding knowledge. Production systems, especially OPS5, offer some additional advantages. These include modularity, modifiability, explainability, simplicity of control, and the ability to learn. Disadvantages include: opaque behavior (difficulty in localizing and debugging), limited communication between control and knowledge (leading to possibly undesirable interaction among rules), limited expressibility and speed (most production systems are, an order of magnitude or more, slower than procedural programs).

Object-oriented languages, such as SMALLTALK [Goldberg83], provide an ease of representation of a variety of closely related objects. This is accomplished through inheritance (properties are inherited from a higher hierarchical class to a lower one) and message passing (automated transfer of information between objects and classes of objects). The advantages of an object-oriented implementation are: ease in spatial description, transparent behavior, and modularity. A distinct advantage of FLAVORS, for example, is having the ability to develop a hybrid environment unique to the needs of a given domain. The principal disadvan-

tages of these systems are that building hybrid environments need development time and object-oriented approaches are slower than rule based systems [Savely85].

Hybrid systems are the highest level languages currently available. Examples include KEE, ART and LOOPS. These are sophisticated AI hybrid environments that combine many of the advantageous characteristics of lower level languages. These include frame based knowledge representation, rule based reasoning, LISP extensibility, interactive graphics, powerful debugging aids, and excellent editors. The price for this excellent development environment is often dedicated AI hardware (such as Symbolics or Lambda machines) and high initial costs (approaching \$100,000). Differences between hybrid systems are many and beyond the scope of this paper; interested readers should find the paper by Richter useful [Richter85].

### **Guidelines**

Problem domains and implementation tools have been identified and discussed. Based on these observations, the following guidelines are offered for designing and implementing expert systems effectively and efficiently:

- If a problem is similar to one that has already been solved and implemented, use as much of the existing shell as possible. The premier example is EMYCIN, a backward chaining, diagnostic system with probabilistic capabilities.
- To the extent possible, define the domain of expertise and the eventual environment of implementation.
- Start at the highest possible programming language. If hybrid systems are available, they will surely lead to an efficient development time.
- For derivation type problems, rule based systems, or hybrid systems with a rule based slant, are a natural selection (since cause and effect relationships are easily expressible as rules).

- For formation type problems, object oriented systems, or hybrid systems with an object-oriented slant, appear more natural than rule based systems. The reason for this is that formation problems often have fewer easily expressible rules and are more easily thought of in terms of goals and subgoals (which are represented as objects).
- Production system approaches offer several advantages to both formation and derivation type problems. Included are expressibility of rules, modularity, modifiability, explainability, ease of learning and portability. However, drawbacks include obscure control, opaque behavior with respect to control strategies and localized debugging, and speed.

These tentative guidelines are offered based on the experience of expert system architects and current technology. Implementing systems with different approaches is certainly feasible and, in fact, is being performed. It is hoped that future endeavors, will modify and improve these general guidelines with the ultimate goal of making effective and efficient development of expert systems possible.

## References

1. Bonissone, P.P.  
DELTA: An Expert System to Troubleshoot Diesel Electrical Locomotives  
In *Proceedings ACM*, New York, NY, pp. 44-45, October 1983.
2. Brownston, L., R.G. Farrell, E. Kant, and N. Martin  
*Programming Expert Systems in OPS5*  
Addison-Wesley, Reading, MA, 1985
3. Buchanan, B.G. and E.A. Feigenbaum  
DENDRAL and meta-DENDRAL: Their applications dimensions  
*Artificial Intelligence*, 11, pp. 5-24, 1978.
4. Culbert, C. and M. Maletz  
Monitoring Real Time Navigation Processes Using the Automated Reasoning Tool (ART)  
*Proceedings of the Aerospace Applications of Artificial Intelligence Conference*, Wright Patterson Air Force Base, Dayton, Ohio, September 1985 (in preparation).
5. Culbert, C., L. Wang and H. Flinn  
ESFAS: An Intelligent User Interface for the Flight Analysis System  
*Proceedings of ROBEXS '85: The First Annual Workshop on Robots and Expert Systems*, Instrument Society of America, NASA/JSC, June 1985.
6. Goldberg, A. and D. Robson  
*SMALL TALK-80, The Language and Its Implementation*  
Addison-Wesley, Reading, MA, 1983.
7. Haran, S., R.H. Allen, R.D. Finch and S.M. Rocha  
Artificial Intelligence in the Acoustic Signature Inspection of Railroad Wheels  
*Proceedings of the 40th Meeting of the Mechanical Failures Prevention Group*, National Bureau of Standards, Gaithersburg, MD, May 1985.
8. Heath, D.W. and M.G. Boarnet  
EXEPS: An Advisory Expert System for Timelining Electrical Power System Activity Blocks  
*Proceedings of ROBEXS '85: The First Annual Workshop on Robots and Expert Systems*, Instrument Society of America, NASA/JSC, June 1985.

9. Malin, J.T. and N. Lance  
An Expert System for Fault Management and Automatic Shutdown Avoidance in a Regenerative Life Support System  
*Proceedings of ROBEXS '85: First Annual Workshop on Robots and Expert Systems*, Instrument Society of America, NASA/JSC, June 1985.
10. McDermott, J.  
R1: A Rule-Based Configurer of Computer Systems  
*Artificial Intelligence*, 19(1)39-88, September 1982.
11. Richer, M.H.  
Evaluating the Existing Tools for Developing Knowledge-Based Systems  
Report No. KSL 85-19, Stanford University, Knowledge Systems Laboratory, May 1985.
12. Savely, R.T.  
*Private communication*, 1985.
13. Shortliffe, E.H.  
MYCIN: *Computer-based Medical Consultations*  
Elsevier, New York, 1976.
14. Sriram, D.  
A Bibliography on Knowledge-Based Expert Systems in Engineering  
Tech. Report DRC-12-23-84, Carnegie-Mellon University, Design Research Center, December 1984.
15. Stefik, M. et al.  
The Organization of Expert Systems: A Prescriptive Tutorial  
Tech. Report VLSI-82-1, Xerox, Palo Alto Research Center, Jan. 1982.
16. Stefik, M.J.  
Planning with constraints  
*Artificial Intelligence*, 16(2)111-140, May 1981.
17. Winston, P.H.  
*Artificial Intelligence*  
Addison-Wesley, Reading, MA 1984.



Evaluating Space Station Applications of Automation and Robotics  
Technologies from a Human Productivity Point of View

by

Jonathan F. Bard

NASA-ASEE Summer Faculty Fellow

National Aeronautics and Space Administration

Johnson Space Center

Houston, Texas

18817

ABSTRACT

The role that automation, robotics, and artificial intelligence will play in Space Station operations is now beginning to take shape. Although there is only limited data on the precise nature of the payoffs that these technologies are likely to afford there is a general consensus that, at a minimum, the following benefits will be realized: increased productivity, increased responsiveness to innovation, lower operating costs, and reduction of exposure to hazards. Nevertheless, the question arises as to how much automation can be justified with the technical and economic constraints of the program? The purpose of this paper is to present a methodology can be used to evaluate and rank different approaches to automating the functions and tasks planned for the Space Station. Special attention is given to the impact of advanced automation on human productivity.

The methodology employed is based on the Analytic Hierarchy Process. This permits the introduction of individual judgements to resolve the conflict that normally arises when incomparable criteria underly the selection process. Because of the large number of factors involved in the model, the overall problem is decomposed into four subproblems individually focusing on human productivity, economics, design, and operations, respectively. The results from each are then combined to yield the final rankings. To demonstrate the methodology, an example is developed based on the selection of an on-orbit assembly system. Five alternatives for performing this task are identified, ranging from an astronaut working in space, to a dexterous manipulator with sensory feedback. Computational results are presented along with their implications. A final parametric analysis shows that the outcome is locally insensitive to all but complete reversals in preference.

KEY WORDS: Multicriteria Decision Making, Analytic Hierarchy Process, Project Evaluation, Expert Opinion

## 1. INTRODUCTION

Under the leadership of the National Aeronautics and Space Administration (NASA) a vigorous effort is now underway to establish a permanent manned presence in space by the early 1990s. Central to this effort is the Space Station and its support systems including the Shuttle, an orbital maneuvering vehicle, unmanned platforms, free-fliers, and attachment facilities for servicing, refueling, and storing satellites. Although the rationale for the Space Station can be adequately expressed in technological terms alone, there is a growing awareness that if the U.S. does not move ahead with this program, whatever related advantages it now possesses will soon give way to the forces of international competition. As such, the climate is right to move from an era primarily centering on exploration to one that encompasses both the scientific and commercial exploitation of space. In order to meet this objective, it will be necessary to reduce the cost and complexity of working and living in space without sacrificing the high level of safety and reliability we have so far been able to maintain.

This injunction has led NASA's Advanced Technology Advisory Committee to conclude that if the Space Station is to succeed it must be highly automated; and to recommend that up to 13 percent of the program's overall budget be spent on research and development in related areas (NASA 1985). In practical terms, a deliberate thrust to incorporate advanced automation and robotics can lead to increased productivity, lower operating costs, more flexibility, improved reliability, and a reduction in life-threatening hazards. Therefore, initial subsystem designs must utilize as much mature automation as technologically feasible without precluding evolutionary growth and expected

innovation. A primary goal will be to optimize the human-machine mix of functions and skills at both the module and subsystem levels (see Zimmerman et al. 1985). This will permit the long-term realizable advances in automation to be easily accommodated, once available.

Of equal importance is the role of humans in space. Because the environment is a difficult one, the risks are great and must be weighed against the promise for new knowledge and new commercial opportunities. But there is a great deal we do not yet understand about either the environment or potential, and it is in just these circumstances that humans function best.

Accordingly, Hall and Wolbers (1984) assert that the human role should be based on what persons are most capable of doing, which is to use their intelligence to perceive, to understand, to redefine continually what has been learned, to take advantage of unforeseen opportunities, to solve unanticipated problems, and to acquire, integrate, and interpret multisensory data. In short, they should function as managers and laboratory scientists rather than as vehicle operators.

Nevertheless, the question arises as to how much automation can be justified within the technical and economic constraints of the program? The purpose of this paper is to develop a model that can be used to evaluate different approaches to automating the functions and tasks that are planned for the Space Station. Chief among these are monitoring and verification, fault management, satellite servicing, space manufacturing, and assembly of external structures. Special attention will be given to the impact of automation on human productivity, as measured by crew time saved, acceptability, health and safety, motivation, and information requirements.

Recognizing that each application of automation and robotics must be carefully weighed against a set of multiple and often incomparable criteria, the model relies on individual judgements to resolve any conflict that appears in the analysis. These judgements take the form of pairwise comparisons between the different factors or criteria reflecting their relative importance with respect to a particular function or task. In order to address the interrelationships between the criteria, as well as establish a means of treating any imprecisions in measurement that may arise, a hierarchical methodology is used (Saaty 1980). The analysis is structured around the following four areas: human productivity, economics, operations, and design. Results are obtained separately and then combined by solving a master problem to arrive at the final rankings. This contrasts with traditional cost-benefit and engineering tradeoff approaches which require a much greater data base before any analysis can be done (e.g, see Bard 1984, and Morgan and Thurgood 1984). The methodology should also be compared with the more general but less comprehensive work of Miller, Minsky and Smith (1982), and the more detailed modeling of Bard et al. (1985).

In the next section, the Space Station concept is defined along with the terms associated with automation. Some related past experience is also outlined. The methodology is presented in Section 3 and a representative analysis is conducted in Section 4. The example concentrates on the task of aligning and fastening mechanical linkages in space. Sections 5 and 6 conclude with a discussion of the results and the potential applications and limitations of the methodology.

## 2. SPACE STATION CONCEPT

Although size and complexity strongly influence the engineering of the Space Station, and suggest a higher degree of autonomy than now exists in most spacecraft, mission diversity is the principal factor driving the design. Current operational concepts include a wide variety of scientific experiments, deep space and earth observation, manufacturing and processing of pharmaceuticals and alloys, and assembly of large-scale structures. Crew time will therefore be a critical resource. A combination of greater demands on both flight and ground crews, coupled with a long-term commitment of manpower and associated ground support, afford a potential for significant cost savings through automation.

### 2.1 Design Requirements

At this time in the program, the mission or customer requirements have been interpreted by NASA (1984) as calling for three separate spacecraft: a permanently manned Space Station in a  $28\text{-}1/2^\circ$  inclination, 270 nmi circular orbit; an unmanned co-orbiting platform in a rendezvous-compatible orbit with both the Space Station and a second platform, itself in a  $98^\circ$ , 430 nmi, Sun synchronous (2 PM) orbit. The manned element will be required to provide at least 50 kW of continuous power, a minimum crew of six with four to service customers, ports for attachment and servicing of two pressurized laboratory payloads and seven unpressurized instrument payloads, and provisions for large space construction and orbital transport vehicle development. The co-orbiting platform will be designed to accommodate payloads for celestial and solar observations, and sensitive microgravity experiments with a minimum of mechanical disturbance and contamination.

The baseline design of the Space Station is envisioned as a set of deployed linear trusses to which pressurized modules, subsystems, and other equipment are attached. The principal structural components are a keel and three booms at right angles to the keel, as shown in Fig. 1. Four of the pressurized modules (two habitation and two laboratory) will be arranged in a quadrangle to provide two access routes for the crew in case of emergency. The Shuttle will berth with the first habitation module to eliminate excessive crew movement in the work area. Similarly, the logistics module will be berthed to the second habitation module to permit unloading with minimum disturbance to laboratory operations.

The Space Station is intended to be manned unless unforeseen circumstances force evacuation. The crew will rotate during the 90 day resupply cycle but there will always be 21 days of reserve provisions to cope with emergencies. Workstations, personal hygiene facilities, private quarters, and a ward room and galley to meet essential health and recreational needs will be provided for a crew of six. Onboard operations will nominally be conducted 24 hours a day, 7 days a week, but management tasks will be divided between onboard and ground personnel to utilize the capabilities of each most effectively. A 10 hour work day is planned.

## 2.2 Definitions

Because there is often confusion in the use of the terms "automation", "robotics", and "artificial intelligence", it will be useful to make precise their meaning, at least for the purposes of this paper (see NASA 1985). In so doing, it should be observed that the underlying fields have grown out of many technologies including computer science, mechanisms, sensors, and controls, so these terms

will have somewhat different connotations depending upon the context. Nevertheless, the following definitions are offered.

Artificial Intelligence is a subfield of computer science concerned with the concepts and methods of symbolic inference and the symbolic representation of knowledge to be used in making inferences. The goal is to make a machine behave in a manner that humans recognize as "intelligent" behavior in each other.

Automation is the use of machines to control or carry out processes in a predefined or modeled set of circumstances without human intervention. Advanced automation will be used to collectively refer to the fields of artificial intelligence, teleoperation, and robotics.

Autonomy is an attribute that allows a system to operate at a specified performance level for given period of time without external intervention. Fault tolerance and reliability are key features of autonomy.

Expert Systems is a subfield of artificial intelligence concerned with developing computer programs that use knowledge and reasoning techniques in specific problem areas to emulate the decision processes of human experts.

Robotics is the study and use of machines capable of manipulation or mobility with some degree of autonomy. The autonomy may be almost complete -- as in the case of an industrial manipulator which follows a sequence of preprogrammed steps, or the Viking Lander which carried out a series of operations during the periods between instructions -- or limited, as with teleoperators used for nuclear power plant or undersea operations.

Teleoperation is the study and use of manipulators which receive instructions from human operators and perform some action based on

those instructions at a remote site.

Telepresence is teleoperation in which feedback of visual, tactile, auditory or other sensory information from the remote work site gives the operator the illusion of being there so that he can exercise better, or more precise control.

In some instances it may be necessary to further refine the above terms to take into account specific functions or tasks. For example, Hall and Wolbers (1984) define supervisory and augmented control for teleoperations while Bard (1985) distinguishes various levels of automation for industrial robots.

In the early years of the program it is likely that artificial intelligence-based systems will be used primarily in an advisory or planning capacity. As crew confidence in automation grows and as technology advances, machines will take on more critical and independent roles. On the other hand, the principal barriers to autonomy levels beyond simple self-regulation, fault diagnosis, adaptive attitude control, and tape management have thus far been the shortage of computational resources. Most of our previous spacecraft have lacked the tools to assist in the implementation of autonomous behavior (e.g., see Soffen 1977). In this regard, commonality of hardware, software, and data protocols throughout the Space Station program will be essential.

### 2.3 Current Developments

The most important initial motivation for telepresence is to enhance crew safety by reducing the need for extravehicular activity (EVA). A second is to increase mission capability by making possible some activities that are now impractical, such as servicing satellites



in high-radiation geosynchronous orbits. Robotic systems are based on the same rationale, but would extend the range of activities to situations where long communication delays hamper telepresence. Further, because one crew member will generally be able to supervise the activities of many robots working simultaneously on different tasks, productivity will rise as less sophisticated systems evolve into advanced automation.

Currently, a number of research programs are under way to determine the most effective means of implementing these technologies. For example, General Electric is building a dexterous manipulator to transfer material between automatic fabrication stations for the production of gallium arsenide (GaAs), a central ingredient in integrated circuits; Martin-Marietta is working on the use of crane manipulators to unstow modular elements, and to help astronauts on EVA assemble them into structures. As evident from Skylab and Shuttle experience, particularly concerning satellite rescue and repair, the automation of manufacturing and satellite servicing will require the most advanced equipment and controls. Because both of these activities involve the precise manipulation of small, asymmetric objects, a great deal of dexterity will be a prerequisite of the design.

### 3. METHODOLOGY

In order to establish a general procedure for evaluating advanced automation alternatives a set of well-defined, uniformly acceptable criteria must be developed. This will be done in a hierarchical framework. The intent is to offer a representation of the system that can be used to examine how changes in priorities at upper levels affect the priority of elements further down the tree. The top of the hierarchy will provide the analytic focus in terms of a problem statement. The example developed below will be concerned with 'Selecting an On-Orbit Assembly System'. At the next level, the major considerations are defined, which, in our case, will include human productivity, economics, design, and operations. This is usually followed by a listing of the criteria for each of the above considerations. For human productivity these will include workload, support requirements, crew acceptability, and issues surrounding man-machine interfaces. Depending upon how much detail is called for in the model, each criteria may then be broken down into individual parameters whose values are either estimated or determined by measurement or experimentation. The bottom level of the hierarchy contains the alternatives or scenarios underlying the problem. With regard to 'Assembly', these might include an astronaut on EVA with tools, a dexterous manipulator under human control, a dedicated manipulator under computer control, a teleoperator maneuvering system with manipulator kit, or a computer controlled dexterous manipulator with vision and force feedback.

Once the hierarchy has been structured, local priorities must be established for each factor on a given level with respect to each factor on the level immediately above it. This step will be carried

out by using the Analytic Hierarchy Process (AHP) of Saaty (1980) which calls for pairwise comparisons between the factors to develop the relative weights or priorities. Because the approach is basically qualitative, it is arguably less burdensome to implement from both a data requirements and validation point of view than the more common multiattribute utility approach of Keeney and Raiffa (1976). That is, independence assumptions need not be substantiated nor preference functions derived. If, however, a more quantitative approach is sought, the exercise required to construct the hierarchy has an inherent value that would likely complement the subsequent analysis (cf. Keefer 1978, Kirkwood and Sarin 1985, Madey and Dean 1985, and White and Sage 1984).

To illustrate the nature of the calculations, observe Fig. 2 which depicts a 3-level hierarchy -- a summary version of the example to be fully analyzed in the next section. Table 1 contains the input and output data for level 2.

TABLE 1. PRIORITY VECTOR FOR MAJOR CONSIDERATIONS

Considerations	1	2	6	4	Priorities	Output Parameters
1) Human Prod.	1	3	3	7	0.521	$\lambda_{\max} = 4.121$
2) Economics		1	1	5	0.204	C.I. = 0.040
3) Design			1	7	0.227	C.R. = 0.045
4) Operations				1	0.047	

When  $n$  factors are being compared,  $n(n-1)/2$  questions are necessary to fill in the matrix. The elements in the lower triangle

(omitted here) are simply the reciprocal of those lying above the diagonal; that is,  $a_{ji} = 1/a_{ij}$ . In this instance, the entries in the matrix at the center of Table 1 are the responses to the 6 ( $n=4$ ) pairwise questions that were asked. These responses were drawn from the 9 point scale shown in Table 2 (see Saaty (1977a) for a further explanation of how this scale was derived). For example, in comparing "human productivity" with "economic" considerations (element  $a_{12}$  of the matrix), it was judged that the first "weakly" dominates the second. Note that if the elicited value for this element were  $1/3$  instead of  $3$ , then the opposite would have been true. Similarly, the value  $7$  for element  $a_{34}$  means that design considerations "very strongly" dominate those associated with operations. After the decision maker supplies all the data for the matrix the following equation is solved to obtain the rankings denoted by  $\underline{w}$ :

$$A\underline{w} = \lambda_{\max}\underline{w}$$

where  $\underline{w}$  is the  $n$ -dimensional eigenvector associated with the largest eigenvalue  $\lambda_{\max}$  of the comparison matrix,  $A$ . The  $n$  components of  $\underline{w}$  are then scaled so they sum to  $1$ . Consistency of response or transitivity of preference is checked by ascertaining whether

$$a_{ij} = a_{ik}a_{kj}, \quad \text{for all } i, j, k. \quad (1)$$

In practice, the decision maker is only estimating the "true" elements of  $A$  by assigning them values from Table 2, so the perfectly consistent case represented by eq. 2 is not likely to occur. "

TABLE 2. SCALE USED FOR PAIRWISE COMPARISONS

Value	Definition	Explanation
1	Equal importance	Both factors contribute equally to the objective or criterion
3	Weak importance of one over another	Experience and judgement slightly favor one factor over another
5	Essential or strong importance	Experience and judgement strongly favor one factor over another
7	Very strong or demonstrated importance	A factor is favored very strongly over another; its dominance is demonstrated in practice
9	Absolute importance	The evidence favoring one factor over another is unquestionable
2,4,6,8	Intermediate values	Used when a compromise is needed
0	No relationship	The factor does not contribute to the objective

Therefore, as an approximation, the elements of  $A$  can be thought to satisfy the relationship  $a_{ij} = w_i/w_j + \epsilon_{ij}$ , where  $\epsilon_{ij}$  is the error term representing the decision maker's inconsistency in judgement when comparing factor  $i$  to factor  $j$ . As such, we would no longer expect  $a_{ij}$  to equal  $a_{ik}a_{kj}$  throughout. Carrying the analysis one step farther, it can be shown that the largest eigenvalue of the matrix  $A$ ,  $\lambda_{\max}$ , satisfies  $\lambda_{\max} \geq n$ , where equality holds for the perfectly consistent case only. This leads to the definition of a consistency index

$$C.I. = (\lambda_{\max} - n)/(n-1) \quad (2)$$

which can be used to evaluate the quality of the matrix  $A$ . To add perspective we compare the C.I. to the index derived from a completely arbitrary matrix whose entries are randomly chosen. Through simulation, Saaty has obtained the following results:

n	1	2	3	4	5	6	7	8	9	10
R.I.	0.00	0.00	0.58	0.90	1.12	1.24	1.32	1.41	1.45	1.49

where n represents the dimension of the particular matrix, and R.I. denotes the random index computed from the average of the C.I. for a large sample of random matrices. It is now possible to define the consistency ratio as

$$C.R. = C.I./R.I.$$

Experience suggests that the C.R. should be less than 0.1 if one is to be fully confident with the results. (There is a certain amount of subjectivity in this assertion much like that associated with interpreting the coefficient of determination in regression analysis.) Fortunately, though, as the number of factors in the model increases the results become less and less sensitive to the values in any one matrix (see Saaty (1980) for ways of dealing with unreasonably high values).

Returning to Table 1, it can be seen that the priorities derived for the major considerations were 0.521 for human productivity, 0.204 for economics, 0.227 for design, and 0.047 for operations. These figures parallel rather closely those obtained in related studies using utility theory (e.g., see Bard et al. 1986, and Dyer and Miles 1976), but tend to emphasize the first consideration more, probably due to the implicit mandate that the Space Station must eventually pay for itself. Finally note that the consistency ratio is well within the acceptable range.

The next step in the analysis is to develop the priorities for the factors on the third level with respect to those on the second. In our

case, we will compare the five alternatives previously mentioned with each of the major considerations. For the moment, assume that the appropriate data have been elicited and that the calculations performed for each of the four comparison matrices, with the results displayed in Table 3. The first four columns of data represent the local priorities derived from the inputs supplied by the decision maker. The global priorities are obtained by weighting each of these values by the local priorities given in Table 1 (note that each column sums to 1). Because there are no more levels left to evaluate, the values shown in the last column of Table 3 represent the final priorities for the problem. Thus, according to the judgements expressed by this decision maker, alternative 2 turns out to be most preferred.

TABLE 3. LOCAL AND GLOBAL PRIORITIES FOR THE PROBLEM OF  
SELECTING AN ON-ORBIT ASSEMBLY SYSTEM

Alternatives*	Local Priorities				Global Priorities
	Human Prod.	Economics	Design	Operations	
1	0.066	0.415	0.122	0.389	0.165
2	0.212	0.309	0.224	0.151	0.232
3	0.309	0.059	0.206	0.178	0.228
4	0.170	0.111	0.197	0.105	0.161
5	0.243	0.106	0.251	0.177	0.214

\*Alternative 1: Astronaut on EVA with Tools  
 Alternative 2: Dexterous Manipulator under Human Control  
 Alternative 3: Dedicated Manipulator under Computer Control  
 Alternative 4: Teleoperator with Manipulator Kit  
 Alternative 5: Dexterous Manipulator with Sensory Feedback



#### 4. ANALYSIS

The 3-level model used for illustrative purposes in the previous section has the advantage of simplicity but captures only the most general properties of the system under study. In developing a more comprehensive model, one must strike a balance between detail, data requirements, and data availability. In practice, straightforward weighting techniques can be effectively used to quickly narrow down a large collection of options so greater attention can be given to the more promising. Miller et al. (1982) take just such an approach in developing a set of advanced automation options for space applications. After identifying 69 space project tasks, they use the following seven criteria in their scoring model: nonrecurring cost, recurring cost, maintenance, time to complete task, failure-proneness, useful life, and development risk. For each task, a judgement was obtained for each criterion based on a 1 to 5 scale with current technology being equal to 3. Rankings were derived by weighting the outcomes by the number of potential applications. Others have taken parallel approaches using similar types of response data, and have met with varying degrees of success. Arbel and Seidmann (1984) have used the AHP to evaluate flexible manufacturing systems and have reported favorable customer reactions; Saaty's experience with the AHP has spanned the gamut of applications as well as results (e.g., see Saaty 1977b).

We will now explore the implications of a full analysis by presenting the data underlying the 3-level 'Assembly' model. The first thing to note is that the number of criteria and factors needed to characterize any real problem is usually too large to neatly structure in a single hierarchy. In our case it was necessary to break the overall problem into four subproblems, each describing one of the major

considerations, and then combine the results. The presentation will therefore follow this course.

#### 4.1 Human Productivity

A major rationale for developing advanced automation applications for the Space Station is that they will increase the productivity of both the ground and flight crews. Benefits will be achieved by eliminating the need for humans to perform repetitive, tedious chores, and by extending the scope of work to include tasks that would ordinarily be impractical for the crew to undertake. For example, the multiplicity of monitoring and calibration functions that must be carried out daily are prime candidates for computer control. Expert systems, or even assistant programs, can be used to guide an astronaut through a complex diagnostic routine as well as manage certain faults by providing facts and procedural information that would be difficult for any individual to remember. For onboard computer repair, such a system might contain a data base of design information, suggest tests, and recommend procedures for recovering from failure. On a more mundane level, an onboard, computerized inventory management system can simplify the task of searching for stored equipment and material. It has been estimated that the amount of time the Shuttle flight crew has spent looking for misplaced items could have already justified the development costs of this system.

A corollary to releasing the crew from low-level monitoring, verification, and calibration functions is that morale will improve, thus enhancing motivation and allowing more time to devote to higher-level decision making and scientific pursuits. Another way automation can result in greater productivity is by reducing the need for frequent, detailed control and direction from the ground. If the

astronauts are more closely involved in the planning and scheduling of day-to-day activities, perhaps through an interactive, onboard scheduler, the best allocation of their time can be more efficiently determined.

With automatic fault diagnosis and recovery, many component failures can be quickly and reliably detected and backup units placed in operation in a manner transparent to the crew. The failed unit can then be replaced or repaired at a convenient time without disrupting the planned work schedule (e.g., see Malin and Lance 1985, and Zorpette 1985). Productivity on the Space Station can also be enhanced by mechanical devices which complement or supplement human functions. For instance, a teleoperated or robotic system could be used to assist an astronaut on EVA by holding tools, moving objects into position, grasping parts being connected, or providing mechanical capabilities a human doesn't possess (e.g., see Wu and Paul 1982). The example that we will examine, 'Selecting an On-Orbit Assemble System' falls in this general category. To begin, let us describe the five alternatives:

1. Astronaut on EVA with Tools - EVA represents current technology, and hence serves as a point of reference in the comparisons. It is extremely man- and time-intensive but requires little research and development (R&D). Although not considered here, an interesting extension of this alternative would be a man-computer vision system. Astronauts would be equipped with TV cameras that would supply quantitative information on an object's size, orientation, and condition to the computer for analysis. The principal issues would concern the miniaturization of computation hardware and design of man-machine interfaces.

2. Dexterous Manipulator under Human Control - Manipulation

technology consists of a well-developed body of kinematic theory for producing any desired movement of an end effector, such as a gripper or tool carried at the end of a robot arm. Dexterity implies a capability to reach and grasp objects in a human manner, and to adapt to a wide number of tasks. Recently, multiple small, three-jointed manipulators have been mounted on a hand to produce the equivalent of true fingers (Jarvis 1984). This system could probably be built with a modular design, so that vision could easily be added; however, because extremely small manipulators for confined spaces and multiply-branched manipulators for complex tasks do not yet exist, the development risk would be high.

3. Dedicated Manipulator under Computer Control - The Remote Manipulator System (RMS) on the Shuttle is an example of the state of the art of teleoperation technology used in existing spacecraft. Although its operations are routinely monitored visually or with TV cameras, it has only limited dexterity and no sensory feedback. Arm control is achieved with a computer program which translates inputs into arm motion through a conventional hand controller. A supervisory control routine has been implemented which permits the arm to follow a predetermined trajectory. This alternative may be thought of as the next generation RMS with force/torque reflection and perhaps tactile feedback. The major difficulty likely to be encountered in its development centers on the computer system, as will be true with the remaining alternatives.

4. Teleoperator Maneuvering System with Manipulator Kit - This would be a remotely controlled device with special-purpose and multifingered end effectors, and an ability to attach itself to handles or fixtures while coordinating its activities with other subsystems.

It would be much more versatile than a dedicated manipulator, possessing an onboard computer with updatable knowledge bases and built in diagnostic and fault-tolerant software. A great deal of R&D would be required, but the payoffs in terms of productivity and technology transfer would be high.

5. Dexterous Manipulator with Sensory Feedback - This system represents the essence of telepresence. It would start with the components of current master-slave manipulators: a control station with one or two master arms; a remote worksite with one or two slave arms geometrically similar to the master arms; and video feedback. It would be expanded, though, to include greater dexterity, stereovision, movable points of view, high resolution zones of focus, as well as force, tactile and thermal feedback. Voice recognition will also be considered in the design. From a development point of view, the man-machine interfaces such as electronic controls and displays, computer graphics, instrumentation engineering, workstation design, and ergonomics will be of primary importance.

Fig. 3 depicts the hierarchy fashioned for the human productivity phase of the analysis. Major considerations for this subproblem include workload, support requirements, acceptability, and man-machine interfaces. At the next level a distinction is made between the onboard and ground crews. This is followed at level 4 by a set of six general criteria which are given explicit definition at level 5 by introducing 16 parameters.

Table 4a displays the input comparison matrix for the level 2 evaluations, and the resultant prioritization. The acceptability factor obtained the highest score of 0.372 but was closely followed by

the man-machine interface factor with a score of 0.366. Tables 4b-4d contain the local and global priorities for levels 3 through 5; the data associated with the last set of comparisons for the 5 alternatives with respect to each of the 16 parameters is shown in Table 4e. The final rankings are enumerated in Table 3. Alternative 3 -- a dedicated manipulator under computer control -- achieved the highest score of 0.309. By tracing the individual comparisons it may be reasoned that high crew acceptability as measured by the six criteria lead to this result. The least preferred alternative was the first -- an astronaut on EVA with tools -- primarily because of the extensive planning required to perform such a task, coupled with the obvious physical hazards. Note that R&D costs, complexity of design, and operational difficulties do not play a significant role in this phase of the analysis.

TABLE 4a. PRIORITIES FOR THE MAJOR CONSIDERATIONS ASSOCIATED WITH SPACE STATION HUMAN PRODUCTIVITY

Considerations	1	2	3	4	Priorities	Output Parameters
1) Workload	1	3	1	1/3	0.203	$\lambda_{\max} = 4.30$
2) Support		1	1/5	1/7	0.059	C.I. = 0.101
3) Accept.			1	2	0.372	C.R. = 0.112
4) Man-Mach.				1	0.366	

TABLE 4b. PRIORITIZATION OF LEVEL 3 FOR HUMAN PRODUCTIVITY SUBPROBLEM

		Local Priorities			Global Priorities
	Crew	Workload	Support	Accept.	Man-Mach.
1) Onboard	0.833	0.875	0.900	0.900	0.885
2) Ground	0.167	0.125	0.100	0.100	0.115

TABLE 4c. PRIORITIZATION OF LEVEL 4 FOR HUMAN PRODUCTIVITY SUBPROBLEM

Criteria	Local Priorities		Global Priorities
	Onboard	Ground	
1) Training	0.029	0.178	0.046
2) Logistics	0.181	0.433	0.210
3) Performance	0.114	0.000	0.101
4) Org. Struct.	0.089	0.084	0.088
5) Health	0.482	0.041	0.431
6) Decision Mkg.	0.105	0.265	0.124

TABLE 4d. PRIORITIZATION OF LEVEL 5 FOR HUMAN PRODUCTIVITY SUBPROBLEM

	PRIORTITIES	
	<u>Local</u>	<u>Global</u>
<u>Training</u>		
1) Regimen	0.246	0.011
2) Time	0.544	0.025
3) Tools	0.141	0.007
4) Support Personnel	0.069	0.003
<u>Logistics</u>		
5) Planning & Scheduling	0.066	0.014
6) Maintenance	0.149	0.031
7) Rescue	0.785	0.165
<u>Performance</u>		
8) Stability in Zero-g	0.167	0.017
9) Working Environment	0.833	0.084
<u>Organizational Structure</u>		
10) Conflict Resolution	0.250	0.022
11) Human Reliability	0.750	0.066
<u>Health</u>		
12) Physical Health	0.875	0.378
13) Psychological Health	0.125	0.054
<u>Decision Making</u>		
14) Intelligence	0.238	0.029
15) Information Processing	0.136	0.017
16) Sensory Load	0.625	0.077
		<u>1.000</u>



TABLE 4e. PRIORITIZATION OF LEVEL 6 FOR HUMAN PRODUCTIVITY SUBPROBLEM

Parameters	LOCAL PRIORITIES				
	Alternatives				
	1	2	3	4	5
1) Regimen	0.038	0.079	0.440	0.230	0.213
2) Time	0.042	0.131	0.534	0.166	0.127
3) Tools	0.049	0.469	0.269	0.133	0.079
4) Support Personnel	0.033	0.233	0.410	0.177	0.147
5) Planning & Scheduling	0.029	0.149	0.510	0.105	0.207
6) Maintenance	0.055	0.479	0.255	0.131	0.080
7) Rescue	0.027	0.285	0.285	0.117	0.285
8) Stability in Zero-g	0.047	0.144	0.557	0.126	0.126
9) Working Environment	0.034	0.113	0.446	0.162	0.226
10) Conflict Resolution	0.049	0.167	0.324	0.125	0.335
11) Human Reliability	0.415	0.119	0.052	0.100	0.315
12) Physical Health	0.027	0.243	0.243	0.243	0.243
13) Psychological Health	0.031	0.124	0.438	0.113	0.294
14) Human Intelligence	0.046	0.103	0.470	0.111	0.270
15) Information Processing	0.422	0.163	0.052	0.110	0.254
16) Sensory Load	0.058	0.140	0.489	0.116	0.197

#### 4.2 Economics

The Space Station is expected to be a vital national resource, not only for scientific experimentation, but for technological innovation and commercialization as well. As such, the Congress has tentatively allocated \$8 billion for the program to be spent proportionately over the next seven years. The goal is to reach the initial operating capability (IOC) outlined in Section 2 by 1992 although it is by no means clear whether the baseline system can be built for this price. Nevertheless, budgetary restrictions and competition for funds from other projects preclude any planning beyond this figure regardless of the present value of the program over its expected 20 year useful life.

In light of this constraint, IOC costs tend to dominate the three other major considerations shown in Fig. 4 -- the hierarchical diagram used in the economic analysis. While long term benefits to the U.S. economy and increased worker productivity are extremely important issues, the first concern is to bring the program in on budget. In fact, advanced automation will play a major role in this regard by permitting a reduction in support personnel through greater autonomy, and introducing improved methods of construction and assembly. Examining recurrent costs, in addition to enhanced crew productivity, cost savings will be realized by lowering the amount of ground resources needed, and by extending the lifetimes and versatility of Space Station systems. Intelligent computer-aided instruction can similarly reduce the costs associated with preflight training, while automatic fault diagnosis, isolation, and recovery can allow partially failed equipment or experiments to remain in operation without having to immediately dispatch a repair team.

Taking a long term view, NASA's tradition of promoting

technologies that have grown out of its basic and developmental research will be taking on an even greater dimension due in part to the decline in the percentage of revenues being spent by U.S. industries on R&D. Cooperation with the private sector will be a key item on the agenda. Accordingly, several areas will be emphasized that to date have hindered the progress and acceptance of automation by many domestic manufacturers (see Ayres and Miller 1983). For example, the lack of standardization in computer systems, as evidenced by a proliferation of languages and disparate intercommunication techniques, has been a principal deterrent to full implementation. It is felt that an impetus by the government toward more universal computer interfaces and software in support of Space Station requirements will facilitate wider acceptance of automation by industry.

Some examples of technology transfer that have now become commonplace include styrofoam insulation and nuclear magnetic resonance imaging used in medicine. Success in meeting Space Station objectives for fault tolerance and recovery techniques will provide the understanding needed by industry to implement automated and autonomous systems on a commercial level. And while the utilization of robotics in space involves considerably different approaches in basic design and qualification testing, research in adaptive control and artificial intelligence is readily transferrable to ground-based firms. Similarly, man-machine interface requirements for robots and teleoperators will apply equally to space and ground applications.

The final point that should be made about the major economic considerations concerns the commercialization opportunities that the Space Station will afford. In particular, working in space provides a variety of unique conditions that may be effectively exploited if

access is available at a reasonable cost. These include

- Microgravity
- High vacuum
- Isolation from disturbances and contamination
- Direct solar energy and cosmic rays
- A synoptic view of the Earth

Because automation will permit more efficient use of the crew's time, it will help reduce operating costs, which in turn will affect the rates that the government will have to charge its customers for using Space Station facilities. Whatever the rates, however, fault-tolerant, highly reliable computers will ensure effective collection of experimental data and support for manufacturing processes.

Returning to Fig. 4, we see that each of the five system alternatives are subsequently compared at level 6 against the following five cost parameters: hardware, software, support equipment and documentation, maintenance, and time saved. It should be noted that in the engineering design phase of any program, these parameters would have to be given much greater definition and their values determined explicitly (see Zimmerman et al. 1985 for more detail). Our concern here, though, is only with relative orders of magnitude, and not specific values.

Because the actual computations closely parallel those described in Section 4.2, the individual results for the economic subproblem will not be presented here. The final rankings for each alternative, however, are displayed in Table 3 where it can be seen that the first -- an astronaut on EVA with tools -- convincingly dominates the others. This result can be traced back to the strong preference placed on IOG costs by the decision maker throughout the analysis. Table 5 presents

the level 2 comparison data which serves to dramatize this point.

TABLE 5. PRIORITIES FOR THE MAJOR CONSIDERATIONS ASSOCIATED WITH SPACE STATION ECONOMICS

Considerations	1	2	3	4	Priorities	Output Parameters
1) IOC Costs	1	5	5	7	0.619	$\lambda_{\max} = 4.240$
2) Recur. Costs		1	1/3	3	0.109	C.I. = 0.080
3) Prod. Improv.			1	5	0.220	C.R. = 0.089
4) Long-Term				1	0.052	

#### 4.3 Design

Fig. 5 depicts the 4-level hierarchy used in the design phase of the evaluation. The following five major considerations were identified at level 2: physical characteristics, safety, technical characteristics, performance, and technological opportunities. In the comparisons, it was found that safety was the predominant concern with performance a far off second. These results are presented in Table 6 while the alternative rankings may once again be found in Table 3. The most advanced alternative, number 5 -- a dexterous manipulator, with sensory feedback -- placed first, primarily due to its high ratings on safety, performance, and technology transfer. The EVA alternative was at the bottom of the list for exactly the opposite reasons.

In general, working in space can pose serious threats to humans because of the hostile surroundings or the nature of the materials and devices involved. Certain fuels are highly toxic or volatile while some facilities require high temperature or pressure environments. Completely automating the accompanying activities would remove humans altogether from potentially hazardous situations, but if the crew must

work outside the Station occasionally, the use of automatic fault diagnosis and response can significantly reduce the dangers.

TABLE 6. PRIORITIES FOR THE MAJOR CONSIDERATIONS ASSOCIATED WITH SPACE STATION DESIGN

Considerations	1	2	3	4	5	Priorities	Output Parameters
1) Physical Chr.	1	1/9	1/5	1/7	1/5	0.028	max = 5.545
2) Safety		1	7	7	9	0.630	C.I. = 0.136
3) Technical Chr.			1	1/3	1/3	0.071	C.R. = 0.122
4) Performance				1	2	0.159	
5) Tech. Opport.					1	0.111	

The reliability of any system may be characterized by the likelihood of failure or process interrupt, the degree or mode of failure, and the effort and time required for diagnosis, repair, and recovery from the degraded condition. While the increased complexity of a highly automated system can be expected to have an adverse effect on component failure rates, automation can improve overall reliability in several ways. Systems for monitoring and control are not subject to fatigue or time dependent error proneness as are humans, and software for automatic fault isolation and recovery can keep a critical system going until an astronaut has time to change out the failed part. In emergencies, automated systems specifically designed for crisis management can bring the troubled equipment to a fail-safe condition before extensive damage occurs. Without automation, humans may more frequently be placed in pressure prone situations such as EVA in which the chances for error increase significantly.

From a strictly design point of view, some of the factors that should be taken in account in the evaluation follows. First, the Space Station should accommodate alternate configurations which readily allow for additions to and deletions from the currently planned mission profiles. Second, all autonomous functions should be capable of being separately enabled, disabled, or updated under the supervisory control of the ground or flight crews. This is necessary to ensure adequate in-flight maintenance, modification, and performance analysis. Finally, because standard retrofit procedures attempted some years after the initial platform is launched would be prohibitively expensive, growth potential must be built into the design from the outset. At a minimum, this implies the incorporation of standard interfaces, the design for ease of assembly and servicing, and the design of an evolutionary computer system architecture. It is not surprising to note that the rankings of the five alternatives reflect these criteria almost exactly.

#### 4.4 Operations

A major goal for the Space Station is to minimize both crew and ground control involvement in system monitoring through onboard automation and platform autonomy. This will maximize crew availability for mission activities which include the servicing of internal and externally attached payloads, supervising laboratory experiments, deploying payloads and upper stages, and assembling large-scale structures. Initial ground control and support will be in the form of flight and system monitoring and assistance during the deployment, assembly, checkout, and verification of each new Space Station element. As time progresses, many of the mission planning activities and data management functions will be assumed by expert systems.

Automation and robotics technologies can increase human performance by decreasing operational requirements and by mechanizing many of the related functions. Skylab and Shuttle experience indicates that the individual productive time available per mission day is on the order of 10 hours (Zimmerman et al. 1985). The remainder of the day is taken up with housekeeping and personal chores. Productive time must include subsystem operation, monitoring, calibration, fault diagnosis and correction, planning, EVA, rendezvous/docking, customer servicing, and other user related activities. As an example, consider the monitoring and verification tasks associated with command and control - these are currently performed by the ground crew. Loftus (1983) reports that roughly 70 percent of the monitoring points are automatically telemetered to the ground. The balance, consisting of approximately 1000 data elements, is monitored onboard. Using a standard scan rate of one second per data element, and monitoring twice a day, a total time of 0.6 hours per day results. If the monitoring function were to be made completely independent from the ground, existing onboard procedures would require an additional hour per day. Thus, the need for automation is clear.

The verification and calibration function is generally more complicated because it requires a variety of steps: repeated instrument readings, a comparison of data with either the ground or other onboard instruments, and possibly a spacecraft control decision which itself must be verified. Both Skylab and Shuttle operational histories suggest that verification and calibration functions will consume approximately 0.3 crew hours per day. Table 7 provides an extrapolated list of associated times for the Space Station.



TABLE 7. ESTIMATED TIMES FOR SPACE STATION VERIFICATION  
AND CALIBRATION FUNCTIONS

Fuctions and Tasks	Approximate time Hours/Day
Plan Mission	0.5
Verify/Calibrate	
- Inertial Unit	0.6
- Docking System	0.3
- Accelerometers	0.3
- Thermal Control Systems	0.3
- Structural and Mechanical Loads	0.3
- Station and Experiment Pointing	0.3
- Power Subsystems	0.1
- ECLS Subsystems	0.1
- Experiment Instrumentation	0.6
- Test Intrumentation	No Value
Parameter Updates and Data Storage	<u>0.1</u>
	Total = 3.5 .

Fig. 6 displays the 6-level hierarchy used to evaluate the issues underlying Space Station operations. Major considerations in this model included administration and management, maintenance, house-keeping, and emergencies. At level 3 a distinction is made between onboard and ground personnel, while levels 4 and 5 contain the criteria and parameters, respectively. Table 8 embodies the input and output data for the first set of evaluations. As can be seen, emergency

considerations strongly dominate the other three, achieving a weight of 0.69. This might suggest that a remote manipulator or robotics system would be most preferred because of the reduced likelihood of emergency situations arising with their use. Nevertheless, the relatively high scores in performance and human factors an astronaut on EVA gets for the assembly task gives alternative 1 a substantial edge in the rankings (see Table 3).

TABLE 8. PRIORITIES FOR THE MAJOR CONSIDERATIONS ASSOCIATED WITH SPACE STATION OPERATIONS

Considerations	1	2	3	4	Priorities	Output Parameters
1) Admin. & Mgt.	1	1/3	3	1/7	0.088	$\lambda_{\max} = 4.264$
2) Maintenance		1	5	1/7	0.178	C.I. = 0.088
3) Housekeeping			1	1/9	0.043	C.R. = 0.098
4) Emergencies				1	0.690	

## 5. DISCUSSION

The final step in the analysis is to derive the overall rankings by combining the results obtained for each of the four subproblems. The collective weights are presented in Table 3 where it can be seen that alternative 2 -- a dexterous manipulator under human control -- slightly outscores alternative 3 -- a dedicated manipulator under computer control. Although the latter is clearly the superior choice when only human productivity is considered, its poor scores in 'economics' and 'operations' reduce its attractiveness. Notice that the first alternative, EVA, turns out to be a rather weak contender despite its high scores in these two areas. This can be traced directly to its unacceptable showing in 'human productivity'. On the other hand, the fifth alternative -- a dexterous manipulator with sensory feedback -- does quite well in all categories, being the system of choice in 'design', but cannot currently be justified from an economic point of view.

In order to test the sensitivity of these findings to variations in judgement, the comparison data in each subproblem were locally perturbed and the individual and collective sets of weights recomputed. It was found that as long as transitivity was preserved, the overall results showed very little variation, with the rankings rarely changing. As would be expected though, the impacts accompanying preference shifts are more pronounced if they occur near the top of the hierarchy. For example, the importance of 'design' would only have to be increased by about 20 percent with respect to 'human productivity' in Table 1 before alternative 5 becomes dominant. This observation conforms directly with the way decisions are made in practice since upper management would be expected to provide the higher level

judgements.

With regard to data collection, it should be mentioned that the interviewing process can be rather time consuming and tedious as the size of the model grows. If the decision maker is unfamiliar with the methodology, it usually takes about 30 minutes of explanation and demonstration before he feels comfortable answering the questions. An additional 45 to 60 minutes are then required to elicit the comparison data for a 6-level hierarchy equivalent in complexity to the human productivity model. Some individuals found it easier to start at the bottom of the hierarchy with the parameters rather than at the top with the more general criteria. Note that all computations were performed in negligible time on an IBM PC using an interactive Basic program. As a benchmark, it takes about 5 seconds to compute the eigenvector of a 6x6 matrix and at most 50 seconds to solve any one of the four subproblems.

From an operational standpoint, rather than do all the analyses during the first interview, it may be more efficient to collect the data off line, then compute the weights, perform a sensitivity analysis, and, if possible, hold a followup session to discuss the results. Even the most experienced analyst makes mistakes, and the time looking for and correcting errors during the interview can only lead to impatience and hasty judgements on the part of the decision maker.

## 6. CONCLUSIONS

It has been shown how the Analytic Hierarchy Process can be used to evaluate automation and robotics applications for the upcoming Space Station. The methodology is completely general, though, and need not be limited to these technologies alone. Other promising areas of application include the selection of the food system, habitat design, and the determination of payload priorities. In this regard, the major considerations, criteria, and parameters developed for each of the four subproblems should not be thought of as fixed. Each new problem will usually require modifications or extensions of these factors to accommodate unique concerns. The flexible nature of the program easily permits such adjustments.

If a more quantitative approach is called for, the AHP is often a good first step in defining and structuring the problem. The fact that it requires only qualitative inputs, though, gives it an advantage over the more formal multicriteria techniques such as multiattribute utility theory and goal programming in that it can be used effectively in the early stages of a program before detailed cost and performance data are available. The time and effort saved at the outset will return dividends throughout the course of development.

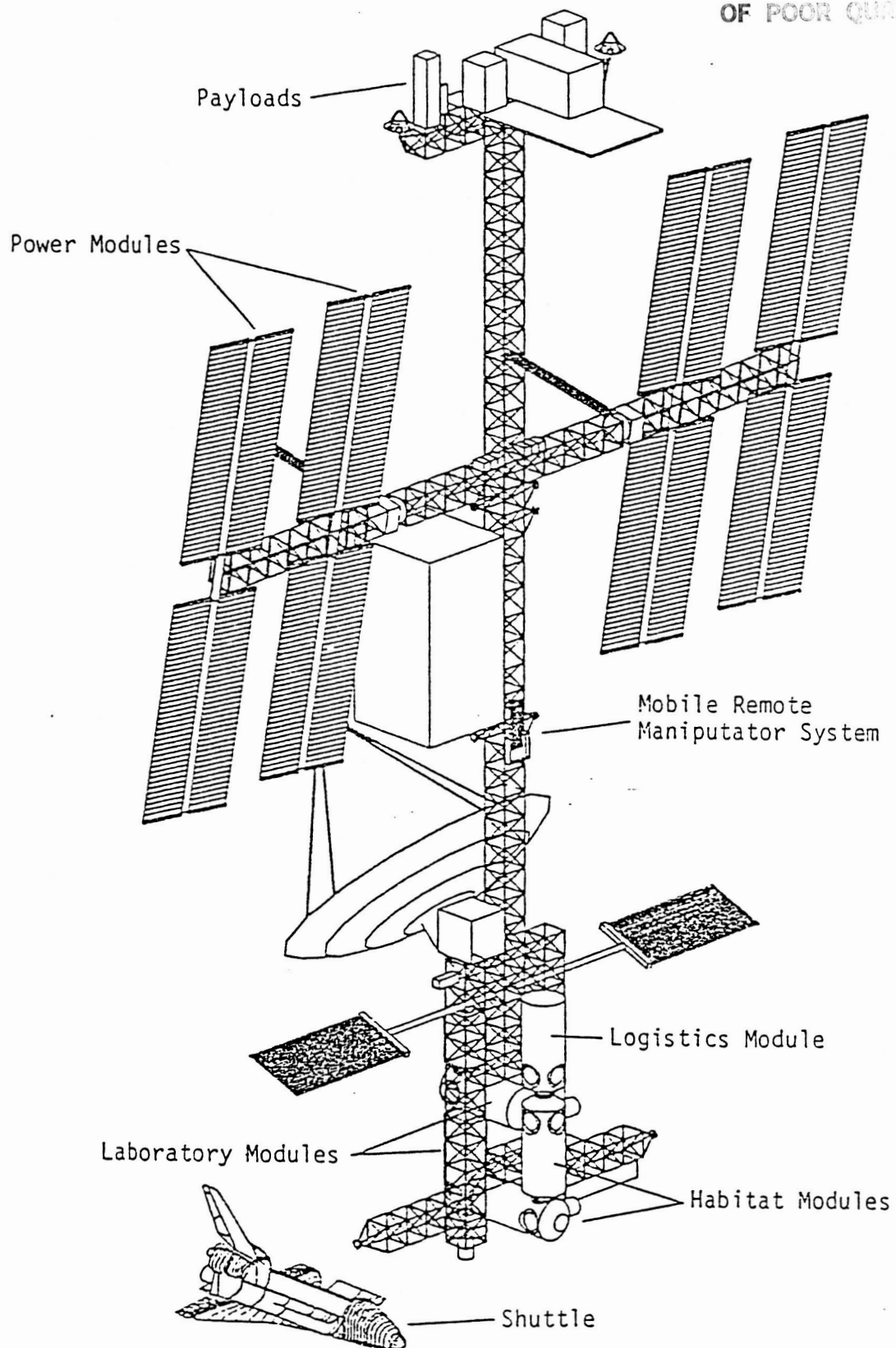


Fig. 1 - Baseline Space Station Configuration

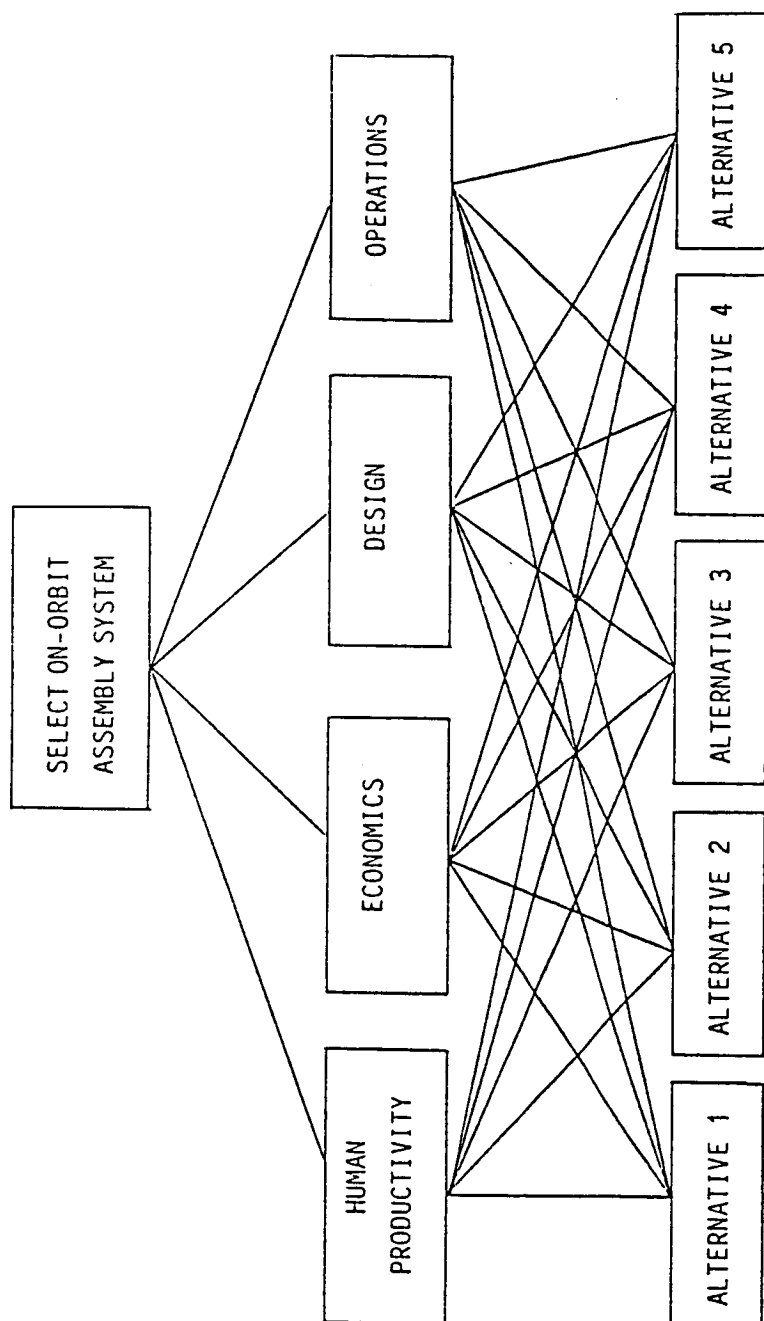


Fig. 2 - Summary 3-Level Hierarchy For Selection Problem

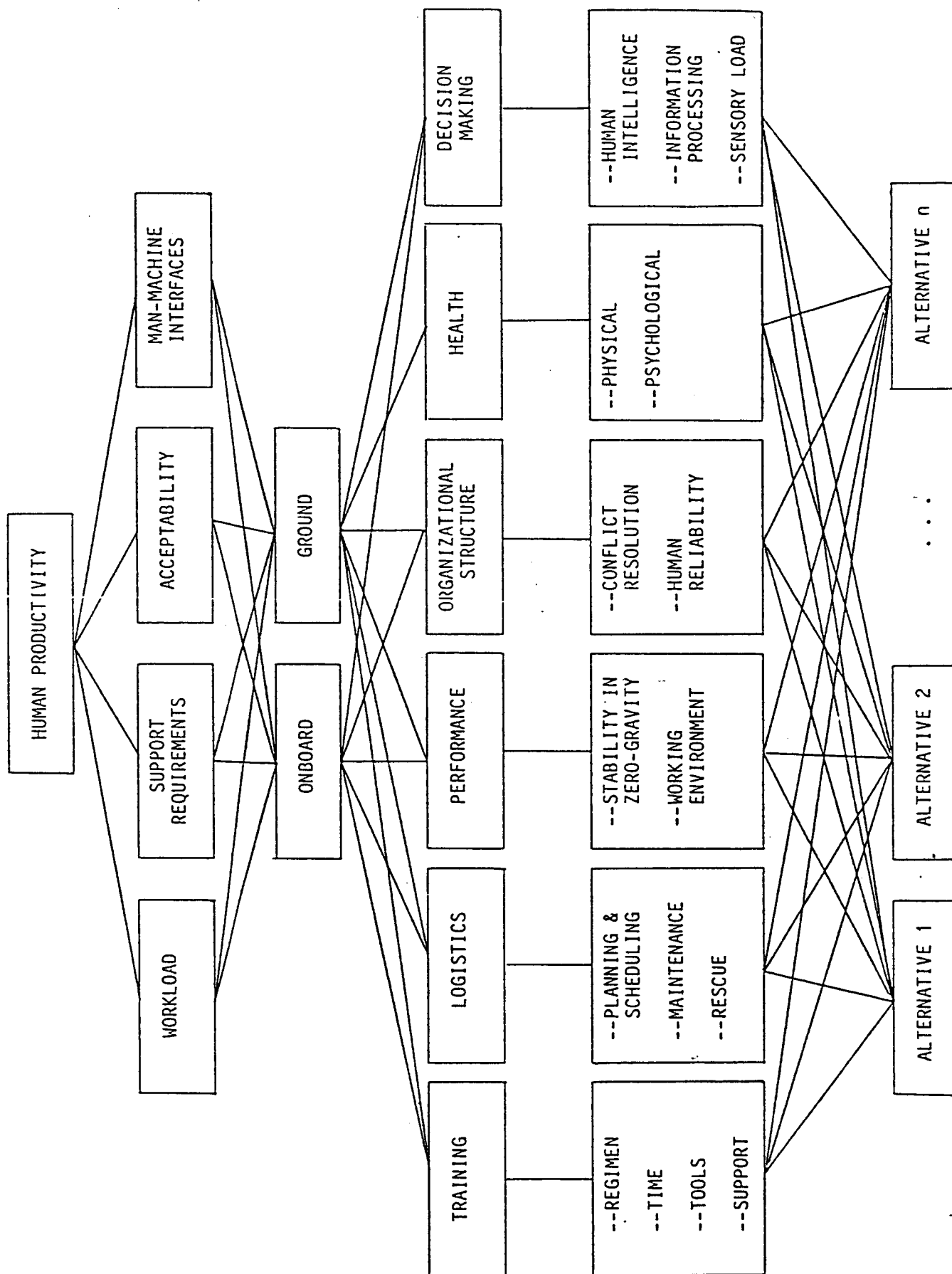


Fig. 3 - Hierarchy For Human Productivity Analysis



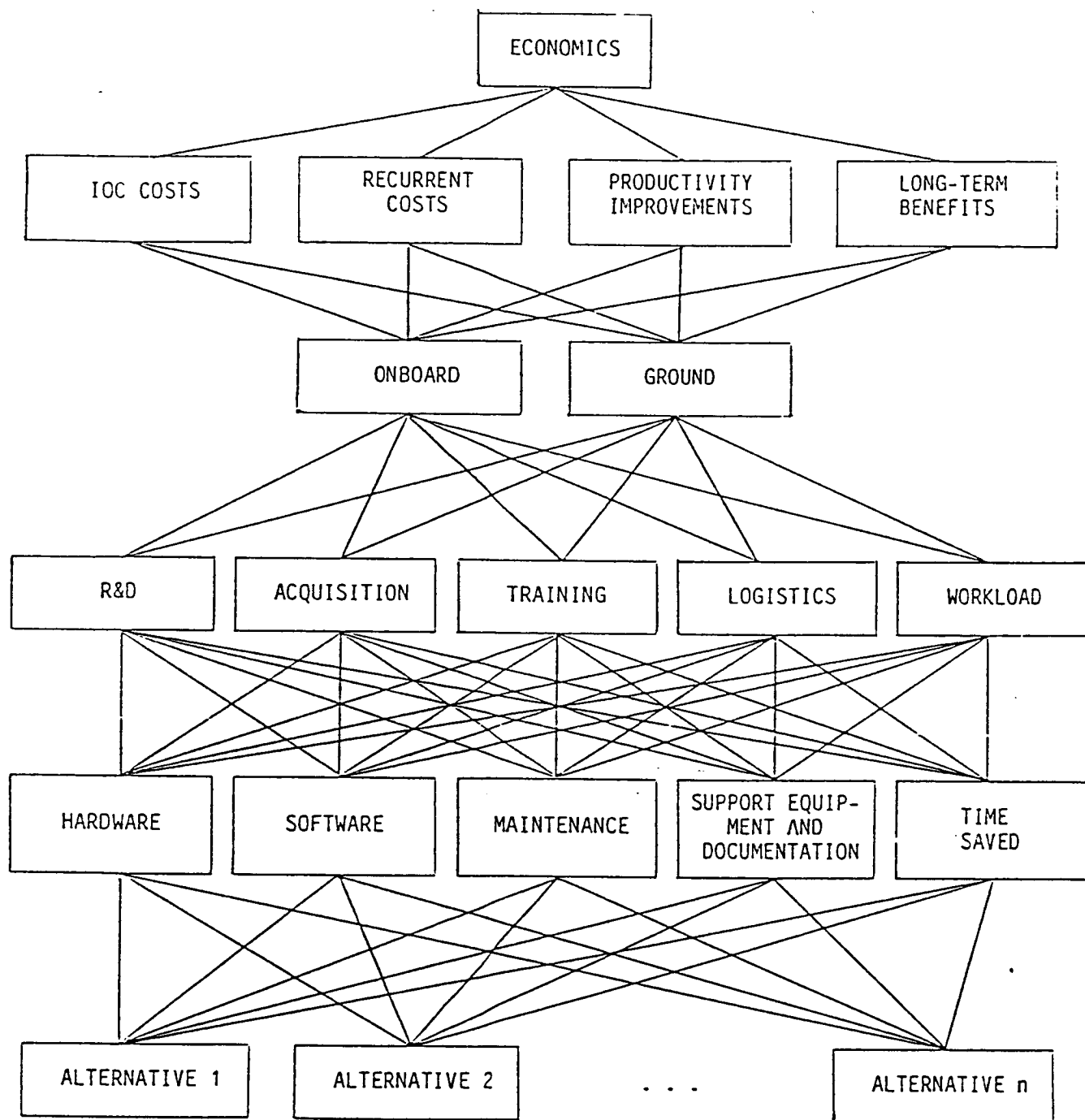


Fig. 4 - Hierarchy For Economic Analysis

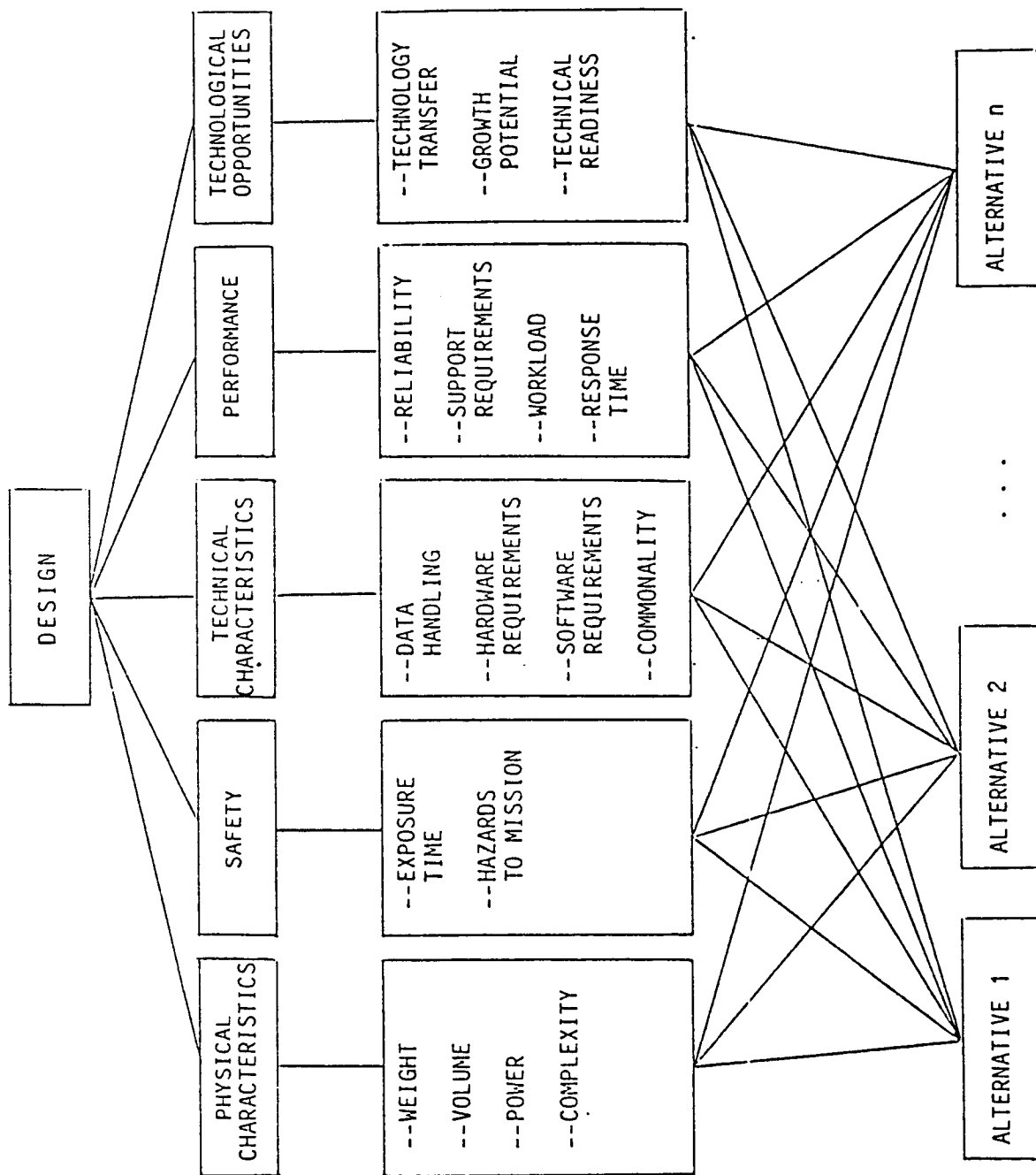


Fig. 5 - Hierarchy For Design Analysis

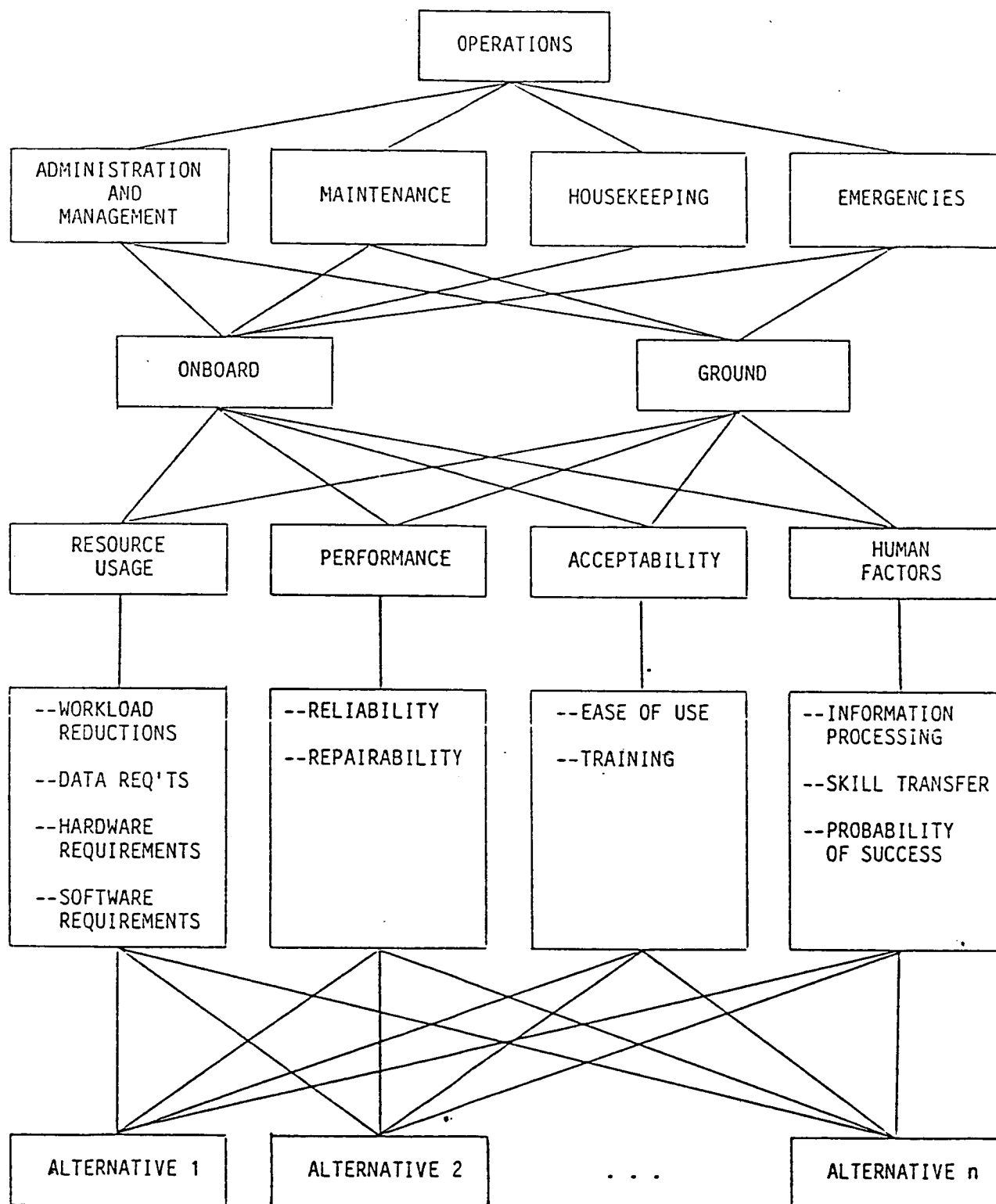


Fig. 6 - Hierarchy For Operations Analysis

## REFERENCES

- Arbel, A. and A. Seidmann, "Performance Evaluation of Flexible Manufacturing Systems," IEEE Trans. Systems, Man, and Cybernetics SMC-14(4) 606-617 (1984).
- Ayres, R.U. and S.M. Miller, Robotics Applications & Social Implications. Ballinger Publishing Co., Cambridge, MA (1983).
- Bard, J.F., "An Assessment of Industrial Robots: Capabilities, Economics, and Impacts," to appear in Journal of Operations Management (1985).
- Bard, J.F., "The Costs and Benefits of a Satellite-Based System for Natural Resource Management," Socio-Economic Planning Science 18(1) 15-24 (1984).
- Bard, J.F., "Designing Large-Scale Multiattribute Systems," in Handbook of Technology Management (D.F. Kocaoglu, ed.) Wiley, NY (1986).
- Dyer, J.S. and R.F. Miles, Jr., "An Actual Application of Collective Choice Theory to the Selection of Trajectories for the Mariner Jupiter/Saturn 1977 Project," Operations Research 24 220-244 (1976).
- Hall, S.B. and H.L. Wolbers, "The Human Role in Space," Seventh Monthly Status Report, NAS 8-35611, DR-2 McDonnell Douglas Astronautics Company, Huntington Beach, CA (May 1984).
- Jarvis, J.F., "Robotics," Computer 17(10) 283-292 (1984).
- Keefer, D.L., "Allocation Planning for R&D with Uncertainty and Multiple Objectives," IEEE Trans. Engineering Management EM-25(1) 8-14 (1978).
- Keeney, R.L. and H. Raiffa, Decisions with Multiple Objectives: Preferences and Value Tradeoffs. Wiley, NY (1976).
- Kirkwood, C.W. and R.K. Sarin, "Ranking with Partial Information: A Method and an Application," Operations Research 33(1) 38-48 (January-February 1985).
- Loftus, J.P., "An Historical Review of NASA Manned Spacecraft Crew Stations," to appear in Journal of British Interplanetary Society (1985).
- Madey, G.R. and B.V. Dean, "Strategic Planning for Investment in R&D Using Decision Analysis and Mathematical Programming," IEEE Trans. Engineering Management EM-32(2) 84-90 (May 1985).
- Malin, J.T. and N. Lance, "An Expert System for Fault Management and Automatic Shutdown Avoidance in a Regenerative Life Support Subsystem," Proceedings of the Instrument Society of America First Annual Workshop on Robotics and Expert Systems, Johnson Space Center, Houston, TX (June 27-28, 1985).

Miller, R.H., M.L. Minsky and D.B.S. Smith, "Space Applications of Automation, Robotics, and Machine Intelligence Systems (ARMIS)," NASA CR-162079, prepared for the NASA Marshall Space Flight Center by the Space Systems Laboratory and Artificial Intelligence Laboratory, MIT, Cambridge, MA (August 1982).

Morgan, T.W. and R.L. Thurgood, "Engineering Tradeoff Problems Viewed as Multiple Objective Optimization and the VODCA Methodology," IEEE Trans. Engineering Management EM-31(2) 60-69 (May 1984).

NASA, "Space Station Reference Configuration Description," JSC-19989 Systems Engineering and Integration Space Station Program Office, Johnson Space Center, Houston, TX (August 1984).

NASA, "Advancing Automation and Robotics Technology for the Space Station and the U.S. Economy," TM-87566, Advanced Technology Advisory Committee (ATAC), Artificial Intelligence Office, Johnson Space Center, Houston, TX (March 1985).

Saaty, T.L., "A Scaling Method for Priorities in Hierarchical Structures," Journal of Mathematical Psychology 15 234-281 (June 1977).

Saaty, T.L., "A Scenario and Priorities in Transport Planning: Application to the Sudan," Transportation Science 11(3) 343-350 (1977).

Saaty, T.L., The Analytic Hierarchy Process. McGraw-Hill, NY (1980).

Soffen, G.A., "The Viking Project," Journal of Geophysical Research 82(28) 3959-3970 (1977).

White, C.C. and A.P. Sage, "A Model of Multiattribute Decisionmaking and Trade-off Weight Determination Under Uncertainty," IEEE Trans. Systems, Man, and Cybernetics SMC-14(2) 223-229 (March/April 1984).

Wu, C.H. and R.P. Paul, "Resolved Force Motion Control of Robot Manipulator," IEEE Trans. Systems, Man, and Cybernetics SMC-12(3) 266-275 (May/June 1982).

Zimmerman, W.F., J.F. Bard and A. Feinberg, "Space Station Automation Tradeoff Analysis," JPL Report 85-13, Jet Propulsion Laboratory, Pasadena, CA (February 1985).

Zorpette, G., "Computers that are 'Never' Down," IEEE Spectrum 46-54 (April 1985).

## ACKNOWLEDGEMENT

This work was performed while the author was an ASEE-NASA summer faculty fellow at the Johnson Space Center. He would like to thank Jeri Brown for suggesting the problem, and his many JSC colleagues for their helpful comments and recommendations for improving the analysis.

## DISTRIBUTED SYNTHETIC APERTURE RADAR SIMULATION

18815

Brian A. Bourgeois

Assistant Professor of Applied Mathematical Sciences

University of Houston-Downtown

Houston, Texas

ABSTRACT

Synthetic aperture radar (SAR) depends primarily on attainable frequency resolution rather than on large physical size of the antenna array. The distributed architecture concept (DSAR) incorporates active elements (amplifiers) at or near the elemental radiators of the array.

Since SAR's are expensive to build and expensive to test, a computer modeling approach is a feasible method of predicting the quality or nature of the SAR image from the proposed system parameters. The goal of this project is to produce a DSAR simulation software package. This report describes the progress made thus far and the work which remains to be done.

Extensive work on this project had been done previously by two NASA contractors. The principal task remaining involved the creation of a suitable interface between these programs and the hardware and software available at the Johnson Space Center. For example, all graphics routines needed to be replaced due to software incompatibility.

## INTRODUCTION

This project is a part of the NASA project MSART, or Multifunction Synthetic Aperture Radar Technology. The objectives of this program are to provide system studies, design approaches, and hardware demonstrations of an antenna system to be used for imaging the earth from the Shuttle, the Spacelab, and satellites. Our particular interest is in two computer programs. The first is an orbital simulation program, whose input is spacecraft geometry, antenna gain pattern, filter processing data, and target information and whose output is a simulated image of that target. This program, called OSS, was created at the Applied Research Laboratories (ARL) at the University of Texas at Austin [Crow and Graf, 1979]. The second program inputs antenna array characteristics along with type and extent of antenna performance failure to produce the antenna gain pattern in graphical or tabular form. This program, called DSAR, was produced at the Physical Science Laboratories (PSL) at New Mexico State University [Jedlicka and Henry, 1985]. The first program was then modified, to input the antenna gain pattern produced as output from DSAR. This work was also done at ARL [Estes, 1985].

These programs, as delivered to NASA, required a great amount of further work in order to be used. All graphics routines had to be replaced because the software packages used were incompatible with those of NASA. In addition, many sections of code needed to be tailored to meet the specific needs of NASA as efficiently as



possible. For example, OSS is general enough to handle an arbitrary orbit about an arbitrary planet, but, for the present, NASA need only concentrate on the Shuttle's orbit about the earth.

## THEORY

There exist two practical methods for obtaining resolution of a signal reflected from two different points. If the points are stationary with respect to the direction of motion of the transmitter, and at different distances, their reflected signals can be distinguished by the time it takes the signal to return. The smaller the duration of the pulse, the better is the resolution. This is the basis for range resolution, the range being perpendicular to the line of motion.

On the other hand, the Doppler theory tells us that if there is a relative line of sight motion between transmitter and reflector, there will be a frequency shift in the received signal proportional to that velocity. Therefore, two points separated in the azimuth direction, that is, parallel to the vehicle motion, will reflect signals with different frequency variations due to their having different velocity components parallel to the motion. This is the basis for azimuth resolution in synthetic aperture radar (SAR).

Unlike convention radar, then, SAR azimuth resolution is independent of antenna beamwidth. Since beamwidth is inversely proportional to antenna length, an impractical physical size is

replaced by complex signal processing equipment. The quality of the SAR image is an involved function of the parameters of the antenna, the signal processor, and the geometry.

The distributed architecture concept (DSAR) incorporates transmit/receive (T/R) modules at or near the elemental radiators of the array. The most important components of the T/R modules are the high power amplifier (HPA) and the low noise amplifier (LNA). The major advantages of this approach include [Jedlicka,1984] :

- 1) enhanced system reliability due to graceful degradation of array pattern performance;
- 2) achievement of high total radiated power with solid state devices;
- 3) improved system noise figure;
- 4) mechanical deformation and motion compensation as well as variable incidence angles (with electronic beam steering option).

## RESULTS

Due to the enormity of the task, the goals for the summer were restricted to work on the DSAR program. Specifically, the goals were

- 1) to load and compile the program on the VAX 11/780 computer;
- 2) to rewrite the graphics routines, both two and three dimensional, using the software package DISSPLA;
- 3) to make the program user-friendly;
- 4) to produce an operator's manual which will enhance 3).

All of these goals were realized. A copy of the program and the manual are available upon request. The only shortcomings, due to time limitations, are in 3) and 4). The program could be made more friendly to the user. The operator's manual is somewhat sketchy in parts, but the essentials are covered sufficiently. In addition, several portions of the program were not thoroughly tested.

#### CONCLUSIONS

One phase of the project has been completed. We now have a working version of the DSAR program, ready to test the effects of component performance degradation and mechanical deformation on the far-field antenna patterns. What remains to be done is a similar job on the lengthier GSS program. It has been loaded on the UNIVAC computer. Graphics must be supplied, the code must be standardized, and an interface with DSAR must be provided.

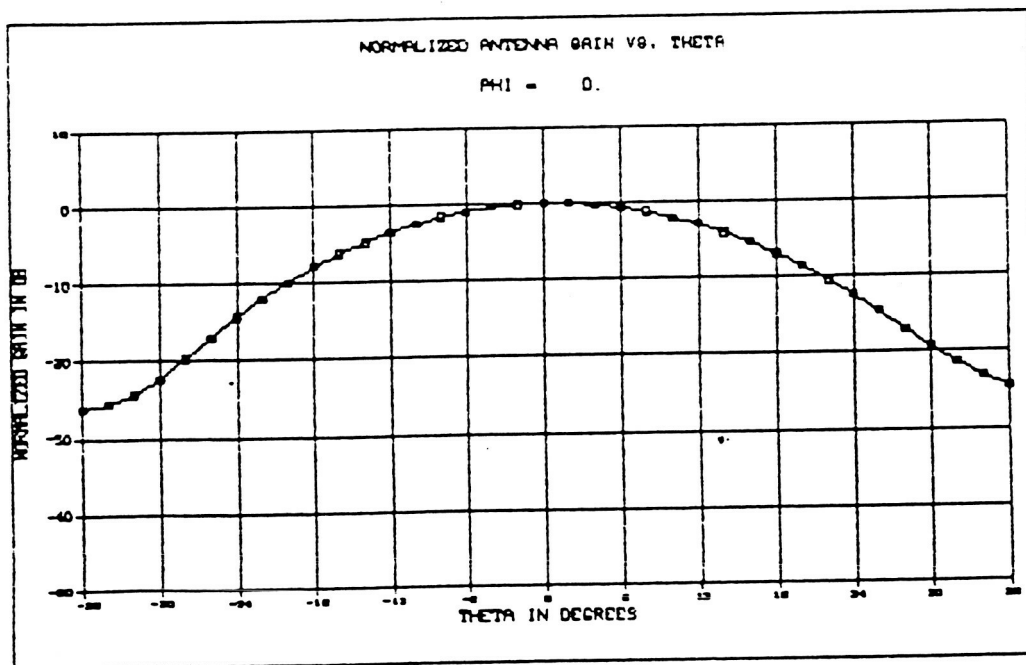
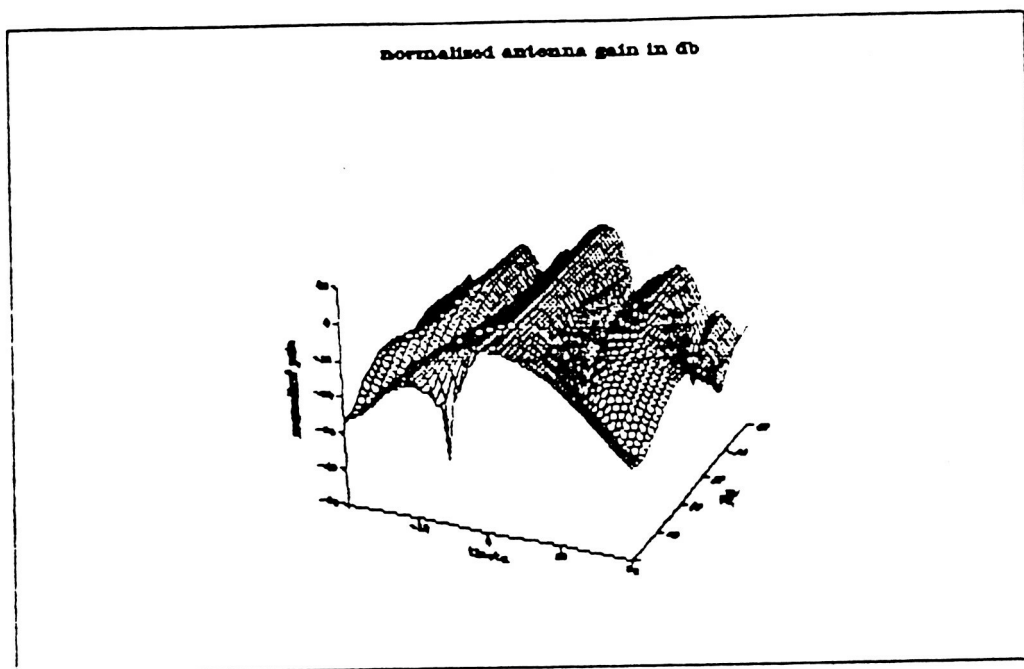
# Sample Input

```

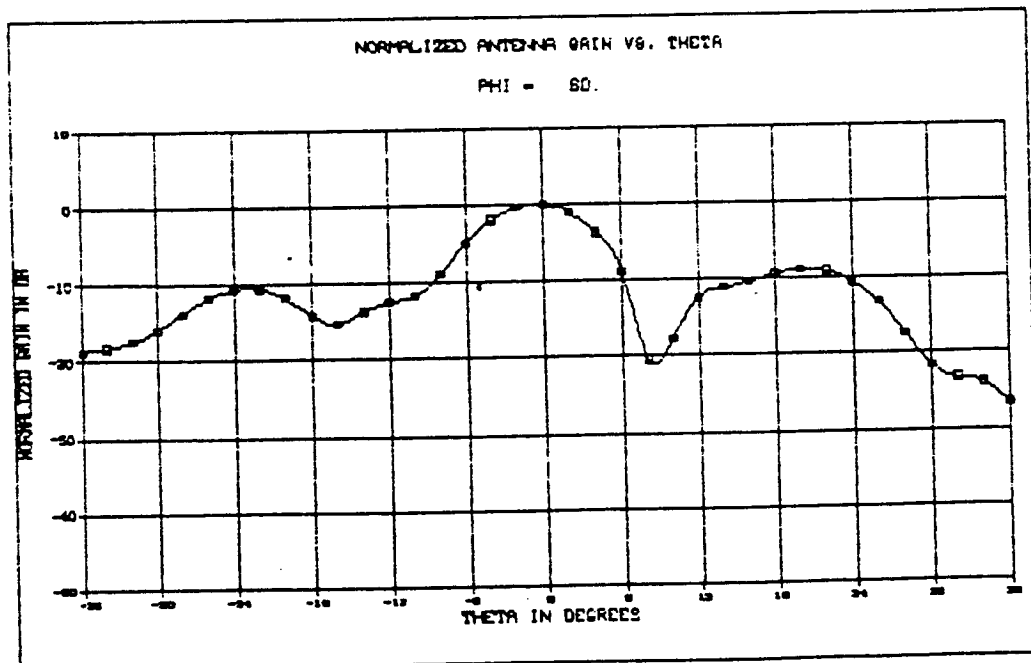
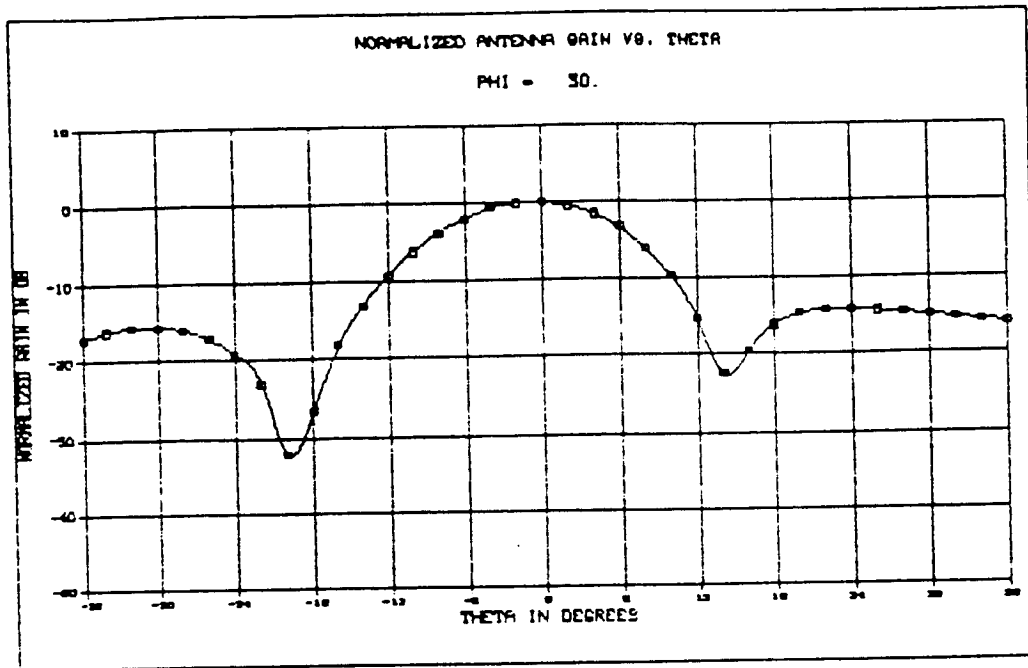
DSAR INPUT TEST
  6 X 12 ELEMENT ARRAY  C-BAND
FREQ F10.0 : 5.300
NUM ELEMS : 6 12 2 3
SPACING : 4.225 4.500 0.0 0.0
STAGGER : 0.0 0.0
NO BITS : 0
RAN QUAN : 0
CO PHAS : 1 1
PANELS : 1 2
ACOL,PCOLX : 1.0 0.0
AROW,PROWY : 1.0 0.0
: -5 22.5
TAPER : 1
DIRECT : X
SIDELOBE : 20.0 20.0
EL PATTERN : 1
ZAP : 2
T/R X,Y : 2 6
NZAP : 3
IRFLAG : 0
ISED2 : 999
ISKIP : 0
2D TICKS : 3
GAIN PHI : 0.0 90.0 2.0
GAIN THETA : -36.0 36.0 2.0
INCREMENTS : 9 9 1 15
3D, IDONT : 1 0
3D TICKS : 9 9
MN,VAR,DEL : 1000. 500. 30.0
AMP,SEED FL : 1 0
90W INFO : 0 0.0 0
STEER : 0.0 0.0 0
ICUT FLAG : 0
3D VIEW PT : 45 -90 70

```

Sample Output



# Sample Output



L. C. Chow

18816

Associate Professor

Mechanical Engineering Department

Washington State University

Pullman, Washington

ABSTRACT

A description of the condensation heat transfer process in microgravity is given. A review of the literature is also reported. The most essential element of condensation heat transfer in microgravity is the condensate removal mechanism. Other important features are also pointed out. In this report, two mechanisms for condensate removal are analyzed by looking into two problems. The first problem is concerned with film condensation on a flat porous plate with the condensate being removed by suction at the wall. The second problem is an analytical prediction of the heat transfer coefficient for condensing annular flows with the condensate film driven by the vapor shear. It is concluded that both suction and vapor shear can effectively drain the condensate to ensure continuous operation of the condensers operated under a microgravity environment. It is recommended that zero-g flight experiments be carried out to verify the prediction made in the present report. The results contained in this report should also aid in the design of future space condensers.

---

NASA Colleague: Richard C. Parish EC2 X4941

## INTRODUCTION

Two-phase heat transfer processes have been investigated extensively in the past. With very few exceptions, these investigations were performed on earth where the heat transfer processes can be significantly affected or even dominated by the earth's gravity. Research in two-phase heat transfer processes under microgravity has potentially a very high payoff in many areas of applications, such as in power generation in space and in spacecraft thermal control and management.

Condensation is the change of phase from the vapor state to the liquid state. It is accompanied by heat transfer because the latent heat of condensation must be removed. In film condensation, the liquid condensate forms a continuous film which covers the condenser surface. The film usually constitutes the dominant resistance to heat transfer for latent heat removal. It is therefore essential to drain the condensate and keep the film as thin as possible. If the condensate is not effectively removed, the condenser may flood and can lead to a halt in further condensation of the vapor. In an earth-based condenser design, drainage of the condenser is typically provided by exploiting the gravitational force. In the absence of gravity, the condensate can be removed by suction, by surface rotation, by shear stress due to vapor flow, by capillary pumping or by a mechanical wiper.

Pertinent literature was reviewed and it was found that data from two-phase heat transfer experiments with reduced gravity forces is very limited. Siegel (1) has summarized the work on the effects of reduced gravity on heat transfer up to November 1966. Eastman et al. (2) have assessed the current status of research in boiling, condensation, and two-phase flow patterns under reduced gravity. Most of the experiments on condensing flows under reduced gravity used mercury (a nonwetting



fluid) as the working fluid (3-5). The experiments were performed on an AJ-2 airplane flying a Keplerian trajectory. The Air Force Flight Dynamics Laboratory has also performed some experiments on forced convection evaporators and condensers in straight, tapered, and vortex tubes in zero-g aircraft flights (6, 7). NASA has also demonstrated that stable condensation can be maintained for zero-g condensation (8). Experiments in two-phase fluid flow regimes were performed aboard a KC-135 aircraft with air and water as working fluids (9). Preliminary design of flight hardware for two-phase fluid research was conducted for NASA-Lewis Research Center (10). This work may eventually lead to space experiments for liquid reorientation, pool boiling, and convective boiling with reduced gravity forces.

As mentioned previously, condensate removal is the key to having stable, steady-state condensation under microgravity. Liquid film removal by suction through a porous plate or a slot has been suggested (11, 12). Another mechanism is to create an artificial gravity for condensate removal by surface rotation (13). For convective condensation, vapor shear can also provide a driving force for moving the condensate film (14 - 16). In a heat pipe, the condensate is removed from the condenser section by capillary pumping provided by the wick structure (17). A mechanical wiper to thin the liquid film has also been suggested (18).

The presence of a small amount of noncondensable gas can lead to a significant reduction in condensation heat transfer (19, 20). When noncondensable gases are present, they move with the vapor towards the condensing surface where the vapor is condensed. Since the gases do not condense, they accumulate in the proximity of the liquid-vapor interface, forming a gas layer. This gas layer retards the movement of vapor to the condensing surface.

It is well known that surface tension or capillary force can be used to thin the condensate layer, thereby enhancing the film condensation rate (21, 22). This method of enhancing the condensation rate is also applicable under a microgravity environment.

The purpose of the present effort is to assess the potential of using suction and vapor shear to remove the condensate for space applications. It is essential to have very effective condensers that are capable of providing high heat fluxes with a small temperature difference. For example, for heat rejection in space, such a condenser will allow a maximum radiator temperature, resulting in lower weights for both the radiator and condenser.

#### CONDENSATION ON A FLAT POROUS PLATE WITH UNIFORM SUCTION

The problem is depicted in Figure 1. Saturated vapor at temperature  $T_s$  is situated above a cooled porous plate maintained at  $T_w$ . The liquid condensate is being sucked into the plate with a velocity  $v_o$  ( $v_o < 0$ ). Under steady-state conditions, the mass condensation rate is the same as the condensate removal rate, and the film thickness  $\delta$  is a constant.

The energy equation is

$$\rho_L c_{pL} v_o \frac{dT}{dy} = k_L \frac{d^2 T}{dy^2} \quad (1)$$

The boundary conditions are

$$\text{at } y = 0, \quad T = T_w$$

$$y = \delta, \quad T = T_s$$

The temperature distribution  $T$  across the film is given by

$$\frac{T - T_w}{T_s - T_w} = \frac{1 - e^{-y/\beta}}{1 - e^{-\delta/\beta}} \quad (2)$$

where

$$\beta = \frac{k_L}{\rho_L c_{pL} v_o} = \frac{\alpha_L}{v_o}$$

and  $k_L$ ,  $\rho_L$ ,  $c_{pL}$  and  $\alpha_L$  are the thermal conductivity, density, specific heat and thermal diffusivity of the liquid condensate, respectively.

The condensate film thickness  $\delta$  can be determined by an energy balance at the interface

$$-\rho_L v_o h_{fg} = k_L \left. \frac{dT}{dy} \right|_{y=\delta} \quad (3)$$

It can be shown that

$$\begin{aligned} \delta &= -\frac{\alpha_L}{v_o} \ln \left[ 1 + \frac{c_{pL} (T_s - T_w)}{h_{fg}} \right] \\ &= -\frac{\alpha_L}{v_o} \ln (1 + Ja) \end{aligned} \quad (4)$$

where  $Ja = c_{pL} (T_s - T_w)/h_{fg}$  is the Jakob number.

For  $Ja < 0.1$ , equation (4) can be approximated to within 5% by

$$\delta = - \frac{\alpha_L}{v_o} Ja \quad (5)$$

and, equation (2) can be rewritten as

$$\frac{T - T_w}{T_s - T_w} = \frac{1 - e^{-yJa/\delta}}{1 - e^{-Ja}} \quad (6)$$

The heat transfer coefficient  $h$  is given approximately by

$$h = \frac{k_L}{\delta} = - \frac{k_L v_o}{\alpha_L Ja} = - \frac{\rho_L c_{pL} v_o}{Ja} \quad (7)$$

For condensation of water vapor, if  $\delta$  can be maintained by suction to 0.5 mm, then the heat transfer coefficient is approximately equal to 1300 W/m<sup>2</sup>K.

#### CONVECTIVE CONDENSATION INSIDE A TUBE

The situation is depicted in Figure 2. Consider a vapor at a temperature of  $T_s$  flowing inside a tube with a velocity of  $u_v$ . The tube wall is kept at a temperature of  $T_w$ , ( $T_w < T_s$ ). The flow regime is very likely to be annular. When the void fraction becomes very low, slug flow and bubble flow may be possible. The vapor

first condenses on the cooler wall and tends to remain there due to surface tension. The only kind of instability that may cause transition to slug or bubble flows is of Kevin-Helmholtz type. These transitions are not likely except when the void fraction is low.

Assuming the flow regime to be annular, in the absence of gravity, the motion of the condensate film is entirely due to vapor shear and momentum transfer due to condensation. We will solve for the motion of the condensate film but will ignore the velocity distribution in the vapor phase. A friction coefficient is specified at the vapor-liquid interface. The approach is similar to the one used in Reference 23.

Assuming the film thickness  $\delta$  is small compared to the tube diameter  $d$ , and ignoring the inertia of the liquid, a momentum balance for a fluid element inside the condensate film is

$$\mu_L \frac{\partial^2 u_L}{\partial y^2} = \frac{dp}{dz} \quad (8)$$

where  $\mu_L$  is the liquid viscosity,  $u_L$  is the liquid film velocity and  $p$  is the pressure.

Due to friction at the wall, it is expected that the pressure will decrease with  $z$ . There is also a small partial pressure recovery due to the decreasing vapor velocity caused by condensation. However, the pressure changes are expected to be very small compared to the absolute pressure. Thus, it is a good approximation to assume the vapor temperature, vapor density and vapor viscosity to be constant.

The velocity  $u_L$  is given by

$$u_L = \frac{1}{\mu_L} \frac{dp}{dz} \left( \frac{y^2}{2} - \delta y \right) + \frac{\tau_\delta}{\mu_L} y \quad (9)$$

The velocity  $u_{L\delta}$  at the interface is

$$u_{L\delta} = \frac{\tau_\delta \delta}{\mu_L} - \frac{1}{\mu_L} \frac{dp}{dz} \frac{\delta^2}{2} \quad (10)$$

In equations (9) and (10),  $\delta$  is the film thickness, and  $\tau_\delta$  is the shear stress at the vapor-liquid interface.

The liquid Reynolds number  $Re_L$  is given by

$$Re_L = \frac{\rho_L u_{L,ave} \delta}{\mu_L} = \frac{\rho_L}{\mu_L^2} \left( \tau_\delta \frac{\delta^2}{2} - \frac{dp}{dz} \frac{\delta^3}{3} \right) \quad (11)$$

where  $u_{L,ave}$  is the average velocity of the condensate.

The mass flow of the condensate increases with  $z$  due to condensation, and the rate of increase of  $Re_L$  is given by

$$\mu_L \frac{d Re_L}{dz} = \dot{m}_c'' \quad (12)$$

where  $\dot{m}_c''$  is the condensation mass flux.

The rate of condensation is determined by the heat transfer rate as the latent heat must be removed,

$$\dot{m}_c'' h_{fg} = \frac{k_L (T_s - T_w)}{\delta} \quad (13)$$

Combining equations (12) and (13),

$$\frac{d Re_L}{dz} = \frac{k_L (T_s - T_w)}{\mu_L h_{fg} \delta} = \frac{Ja}{Pr_L \delta} \quad (14)$$

where Ja is the Jakob number and  $Pr_L$  is the condensate Prandtl number.

Momentum balance for the vapor yields

$$\frac{dp}{dz} \sim \frac{\tau_\delta}{d} \quad (15)$$

This implies that the pressure gradient terms in equations (10) and (11) are smaller than the shear stress terms by a factor of  $\delta/d$ . Since  $\delta/d$  is very small, one can simplify the expressions for  $u_{L\delta}$  and  $Re_L$  as

$$u_{L\delta} \cong \frac{\tau_\delta \delta}{\mu_L} \quad (16)$$

$$Re_L \cong \frac{\rho_L}{\mu_L^2} \frac{\tau_\delta \delta^2}{2} \quad (17)$$

As the vapor condenses, the vapor mass flow rate decreases. Assuming the quality is unity at the inlet, then

$$\dot{m}_V + \dot{m}_L = \dot{m}_{VO} \quad (18)$$

where  $\dot{m}_V$  and  $\dot{m}_L$  are the vapor and liquid mass flow rates at any position  $z$  and  $\dot{m}_{VO}$  is the vapor mass flow rate at the inlet. From this, it can be shown that the vapor Reynolds number is

$$Re_V = \frac{\rho_V u_V d}{\mu_V} = Re_{VO} \left( 1 - \frac{4 Re_L}{Re_{VO}} \mu_R \right) \quad (19)$$

where  $Re_{VO}$  is the vapor Reynolds number at the inlet ( $= \rho_V u_{VO} d / \mu_V$ ), and  $\mu_R$  is the ratio of the viscosity of liquid to that of vapor ( $= \mu_L / \mu_V$ ). Since the vapor density and viscosity are assumed to be constant,

$$u_V = u_{VO} Re_V / Re_{VO} \quad (20)$$

As mentioned previously, the motion of the condensate is driven by the shear stress



at the interface.

$$\tau_{\delta} = \left( \frac{C_f}{2} \right)_E \rho_v (u_v - u_{L\delta})^2 + \dot{m}''_c (u_v - u_{L\delta}) \quad (21)$$

where the first term in equation (21) is due to the frictional drag between the vapor and the liquid, and the second term is due to the faster moving vapor condensing onto the slower moving liquid.

For laminar vapor flow ( $Re_v < 2300$ ), the frictional coefficient is given by

$$\left( \frac{C_f}{2} \right)_E = \frac{8}{Re_v} \quad (22)$$

For turbulent vapor flow ( $Re_v > 2300$ ),  $\left( \frac{C_f}{2} \right)_E$  is given by Henstock and Hanratty (24),

$$\left( \frac{C_f}{2} \right)_E = \left( \frac{C_f}{2} \right) (1 + 850 F) \quad (23)$$

where  $\frac{C_f}{2} = 0.023 Re_v^{-0.2}$

$$F = \frac{\delta \mu_R}{\sqrt{\rho_R} Re_v^{0.9}}$$

$$\rho_R = \rho_L / \rho_v$$

$$\gamma = [(0.707 \text{ Re}_{LF}^{1/2})^{2.5} + (0.0379 \text{ Re}_{LF}^{0.9})^{2.5}]^{0.4}$$

$$\text{and } \text{Re}_{LF} = 4\text{Re}_L$$

Nondimensionalizing distances and velocities by the tube diameter  $d$  and the inlet vapor velocity  $u_{v0}$ , respectively,

$$\bar{u}_v = \frac{u_v}{u_{v0}}, \quad \bar{u}_L = \frac{u_L}{u_{v0}}$$

$$\bar{z} = \frac{z}{d}, \quad \bar{\delta} = \frac{\delta}{d}$$

(24)

and defining a nondimensional shear stress  $M$ , one can rewrite equations (14), (16), (17), (20) and (21) as:

$$\frac{d \text{Re}_L}{d \bar{z}} = \frac{\text{Ja}}{\text{Pr}_L} \frac{1}{\bar{\delta}} \quad (14a)$$

$$\bar{u}_{L\delta} = M\bar{\delta} \quad (16a)$$

$$Re_L = \frac{M \rho_R Re_{vo}}{\mu_R} \frac{\bar{\delta}^2}{2} \quad (17a)$$

$$\bar{u}_v = Re_v / Re_{vo} \quad (20a)$$

and

$$M = \frac{\tau_s d}{\mu_L u_{vo}} = \left( \frac{c_f}{2} \right)_E \frac{Re_{vo}}{\mu_R} (\bar{u}_v - \bar{u}_{L\delta})^2 + \frac{Ja}{Pr_L \bar{\delta}} (\bar{u}_v - \bar{u}_{L\delta}) \quad (21a)$$

Equations (14a), (16a), (17a), (19), (20a), (21a) and (22) or (23) are used to find  $\bar{\delta}$ ,  $Re_L$ ,  $Re_v$ ,  $\bar{u}_v$ ,  $\bar{u}_{L\delta}$  and  $M$  as functions of  $\bar{z}$ . The heat transfer coefficient  $h$  is given by  $k_L/\delta$ . Hence, the Nusselt number is

$$Nu = \frac{hd}{k_L} = \frac{1}{\bar{\delta}} \quad (25)$$

From the nondimensional equations, it is clear that the quantities  $\bar{\delta}$ ,  $Re_L$ ,  $Re_v$ ,  $\bar{u}_v$ ,  $\bar{u}_{L\delta}$  and  $M$  are functions of  $\bar{z}$  with  $Re_{vo}$ ,  $Ja/Pr_L$ ,  $\rho_R/\mu_R$  as parameters.

We will present results only for the case of steam condensing at one atmosphere, ( $T_s = 100^\circ\text{C}$ ). The wall temperature is assumed to be at either  $85^\circ\text{C}$  or  $70^\circ\text{C}$ . Two vapor Reynolds numbers are chosen, namely, 5000 and 50000. The liquid properties are chosen to be at the average film temperature,  $1/2 (T_s + T_w)$ . The values of the parameters are listed in Table 1.

The film thickness and the vapor Reynolds number for  $Re_{v0} = 5000$  are plotted as functions of  $\bar{z}$  in Figure 3. The solid lines are for  $\Delta T = 15^\circ\text{C}$ , while the dashed lines are for  $\Delta T = 30^\circ\text{C}$ . The vapor Reynolds number gives an indication of the amount of vapor that remains at a given  $\bar{z}$ . For  $\Delta T = 15^\circ\text{C}$ , about 50% of the vapor remains at  $\bar{z} = 8$ , while it only takes  $\bar{z} = 3$  to condense 50% of the vapor <sup>for  $\Delta T = 30^\circ\text{C}$</sup> . It can also be seen from Figure 3 that the film thickness is indeed very small, with  $\bar{\delta} < 0.01$ .

Similar results for  $Re_{v0} = 50000$  are plotted in Figure 4. However, it takes up to  $\bar{z} = 50$  to condense 50% of the vapor with a  $\Delta T$  of  $15^\circ\text{C}$ . The corresponding condensing length for a  $\Delta T$  of  $30^\circ\text{C}$  is approximately 20.

For  $Re_{v0} = 50000$ , the vapor velocity  $\bar{u}_v$  and the liquid velocity at the interface  $\bar{u}_{L\delta}$  are plotted in Figure 5. Again, the solid lines indicate the results with a  $\Delta T$  of  $15^\circ\text{C}$  while the dashed lines are the results with  $\Delta T = 30^\circ\text{C}$ .

## CONCLUSIONS

This report has addressed two possible mechanisms of condensate removal for condensers operated in a microgravity environment. It is concluded that both suction and vapor shear can effectively drain the condensate to ensure continuous operation of the condensers. It is recommended that zero-g flight experiments be carried out to verify the prediction of the heat transfer coefficient for the case of convective condensation. The results contained in this report should also aid in the design of future space condensers.

## References

1. R. Siegel, "Effects of Reduced Gravity on Heat Transfer", Advances in Heat Transfer, Vol. 4, pp. 143-228, 1967.
2. R. E. Eastman, C. J. Feldmanis, W. L. Haskin and K. L. Weaver, Two-Phase Fluid Thermal Transport for Spacecraft, AFWAL-TR-84-3028, October 1984.
3. J. A. Albers and R. P. Macosko, Experimental Pressure-Drop Investigation of Non-Wetting, Condensing Flow of Mercury Vapor in a Constant-Diameter Tube in 1-G and Zero-Gravity Environments, NASA TN D-2838, June 1965.
4. J. A. Albers and R. P. Macoski, Condensation Pressure Drop of Non-Wetting Mercury in a Uniformly Tapered Tube in 1-G and Zero-Gravity Flight Environments, NASA TN D-3185, January 1966.
5. D. Namkoong, H. B. Block, R. P. Macosko and C. C. Crabs, Photographic Study of Condensing Mercury Flow in 0- and 1-G Environments, NASA TN D-4023, June 1967.
6. C. J. Feldmanis, Performance of Boiling and Condensing Equipment Under Simulated Outer Space Conditions, ASD-TDR-63-862, November 1963.
7. C. J. Feldmanis, "Pressure and Temperature Changes in Closed Loop Forced Convection Boiling and Condensing Processes Under Zero Gravity Conditions", Presented at the 1966 Annual Technical Meeting of the Institute of Environmental Sciences.

8. J. L. Williams, E. G. Keshock and C. L. Wiggins, "Development of a Direct Condensing Radiator for Use in a Spacecraft Vapor Compression Refrigeration System ", Journal of Engineering for Industry, Vol. 95, pp. 1053-1064, 1973.
9. D. B. Heppner, C. D. King and J. W. Littles, "Zero-G Experiments in Two-Phase Fluids Flow Regimes", ASME Paper 75-ENAS-24, 1975.
10. D. C. Hustvedt and R. L. Oonk, Preliminary Design of Flight Hardware for Two-Phase Fluid Research, NASA CR-168072, February 1982.
11. N. A. Frankel and S. G. Bankoff, "Laminar Film Condensation on a Porous Horizontal Tube with Uniform Suction Velocity", Journal of Heat Transfer, Vol. 87, pp. 95-102, 1965.
12. W. S. McEver and H. Hwangbo, "Surface Tension Effects in a Space Radiator Condenser with Capillary Liquid Drainage", AIAA Paper 83-1525, 1983.
13. E. M. Sparrow and J. L. Gregg, "A Theory of Rotating Condensation", Journal of Heat Transfer, Vol. 81, pp. 113-120, 1959.
14. R. D. Cess, "Laminar-Film Condensation on a Flat Plate in the Absence of a Body Force", Z. Angew. Math. Phys., Vol. 11, pp. 426-433, 1960.
15. J. C. Y. Koh, "Film Condensation in a Forced-Convection Boundary-Layer Flow", Int. J. Heat Mass Transfer, Vol. 5, pp. 941-954, 1962.
16. I. G. Shekriladze and V. I. Gomelauri, "Theoretical Study of Laminar Film

Condensation of Flowing Vapor", Int. J. Heat Mass Transfer, Vol. 9, pp. 581-591, 1966.

17. C. L. Tien, "Fluid Mechanics of Heat Pipes", Annual Review of Fluid Mechanics, Vol. 7, pp. 167-185, 1975.
18. E. L. Lustenader, R. Richter and F. J. Neugebauer, "The Use of Thin Films for Increasing Evaporation and Condensation Rates in Process Equipment", Journal of Heat Transfer, Vol. 81, pp. 297-307, 1959.
19. E. M. Sparrow and S. H. Lin, "Condensation Heat Transfer in the Presence of a Noncondensable Gas", Journal of Heat Transfer, Vol. 86, pp. 430-436, 1964.
20. E. M. Sparrow, W. J. Minkowycz and M. Saddy, "Forced Convection Condensation in the Presence of Noncondensables and Interfacial Resistance", Int. J. Heat Mass Transfer, Vol. 10, pp. 1829-1845, 1967.
21. R. Gregorig, "Hautkondensation an feingewellten Oberflächen bei Berücksichtigung der Oberflächenspannungen", Zeitschrift für angewandte Mathematik und Physik, Vol. V, pp. 36-49, 1954.
22. H. Honda, S. Nozu and K. Mitsumori, "Augmentation of Condensation on Horizontal Finned Tubes by Attaching a Porous Drainage Plate", Proceedings of the ASME/JSME Thermal Engineering Joint Conference Vol. III, pp. 289-296, 1983.
23. R. A. Seban and J. A. Hodgson, "Laminar Film Condensation in a Tube With Upward Vapor Flow", Int. J. Heat Mass Transfer, Vol. 25, pp. 1291-1300, 1982.



24. W. H. Henstock and T. J. Hanratty, "The Interfacial Drag and the Height of the Wall Layer in Annular Flows", AIChE Journal, Vol. 22, pp. 990-1000, 1976.

Table 1. Parameters Chosen for Convective Condensation

	$\Delta T = 15^{\circ}\text{C}$	$\Delta T = 30^{\circ}\text{C}$
$\mu_R$	24.92	25.98
$\rho_R$	1614	1620
Ja	0.02797	0.0559
$Pr_L$	1.91	1.99
$Re_{vo}$	5000 or 50000	5000 or 50000

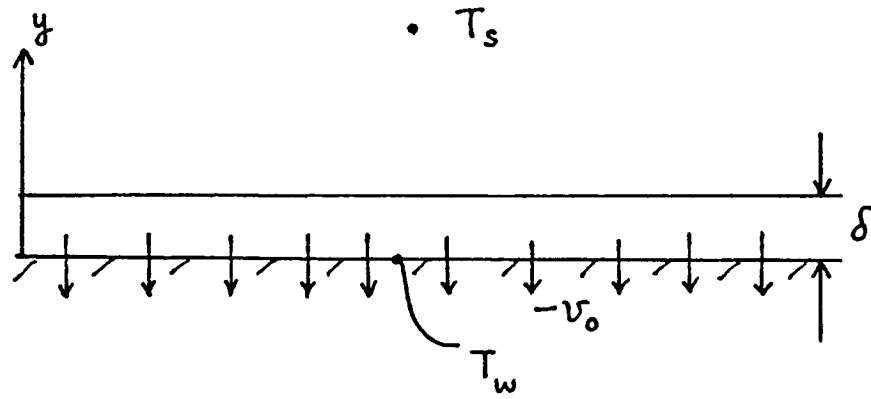


Figure 1

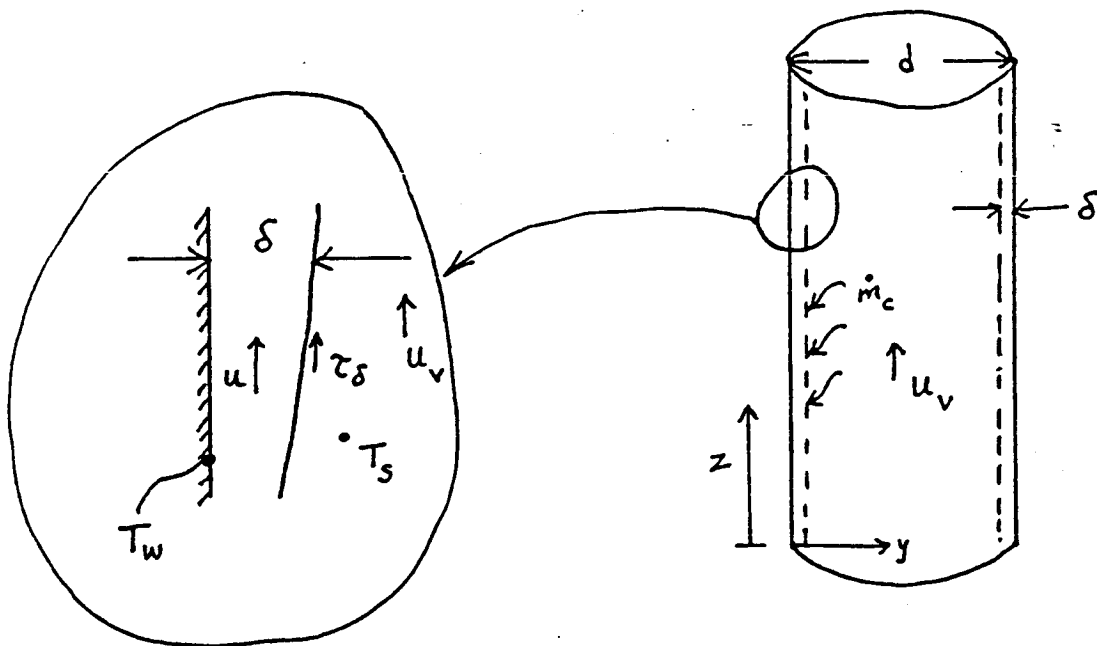


Figure 2

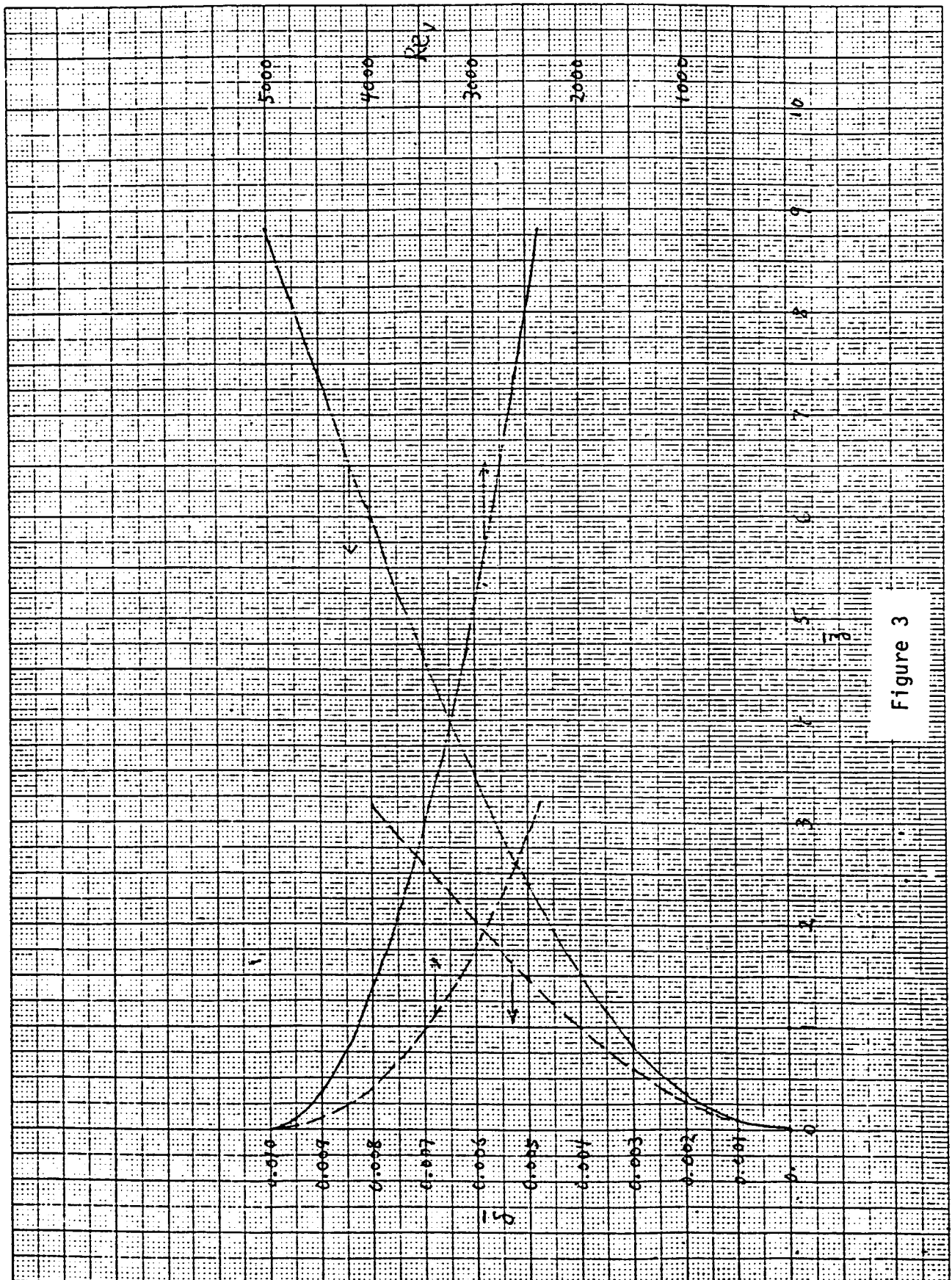


Figure 3

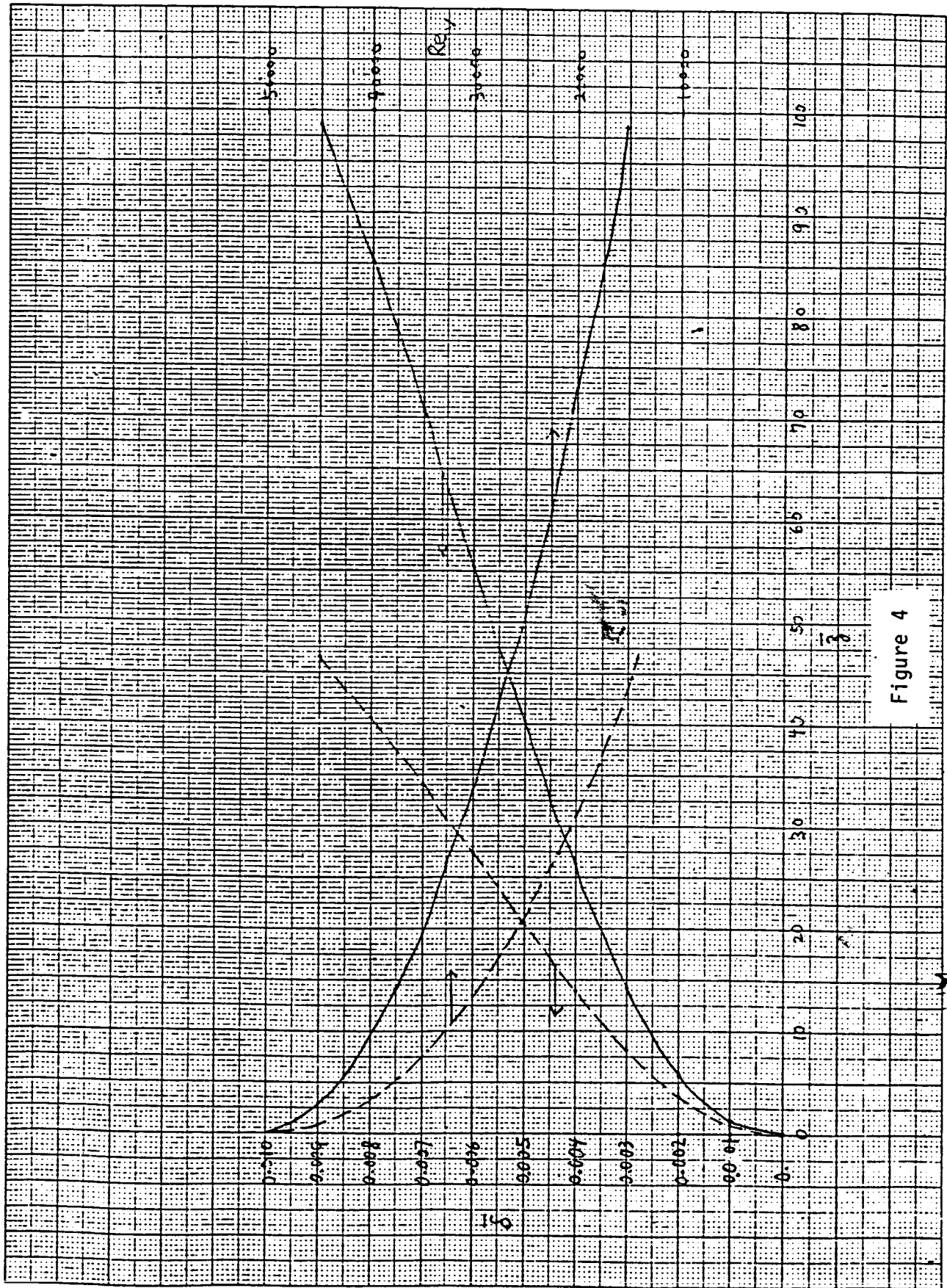


Figure 4

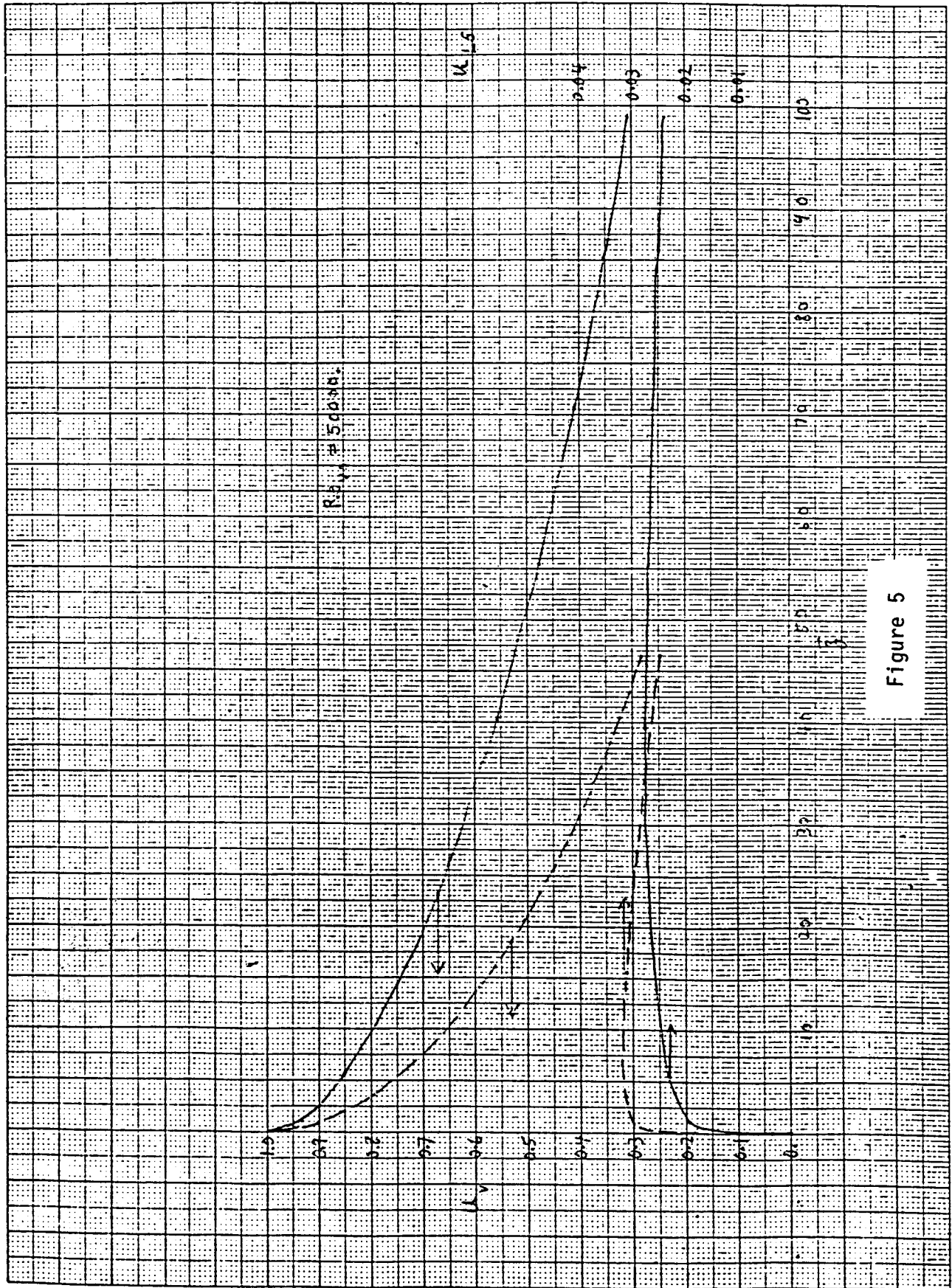


Figure 5

Chronology and Isotopic Geochemistry of Apollo 14  
Basalts and Skaergård Gabbro, Eastern Greenland  
LP.

E. Julius Dasch 18817

ASEE/NASA 1985 Summer Faculty Fellow

Final Report

August 1985

## 1. Apollo 14 basalts

Work completed on Apollo 14 basalts during my first year as a Summer Faculty Fellow has been presented and published (Dasch, et al., 1985). The two dates obtained from these rocks comprised the oldest and two of the three oldest ages (4.1 and 4.3 billion years) known for lunar maria basalts; thus their ages are important in understanding moon's earliest history.

Owing to the antiquity of these rocks, two more fragments have been dated as part of my second ASEE/NASA SFF program. The new ages are 3.95 and 4.12 billion years, thus further establishing and amplifying the earlier results (see attached figures 1, 2 and table 1). This work, although perhaps more interesting for its chronologic information, was begun as a test of chemical and petrographic models by Dickinson, et al., (1984). These workers placed fragments of Apollo basalt into five categories, based on petrologic and chemical, especially rare-earth element, composition. Our isotopic studies were begun in an attempt to determine if the five groups of basalts were related by age or initial isotopic composition (isotopic composition of lava at time of extrusion). As figure 3 shows, although a few of the representatives of the five groups have the same age (T) and/or initial strontium-isotopic composition (I), within the analytical uncertainties, most apparently are unrelated. Petrologic implications of these data will be published in an appropriate journal.

## 2. Skaergård gabbro, Eastern Greenland

Ten samples of plagioclase separated from Skaergård gabbro were analyzed isotopically during my 1984 Summer Faculty Fellowship Program. These data were presented in an abstract (Dasch, et al., 1985) and are being prepared for publication. Based on this work, I joined the final (just returned) American expedition to the Skaergard outcrop, led by A.R. McBirney, University of Oregon (expenses for this travel were provided by my home institution, Oregon State University).

About 25 samples of rock were collected for isotopic analysis in an attempt to: study further the origin of distinctive gabbroic pegmatite: origin and evolution of layering; age of a coarse-grained ilmenite rock; and to determine if the three main parts of the intrusion (Layered Series, Marginal Border Group, Upper Border Group) evolved separately. This work will be completed during the month of September. Publication of the 14-year restudy of the Skaergard Intrusion including this isotopic work, will be in a series of papers in a special issue of the Journal of Petrology.

### References

Dasch, E.J., Shi, C.-Y., Bansal, B.M., Wiesmann, H., and Nyquist, L.E., 1985, Isotopic provenance of aluminous mare basalts from the Fra Mauro Formation: 16th Lunar and Planetary Science Conference, p. 163, 164.

Dasch, E.J., Hoover, J.D., and Kays, M.A., 1985, Omnipresent contamination in the Skaergaard Intrusion, Eastern Greenland: Geol. Soc. America (South-Central Section) Ann. Meetings Program.



Figure 1

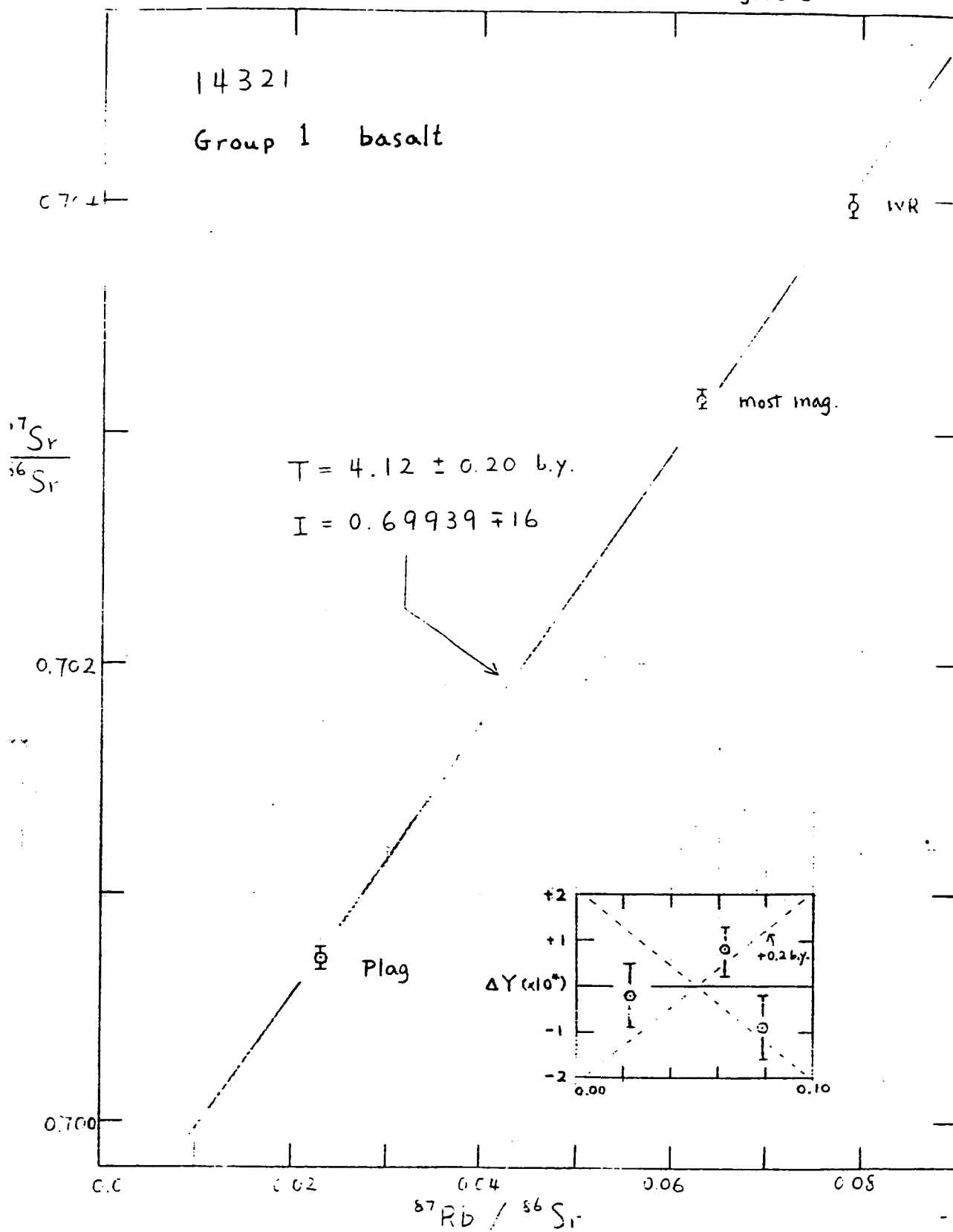


Figure 2

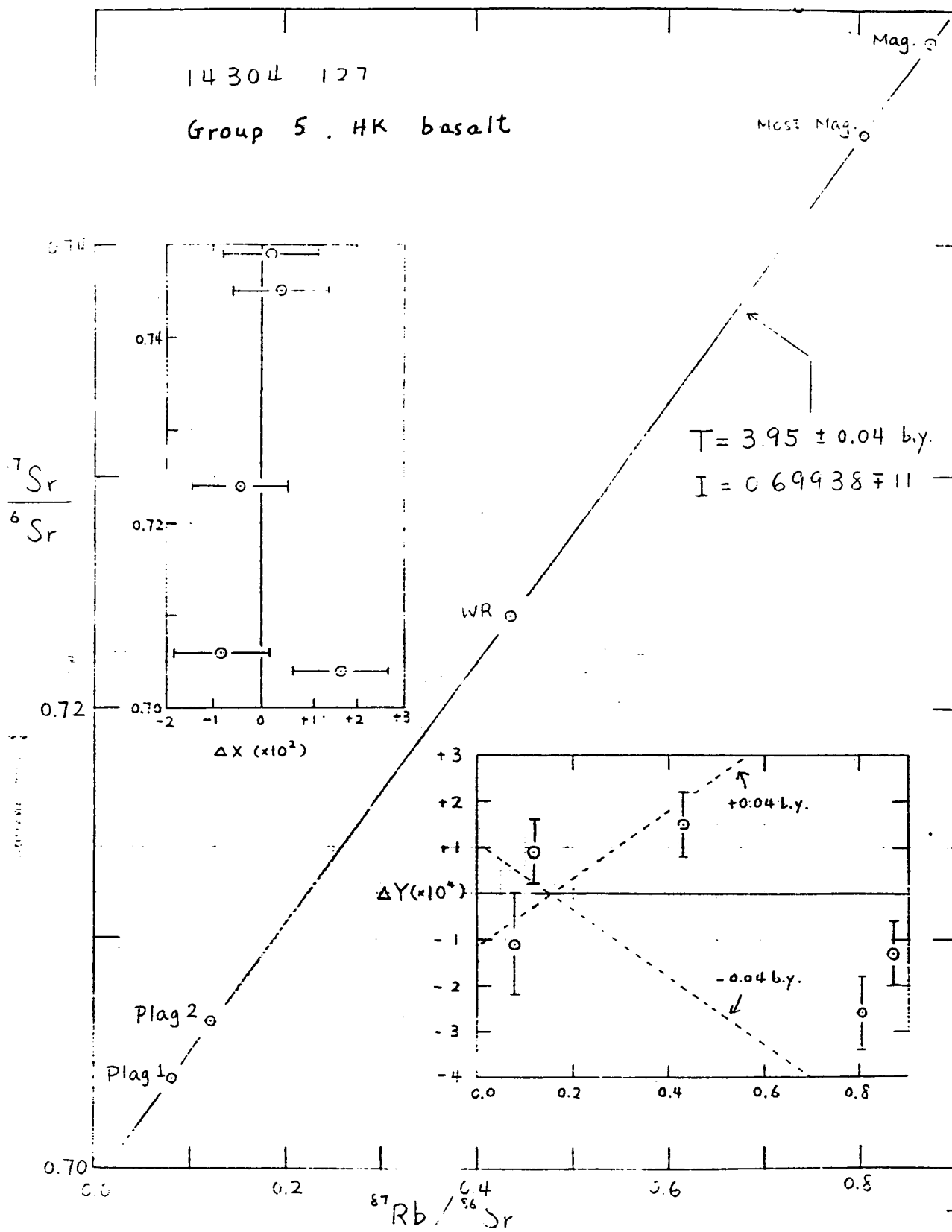
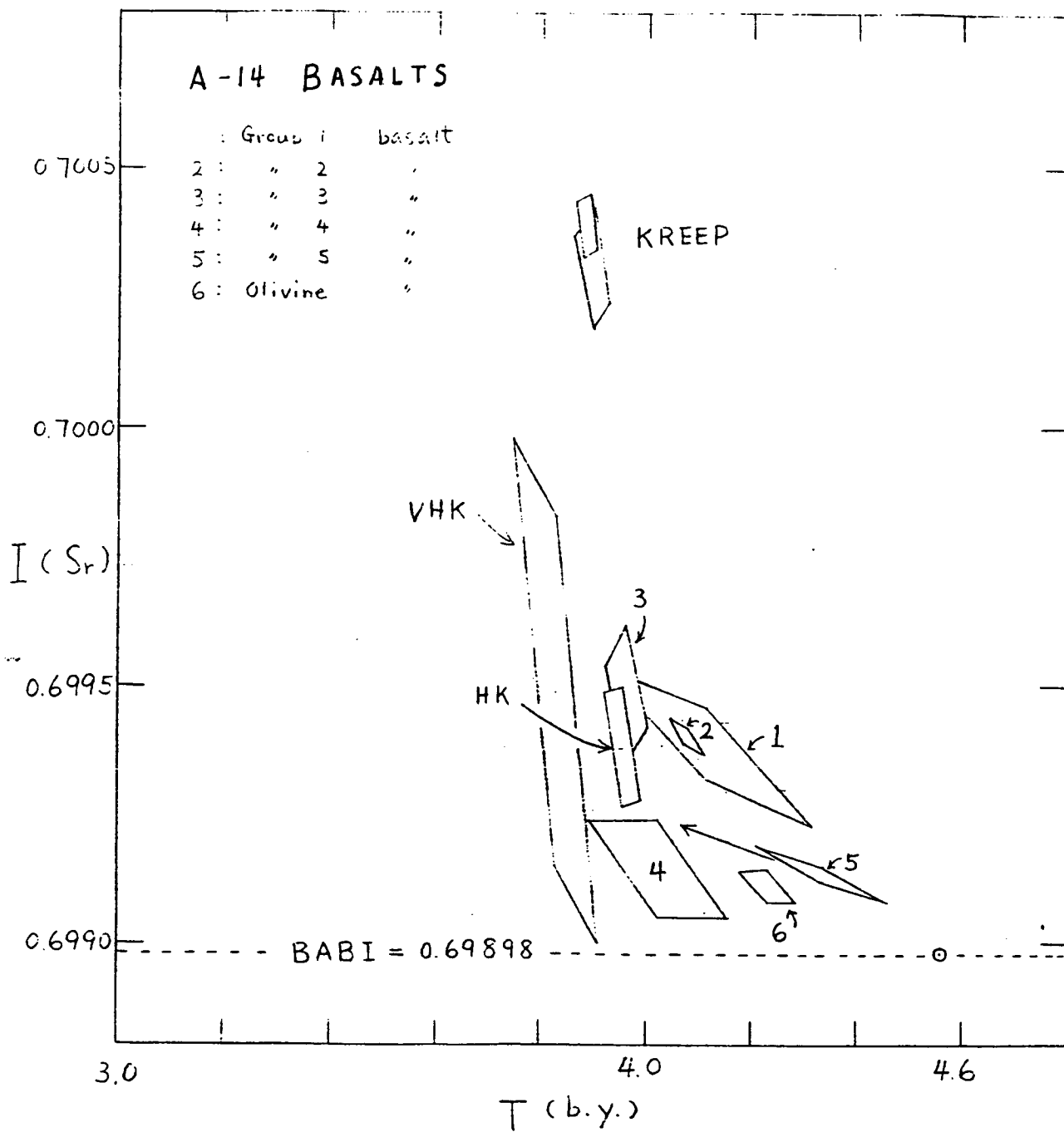


Figure 3



Table

## Rb-Sr Results for Apollo 14 Basaltic Clasts

Sample	Wt(mg)	Rb(ppm)	Sr(ppm)	87Rb/86Sr	87Sr/86Sr <sup>a</sup>	T <sub>BAB1</sub> (b.y.) <sup>e</sup>	T <sub>LUN1</sub> (b.y.) <sup>f</sup>
<hr/>							
1. 14321 (Group 1 Basalt)							
WR	18.1	2.83	103.6	0.0791	0.70398±5	4.41±0.06	4.37±0.06
Plag	2.9	0.988	124.9	0.0229	0.70072±5		
Most Mag	20.3	1.79	82.19	0.0630	0.70315±4		
(T = 4.12 ± 0.20 b.y., I(Sr) = 0.69939 ± 0.00016) <sup>b</sup>							
<hr/>							
2. 14321, 9056 (Group 2 Basalt)							
WR	17.5	2.95	105.6	0.0809	0.70414±4	4.45±0.06	4.41±0.06
Non Mag	1.3	0.515	160.5	0.00928	0.69995±6		
Mag	26.4	1.56	69.43	0.0651	0.70318±3		
Most Mag	16.2	5.61	128.7	0.126	0.70675±4		
(T = 4.07 ± 0.03 b.y., I(Sr) = 0.69940 ± 0.00003) <sup>b</sup>							
<hr/>							
3. 14321, 9059 (Group 5 Basalt)							
WR	19.5	0.685	77.68	0.0255	0.70073±3	4.78±0.10	4.64±0.10
2.85-3.3 <sup>d</sup>	15.9	0.722	113.3	0.0185	0.70027±4		
>3.3	19.9	0.586	41.81	0.0406	0.70165±3		
(T = 4.33 ± 0.13 b.y., I(Sr) = 0.69913 ± 0.00005) <sup>b, c</sup>							
Non Mag	1.5	0.481	112.9	0.0123	0.70065±6		
<2.85	0.9	2.08	186.7	0.0323	0.70073±7		
<hr/>							
4. 14304, 127 (Group 5, HK Basalt)							
WR	38.9	6.86	45.79	0.4334	0.72398±5	4.04±0.04	4.03±0.04
Plag 1	0.9	3.87	137.9	0.0813	0.70390±8		
Plag 2	5.9	6.07	142.4	0.1233	0.70641±5		
Mag	20.3	8.24	27.29	0.8731	0.74862±5		
Most Mag	6.6	14.2	51.12	0.8054	0.74470±6		
(T = 3.95 ± 0.04 b.y., I(Sr) = 0.69938 ± 0.00011) <sup>b</sup>							

NBS SRM 987 (8 analyses)

0.71019±2

<sup>a</sup>Normalized to 88Sr/86Sr=8.37521 and uncertainties correspond to last figures and are 2  $\sigma$  errors.

<sup>b</sup>Mineral Isochron calculated for  $\lambda(87\text{Rb})=0.0139$  (b.y.)<sup>-1</sup>.

<sup>c</sup>Excluding Non Mag and <2.85 fractions.

<sup>d</sup>Density in g/cm<sup>3</sup> for all mineral separates obtained using heavy liquids.

<sup>e</sup>Relative to I(Sr) = BAB1 = 0.69898.

<sup>f</sup>Relative to I(Sr) = LUN1 = 0.69903.

N86 - 31416

D7  
697

18818

APPLICATION OF COMPUTER IMAGE ENHANCEMENT TECHNIQUES  
TO SHUTTLE HAND-HELD PHOTOGRAPHY

DR. BRUCE E. DAVIS  
ASEE SUMMER FACULTY FELLOW

DEPARTMENT OF GEOGRAPHY  
UNIVERSITY OF HAWAII  
HILO, HAWAII  
96720

011010-1000

With the advent of frequent Space Transportation System Shuttle missions, photography from hyperaltitudes stands to become an accessible and convenient resource for scientists and environmental managers. As satellite products (such as Landsat) continue to spiral in costs, all but the most affluent consumer is finding Earth imagery from space to be more and more unavailable. Therefore, the potential for Shuttle photography to serve a wide variety of users is increasing. However, despite the popularity of photos from space as public relations tools and report illustrations, little work has been performed to prove their scientific worth beyond that as basic mapping bases. It is the hypothesis of this project that hand-held Earth photography from the Space Shuttle has potentially high scientific merit and that primary data can be extracted. In effect, Shuttle photography should be considered as a major remote sensing information resource.

Space photography is not typically considered equally comparable to normal satellite scanner systems. While scanners provide digital data in multiple bands, essentially ready for processing and analysis by computerized techniques, photography is thought to be a single-image, relatively narrow and inflexible sensor that is heavily affected by atmospheric scattering, particularly in the visible range of the electromagnetic

spectrum. Consequently, photography from space is not a favored imagery format for most scientific research.<sup>1</sup>

There are numerous studies utilizing Shuttle hand-held photography (herein referred to as SP) as support imagery, but there seems to be a paucity of research employing it as the (or even a) primary data extraction mechanism.<sup>2</sup> (In this sense, primary data refers to information either previously unknown or as the major evaluation mechanism.) The major exception is the use of photography for mapping. As a discipline, remote sensing is engaged in multispectral, multiband computer-oriented techniques, basically in discriminating spectral signatures. There seems to be much more benefit to employing sensors which give a much larger and more detailed informational content than does visual, emulsion-based photography, especially in terms of quantitative data. However, the fundamental problem is in the perception of SP as a single band image that can, at best, be manipulated photographically, in the development and printing stage (dark room processing and analysis). The solution, therefore, is to render the photography compatible to computer analysis. The focus of this project has been to that aim.

One of the essentials of color photography is that it has three chemical layers (emulsions) that have different electromagnetic sensitivities. The primary colors of the emulsion's responses

are red, green, and blue (in decreasing wavelengths). If each of the layers can be separated and computerized, then the photography would be comparable to a multiband digital scanner system, albeit with limited spectral qualities. Fortunately, color separation is relatively easy with the use of red, green, and blue filters. The process involves projecting (or sensing) the image through each filter separately, obtaining three monochrome images of varying tonal and contrast information.<sup>3</sup> Putting the photographs through filters and digitizing them will thus convert them to computer format. Once in digital form, numerous manipulations and "tricks" can extract previously undetected information.

Four fundamental prefaces are necessary at this point:

1. Computerization of data, particularly imagery, is not a solution to any problem, only a convenient assistance. Hence, production of digital data from SP is not, in itself, necessarily any more valuable than when left in an eye-interpretation format. Because there has been virtually no digitizing of SP in published literature (none was found in a search) it cannot be said at this time, aside from hypothesizing, that digital SP data is highly valuable for most investigations. However, the working premise is that computerization can offer another dimension to the standard product.



2. While computers offer highly sophisticated analytical techniques and can present a very high level of informational discrimination, there is not always a direct compatibility between the eye and the computer. That is, the eye operates on a contrast basis for spatial detection and spectral and albedo separation, while computers sense numerical differences as defined initially by a CRT sensor in terms of tonal variation; the two methods may produce similar results, or they may differ so that either does not necessarily recognize the same characterization of information. As will be stated, the eye is not always the best guide as to which imagery versions will produce good computer information, and vice versa--good computer products are not always pleasing or even understandable to the eye. Contrast, then, is relative to the sensor.

3. Digitization of photography is not particularly new nor particularly clever, but for SP it is novel. If computerization of SP proves to be an original data source (or at least a major supplemental resource), then a new and potentially valuable product becomes available. This lends itself to the next point:

4. As inferred, most research utilizes technically superior sensors and associated equipment; apparently there has been little need of or thought to digital SP. But as world problems

become less and less provincial in nature, there is more and more demand for world imagery coverage as part of the concerted effort to understand and resolve global issues. The synoptic perspective of space-borne imagery offers an ideal platform from which to sense the manifestations of many problems. However, along with the indicated rising costs of satellite products, there is also the physical availability factor--digital space data are becoming less and less available. For example, Landsat 4 imagery is primarily relegated to the continental U.S. because, unlike earlier Landsats, it does not carry a recorder for time-delay transmission. Coverage of other parts of the world is either lacking or in the hands of those few nations which operate a receiving station. On the other hand, the library of SP is increasing dramatically as missions become more frequent and more science-oriented. Although SP cannot replace the more versatile Landsat or SPOT (or other similar systems), its relatively low cost and high availability, along with its near-global coverage and potential for digital conversion, may offer an acceptable, even desirable, alternative.

#### METHODOLOGY

A Gould IP8500 Image Processing System, using LIPS software (Library of Image Processing Software) at the Lunar and Planetary Institute provided an efficient and rapid mechanism for

computerizing SP imagery. Using its video camera and photographic filters, an image (print or transparency) can be digitized, i.e., reduced to a 512 x 512 pixel format (262,144 pixels for each image). Once saved, the images can be processed and analyzed in numerous ways, from simple combination to complex algebraic manipulations.

The basic methodology employed is detailed in an accompanying tutorial manual prepared as part of this project. Briefly, the first step is to reduce the image to its primary color components by the use of filters over the camera lens, thereby producing three images with distinctive pixel values. If no image displacement has occurred in the process, a given pixel in one image corresponds to the exact location and pixel of its counterparts. For example, pixel number 1 of image A is spatially compared to pixel 1 in image B.

The range of pixel value tones varies between 0 (pure black) and 255 (pure white). In effect, the technique is to change pixel values without losing the fundamental relationships of each with all others. Processing and analytical functions used in this research included addition, subtraction, multiplication, ratioing, contrast stretching, histogram equalization, principal component analysis, and their various combinations. These steps are supported by density slicing and pseudocoloring (artificial

color assignment--to be discussed). Spatial filtering is available on LIPS but was not used.

Standard algebraic functions of addition, subtraction, multiplication, and ratio operate on a pair of images, processing the common pixel from each with an established algorithm. Addition and multiplication have constants that can be manually set to change results. Inherent factors prevent under- and over-run of values in the 0-255 range. Any pair of images may be used, so long as they have corresponding pixel coordinates.

Contrast stretching is a process of redistributing the pixel values of an image over a larger range of the 0-255 scale than occurs originally so that greater contrast can be achieved. Five types of stretch are available in LIPS but only two are used regularly--linear and piecewise linear, both of which allow the user to select the limits of pixel (or density number--DN) values that are to be stretched, thereby offering considerable control over the nature of the resulting image.

Histogram equalization is an automatic (uncontrolled) operation of spreading the input pixel values so that each DN of the 0-255 range contains an equal number of pixels. The resulting image is usually excellent in terms of perceivable information, typically much better than the input image.

Principal component analysis (PCA) is a rather complex (though easily produced on LIPS) function which, in effect, constructs the best, most contrasting image from a set of two to four input images. Although to the eye the resulting image may be no better than other manipulations, it may possess superior digital data.

Density slicing and pseudocoloring involves manual selection of DN ranges (of the 0-255 scale) and assignment of colors to each segment. The size and color of the slice is determined by the user, basically in an attempt to isolate some feature or phenomenon. Three "canned" schemes exist in LIPS and others are constructed easily and interactively. Once created, the schemes are entered into a "look-up table", or LUT, and can be recalled and applied to any other image with a single command.

LIPS has several useful analytical support functions, each interactively controlled by the operator. A floating cursor takes individual pixel values and is ideal for sampling features such as lava flows. Pixel value profiles, from one point to another (placement and length controlled by the user), can be obtained easily and is useful for cross-section sampling. A controlled box (size and placement) collects encompassed pixels and reports basic statistics and displays a histogram. All of these were used in evaluating strengths and weaknesses of various

scenes as well as in gaining new information of selected ground features. Other support functions of LIPS, such as graphics, on-screen writing, measuring, etc., can be found in the accompanying tutorial and in the LIPS manual.

Two elemental approaches to image enhancement and analysis exist: photographic and algebraic. Photographic techniques consist of manipulations that conceivably can be performed in the darkroom, e.g., tonal variations, filter exchange, etc. LIPS can accomplish such tasks easily and rapidly. For instance, display of the three images combined into one and application of their respective filters will produce normal color. Swapping filters (or more precisely, exchanging images under set color guns) makes false color renditions. Some features may be enhanced and/or others suppressed but basically, these operations were largely unsatisfactory. Therefore, most of the work focussed on the algebraic functions.

The procedure generally employed for complete processing included the following steps, generally in order (other possible combinations were found to be non-productive and are not listed):

Digitizing

Contrast Stretch

Histogram equalization

Photographic-style Manipulations

## Density Slicing & Pseudocoloring

Addition

Subtraction

Multiplication

Ratioing

Addition + Subtraction

Addition / Subtraction

Multiplication / (Addition / Subtraction)

Principal Component Analysis

Each step could involve changing factor scales to produce slightly different versions (especially in the contrast stretching), assignment of different pseudocolor schemes, or arbitrary combination with other products. The range of possibilities is enormous.

## ANALYSIS AND RESULTS

Rather than attempting a single interpretative objective, the primary emphasis is on the potential scientific value of SP computerized image analysis, especially in terms of production of primary data. Consequently, results tend toward an evaluation of various techniques and selection of useful imagery manipulation

versions. Demonstration of the types of information and forms of analysis is presented as mechanisms in the evaluation. The major working interpretative goal is the analysis of the island of Hawaii (The Big Island), particularly regarding lava flow information. Several secondary projects were also pursued and will be discussed toward the end of this report. Both the methodological interests and Big Island interpretation are discussed together, with emphasis on the former but high interest on the latter. In this way, it is hoped that the scientific value of SP and the techniques employed can be shown.

#### BIG ISLAND

The island of Hawaii, the largest in the Hawaiian archipelago, is a dynamic landscape. Two active volcanoes are present, Kilauea and Mauna Loa, the former being perhaps the most active in the world. There is a wide range of climates and environments, controlled primarily by the imposing (nearly 4200 meters above sea level) Mauna Kea and Mauna Loa. An extremely wet windward side (750+ cm of precipitation) contrasts with the very dry leeward (Kona) side (down to less than 4 cm of rain). As a consequence, the island presents a variety of environmental influences on lava flow aging. For example, on the wet side, the luxuriant vegetation quickly masks flows of recent vintage. On the Kona side, however, flows of several hundred years age



seems to be relatively new. Also, the elevational effects of temperature and vegetation result in variations of weathering even on a single flow.

The complex of factors affecting remote sensing signatures of lava flows is intriguing and worthy of investigation. Therefore, a primary intention of the research is to see if flows of apparent visual similarity can be separated and if additional information of their morphology and signature can be gained. In association, other types of Big Island landscapes were examined to assess SP in interpretation and analysis of various environments (albeit with less detail than in the flows).

Discussion of analysis and results will first focus on production and interpretation of imagery, followed by quantitative assessment. For the sake of brevity and clarity, not all steps of the research and results are reported here; emphasis is on the general structure of investigation, representation of procedures and data, and basic conclusions. Polaroid prints are included as selected illustrations but unfortunately, they do not duplicate monitor screen colors or contrast very well. Coloration is more vivid and interpretable on the screen and 35mm slides.

SP imagery used included: S19-35-013, S09-46-1841, S09-31-1015,

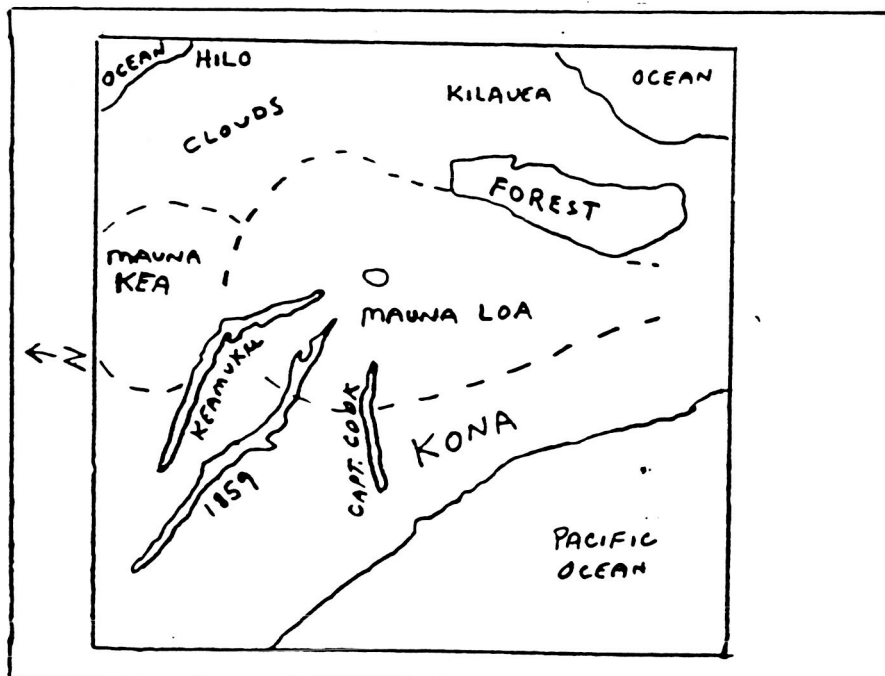
and S84-14-44-93. Because every scene produced was not photographed for this report, there may be a mix of scenes (areas from different SP photos) in a sequence of illustrations. Additionally, because of the expense of Polaroid film, many images were not photographed as prints; most of the important ones were taken as slides but are not included as examples in this report. Moreover, there is a lack of complete sequence illustrations due to problems with tape storage replay. A combination of hardware and software problems prevented recall of stored images from which further processing, analysis, and comparisons with later images were to be performed. Approximately 50 scenes are "frozen" and are inaccessible at this time. The project remains incomplete.

Figure 1 is a color combined version of the original SP image. Although the color is poorly represented on the print, there is useful information evident. Areas of interest include the forest and surrounding vegetation, Mauna Loa radial flows, and Mauna Kea glacial debris and old volcanic landforms. Primary interest is on the three delineated lava flows, from north to south (left to right): Keamuku flow, 1859 flow, and the Captain Cook flow (unofficial name). Ages of the three respectively are approximately 335 years old, 125 years, and approximately 545 years old (approximate years via Dr. Jack Lockwood, Hawaiian Volcanoe Observatory scientist, personal communications).

ORIGINAL PAGE IS  
OF POOR QUALITY



FIGURE 1



Apparent is a detectable tonal difference in the three flows. Although albedo is a prime characteristic of age (the darker a flow, generally the younger it is presumed to be), these flows do not follow the established progression. According to Lockwood the Keamuku flow is in a distinctively drier zone and therefore has less vegetation and weathering than do the other two flows. Also, note some tonal differentiation in the forest and on Mauna Kea. The Mauna Loa radial flows seem to have similar tones and are very difficult to separate visually.

Figure 2-A is the red channel of original data (from another SP photograph). Despite the apparent contrast and reasonably good information, the image fails to discriminate several important lava flows and is poor in distinguishing much of the glacial and residual glacial covering of Mauna Kea.<sup>4</sup> Figure 2-B is the green band of original data and has less visual contrast than does the red. Figure 2-C, blue, has seemingly very poor information. However, as indicated and as will be discussed, this is not necessarily a valid perception when considering digital data.

When histograms are taken of the original images, they have a relatively short range on the 0-255 scale. Contrast stretching expands the range of pixels along the scale, thereby creating more contrast. Figures 3-A and 3-B show before and after

ORIGINAL PAGE IS  
OF POOR QUALITY

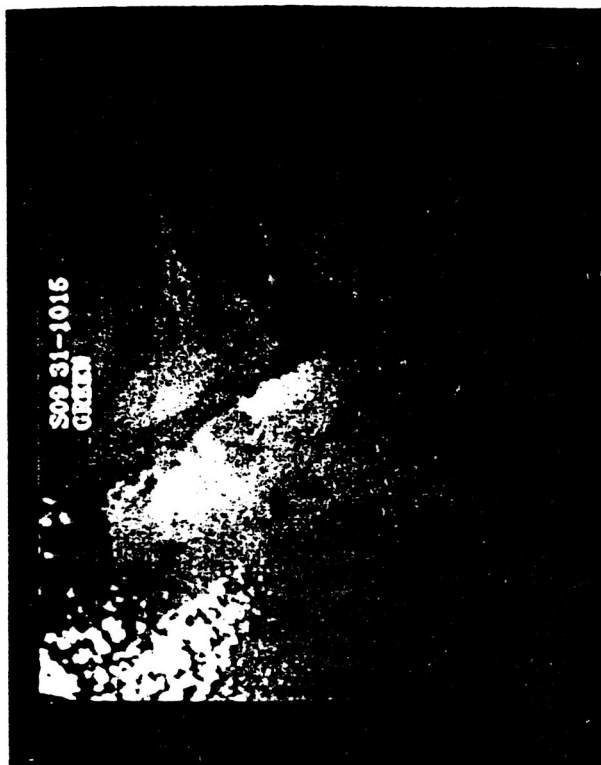
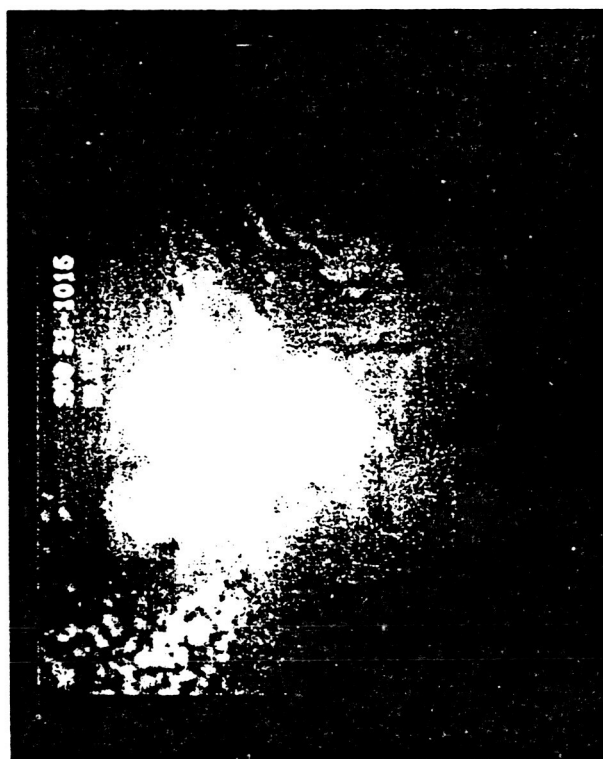
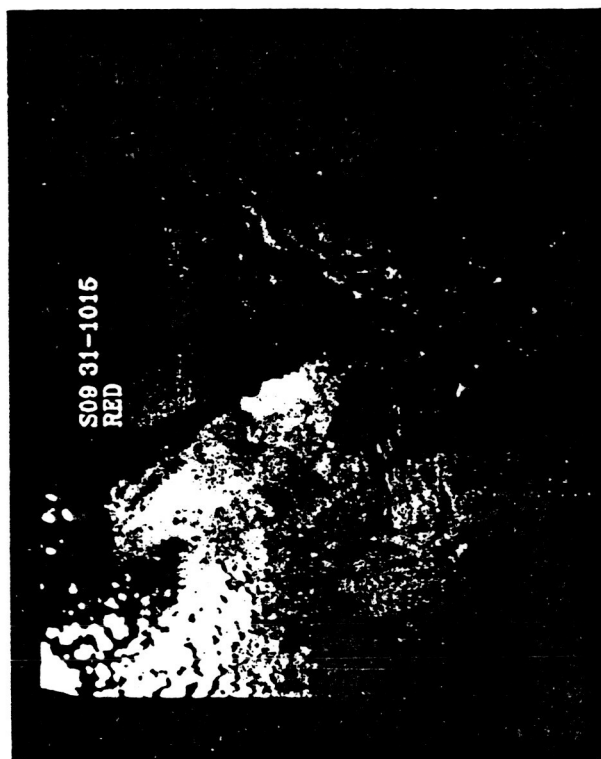


FIGURE 2-A: Red  
FIGURE 2-B: Green  
FIGURE 2-C: Blue



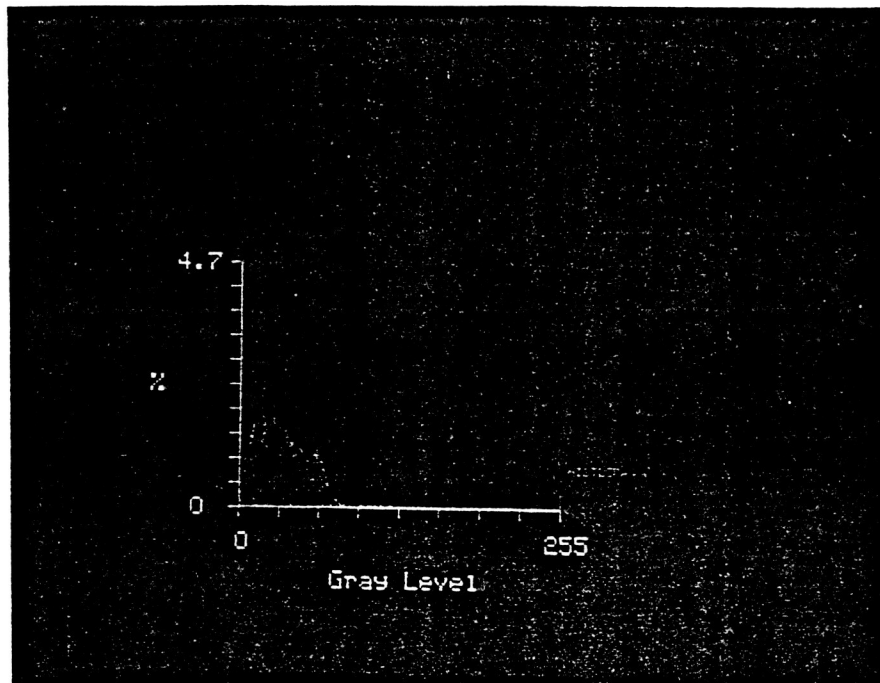


FIGURE 3-A

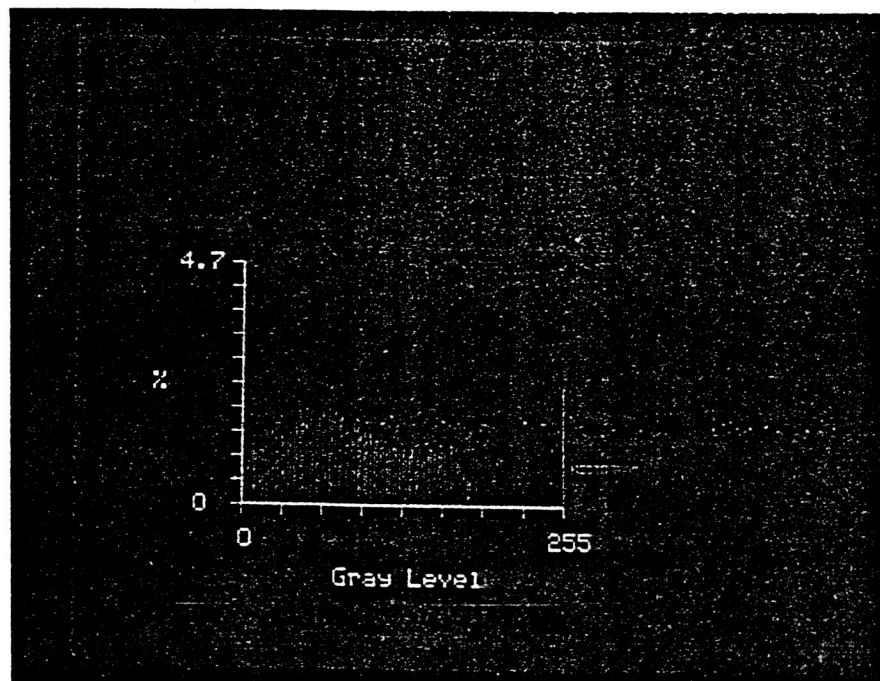


FIGURE 3-B

histograms of original and contrast stretched (CS) red band data. Figures 4-A, B, C show the contrast stretched versions of the original images. Compare 2-A and 4-A (red) and note that while some areas have better information in the CS version, other areas have been reduced in detail. Because there was more interest in the lava flows, the stretch was manipulated to maximize the darker portion of the scene. The green bands (2-B and 4-B) are better examples of increased information through stretching. The blue remains rather poor visually despite the enhancement.

Figure 5 is a color combination of the three CS images. Despite this poor rendition (monitor and slide versions are much better), color CS images offer significant visual and informational improvement over original color scenes. Color combinations through filter swapping offered interesting views, but did not present better information. For a more detailed analysis, quantitative data were taken to determine possible variation within a given color. Figure 6-A shows the sample sites of Mauna Loa flows near Saddle Road (between Mauna Loa and Mauna Kea). Figure 6-B depicts profiles of kipukas (islands left by flowing lava) and histogram sites are presented on 6-C. Numerous other sites on other images were analyzed using these techniques. Graphed data are discussed further on.

ORIGINAL PAGE IS  
OF POOR QUALITY

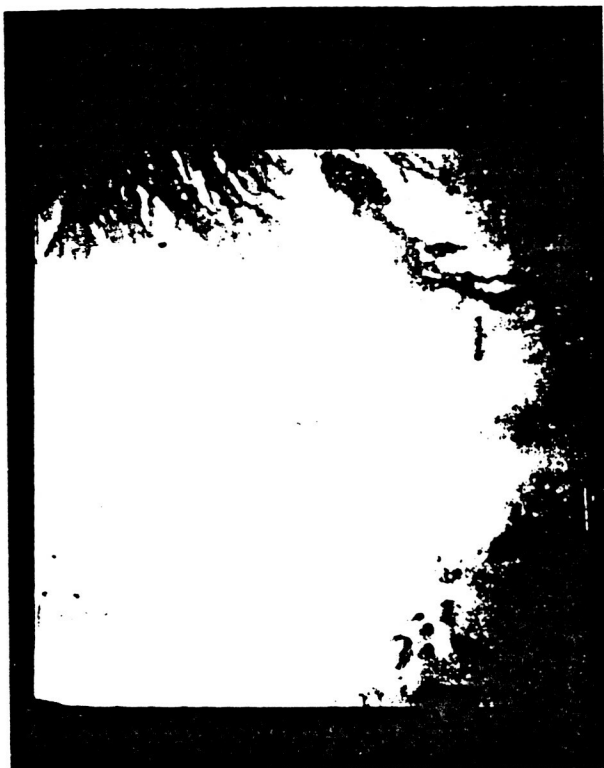
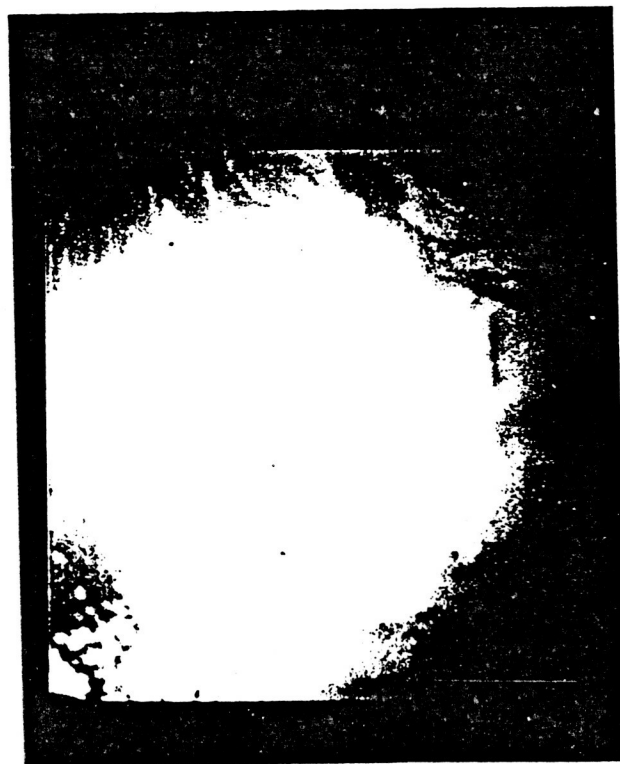
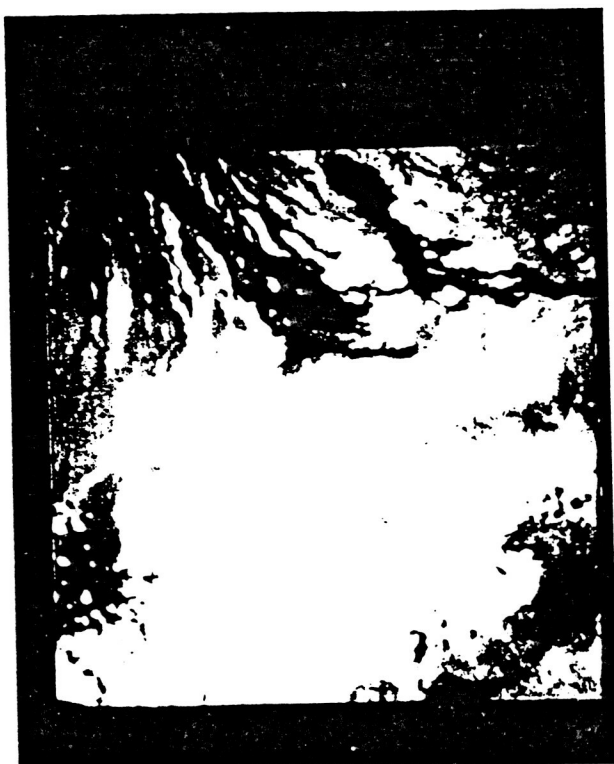


FIGURE 4-A: CS RED  
FIGURE 4-B: CS GREEN  
FIGURE 4-C: CS BLUE





ORIGINAL PAGE IS  
OF POOR QUALITY

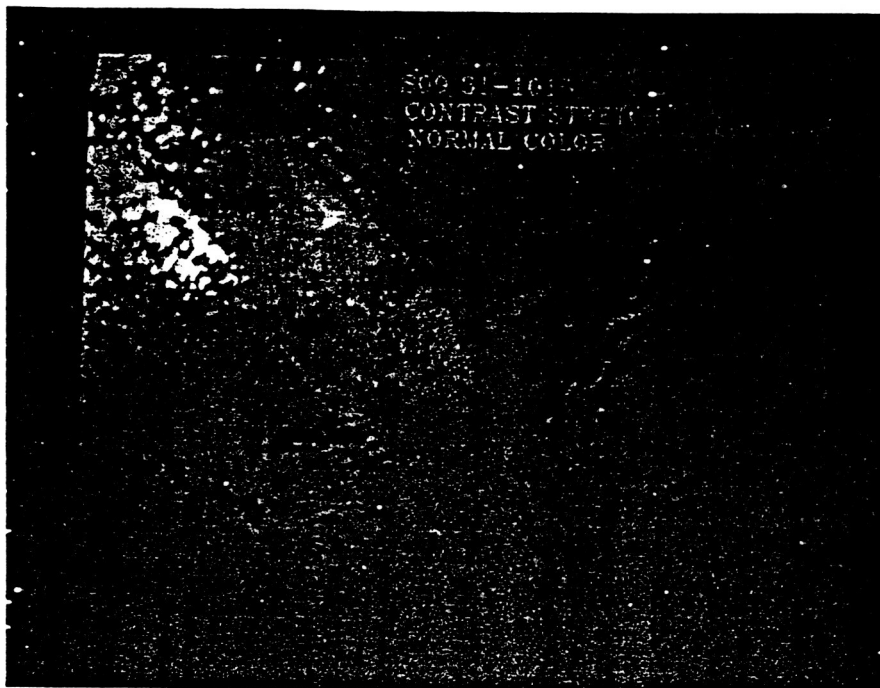


FIGURE 5

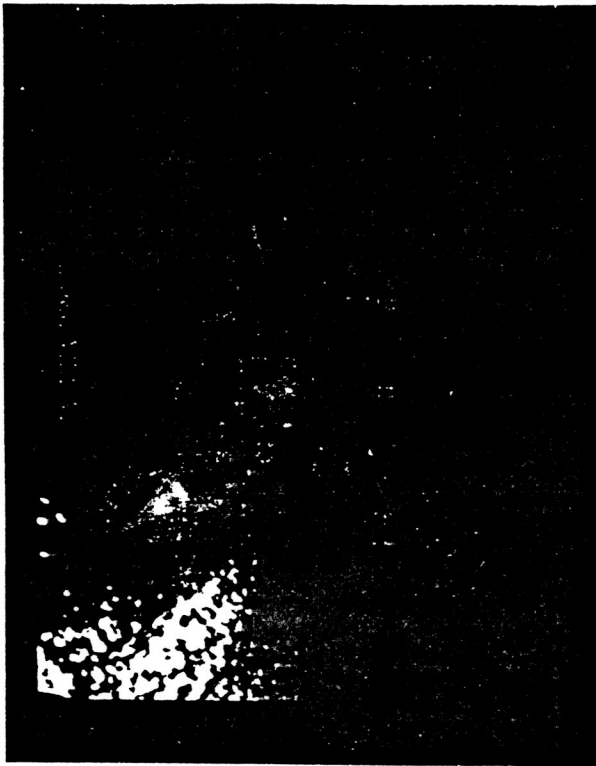


FIGURE 6-A: SAMPLE SITES  
FIGURE 6-B: KIPUKA PROFILES  
FIGURE 6-C: HISTOGRAM SITES



Once pixel, profile, and histogram data reveal variations within visually similar features, the next step is either to reconfigure contrast stretch increments (particularly using pixel values of select features as guides) or to find algebraic manipulations that may show better discrimination. Figure 7 is an addition-- red + green. (Contrast bands green are used herein and may not be always referred to as CS). A "canned" color scheme ("Barl2") is applied to the image and divides the DN scale into twelve even increments. Immediately noticable is the separation of the three lava flows into distinctive color coding. Even more useful is the revelation of separation within the flows, meaning that each flow has appreciable morphologic and/or spectral variation. The cause is unknown and explanation awaits ground investigation. This is the first indication of important primary data from these images.

Also noticable in Figure 7 is considerable coloring of the forest, which is indicative (or at least suggestive) of vegetational and/or environmental variety. The radial flows of Mauna Loa are now separated and present information not apparent on previous scenes. Despite the simplicity of the addition function, this version is one of the best, as will be discussed.

Figure 8 depicts a multiplication--red x green, with Barl2 used again. There seems to be much less informational separation than

ORIGINAL PAGE IS  
OF POOR QUALITY

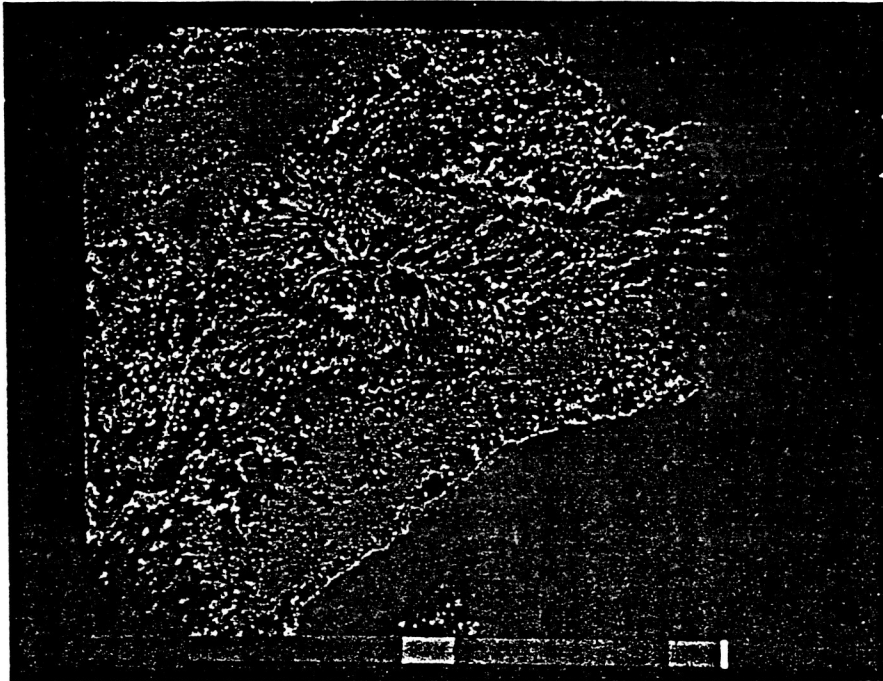


FIGURE 7

in the addition, e.g., note the basic rendition of the forest and radial flows. The three lava flows still show individuality, but not with the detail of Figure 7. Of course, generalization often has merit over fine detail, particularly in mapping tasks. For some purposes, Figure 8 may be the desirable compromise between enhancement and generalization. Further, with the application of another color scheme, multiplication may prove to be a better discriminator of some features than is addition. In fact, this was the case in other images.

Figure 9 shows red x green as applied to the flows on another SP photograph. Also, a designed color scheme (CSLUT2--for Contrast Stretch Look-Up Table 2) is used. The level of detail is much better than in Figure 8. Although the Captain Cook flow is almost lost in the confusion, the other two flows show information useful for ground investigation--another indicator of lava flow differences. As will be discussed, multiplication is one of the better versions of enhancement.

Ratioing is one of the favorite techniques of Landsat data and much use has been made of it. Therefore, considerable time was spent in ratio versions of SP imagery. However, one of the prime values of Landsat is the utilization of the near infrared and most ratios depend on those bands for good results. SP imagery rarely uses infrared, basically because the Shuttle windows

ORIGINAL PAGE IS  
OF POOR QUALITY

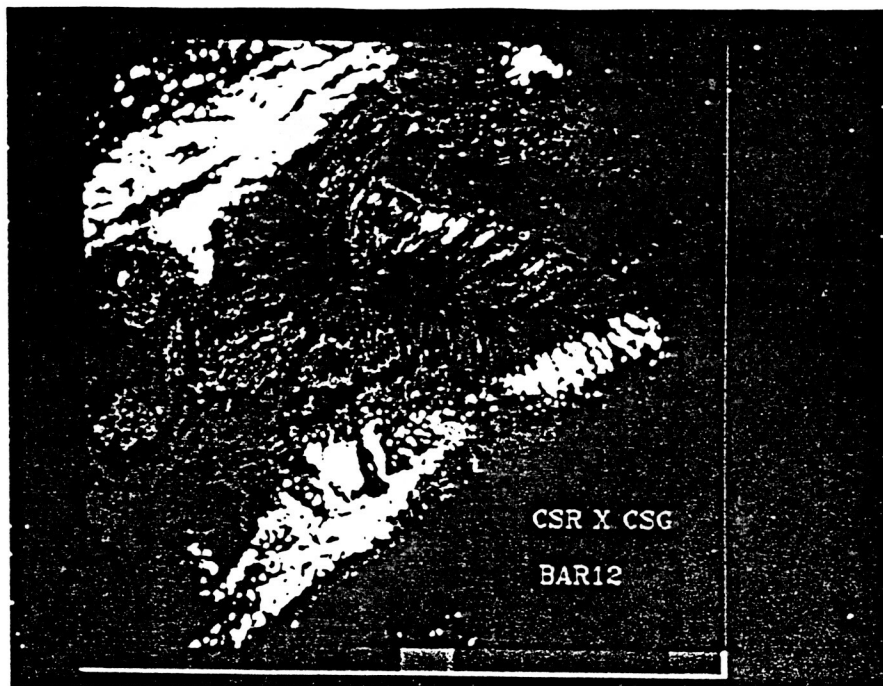


FIGURE 8

ORIGINAL PAGE IS  
OF POOR QUALITY

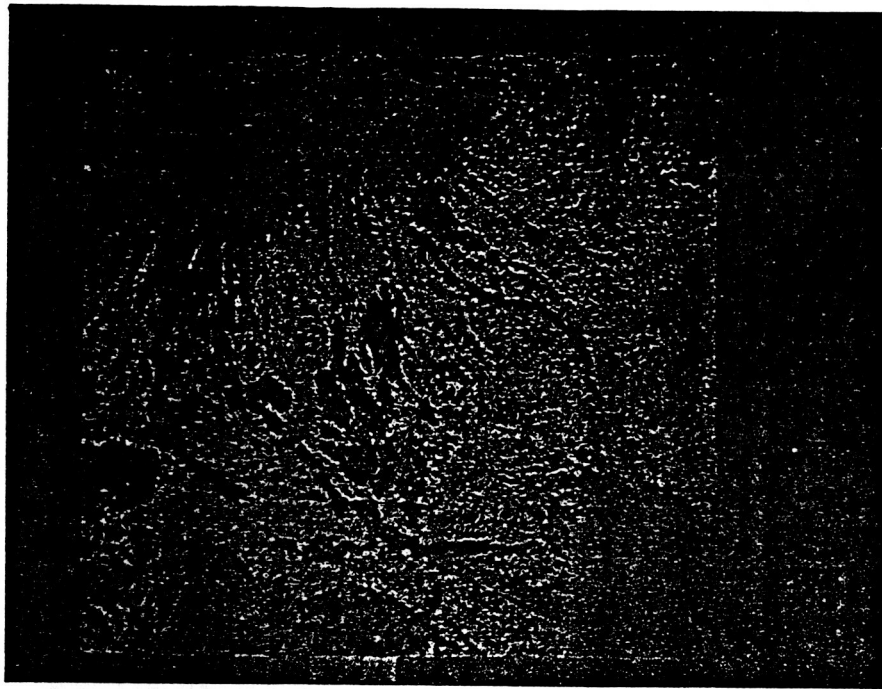


FIGURE 9

attenuate all but a small slice of that portion of the electromagnetic spectrum. Figure 10 is red / green, using CSLUT 1. The mix of colors is not as impressive as has been seen on previous illustrations, but the potential informational content, especially in digital form, cannot be discounted at first impression. Close examination may reveal highly useful data. For example, the large oval in the lower center is seen as a very bright, indiscriminate feature in visual, but is separated into green, yellow, and gold in this ratio. The focus of the view is the 1984 Mauna Loa flow, stretching from upper center to low center left. Ratioing reveals a little tonal distinction in the flow but better versions are available.

Subtraction was found to be visually inferior, usually resulting in very bright and poorly separated tones. Nonetheless, because the eye may not be the best judge of value for the computer, subtraction is retained. One of the uses of subtraction is its combination with other versions. Thus, the step following single algebraic functions is the creation of complex, multiple algebra renditions. Such manipulations are not inherently predictable but can be derived either through experimentation or experience.

Figure 11 is an "addsub"--an addition ratioed to a subtraction (a reasonably successful version in many cases). Shown is red +



ORIGINAL PAGE IS  
OF POOR QUALITY

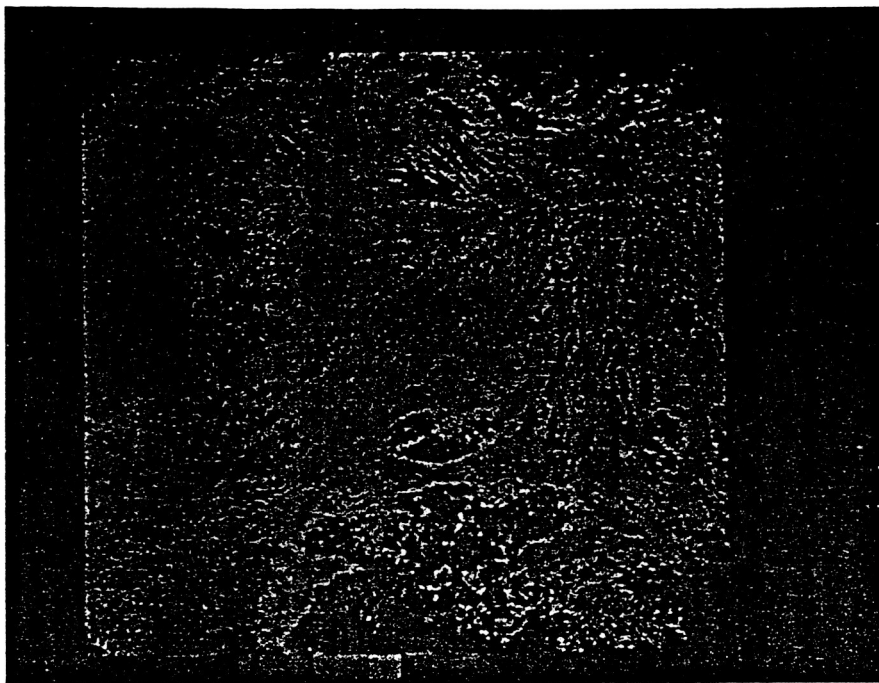


FIGURE 10

ORIGINAL PAGE IS  
OF POOR QUALITY

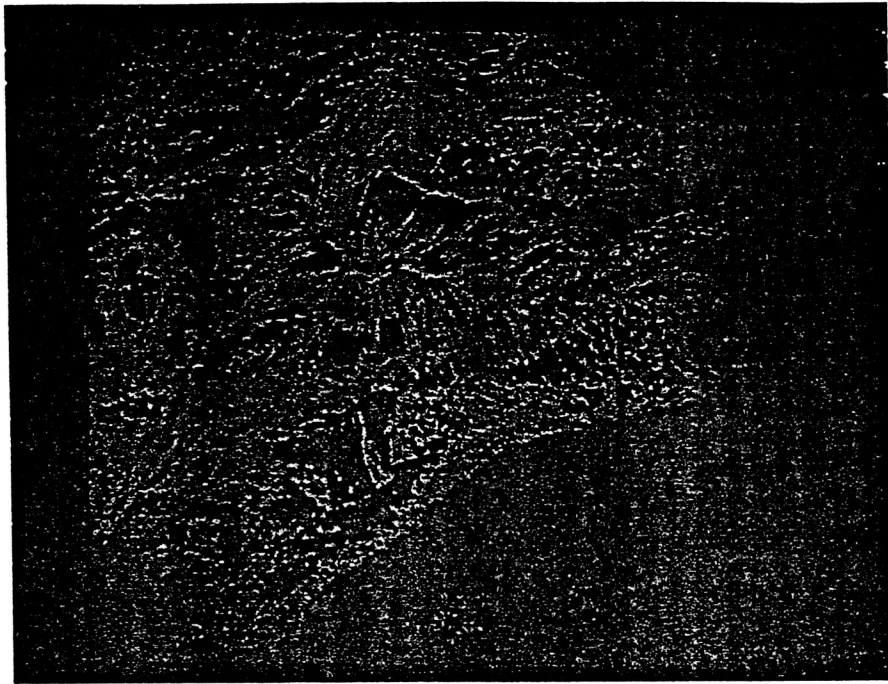


FIGURE 11

green ratioed against red - green. There is good information in the forest, albeit a blending of one lobe with the ocean is a problem. Fine tuning of color intervals possibly could eliminate the merging. The radial flows of Mauna Loa are presented in several color patterns, which is very interesting considering their apparent uniformity. The three study flows have informational individuality, although the Captain Cook flow is almost singular in tone, but with some "tweaking" of the LUT design, perhaps better internal differentiation can be produced.

Figure 12 is the same ratio but with CSLUT2 applied and Figure 13 has CSLUT3, each with succeeding finer separations of darker tones and assignment of moderate and bright tones into larger segments. The Captain Cook flow is better represented with CSLUT2 and even better internal information is seen with CSLUT3. On the other hand, CSLUT2 loses the other two flows for analytical purposes. CSLUT3 offers better flow delineation but Keamuku and the 1859 flows are not well detailed within. Obviously, the three flows have differing characteristics and certainly are worth investigating further, both in the field and from other sensors (including additional Shuttle photography from varying look and sun angles).

Versions of multiple algebra can be infinite and there is no practical guide suggesting which ones are best for which

ORIGINAL PAGE IS  
OF POOR QUALITY

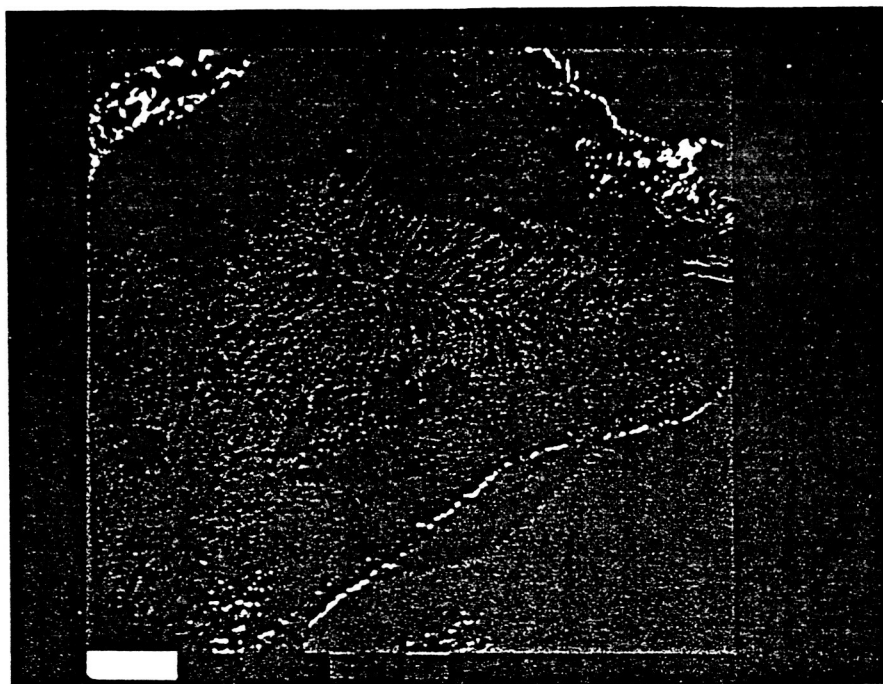


FIGURE 12

ORIGINAL PAGE IS  
OF POOR QUALITY



FIGURE 13

purposes.<sup>5</sup> Figure 14 is a final manipulation and depicts a complex red x green / (red + green / red - green), herein referred to as x/+- . X/+- was derived as a rough approximation to a Landsat vegetation index and proved to be useful for several purposes. Although this image seems very busy it separates some lava flows not previously distinguished on other manipulations. For example, the large red area at right center is separated from a fringing green--1871 versus 1935 flows. Mauna Kea slopes are well defined and will be compared to existing geologic maps in forthcoming research.

Another technique available from LIPS is the creation of principal component analysis images--PCA. As indicated, PCA involves a complicated algorithm which strikes the best balance within the input scenes to produce the best contrasting image.<sup>6</sup> Visually, the views are not particularly remarkable after experiencing previous images, but for the computer, PCA offers excellent information. Figure 15 shows one PCA and CSLUT2. As will be discussed in the following section on quantitative information, four PCAs were produced, each using either a different set of input images and/or a different ground area for principal components statistics. The 1984 flow is well defined and reveals surprising internal information. Some radial flow zonation can be seen on Mauna Loa.

ORIGINAL DISC IS  
OF POOR QUALITY



FIGURE 14



FIGURE 15



ORIGINAL PAGE IS  
OF POOR QUALITY

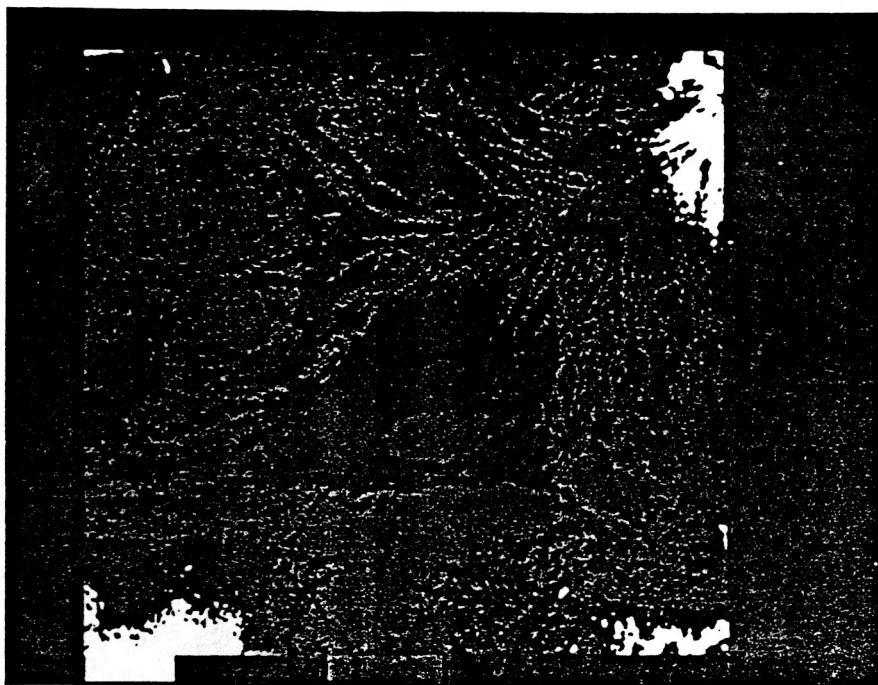


FIGURE 16

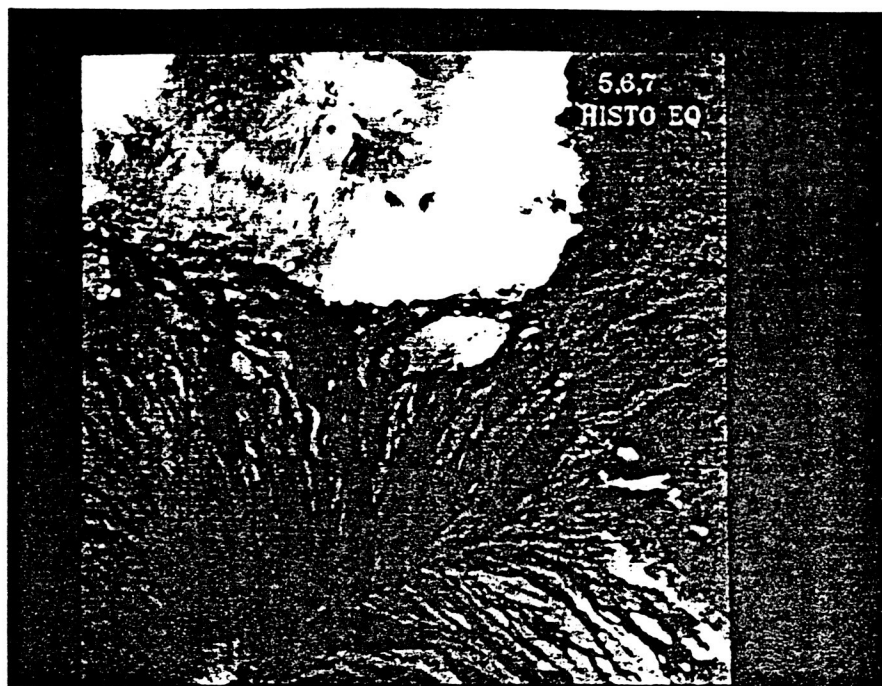


FIGURE 17

Figure 16 is a different PCA, with CSLUT2, which shows excellent 1984 flow data. This makes a very good field guide to potential morphologic and/or spectral sample sites. The radial flow zonation is well marked. Therefore, these images are superb data sources, especially when combined with even better detailed information from pixel value, profile, and histogram functions.

A final manipulation, which really could be one of the first employed, is histogram equalization. Its simplicity of use essentially hid it from obvious view when first exploring the system--it is a subsidiary sub-command in the Histogram operation. Consequently, it was not utilized until very late into the project and the only print (though not slide) version is of a Landsat scene. However, it well represents SP histogram equalizations. The version shown here<sup>(Fig. 17)</sup> is the combination and coloring of three bands. Application of LUTS to monochrome versions results in images of similar caliber to previous manipulations.

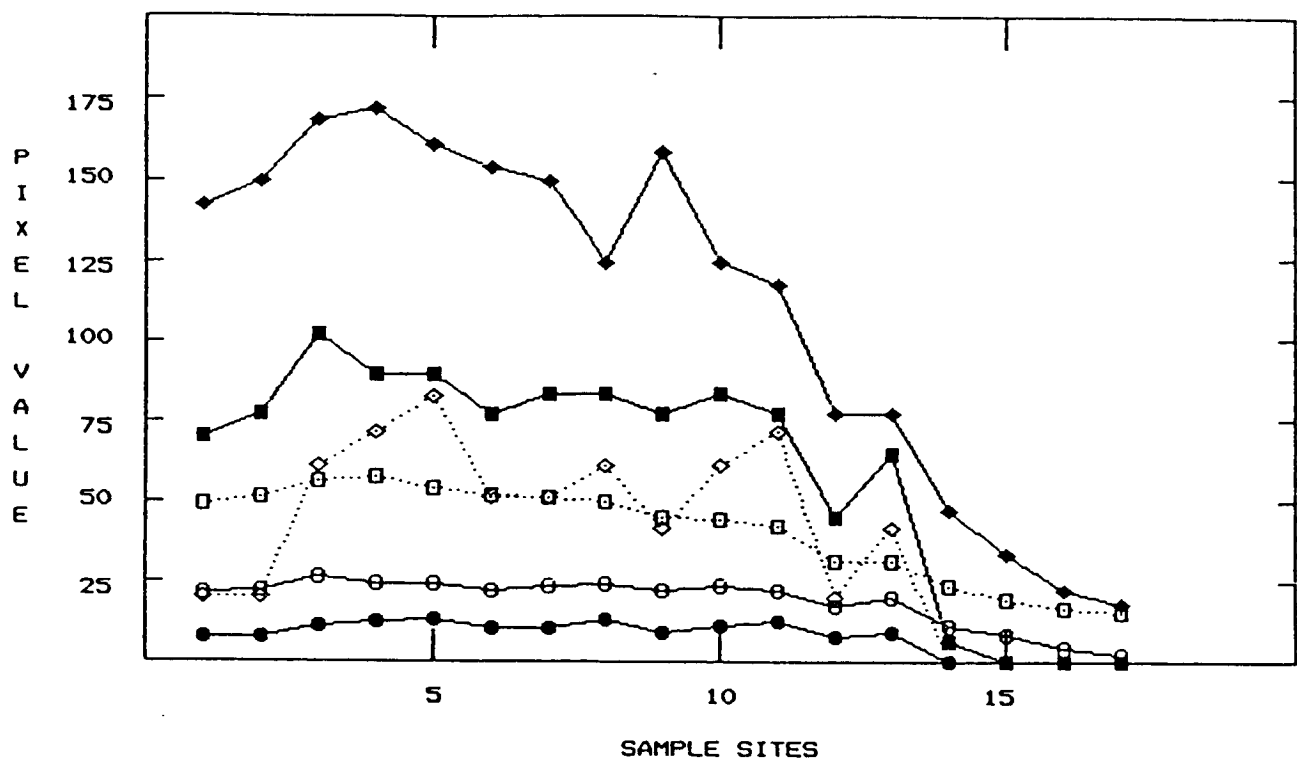
## GRAPHS

Imagery is meant for the eye and despite sophisticated computer techniques, the human interpreter cannot be dismissed.

Nonetheless, the use of quantitative data in imagery analysis cannot be underscored. Visual information can be rendered understandable with relatively simple mathematical and statistical techniques. Therefore, a major objective of this project is to produce useful quantitative analysis of SP imagery.

One of the most basic, yet most valuable techniques, is to construct transects of pixel values. Using the floating cursor, sites of convenience and potential value are selected on various images and pixel values at each location are noted. The Keamuku flow is presented in Figure 18. It contrasts the responses of original and CS versions along the flow.

Several surprises are evident. First, while the CS images would be expected to offer a greater range of values (and thus greater contrast from which to perform further enhancement and analysis), they do not always "win" over original data (or so it seems here). Original red and green show rather flat trends, indicating low contrast, but surprisingly, blue, which is visually poor, gives the best original contrast in digital format, even better than CS red and perhaps better than CS green. CS blue presents the widest range of contrast. The explanation is either that blue is digitally more informative or that the image analyzed here contained much noise in the blue.



# KEAMUKU FLOW VALUES

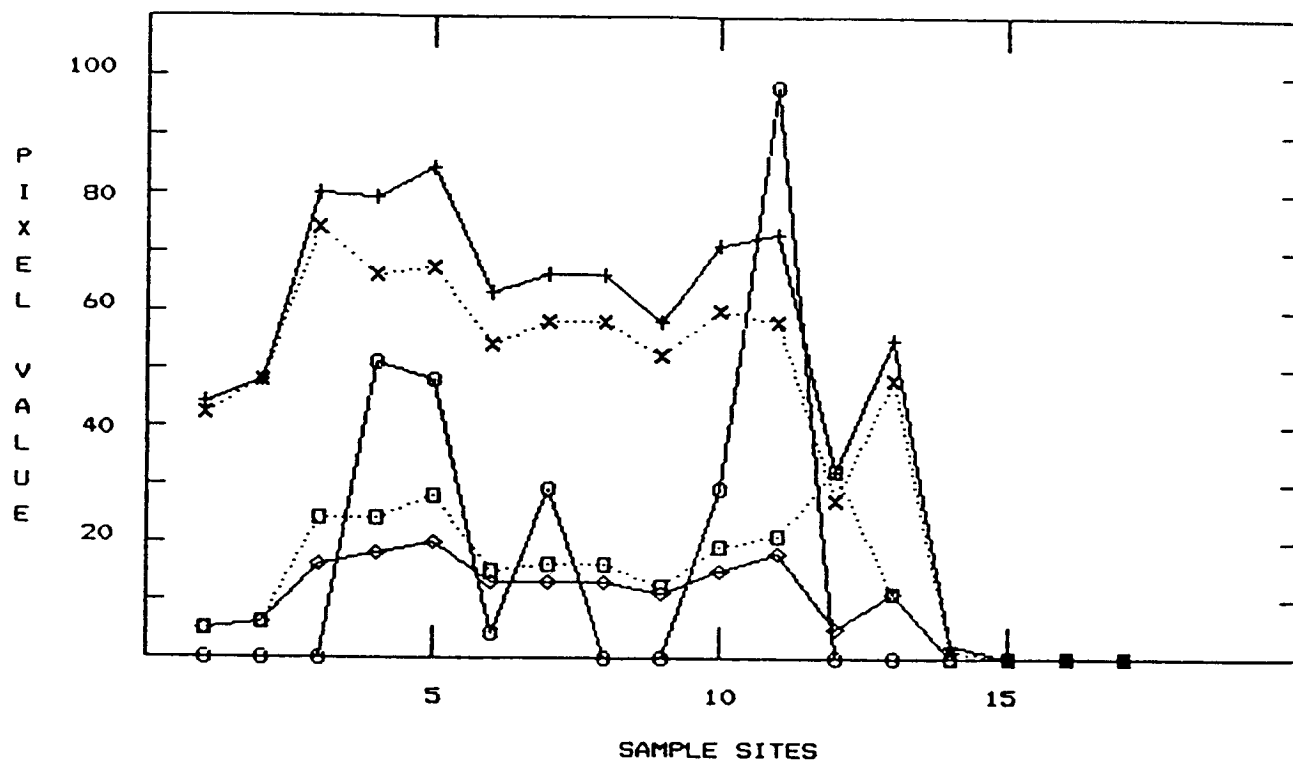
RAW AND CONTRAST STRETCHED RED, GREEN, BLUE

- RED
- GREEN
- ◇ BLUE
- CS RED
- CS GREEN
- ◆ CS BLUE

FIGURE 18

The latter is credible given that the blue filter is very dense visually and requires considerable electronic "push" for production of a semi-useful image. For example, much more contrast must be applied, the vidicon camera's diaphragm must be open to the maximum, and often the gain and blank of the camera's control box must be shifted. All of these manipulations are potentially inherently noisy. Further work needs to solve this question.

Figure 19 shows five red-green algebraic versions and the same pixel value locations as in Figure 18. Note the wider range and variation of values in most of these versions. Red + green has high tones and varies considerably, as does the addsub. Perhaps the poorest of this set is the  $x/\pm$ , but it is still a useful variation that could be separated with careful density slicity and LUT construction. The ratio version is extremely variable and actually may fluctuate too much to be useful. The smoother trends in the other images are suggestive of a relatively uniform change, but the gyrations of the ratio cast suspicion on its utility. This problem shows the value of using multiple images in analysis and the disadvantage of depending upon a single image for information. Also notable in both Figures 18 and 19 is the decrease in pixel value downstream. The exact cause of this trend is unknown at present, perhaps tonal degradation toward the frame edge caused by intrinsic lighting conditions on the



# KEAMUKU FLOW VALUES

ENHANCED IMAGES

- R / G
- R x G
- ◇  $R \times G / (R+G / R-G)$
- X  $(R+G) / (R-G)$
- + R + G

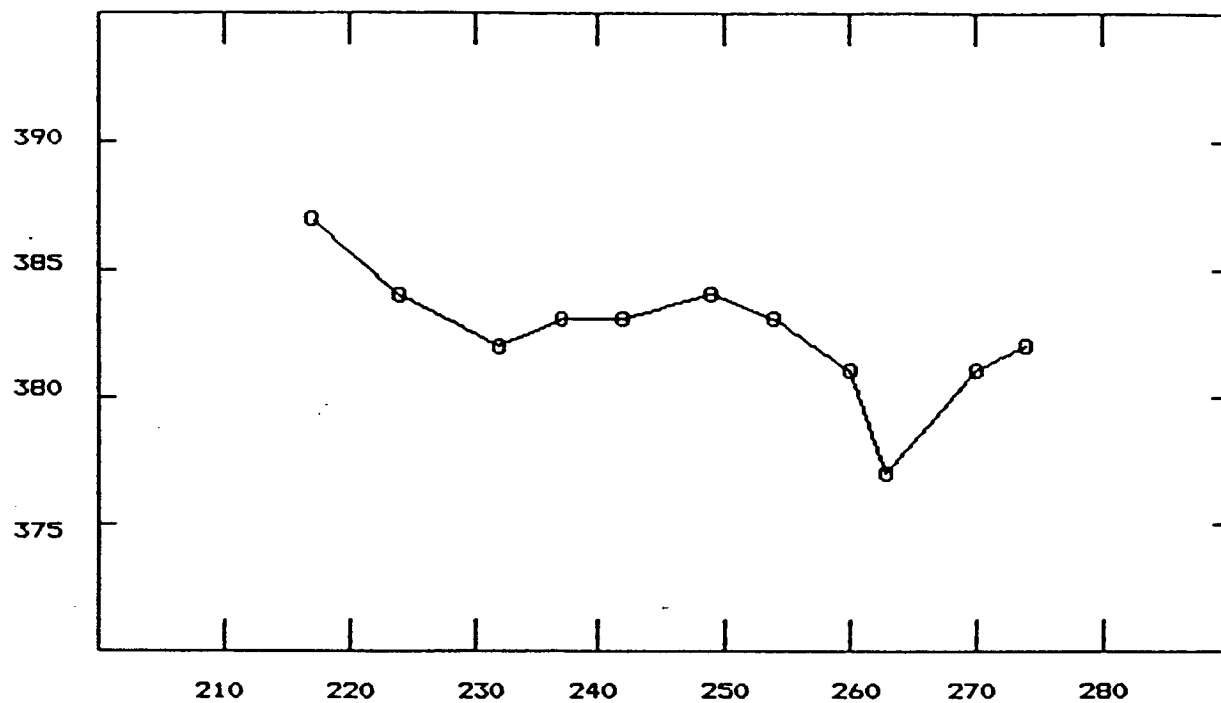
FIGURE 19

original photograph or lighting conditions during digitizing, or perhaps a real darkening along the flow. It is sufficiently intriguing to stimulate intensive field work.

Another transect performed was along Saddle Road--Saddle Road Profile A. A series of short pixel value profiles were performed--similar to but not be confused with the profile operation which runs an automatic continues line between points. Screen coordinate mapping is given in Figure 20 and helps to locate sample points in the field. Four images were used and are presented in Figure 21. There is a similarity in trends but subtle differences or changes are interesting. For example, why does green CS dip lower at sites 4, 7, and 9 than the others? Also, note the bright spot at site 2--worth investigating.

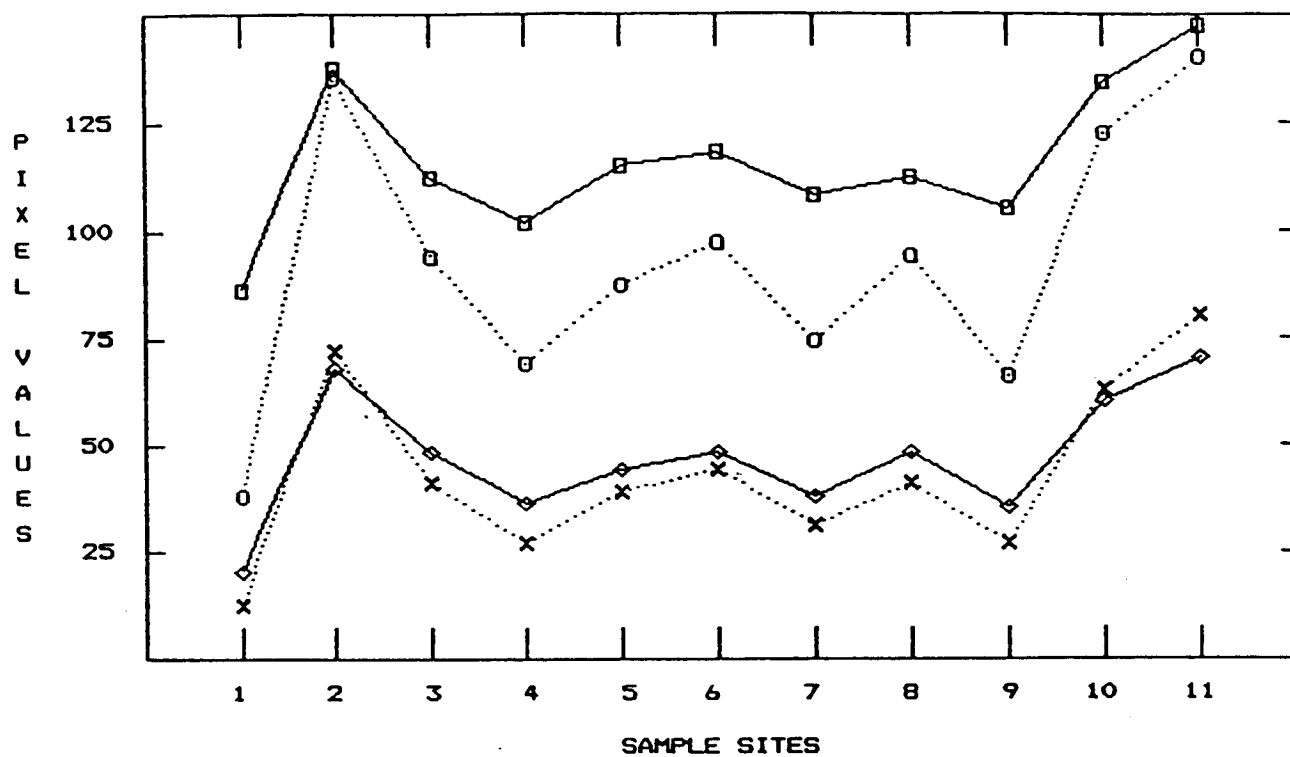
Figure 22 depicts the 1984 flow pixel value transect from seven images. Again, there is a similar trend along the flow and notable changes at sites 7, 20, and 24--further information for field analysis. The red x green has the darkest response, but informationally presents a greater range of values than several other versions, especially greater than the x/+ adjacent to it on the graph. The brightest image is the green CS, which contains good contrast, but probably does not perform any better in terms of contrast trends than the other versions.





SADDLE ROAD PROFILE A  
SCREEN COORDINATES

FIGURE 20



SADDLE ROAD PROFILE A

- RED CS
- GREEN CS
- ◇ RxG / (R+G / R-G)
- x RED x GREEN

FIGURE 21

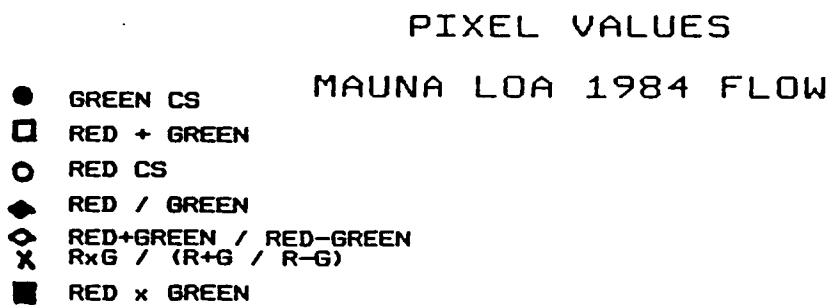
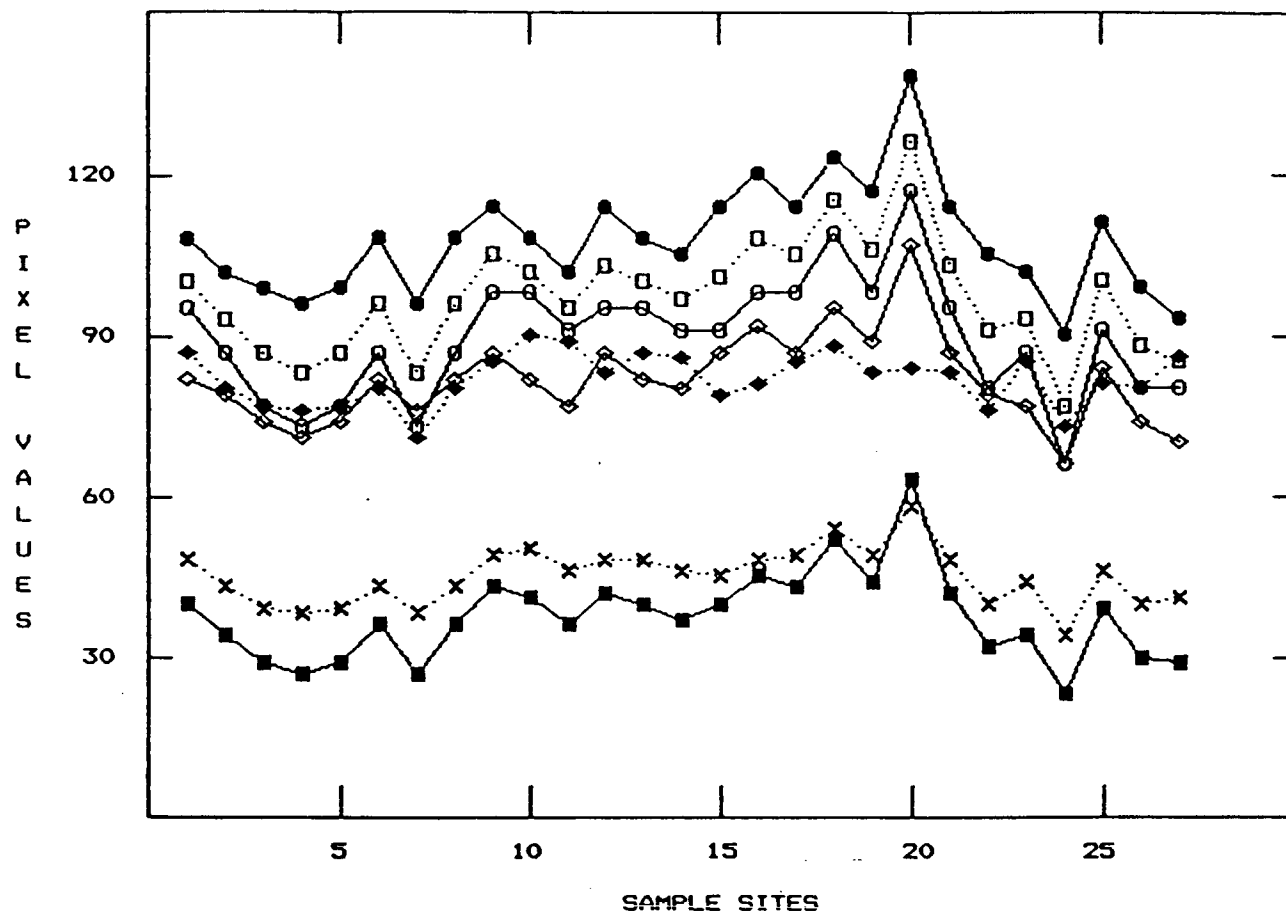
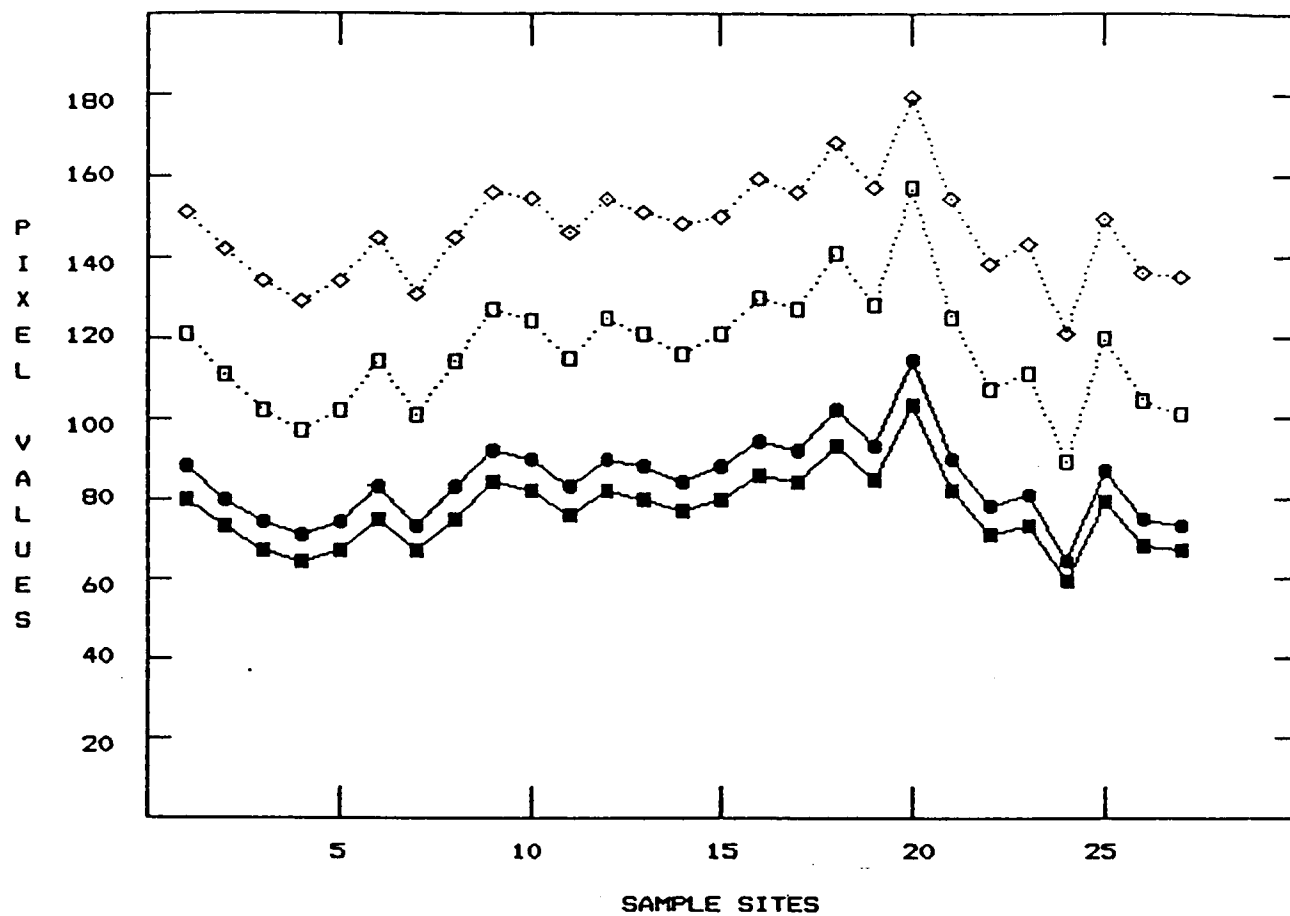


FIGURE 22

When select images are put into PCA, there is potentially high quantitative data. Figure 23 shows four PCA versions. PCA1 (annotated as just PCA on some photography) is based not on the whole image but only on the volcanic landscape area, avoiding Mauna Kea's bright glacial debris. As indicated, LIPS's PCA option allows the user to select a small portion of the image from which to base PCA statistics. PCA1 uses two non-algebra images of CS red and CS green, and two algebraic images of red x green and  $x/\pm$ . PCA2 uses the flow area for PCA data sample and employs four other images (which are also used for PCA3): red/green, addsub, red CS, and red x green. Their selection was based on previous performance, e.g., as on Figure 22. However, even arbitrary selections should produce similar results, as will be discussed in the next paragraph.

PCA3 was based upon Mauna Kea's very bright area near Saddle Road. PCA4 used only three images: red/green, red + green, and addsub, and the same flow area as PCA2. Interestingly, despite the variety of PCA bases, the resulting trends shown in Figure 23 are very similar, differing only in brightness. Therefore, it appears that the lava flow, if not the entire image, will respond in a rather uniform manner regardless of PCA versions used. This is stated with only little evidence and in the belief that some algebraic renditions possibly could have dramatic effect on principal components analysis. On the other hand, perhaps the



PC PIXEL VALUES  
MAUNA LOA 1984 FLOW

- PC1
- PC2
- PC3
- ◇ PC4

FIGURE 23

generalizing and compromising nature of PCA subdues remarkable responses. Sample sites 7 and 20 and possibly 24 stand out as slight anomalies in this graph and may be worth investigating in the field.

In further assessment of the varying PCAs' responses, with interest on the subtle trend differences, all four were set to zero at site one and changes in value from one site to the next were plotted (Figure 24). Whereas the graph substantiates the general similarity of their trend (as reckoned by the eye from Figure 23) some deviations are evident. For example, PCA2 and PCA4 (both based on the very dark lava flow) have greater change between sites 3-5 and at site 24 than the other two versions. No explanation is offered at this time but both field checking and more thought into the construction of the PCAs are in order.

Plotting the averages of the PCAs against the important algebraic versions, using the 1984 lava flow as a medium, Figure 25 shows that PCAs have high tonal values but a similar trend curve as that of the algebra. Does this mean that, indeed, PCAs really are no better than algebraic functions despite the supposed superiority?

One means of judgement is to check the potential for contrast and Figure 26 presents one rather simple way. Changes from one

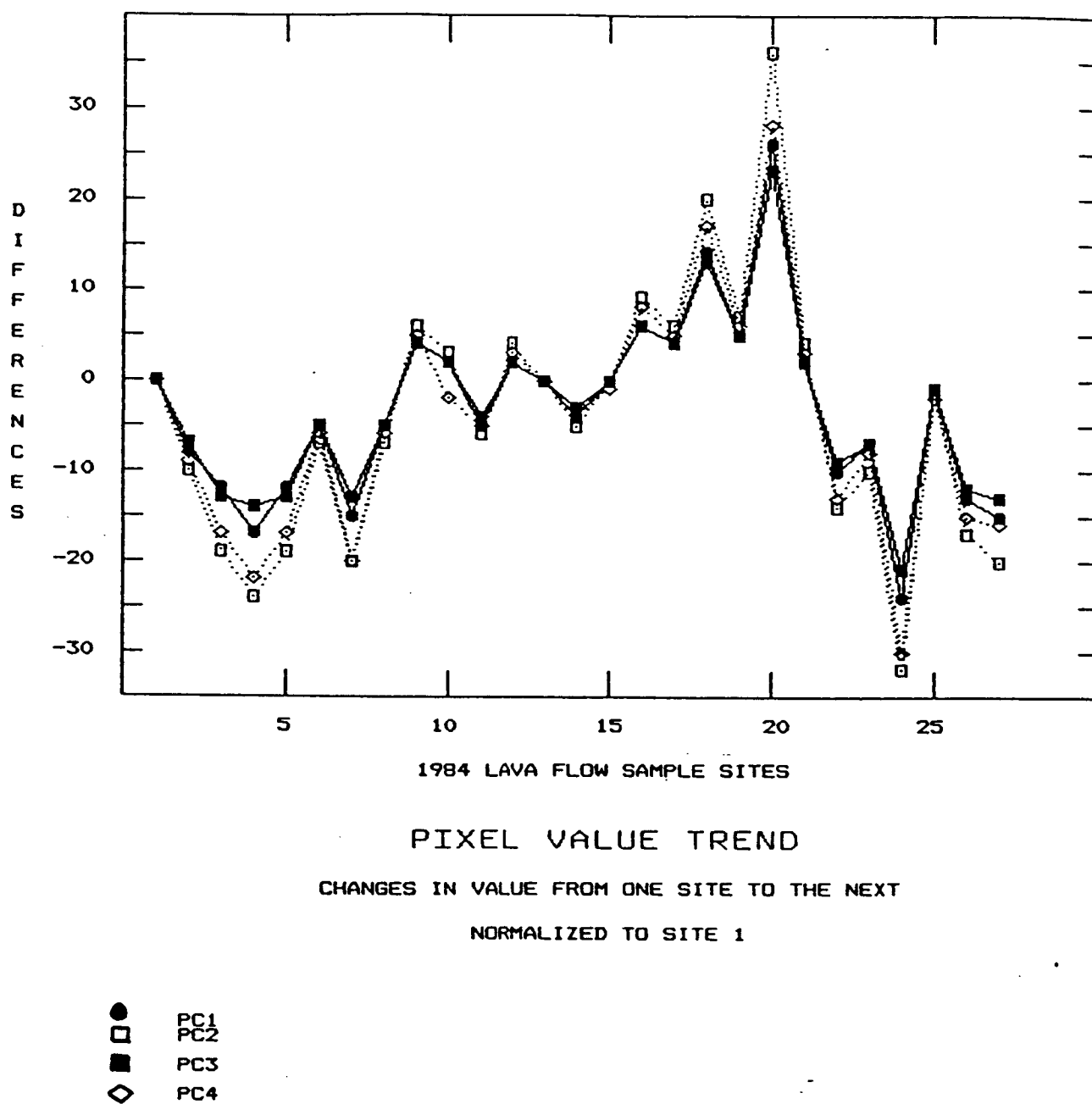
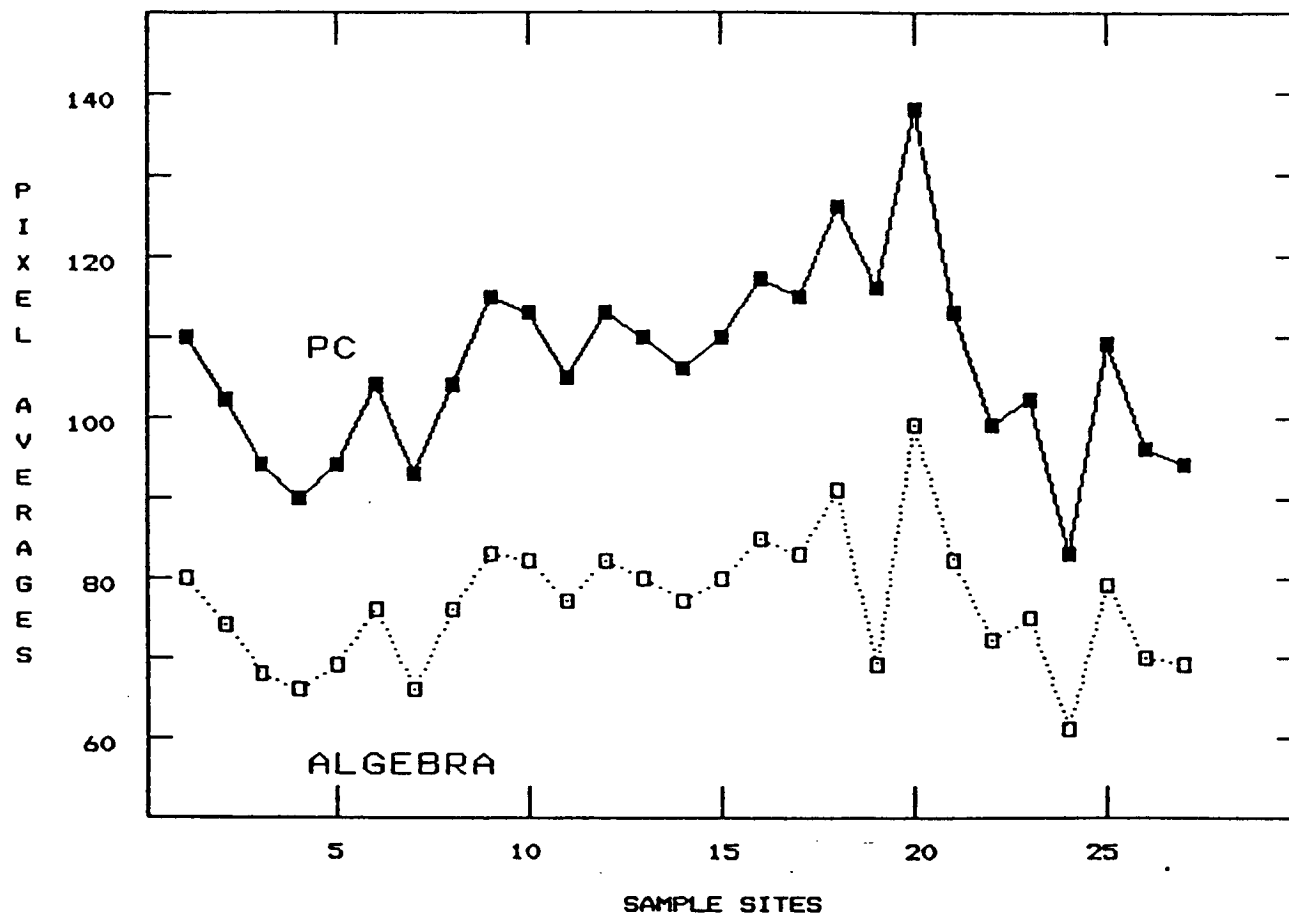


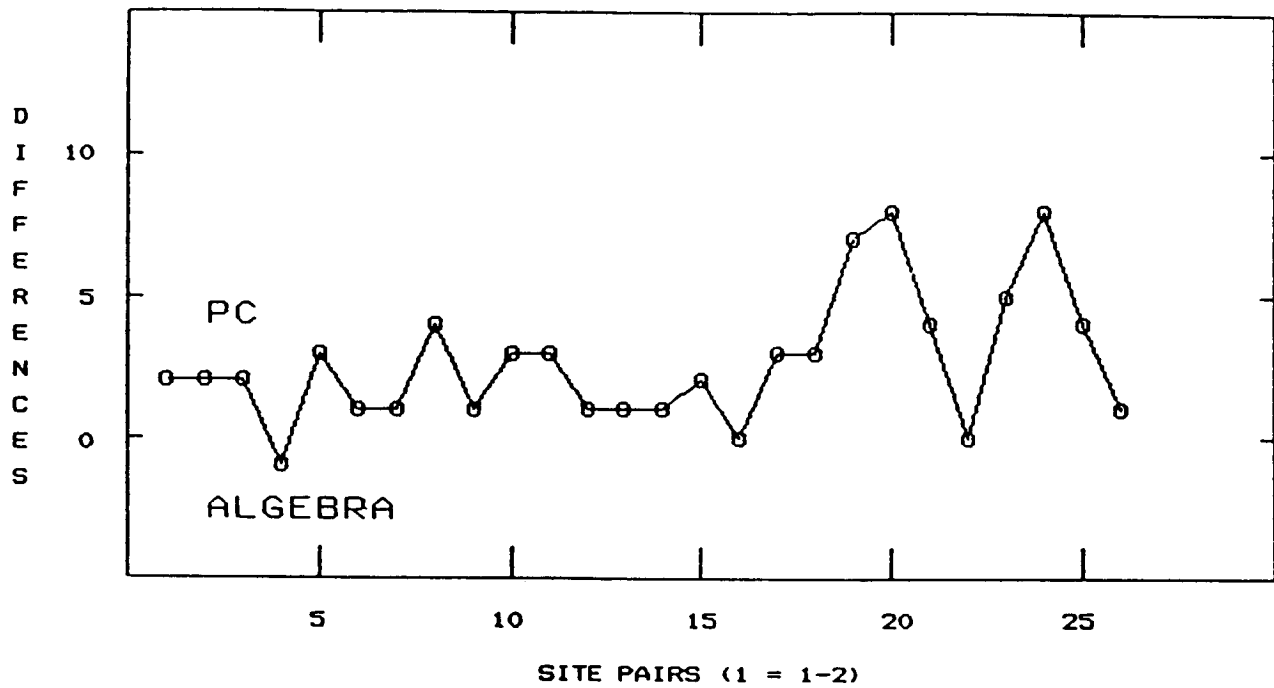
FIGURE 24



PIXEL AVERAGES  
ALGEBRA & PC VERSIONS

FIGURE 25





# DIFFERENCES IN CHANGES FROM ONE SITE TO THE NEXT

AVE. PC VERSIONS - AVE. ALGEBRA VERSIONS

- > 0 = PC OFFERS MORE CONTRAST
- < 0 = ALGEBRA OFFERS MORE CONTRAST

FIGURE 26

site to the next on any transect shows the degree of progressive tonal contrast. As seen in previous graphs, comparing that change among several image renditions indicates which image probably presents the greatest useful contrast for the subject under investigation. The base for Figure 26 was a site difference plot derived from Figure 25. Then the algebra differences were subtracted from PCA differences for comparison. Where both versions (i.e., their composite averages) change identically from one site to the next, there is no variance between them; there is zero value. Where the PCA has greater change, the graph number is positive and where the algebraic functions have greater difference, the number is negative. Figure 26 shows that only at site 4-5 does the algebra perform slightly better than PCAs. At other sites there is either no difference or PCAs out-contrast the algebra. Therefore, principal components images seem to present the best interpretative information, although algebraic renditions are also useful.

#### VISUAL EVALUATION

Because the human element of interpretation is deemed important, a visual comparison of thirty algebraic and PCA versions, from four original photographs, was performed. Eighteen sites of varying nature (vegetation, lava flow detail

and discrimination, glacial debris, etc.) were examined and rated on each image as poor (useless), moderate (possible utility), or good (worth using for investigation). Two basic assessments were employed: overall scoring and double weight for lava flow information. Ultimate evaluation was in the form of a ranking of each rendition and results are presented in the Conclusions portion of this report (but quantitative results are not itemized). In essence, monochrome scenes ranked poorly while LUT versions were the best, as would be expected. Also unsurprising is that PCAs and histogram equalizations are deemed visually superior, but are followed closely by several algebraic functions, such as multiplication and addition.

#### OTHER WORK

The bulk of the project's time was spent on the work detailed above, but because the basic goal was to explore the digital possibilities of SP, several secondary projects were pursued intermittently. They remain incomplete but the potential of each can be assessed.

Because many of the enhancements seemed promising for landscape mapping and analysis, mapping of Mauna Kea's glacial and volcanic

deposits was attempted, using Porter's map as reference (see Footnote 3). The map was reduced to an outline format by hand tracing and digitized into LIPS. Using the Coregistration program the map was registered to image number 84-14-44-93. An inadequate fit resulted, probably from operational errors, which caused problems of comparison. Preliminary examination revealed numerous tonal discrepancies between CS red and corresponding map divisions. However, many other renditions are available for testing once the map is properly registered.

Using the same scene as above, land use and land cover analysis of the Hamakua (windward east) coast will be performed. There is a band of sugar cane (under various growth conditions) and a distinct elevational zonation of vegetation upslope. The coast is often cloud-covered and clear imagery is relatively rare. Combined with one of the few useful Landsat scenes, change analysis and multisensor analysis can be accomplished. Preliminary examination of several enhancements showed promise.

An applied investigation is delineation of deforestation of Grand Comoro island, Comoros. Losses of forest resources in many nations is alarming, and perhaps no more so than in Comoros, where on one island there has been a 66% decrease over a ten year period. Although Landsat's simulated color infrared would be ideal in mapping the forest distribution, the imagery is stored

and dispensed from South Africa, making procurement difficult. Also, from Landsat records it is seen that heavy cloud covers predominant over the islands and there is no image with less than 30% clouds. However, the Shuttle's frequent overflights gives it access and astronaut monitoring and photograph selection can obtain cloud-free or special site visual opportunities (as opposed to Landsat's automatic chance imaging).

One SP image of Grand Comoro (S09-39-2516) is a near vertical and is ideal for mapping. Enhancement of the image is necessary in that there is heavy attenuation in the blue on the original. Comparison with existing 1949 and 1950 airphotos was begun but difficulties in airphoto mapping due to significant displacement problems (common steep slope landscapes) prevented completion of the comparison in the short time available. Initial examination shows that if the traditional mapping can be completed, good comparisons can be made. As such, a valuable service can be performed.

Reunion island, also in the Indian Ocean, is seldom seen or investigated. Like Landsat of Comoros, satellite imagery of Reunion is practically inaccessible. Several SP scenes are available, however, and are to be enhanced to remove the heavy attenuation. For example, S13-39-2002 shows part of Piton La Fournaise, a large breached caldera, and application of lava

enhancement experience from Hawaii will be interesting. Also, because of world sugar economic problems, the island's monocrop dependence on cane (approximately 90% of arable land on the island) is threatened. Mapping of sugar cane cultivation (based on experience from sugar cane interpretation on Hawaii) and comparison with earlier maps may reveal important economic and environmental changes. Further, since the two SP shots are partially (but spatially-opposed) cloud covered, the opposing cloud-free halves can be separated from their original scene, registered to a common planimetric format, and then mosaicked with each other to produce a rare cloud-free, rectified space image, which subsequently can be digitally enhanced for analysis heretofore unavailable.

The San Joaquin Valley of California presents an ideal agricultural landscape from which to study computerized SP analysis. It was hoped that the University of Santa Barbara's Geography Remote Sensing Unit would have current field data on imaged areas of the southwestern part of the valley. However, their data collection is to be performed too late into this project for application to imagery. Initial inspection and manipulations of 51B-147-038 reveal a wealth of information and significant possibilities for image analysis. This project awaits UCSB's field data and access to other ground information.

Comparison of SP with Landsat was begun but because of mentioned tape storage and recall difficulties, systematic investigation was prevented. Initial manipulations showed excellent potential for data gathering. Subjective (and very preliminary) judgement, however, indicated that SP is as good (perhaps better?) in some lava flow discrimination, but much more work is needed. The infrared quality of Landsat is sure have advantage over SP for some purposes but the effect on unvegetated lava flows is to be determined.

When the tape recall problems are solved and access to the image analyzer is regained, more systematic comparisons of varying look angles and environmental conditions, as well as comparison of SP and Landsat, can be performed. Initial assessment shows that different look angles and scales provide varying details of information, as would be expected. Obviously, larger scale produces higher potential for increased information, primarily due to the higher resolution and resulting number of pixels for a given feature (and therefore, presumably more values to work with).

Also, it was seen that contrasting Sun angles affect lava signatures, which is to be expected, but the changes, if any, in relationships within or between flows under such conditions should be researched. That is, under one Sun angle (and/or other

environmental conditions and/or under different look angles) the pixel value difference between specific points within a flow and/or the pixel value differences between flows may show a particular or numerical relationship, but under other conditions, that relationship may change. Further complexity is added by introducing and analyzing various enhancement renditions. There is a potential wealth of analysis and information available which has yet to be investigated.

Other projects that could be pursued involve the effect of spatial filtering on SP, inclusion of SP color infrared (however poor the imagery), and change analysis using SP shots from different times. Also, expansion of subject matter is in order, e.g., further investigation into forest sites of Hawaii or application of the enhancement techniques to other areas of the world.

## CONCLUSIONS

Conclusions, at this stage, are in the form of suggestions for use of SP on LIPS and suggestions for specific versions. Quantitative and visual data proved the following images to be superior in delineation and discrimination of Hawaii volcanic landscapes (application to other sites and features is to be determined):



PCA  
Histogram Equalization

Followed by (all contrast stretched):

$$\begin{array}{l} \text{Red} + \text{Green} / \text{Red} - \text{Green} \quad [\text{Addsub}] \\ \text{Red} \times \text{Green} \\ \text{Red} + \text{Green} \end{array}$$

and sometimes:

$$\begin{array}{l} \text{Red} \times \text{Green} / (\text{Red} + \text{Green} / \text{Red} - \text{Green}) \quad [\text{X}/+ -] \\ \text{Monochrome Red CS} \end{array}$$

PCA and histogram equalization are extremely easy to create, requiring only a few simple commands (but mathematically are not necessarily comprehensible, though that is not considered significant at the applications stage). Algebraic versions are not difficult to produce but do require more steps, care and systematic treatment, and more understanding of signatures and LIPS creations that do the first two versions.

There is a great deal of analytical capability of SP using computerized techniques. The Gould image analyzer and LIPS software are relatively easy to learn and use and should be utilized in both further evaluation of SP and in research previously dependent upon traditional manual/eye interpretation of scenes. Other image analyzers, even microcomputer systems, can perform useful analysis. Not only are subtle signature differences rendered more appreciable but new, primary data can be revealed. Consequently, there is much unrecognized scientific

merit to Shuttle hand-held photography and perhaps a new dimension in its use and application can be employed.

## FOOTNOTES

1. Compounding this rather subordinate reputation is the difficulty in obtaining truly vertical photos that may be used for planimetric mapping. Whereas satellites retain continual nadir pointing and are ideal for precision mapping, Shuttle astronauts are seldom able to provide zero degree verticality (or, more technically correct, they choose and frame select targets which rarely occur directly beneath the Shuttle when it is in a perfect attitude).

Nonetheless, there are sufficient advantages of photography over satellites, such as the "man-in-the-loop" concept where astronauts make immediate decisions on targets, lens, framing, and exposures. Further, although satellites usually are limited to single sun-time lighting, Shuttle photography encompasses a wide range of light conditions, from very low to very high sun angles.

2. See for example, R. Steven Nerem and Robert Holz, "The Use of NOAA AVHRR Satellite Data and Hand-Held Earth Photography From Space in a Multi-Data Study of the Nile Delta." Technical Papers, 1984 ASP-ACSM Fall Convention, San Antonio, Texas, 1984,

pp. 722-736. Also, Gellegos, S., R. Nerem, et. al. "Vegetative Responses From a Great Barrier Reef Surface Water Feature Detected By Space Shuttle Photography." Proceedings: 1984 ASP-ACSM Fall Convention. 1984. 699-707. Some visual Skylab projects were completed. See for example Richard Ellefsen and Duilio Peruzzi, "Land-Use Change Detection from LANDSAT and Skylab Satellites." 13th International Congress for Photogrammetry, Helsinki, Finland, 1976, NASA TM A78-16550. Also, H. F. Lins, "Land-use Mapping from Skylab S-190B Photography." Photogrammetric Engineering and Remote Sensing 42(3): 301-307; 1976.

3. As 19th century photographers demonstrated, reprojection and registration of the black and white images, through their respective filters will, converse to the separation process, combine to make a color rendition. Such a premise is used on the computer by effectively reprojecting various bands through red, green, and blue "guns" to reconstruct the natural color, or by mixing the combinations, creating false-color renditions.

4. Porter, Stephen. "Stratigraphy and Chronology of Mauna Kea, Hawaii: A 380,000-Yr. Record of Mid-Pacific Volcanism and Ice Cap Glaciation." Geological Society of America, Bulletin, Part II, Vol. 90 (July, 1979): 908-1093. His map is published as: Porter, Stephen, 1979. "Geologic Map of Mauna Kea Volcano,

Hawaii." Geologic Society of America Map MC-30. Also, see Stephen Porter, M. Stuiver, and I. Yang. "Chronology of Hawaiian Glaciations." Science, 195 (Jan. 7, 1977): 61-63.

5. There's very little published information or guides on selecting band combinations or versions for given features. One of the most recent is: Sheffield, Charles. "Selecting Band Combinations From Multispectral Data." Photogrammetric Engineering and Remote Sensing, 51,6 (June, 1985): 681-687.

6. Principal component analysis is discussed in various references. Two of the most recent and useful for this type of project are: Canas, A. and M. Barnett. "The Generation and Interpretation of False-Colour Composite Principal Component Images." International Journal of Remote Sensing, 6,6 (1985): 867-881. Singh, A. and A. Harrison. "Standardized Principal Components." International Journal of Remote Sensing, 6,6 (1985): 883-896. Also see: Schowengerdt, Robert. Techniques for Image Processing and Classification in Remote Sensing. New York: Academic Press. 1983: 159-164.

## BIBLIOGRAPHY

Blodgett, H. and G. Brown, 1982. "Geological Mapping By Use of Computer-Enhanced Imagery in Western Saudia Arabia." U.S. Geological Survey Professional Paper 1153. Washington.

Blodgett, H. and G. Brown, 1984. "Age Discrimination Among Basalt Flows Using Digitally Enhanced Landsat Imagery." NASA Techical Memorandum 86141.

Canas, A. and M. Barnett, 1985. "The Generation and Interpretation of False-Colour Composite Principal Component Images." International Journal of Remote Sensing, 6 (6): 867-881.

Duggin, M. J., 1985. "Factors Limiting the Discrimination and Quantification of Terrestrial Features Using Remotely Sensed . Radiance; A Review Article." International Journal of Remote Sensing, 6 (1): 3-27.

Ellefsen Richard and Duilio Peruzzi, 1976. "Land-Use Change Detection from LANDSAT and Skylab Satellites." 13th International Congress for Photogrammetry, Helsinki, Finland, Also is NASA TM A78-16550.

Gellegos, S., R. Nerem, et. al., 1984. "Vegetative Responses From a Great Barrier Reef Surface Water Feature Detected By Space Shuttle Photography." Proceedings: 1984 ASP-ACSM Fall Convention: 699-707.

Goetz, Alexander and L. Bowen, 1981. "Geologic Remote Sensing." Science, 211: 781-791.

Ingebritsen, S. and R. P. Lyon, 1985. "Principal Component Analysis of Multitemporal Imager Pairs." International Journal of Remote Sensing, 6 (5): 687-696.

Lins, H. F., 1976. "Land-use Mapping from Skylab S-190B Photography." Photogrammetric Engineering and Remote Sensing 42(3): 301-307.

Lipman, Peter, 1980. "The Southwest Rift Zone of Mauna Loa: Implications for Structural Evolution of Hawaiian Volcanoes." American Journal of Science, 280-A: 752-776.

Lord, D. and R. Desjardins, et. al., 1985. "Variations of Crop Canopy Spectral Reflectance Measurements Under Changing Sky Conditions." Photogrammetric Engineering and Remote Sensing, 51(6): 689-695.

Malin, Michael, 1980. "Lengths of Hawaiian Lava Flows." Geology, 8: 306-308.

Nerem, R. S. and Robert Holz, 1984. "The Use of NOAA AVHRR Satellite Data and Hand-Held Earth Photography From Space in a Multi-Data Study of the Nile Delta." Technical Papers, 1984 ASP-ACSM Fall Convention: 722-735. San Antonio, Texas.

Porter, Stephen, 1979. "Stratigraphy and Chronology of Mauna Kea, Hawaii: A 380,000-Yr. Record of Mid-Pacific Volcanism and Ice Cap Glaciation." Geological Society of America, Bulletin, Part II, 90: 908-1093.

Porter, Stephen, 1979. "Geologic Map of Mauna Kea Volcano, Hawaii." Geologic Society of America Map MC-30.

Porter, S., M. Stuiver, and I. Yang, 1977. "Chronology of Hawaiian Glaciations." Science, 195: 61-63.



Sheffield, Charles, 1985. "Selecting Band Combinations From Multispectral Data." Photogrammetric Engineering and Remote Sensing, 51 (6): 681-687.

Rowan, L., P. Wetlaufer, et. al., 1974. "Discrimination of Rock Types and Detection of Hydrothermally Altered Areas in South-Central Nevada by the Use of Computer-Enhanced ERTS Images." U.S. Geological Survey Professional Paper 883. Washington.

Schowengerdt, Robert, 1983. Techniques for Image Processing and Classification in Remote Sensing. New York: Academic Press, 159-164.

Singh, A. and A. Harrison, 1985. "Standardized Principal Components." International Journal of Remote Sensing, 6 (6): 883-896.

Smedes, H. and H. Linnerud, et. al., 1971. "Digital Computer Mapping of Terrain by Clustering Techniques Using Color Film as a Three-Band Sensor." EG&G Technical Memorandum B-542. Bedford, MA: EG&G Incorporated.

N86 - 31417

D8  
49.

ASEE Summer Faculty Research Program

FINAL REPORT

12819

INVESTIGATION OF LOCAL AREA NETWORKS  
FOR AN ORBITING SPACE STATION

Louis A. DeAcetis, Ph.D.  
Professor of Physics  
Bronx Community College  
of the City University of New York  
Bronx, NY 10453

Abstract

An investigation and test of various equipment was conducted to determine its state of repair and suitability for use in a test-bed computer network (to be used to simulate a space station configuration of computers for control and monitoring).

A research study was also made of various network types, including the IEEE network standards:

- 802.3- Carrier Sense Multiple Access with Collision Detection.
- 802.4- Token Passing Bus
- 802.5- Token Passing Ring,

and the draft ANSI standard for a High Speed Local Network:

ANS X3T9.5- CSMA with Collision Avoidance.

No firm conclusions were possible at this time as to which would be most suitable.

An evaluation of the user interface of a space station database program, FREDSS (Formatted Retrieval and Entry of Data for Space Station, preliminary version), was also conducted and recommendations were made for possible improvements.

NASA Colleague: Oron L. Schmidt, EE7 X6301

## INTRODUCTION

The Johnson Space Center ESTL facility had in recent years acquired an optical ethernet system whose reliability and state of repair had become questionable. It was decided that an evaluation of this equipment would be important in determining future acquisitions. A major portion of this fellowship was involved with this assessment. A study of the various types of networks and the IEEE standards 802.x was also undertaken in conjunction with the equipment evaluation.

Another evaluation involved the user interface of a proposed database system for the space station. A database accessing program, FREDSS, had been written to permit the entry of pertinent data for equipment on a space station, as well as retrieval of same.

## THEORY

The IEEE 802.x standards represent a family of specifications for Local Area Networks (LANs). These standards deal with the Physical and Data Link Layers as defined by the International Standards Organization (ISO) Open System Interconnection (OSI) Reference Model. The standards in particular deal with the following access methods:

- 802.3- Bus utilizing CSMA/CD
- 802.4- Bus utilizing token passing
- 802.5- Ring utilizing token passing.

In addition, a draft standard by the American National Standards Institute (ANSI), ANS X3T9.5, deals with High Speed Local Network (HSLN's), being designed specifically for bulk file

transfer between computers and peripherals [Stallings, 1984]. Any one of these standards, or a combination, is a candidate for a space station network. A quick review of available literature indicated that all access methods are currently undergoing modeling and study to determine performance under a variety of conditions [Cheng, 1982; Stallings, 1984].

The network equipment that underwent assessment was for an "Ethernet" network which essentially conforms to the IEEE 802.3 standard for a CSMA/CD system. This and related equipment are intended for use in a test-bed network employing VAX and MICROVAX computer systems to simulate a space station computer facility.

#### RESULTS and CONCLUSIONS

The equipment assessment results are detailed in a memorandum to Oron L. Schmidt/EE7, dated July 24, 1985, and are not included here. Likewise, the assessment of the user interface of FREDSS is contained in a memorandum to Eric Barnhart/LEC, dated July 29, 1985.

A review of Local Area Network access methods and protocols was presented at the Final Oral Presentation given on August 5, 1985. In general, various network configurations are only now being modeled and studied in detail. No clear choices exist at this time concerning what is most suitable in a given case. It appears that further investigation and evaluation of the various 802.x systems and the ANS X3T9.5 draft standard will be needed, along with a clearer specification of the computer facility for the space station, before any clear choice can be made.

## REFERENCES

1. Cheng, Wu-Yeh, "Performance Evaluation of Token Control Networks," Ph.D. Thesis, Department of Computer Science, University of Illinois at Urbana-Champaign, 1982.
2. IEEE Standard 802.3: "Carrier Sense Multiple Access with Collision Detection (CSMA/CD) Access Method and Physical Layer Specifications," 1985.
3. IEEE Standard 802.4: "Token-Passing Bus Access Method and Physical Layer Specifications," 1984.
4. IEEE Draft Standard 802.5: "Token Ring Access Method and Physical Layer Specifications," February 29, 1984.
5. Stallings, William, Local Networks, Macmillan Publishing Co., New York, NY (1984).

## ACKNOWLEDGEMENT

I would like to acknowledge the support and encouragement of Oron L. Schmidt, my "NASA colleague" and advisor. In any large organization, there are the many, and then there are the few without whom the organization could accomplish very little, if anything. Oron is clearly a part of that select few.

Additional thanks to Chuck Allen, Eric Barnhart, and Hector Reyna for their complete cooperation and assistance throughout my stay.

N86 - 31418

Dg  
288.

AN IBM PC-BASED MATH MODEL FOR SPACE STATION  
SOLAR ARRAY SIMULATION

18820

Ervin M. Emanuel, P. E.  
Assistant Professor of  
Electrical Engineering  
Prairie View A&M University  
Prairie View Texas

ABSTRACT

This report discusses and documents the design, development, and verification of a microcomputer-based solar cell math model for simulating the Space Station's solar array Initial Operational Capability (IOC) reference configuration. The array model is developed utilizing a linear solar cell dc math model requiring only five input parameters: short circuit current, open circuit voltage, maximum power voltage, maximum power current, and orbit inclination. The accuracy of this model is investigated using actual solar array on orbit electrical data derived from the Solar Array Flight Experiment/Dynamic Augmentation Experiment (SAFE/DAE), conducted during the STS-41D mission.

This simulator provides real-time simulated performance data during the steady state portion of the Space Station orbit (i.e. array fully exposed to sunlight). Eclipse to sunlight transients and shadowing effects are not included in the analysis, but are discussed briefly.

Integrating the Solar Array Simulator (SAS) into the Power Management and Distribution (PMAD) subsystem is also discussed.

---

NASA Colleague: Charles R. Price EH5 X2766

## 1.0 INTRODUCTION

Mathematical models for predicting the performance characteristic of terrestrial and space arrays have been utilized since the advent of the solar cell. The development of a relatively simple yet accurate model which could produce performance data over a wide range of environmental conditions is a complex task involving a multitude of factors. A thorough treatment and analysis of these factors contributing to the solar cell performance are discussed in research documents by J. Sandstorm (3), W. D. Brown et al (14), C. H. Liebert and R. R. Hibbard (4), R. E. Patterson and R. K. Yasui (8), W. W. Hough and B. D. ElRod (6), and H. S. Rauschenbach (1). Many others are shown in the list of references.

Hans Rauschenbach the author of a solar cell array design Handbook, discloses a complete procedure for producing space arrays electrical performance predictions. This process contains the following elements: (1) Solar cell electrical performance characterization, determination of the degradation factor related to solar cell array design and assembly, conversions of environmental considerations and criteria into solar cell operating temperature, and calculating of solar cell array power output capability. The complexity of correlating the effect of all elements affecting the cells' output has demanded the use of a main frame computer; of course not all the input data and supporting analysis are required by all designs and missions, but this generalized approach provides a strong base for developing mission-dependent (i.e. orbiting Space Station) electrical performance data.

This research report discusses the development of a streamlined approach, incorporating empirical data for determining the solar cell electrical characteristics, predetermined mission parameters, and array geometry and attitude, thus making a personal computer a perfect candidate for use as an analysis tool and Solar Array Simulator (SAS).

## 2.0 SPACE STATION ELECTRIC POWER SYSTEM

The IOC reference configuration power system consists of eight solar array wings, four regenerative fuel cell (RFC) modules, four heat rejection systems (for cooling the RFC modules and power conditioning equipment outboard of the alpha joint), and a power management and distribution (PMAD) system (11). The IOC baseline reference configuration is shown in figure (1).

### 2.1 IOC SYSTEM SIZE

The Solar Array must deliver 172 KW of power during the sun period of the orbit in order to provide 75 kilowatts of continuous power to the bus. These values were based on an orbital period of 94 minutes, a sun period of 59 minutes, and an energy storage efficiency of 55 percent for regenerative fuel cells.

Table one shows the derivation of the solar array power/area factor for sizing the IOC array. All factors influencing the output power of the array are shown. Applying these factors to the initial input power at AMO and LAU yields an output value of 9.6 watts per square feet, thus requiring a total array active area of 17,969 square feet to produce 172.5 kw of power at EOL (end of life).

### 2.2 ARRAY GEOMETRY

The Solar Array System will employ flexible, planar, large area (5.9 cm X 5.9 cm) of Silicon cells. The cells will be attached to a flexible Kapton (or similar material) substrate and welded to the attached circuitry in order to provide better resistance to thermal cycling that will be experienced in LEO (11). The complete system will be interconnected as cells, panel/module, blankets, and wings.

The baseline IOC panel/module configuration will contain 1 panel per module. A panel will contain 360 cells in series. The panel dimensions are shown in figure (2). The blankets will contain 66 panels and the wings will employ two blankets per wing. The entire array will contain 1056 panels (380,160 cells).



### 3.0 SOLAR ARRAY SIMULATOR DEVELOPMENT

#### SOLAR CELL DC MODEL

A lumped parameter solar cell, DC model is shown in figure (3). This model has been widely used for solar array analysis and is suitable for computer simulation.

The I-V characteristics are defined by the following equations. (1)

$$I = I_L - I_0 \{ \exp[KO(V + R_S I)] - 1 \} - (V + I R_S) / R_{SH}$$

$$V = R_{SH}(I_L - I - I_0 \{ \exp[KO(V + R_S I)] - 1 \}) - I R_S$$

Where

$I$  = Current through the load

$I_L$  = Photovoltaic current across the junction

$R_S$  = Series resistance

$R_{SH}$  = Shunt resistance

$KO = E / AKT = e =$  coefficient of exponential

$K$  = Boltzmann's constant

$T$  = Absolute temperature, K

$E$  = Electronic charge,  $1.6 \times 10^{-19}$  coulombs

$A$  = A curve fitting constant

$I_0$  = Reverse saturation current of the ideal diode characteristic.

The current through the shunt branch of the DC model is neglected and the I-V characteristics equations are altered and are expressed in terms of four common cell parameters,  $I_{SC}$ ,  $I_{MP}$ ,  $V_{MP}$  and  $V_{OC}$ . The final equations describing a computer simulation model are shown below.

$$I = I_{SC} (1 - C_1 (\exp[V / (C_2 V_{OC})] - 1))$$

$$C_1 = [1 - (I_{MP} / I_{SC})] (\exp[V_{MP} / (C_2 V_{OC})])$$

$$C_2 = [(V_{MP} / V_{OC} - 1) / \ln(1 - I_{MP} / I_{SC})]$$

Solar cell design analysis and applications have involved many different disciplines (i.e. Physicist, Engineers, Material Scientist). Because of this, several terms currently in use have similar definitions. Appendix A lists the most commonly used terms and their definitions.

Typical I-V solar cell characteristics are shown in figures (4,5,6); maximum power is available at the output terminals of the cell when it is operated at a point called the knee of the curve and is denoted by PMP. The maximum power point PMP, corresponds also to a point located where the rectangle, having the largest area, can be drawn inside the I-V curve. The voltage and current at maximum power is always less than the open circuit voltage and short circuit current, respectively.

#### 4.0 THERMAL ANALYSIS

The solar cells' operating efficiency and maximum power output strongly depend on the cells' operating temperature. Thermal predictions can be made by utilizing a straightforward computer model. This model solves a heat balance equation by incorporating several known thermal properties of the solar cell.

An approximate steady solution hand calculation is shown in the appendix.B. This information was taken directly from a Lockheed Missile & Space Company interdepartmental communication document prepared by P. S. Lynch. A discussion of this analysis can also be found in a final report by Lockheed Missiles and Space Company, prepared for NASA under contract. NAS-915595 and LMSC-D7612240, "Power Extension Package System." Orbital steady state and transient temperature predictions are shown in figure (7).

#### 5.0 IOC SOLAR ARRAY ORBITAL ANALYSIS

The IOC Space Station will be placed in a Low Earth Orbit (LEO) at approximately 270 nautical miles altitude, at a 28.5 degree inclination.

The solar array wings will be gimbaled to provide two-dimensional sun tracking capabilities for maintaining the solar cell face perpendicular to a solar vector; this along with other environmental conditions provides maximum power and a solar cell light incident angle of zero. The alpha gimbal will be rotated at orbital rate while the beta gimbal will be a slow adjustment for tracking the Sun's motion relative to orbit plane (11). A stream line and normal orientation configuration for gravity gradient stability control is shown in figures (8,9).

## 6.0 SHADOW ANALYSIS

A shadow is defined as the absence of solar illumination on a solar cell array due to a blocking of the sunlight by a shadow-casting object (1). Solar array shadowing can be caused by either Space Station appendages or IOC payloads. When high voltages in excess of 40-50 volts are present in a solar cell string, the potential exists for high power dissipation in individual solar cells due to reverse voltage bias across that cell or cells causing high power dissipation over a small cell area (hot spots). This condition could be brought about by any imbalance between cells, including large cell mismatch, broken cells, or shadowing of parts of the solar panel. Consequence of these effects can range from temporary power reduction to cell damage leading to loss of a complete solar cell string (12). Blocking diodes will be used to eliminate this potential problem.

## 7.0 SOLAR ARRAY SIMULATOR

The flow diagram for a microcomputer-based Solar Array Simulator is shown in figure (10). The source code listing is presented in appendix C. This code was developed using a TRS80 model 100 portable computer. A TRSDOS version basic is utilized. This code runs directly on a Tandy 200 portable computer with minor changes in the screen's print positions. It also runs on an IBM-PC with similar minor changes.

### 7.1 INTERGRATING THE SAS INTO PMAD

Recent versions of Microsoft basic allow communication with the outside world via basic source code. The key feature in these new versions is the ability to "open" an RS-232 port as a file, and, hence, read and write data to the RS-232 lines in much the same way that data can be written to a disk file. Ultimately the SAS will talk to a PMAD Control Power Source Computer (CPSC).

## 8.0 CONCLUSIONS

The personal computer has again demonstrated it's ability to perform various mathematical tasks with accuracy, speed, and efficiency. The Space Station Reference Configuration Electric Power System was simulated in real-time and performance data was generated for the steady-state portion of the orbit. Transient conditions were not analyzed, but could be included in the model with no major problems. Future model enhancements will include a transient analysis and a battery energy storage routine.

Several computer simulation techniques are currently in use. The accuracy of any computerized array analysis is usually highest for those operating conditions for which actual solar cell test data are used as inputs to the model.

The accuracy of the model is approximately within the plus or minus .1 percent range when using the data extracted from the Solar Array Flight Experiment/Dynamic Augmentation Experiment (SAFE/DAE) conducted during the STS-41D mission.

The streamline approach utilized during this research effort demonstrated great potentials for use as an analysis and design tool for Space Station Solar Arrays.

## References

1. Rauschenbach, H. S.: Solar Cell Array Design Handbook. Van Nostrand Reinhold Company, 1980.
2. Rauschenbach, H. S.: "Electrical Output of Shadowed Solar Arrays," Conference Records of the 7th IEEE Photovoltaic Specialists Conference, Pasadena, California, November 1968.
3. Sandstorm, J. D.: "Electrical Characteristics of Silicon Solar as a Function of Cell Temperature and Solar Intensity," IEEE Intersociety Energy Conversion Engineering Conference, Boulder, Colorado, August 1968.
4. Liebert, C. H. and Hibbard, R. R.: "Theoretical Temperatures of Thin Film Solar Cell in Earth Orbit." NASA TND-4331, January 1968.
5. Merrill, W. C., Blaha, R. J., and Pickrell, R. L.: "Dynamic Analysis of a Photovoltaic Power system with Battery Storage Capability." DOE/NASA/20485-79/4, NASA TM-79209, July 1979.
6. Hough, W. W. and Elrod, B. D.: "Solar Array Performance as a Function of Orbital Parameters and Spacecraft Attitude," Journal of Engineering for Industry, February 1969.
7. Sandstorm, J. D.: "A Method for Predicting Solar Cell Current-Voltage Curve Characteristic as a Function of Incident Solar Intensity and Cell Temperature," Records of the IEEE 6th Photovoltaic Specialists Conference, Cocoa Beach, Florida, March, 1967.
8. Patterson, R. E., and Yasui, R. K.: "Parametric Performance Characteristics and Treatment of Temperature Coefficients of Silicon Solar Cells for Space Application," Technical Report 32-1582, Jet Propulsion Laboratory, Pasadena, California, May, 1973.

9. Tada, H. Y., Carter J. R., Anspaugh, B. E., and Dowing, R. G.: "Solar Cell Radiation Handbook," JPL Publication 82-69, Jet Propulsion Laboratory, Pasadena, California, November 1982.
10. NASA SP-33, Part-3, "Orbital Flight Handbook", 1963
11. NASA, JSC 19989, "Space Station Reference Configuration Description," Johnson Space Center, Houston, Texas, August 1984.
12. Lockheed Missiles and Space Company, "Planar Solar Arrays for Space Station," Sunnyvale, California, October 1984.
13. Marshall Space Flight Center, "Solar Array Flight Experiment/Dynamic Augmentation Experiment," Huntsville, Alabama, October 1984.
14. Brown, W. D., et al: "Computer Simulation of Solar Array Performance," Report No. SSD 70135R, Hughes Aircraft Co.
15. Emanuel, Ervin M.: "Digital Readout of Polyphase Induction Motor Test Values," M.S. Thesis, Iowa State University, 1976.
16. Emanuel, Ervin M.: "Apparatus for Testing the Performance of Electric Machines," U.S. Patent No. 4091662 (1978).
17. Emanuel, Ervin M.: "A Digital Instrumentation System for Test and Control of AC Machines," Proceedings of the 1978 Midwest Power Symposium, University of Nebraska, Lincoln, Nebraska, 1978.
18. Emanuel, Ervin M.: "Apparatus and Method for Testing the Performance of Electrical Machines," U.S. Patent No. 4348892 (1982).

ORIGINAL PAGE IS  
OF POOR QUALITY

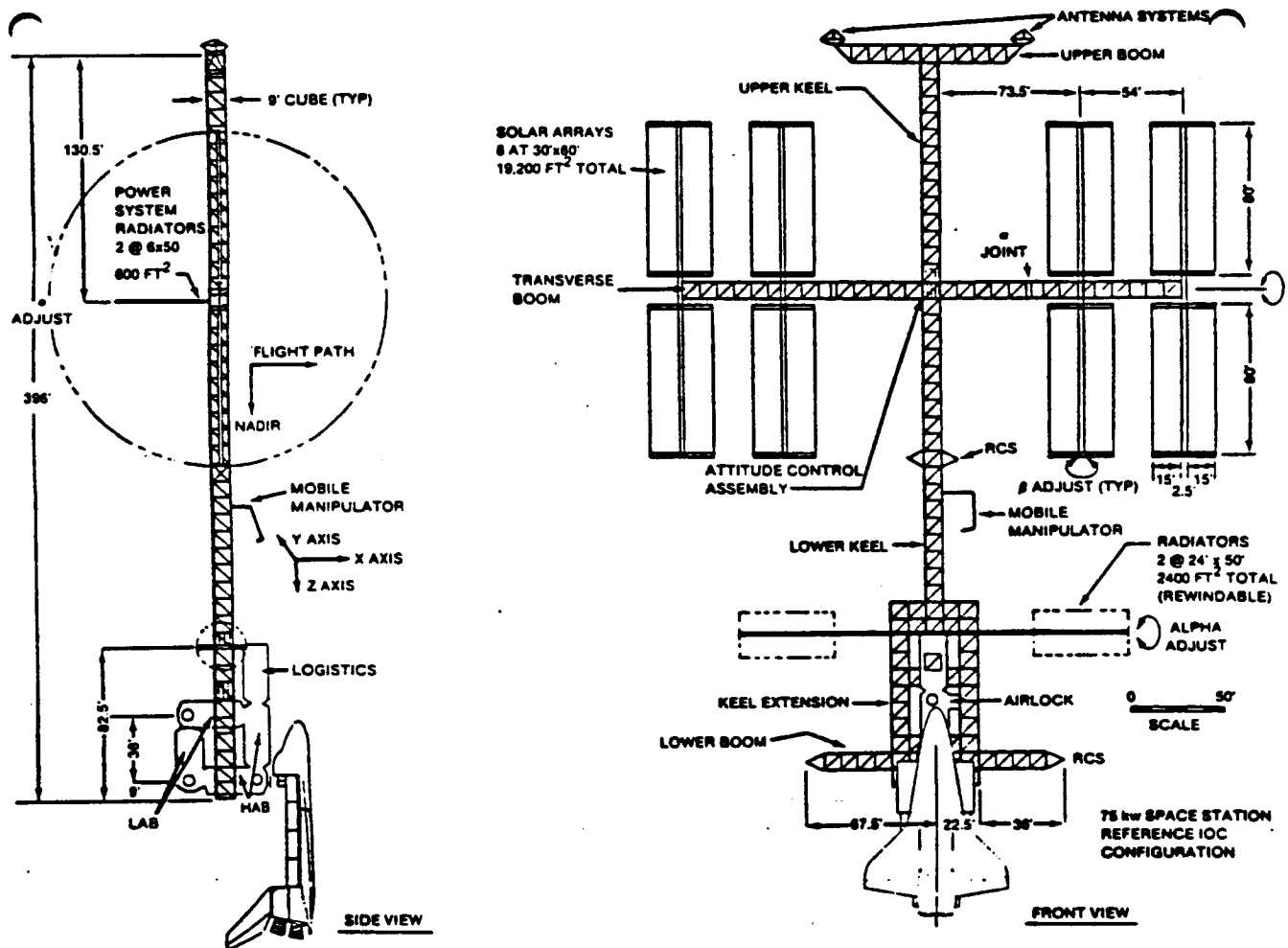


FIGURE 1. IOC REFERENCE CONFIGURATION

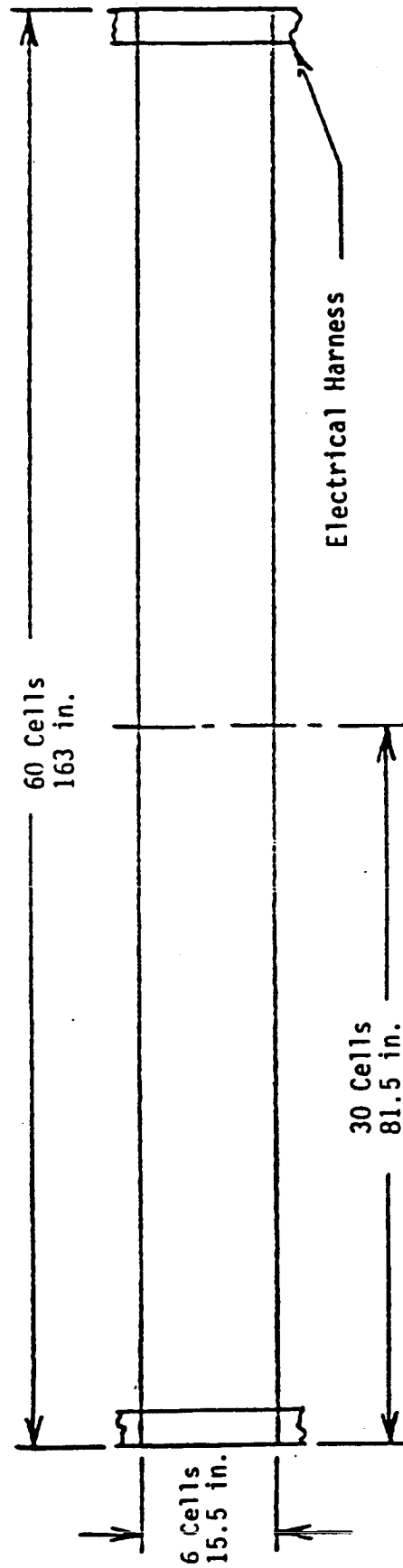


FIGURE 2. BASELINE PANEL DIMENSIONS



SOLAR CELL DC MODEL

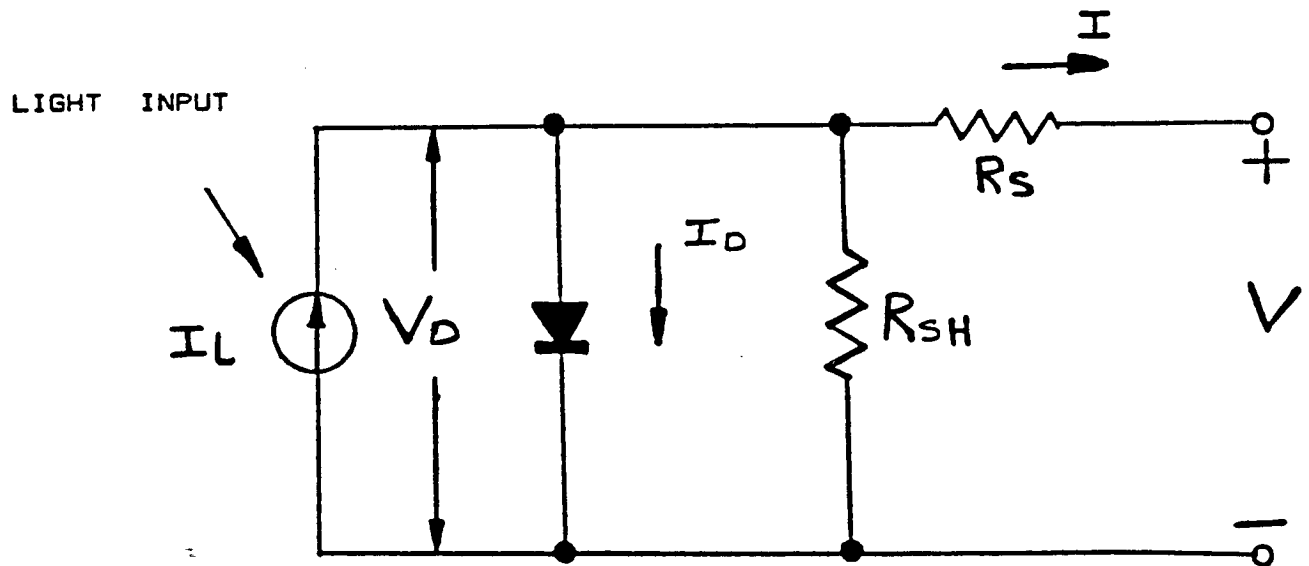


FIGURE 3. SOLAR CELL DEC MODEL

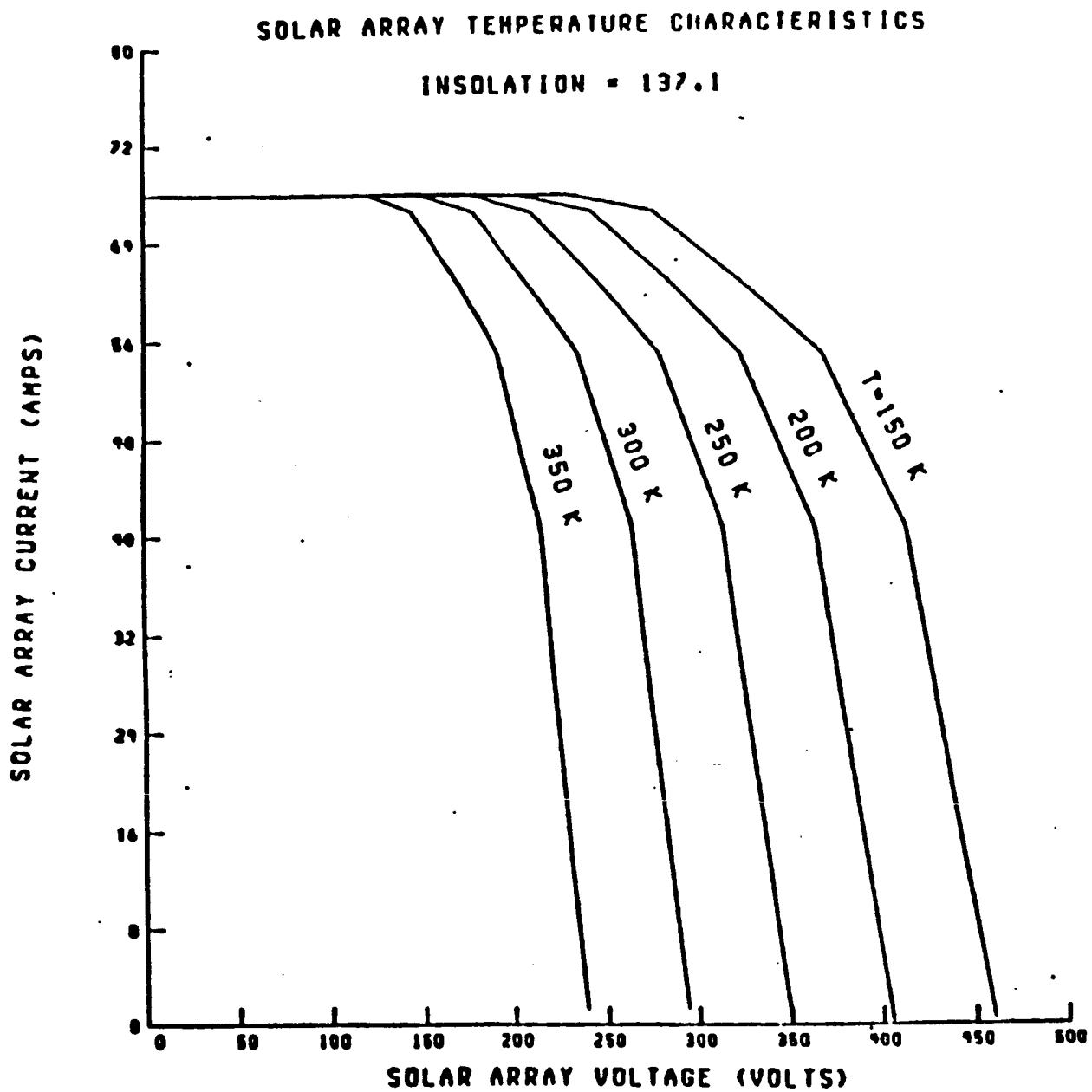


FIGURE 4. SOLAR CELL TEMPERATURE CHARACTERISTIC

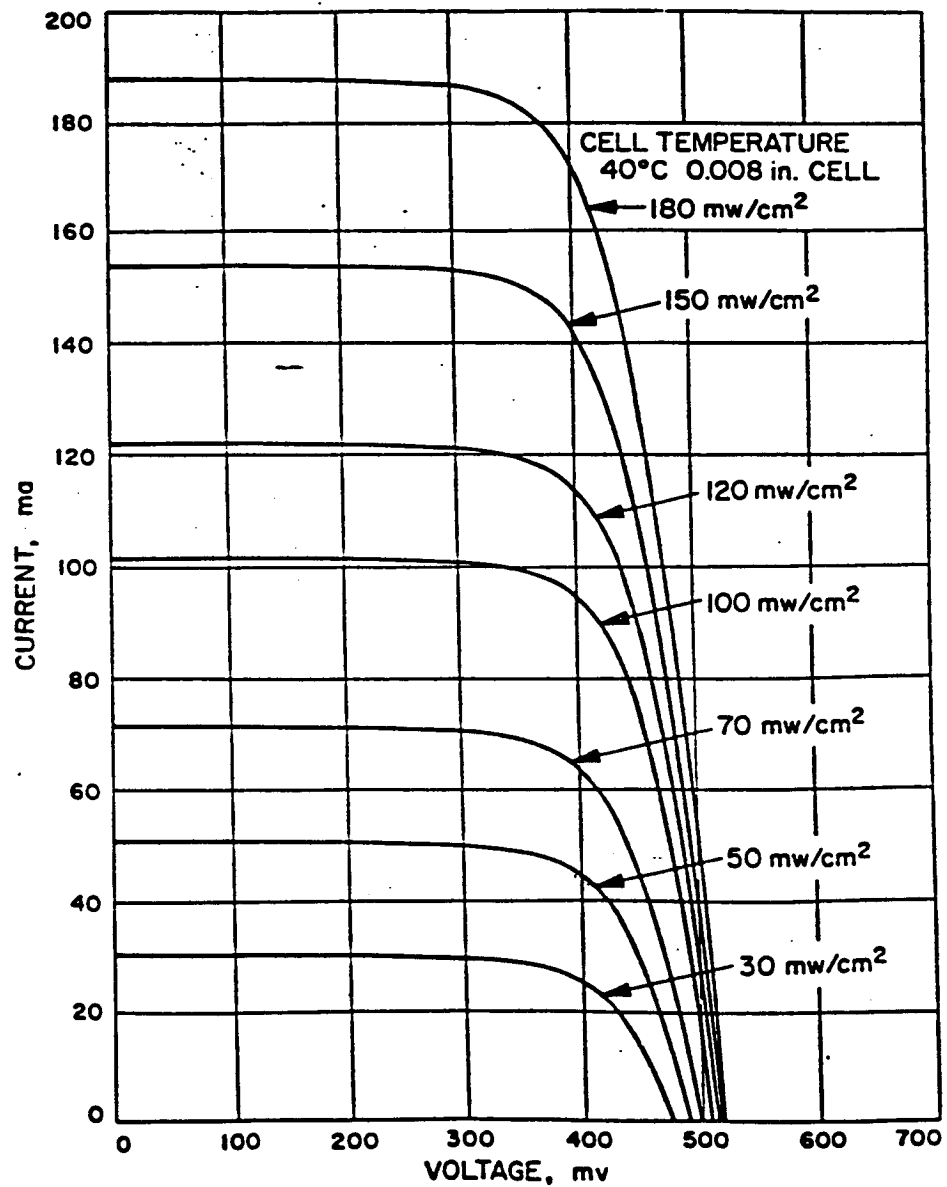


FIGURE 5. N/P SILICON CELL CHARACTERISTICS AS A FUNCTION OF INCIDENT INTENSITY

ORIGINAL PAGE IS  
OF POOR QUALITY

2006.4 SECONDS FROM 246:11:27:54.0

NTI

TEST NO	SAE W/C RS19	NOFFT	1
REF TIME	8:22:46:33.0	FFTSU-MZ	0.00000
TIME OFFSET	501.500	FFTER	0.00
TOTAL TIME	0.800	FFTIM	0.00
SAMPLE RATE	0.1000E+02	FFTLIN	0

SI 10-31-84  
VI 10-17-85

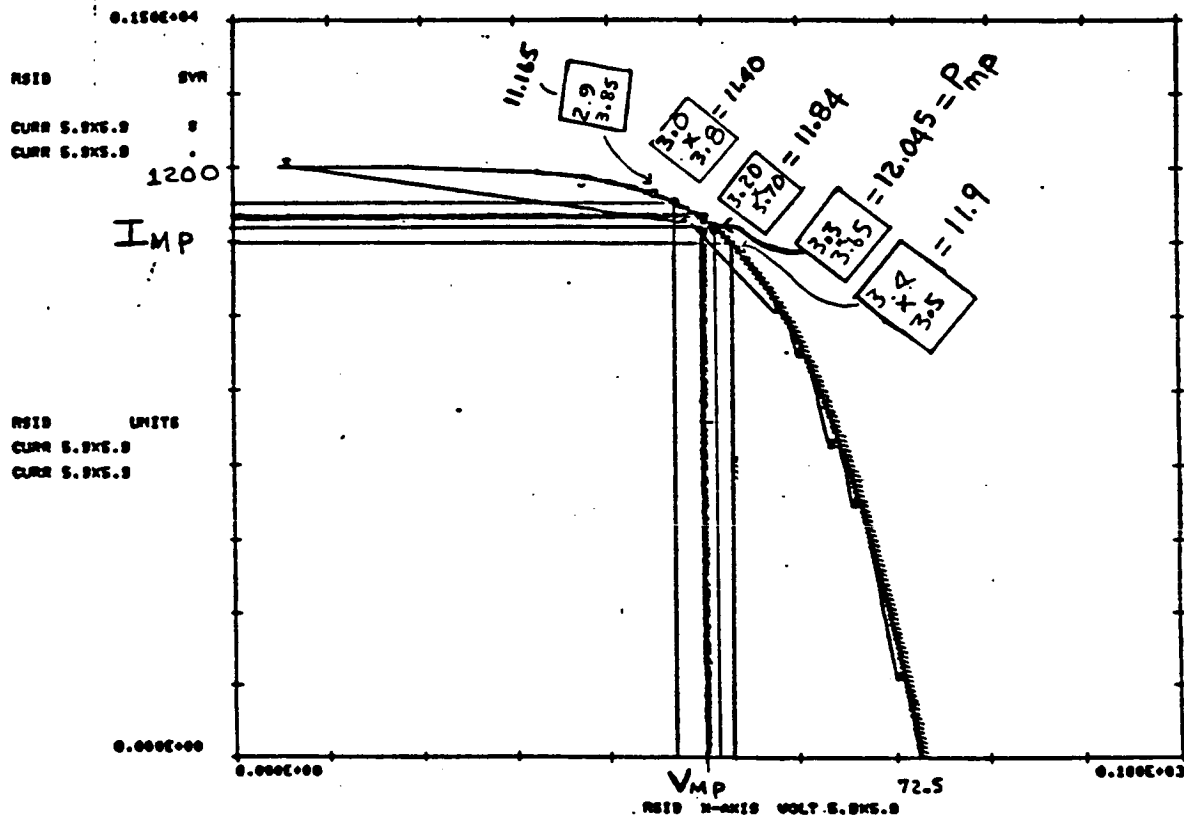


FIGURE 6. SOLAR MODULE I-V CURVE, ON ORBIT FLIGHT EXPERIMENT DATA FROM STS-51D

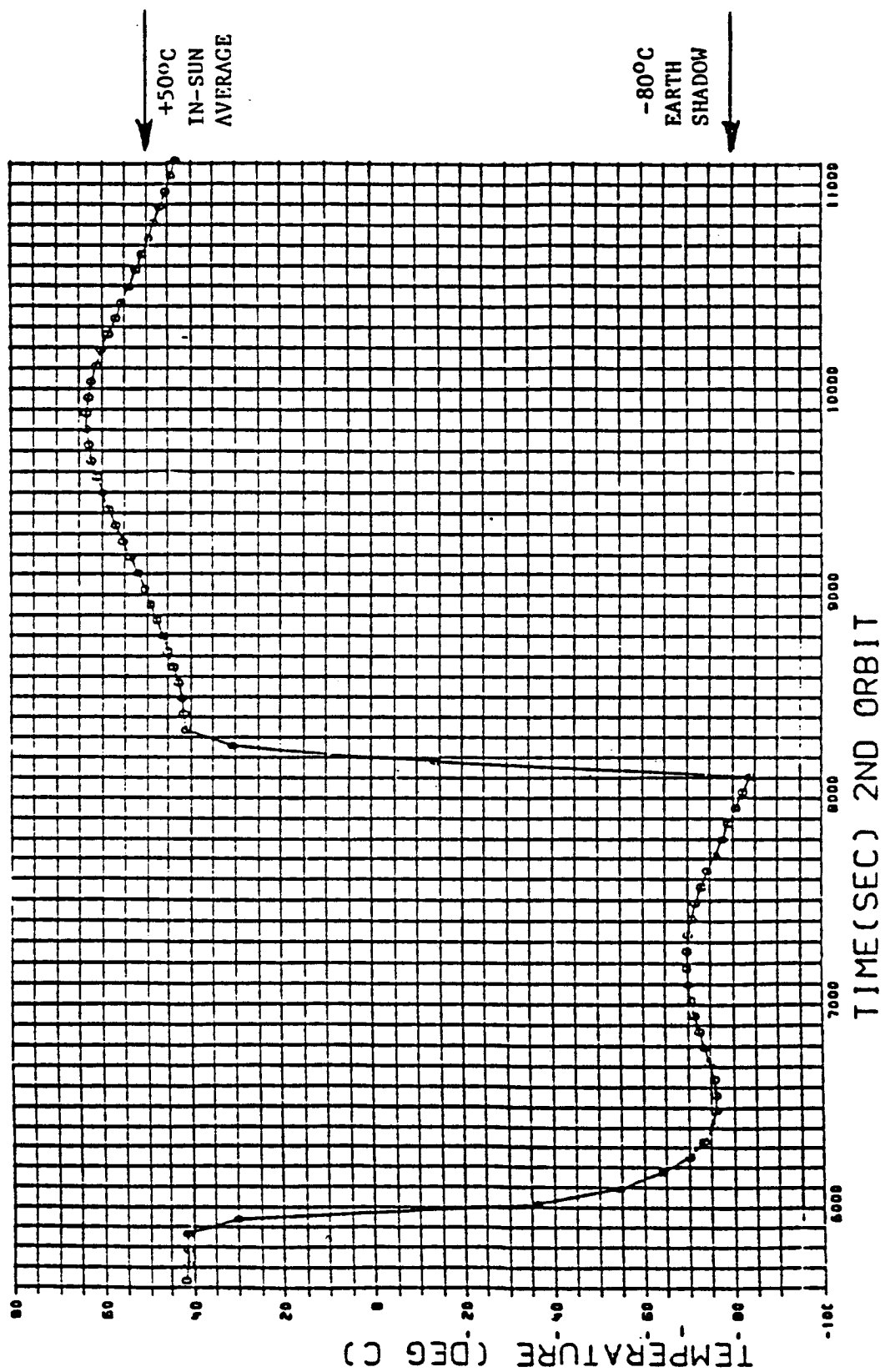


FIGURE 7. SOLAR CELL TEMPERATURE PREDICTIONS, 235 MILES ORBIT

ORIGINAL PAGE IS  
OF POOR QUALITY

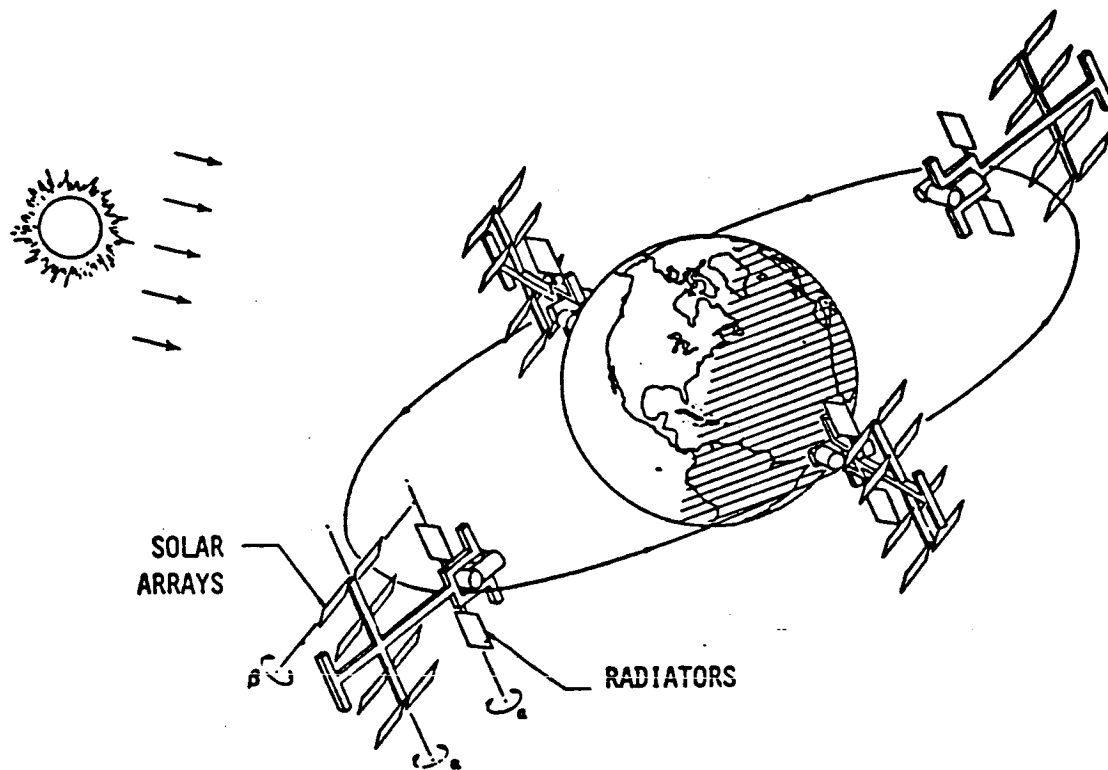


FIGURE 8. NORMAL ORIENTATION

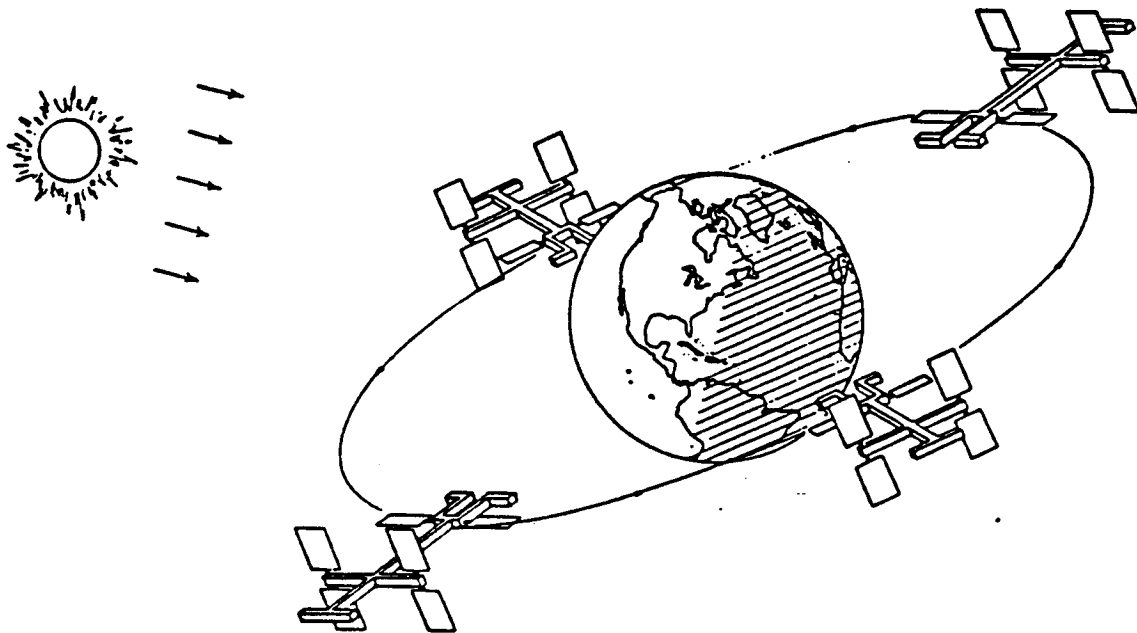


FIGURE 9. STREAMLINED ORIENTATION

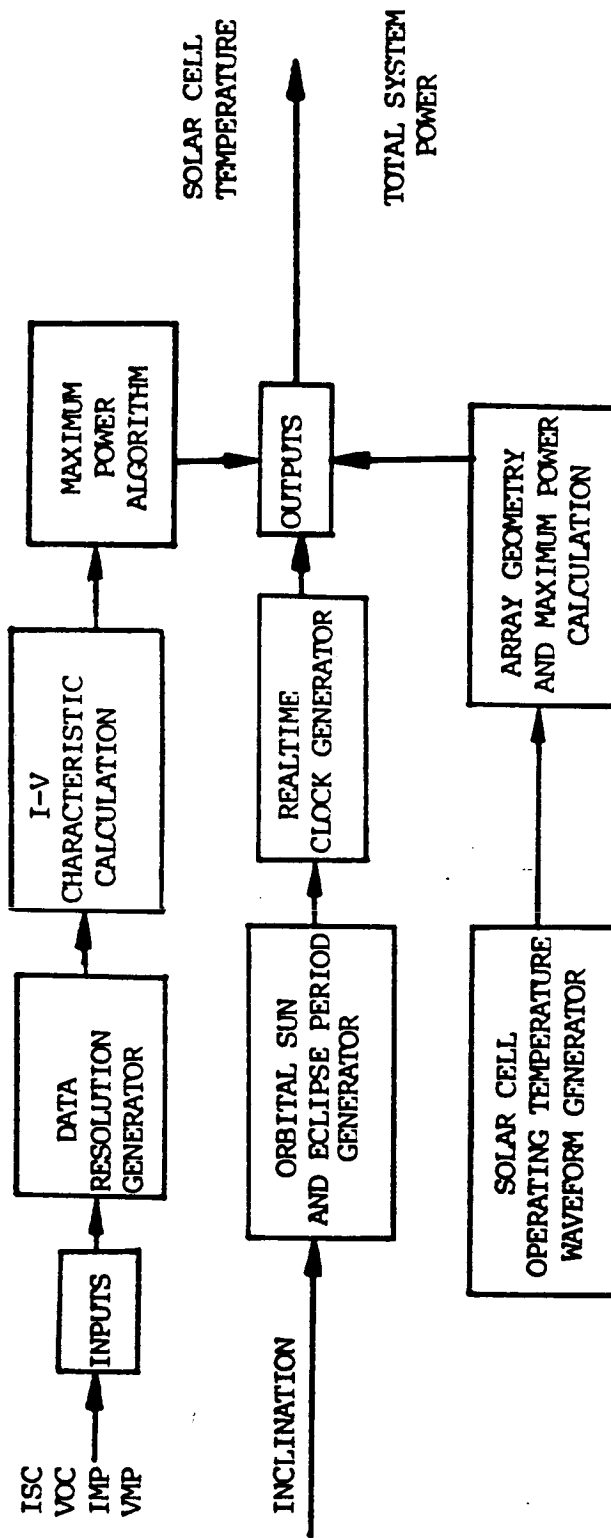


FIGURE 10. MICROCOMPUTER BASED SOLAR ARRAY SIMULATOR BLOCK DIAGRAM



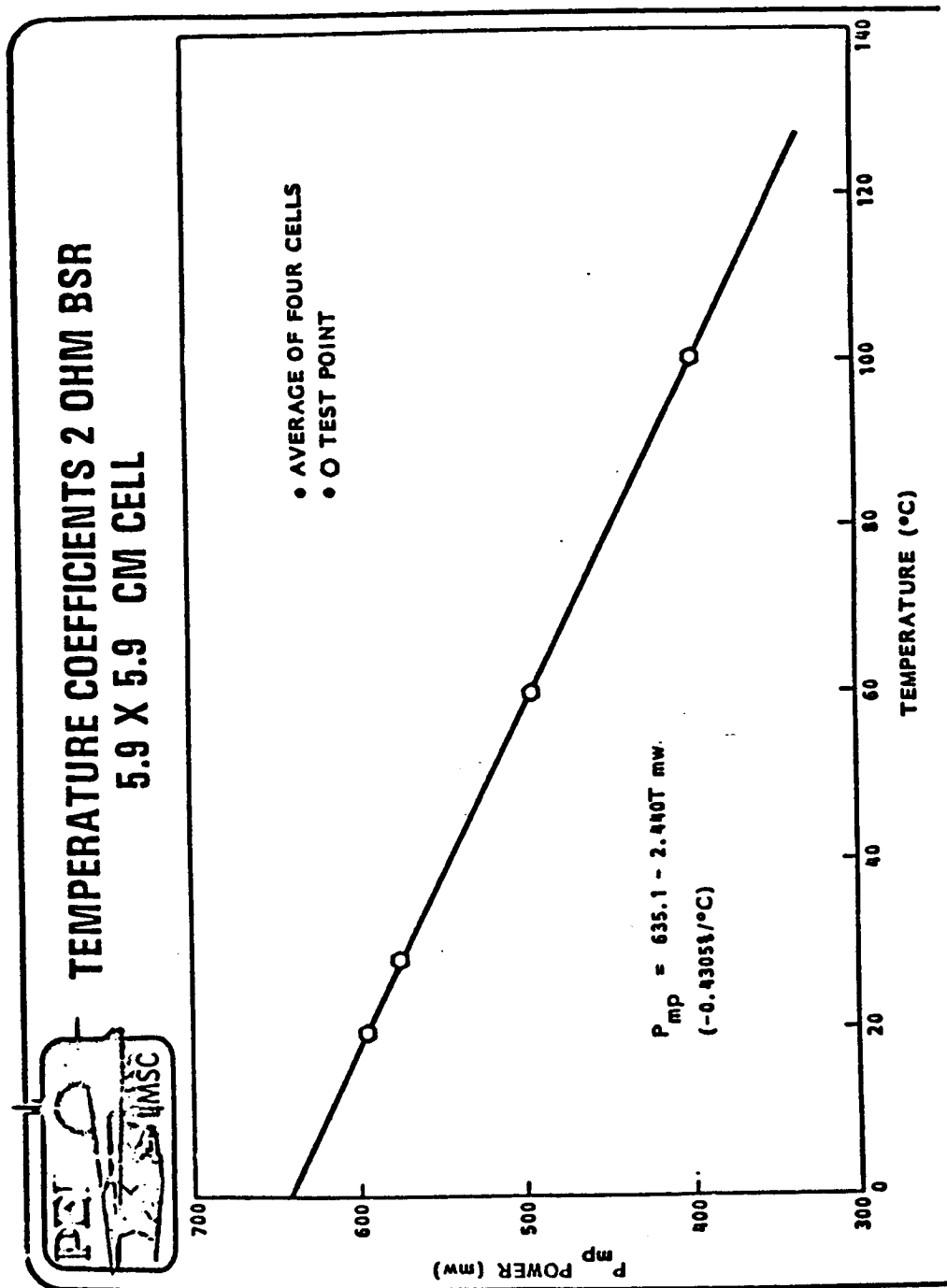


FIGURE 11. TEMPERATURE COEFFICIENTS TWO OHM BSR 5.9x5.9 CM SOLAR CELL

ORIGINAL PAGE IS  
OF POOR QUALITY

**NASA** National Aeronautics and  
Space Administration

1 - 1 2 1

Lyndon B. Johnson Space Center  
Houston, Texas 77058

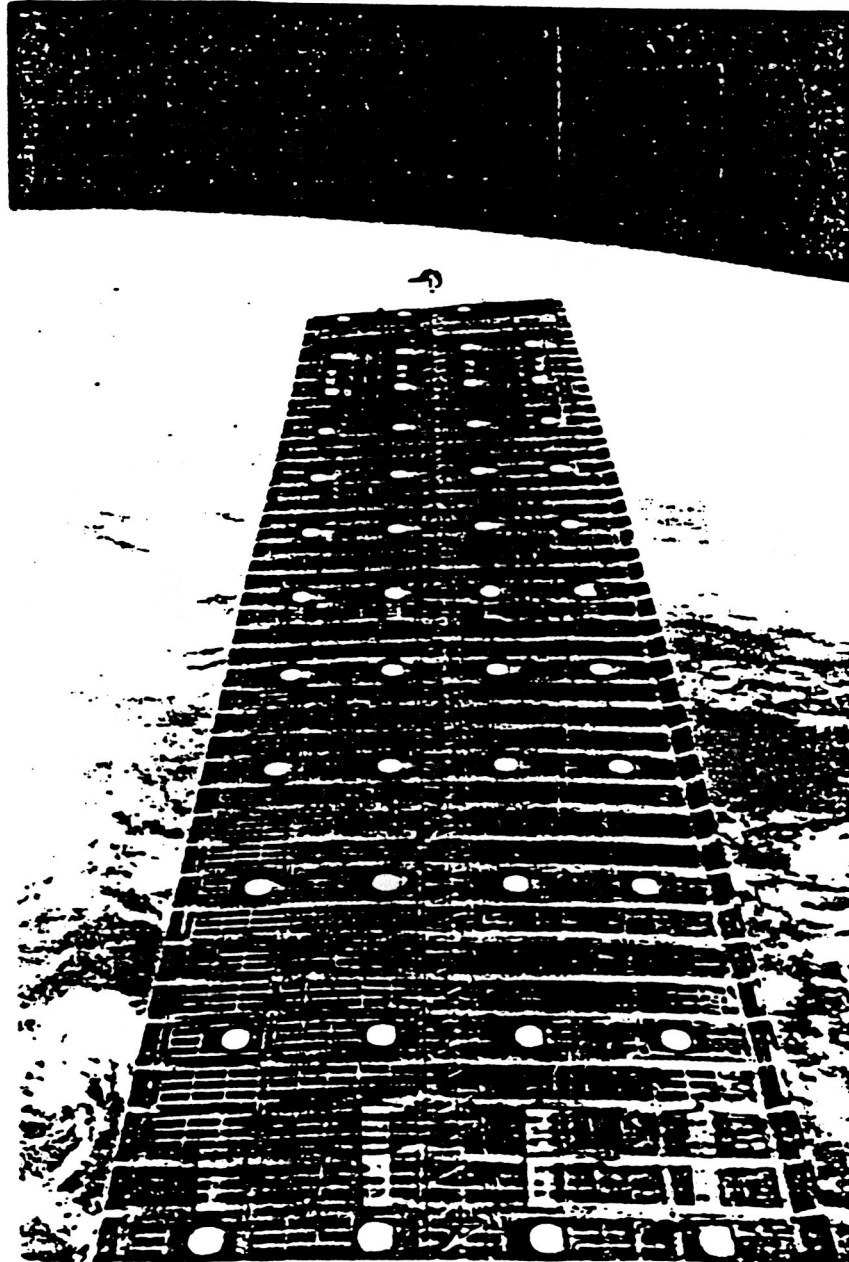


FIGURE 12. DEPLOYED SAFE ARRAY IN ORBIT

TABLE ONE

## POWER/AREA FACTOR DERIVATION

	FACTOR	WATTS/FT <sup>2</sup>
Solar power input at 1 A.U. and air mass zero	--	125.7
Solar power seasonal variation	.970	121.9
Solar cell output at 28°C and beginning of life	.128	15.6
Solar array blanket packing	.764	11.9
Ultraviolet degradation	.980	11.7
Harness voltage drop	.980	11.5
Interconnect voltage drop	.980	11.2
Cell mismatch	.990	11.1
Temperature effect at 50°C	.905	10.1
EOL radiation at 5E13 equiv. 1 MeV electron fluence	.958	9.6

## Appendix A

### SOLAR ARRAY TERMINOLOGY

SOLAR CELL	A silicon photovoltaic cell that converts solar energy directly into electrical energy.
PHOTOVOLTIC	Capable of generating a voltage when exposed to visible or other light radiation.
SOLAR MODULE	One or more interconnected solar cells.
SOLAR ARRAY	One or more interconnected solar modules [planar (flat) and concentrator (parabolic)].
INSOLATION	The rate of delivery of all direct solar energy per unit of horizontal surface.
IRRADIATION	Emission of radiant energy.
IRRADIANCE	Radiant flux density on a given surface, expressed in watts per square centimeter or square meter.
ILLUMINATION	The luminous flux per area on an intercepting surface at any given point.
SOLAR CONSTANT	The total energy received from the sun on a unit area perpendicular to the sun's rays at the mean earth-sun distance, termed an astronomical unit ( $1.000\text{AU} = 1.496 \times 10^8 \text{ M} = 92,959,670$ miles)
AMO	Air mass zero (the absence of any atmospheric attenuation or modification of the sun radiation). At AMO the optical air mass is zero.

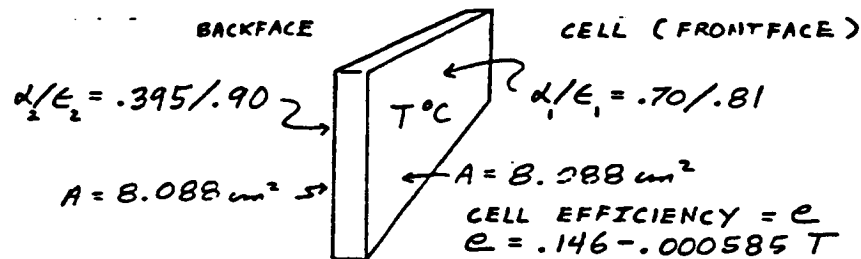
BOL                    Beginning of life

EOL                    End of life

BLOCKING DIODE    A diode used to block reverse flow of current into a photovol-  
taic source circuit.

APPROXIMATE STEADY STATE SOLUTION  
BY HAND CALCULATION

CONDITIONS:  $\beta = +60^\circ$  Orbit Time = 4194 sec.  
Subsolar Point, ZERO CELL-SUBSTRATE RESISTOR  
(COMPARE THIS WITH THE RESULTS PRESENTED IN FIGURE 39)

HEAT INPUT

FROM TABLE B at Time 4194.4 sec

$$\begin{aligned} Q_{\text{SOLAR FRONT}} &= .1356 \text{ Watts/cm}^2 \text{ sec} = Q_{\text{SF}} \\ Q_{\text{ALBEDO FRONT}} &= .002758 = Q_{\text{AF}} \\ Q_{\text{EARTHSHINE FRONT}} &= .002490 = Q_{\text{EF}} \\ Q_{\text{SOLAR BACK}} &= .0000 = Q_{\text{SB}} \\ Q_{\text{ALBEDO BACK}} &= .01233 = Q_{\text{AB}} \\ Q_{\text{EARTHSHINE BACK}} &= .01502 = Q_{\text{EB}} \end{aligned}$$

$$Q = A[(\alpha_1 - e)(Q_{\text{SF}} + Q_{\text{AF}}) + \epsilon_1 Q_{\text{EF}} + \alpha_2(Q_{\text{SB}} + Q_{\text{AB}}) + \epsilon_2 Q_{\text{EB}}]$$

assume  $T = 50^\circ\text{C}$  then  $e = .1168$

$$Q_{\text{IN}} = .8177 \text{ Watts/sec heat input}$$

HEAT LOSS TO SPACE

$$Q_{\text{OUT}} = (A\epsilon_1 V_1 + A\epsilon_2 V_2) \sigma T^4, \quad V_1 = V_2 = 1.00 \text{ View Factors}$$

$$\sigma = 5.670 \times 10^{-12} \text{ Watts/cm}^2 \text{ } ^\circ\text{K}^4$$

$$Q_{\text{OUT}} = 7.842 \times 10^{-11} T^4$$

$$Q_{\text{IN}} = Q_{\text{OUT}}, \quad .8177 = 7.842 \times 10^{-11} T^4$$

$$T = (.8177 / 7.842 \times 10^{-11})^{1/4} = 319.6^\circ\text{K} = 46.4^\circ\text{C}$$

# SOURCE CODE LISTING

```

14 CLS
15 PRINT@11,"WELCOME TO EH5"
17 PRINT@63,"DATE ="DATE$ " TIME ="TIME$
19 PRINT@166,"POWER DISTRIBUTION DISPLAY"
21 PRINT@250,"AND CONTROLS"
32 PRINT@323,"BRANCH CHIEF: CHARLES PRICE"
43 PRINT@443,"SECTION HEAD: DICK BURGHDOFF"
54 PRINT@523,"LEAD ENGR. : LARRY MOON"
64 PRINT@683,"RESEARCH FELLOW: ERVIN M EMANUEL,P.E."
77 PRINT:PRINT:PRINT:PRINT
88 PRINT "PRESS ANY KEY AND ENTER TO CONTINUE"
93 INPUT C$
100 CLS: PRINT@203,"SPACE STATION SOLAR ARRAY SIMULATOR"
110 LINE(5,20)-(5,50):LINE -(238,60):LINE-(238,20):LINE-(5,20)
120 PRINT:PRINT:PRINT:PRINT:PRINT:PRINT:PRINT:PRINT:PRINT:PRINT:PRINT PRE
SS ANY KEY AND ENTER TO CONTINUE"
130 INPUT D$
140 CLS
150 BEEP
160 DEF SNG A=Z
170 PRINT "ENTER SHORT CIRCUIT CURRENT"
180 PRINT"ISC(MILLIAMPS)"
190 INPUT ISC
195 PRINT:PRINT
200 PRINT "ENTER OPEN CIRCUIT VOLTAGE"
210 PRINT "VOC(MILLIVOLTS)"
220 INPUT VOC
225 PRINT:PRINT
230 PRINT "ENTER CURRENT AT MAX POWER"
240 PRINT "IMP(MILLIAMPS) LABELED AIMP"
250 INPUT AMP
255 PRINT:PRINT
260 PRINT" ENTER VOLTAGE AT MAX POWER"
270 PRINT "VMP(MILLIVOLTS)"
280 INPUT VMP
285 PRINT:PRINT
290 FOR K =1 TO 1
300 PRINT "ENTER VOLTAGE DATA RESOLUTION"
310 PRINT "(NUMBER OF DATA POINTS FOR )"
320 PRINT "I-V CURVE PLOTTING(XNDPIV)"
330 INPUT NDPIV
340 VC=VOC/NDPIV
350 K=NDPIV +1
360 DIM V(K),AI(K),P(K)
370 C=0
375 CLS: PRINT@41,"NOW SEARCHING FOR MAXIMUM POWER POINT":PRINT@205,"SOLAR CELL I-V CHARACTERISTICS":PRINT@283,"VOLTAGE(V) CURRENT(A) POWER(W)"
380 C2=((VMP/VOC)-1)/(LOG(1-AMP/ISC))
390 C1=(1-(AMP/ISC))*EXP(-VMP/(C2*VOC)))
400 C=C+1
410 IF C=S THEN 505
420 K=NDPIV +1
435 FOR K=1 TO NDPIV +1
440 V(K)=VC*(K-1)
445 AI(K)=ISC*(1-C1*(EXP(V(K)/(C2*VOC))-1))
450 NEXT K
455 FOR K=1 TO NDPIV +1
460 P(K)=V(K)*AI(K)

```

## SOURCE CODE LISTING CONT.

ORIGINAL PAGE 10  
OF POOR QUALITY

```

465 NEXT K
470 FOR K=1 TO NDPIV +1
475 L=K+1
480 IF P(K)>P(L) THEN 500
490 NEXT K
500 L=K:VMP=V(L):AMP=AI(L): PRINT@362,"VMP=" V(L);:IMP="AI(L);:PMP="P(L):GOTO 380
505 CLS:PRINT@43,"SOLAR CELL I-V CHARACTERISTIC":PRINT@123,"VOLTAGE(V) CURRENT(A) POWER(W)";:PRINT@202,"VMP=" V(L);:IMP="AI(L);:PMP="P(L)
510 FOR K =1 TO 1
520 PRINT "      "V(K);"      " AI(K)"      "P(K)
530 NEXT
535 FOR K=2 TO NDPIV +1
540 PRINT USING "#####.###";V(K);AI(K);P(K)
545 NEXT K
550 A1$="Y"
555 PRINT: PRINT "ENTER Y IF YOU WANT TO ABORT TO":PRINT:PRINT"BEGINNING(DATA ENTRY POINT)"
:PRINT:PRINT" OR PRESS ENTER TO CONTINUE"
560 INPUT B$
565 IF B$=A1$ THEN 140
570 CLS
575 PRINT@123, "YOU ARE NOW READY TO ENTER":PRINT@203,"THE MISSION PARAMETERS":PRINT@243,"THIS MODEL USES THE BETA"
580 PRINT@283,"ANGLE ONLY.THIS IS CALLED":PRINT@323,"INCLINATION.FUTURE MODEL"
585 PRINT@363,"ENHANCEMENTS MAY REQUIRE":PRINT@403,"MORE INFORMATION"
590 PRINT@483,"ENTER BETA (MEASURED IN DEGREES)"
600 INPUT B
605 IF B=28.5 THEN 615
610 PRINT "ENTER BETA AGAIN":GOTO 600
615 SP =3540
620 CLS
622 PRINT@98,"EPDC":PRINT@27,"DATE="DATE$:PRINT@162,"SPACE STATION SOLAR ARRAY SIMULATOR":PRINT@244,"ON ORBIT ELECTRICAL PERFORMANCE":PRINT@380,"ORBIT ELASPE TIME":PRINT@603,"POWER(KW) VOLTAGE(V) CURRENT(A)":PRINT@680,"AJ1":PRINT@800,"AJ2"
623 PRINT@362,"SOLAR CELL":PRINT@404,"TEMP":PRINT@880,"TOTAL SYSTEM POWER"
625 TIME$="00:00:00"
630 A$=TIME$
635 PRINT@430, A$
640 SEC$ =RIGHT$(TIME$,2)
645 MIN$ =MID$(TIME$,4,2)
650 HR$=LEFT$(TIME$,2)
655 PRINT@467," "HR$" " MIN$" "SEC$
660 TEL= VAL( HR$)*3600 +VAL(MIN$)*60 +VAL(SEC$)
670 PRINT@510," "TEL
1500 SP =3540
1510 AV =.000887324
1515 WT =AV*TEL
1520 SN =40.06 +20*SIN(WT)
1525 PFMP=((P(L) +146.4) -2.44*SN)*380160
1530 IF TEL =SP GOTO 1540
1535 PRINT@482, SN:PRINT@922,PFMP/100000:PRINT@932,"KW"
1537 GOTO 630
1540 STOP
2000 CLS:PRINT@125,"THIS SIMULATOR HAS ARTIFICIAL,":PRINT@207,"INTELLIGENCE CAPABILITIES"
2010 PRINT@328,"ERROR DIAGNOSIS:":PRINT@448,"THE ELEC. VALUES YOU HAVE":PRINT@488,"ENTERED ARE MATHEMATICALLY":PRINT@528,"IMPOSSIBLE"
2030 BEEP:BEEP
2040 END
2050 CLS
2060 BEEP
2070 LINE(40,0)-(40,100):LINE -(239,100)

```



This research report contains the results of the research conducted during a ten week ASEE (American Society of Engineering Education) Research Program. This program is sponsored jointly by ASEE and the National Aeronautics and Space Administration, Washington D. C. The program is administered by the Texas A&M University Research Foundation. Jointly directed by Professor Bob Chilton, Texas A&M University, Department of Aerospace Engineering, and Clarence Williams, University Programs Office, NASA Johnson Space Center.

N86 - 31419 D10

148

FIRE CONTROL METHOD AND ANALYTICAL  
MODEL FOR LARGE LIQUID HYDROCARBON POOL FIRES

Donald L. Fenton  
Professor of Mechanical Engineering  
New Mexico State University  
Las Cruces, New Mexico

1882#

ABSTRACT

The dominate parameter governing the behavior of a liquid hydrocarbon (JP-5) pool fire is wind speed. The most effective method of controlling wind speed in the vicinity of a large circular (10 m dia.) pool fire is a set of concentric screens located outside the perimeter. Because detailed behavior of the pool fire structure within one pool fire diameter is unknown, an analytical model supported by careful experiments is under development. As a first step toward this development, a regional pool fire model was constructed for the no-wind condition consisting of three zones -- liquid fuel, combustion, and plume -- where the predicted variables are mass burning rate and characteristic temperatures of the combustion and plume zones. This zone pool fire model can be modified to incorporate plume bending by wind, radiation absorption by soot particles, and a different ambient air flow entrainment rate. Results from the zone model are given for a pool diameter of 1.3 m and are found to reproduce values in the literature.

## INTRODUCTION

The heat source used for the fast cook-off tests of Naval ordinance is a JP-5 liquid pool fire approximately 10 m in diameter. The pool fire duplicates the conditions involved with the shipboard fire threat -- especially an aircraft carrier flight deck where weapons are usually installed on airplanes. A pool fire originates from the spill of liquid fuel onto a flat horizontal surface and the subsequent combustion of the fuel vapors.

### Objective

Repeatability of these cook-off tests is dominated by ambient wind as these tests are conducted outdoors. The standard cook-off test must last 5 minutes and maintain a temperature of 870°C. If sufficient wind exists during the cook-off test, the pool fire flames will bend in the direction of the wind and expose the weapon. This invalidates the cook-off test. The objective of this work is to develop a method that mitigates the wind's influence on the structure of a pool fire and therefore improve the repeatability of the cook-off test.

In conjunction with developing a wind mitigation method, an analytic pool fire model is required. The model is important because the pool fire structure (temperature, velocity, and species concentration profiles), as influenced by the wind or the wind mitigation method, can be predicted.

Additionally, the model can estimate the pool fire conditions in the vicinity of the test article and thus be used to determine the suitability of conducting a cook-off test on a given day.

A computerized literature search was conducted regarding the behavior of pool fires. Several data bases were searched and most of the pertinent documents and articles obtained. The most extensive experimental data found characterizing large diameter pool fires were reported by [Johnson, 1982], [Kung, 1982], [Alger, 1979], and [Blinov, 1957] where wind speed was minimized by careful test time selection. The Naval Weapons Center, [Tozer, 1983] experimentally investigated the improvement of cook-off test repeatability for windy days by using aerodynamic jets and found that the entrainment of fuel vapor into the jet significantly changed the pool fire structure. Consequently, an alternative wind control method is necessary. Experimentally determined empirical correlations concerning wind on pool fires were given by [Moorhouse, 1984], [Kalghatgi, 1983] and [Welker, 1965].

The reported analytical pool fire models fell into three categories: regional, integral, and two-dimensional. The regional model divides the pool fire into zones and consists of algebraic equations describing the behavior of the zones and their interfaces. The only pool fire zone/model found was by [Ndubizu, 1983] and employed three zones (liquid fuel, combustion, and plume) where the mass burning rate, combustion temperature and plume temperature were predicted. The integral model breaks the pool fire into a collection of infinitesimally thin stacked disks each equal in diameter to the pool fire at the particular elevation. This approach was taken by [McCaffrey, 1983], [Raj, 1981], and [Steward, 1970] where the turbulent fire plume was governed by buoyancy and chemical reaction. Obtained from the integral approach were the so-called "top hat" profiles (variations neglected across the plume of time-averaged values) of burning rate, temperature, fuel mass fraction, oxygen mass fraction, vertical velocity, plume radius, and entrainment rate. Factory Mutual Research

[Tamanini, 1981] developed an integral model for turbulent fire plumes where the "unmixedness" of turbulent reacting flows was included.

Tamanini's approach therefore, calculated composition fluctuations due to molecular diffusion and entrainment of ambient air based on the k-E-g standard turbulence model [Spalding, 1971] and should be applicable to pool fires. The third category, two-dimensional pool fire models, has two representatives where in both the governing equations are reduced to partial differential equations of the parabolic type (boundary layer equations) [Harsha, 1981] and [Schneyer, 1975]. In reality, only the model developed by Harsha, et.al., was completed and compared with pool fire data [Johnson, 1982]. Comparisons were within experimental errors for downstream distances greater than one pool diameter. Because the cook-off test involves the pool fire structure at 1.5-to-2.0 m above the liquid surface (0.1-to-0.2 pool diameters), further pool fire modeling work is required to accurately predict temperatures, velocities, etc., at the location of the test article.

### THEORY

Two efforts are required in this investigation concerning the improvement of test repeatability. The first is technique for mitigating the wind effects and the second is the development of an analytical model for large pool fires that includes ambient wind.

#### Wind Control Method

A technical review of the available concepts for control of wind effects on pool fires was conducted to select the best candidates. These included: the downward-directed aerodynamic jet, multiple concentric screens, earth berm, and an analytical correction procedure that increases the actual cook-off test time such that the thermal conditions of the standard test

are achieved. Each of these approaches were developed at the conceptual level and reviewed again. The use of multiple screens was determined to provide good wind control with little influence on the pool fire structure.

With the conceptual development of screens, the following assumptions were made: steady potential flow, downstream jet coalescence, and equal velocity decrease through each screen. Using Bernoulli's equation upstream and downstream of the screen in conjunction with the solidity ratio (fractional degree to which the screen obstructs the flow).

$$S = 1 - A_o/A_t$$

yields [Baines, 1951],

$$\frac{\Delta P}{\rho V_o^2/2} = \left[ \frac{1}{C_c(1-S)^{-1}} \right]^2$$

The symbols are defined in the nomenclature where Table 1 summarizes the calculations associated with the flow through screens appropriate for this application. Since the screens are in the form of a circle, the projected area of the circular holes decreases by the factor  $\cos \theta$  ( $\theta$  is the angle between the wind direction and the plane containing the hole).

Additionally, the hole density on the projected area increases by the same factor,  $\cos \theta$ . This causes the flow rate/unit area projected of screen to be the same and leads to the velocity profiles upstream and downstream being uniform or flat.

The screen height must be sufficient to protect the test article from ambient wind. At the top of the screen, a turbulent mixing layer develops and thickens in the downstream direction. Carefully combining the

analytical results of [Townsend, 1976] and [Schlichting, 1955] with the experimental results of [Hakuro, 1984], [Oster, 1982], and [Brown, 1974] the following relation is found for the mixing layer half-width,

$$b = 0.138 x$$

where  $x$  is the downstream distance from the screen. Also important is the vertical location of the pool fire. The Handbook of Snow [Gray, 1981] summarizes flow through a snow fence (similar to this application) and presents a correlation between fence height and reattachment length of the mixing layer. Thus, to protect a height of 2 m near the center of the pool fire where the mixing layer widens to about a 0.7 m half width and drops about 0.7 m, a height of 1.1 m about 2 m or 3.1 m is required for the screens. This is conservative as the pool fire plume, due to buoyancy, possesses vertical motion.

### Pool Fire Modeling

The zone model reported in the literature [Ndubizu, 1983] consists of a system of three coupled non-linear algebraic equations the solution of which yields the mass burning rate, combustion zone temperature, and plume zone temperature. Figure 1 is a schematic diagram illustrating the three zones and their relative interfaces. The governing equations for the three zones are:

$$\text{Fuel zone: } \dot{m}_v = \frac{[A_s h_s (T_f - T_s) + \dot{q}_{rs, net}]}{\Delta H_v + C_{fuel} (T_s - T_b)}$$

$$\text{Combustion zone: } \dot{q}_{gen} + \dot{m}_{af} C_a T_a + \dot{m}_v C_v T_s = \dot{m}_{ss} C_g T_f + A_s h_s (T_f - T_s) + \dot{q}_{rf, net}$$

$$\text{Plume zone: } \dot{m}_{ss} C_g T_f + \dot{m}_{ap} C_a T_a = \dot{m}_p C_p T_p + \dot{q}_{rp, net}$$

where the variables are defined in the nomenclature. Results that duplicate the values obtained by [Ndubizu, 1982] with acceptable computational accuracy are shown in Table 2. The calculation algorithm used in the program is due to [Powell, 1970].

Modifications and extensions currently in progress for the zone model include: different entrainment rate for combustion and plume zones such as those by [Delichatsios, 1984] and [Zukoski, 1981], plume bending by ambient wind utilizing a reported correlation, and radiation absorption in the combustion and plume zones by soot particles. Further effort will involve the development of an integral model and a detailed two-dimensional model incorporating the elliptic behavior of the pool fire near the fuel surface.

### CONCLUSIONS

1. Wind control method is four concentric screens 3 m tall around the fuel surface perimeter. Table 1 summarizes acceptable parameters for the screens where the protected height is 2 m.
2. Pool fire zone model is correct for pool diameters up to 2 m. Further work is necessary to improve calculations for larger pool diameters and include wind effects, improved entrainment rates, and soot particle radiation absorption. Integral and two-dimensional models are required for detailed fire structure appropriate for analysis of the cook-off test.



## NOMENCLATURE

A	area ( $\text{m}^2$ )
$A_o$	screen open area ( $\text{m}^2$ )
$A_t$	screen total area ( $\text{m}^2$ )
b	mixing layer half-width (m)
C	specific heat at constant pressure ( $\text{W} \cdot \text{s}/\text{kg} \cdot \text{K}$ )
$C_c$	coefficient of jet contraction
d	diameter of fuel container
$h_s$	convective heat transfer coefficient ( $\text{W}/\text{m}^2 \cdot \text{K}$ )
$\Delta H_v$	latent heat of vaporization of fuel ( $\text{W} \cdot \text{s}/\text{kg}$ )
$\dot{m}$	mass flow rate (kg/s)
$\dot{m}_v$	fuel evaporation rate (kg/s)
$\Delta P$	pressure drop across screen ( $\text{N}/\text{m}^2$ )
$\dot{q}$	power (W)
$\dot{q}_{\text{gen}}$	actual heat release rate by combustion (W)
$\dot{q}_{\text{rf, net}}$	net radiant heat loss from combustion zone (W)
$\dot{q}_{\text{rp, net}}$	net radiant heat loss from plume zone (W)
$\dot{q}_{\text{rs, net}}$	net radiant heat gain (W)
S	screen solidity ratio
T	temperature (K)
$V_o$	free stream mean velocity (m/s)
x	downstream horizontal distance (m)
$\rho$	fluid density (kg/m)

## Subscripts

a	environmental air
b	fuel
c	combustion
f	combustion zone
p	plume zone
r	radiation
s	fuel surface
ss	combustion zone - plume interface
v	vapor
fuel	fuel

## REFERENCES

1. Alger, R. S., Corlett, R. C., Gordon, A. S., and Williams, F. A., "Some Aspects of Structures of Turbulent Pool Fires," *Fire Technol.*, V15, n2, pp. 142-156, May 1979.
2. Baines, W. D. and Peterson, E. G., "An Investigation of Flow Through Screens," *Trans. ASME*, pp. 467-480, July 1951.
3. Blinov, V. I. and Khudiakov, "Certain Laws Governing the Diffusive Burning of Liquids," *Academiia Nauk, SSR Doklady*, V113, pp. 1094-1098, 1957.
4. Brown, G. L. and Roshko, A., "On Density Effects and Large Structures in Turbulent Mixing Layers," *J. Fluid Mech.*, V64, pp. 775-816, 1974.
5. Gray, D. M. and Male, D. H. (eds.), Handbook of Snow, Pergamon Press, Toronto, Canada, pp. 338-358 and 630-647, 1981.
6. Hakuro, H. and Inoue, O., "Mixing Layer Produced by a Screen and Its Dependence on Initial Conditions," *J. Fluid Mech.*, V 142, pp. 217-231, 1984.
7. Harsha, P. T., Bragg, W. N., and Edelman, R. B., "A Mathematical Model of a Large Open Fire," Contract No. N60530-80-M-NA76, Science Applications, Inc., Canoga Park, California, April 1981.
8. Johnson, H. T., Linley, L. J., and Mansfield, J. A., "Measurement of the Spatial Dependence of Temperature and Gas Soot Concentrations Within Large Open Hydrocarbon Fuel Fires," NASA Tech. Mem. 58230, Johnson Space Center, Houston, Texas, March 1982.
9. Kálghatgi, G. T., "The Visiple Shape and Size of a Turbulent Hydrocarbon Jet Diffusion Flame in a Cross-Wind," *Comb. and Flame*, V52, pp. 96-106, 1983.
10. Kung, H. and Stavrianidis, P., "Buoyant Plumes of Large-Scale Pool Fires," *Nineteenth Symp., The Combustion Institute*, pp. 905-912, 1982.
11. McCaffrey, B. J., "Momentum Implications for Buoyant Diffusion Flames," *Comb. and Flame*, V52, pp. 149-167, 1983.
12. Moorhouse, J., "Scaling Criteria for Pool Fires Derived From Large Scale Experiments," *EFCE Publ. Series*, n25, Inst. of Chem. Engr. (Symp. Ser. n71), Rugby, Warwickshire, England, pp. 165-179, 1982.
13. Ndubizu, C. C., Ramaker, D. E., Tatem, P. A., and Williams, F. W., "A Model of Freely Burning Pool Fires," *Comb. Sci. and Technol.*, V31, pp. 233-247, 1983.
14. Powell, M. J. D., "A Fortran Subroutine for Solving Systems of Nonlinear Algebraic Equations" in Numerical Methods for Nonlinear Algebraic Equations, Rabinowitz, P. (ed.), Gordon and Breach, New York, pp. 115-161, 1970.

15. Oster, D. and Wagnanski, I., "The Forced Mixing Layer Between Parallel Streams," J. Fluid Mech., V123, pp. 91-130, 1982.
16. Raj, P. K., "Analysis of JP-4 Fire Test Data and Development of a Simple Fire Model," ASME Pap. 81-HT-17, 20th Joint ASME/AICHE National Heat Transfer Conference, Milwaukee, Wisconsin, August 2-5, 1981.
17. Schlichting, H., Boundary Layer Theory, Pergamon Press, New York pp. 488-492, 1955.
18. Schneyer, G. and Laird, D., "Development of Analytical Fire Models," Contract No. NAS2-8339, Systems, Science and Software, Inc., La Jolla, California, April 1975.
19. Spalding, D. B., "Concentration Fluctuations in a Round Turbulent Free Jet," Chemical Engr. Sci., V26, pp 95-17, 1971.
20. Steward, F. R., "Prediction of the Height of Turbulent Diffusion Buoyant Flames," Comb. Sci. and Technol., V2, pp. 203-212, 1970.
21. Tamanini, F., "An Integral Model of Turbulent Fire Plumes," Eighteenth Symp., The Combustion Institute, pp. 1081-1090.
22. Tozer, B. L., "An Investigation to Improve JP-5 Fuel Pool Fire Test Repeatability," NWC Tech. Mem. 5202, Naval Weapons Center, China Lake, California, November 1983.
23. Townsend, A. A., The Structure of Turbulent Shear Flow, 2nd ed., Cambridge University Press, Cambridge, U.K., pp 188-258, 1976.
24. Welker, J. R. and Sliepcevich, C. M., "The Effect of Wind on Flames," Tech. Rept. No. 2, Research Institute, Univ. of Oklahoma, NBS Contract CST 1142, Nat'l. Bureau of Standards, Washington, D.C., November 15, 1965.

Table 1

Wind Speed Reduction Using  
Multiple Concentric Screens

Wind Speed = 6.68 m/s

Height of Screen = 3 m

Number of Screens = 4

Distance Between Screens = 2.5 m

Parameter \ Screen No.	1 (Outer Screen)	2	3	4 (Inner Screen)*
Velocity After Screen (m/s)	5.23	3.78	2.33	0.88
Pressure Drop Across Screen (Pa)	8.6	6.5	4.4	2.3
Solidity Ratio, S	0.36	0.33	0.29	0.30
Drag Force (N)	611	372	127	128
Diameter of Opening	0.1	0.1	0.1	0.1
Number of Openings	17,520	15,670	13,775	11,860

\* Inner screen located 2.5 m outside pool fire perimeter.

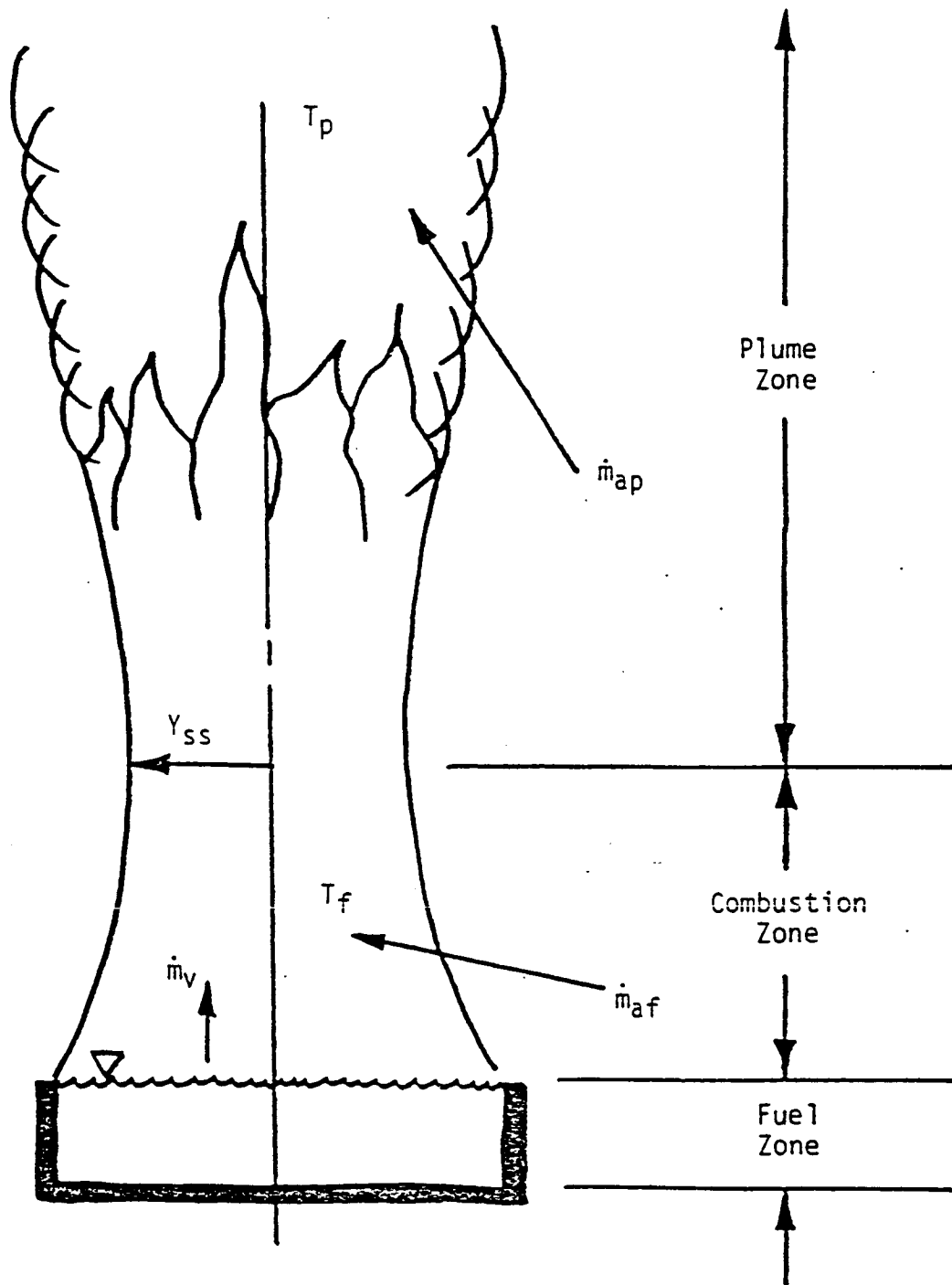


Figure 1: Pool Fire Zone Model

Table 2

## Predicted Characteristics of a 1.3 m Diameter

Fuel:	Kerosene	
Fuel Properties:	Specific Heat (liquid)	2090 W s/kg K
	Boiling Point	499.7 K
	Stoichiometric Air/Fuel Ratio	14.99
	Heat of Combustion	$4.3 \times 10^7$ W s/kg
	Heat of Vaporization	$2.0 \times 10^5$ W s/kg
	Molecular Weight	154
	Liquid Density at Boiling Point	740.2 kg/m <sup>3</sup>
Predictions:	Fuel Evaporation Rate	0.033 kg/m <sup>2</sup> s
	$T_f$	1135 K
	$T_p$	559 K
	$\dot{q}_{gen}$	1223 kW
	$\dot{q}_{rf, net}$	312 kW
	$\dot{q}_{rs, net}$	25 kW
	$A_s h_s (T_f - T_s)$	2.1 kW
	Plume Zone Height	3.27 m
	Combustion Zone Height	1.47 m
	$\dot{m}_{af}$	0.978 kg/s
	$\dot{m}_{ap}$	2.90 kg/s

omit

MICHAEL C. GREENISEN

PAPER UNAVAILABLE



N86 - 31420

D11  
5P.

DEVELOPMENT OF A NUMERICAL PROCEDURE TO  
MAP A GENERAL 3-D BODY ONTO A NEAR-CIRCLE

18822

Dr. Mark J. Hommel, P.E.  
Associate Professor  
Department of Mechanical Engineering  
Prairie View A&M University  
Prairie View, Texas

ABSTRACT

Conformal mapping is a classical technique which has been utilized for solving problems in aerodynamics and hydrodynamics for many years. Conformal mapping has been successfully applied in the construction of grids around airfoils, engine inlets and other aircraft configurations. These shapes are transformed onto a near-circle image for which the equations of fluid motion are discretized on the mapped plane and solved numerically by utilizing the appropriate techniques. In comparison to other grid-generation techniques such as algebraic or differential type, conformal mapping offers an analytical and accurate form even if the grid deformation is large. One of the most appealing features is that the grid can be constrained to remain orthogonal to the body after the transformation. Hence, the grid is suitable for analyzing the supersonic flow past a blunt object. The associated shock as a coordinate surface adjusts its position in the course of computation until convergence is reached.

The present work applies conformal mapping to 3-D bodies with no axis of symmetry such as the Aerobraking Flight Experiment (AFE) vehicle, transforming the AFE shape onto a near-circle image. A numerical procedure and code have been developed for generating grids around the AFE body. Two different approaches have been explored: a Karmen-Trefftz transformation, and a Schwartz-Christoffel type transformation. The advantages and disadvantages of both methods are discussed, as well as the trade-offs involved in utilizing either one.

Center Research Advisor: Dr. Chien Li

CONCLUSIONS

Two different conformal mapping approaches were utilized:

- (a) Karmen-Trefftz
- (b) Schwarz-Christoffel

Computer programs were written to implement both approaches, and the methods were compared. It was seen that the primary advantage of the Karmen-Trefftz method lies in its ease of programming, as well as its inherent property of providing a finer mesh at corner locations of the body to be mapped. However, the Karmen-Trefftz transformation has the disadvantage of not constraining the transverse coordinate to be perpendicular to the mapped body. The Schwarz-Christoffel transformation was then utilized with the hope of overcoming the latter disadvantage. The Schwarz-Christoffel transformation is not as straightforward to program, nor does it possess the inherent fineness of grid at body corners which the Karmen-Trefftz transformation possesses. However, the mesh is constrained with the Schwarz-Christoffel transformation to be perpendicular to the body. It is seen that both methods have advantages, and a given application may dictate which method is more useful.

Attached are examples of a mapped grid surrounding an AFE-type body, utilizing the two methods.

#### REFERENCES

1. Moretti, G., "Conformal Mappings for Computations of Steady, Three-Dimensional, Supersonic Flows," Numerical/Laboratory Comp. Methods in Fl. Mech., ASME, 13, pp.13-28, 1976.
2. Hall, D.W., "A Three-Dimensional Body-Fitted Coordinate System for Flow Field Calculations on Asymmetric Nosedips," Numerical Grid Generation Techniques, NASA Conference Publication 2166, Langley Research Center, October 6-7, 1980.

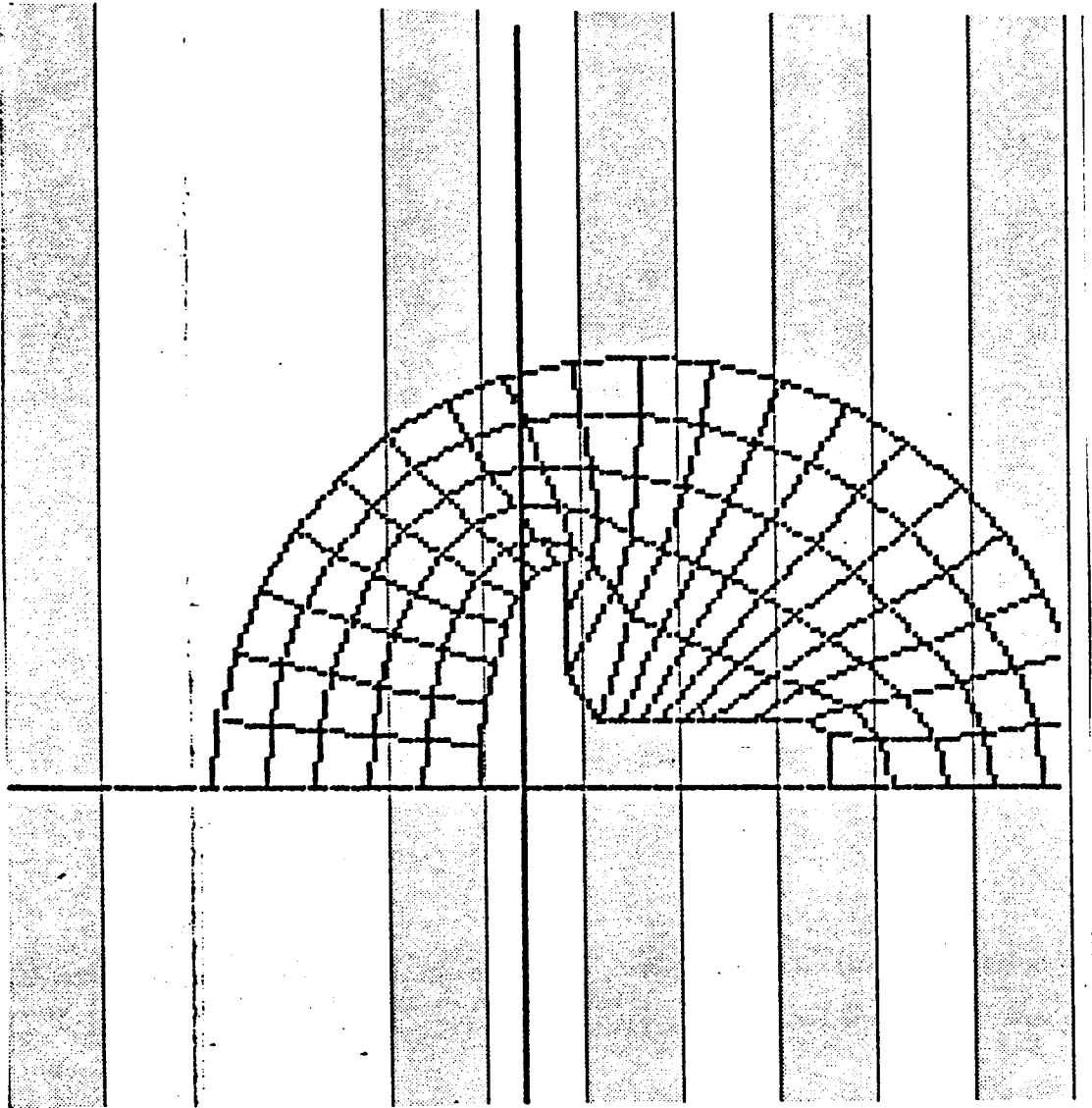


Figure 1--Karmen-Trefftz Transformed Grid

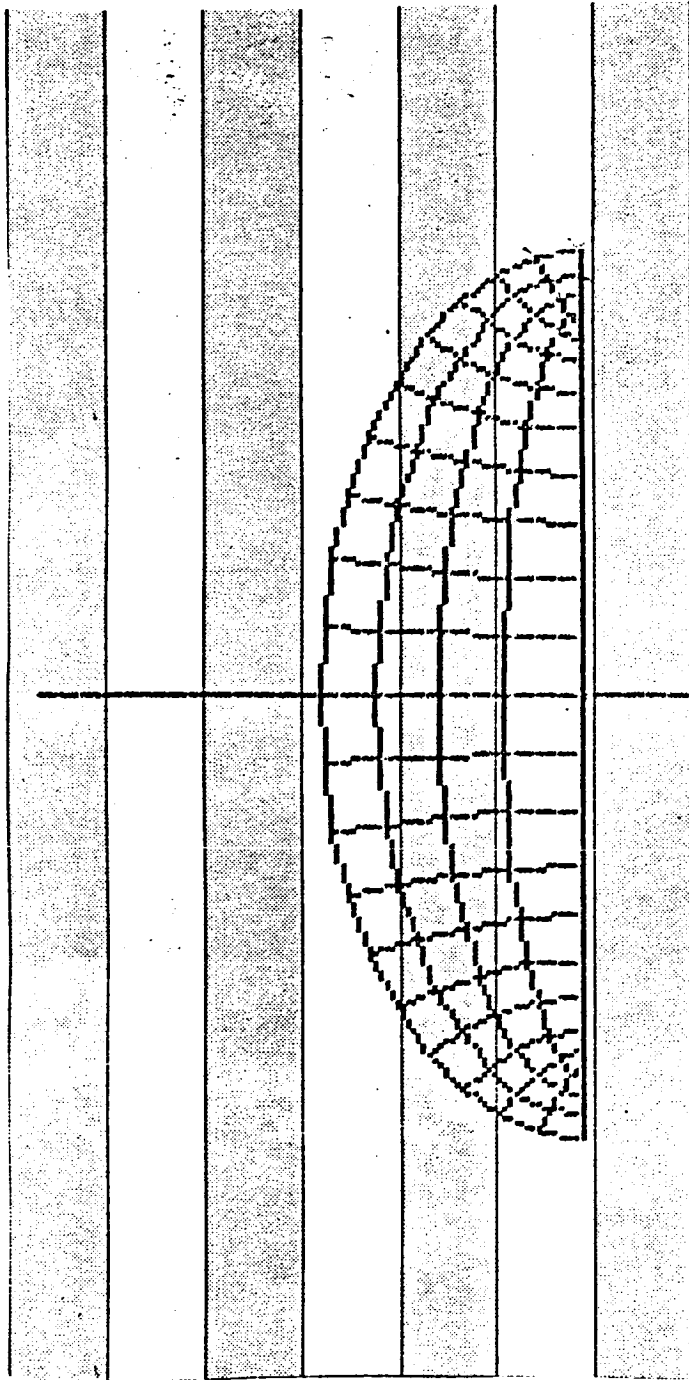


Figure 2--Schwarz-Christoffel Transformed Grid

N86 - 31421

D12  
12P.

Effects of Lunar Soil, Zagami meteorite, and  
Ocean Ridge Basalt on the Excretion of Itoic Acid,  
a Siderophore, and Coproporphyrin by Bacillus subtilis

Takeru Ito  
Professor of Biology  
East Carolina University  
Greenville, North Carolina 27834

18823

ABSTRACT

Samples of lunar soil (10084,151), Zagami meteorite, postulated to be ejected from Mars, and ocean ridge basalt, the most abundant volcanic rock on earth, all completely inhibited the excretion of itoic acid and of coproporphyrin by Bacillus subtilis, a common air born bacterium. Since such inhibition has been known to occur only under iron rich growth condition (the excretion of these compounds occurs under iron deficient growth conditions), the result indicated that the organism was capable of extracting iron quite readily from these materials.

A sample of synthetic ilmenite completely failed to inhibit the excretion of coproporphyrin, and inhibited the excretion of itoic acid only slightly. The result suggested that much of the iron extracted by the organism must have come from other iron sources, such as pyroxenes and olivines, than ilmenite in these natural materials tested.

Center Research Advisor: Donald L. Henninger, Ph. D.

## INTRODUCTION

Solving the problem of how a "terrestrial-like" soil can be generated from lunar soil that would support growth of living organism is an important issue in successful establishment of a future lunar base, since it may depend on at least a partial satisfaction of the needed foods met by growing them at the base. Solubilization of iron, which is a major element in the lunar soil (Morris, et al., 1983), is one of the most important aspects of the "soil genesis", since iron is required for all living organisms. It is reasonable to expect that the interaction of the lunar soil with microorganisms is necessary in order to facilitate the solubilization process, in view of the fact that many microorganisms are involved in weathering of the minerals containing iron on earth (Nealson, 1983).

Since the ferric form of iron is extremely insoluble in water, most all microorganisms especially under iron deficient growth conditions excrete iron-binding compounds generally known as siderophores, which in effect "solubilize" the iron making it available for transport into microbial cells (Neillands, 1974, Emery, 1982). In

particular, Bacillus subtilis, when grown under iron deficient growth conditions, excretes itoic acid, a siderophore, and coproporphyrin, a precursor of cytochrome biosynthesis. The excretion of these two compounds is extremely sensitive to the iron concentration in a growth medium, and stops as the iron concentration rises (Ito and Neillands, 1958).

This study was undertaken in order to learn whether lunar soil inhibits excretion of itoic acid and coproporphyrin by the organism when included in an iron deficient culture medium. The effects of lunar soil were compared with that of other natural materials, a Mars origin meteorite, terrestrial ocean ridge basalt, and natural and synthetic ilmenite.

#### MATERIALS AND METHODS

Minerals: 1) Lunar soil sample, (10084,151), 2) Zagami meteorite, 3) Gorda ridge ocean basalt, 4) Quebec ilmenite, and 5) synthetic ilmenite were obtained from the Solar Exploration Division of the Johnson Space Center, Houston, Texas.

Growth of Organism and Determination of Itoic Acid and Coproporphyrin: The organism used for this study was Bacillus subtilis (NRRL B1471, ATCC 15933). The 250 ml



flasks each containing 50 ml iron deficient growth medium (GM) (Ito and Neillands, 1958) with or without 10 mg minerals listed elsewhere were autoclaved ( $120^{\circ}$ , 20 lb. pressure), and inoculated with 5 drops of a freshly grown culture in GM. In some experiments, after autoclaving, the growth media were filtered through disposable Millipore filter apparatus before the inoculation of the organism into the filtrate. In other experiments, the lunar soil was sterilized by immersing in 50 ml 95% ethanol for one day in 250 ml flasks, and decanting the ethanol out while rinsing the inner wall of the flasks thoroughly as the ethanol was poured out. To each flask, 50 ml autoclaved GM was added before the inoculation of the organism. The inoculated flasks were incubated for three days at  $30^{\circ}$  in a gyratory shaker at about 50 cycles/min. The cells were removed by centrifugation at 10,000 g for 10 min., and the absorbance of each supernatant after diluted to five folds was read at 320 nm and 405 nm for the measures of itoic acid and coproporphyrin respectively (Ito and Neillands, 1958; Townsley and Neillands, 1957) with a Beckman ACTA III UV-Visible spectrophotometer with 1-cm light path cuvettes. All flasks containing GM were previously rinsed thoroughly with 6 N HCl in order to remove any possible iron contamination on the inner wall of the flasks.

## RESULTS AND DISCUSSION

The spectra of the supernatants of the three day old culture grown in GM and GM to which 100 micrograms Fe/50 ml was added in the form of ferric chloride are shown in Fig. 1. Two absorption peaks, one at 320 nm for itoic acid (Ito and Neilands, 1958) and another at 405 nm for coproporphyrin (Townesley and Neilands, 1957), were observed with no addition of ferric chloride, but disappeared with the addition of iron. The intense pink color developed in the three day old iron deficient culture was obviously indicative of the coproporphyrin accumulation (Ito and Neilands, 1958).

The lunar soil (10084,151), collected during the Apollo 11 mission (Morris et al., 1983), the Zagami meteorite, postulated to be of Mars origin (Nyquist et al., 1979), and the Gorda ridge basalt (Kay et al., 1970), the most abundant volcanic rock on earth, all completely inhibited the excretion of itoic acid and coproporphyrin. No inhibition of coproporphyrin excretion and slight inhibition of itoic acid excretion by the synthetic ilmenite were observed. The Quebec ilmenite inhibited the excretion of both, but not to the extent by the other three natural samples tested (Table 1). It was obvious from the result that iron was released from these natural samples, and evidently utilized by the organism. However, much of the iron that was released from these samples and utilized by the organism must have

originated from types of iron sources other than ilmenite, such as pyroxenes and olivines, all of which are abundant in the lunar soil, the Zagami meteorite and the ocean ridge basalt. The inhibition of the excretion of these two compounds by the Quebec ilmenite indicated that this ilmenite sample was contaminated with other iron sources.

The release of iron observed above, however, may have occurred through two ways. One is the solubilization of the iron from these natural samples during the autoclaving to sterilize the liquid growth media. Another way is through the action of the organism. To test if an appreciable amount of iron was released from the mineral samples by mere autoclaving, the mineral samples and the GM, after autoclaving together, were aseptically filtered, and the filtrate was inoculated with the organism. The result showed that a considerable amount of iron was released from the lunar soil and the basalt upon mere autoclaving, although some iron also was released from the filtration apparatus (Table 2).

In order to learn if the iron was released by the action of the organism not merely by the autoclaving, autoclaved GM was added to the lunar sample sterilized by ethanol as described in MATERIALS AND METHODS. It was clear that the organism did facilitate the release of iron from the lunar soil, but from the ethanol as well, which must

have been contaminated with much iron. (Table 3).

Autoclaving in a sense can be considered an accelerated weathering condition, since the high temperature ( $120^{\circ}$ ) used for autoclaving is expected to speed up the solubilization process which undoubtedly occurs under natural conditions but at a much slower rate (Keller and Huang, 1971). The results presented here suggest that iron may be released quite readily from minerals not only by natural chemical weathering alone but also by the action of microorganisms. It can be surmised that the ready extraction of iron by the organism from these natural samples tested was presumably mediated by itoic acid, a specific siderophore of Bacillus subtilis, in the light of the finding that a siderophore rhodotorulic acid produced by Rhodotorula facilitated release of iron without the action of living organisms from a volcanic ash and other silicate rocks (Akers and Magee, 1985).

Table 1. Itoic Acid and Coproporphyrin Excretion by Bacillus subtilis with various minerals. Each number without parentheses represents the mean absorbance of four determinations, at approximate absorption maxima of itoic acid (320 nm) and coproporphyrin (405 nm). The ranges are given in parentheses.

Addition to GM before Autoclaving	Absorbance of Supernatants at			
	320 nm		405 nm	
None	5.00	(5.32-4.70)	1.07	(1.23-0.925)
Lunar Soil	0.661	(0.690-0.625)	0.216	(0.225-0.210)
Zagami Meteorite	0.584	(0.615-0.555)	0.196	(0.205-0.190)
Gorda Ridge Basalt	0.663	(0.680-0.655)	0.215	(0.225-0.200)
Quebec Ilmenite	1.14	(1.24-1.05)	0.615	(0.830-0.500)
Synthetic Ilmenite	3.17	(3.53-2.71)	1.58	(2.09-1.13)

Table 2. Release of Soluble Iron from from the Lunar Soil and the Gorda Ridge Basalt upon Autoclaving. \*These growth media were autoclaved and filtered aseptically before the inoculation of the organism as described in the text. #Mean of two determinations. See Table 1 for other explanations.

Addition to GM before Autoclaving	Absorbance of Supernatants at			
	320 nm		405 nm	
None	4.74	(4.89-4.61)	2.28	(2.44-2.04)
None*	#4.16	(4.47-3.86)	#0.835	(0.890-0.780)
Lunar Soil*	0.640	(0.675-0.615)	0.315	(0.340-0.305)
Basalt*	0.661	(0.680-0.645)	0.223	(0.300-0.180)

Table 3. Release of Iron (without autoclaving) from the Lunar Soil by Bacillus subtilis during Its Growth. \*Ethanol sterilized flasks. \*\*Lunar Soil sterilized by ethanol. #Mean of two determinations. See other details in Table 1 and the text.

Autoclaved GM Added to	Absorbance of Supernatants at			
	320 nm		405 nm	
None	4.00	(4.13-3.71)	4.84	(5.62-3.86)
None*	#1.31	(1.57-1.04)	#1.18	(1.47-0.895)
Lunar Soil**	0.586	(0.630-0.530)	0.180	(0.210-0.150)

## REFERENCES

Akers, H. A., and K. P. Magee, 1985. The Siderophore Mediated Release of Iron and Magnesium from Mt St. Helens' Ash and Silicate Rock Standards. *Experientia*, 41, 522.

Emery, T., 1982. Iron Metabolism in Humans and Plants. *American Scientist*, 70, 626.

Ito, T., and J. B. Neilands, 1958. Products of Low Iron Fermentation with Bacillus subtilis: Isolation, Characterization, and Synthesis of 2,3-Dihydroxybenzoylglycine. *J. Am. Chem. Soc.*, 80, 4645.

Kay, R., N. J. Hubbard, and P. W. Gast, 1970. Chemical Characteristics and Origin of Oceanic Ridge Volcanic Rocks. *J. Geophys. Research*, 75, 1585.

Keller, W. D., and W. H. Huang, 1971. Response of Apollo 12 Lunar Dust to Reagents Simulative of Those in the Weathering Environment of Earth. *Proceedings of 2nd Lunar Science Conference*, vol. 1, p. 973.

Morris, R. V., R. Score, C. Dardano, and G. Heiken, 1983. *Handbook of Lunar Soils, Part I: Apollo 11-15. Planetary*

Materials Branch Publication 67, p. 10.

Nealson K. H., 1983. The Microbial Iron Cycle. In Microbial Geochemistry. ed. by W. E. Krumbein, Blackwell Scientific Publications, Oxford, p. 159.

Neilands, J. B., 1974. Iron and Its Role in Microbial Physiology. In Microbial Iron Metabolism, ed. by J. B. Neilands, Academic Press, New York, p. 3.

Nyquist, L. E., D. D. Bogard, J. L. Wooden, H. Wiesmann, C.-Y. Shih, B. M. Bansal, and G. A. McKay, 1979. Early Differentiation, Late Magmatism, and Recent Bombardment of the Shergottite Parent Planet. *Meteoritics*, 14, 502.

Townsley, P. M., and J. B. Neilands, 1957. The Iron and Porphyrin Metabolism of Micrococcus lysodeikticus. *J. Biol. Chem.*, 224, 695.



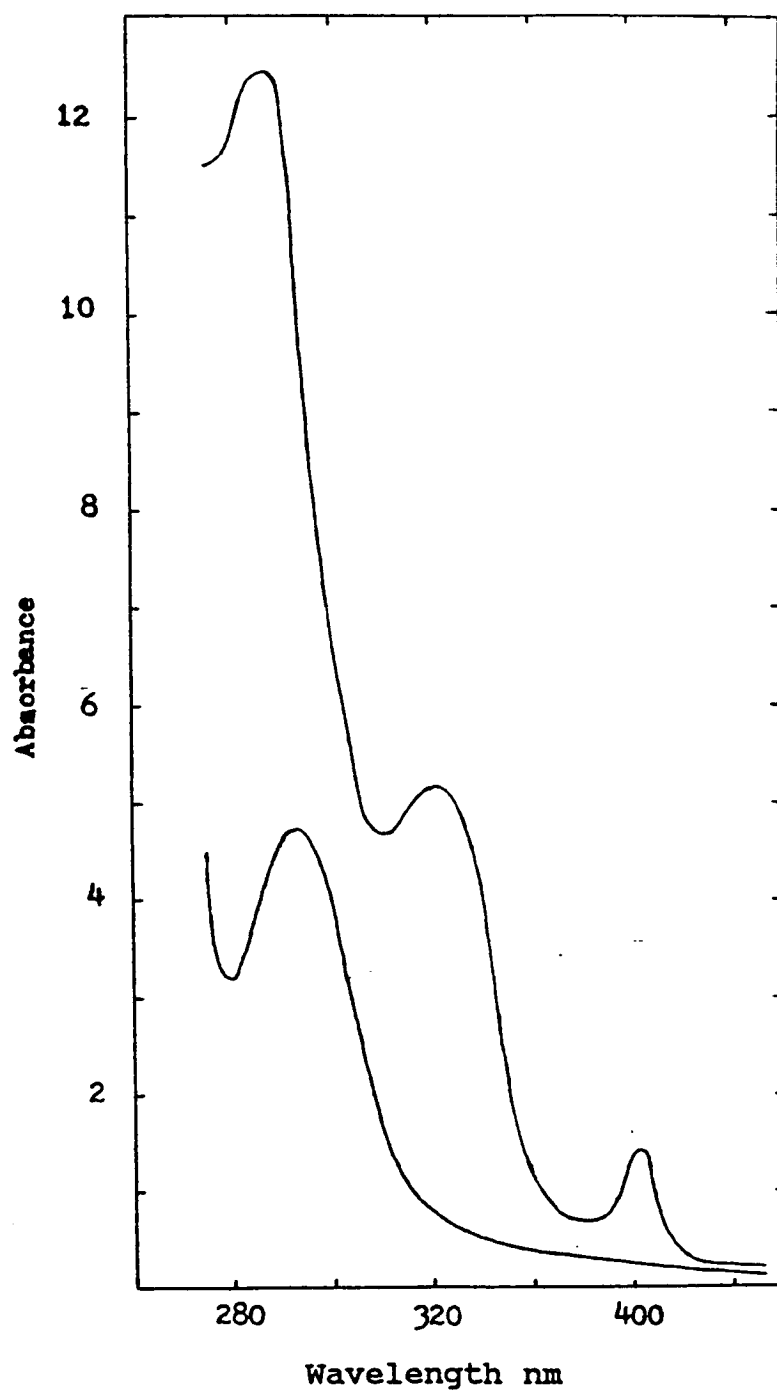


Fig. 1. Effect of Iron on the Excretion of Itoic Acid and Coproporphyrin. Upper curve, no iron added to GM; Lower curve, 100 micrograms iron/liter added to GM.

N86 - 31422

D13  
49P.

DEFINING RECLAIMED WATER POTABILITY REQUIREMENTS

Daniel S. Janik, MD, MPH  
Rocky Mountain Center for Occupational and Environmental Health  
University of Utah  
Salt Lake City, UT 84132

18824

Abstract. Water used during previous space missions has been either carried or made aloft. Future human space endeavors will probably have to utilize some form of water reclamation and recycling. There is little applied experience in either the US or foreign space programs with this technology. Water reclamation and recycling constitutes an engineering challenge of the broadest nature and will require an intensive research and development effort if this technology is to mature in time for practical use on the proposed US spacestation. In order for this to happen, reclaimed/recycled water specification will need to be devised to guide engineering development. Perhaps the most stringent specifications will involve water to be consumed. NASA's present Potable Water Specifications are not applicable to reclaimed or recycled potable water. No specifications for reclaimed or recycled potable water presently exist either inside or outside NASA. NASA's past experience with potable water systems is reviewed, limitations of the present Potable Water Specifications are examined, present world expertise with potable water reclamation/recycling systems and system analogs is reviewed, and an approach to developing pertinent Reclaimed/Recycled Potable Water Specifications for spacecraft is presented.

Up to the present, the air, food and water necessary to support human life in space has either been carried or generated aloft. This probably reflects the short duration of the missions (Mercury/Vostok, Gemini/Voskhod, Apollo/Soyuz), lack of need to conserve mass during orbital insertion (Skylab), or existence of a dependable reprovisioning system (Soyuz/Salyut/Progress). In each case, however, human space activities have been constrained primarily by the limitations of the human life support system (environmental control and life support system, or ECLSS) employed. The proposed United States (US) spacestation, scheduled for implementation on or before 1994, is being designed to support a permanent manned presence in space (1). Present plans call for it to be capable of supporting commercial/industrial applications, be assembled from a minimum number of modules within the size and weight limitations imposed by the US space transportation system (Shuttle), and be as independent of ground-support as possible (1,2). Limitations imposed by present ECLSS technology will therefore likely prove unacceptable.

Of the different ECLSS constituents, water occupies first place by weight (3). Indeed, the human body's daily weight requirement for water exceeds that of oxygen and food substances combined (4). The minimum amount of water necessary to support human life in space is about 2.5 liters per sedentary crewmember per day (3). US and Union of Soviet Socialist Republics (USSR) experiments indicate that up to 6 liters per crewmember per day may be necessary to support vigorous activity in space. The minimum amount of water necessary to support a manned space mission is roughly proportional to the duration of the mission; all of this water must be consumable, or potable. Potable water (PW) may be used for other purposes such as handwashing, cooling, oxygen generation or even fuel (hydrogen) generation. If PW is used

for multiple purposes, it can become the principal mission delimiter.

TABLE 1 - SOME ECLSS CONSTITUENTS REQUIRED TO SUPPORT A SINGLE PERSON IN SPACE (3,4).

<u>Constituent</u>	Amount (kilograms per person)		
	<u>per day</u>	<u>per year</u>	<u>per lifetime</u>
Food (dry)	0.6	219	15,300
Oxygen	0.9	239	23,000
Water			
-drinking*	2.5	913	73,120
-sanitary	2.3	840	58,800
-domestic	16.8	6,132	429,240

\* includes food rehydration.

In either case, one method under consideration for providing PW for longer duration missions such as the spacestation is reclamation and recycling of previously-used water (e.g. humidity condensate, washwater, food wastes, urine or feces). This represents a major departure from the fill-and-draw type PW systems used on all previous spaceflights.

-----

1. Froehlich W: Spacestation - The next logical step. (NASA document #EP-213, Superintendent of Documents, Government Printing Office, Washington DC 20402, 1985).

2. Office of Technology Assessment: Civilian Space Stations and the U. S.

Future in Space. (OTA document #OTA-STI-241, Superintendent of Documents, United States Government Printing Office, Washington DC 20402, Nov 1984).

3. Popov IG: Food and water supply. In Calvin M and Gazonko OG: Foundations of Space Biology and Medicine Vol. III (Stock #033-000-00608-0, United States Government Printing Office, Washington DC 20402, 1975).

4. Spurlock J et al: Research planning criteria for regenerative life-support system applicable to space habitats. In Billingham J and Gilbreath W: Space Resources and Space Settlements (Stock #033-000-00765-5, United States Government Printing Office, Washington DC 20402, 1979).

## PW SYSTEMS USED IN SPACE

NASA PW Systems. All US spacecraft have thus far carried some variant of a fill-and-draw type PW system, and have used PW for all water needs. In general, a spacecraft's PW system is prepared as necessary well in advance of a launch by steaming, flushing with chlorinated/distilled water, flushing with ethanol/distilled water, or some combination thereof. Spacecraft water is usually obtained from a public water source, filtered, polished, tested and certified potable using prevailing NASA PW Specification criteria. The water is then supplied to the spacecraft and periodically monitored for chemical/microbiological purity using prevailing NASA PW Test Procedures. Immediately prior to launch (usually T minus 4 days) a bacteriocide is re-introduced, final tests are taken, and the PW system is officially certified for launch. Once aloft, the water is used and either vented to space, destroyed with the spacecraft on reentry or returned to earth. Beginning with Gemini 2, routine postflight testing was instituted; on later flights, inflight testing and re-disinfection was introduced.

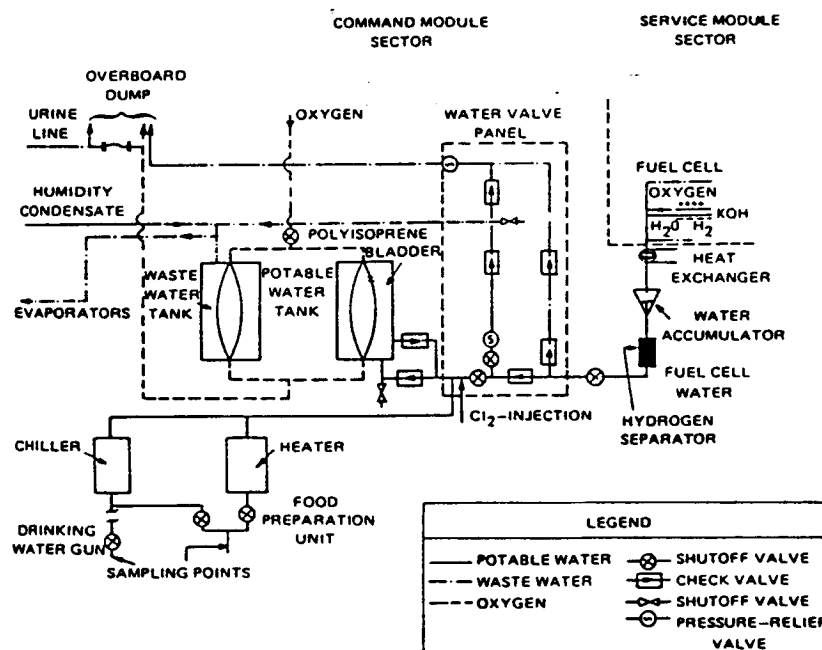
During Mercury, the PW system was divided into 2 independent subsystems. A 2.7-liter, passively-pressurized, plastic pouch supplied drinking water through a flexible tube inserted, when desired, into the astronaut's pressure-helmet via a one way flap-valve. Water for food reconstitution was supplied from a separate container pressurized by manually squeezing a bulb (4,5).

Gemini utilized a single, integrated PW system divided into 2 inter-related subsystems corresponding to the spacecraft's command (crew and reentry) and supply modules. A single, 7-liter holding tank, located between the crew-seats delivered PW for drinking and food reconstitution via a system

similar to Mercury. A second PW tank located in the supply module replenished the holding tank as necessary. A third water tank, also located in the supply module, was originally designed to receive water produced from fuel-cells. However, the fuel-cell water was not able to meet NASA PW Specifications. Instead, the third tank was filled with ground-supplied water (GSW) and fuel-cell water was used with nitrogen gas to pressurize the PW system. Upon reentry, the supply module was jettisoned. PW provided spacecraft cooling, spacesuit cooling and humidity (5,6).

Like Gemini, Apollo spacecraft utilized a single, integrated PW system divided into 2 inter-related subsystems corresponding to command and service modules (FIGURE 1). A single, 16-liter holding tank was located in the

FIGURE 1 - POTABLE WATER SYSTEM FOR APOLLO COMMAND/SERVICE MODULES (9).



command module and supplied hot and cold water to the crew via drinking water and food rehydration injection ports. Unlike Gemini, Apollo fuel-cell water

was able to meet NASA PW Specifications and was used to continuously replenish PW stores. Fuel-cell water was secondarily directed towards a second 16-liter (wastewater) holding tank which also received humidity condensate from the spacecraft and spacesuits. Either or both tanks could supply water for spacecraft or spacesuit cooling, or be vented overboard via common distribution lines (9,10).

The Apollo Lunar Module (LM) had a separate PW supply also divided into 2 subsystems. PW loaded in the LM prior to launch was stored in two 19-liter holding tanks located in the upper, ascent module and one or two 151-liter tanks in the jettisonable, lower, descent module. LM provided PW for drinking, food reconstitution, spacecraft cooling and spacesuit cooling during travel to, on and return from the moon. The system was pressurized by nitrogen gas and was independent of the wastewater system (3,5,9,10).

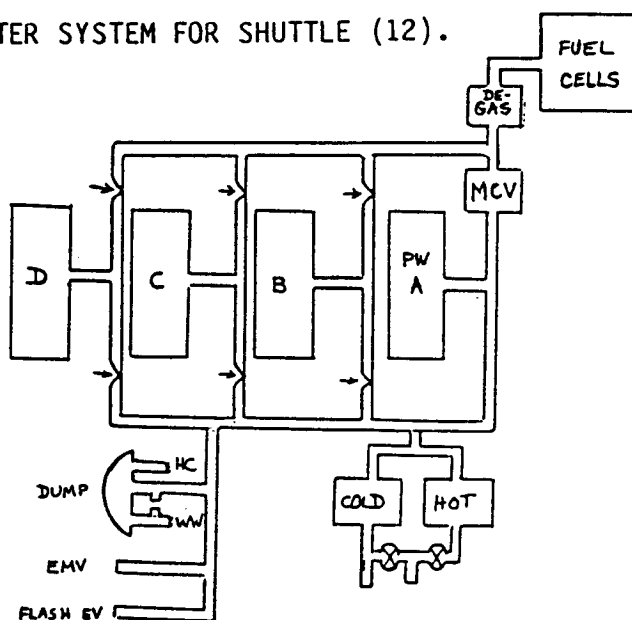
Skylab represents the US's first longer-duration, multi-crewed spacecraft. Skylab's Orbital Workshop (OWS) had three independent PW subsystems. Water for drinking and food reconstitution (wardroom water) was supplied at any one time from one of six 278-liter tanks. Three additional tanks supplied personal hygiene/waste management, and another airlock servicing/contingency water. A 12.7-liter, portable PW tank provided emergency water. All tanks were launched fully-charged with PW; water was not generated inflight. During each of the three manned Skylab missions (Skylabs 2, 3 and 4), the crew had to first reconnect and fill the wardroom water distribution system, then check disinfectant residuals, add iodine disinfectant as necessary, and draw samples for testing prior to use. After completion of a mission, the crew had to disconnect, vent and seal the wardroom water distribution system for subsequent use. Wardroom water was



used only for drinking and food reconstitution. The water systems were pressurized by nitrogen gas (5,7,8).

The present Shuttle spacecraft PW system similar to Apollo's but is more highly integrated. Three, parallel, prefilled water tanks are continuously replenished with fuel-cell water. Fuel-cell water to the first tank is degassed, passed through an iodine/anion-exchange microbial check valve (MCV) on its way to the holding tank, and preferentially supplies hot and cold PW inflight for drinking and food reconstitution. The second and third tanks receive degassed water routed to bypass the MCV. Water from these tanks is preferentially directed towards the waste management system, spacecraft coolers, spacesuit cooling system and/or vented overboard as needed. Interconnections between the tanks allow reshunting of water from and to various tanks as needed. Non-potable water from the second and third tanks may be backwashed through the MCV valve into the first tank. Used water is kept separate from PW by the absence of a quick-connect line which may be reconnected in an emergency. The Shuttle's PW system is pressurized by gaseous nitrogen (11,12).

FIGURE 2 - POTABLE WATER SYSTEM FOR SHUTTLE (12).



Soviet PW Systems. Soviet Vostok, Voskhod, Soyuz and Salyut spacecraft utilize fill-and-draw technology roughly analagous to their Mercury, Gemini Apollo and Skylab counterparts (3,14). However, Salyut, which the Soviet's describe as a spacestation, may augment stored wardroom water with reclaimed urine water. What portion, if any, of the PW is actually regenerated is not well described. However, Salyut's stores of PW are regularly reprovisioned with GSW from the Progress cargo ship (15).

Summary. In summary, the US and USSR have extensive spaceflight experience with fill-and-draw PW systems. The US, in addition, has experience with inflight generation of PW. At this time, however, there is little spaceflight experience with regard to regenerated, reclaimed or recycled PW systems to draw upon in the design and development of a reclaimed PW system for the proposed US spacestation.

-----

5. Sauer RL and Bustamante RB: Water supply and waste management in spacecraft - past, present, and future. Unpublished document # MSC-04269 dated 1971 available from R. L. Sauer, Biomedical Research Section (Code SD 3), NASA/Johnson Space Center, Houston, TX 77058.

6. Frost RL, Thompson JW and Bell LE: Environmental control system. In Gemini Midprogram Conference including Experimental Results. (NASA #SP-121, United States Government Printing Office, Washington DC 20402, 1966).

7. Johnston RS: Skylab Medical program overview. In Johnston RS and

Dietlein LF: Biomedical Results from Skylab (Stock #033-000-00648-9, United States Government Printing Office, Washington DC 20402, 1977).

8. Skylab Program Office (Marshall Flight Center): Skylab Vol III. (NASA Technical Memorandum #TM X 64813, National Scientific and Technical Information Office, National Aeronautics and Space Administration, Washington DC 20546, May 1976).

9. Sauer RL and Calley DJ: Potable water supply. In Johnston KS, Dietlein LF and Berry CA: Biomedical Results of Apollo. (Stock #003-000-00628-4, United States Government Printing Office, Washington DC 20402, 1975).

10. Sauer RL: Potable water. In Nicogossian AE: The Apollo-Soyuz Test Project Medical Report. (NASA #SP-411, National Technical Information Service, Springfield, VA 22161, 1977).

11. Sauer, RL: The potable water. In Pool SL, Johnson PC and Mason JA: STS-1 Medical Report. (NASA Technical Memorandum #58240, Scientific and Technical Branch, National Aeronautics and Space Administration, Washington DC 20546, Dec 1981)

12. Sauer, RL: Potable water. In Pool SL, Johnson PC and Mason JA: Shuttle OFT Medical Report. (NASA Technical Memorandum #58252, Scientific and Technical Branch, National Aeronautics and Space Administration, Washington DC 20546, July 1983).

13. Crew Systems Division: Supply Water Storage. Unpublished document dated

25 Jan 1984 available from R. L. Sauer, Biomedical Research Branch (Code SD 3), NASA/Johnson Space Center, Houston, TX 77058.

14. Radchenko N: Water supply of cosmonauts. Translation of Vodoobespcheniye Kosmonavtov in Aviatsiya i Kosmonavtika 1:31, Sept 1970. (NASA document #NASA TT F-13-634, National Aeronautics and Space Administration, Washington DC 20546, undated).

15. Office of Technology Assessment: SALYUT - Soviet steps towards permanent human presence in space. (OTA document #OTA-TM-STI-14, United States Government Printing Office, Washington DC 20402, Dec 1983).

## PW SPECIFICATIONS

NASA PW Specifications. NASA's PW specifications (APPENDIX A) were initially formalized during Apollo for the testing and certification of GSW (1). They were later used for testing and evaluation of pre- and post-flight PW samples, and were revised in 1970 and again in 1971 primarily to incorporate a more testable definition of microbial sterility. They do not specifically address reclaimed or recycled water (2,3).

The United States primary and secondary drinking water standards (DWS) as amended, and the National Academy of Sciences water quality standards for manned space missions recommendations (WQS) served as major source-documents in development of these specifications (4,5,6,7). As such, the present NASA PW specifications reflect assumptions inherent to the source-documents, namely:

- 1-Humans are the PW consumers,
- 2-Spacecraft PW systems are similar to public PW systems, and
- 3-Other exposure(s) are known or insignificant.

The DWS and WQS addressed substances associated with human disease (4,5,6,7). PW engineered for human consumption may be similar to, different from or incompatible with other lifeforms (e.g. animals, plants, bacteria). If the lifeforms are spacecraft cohabitants, the ecological milieu will undergo change until an ecological equilibrium is established. The resulting equilibrium may favor the human crew, cohabitant lifeforms, or other lifeforms as they are introduced. If cohabitant lifeforms are participants in metabolic, medical or ecological research studies, the studies will be significantly but insidiously affected.

DWS and WQS defined human exposure whenever possible in terms of maximum

allowable concentrations (MAC) (4,5,6,7). MACs are based on an "average," terrestrial PW consumption of less than 2 liters per person per day. Consumption of more than this amount by astronauts especially during vigorous activity, will result in substantially increased exposures.

MAC's do not apply well to situations where cohabitant lifeforms are involved in a food chain. For instance, if a plant preferentially bioaccumulates a particular substance, even though the substance might be present in PW in concentrations well below the MAC, an astronaut consuming the plant would experience an increased and otherwise difficult to explain exposure to the substance.

DWS and WQS did not address minimum necessary concentrations (MNC), or optimal concentrations (MOC) associated with health. MNC and MOC are of critical importance in maximizing yield and quality whenever animals are raised or plants cultivated for consumption or commercial use.

DWS and DQS organoleptic data are based on rudimentary studies of substances which when present in PW will make it unpalatable. They do not address organoleptic substances which may make PW preferential. Such criteria will, however, determine the form and method of total water ingestion.

DWS and WQS are directed at substances commonly found in terrestrial surface water (4,5). GSW, inflight-generated and reclaimed spacecraft PW is considerably different in physical, chemical, microbiological and radiological makeup than surface waters. Some substances common to terrestrial, surface water will not be present at all in spacecraft PW water. Negative results of tests for such substances may inappropriately infer purity. Spacecraft PW will, however, contain a variety of unique substances, determined to large extent by the materials used in construction of the spacecraft and PW system, the route(s) and mode(s) of introduction into the PW system, and interaction

with environmental reservoirs (sinks) present in the ecological system. If the water is recycled, these substances (which may or may not have been present in GSW or inflight-generated water) will slowly increase in concentration until a new chemical ecological equilibrium is attained.

Spacecraft PW systems are similar to terrestrial, public PW systems in that both involve primary water treatment, disinfection, temporary storage, and distribution (4,5,8). However, because of weight, size and independence restrictions, unique technologies are used in space applications; system byproduct, wear-and-tear and component-failure contaminants will contribute significantly to the water.

DWS and WQS are based on the assumption that the non-PW sources of human exposure (e.g. food, air) are insignificant or quantifiable (5). Average human exposures from substances found in both food and water, for example, were generated from US Food and Drug Agency data on the composition and use of common, public consumables (5). Exposures from substances found in air were similarly derived from urban, ambient air pollution information prepared by the National Academy of Sciences for the US Environmental Protection Agency (8). These resource data are not directed at a spacecraft environment and do not incorporate even terrestrial indoor or occupational exposure data, applicable to a permanently-manned, commercial/industrial spacestation.

The National Academy of Sciences (NAS) recently completed a monograph on quality criteria for water reuse. In it they question several additional assumptions including:

- Total organic carbon as an indicator of organic chemical toxicity,
- Coliforms as indicators of microbial contamination, and
- Applicability of fill-and-draw criteria to reclaimed PW.

NAS quality criteria for water reuse have not been incorporated into current

NASA PW Specifications (9).

Soviet PW Specifications. The Soviet All-Union State Standards (GOST) have been repeatedly applied to reclaimed/recycled PW without substantive change. They do not, however, address or apply to such. GOST are similar to US primary and secondary drinking water standards, and incorporate the same basic assumptions discussed above (10).

Summary. Present NASA PW Specifications are based on data originally compiled for terrestrial applications. These data have marginal applicability to a spacecraft environment. They do not address recycle systems, but do incorporate assumptions in conflict with recycle systems and applications of the proposed spacestation.

- 
1. Biomedical Research Office: Potable water specification. Document #MSC-PF-SPEC-1, National Aeronautics and Space Administration, Johnson Space Center, Houston, TX 77058, May 17, 1968.
  2. Biomedical Research Branch: Water, potable, specifications for. (NASA document #JSC-SPEC-SD-W-0020, National Aeronautics and Space Administration, Johnson Space Center, Houston, TX 77058, May 16, 1970).
  3. Biomedical Research Branch: CSM/LM/OWS potable water specification & test procedures. (NASA document #PF-SPEC-1-REV D, National Aeronautics and Space Administration, Johnson Space Center, Houston, TX 77058, July 1971).



4. United States Public Health Service: Public Health Service Drinking Water Standards. (USPHS Document #956, United States Government Printing Office, Washington DC 20402, 1962).
5. Safe Drinking Water Committee: Drinking Water and Health. (Printing and Publishing Office, National Academy of Science, 2102 Constitution Ave, Washington DC 20418, 1984).
6. Space Science Board: Report of the ad hoc panel on water quality standards for long-duration manned space missions. (Printing and Publishing Office, National Academy of Science, 2102 Constitution Ave, Washington DC 20418, Sept 1967).
7. Committee on Toxicology: Report of the panel on potable water quality in manned spacecraft. (Printing and Publishing Office, National Academy of Science, 2102 Constitution Ave, Washington DC 20418, Aug 1972).
8. Committee on Medical and Biological Effects of Environmental Pollutants: Medical and Biological Effects of Environmental Pollutants (Series). (Printing and Publishing Office, National Academy of Science, 2102 Constitution Ave, Washington DC 20418, 1966 - 1978).
9. Panel on Quality Criteria for Water Reuse: Quality Criteria for Water Reuse. (Printing and Publishing Office, National Academy of Science, 2102 Constitution Ave, Washington DC 20418, 1982).
10. Siniak YY and Chizhov SV: Regeneration of water in the spaceship cabin.

Prob Space Biol 3:104, date unknown.

## PW RECLAMATION/RECYCLING TECHNOLOGY

Water may be used once and disposed of, reused without reprocessing, or reprocessed and reused (reclaimed). Reclaimed water may be used for the same purpose for which it was previously used (e.g. used washwater reclaimed to washwater for reuse), or for different purposes (e.g. used washwater to PW). Water reprocessed and reused for the same purpose is termed recycled. To some extent the concept of recycling depends on perspective. For example, urine which is reprocessed and reused as PW could be called recycled if one considers that urine is only an intermediate step in the PW cycle (PW to urine to PW). For this reason, it is probably better to specify the immediate influent and effluent of a particular water processing system, and then categorize it as a reclamation or recycling system in the broader context. In addition, recycled water systems may be configured to diminish or entirely eliminate the need for outside resupply. A recycled water system which entirely eliminates the need for outside resupply is called a closed-loop system. The US and USSR have yet to demonstrate a spaceflight-tested, reclaimed, recycled or closed-loop PW system.

NASA Technology. Several PW reclamation systems are being ground-tested by NASA for possible use on the spacestation:

- 1-Air evaporation wick (WICK) PW system,
- 2-Vapor compression distillation (VCDS) system, and
- 3-Thermal, integrated, membrane-evaporative (TIMES) system.

WICK is the oldest, best described and most thoroughly tested PW system. Used water is stabilized and fed into an array of solid or molecular-sieve wicks. Water vapor is captured by air passed over the wicks, condensed,

disinfected, filtered and polished for reuse. The wicks require either regular replacement or servicing. Mixed urine/humidity condensate to PW recycling, and used washwater to washwater recycling have been tested in partially-closed 60 and 90 day manned ground-tests (1,2).

Presently, a third-generation, advanced VCDS preprototype (VCD2A) is undergoing testing. Used water is stabilized and boiled under high pressure on the inside of a rotating drum. Water vapor is condensed under low pressure on the outside of the drum, filtered, polished and disinfected for reuse. The residual sludge is collected and reintroduced into the influent (concentrator loop) for increased system efficiency. The drum and housing require regular servicing. Urine to PW recycling has been demonstrated and tested to some extent; used washwater to PW reclamation is being considered (2,3).

A TIMES prototype is also undergoing testing, primarily for urine to PW reclamation. The urine is stabilized, pasteurized in the hot side of a heat exchanger, and fed into a bundle of tiny, hollow, tubular membrane filters. Low pressure is maintained outside of the filters, causing low temperature vaporization and migration of the water vapor across the membranes. The water vapor is fed through and condenses on a chilled, porous plate on the cold side of the heat exchanger. Liquid water is filtered, polished and disinfected for reuse. Residual sludge is collected and reintroduced using a concentrator loop. The membranes require regular replacement or servicing (4,5).

NASA has recently announced plans for a partially-closed, unmanned 15 to 30-day test of an integrated air and water reclamation system based on the VCDS preprototype. 30 and 90-day manned, closed-loop testing is tentatively scheduled for 1988 (6).

Soviet Technology. Soviet PW reclamation/recycling technology is not well

described in the literature. It is possible that a humidity condensate and/or urine to PW reclamation system may have been tested on Salyut. If so, it is likely that it would represent a partially-closed system, as PW is regularly resupplied to the spacecraft (7). A 1-year, manned, closed-loop life support system incorporating humidity condensate/urine to PW recycling has been reported. Further details, however, are lacking (8).

Freeze-drying, vacuum distillation, lyophilization and catalytic processes have been reportedly used for urine to PW reclamation and mixed humidity condensate/urine/washwater to PW recycling. In the lyophilization process, urine is subjected to low pressure in the presence of heat. Water vapor is condensed, filtered and polished. Descriptions of the freeze-dry, vacuum distillation and catalytic processes were not available to the author at the time of this report (9,10).

The Soviets have reported spaceflight-testing of a humidity condensate/used washwater to washwater recycling system on Salyut (7). In addition, they claim to have spaceflight-tested various partially-closed, unmanned, "higher lifeform habitats" (11).

Experimentation with long-duration (up to 1 year), manned, closed-loop hermetically-sealed "habitats" including other higher lifeforms have been conducted (BIOS 1-3) (11).

Other Technologies. The US Environmental Protection Agency has expressed interest in developing and testing PW reclamation systems for public use. However, no reports of such were found in the literature at the time of this paper (12).

The US Department of Defense (DOD) has also indicated interest in reclaimed PW systems for possible use at advanced, remote military sites (US

Army) and for desalinization (US Navy). No reports of such were found in the literature at the time of this paper, however (12).

Various other PW reclamation/recycling analogs exist. The US Center for Disease Control and state public health departments have had extensive experience with recycled swimming pool and hydro-therapy water. Numerous reports in the medical literature have been directed at recycled humidifier condensate.

Summary. Water reclamation and recycle technology is uncommon, largely experimental, and poorly developed especially with regard to PW systems. PW reclamation and recycle preprototypes are under evaluation at NASA, and probably within the USSR. Efforts, however, are mainly directed towards developing water reclamation concepts in general. Some analogs to PW reclamation systems exist within the public and private sectors which may provide additional information useful in determining reclaimed PW specifications.

-----

1. McDonnell Douglas Astronautics Company: 60-day manned test of a regenerative life support system with oxygen and water recovery. MD document #CR-98500 available from R. L. Sauer, Biomedical Research Branch (Code SD 3), NASA/Johnson Space Center, Houston, TX 77058, Dec 1968).

2. McDonnell Douglas Astronautics Company: Test report - Test results - Operational ninety-day manned test of a regenerative life support system. MD document #CR-111881 available from R. L. Sauer, Biomedical Research Branch

(Code SD 3), NASA/Johnson Space Center, Houston, TX 77058, Sept 1970).

3. Zdankiewicz EM and Schubert FH: Development of an advanced preprototype vapor compression distillation subsystem (VCDS) for water recovery. Life Sciences Inc document #LSI-TR-471-4 available from R. L. Sauer, Biomedical Research Branch (Code SD 3), NASA/Johnson Space Center, Houston, TX 77058, undated.

4. Hamilton Standard/United Technologies: Untitled, unnumbered report available from T. Naglak, Crew Systems Division (Code S ), NASA/Johnson Space Center, Houston, TX 77058, undated.

5. Roebelen GJ and Lysaght MJ: Hollow fiber membrane systems for advanced life support. Document #SVHSER 7100 available from R. L. Sauer, Biomedical Research Branch (Code SD 3), NASA/Johnson Space Center, Houston, TX 77058, Oct 1976.

6. Behrends A, personal communication 30 July 85. Crew Systems Division, Engineering Directorate, National Aeronautics and Space Administration, Johnson Space Center, Houston, TX 77058.

7. Office of Technology Assessment: SALYUT - Soviet Steps towards Permanent Human Presence in Space. Op Cit.

8. Radchenko N: Water supply of cosmonauts. Op Cit.

9. Siniak YY and Chizhov SV: Regeneration of water in a spacecraft cabin.

Op Cit.

10. Moiseyev AA et al: Water supply for the crew during spaceflights. Prob Space Biol 7: 362, May 1969.
11. Lissovskiy GM (Ed): Zamknutaya Sistema: Chelovek - Vysshee Rastenye (translation: Closed Systems: Man - Higher Plants). (Nauka, Novosibirsk, USSR, 1979). Translation in progress by Timacheff, Biomedical Research Branch (Code SD 3), NASA/Johnson Space Center, Houston, TX 77058.
12. Flory DS and Weir FW: Development of reclaimed potable water quality criteria. NASA document #NAS9-15368, National Aeronautics and Space Administration, Johnson Space Center, Houston, TX 77058, Dec 1978.



## EXPERIENCE RELEVANT TO RECLAIMED/RECYCLED PW

NASA Flight Experience. During Gemini, it was found that bacteria could often be cultured from GSW meeting NASA PW Specifications. Bacteria could persist and in some instances multiply apparently irrespective of prechlorination even during short-duration missions. Bacteria identified were non-coliforms except during Gemini 11 where it was concluded that fecal contamination via spacesuit condensate had been introduced into the PW system (1).

The Apollo CM/SM experienced problems with PW production (fuel cell failure), inflight chlorination, gas bubble formation and PW palatability. Of the inorganic chemicals specified in the NASA PW Specifications, nickel, cadmium, aluminum and manganese were present in excessive levels. Approximately 150 organic compounds were detected in inflight "grab" air samples from Apollo 7-17 spacecrafts but corresponding PW samples were not obtained. Pre and post-flight bacterial cultures were frequently positive. Flavobacterium and Pseudomonas, both conditional human pathogens, were most commonly identified. No coliforms were cultured. The highest plate counts and greatest number of positive cultures were consistently obtained from the crew hot-water dispenser. Postflight PW bacterial species did not correspond well with those found on crew skin, mucous membranes, clothing or spacecraft environmental surfaces (2,3,4).

The Apollo LM experienced gas bubble formation and increased nickel levels. No bacterial contamination problems were identified. It was concluded that iodine disinfection as used in the LM was superior to chlorination (2,3,4).

On Skylab, over 300 low molecular weight organic compounds were detected in inflight air samples. Again, corresponding PW sampling was not done. OWS

PW data further supported the use of iodine as a disinfectant. As long as effective iodine residuals were maintained, PW inorganic and bacterial contaminants were maintained within NASA PW specifications (2,3,5,6).

On shuttle flight STS-8, an experiment suffered contamination by Pseudomas and Flavobacterium in spite of extensive preflight sterilization precautions. Combined shuttle data are presently under evaluation (7,8,9).

Soviet Flight Experience. Information on Soviet spacecraft PW quality was not available to the author at the time of this report. Unsubstantiated reports within NASA suggested that Salyut has experienced repeated problems with fecal coliform contamination.

Other NASA Experience. NASA's experience with PW reclamation systems is limited to experimental, ground-based systems. In the McDonnell Douglas 60-day, 3-man test of the WICK system, mixed humidity condensate/urine was reclaimed to PW and recycled. Bacterial movement of a "gram negative rod of the Achromobacter group" was noted to occur starting at a filtration devise and eventually contaminating the entire distribution system forcing a temporary system shutdown approximately mid-test (10). Similar problems were experienced during the 90-day, 4-man test of WICK/VCD systems on about the 30th and 60th days. The offending organism(s) in these instances were not reported. In addition, a gradual rise in PW conductivity, total organic carbon and ammonia were reported starting at about the 30th day and continuing until system shutdown (11). Data from 1200 hours of non-continuous operation of the VCD1 system, where urine was reclaimed to PW but was not recycled, suggested similar problems. A variety of non-coliform bacteria were isolated; Flavobacterium and Pseudomonas species predominated. Fungal cultures revealed

Aspergillus, Cephalosporium, and Candida species (12,13). Ten and 30-day non-continuous operation of the advanced VCD2 preprototype system, where urine was reclaimed to PW but not recycled, showed similar problems (13). Over 100 low molecular weight organics (incl. halobenzenes and nitrobenzenes) have been detected in TIMES and VCDS effluent reclaimed from batches of mixed human urine. About 25% of these compounds were also reported in shuttle air samples; 30% were reported present in atmospheric condensate samples from shuttle flight STS-9. TIMES and VCDS tests did not include human recycling. Data on urine organic composition was not reported (13).

Other Soviet Experience. Soviet experience with PW reclamation systems appears limited to experimental, ground-based systems. A 3-month, rat test and a 30-day, 3-man test of a "catalytic method" was described. In each case mixed humidity condensate/urine/washwater was reclaimed to PW and recycled. PW was reported to meet select physical/chemical Soviet All Union State (GOSH) Standards and several NASA PW specifications. "Clinical and physiologic" tests performed revealed "no pathological changes or manifestations of toxicoses." PW organoleptic properties were judged to be poor and salt was added "with the aim of giving it the customary taste properties" (14).

Public experience. Public PW reclamation experience is largely based on systems which reclaim mixed fecal/urine/washwater/industrial/commercial water to effluent meeting secondary or tertiary EPA standards which is subsequently diluted, percolated into soils, or injected into groundwater aquifers. These systems, therefore, more accurately represent pass-through systems with partial, indirect recycle. Examined together with other public pass-through systems, a number of observations are, however, relevant.

Inorganic chemicals found in undiluted effluent are related primarily to the chemical composition of the influent. Inorganics from the wear-and-tear of system components are of importance in recycling systems. While the types of inorganics are determined by influent and processing system materials composition, the concentrations of the specific inorganics are related more to the particular reclamation process employed. Inorganic contaminants exert a strong influence on the types and numbers of microorganisms, their virulence, resistance and byproduct (e.g. exotoxin, aflatoxin) production. Corrosion appears to play an increasingly important role as a particular system ages. Corrosion selectively consumes (sink) and releases inorganic chemicals. It can afford bacteria a convenient surface on which to multiply, the trace inorganics necessary for their multiplication, and protection from disinfectants. Bacteria embedded within a slime-corrosion coat may be undetectable by routine plate counts, but may be infective after passing through an acid solution, such as gastric acid. Inorganics are often removed from primary effluents by adsorption onto granular activated carbon (GAC) filters or ion-exchange resins. It appears that inorganics may be adsorbed, concentrated on and selectively desorbed in pulses from GAC filters. Hence, consumers of GAC filtered PW may periodically receive slugs of contaminants due to selective desorption which might not be detected in periodic PW samples. The methodology for identification and quantification of inorganics is well defined, although realtime monitoring devices are only now being developed (15-17).

The types and concentrations of organic chemicals in PW are similarly determined, except that in addition they may be associated with water-soluble organics adsorbed onto atmospheric particulates, in atmospheric humidity condensate and gas (e.g. smoking). They are strongly affected by the

particular biological participants within a recycle system. Biological organisms are efficient, selective sinks and producers of organic chemicals. Organics can exert a profound effect on all or selective lifeforms. This is especially true if a food chain is involved. When passed through a GAC filter, organics are probably subject to the same pulsing phenomenon as are inorganics. Interactions on the surface of the granulated carbon particles with other inorganics, human organic byproducts, bacteria, bacterial byproducts, viruses, fungi and fungal byproducts greatly complicate this situation however. Identification and quantification of biochemical compounds is still largely experimental; sampling technology may be the biggest problem at present (15-18).

Organolepsis and the characterization of organoleptic properties of PW are both highly experimental. Organoleptic properties, however, will determine the particular ways that PW will be consumed (e.g. drinking water, juice, food) and ultimately affect total human exposures (19,20,21).

Recent epidemiologic evidence suggests that public outbreaks of waterborne diseases are increasing in frequency. Standard tests for bacteria have identified an etiologic organism in less than 5% of outbreaks. Up to 60% of outbreaks have occurred in the presence of repeated, negative bacterial tests. There is some evidence that encysted or spore-forming protozoa, bacteria and fungi may be favored in reclamation/recycle systems. Coliform tests are and will continue to be of use in detecting heavy sewerage contamination in the presence of inadequate disinfection. However, it is likely that, in the absence of a fecal contamination event, "environmental" bacteria such as Pseudomonas, Flavobacteria, Legionella, Proteus or Serratia will pose the greatest bacteriological challenge to PW recycle systems. Standard plate counts consistently underestimate these particular bacteria

(22-25).

Pseudomonas is a ubiquitous and hardy organism which has been identified as a contaminant in "sterile" distilled water, chlorinated swimming pools and whirlpools, faucets, public PW stores, space experiments and spacecraft PW supplies. Different species are associated with a wide variety of human, animal and plant diseases, including urinary tract infection in a US astronaut (26,27,28).

Flavobacteria have been cultured from distilled water, distilled water lines, drinking fountains, faucets and humidifier water. They are sensitive to heat. Flavobacteria have been implicated in hospital deaths (29).

During outbreaks, Legionella have been associated with cooling tower water, evaporative cooler water, evaporative condenser condensates, hot water tanks and public PW supplies. Legionella have not been cultured from spacecraft PW supplies or during PW reclamation system ground-tests. They have, however, been demonstrated to grow in nutritionally deficient media in the presence of Flavobacteria and may prove to be a commensal or secondary invader of clinical significance in PW recycling systems (30,31).

Environmental bacteria such as those mentioned above have been shown to grow, multiply and spread in plastic, corrosion tubercles, corrosion pits, PW pipe coatings, granular activated charcoal (GAC) filters and ion exchange resins. GAC filter devices may act much like biological trickle filter beds in providing a medium onto which such bacteria can attach. Adsorbed inorganic/organic chemicals provide nutritent. Slime coats and multiple layers of bacteria can provide protection from disinfectants. A contaminated GAC may serve as an area for virulence (V) and/or resistance (R) plasmid selection and transmission. Seeding of a recycle system would proceed from this site and could rapidly result in system overgrowth (32-35).

Most environmental bacteria produce metabolic byproducts which are offensive, irritating, toxic or mutagenic to humans, animals or plants. It is likely that PW recycle systems will selectively concentrate specific endotoxins, exotoxins and other pyrogens depending on the physiochemical characteristics of the byproducts and the particular treatment method employed (36).

It has been said that viruses are almost entirely person-to-person fomite spread. However, if relatively small quantities of virus are being ingested by relatively small numbers of people on a daily basis, this would result in an epidemiological picture consistent with person-to-person spread. In fact, waterborne transmission has been demonstrated for hepatitis A, polio and several viral gastroenteritidities. No public or spacecraft PW standards exist for viruses. It is generally assumed that if coliforms are absent, so are pathological viruses. However, infective viruses have been recovered from public PW treatment plants in the presence of negative coliform and plate counts, and in groundwater which has received reclaimed PW. Active poliovirus has been recorded in public PW treatment plant effluent to increase 24-fold following community-wide Sabin poliovirus immunization. Animal tumor and plant disease viruses have been isolated from public PW treatment plant effluents. Friend Disease virus, a reticulum cell leukemia virus similar in many respects to the Acquired Immune Deficiency Syndrome virus, has been transmitted to mice via PW. Many viruses are shed primarily in feces. Some viruses, like cytomegalovirus, are shed in large quantities in human urine. Viruses may serve as V or R plasmid carriers. In addition, viruses are capable of concentrating and surviving on GAC filters, electropositive filters and ion exchange resins. Such devices may serve as sites for viral seeding within a recycle system (37,38).

Cephalosporium fungi are ubiquitous, hardy and some species are capable of producing potent exotoxins and endotoxins. Some Aspergillus species, in addition, may produce aflatoxins, extremely potent human carcinogens. Various Candida fungi produce metabolic byproducts which have been shown to stimulate co-bacterial infection and enhance the effects of bacterial toxins. Fungal metabolic byproducts, like bacterial byproducts, can be selectively concentrated within a recycle system depending on the characteristics of the byproduct and the particular reclamation process utilized (39,40).

The mechanisms of action, sinks and chemical properties of the disinfectant iodine are only poorly understood. Pseudomonas has been cultured in iodine bactericide ampules. Little is known about iodine's interreaction with residual organics and resultant trihalomethanes. Trihalomethanes may be carcinogenic to man. The effect of residual iodine on human and animal metabolism is only partially known (41,42,43).

Summary. World experience with reclaimed PW is extremely limited. NASA expertise is restricted to uncontrolled engineering tests of preprototype hardware. Organic chemical and microbacteriological quality specifications and testing procedures are of greatest concern as these have already been shown to be insufficient or inappropriate.

-----

1. Gemini water reports (Gemini 2-12). Unpublished reports available from R. L. Sauer, Biomedical Research Section (Code SC 3), NASA/Johnson Space Center, Houston, TX 77058, undated.



2. Apollo water reports (Apollo 1-17 and ASTP). Unpublished reports available from R. L. Sauer, Biomedical Research Section (Code SD 3), NASA/Johnson Space Center, Houston, TX 77058, undated.
3. Johnston KS, Dietlein FL and Berry CA: Biomedical Results of Apollo. Op Cit.
4. Leslie SA and Sauer RL: ASTP manned space flight chemical and microbiological analyses of potable water. NASA document #DE-ASTP-047, available from R. L. Sauer, Biomedical Research Section (Code SD 3), NASA/Johnson Space Center, Houston, TX 77058, undated.
5. Skylab water reports (Skylab 1-4 and Apollo 116-118). Unpublished reports available from R. L. Sauer, Biomedical Research Section (Code SC 3), NASA/Johnson Space Center, Houston, TX 77058, undated.
6. Comprehensive Skylab chemical and microbiological analysis of potable water. NASA document #SE-SL-076, National Aeronautics and Space Administration, Johnson Space Center, Houston, TX 77058, 10 June 77.
7. Perryman BT: Shuttle iodine - Microbiological results. Technology Inc internal memorandum dated 13 March 85, available from Technology Inc, 17625 El Camino Real #311, Houston, TX 77058.
8. Oral communication with Dr. Charles Willis, Technology Inc, 30 July 85.
9. Morrison DR et al: Electrophoretic separation of kidney and pituitary

cells on STS-8. Adv Space Res 4:67, 1984.

10. McDonnell Douglas Astronautics Company: 60-day manned test of a regenerative life support system with oxygen and water recovery. Op Cit.
11. McDonnell Douglas Astronautics Company: Test report - Test results - Operational ninety-day manned test of a regenerative life support system. Op Cit.
12. Vapor compression distillation (VCD1) subsystem test report (1978-1981). NASA document #JSC-17683, National Aeronautics and Space Administration, Johnson Space Center, Houston, TX 77058, 6 May 1982.
13. Zdankiewica EM and Schubert FH: Development of an advanced preprototype vapor compression distillation subsystem (VCDS) for water recovery. Op Cit.
14. Moiseyev AA et al: Water supply for the crew during spaceflights. Problems of Space Biology 7: 362, May 1969.
15. Panel on Quality Criteria for Water Reuse: Water Criteria for water reuse. Op Cit.
16. Safe Drinking Water Committee: Drinking Water and Health. Op Cit.
17. Reynolds TD: Unit Operations and Processes in Environmental Engineering. (Brooks/Cole Engineering Division, Wadsworth Inc, Belmont, CA 94002, 1982).

18. Steel EW and McGhee TJ: Water Supply and Sewerage. (McGraw-Hill Book Company, New York, New York, 1979).
19. Thacker WE, Snoeyink VL and Crittenden JC: Desorption of compounds during operation of GAC adsorption systems. JAmWWA 75:144, Mar 83.
20. El'piner LI: Physiological-hygienic evaluation of regenerated drinking water. Space Biol and Med 5:73, 1971 (translated from Russian).
21. Zoeteman BCJ, Piet GJ and Postma L: Taste as an indicator for drinking water quality. JAmWWA 72:537, Sept 80.
22. Craun GF: Outbreaks of waterborne disease in the United States 1971-1978. JAmWWA 73: 360, July 81.
23. Lippy EC and Waltrip SC: Waterborne disease outbreaks - 1946-1980 - A thirty-five-year perspective. JAmWWA 76: 60, Feb 84.
24. Stanridge JH and Delfino JJ: Underestimation of total-coliform counts by the membrane filter verification procedure. Appl Environ Microbiol 44:1001, Oct 82.
25. Space Science Board: Infectious Disease in Manned Spaceflight - Probabilities and Countermeasures. (Space Science Board, National Academy of Sciences, 2101 Constitution Ave, Washington DC 20418, 1970).
26. van der Kooij D, Oranje JP and Hijnen WAM: Growth of Pseudomonas

aeruginosa in tap water in relation to utilization of substrates at concentrations of a few micrograms per liter. Appl Environ Microbiol 44:1086, Nov 82.

27. Favero MS et al: Pseudomonas aeruginosa: Growth in distilled water from hospitals. Science 173:836, 27 Aug 71.

28. Khabbaz RF et al: Pseudomonas aeruginosa serotype 0:9 - New cause of whirlpool-associated dermatitis. Am J Med 74:73, Jan 83.

29. Herman LG and Himmelsbach CK: Detection and control of hospital sources of Flavobacteria. Hospitals 39: (page unknown), 16 June 65.

30. Dufour AP and Jakubowski W: Drinking water and Legionaire's Disease. JAmWWA 74:631, Dec 82.

31. Plouffe JF, Webster LR and Hackman G: Relationship between colonization of hospital buildings with Legionella pneumophila and hot water temperatures. Appl Environ Microbiol 46:769, Sept 83.

32. Ellgas WM and Lee R: Reservoir coatings can support bacterial growth. JAmWWA 72:693, Dec 80.

33. Allen MJ, Taylor RH and Geldreich EE: The occurrence of microorganisms in water main encrustations. JAmWWA 72:614, Nov 80.

34. Wilcox DP et al: Microbial growth associated with granular activated

carbon in a pilot water treatment facility. Appl Environ Microbiol 46:406, Aug 83.

35. Mach PA and Grimes DJ: R-plasmid transfer in a wastewater treatment plant. Appl Environ Microbiol 44:1395, Dec 82.

36. Spira WM and Fedorka-Cray PJ: Enterotoxin production by Vibrio cholerae and Vibrio mimicus grown in continuous culture with microbial recycle. Appl Environ Microbiol 46:704, Sept 83.

37. Berg G (Ed): Transmission of Viruses by the Water Route. (Interscience Publishers, New York, NY 1965).

38. Keswick BH: Survival of enteric viruses adsorbed on electropositive filters. Appl Environ Microbiol 46:501, Aug 83.

39. Wicklow DT and Shotwell OL: Intrafungal distribution of aflatoxins among conidia and sclerotia of Aspergillus flavus and Aspergillus parasiticus. Can J Microbiol 29:1, 1983.

40. Carlson E: Enhancement by Candida albicans of Staphylococcus aureus, Serratia marcescens and Streptococcus faecalis in the establishment of infection in mice. Inf Immun 39:193, Jan 83.

41. Anderson RL et al: Investigations into the survival of Pseudomonas aeruginosa in poloxamer-iodine. Appl Environ Microbiol 47:757, Apr 84.

42. Fina LR et al: Viricidal capacity of resin-triiodide demand-type disinfectant. Appl Environ Microbiol 44:1370, Dec 82.

43. Dore M et al: Reactivity of halogens with aqueous micropollutants: A mechanism for the formation of trihalomethanes. JAmWWA 74:103, Feb 82.

## SUMMARY AND RECOMMENDATIONS

Summary. Present NASA PW Specifications are inappropriate for reclaimed/recycled (RR) PW systems. Based on present NASA priorities, it seems unlikely that RR PW Specifications will be defined in time to direct spacestation ECLSS development. If this were to occur, spacestation may ultimately have to utilize ground-supplied PW, like Salyut, until RR Specifications and related engineering technology mature, or be forced to utilize first-application RR technology with its attendant risks.

Recommendations. In order to provide timely RR PW Specifications, an intensive, joint, priority effort between Johnson Space Center Engineering and Life Sciences Directorates will have to be undertaken to:

- 1-Rapidly develop a knowledge base on RR PW
- 2-Define Interim RR PW Specifications
- 3-Define and complete some basic sciences experiments
- 4-Design and implement joint tests of existing hardware
- 5-Develop and standardize RR PW testing and monitoring techniques
- 6-Plan and implement closed-loop testing of integrated ECLSS hardware

Knowledge Base. This paper was meant to serve as the basis for developing an engineering/life sciences knowledge base on PW RR technology. It should include contact information for US and foreign PW RR systems and system analogs. Requests for information will need to be made. A request to the National Academy of Sciences regarding spacecraft PW RR concerns should be considered. US Environmental Protection Agency scientists involved in public PW RR system research need to be identified. US Department of Defense

classified literature needs to be searched for information on RR PW experience with closed-environments such as submarines, missile launch facilities, hardened command facilities. A request for foreign information needs to be submitted through official channels to the US Central Intelligence Agency. National/international meetings on PW RR or RR technology need to be identified. Key research sites, groups, scientists or meetings need to be selected, visited and informed of NASA's interests. Hard-copy reference materials need to be available to NASA PW RR scientists.

Interim RR PW Specifications. A decision needs to be reached regarding who the RR PW Specifications will be developed for, i.e. humans, animals, plants. Metabolic requirements for RR PW users need to be determined and updated based on NASA spaceflight experience. Coexposures from food and air need to be recalculated based on cumulative terrestrial exposure and projected mission exposure. Mission exposures need to be calculated based on an assumed 24-hour exposure, need to include contaminants likely to occur from spacecraft and PW system construction materials, and need to reflect NASA and Soviet PW RR system prototype experience. National Academy of Sciences quality criteria for water reuse data need to be incorporated where appropriate. Preferential qualitative and quantitative PW organoleptic specifications need to be determined. A set of Interim RR PW Specifications based on recalculated MAC's (and where appropriate MNC's and MOC's) which take into account NASA PW consumption and coexposure data need to then be formalized. Specifications need to be directed at influent, effluent and/or "at the tap" testing, with special emphasis on organic, bacterial, viral and fungal contaminants. Appropriate indicators need to be identified to allow PW RR system testing and evaluation. Indicators for low molecular weight, volatile organics (which may



be "carried over" with water in the PW reclamation process), high molecular weight organics (e.g. steroids, antibiotics), inorganic/organic substances which are selectively retained in the concentrator loop (present in effluent with wear-and-tear), key bacterial contaminants (incl. Pseudomonas, and/or Flavobacterium), viruses, and fungi will need special consideration. The best bacterial and fungal indicators may be unusual metabolic byproducts. The best viral indicators may be oral vaccine viruses introduced periodically into influent.

Basic Science Experiments. Several areas of concern have been established which could be of fundamental importance to application, testing or evaluation of PW RR Specifications to spacestation:

1-Properties of liquids moving in pipes in zero-gravity (ZG)

- a) corrosion buildup
- b) particle deposition

2-Properties of ZG colloidal suspensions

- a) gas bubbles in water
- b) liquid droplets in water
- c) solid particles and aggregates in water
- d) mixed colloids interactions

3-Properties of substances adsorbed onto surfaces

- a) piping and joints
- b) GAC filters and ion-exchange resins
  - 1) pulsing phenomenon
  - 2) ZG bacterial/viral activities
  - 3) plasmid interchange

4-Properties of surfactants in ZG

Specific research experiments need to be devised and executed to elucidate the effect, if any, these particular physical properties might have on RR PW systems and quality testing.

Testing Existing Hardware. Interim PW RR Specifications need to be tested against existing system prototype hardware. Techniques for sampling, testing, quality-assurance and evaluation of PW RR Specifications and hardware operation need to be critically defined, pretested, documented and rehearsed. The system hardware will need to be examined and adapted for sampling. Whenever possible closed-system sampling methodology should be incorporated. Mechanisms for sensing, sampling and examination of components without interruption of operation need to be evaluated and incorporated into systems engineering.

Initially, unmanned PW reclamation tests need to be done on paired influent/effluent samples taken at fixed intervals during continuous system operation. Samples should be taken until influent, effluent and microbiological equilibriums are established. Similar testing will need to be begun as soon as possible for the specified life expectancy of the system. Hardware and Interim PW RR Specifications will probably need to be revised periodically throughout this phase to reflect experience with actual PW RR hardware.

Unmanned PW reclamation tests need to be performed challenging prototype system hardware with specific substances which have been identified to be of special concern. Sterile distilled water (or other appropriate negative controls) will probably need to be used for comparison purposes. Challenge substances could include:

- 1-Concentrator loop water

- 2-Particulate colloidal solutions
- 3-Solvents which will probably be used on spacestation
- 4-Organics which tend to volatilize like water
- 5-Human steroids (e.g. premarin)
- 6-Antibiotics commonly excreted in urine (e.g. ampicillin)
- 7-Atmosphere humidity condensate
- 8-Spacesuit coolant concentrate
- 9-Spacesuit humidity condensate
- 10-Washwater
- 11-Spacecraft wastewater
- 12-Lactobacillus or E. coli bacteria
- 13-Pseudomonas bacteria
- 14-Sabin oral poliovirus (vaccine)
- 15-Aspergillus fungi
- 16-Endotoxin/exotoxin analogs.

During this period, bioaccumulator plants which preferentially bioaccumulate substances of concern should be identified.

Testing and Monitoring. As open-loop testing nears completion, testing methodologies need to be revised for micromputerized, online, realtime monitoring whenever possible. Prototype systems may need to be reengineered to accommodate monitoring.

Unmanned, closed-loop, integrated ECLSS system recycle tests using animals, bioaccumulator plants and plants which may be cultivated for human consumption on spacestation need to be conducted. Atmospheric contamination tracer tests will need to be considered if humidity condensate to PW reclamation is to be considered. Testing should be done in situ and should

allow parallel evaluation of monitoring techniques. These tests will need to be run continuously until system equilibrium is reached. Test animals, test plants, cultivated plants, and effluent equilibrium concentrates will need to be subjected to standardized, toxicological testing at this point. Determination of common and biologically significant substances and the establishment of their dose-response curves will need to be accomplished to substantiate MAC's and interim PW RR Specifications. It is likely that PW RR Specifications will undergo major revision at this stage. Hardware, monitoring and testing may need corresponding revision. A reasonable list of organic substances of concern for spacecraft PW RR should result. Final PW RR Specifications will need to be promulgated. Specific plant bioaccumulators will need to be chosen to act as total accumulated exposure indicators for key substances.

Manned, Closed Testing of Integrated ECLSS System. Similar, continuous, closed-loop, integrated ECLSS system recycle tests using human test subjects and bioaccumulator test plants will need to be conducted until system equilibrium, and should be considered for the duration of likely exposure on spacestation. Select biomedical tests including enzyme-activity assays for key organ systems (e.g. fat, muscle, bone, liver), hair, nail and other analyses need to be correlated with bioaccumulator plant results.

SUPERSEDES MSC-SPEC-C21A DATED JUNE 19, 1967

MANNED SPACECRAFT CENTER  
NATIONAL AERONAUTICS AND SPACE ADMINISTRATION

This specification has been approved by MSC for use by MSC Contractors, MSC, and other Centers, as appropriate, involved in manned spacecraft design, testing and operations at Contractor sites, KSC, and MSC utilizing potable water.

## 1.0 SCOPE

This specification establishes the requirements for water used in servicing potable water systems, generated on-board spacecraft, and obtained from spacecraft water reclamation systems.

## 2.0 APPLICABLE DOCUMENTS

The following documents form a part of this specification to the extent indicated herein. In case of conflict between these documents (latest revisions) and this specification, this specification shall prevail:

### STANDARDS

#### Manned Spacecraft Center

MSC-STD-C-1

Definitions for Contamination Programs

#### Non-Governmental

##### Society of Automotive Engineers

SAE-ARP 598

Procedures for Determination of Particulate Contamination of Hydraulic Fluids by the Particulate Count Method

##### American Society for Testing and Materials

ASTM D 1293-65

Methods of Test for pH of Industrial Water and Industrial Wastewater

ASTM D 1888-67

Tentative Methods of Test for Suspended and Dissolved Solids in Industrial Water

ASTM D 1889-66

Tentative Methods of Test for Turbidity of Industrial Water

American Public Health AssociationAmerican Water Works AssociationWater Pollution Control Federation

Standards Methods for the Examination of Water and Wastewater  
N. Y., 12th Edition, 1965.

### 3.0 DEFINITION

MSC-STD-C-1 lists definitions used in the MSC Contamination Program. In case of conflicts, the MSC-STD-C-1 definitions will govern in this specification unless otherwise noted. The following definition is included to clarify this specification:

Microorganism - An organism of microscopic size, limited to bacteria, fungi, including molds and yeasts and algae and protozoa, either active or dormant.

### 4.0 REQUIREMENTS

#### 4.1 Water Properties

The potable water shall meet the following specific requirements:

Properties	Limits:	
	Maximum Allowable Concentrations	Test Para.
pH	6.0-8.0 at 25°C (77°F)	4.3.1.1
Total Solids	TBD but <500 mg/liter	4.3.1.2
Total Organics	TBD	4.3.1.3
Taste & Odor	None at Threshold (Odor No. of 3)	4.3.1.4
Turbidity	11 Units	4.3.1.5
Color, True	15 Units	4.3.1.6
Particulate	TBD	4.3.1.7

#### Ionic Species

Cadmium	0.01 mg/liter
Chromium (Hexavalent)	0.05 mg/liter
Copper	1.0 mg/liter
Iron	0.3 mg/liter
Lead	0.05 mg/liter
Manganese	0.05 mg/liter
Mercury	0.005 mg/liter
Nickel	0.05 mg/liter
Silver	0.05 mg/liter
Zinc	5.0 mg/liter
Selenium	0.01 mg/liter

## Microbial Control

Positive microbial control is required throughout the potable water system. The agent or mechanism of this control shall be determined by system requirements and shall require the approval of the MSC Medical Research and Operations Directorate.

### Sterility

Free of viable organisms 4.3.2  
(as defined in paragraph 3.0)

Note: Specific system designs may necessitate the inclusion of other water property requirements in the above listing.

## 4.2 Sampling

### 4.2.1 Containers for Samples

The water samples for analysis shall be collected in containers approved by the MSC Medical Research and Operations Directorate. The collection containers shall be chemically inert and nonbreakable and shall be prepared according to instructions supplied by MSC.

### 4.2.2 Sampling Technique

Standard aseptic technique will be used in collecting water samples for analysis.

## 4.3 Analyses

Analysis of the water shall conform to established laboratory methods and shall be performed by a laboratory approved by the Medical Research and Operations Directorate.

### 4.3.1 Chemical and Physical Analyses

#### 4.3.1.1 pH

The pH shall be determined per ASTM D 1293, taking special precautions to exclude the atmosphere during test. On line on-site analysis shall be performed where possible.

#### 4.3.1.2 Total Solids

Total solids shall be determined by a gravimetric technique. The maximum allowable concentration will be established by system operational requirements yet must not exceed 500 mg/l.

#### 4.3.1.3 Total Organics (COD, BOD, TOC)

Total organics shall be determined by standard laboratory technique. The maximum allowable concentration will be established by specific system requirements, yet shall not exceed 100 mg/l.

#### 4.3.1.4 Taste and Odor

Taste and odor shall be determined per the method described on page 304 of Standard Methods for the Examination of Water and Wastewater, (12th Edition).

#### 4.3.1.5 Turbidity

Turbidity shall be determined using the nephelometric turbidity procedure described in ASTM D 1889.

#### 4.3.1.6 Color

Color shall be determined using the method described in paragraph 1.4 on page 127 of Standard Methods for the Examination of Water and Wastewater.

#### 4.3.1.7 Particulate

The particulate levels shall be determined by standard particle count methods. The maximum allowable concentration will be established by individual system operational requirements.

### 4.3.2 Sterility/Microbiological Analyses

If samples for microbiological analyses are not processed within 30 minutes following collection, the samples must be refrigerated at 4° - 6°C. If the water contains chlorine or iodine, a sufficient amount of 0.1% solution of sterile sodium thiosulfate is added to the sample container to result in a concentration of 100 mg/liter of the sodium thiosulfate.

General: Aseptic technique within a Class 100 clean bench or equivalent will be employed throughout the analyses. Any organisms cultured at KSC in the following analyses will be shipped to MSC in biological shipping containers for identification.

#### 4.3.2.1 Aerobic Analysis

The three 150 ml aliquots for the following microbiological analyses shall be obtained from a 500 ml minimum volume microbiological sample. Each aliquot shall be passed through a 35 mm 0.45 micron membrane filter, Millipore HAWG (for yeast and molds) or equivalent.

##### 4.3.2.1.1 Total Bacterial Count

Total bacteria count shall be performed according to procedures described in Standard Methods for the Examination of Water and Wastewater, N.Y., 12th



#### 4.3.2.1.1 Total Bacterial Count (continued)

Edition, 1965, and/or by the following membrane filter method: Filter, aseptically 150 ml of the water sample through a membrane filter monitor. Remove excess water from the membrane filter monitor using a syringe and extracting the water from the discharge end of the monitor. Disconnect the syringe and add 0.8 ml of M-TGE Broth (Difco or equivalent) into the discharge end of the monitor. Replace monitor plugs, invert, and incubate at  $350 \pm 0.50^{\circ}\text{C}$ . (Membrane filters should always be incubated in 100% humidity). Count total number of bacteria on pad at 24 and 48 hours. Report out as the number of colonies per 150 ml of water. Serial dilutions of a minimum of 1:100 and 1:10,000 will be conducted in addition to the zero dilution above. If growth is observed, the sealed monitor will be shipped to MSC.

#### 4.3.2.1.2 Coliform Counts

Coliform counts shall be performed according to procedures outlined in Standard Methods for the Examination of Water and Wastewater, N.Y., 12th Edition, 1965, and/or by the following membrane filter method: Filter, aseptically, 150 ml from the sample container through the membrane filter monitor. Remove excess water from membrane filter monitor using a syringe and extracting the water from the discharge end of the monitor. Disconnect the syringe and add 0.8 ml of M-F Endo Broth into the discharge end of the monitor. Replace monitor plugs, invert, and incubate at  $350 \pm 0.50^{\circ}\text{C}$ . Count total number of coliform colonies at 18 to 24 hours and report out as the number of colonies per 150 ml of water. If growth is observed, the sealed monitor will be shipped to MSC.

#### 4.3.2.1.3 Yeast and Mold

Filter, aseptically, 150 ml from the sample container through the membrane filter monitor with black filter (Millipore MHBG or equivalent). Remove excess water from the membrane filter monitor using a syringe and extracting the water from the discharge end of the monitor. Disconnect the syringe and add 0.8 ml of M-Green Yeast and Mold (Difco or equivalent) into the discharge end of the monitor. Replace monitor plugs, invert, and incubate at  $300 \pm 10^{\circ}\text{C}$  for 48 hours. Count and report number of yeasts and molds per 150 ml of water sample. Cultures will be transferred to Sabouraud agar slants prior to shipment to MSC.

#### 4.3.2.2 Anaerobic Analysis

An anaerobic analysis will be conducted by transferring, aseptically, 1 ml of water into a tube of fluid thioglycollate medium which has been freshly prepared. Do not mix. Incubate at  $35^{\circ} \pm 0.5^{\circ}\text{C}$  for 48 hours. Examine for growth. Report growth as positive or negative growth. If any growth is observed, a portion of the growth will be transferred with a sterile loop to a tube of transport medium (Stuart or equivalent) and incubated for at least 12 hours prior to shipping to MSC.

- 4.4 If the ground test or flight mission purpose does not involve verification of acceptance for human consumption or will not be used for human consumption, the water need not meet the requirements of paragraph 4.1.

Notice - When Government drawings, specifications, or other data are used for any purpose other than in connection with a definitely related Government procurement operation, the United States Government thereby incurs no responsibility nor any obligation whatsoever; and the fact that the Government may have formulated, furnished, or in any way supplied the said drawings, specifications, or other data is not to be regarded by implication or otherwise as in any manner licensing the holder or any person or corporation.

Prepared by:

DC/Preventive Medicine Division.

N86 - 31423

D14  
197

REVIEW AND ANALYSIS OF HIGH TEMPERATURE CHEMICAL REACTIONS  
AND THE EFFECT OF NON-EQUILIBRIUM CONDITIONS

18825

Richard E. Johnson  
Professor of Chemistry  
LeTourneau College  
Longview, Texas

LM362800

ABSTRACT

Chemical reactions at high temperatures have been considered extensively because of their importance to the heating effects on re-entry of space vehicles. Data on these reactions however, are not abundant and even when found there are discrepancies in data collected by various investigators. In particular, data for recombination reactions are calculated from the dissociation reactions or vice versa through the equilibrium constant. This involves the use of the principle of "detailed balancing." This principle is discussed in reference to conditions where it is valid as well as to those where it is not valid. Related topics that merit further study or for which applicable information was available are briefly mentioned in an appendix to this report.

---

NASA Colleague: Carl D. Scott, Ph.D. ED331 713-483-3905

## INTRODUCTION

The re-entry of transport vehicles into upper levels of the atmosphere at high velocities results in the production of high energy shock waves. Because of the velocities involved and the low pressure of the atmosphere, there is chemical and thermodynamical nonequilibrium in the shock layer flow around the vehicle. The heating effects due to these chemical phenomena may result in an added heat load of about of 50%.<sup>1</sup> Much has been written about this effect including experimental data from some Shuttle flights and arc jet laboratory experiments.<sup>2,5</sup> There is interest in predicting heat transfer rates to future vehicles such as the AOTV where re-entry velocities are even higher and therefore these nonequilibrium effects could become even more significant.<sup>6</sup>

This study focuses on the chemical reactions and in particular the effect of nonequilibrium and the use of the principle of detailed balancing for these transient conditions. This will be approached by looking generally at thermodynamics and kinetics to see how they are applied. Then the principle of detailed balancing will be defined along with the high temperature reactions found in re-entry conditions and finally some conclusions will be drawn.

## THERMODYNAMICS AND KINETICS

These two major fields of study have provided much information about the chemistry and physics of processes and have been invaluable tools for engineers in design work. In general, thermodynamics is dealing with quantities of enthalpy, entropy, free energy and work, and is useful in measuring or predicting these quantities as they relate to the beginning and the end of a

process or reaction. As such they are generally classified as state functions in that they depend on the initial and final state of a system and not how the system moves from the initial to the final state. Also, these properties are not time dependent. Now work and heat may be path dependent, but they can be evaluated with thermodynamical relationships and are not independent of one another.

Kinetics, as its name implies, is a study of time-dependent quantities and how a system moves from one state to another. It has to do with the rate of a reaction and the mechanism or series of steps by which reactants are moved toward the desired products.

As an example consider the system of hydrogen gas, oxygen gas, and liquid water. This is represented in Figure 1.

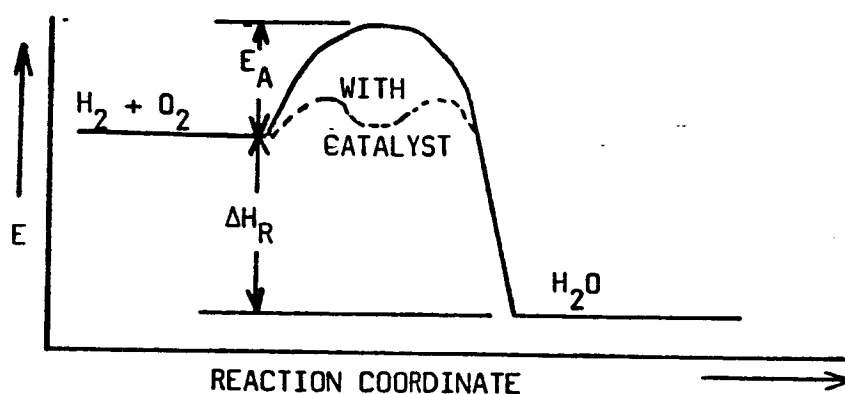


Figure 1. - Energy-Reaction Diagram for Reaction  $\text{H}_2 + \text{O}_2 \longrightarrow \text{H}_2\text{O}$

Thermodynamically, water is lower in enthalpy than the reactants hydrogen and oxygen and thus the systems would be expected to produce water when hydrogen and oxygen are mixed. However, kinetically, the reaction is so slow at ordinary temperatures, that hydrogen and oxygen mixtures are stable almost indefinitely unless some energy is put into the system by an electric spark or heat to get the reactants over the activation energy barrier. Once the reaction is started,

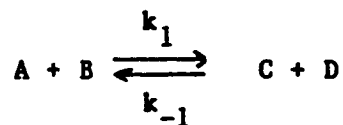
the reaction is so exothermic that it proceeds explosively to produce the product water. Other examples could be found where the reaction is thermodynamically unfavorable, but kinetically a very fast reaction. Thus a product can be formed by continuously removing it and forcing the reaction to go against a thermodynamically uphill path.

It seems intuitively obvious though, that at the molecular level, when one molecule is dissociating or two or more molecules colliding, a relationship should exist in a one-step reaction between how fast the reaction proceeds in either direction and the energy involved in that reaction. Hence, a relationship should exist between thermodynamical quantities and kinetics quantities. Indeed, this relationship can be seen in the principle of detailed balancing which is defined in the next section.

#### PRINCIPLE OF DETAILED BALANCING

##### DEFINITION:

This principle is succinctly defined by Benson<sup>7</sup> as follows: "The principle of detailed balancing asserts that at equilibrium, the specific rate of every elementary collision process is exactly equal to the specific rate of its inverse, or reverse process." This principle when applied to the molecular level is also referred to as the principle of microscopic reversibility. If the reaction for a molecular process can be pictured as a path that was shown in Figure 1, then this principle implies the obvious conclusion that proceeding from products to reactants should be retracing the path that led from reactants to products. Consider the following reaction of elementary particles (atoms, molecules, or ions) which occurs as a single step,



where A and B are reactants and C and D are products. The forward rate of the reaction is given by  $k[A][B]$  where  $k$  is the rate constant and  $[ ]$  refers to concentration of the species in the brackets. The reverse rate is given by  $k_{-1}[C][D]$ . At some point in time these two rates will become equal to each other regardless of which direction the reaction started from. At this point the reaction has reached a steady-state or equilibrium condition. This equilibrium is a dynamic one, however, in which the reactions in both directions are still proceeding. At this point, the equality of reaction rates can be expressed as,

$$k_1[A][B] = k_{-1}[C][D]$$

which can be rearranged to,

$$\frac{k_1}{k_{-1}} = \frac{[C][D]}{[A][B]} \quad (1)$$

however,  $[C][D]/[A][B] = K$  is the definition of the equilibrium constant. The equilibrium constant,  $K$  is a thermodynamic quantity. The above equality, in equation (1), also implies that the equilibrium constant is related to the kinetic rate constants as follows:

$$K = k_1/k_{-1} \quad (2)$$

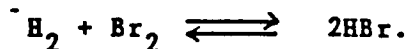
and this relationship is the mathematical formulation of the principle of detailed balancing. Often in kinetic studies, the rate constant in one direction of a reaction is determined experimentally and then through the equilibrium constant, by means of equation (2), the rate constant for the other direction of the reaction is calculated.

## CONDITIONS FOR THE PRINCIPLE OF DETAILED BALANCING:

In the definition of the principle of detailed balancing, it was assumed that the reaction was an elementary one-step reaction in equilibrium. This implies constant temperature and pressure as well as steady state concentrations of reactants and products.

O. K. Rice<sup>8</sup> in a classic paper has shown that even if the reaction involves more than one step, the relationship of  $K = k_f/k_r$  must still hold where  $k_f$  is the overall forward rate constant and  $k_r$  is the overall reverse rate constant. This must be true so that  $K$  is still a state function and does not depend on the path of the reaction.

An example of this is the reaction,



By experimental methods, the forward rate is given by,

$$\frac{k_1[\text{H}_2][\text{Br}_2]^{0.5}}{1 + k_2[\text{HBr}]/[\text{Br}_2]}$$

Since  $K = [\text{HBr}]^2/[\text{H}_2][\text{Br}_2]$ , then the reverse rate of the reaction must be given by an expression such that when the two rates are set equal to each other, they will give the expression for  $K$ . This implies that the reverse rate must be given by

$$\frac{k_{-1}[\text{HBr}]^2/[\text{Br}_2]^{0.5}}{1 + k_2[\text{HBr}]/[\text{Br}_2]}$$

The principle of detailed balancing can then be used to calculate the rate in one direction of a reaction when it is only feasible to measure the rate in the other direction.



Also, Rice, Benson<sup>7,8</sup> and others have shown that even if the system is far removed from equilibrium, the relationship,  $K = k_f/k_r$  must still hold if the  $k$ 's are measured under the same conditions, since the  $k$ 's do not generally depend upon concentration, or upon the fact that both forward and reverse reactions are proceeding at the same rate. Even when alternate reaction paths are available, such as when a catalyst is used, the relationship for  $K$  and thus detailed balancing still holds, since  $K$  is a state function and the energy relationships between reactants and products have not changed.

#### CONDITIONS WHERE DETAILED BALANCING PRINCIPLE DOES NOT APPLY:

The principle of detailed balancing does have limitations. If the temperature is changing very rapidly, then at a given instant the principle may apply, but in a finite time the forward and reverse rates are a function of temperature and if they are measured at two different temperatures, they will not be related by the equilibrium constant.

Also, for very high temperature reactions, where the temperature is changing very quickly, such as in a shock wave, the relaxation time between internal energy states and the translational energy becomes equal to or greater than that of reaction times of the particles. This results in an incubation time where the internal energy states attempt to equalize with translational energies. This incubation time has been called a pre-quasistationary time by Troe and Wagner.<sup>11</sup> This effect is explained by the so called "bottle-neck" mechanism. This mechanism recognizes that at high temperatures there is a point where vibrational relaxation time becomes comparable to the dissociation relaxation time. When this occurs, then a limiting step in the process, which

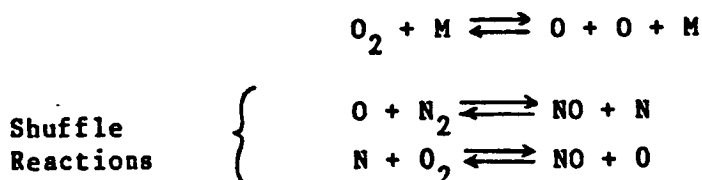
might be a vibrational transitions or dissociation itself, becomes the rate determining step. This then is the "bottleneck" in the overall dissociation reaction. Steps in the reaction before and after this "bottleneck" or rate-limiting step are in a quasistationary state and in that state the principle of detailed balancing does apply. However, upon an initial transient in temperature, such as in shock wave, there is an incubation time period while the energy levels (either vibrational or dissociative) build up to this quasistationary state where one step becomes the bottleneck step. During this incubation period or pre-quasistationary state, in which a redistribution of state populations occurs, the principle of detailed balancing does not hold since the rate constants are changing with time and it is questionable whether there is even a clear definition of a rate constant at this point. This incubation time or pre-quasistationary state has been found by other investigators as well.<sup>9,10</sup> Extrapolation of rate constants to higher temperatures have indicated higher values than actual measured values because of this relaxation effect. A second order effect related to this is that the high vibrational levels are lowered in population due to reaction and this lowers the observed reaction rate even further. This does not violate the principle of detailed balancing, but it does mean that this principle cannot be applied where there is a pre-quasistationary period and the rate constant is undergoing an incubation period. Troe and Wagner<sup>11</sup> state it as follows, "In comparing experimental dissociation results with the corresponding reverse recombinations,---the relationship,  $K = k_d/k_r$  was always used. It is clear that this equation cannot be valid under all circumstances: it is, for example, meaningless in the initial pre-quasistationary period of the reaction where  $k$  is time dependent."

## APPLICATION TO HIGH TEMPERATURE REACTIONS

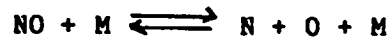
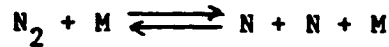
Research into the chemical reactions occurring during combustion and more recently, reactions occurring in shock waves of re-entry vehicles have generated much data on chemical reactions at high temperatures. In recent years, more attention to careful experimental and theoretical work has removed some of the inconsistencies in data that differed by orders of magnitude for given reactions. Advancements in shock tube studies, combustion research, arc jet experiments and re-entry flights have generated data over wide temperature ranges for forward and reverse reactions of many types. However, more work is still needed in these areas and where experimental data is missing, rate constants are often calculated through the equilibrium constant.<sup>12</sup> This should be evaluated in light of the limitations on the principle of detailed balancing.

According to Troe and Wagner,<sup>11</sup> the pre-quasistationary stage has been observed only at high temperatures for a few diatomic molecules. However, two diatomic molecules that exhibit this behavior are oxygen and nitrogen molecules. A useful measure of temperature given in reference 11 is  $D_0/RT$  where  $D_0$  is the dissociation energy of the molecule at 0 K. If this ratio is less than 10, then vibrational relaxation is important during the reaction and the incubation time of the rate constant must be considered. If this ratio is greater than 10, vibrational relaxation is complete before appreciable dissociation occurs and need not be considered. At a temperature of 15,000 K, this ratio is 3.9 for oxygen and 7.5 for nitrogen and therefore the vibrational relaxation effect on the dissociation rate should be considered for more accurate results. Experimental work at higher temperatures indicates that this effect must be taken into account to match theory with data. For the dissociation of oxygen up

to 18,000 K, Wray fit experimental data with explanations of the effect of translational, rotational, vibrational and dissociation relaxation times.<sup>13</sup> At Mach numbers from 3-10, translational and rotational relaxation is important; at Mach numbers from 10-16, vibrational relaxation must also be considered; above Mach 16 translational, rotational, vibrational, and dissociation relaxation times are all involved. In a similar fashion, Koshi, et.al., studied the dissociation of nitric oxide in shock waves up to 9,000 K and matched the data fairly well with the CVDV model (coupling of vibration excitation with dissociation including the effects of dissociation on vibration).<sup>14</sup> From their work, the vibrational temperatures were significantly lower than translational temperatures above 5,000 K. Also, some abnormal depopulation of vibrational levels near the eighth level indicated that multi-quantum jumps of less than five levels were possible at these temperatures. It is usually assumed that a step-ladder type of mechanism excites the vibrational energy levels from adjacent levels. The chemical reactions encountered by the Shuttle or AOTV in re-entry are complicated by the fact of interactions between nitrogen and oxygen and also by the non-equilibrium of the shock wave produced. At altitudes of less than 100 km, the predominant species in air are still molecular nitrogen and oxygen.<sup>15</sup> The energy from the shock wave produces many other atomic, molecular and ionized species. The Zeldovich mechanism for nitric oxide formation is certainly activated and proceeds as follows:<sup>16</sup>



However, at high temperatures, the higher energy reactions below would also take place.



Ionization reactions involving many of these species are also possible. The ionization of NO is thought to be responsible for the communications blackout with the vehicle upon re-entry. This rapid change of energy produces at least three different temperatures in the gas: the translational temperature, the vibrational temperature, and the electron temperature. These temperatures have been calculated for nitrogen shock waves by Prud'homme and Rowe.<sup>17</sup> They indicate that for a step function increase in the translational temperature, the vibrational temperature slowly increases to approach the final equilibrium temperature. The electron temperature exponentially increases and overshoots the equilibrium value then drops back to the final equilibrium temperature. Parks has attempted to apply a two temperature model to re-entry heating.<sup>12</sup> In this model rotational and translational temperatures were assumed to be the same and vibrational and electronic temperatures were assumed to be the same and were the second temperature used. This may be a good approach, but the agreement with actual radiation measurement data is not good. It may be that the model needs to be modified to the "bottleneck mechanism" presented earlier. Thus one step in the vibrational transitions may be rate-limiting instead of the dissociation step itself.

Another approach to these calculations would be to consider the "master-equation" approach as defined by Troe and Wagner<sup>11</sup> and by Levine and Bernstein.<sup>25</sup> This approach considers the net rate of transfer of molecules from

the ith level of vibrational energy states as given by the equation below. A schematic of this process is shown in Figure 2. This equation gives the net transfer of molecules out of the ith vibrational state by considering the sum of all the rates of transfer in from various vibrational levels and subtracting from that all the transfers from the ith level to other vibrational levels and finally subtracting the rate of actual dissociation from the ith level. This equation could be used if all rate constants were known for all dissociating gases.

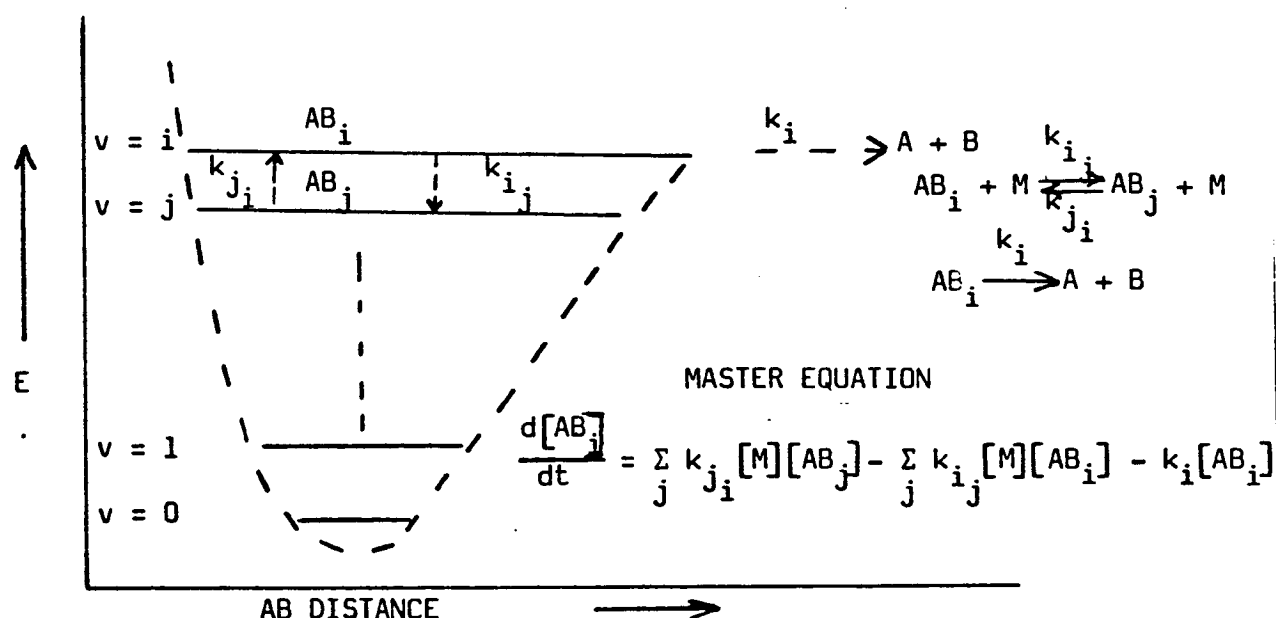


Figure 2. - Diagram Illustrating the Master Kinetic Equation

Some values for oxygen and nitrogen have been published.<sup>26</sup> However, this is further complicated when the gas is a mixture such as air and there is interaction between the elemental gases. Possibly some assumptions could be made that would reduce even this mixture to a few independent reacting species. This could be worth further study.

The conditions in a shock wave change so rapidly that equilibrium is certainly questionable. It may be that some species near the stagnation point

pre-quasistationary state where the principle of detailed balancing cannot be used and yet further down the vehicle, steady-state conditions may be reasonably assumed.

## CONCLUSIONS

The principle of detailed balancing has been used extensively in theoretical calculations as well as calculations involving experimental data to determine rate constants for reverse reactions by means of the forward rate constants and the equilibrium constant. In the majority of cases this is justified since the reactions are normally in a steady-state relationship or quasistationary state with some predictable distribution of energy among internal energy states. However, there is a small but finite time in which a gas system such as air with a low density is in a pre-quasistationary state when subjected to a high temperature shock wave. Under these conditions the equilibrium constant is not defined since the rate constants are changing with time and the principle of detailed balancing does not hold. This may be present near the forward part of a re-entry vehicle in the vicinity of a strong shock wave. Steady state or relaxation to an equilibrium distribution of internal energy states may be established further down the vehicle due to expansion of the gas and lowering of the temperature again.

The assumptions of detailed balancing and the use of equilibrium constants have been used even in the two-temperature models to date. However, these models should be re-evaluated since these assumptions may not be valid at least for a part of the entry vehicle.

Two other approaches to solving this non-equilibrium heat transfer of chemically reacting species would be to consider (a) the "bottleneck mechanism" on the basis of finding the limiting step in vibrational or dissociation steps

for each dissociating species or (b) using the "master-equation" approach of summing up rate constants over all possible reaction steps for vibration and dissociation. This would take some selection of important reactions since it would be too complicated to consider all species and all possible interactions.

#### ACKNOWLEDGEMENTS

I would like to express my appreciation to NASA and ASEE for sponsoring this summer faculty program which provided the opportunity for this study. This has been a learning experience for me and it will enrich my teaching experience as well as enhance my enthusiasm for the ongoing space research programs at NASA. I also wish to thank my NASA Colleague, Dr. Carl Scott for his suggestion of this study and his encouragement and support on this project.



## REFERENCES

1. Menees, G. P.: "Trajectory Analysis of Radiative Heating for Planetary Missions with Aerobraking of Spacecraft," J. Spacecraft and Rockets 22, 37-45, 1985.
2. Scott, C. D.: "Catalytic Recombination of Nitrogen and Oxygen on High Temperature Reusable Surface Insulation," in Aerothermodynamics and Planetary Entry, ed. by L. Crosbie, Vol. 77 of Progress in Astronautics and Aeronautics, 1981, pp 192-212.
3. Scott, C. D.: "Effects of Nonequilibrium and Catalysis on Shuttle Heat Transfer," AIAA 18th Thermophysics Conference, 1983.
4. Scott, C. D. and Derry, S. M.: "Catalytic Recombination Space Shuttle Heating," in Entry Vehicle Heating and Thermal Protection Systems, ed. by Bauder and Collicott, Vol. 85, Progress in Astronautics and Aeronautics, 1983, pp. 123-148.
5. Rakich, J. V. and Stewart, D. A.: "Catalytic Efficiency of the Space Shuttle Heat Shield," in Entry Vehicle Heating and Thermal Protection Systems, ed. by Bauer and Collicott Vol. 85, Progress in Astronautics and Aeronautics, 1983, pp. 97-122.
6. Scott, C. D.; Ried, R. C.; Maraia, R. J.; Li, C. P.; and Derry, S. M.: "An AOTV Aeroheating and Thermal Protection Study," in Thermal Design of Aeroassisted Orbital Transfer Vehicles, ed. by H. F. Nelson, Vol. 96, Progress in Astronautics and Aeronautics, 1985, pp. 309-337.
7. Benson, S.: Thermochemical Kinetics, J. Wiley and Sons, NY, 1968, pp. 1-6.
8. Rice, O. K.: "On the Relation Between an Equilibrium Constant and the Nonequilibrium Rate Constants of Direct and Reverse Reactions," J. Phys. Chem. 65, 1972-1976, 1961.
9. Greene and Toennies, Chemical Reactions in Shock Waves, Academic Press, NY, 1964, pp. 72-85.
10. Luther, K. and Troe, J.: "Influence of Temperature on Unimolecular and Termolecular Reactions," in Reactions of Small Transient Species, ed. by Fontijn and Clyne, Academic Press, NY, 1983, pp. 65-76.
11. Troe, J. and Wagner, H. G.: "Unimolecular Dissociation of Small Molecules," in Physical Chemistry of Fast Reactions-Vol. 1 Gas Phase Reactions of Small Molecules, ed. by B. P. Levitt, Plenum Press, NY, 1973, pp. 1-80.
12. Park, Chul: "On Convergence of Computation of Chemically Reacting Flows," NASA Ames Research Center, Moffett Field, CA (No Publication Date).
13. Wray, K. L.: "Kinetics of Oxygen Dissociation and Recombination," Tenth Symposium (International) on Combustion, The Combustion Institute, Pittsburgh, PA., 1965, pp. 523-537.

14. Koshi, M. et al: "Dissociation of Nitric Oxide in Shock Waves," Seventeenth Symposium (International) on Combustion, The Combustion Institute, Pittsburgh, PA 1978, pp. 553-562.
15. McEwan and Phillips, Chemistry of the Atmosphere, J. Wiley and Sons, NY 1975, p. 7.
16. Greene, E. F.: Chemical Reactions in Shock Waves, Academic Press, NY, 1964, p. 300.
17. Prud'homme, R. and Rowe, B.: "Partial Equilibrium and Relaxation in a Plasma," Acta Astronautical 6, 491-498, 1979.
18. Levine, R. D.: "Information Theory Approach to Molecular Reaction Dynamics," in Annual Review of Physical Chemistry, ed. by B. S. Rabinovitch, Vol. 29, 1978, Annual Reviews Inc., Palo Alto, CA, pp. 59-92.
19. Benson, S. W.: "Energy Transfer Processes and Chemical Kinetics at High Temperatures," Ninth International Symposium on Combustion, The Combustion Institute, Pittsburgh, PA., 1963, pp. 760-767.
20. Glanzer, K. and Troe, J.: "Vibrational Relaxation of NO by Atomic Oxygen," Tenth International Shock Tube Symposium, Shock Tube Research Society, Japan, 1975, pp. 575-578.
21. Merzkirch, W. and Erdman, W.: "Precise Measurement of Local Shock Wave Velocity Using a Modified Laser-Doppler Interferometer," Tenth International Shock Tube Symposium, Shock Tube Research Society, Japan, 1975, pp. 808-812.
22. Waterston, R. M. and Chou, H. P.: "A Crossed Laser Beam Technique for Particles Sizing and its Application to Shock Tube Experiments," Tenth International Shock Tube Symposium, Shock Tube Research Society, Japan, 1975, pp. 788-795.
23. Hansen, R. K. et al: "Decomposition of NO Studied by Infrared Emission and CO Laser Absorption," Tenth International Shock Tube Symposium, Shock Tube Research Society, Japan, 1975, pp. 536-543.
24. Wray, K. L.: "Shock-Tube Study of the Vibrational Relaxation of Nitric Oxide," J. Chem. Phys. 36, 2597-2603, 1962.
25. Levine, R. D. and Bernstein, R. B.: Molecular Reaction Dynamics, Clarendon Press, NY, 1974, pp. 146-148.
26. Duff, R. E.: "Calculation of Reaction Profiles Behind Steady State Shock Waves: II. The Dissociation of Air," J. Chem. Phys. 31, 1018-1027, 1959.

## APPENDIX

The appendix will describe briefly some other related areas to this study.

1. Information theory approach to molecular reaction dynamics.<sup>18</sup> This review by Levine seems to bring forth a new approach to molecular dynamics. He notes that the distribution of available energy among the final products in collision reactions was by no means chaotic. Rather, it was surprisingly specific. Among all distributions of quantum states the prior distribution is of maximal entropy. The entropy deficiency is the difference between the entropies of the prior and the observed distribution and can be calculated. The entropy deficiency is an average of the local deviance of the observed frequency of the final state from its prior probability. This local measure of deviance is termed the surprise. Surprisal syntheses is the logical outcome of surprisal analysis. It has now been shown that it is indeed possible to rewrite quantal or classical collision theory so as to determine the surprisal directly as the primary output of the computation. This might be a useful technique in analyzing chemical reactions at high temperatures since this technique deals with translational, rotational, vibrational and electronic energy transfers.

2. Gas phase recombination of atoms and surface recombination of atoms. Scott<sup>3</sup> has shown that recombination coefficients for oxygen and nitrogen increase with increasing temperature upon surfaces. Other workers such as Benson<sup>19</sup> have shown that gas-phase recombination of atoms decreases in rate as the temperature increases. The effect of these opposing changes in rates upon heat transfer to vehicle surfaces is not known and these changes may even produce compensating heating effects.

3. Vibrational relaxation of gases. The vibrational relaxation constant of a gas determines the rate at which energy transfers from vibrational to translational energy. When this value is comparable to reaction time, it causes the reaction to be in a pre-quasistationary state and kinetic laws are difficult to apply. This was specifically mentioned for the principle of detailed balancing. At high temperatures this problem is worse. However, experimental studies have shown that relaxation time is lower in air for both oxygen and nitric oxide than it is in the pure gases. This is felt to be due to formation of  $\text{NO}_2$  and  $\text{O}_3$  complexes that relax faster than the molecules in the pure gases. In the specific case of the relaxation of NO by oxygen atoms, the rate of relaxation was 10 times faster than with argon. This approached the rate of the reaction of  $\text{NO} + \text{O} \rightarrow \text{NO}_2$  and from this was inferred that  $\text{NO}_2$  might be involved in the rapid relaxation of NO by oxygen atoms. This could result in reaching equilibrium in air faster than would be expected for the pure gases.<sup>28</sup>

4. Laser applications to velocity measurements<sup>21</sup> and to particle size measurements in shock tubes.<sup>22</sup> These are articles of general interest that might be useful for reference.

5. Techniques for monitoring species in high temperature processes. NO was measured by infrared emission at 5.3 microns which is the fundamental vibration-rotation band of NO. Also a CO tunable laser was used to measure by absorption the  $1935.482 \text{ cm}^{-1}$  line that corresponded to the 7-6 vibration level and the J transition of 12-13.<sup>23</sup> These two measurements correlated well.

Wray used the 1270 Angstrom line to monitor NO. This line has absorption that increases almost linearly with the vibrational excitation of NO.<sup>24</sup> Koshi used two detectors,<sup>14</sup> one at 4.87 microns and the other at 5.22 microns to monitor NO. This discriminated between NO molecules in vibrational ground state from those in higher levels of vibrational excitation.

Greene<sup>16,p303</sup> reports that at 2465 Angstroms, the 0 to 2 vibrational transition of NO can be followed. Also, in Greene<sup>16p299</sup> absorption at 1470 Angstroms in high temperature air is due almost entirely to oxygen in its ground state.

Wray<sup>13</sup> indicates, however, that oxygen absorbs at both 1470 and 1270 Angstroms. Evidently, the 1270 line does not discriminate between nitric oxide and oxygen.

N86 - 31424

D15  
74P.

An Analysis of Ullage Heat Transfer  
in the Orbital Refueling System

David Kauffman, Ph. D.  
Chemical and Nuclear Engineering Department  
The University of New Mexico  
Albuquerque, New Mexico

18826

ABSTRACT

The Orbital Refueling System was an experiment flown on Shuttle Mission STS 41-G in October, 1984. Liquid hydrazine fuel was transferred back and forth from one spherical bladder tank to another using pressurized nitrogen as the driving force. Compressive heating of the ullage gas in the receiving tank could lead to a hazardous situation if any hydrazine leaked through to the ullage side of the bladder and was heated above about 175°F, where it can undergo spontaneous exothermic decomposition. Early analysis of the flight data indicated that the ullage compression process was much closer to an isothermal than an adiabatic one.

In this study, a thorough review of the pertinent literature was used to make an a priori best-estimate for the ullage gas heat transfer coefficient (defining the Nusselt Number as a function of Reynolds and Rayleigh Numbers). Experimental data from the flight were analyzed in detail. It is evident that there is considerably more heat transfer than can be accounted for by conduction alone, but the observed increases do not correlate well with Reynolds Number, Rayleigh Number or vehicle acceleration.

There are large gaps in the present understanding of convective heat transfer in closed containers with internal heat generation, especially in the presence of vibrations or other random disturbances. A program of experiments to fill in these gaps is suggested, covering both ground and orbital environments.

PRECEDING PAGE BLANK NOT FILMED

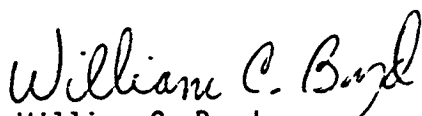
## FOREWORD

The ability to accurately predict fluid system performance and capability, along with fluid conditions, is an important part of the design of on-orbit fluid management systems. This aspect of system design will take on an even greater role in the design and evaluation of the numerous fluid systems required to manage the variety of earth storable and cryogenic fluids involved in the operation of the Space Station and its interfacing elements, such as OMV (Orbital Maneuvering Vehicle), OTV (Orbital Transfer Vehicle), and OSCRS (Orbital Spacecraft Consumables Resupply System). One such operation, as demonstrated with the ORS (Orbital Refueling System) experiment, is the replenishment of propellant for Space Station and satellite propulsion systems.

The procedures and techniques for accomplishing on-orbit resupply are now being formulated, as are methods for overcoming the many associated problems. A particularly interesting one is the impact on refueling timelines due to the requirement to limit the recompression temperature rise in the ullage gas during resupply of hydrazine propellant tanks. Analyses of heat generation and dissipation are necessary aspects of the work required in this area.

However, there are large gaps in the present understanding of convective heat transfer in low gravity environments. Data from the ORS has provided insight into this process.

The work of Dr. Kauffman, and the results of his work as described herein, represent a significant first step in an attempt to analytically describe the mechanism of internal propellant tank heat transfer. In just ten weeks during the Summer of 1985 at JSC, Dr. Kauffman was able to familiarize himself with the ORS, the available analytical tools, and the flight data in sufficient degree to produce a quite interesting study of this little-known area.



William C. Boyd  
Johnson Space Center  
Houston, Texas  
October, 1985

## SUMMARY

During orbital refueling operations, ullage gas in the receiving tank is compressed and therefore heated. In order to insure safe, efficient transfer of fluids on orbit, it is necessary to understand the nature of heat transfer from the ullage gas to the tank walls. In the Orbital Refueling System, an experiment flown on Shuttle Mission 41-G in October, 1984, hydrazine was transferred back and forth from one tank to another. Preliminary analysis of the data indicated that there was considerably more heat transfer from the gas than could be accounted for by conduction alone. This study analyses the problem and the flight data in more detail.

Section 2 of the report contains a survey of applicable heat transfer theory. Conduction, forced convection and natural convection heat transfer mechanisms and correlations are reviewed. Only a very limited amount of information is available on non-steady-state natural convection and on natural convection inside closed containers. A method is suggested for combining various heat transfer mechanisms to give an a priori estimate of the overall heat transfer for the ORS ullage gas.

Section 3 of the report contains a brief description of the ORS equipment and instrumentation, with emphasis on the items directly involved in analyzing the ullage gas heat transfer problem. It includes a summarized schedule of events for the orbital experiment. Order-of-magnitude calculations show the energy flows associated with the ullage heat transfer problem. The ORSCOMP computer program was used in the analysis. Heat transfer analysis methods and data are presented for the two approaches used, constant and variable Nusselt Numbers. Vehicle accelerations are calculated from thruster firing data for a few selected portions of the experiment.

Section 4 presents an analysis of the ORS experiment heat transfer data. Low Reynolds Number and High Reynolds Number events are grouped separately to examine various correlations. In neither group are there significant correlations between heat transfer coefficients calculated from the data and



either Rayleigh or Reynolds Numbers. Heat transfer does not correlate with vehicle acceleration data either for the few events for which it was calculated. An "uncertainty analysis" is used to illustrate the high sensitivity of heat transfer coefficient values to small random or systematic errors in the pressure vs. time data and in the initial calculation of the amount of ullage gas present in a tank. Some of the basic limitations of the ORS experiment are reviewed.

Section 5 summarizes the present knowledge applicable to on-orbit ullage gas heat transfer. Two heat transfer modeling approaches are recommended, one which gives a conservative lower bound on the heat transfer, thus an upper bound on the maximum temperature, and one which is more realistic but less certain. The former is based on pure conductive heat transfer, taking advantage of various geometric features. The latter uses a constant Nusselt Number for each type of operation; this is the best correlation that the present data can justify. The major gaps in existing knowledge related to the problem are outlined.

Two approaches for an experimental program to provide information for ullage gas heat transfer are presented in Section 6. The first approach emphasizes obtaining fundamental engineering correlations for the individual processes involved. The second approach is based more on direct simulation and scale-up procedures. Advantages and disadvantages of each are presented, along with some guidelines on the ranges of key variables for any comprehensive experimental program.

## 1.0 INTRODUCTION

Orbital refueling of satellites and other space vehicles will be required for many future space programs. Many different technologies are involved in developing the capability to provide routine, safe, efficient on-orbit resupply of fluids: flow measurement, tank gauging, coupling design and standardization, etc. One key feature from a safety and operational standpoint relates to the compressive heating of the ullage gas in a tank as it is filled with liquid. That is the principal topic of this report.

### 1.1 Typical Refueling Operations

A typical satellite refueling operation is shown schematically in Figure 1-1. Liquid from the supply vehicle is moved to an empty bladder tank using compressed gas as the driving force. As the filling proceeds, the ullage gas in the receiving tank is compressed and thereby heated. The maximum

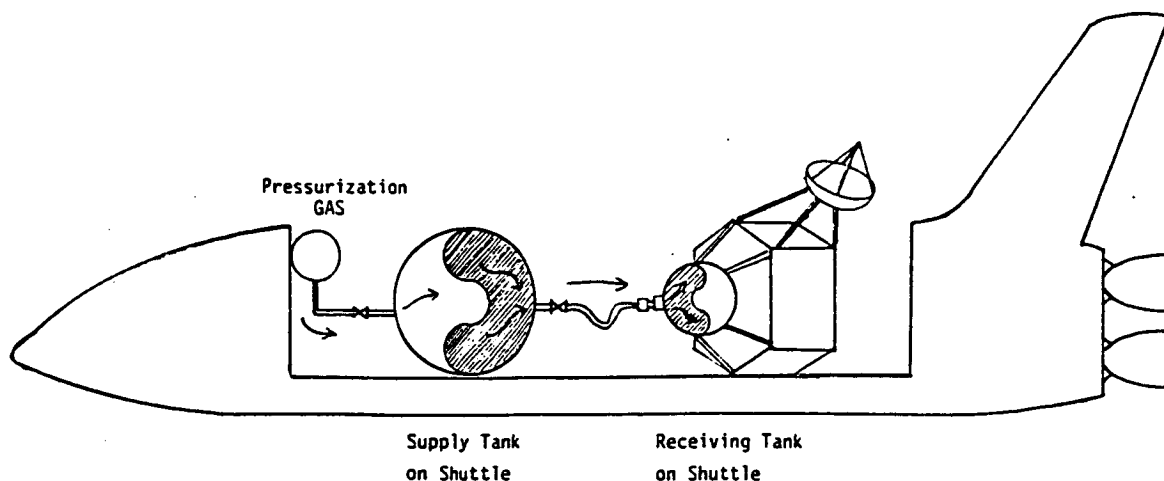


Figure 1-1. Typical Satellite Refueling System

temperature that the ullage gas can reach is that associated with adiabatic compression. For an ideal gas it is given by:

$$T_2 = T_1 \left( \frac{P_2}{P_1} \right)^{\frac{\gamma-1}{\gamma}} \quad (1-1)$$

In practice, there will be heat transfer from the gas to the vessel walls and surroundings, so the observed temperature rise will be less than that for a true adiabatic compression.

A major potential hazard arises when certain fuels are transferred in this manner. Hydrazine, commonly used as a fuel on spacecraft, decomposes spontaneously at temperatures around 200°F, with release of a great deal of energy. If a small amount of hydrazine accidentally leaked to the ullage side of the bladder, it could easily be heated above 200°F by too-rapid filling of the tank. The ullage gas is heated by compression; it is cooled by heat transfer to the tank walls and, in turn, to the surroundings. Higher heat transfer rates, then, can lead to higher safe tank fill rates. Safety is of prime concern in orbital operations, but time is also critical. Better knowledge of the heat transfer phenomena involved in tank filling is needed in order to operate at the maximum safe flow rates.

## 1.2 The Orbital Refueling System Experiment

The Orbital Refueling System (ORS) experiment was built in-house by NASA-JSC and flown on Shuttle Mission 41-G in October 1984. The overall objective of the project was to develop initial design concepts and criteria to permit future use of the Space Shuttle as a carrier of a propellant or consumables "tanker" for satellites and other space vehicles (NASA, 1983; Griffin, 1985). From a technical standpoint, it had several specific objectives:

- (a) Demonstrate extravehicular activity (EVA) tool/valve interface for typical existing satellite propellant and pressurant servicing valves that were not designed for in-flight resupplying.

- (b) Demonstrate Orbiter-to-satellite interface for control of fluid transfer from the Orbiter aft flight deck. Establish procedures for transferring hydrazine in the payload bay.
- (c) Establish procedures for crew EVA operations on a hydrazine system with potential crew/Orbiter exposure to hydrazine.
- (d) Fabricate a system which, with minor modifications, could be reflown to permit orbital propellant refueling of a satellite such as LANDSAT.

As the program design and ground test work proceeded, it became evident that low-gravity heat transfer would have a major impact on the experiment and on any operational refueling system. The experiment was not designed, however, with a primary objective of obtaining heat transfer data.

The system was designed and built to be "two-failure tolerant." That is, it would not pose any imminent hazard to crew or mission in the event of any two simultaneous component failures. For each transfer, the maximum possible adiabatic temperature increase was calculated. Flow was stopped at the point where a purely adiabatic compression would have raised the ullage gas temperature to 150°F. The operations were carried out by remote control from inside the Orbiter cabin. For the fifth transfer, two crew members went outside the cabin and installed the "mod-kit" piping using specially designed tools. All transfers were carried out satisfactorily.

### 1.3 Early ORS Analysis

Pressures, tank-wall temperatures and flow rate data were recorded continuously for the ORS experiment. Using a previously developed program, plots of pressure vs. time and pressure vs. amount transferred were made (Boyd, 1984). The data indicated conditions much closer to isothermal than adiabatic. Figure 1-2 is typical of this early data analysis. Calculated adiabatic and isothermal lines give upper and lower bounds to the expected receiving tank pressure data. The dotted line is one calculated assuming conductive heat transfer only. Clearly the data indicate more heat transfer than conduction alone could provide.

— ADIABATIC/ISOTHERMAL LIMITS  
 - - - PREDICTED  
 XXXXX FLIGHT DATA

P2 = SUPPLYING TANK PRESSURE  
 P1 = RECEIVING TANK PRESSURE

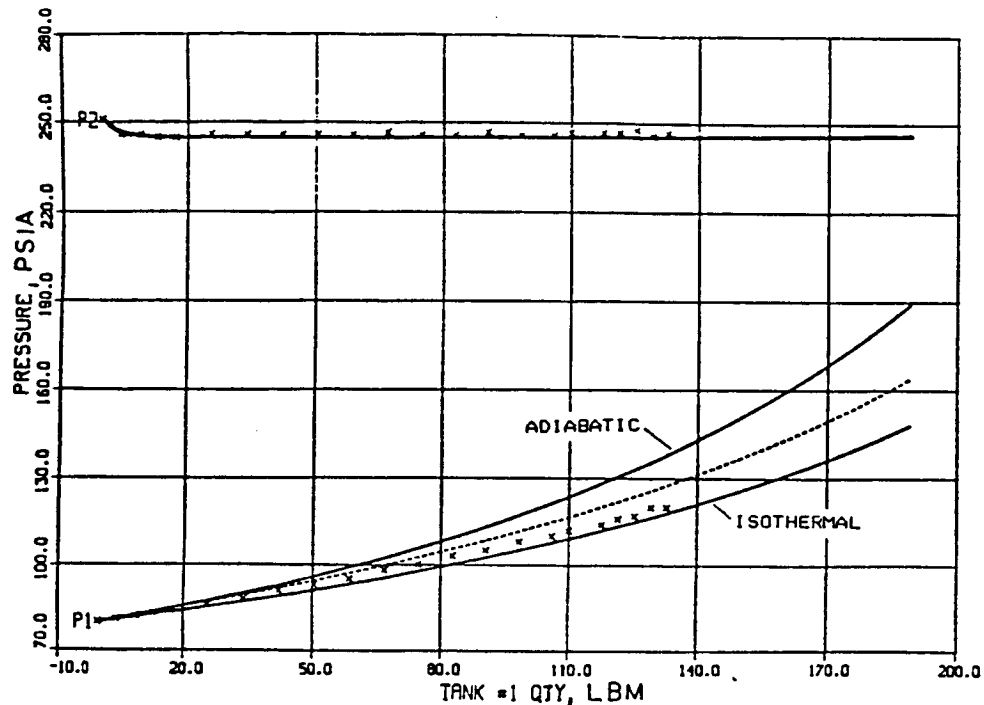


Figure 1-2. Pressure vs. Quantity Transferred for Transfer #2a

The ORS test operations and data are discussed in Section 3. An analysis of the data is presented in Section 4.

#### 1.4 Scope of This Study

This study includes a theoretical analysis and review of associated literature for heat transfer mechanisms of the type found in the ullage gas. It includes extensive review and analysis of the ORS test data.

This study does not address alternate means of solving the basic ullage gas heating problem. Several approaches, however, might be examined in the future. The ones listed below all offer some advantages in terms of minimizing ullage gas heating, but they also have associated penalties of weight and/or mechanical complexity.

- (a) Use of ullage gases other than nitrogen. A gas with a higher molar heat capacity would have a lower specific heat ratio and thus a lower temperature increase for any given pressure increase.

- (b) Carbon-tetrafluoride,  $\text{CF}_4$ , for instance, has a specific heat ratio of 1.16, compared to 1.40 for nitrogen. Doubling the pressure for nitrogen adiabatically, starting at 70°F, leads to a 116°F rise. For  $\text{CF}_4$ , the rise is only 52°F.
- (c) Use of a two-phase, single component ullage fluid. For instance, if saturated propane vapor is compressed, a portion of it condenses. There is some heating, but not as much as with most totally gas systems. For instance, halving the total volume of saturated propane vapor at 80°F and 147 psia in an adiabatic compression results in a two-phase mixture at 132°F and 241 psia.
- (d) Venting of the ullage gas during tank filling. This obviously avoids pressurization and heating. The associated loss of pressurant gas, however, may be too great a penalty to pay.
- (e) Active cooling of the ullage chamber. Heat transfer could be enhanced by active mixing of the ullage gas or by providing more heat transfer area.

## 2.0 THEORETICAL ANALYSIS

### 2.1 Heat Transfer Mechanisms

There are three heat transfer mechanisms that must be considered in analysing any heat transfer problem: conduction, convection and radiation.

- (a) Conduction heat transfer will always be present except in a vacuum, though it is frequently not the predominant heat transfer mechanism. For the ORS experiment, it provides a minimum lower bound to possible heat transfer rates. It is discussed further in Section 2.2.
- (c) There are two types of convective heat transfer that could be significant, forced convection and natural, or free, convection. In forced convection, heat is transferred due to the already-existing motion of a fluid. In natural convection, heat is transferred by a fluid which is set in motion due to a temperature, and thus density, gradient. On orbit, forced convection is a major mode of heat transfer when fluids are moved through pipes at reasonably high velocities. Natural convection should not exist in a perfect zero-g environment, but it can nevertheless be significant on orbit, even though it is much less significant than it is on the ground. Forced convection heat transfer is discussed in Section 2.3. Natural convection is discussed in Section 2.4.
- (d) Radiation heat transfer is frequently significant in space activities, but it should not be significant inside the tanks of the ORS system. Wall temperatures were fairly uniform, due to the high thermal conductivity of the metal tanks as compared to that of the nitrogen pressurization fluid. Nitrogen itself does not absorb radiation in the energy region corresponding to black-body radiation at the temperatures encountered in the experiment. Radiation was therefore assumed to be negligible in analysing the ORS experiment.

In many practical situations, not one, but several, heat transfer mechanisms are involved simultaneously. In some simple cases, such as combined radiation and conduction, there are straight-forward methods for combining the mechanisms in an overall energy balance equation. In many other cases, especially those involving natural convection, the appropriate methods for combining heat transfer mechanisms are subject to considerable uncertainty. This problem is discussed further in Section 2.5. An overall best estimate of the heat transfer situation for the ORS system, based on theory and existing correlations, is presented in Section 2.6.

It is convenient to use five dimensionless groups when analysing heat transfer problems:

- (a) Nusselt Number, a ratio of convective to conductive heat transfer:

$$Nu = hL/k \quad (2-1)$$

- (b) Reynolds Number, a ratio of inertial to viscous forces in fluid flow:

$$Re = Lv\rho/\mu \quad (2-2)$$

- (c) Prandtl Number, a ratio of momentum transport to thermal energy transport:

$$Pr = C_p \mu/k \quad (2-3)$$

- (d) Grashof Number, a ratio of bouyant forces to viscous forces in fluid flow:

$$Gr = L^3 \rho^2 g \beta \Delta T / \mu^2 \quad (2-4)$$

- (e) Rayleigh Number, the product of the Grashof and Prandtl Numbers, a ratio of natural convection heat transfer to conductive heat transfer:

$$Ra = L^3 \rho^2 g C_p \beta \Delta T / \mu k \quad (2-5)$$



## 2.2 Conductive Heat Transfer

Conductive heat transfer occurs when hotter, more energetic molecules transfer some of their energy to neighboring, cooler ones by collision processes. There is no net movement of the material involved. Except in a vacuum, where there are no neighboring molecules, conductive heat transfer will always occur whenever there is a temperature difference in a system. The rate of heat transfer is proportional to the temperature gradient and to the thermal conductivity of the material through which heat is passing. The equations describing the process are fairly simple, often leading to analytic solutions.

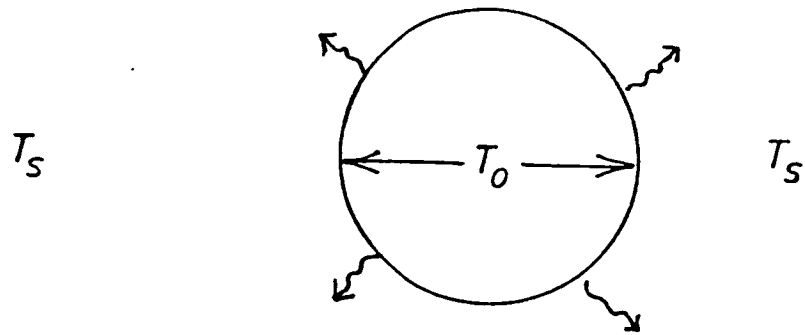
### 2.2.1 Spherical Geometry

In spherical coordinates, the basic conductive heat transfer equation is:

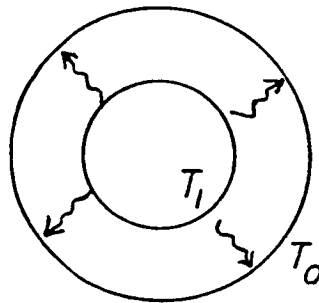
$$\rho C_v \frac{\delta T}{\delta t} = \frac{k}{r^2} \frac{\delta}{\delta r} \left[ r^2 \frac{\delta T}{\delta r} \right] + q_i \quad (2-6)$$

At steady state, of course, the left-hand side is equal to zero.

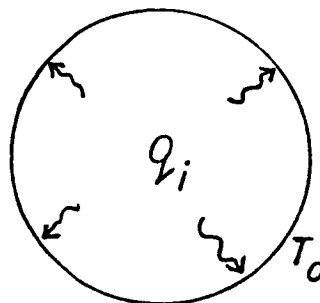
It is frequently reported in the literature that the limiting Nusselt Number for a sphere, using the sphere diameter as the length parameter, is 2.0 (Churchill, 1977; Chow and Akins, 1975). This limit takes effect when there is no convective heat transfer at all; the heat transfer is due to conduction only. This is true, however, only in a limited number of cases, depending upon the particular boundary conditions for the problem. It is true for a sphere held at constant temperature,  $T_0$ , with heat to or from infinite surroundings initially at constant temperature,  $T_s$  (See Figure 2-1.a.). It also holds true for heat transfer between concentric spheres held at constant temperatures, but only in the limit as the ratio of the two sphere diameters approaches 1 (See Figure 2-1.b.). Note that for this latter case the length term used in the Nusselt Number is the difference of the two radii, not the diameter of either of the spheres.



A. Heat Transfer to External Sink



B. Heat Transfer between Concentric Spheres



C. Heat Transfer with Internal Heat Generation

Figure 2-1. Spherical Geometry Heat Transfer

For the case at hand, we are interested in heat transfer from an enclosed body of gas to its container, with heat generation taking place uniformly within the gas (See Figure 2-1.c.). For this situation, the appropriate steady-state differential equation is:

$$\frac{\delta}{\delta r} \left[ r^2 \frac{\delta T}{\delta r} \right] = - \frac{r^2 q_i}{k} \quad (2-7)$$

The simplest boundary conditions for a realistic problem are:

$$T = T_o \quad \text{at } r = r_o \quad (2-8)$$

$$\frac{\delta T}{\delta r} = 0 \quad \text{at } r = 0 \quad (2-9)$$

The analytic solutions for  $T$ ,  $\bar{T}$  and  $T_{\max}$  are:

$$T = T_o + \frac{q_i}{6k} (r_o^2 - r^2) \quad (2-10)$$

$$\bar{T} = T_o + \frac{q_i r_o^2}{15k} \quad (2-11)$$

$$T_{\max} = T_o + \frac{q_i r_o^2}{6k} \quad (2-12)$$

We can define two different heat transfer coefficients, depending on the selection of the temperature difference:

$$h_1 = \frac{Q}{A} (\bar{T} - T_o) \quad (2-13)$$

$$h_2 = \frac{Q}{A} (T_{\max} - T_o) \quad (2-14)$$

Using a temperature difference of  $(T - T_0)$  and the sphere diameter as the length parameter, the Nusselt number is then given by:

$$Nu_c = hD/k = 10.0 \quad (2-15)$$

From this we conclude that the minimum possible heat transfer coefficient, based on the difference between average fluid temperature and wall temperature, is  $10k/D$ . The maximum possible temperature difference between any point in the fluid and the wall is 2.5 times the difference of the average fluid temperature and the wall temperature.

### 2.2.2 Cylindrical Geometry

Conductive heat transfer in cylindrical geometry can be handled in an analogous fashion to that for spherical geometry. The steady-state equation for heat transfer with uniform internal heat generation and insulated (no heat transfer) ends is:

$$k \frac{\delta}{\delta r} \left[ r \frac{\delta T}{\delta r} \right] = - r q_i \quad (2-16)$$

The boundary conditions are the same as those for the spherical case:

$$T = T_0 \quad \text{at } r = r_0 \quad (2-17)$$

$$\frac{\delta T}{\delta r} = 0 \quad \text{at } r = 0 \quad (2-18)$$

The solutions for  $T$ ,  $\bar{T}$  and  $T_{\max}$  are:

$$T = T_o + \frac{q_i}{4k}(r_o^2 - r^2) \quad (2-19)$$

$$\bar{T} = T_o + \frac{q_i r_o^2}{8k} \quad (2-20)$$

$$T_{\max} = T_o + \frac{q_i r_o^2}{4k} \quad (2-21)$$

If we again define  $h_1$  as the heat transfer coefficient based on the difference between the average fluid temperature and the wall temperature, then the limiting value of the Nusselt Number due to conduction only is 8.0. The maximum temperature difference is twice the average temperature difference.

The above analyses for spherical and cylindrical heat transfer are, of course, highly idealised. In the ORS experiment, the tanks were spherical, but the gas space was not; it was constantly changing shape as the bladder moved in or out due to liquid movement. This analysis, however, can help by determining some lower bounds on the heat transfer coefficients. Furthermore, it establishes the values that would be calculated from flight data if the only heat transfer mechanism in operation was conduction.

### 2.3 Forced Convection Heat Transfer

Forced convection heat transfer is the movement of heat from one point to another by the action of a fluid put in motion by external forces. It is the principal heat transfer mechanism for fluids flowing in pipes at moderate to high Reynolds Numbers.

There are many available correlations for heat transfer coefficients for flow in pipes and ducts of various geometries. Likewise, there are numerous correlations for flow past solid objects: plates, spheres, cylinders, etc.

There are no available correlations for forced convection flow inside closed boundaries, mainly because there are very few situations where there are significant convection currents inside a closed container.

For the purposes of this study, Churchill's correlation for the Nusselt Number for flow outside of a sphere was used for heat transfer estimation inside a sphere-like container (Churchill, 1977):

$$Nu_f = 0.347 Re^{0.5} \quad (2-22)$$

For flow past a sphere, the Reynolds Number is based on the sphere diameter and the free-stream velocity far from the sphere. It is not immediately evident just what length and velocity parameters should be used in the study at hand. This point is discussed further in Section 3.5.

Another possible way of examining the forced convection heat transfer in the ullage section of the ORS tanks would be to use an approach based on free jet mixing. No such analysis was made in the course of this study. It could apply only to the supply tank, with its high-velocity injection of nitrogen; it would not apply to the receiving tank, where Reynolds Numbers are very low. A number of different studies could be used as a starting point, but considerable analysis would be required (e.g., Martin, 1977; Sparrow and Lovell, 1980).

## 2.4 Natural Convection Heat Transfer

Natural, or free, convection heat transfer is the movement of heat from one point to another by a fluid set into motion by the density-difference driving force induced by a temperature gradient. Under true zero-gravity conditions there would be no natural convection since the driving force is proportional to the fluid density difference, which would be present, and to the local body force field, which would be zero. Even for a satellite in orbit, however, the body force field does not reach zero. A small gravitational force will exist at any point on the satellite which is at an elevation above the earth's center of mass different from that of the center of mass of the satellite. More importantly, various activities on the

satellite (attitude thruster firings, movement of equipment or structural members, crew motion on manned satellites, etc.) can cause accelerations on the order of  $10^{-6}$  g to  $10^{-3}$  g (Olsen and Mockovciak, 1981; and Kullas, 1979). Natural convection cannot, then, be ignored a priori for heat flow in orbiting spacecraft systems.

#### 2.4.1 Theory

The theory for natural convection heat transfer to or from a vertical flat plate at steady state with the moving fluid film in laminar flow has been extensively studied (e.g., Burmeister, 1983). Dimensional analysis shows that the Nusselt Number for such a case should be a function of only the Rayleigh and Prandtl Numbers. For any given fluid, the Prandtl Number depends only on properties of the fluid at rest; so the Nusselt Number becomes a function of the Rayleigh Number alone. Numerical solutions of this function have been made. The general form of the solution is:

$$Nu_n = A(Pr)Ra^{0.25} \quad (2-23)$$

For air at ambient conditions, A has the value of 0.517. Purely theoretical solutions are virtually non-existent for other geometries.

#### 2.4.2 Nusselt Number Correlations

Experimental data for Nusselt Number/Rayleigh Number correlations have been obtained for many different fluids and many different geometries. Most frequently, the functional form

$$Nu_n = C Ra^n \quad (2-24)$$

is used. It reduces to the theoretical form for laminar natural convection past vertical plates. It fits many other situations very well: vertical cylinders, both inside and outside; horizontal cylinders, both inside and outside, sometimes with a correction factor to account for variations with

angular position; and outside of spheres, again with an appropriate angular-dependent function for point heat-transfer values. In nearly all cases the exponent of 0.25 is satisfactory for correlating data in the laminar flow range. In this range the value of C depends on geometry and, to a lesser extent, on Prandtl Number. A large number of cases give values ranging from 0.50 to 0.64. In this study, a value of 0.59 is used except when there are data indicating otherwise, as suggested by Eckert (1954). The flow generally starts to become turbulent at Rayleigh Numbers of about  $10^9$ . In the turbulent range, the exponent tends to be larger than 0.25, typically 0.3 to 0.5.

Very few experimental data are available for natural convection correlations inside closed spheres. The only laboratory data found in an extensive literature search are those of Chow and Akins (1975). Their data are plotted in Figure 2-2. They reported a least-squares fit to the data of:

$$Nu_n = 0.8 Ra^{0.3} \quad (2-25)$$

A recalculation of the least-squares fit by the present author gave different values to the constants:

$$Nu_n = 1.9 Ra^{0.236} \quad (2-26)$$

A least-squares fit with the exponent fixed at 0.25 gives:

$$Nu_n = 1.59 Ra^{0.25} \quad (2-27)$$

As can be seen in Figure 2-2, there is considerable scatter in the data, and any of these lines could be considered reasonable. Note, too, that the data tend to be considerably higher than the expected correlation based on Equation 2-24 with a constant of 0.59 and exponent of 0.25.

A further complication arises at low Rayleigh Numbers with regard to the thickness of the boundary layer set in motion by the thermal gradient.



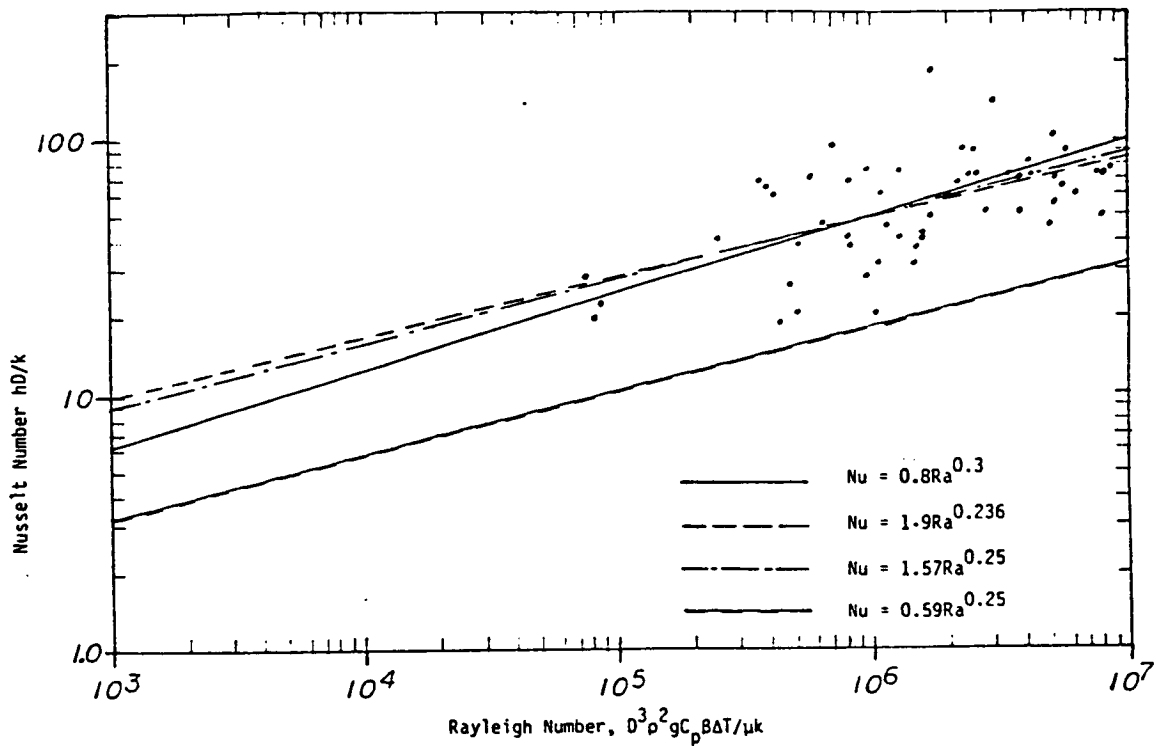


Figure 2-2. Chow-Akins Data for Natural Convection Inside Spheres

Combined solutions of boundary layer flow equations and heat transfer equations for vertical flow past a flat plate leads to the following estimate of the boundary layer thickness (Siegel, 1967):

$$\frac{\delta}{x} = \frac{3.93(0.952 + Pr)^{0.25}}{(RaPr)^{0.25}} \quad (2-28)$$

Bergholz (1980) concluded that the lower bound for stability for natural convection inside a closed container corresponded to a Rayleigh Number of about 100,000. At lower values, the boundary layers interfere with each other. For the low Rayleigh Numbers expected on orbit, the boundary layer thickness calculated from this correlation can be a significant part of the total system size. For instance, for nitrogen at 70°F and a Rayleigh Number of 20,000, the boundary layer thickness is 40% of the height of the plate.

Jahn and Reineke (1974) reported experiments involving natural convection inside closed containers with internal heat generation. This is somewhat closer to the situation of interest in this report. Data were quite limited and were restricted to two very simple geometries. They correlated their data in terms of the product of the Rayleigh Number and the Dammkohler Number.

$$Da = q_i L^2 / k \Delta T \quad (2-29)$$

$$Nu_n = C(DaRa)^n \quad (2-30)$$

#### 2.4.3 Time Needed to Approach Steady-State

All of the theory and correlations given above are based on steady-state solutions and measurements. Natural convection, however, goes through two "start-up" phases before reaching steady-state conditions (Ede, 1967). In the first of these phases, there is no fluid motion. Heat transfer is starting, but it occurs by conduction only. This phase, known as the conduction phase, continues until such time as a large enough density gradient has been established to set the fluid in motion. In the second phase, known as the transition phase, fluid flow at the boundary has started, but it has not reached a steady-state flow pattern. The moving film thickness is thinner than that which exists at steady-state. Correlations have been determined experimentally for the length of time these two phases exist for natural convection heat transfer from vertical walls. The conduction/transition time is given by:

$$t_1 = 1.80(1.5 + Pr)^{0.5} \left( \frac{x}{g \beta \Delta T} \right)^{0.5} \quad (2-31)$$

The transition/steady-state time is given by:

$$t_2 = 5.24(0.952 + Pr)^{0.5} \left( \frac{x}{g \beta \Delta T} \right)^{0.5} \quad (2-32)$$

During the initial conduction period for a step change in wall temperature, the heat transfer coefficient is given by:

$$h = \left( \frac{\rho C_p k}{\pi t} \right)^{0.5} \quad (2-33)$$

Even though these correlations are for vertical plates, they can be used to give an approximate estimate of the time needed to establish steady natural convective heat transfer conditions for other geometries. Equation 2-33 can be used qualitatively to estimate trends in the initial heat transfer rate. Note that the initial rate predicted by this correlation is much higher than the steady-state rate.

Whitley and Vachon (1972) did a comprehensive computational analysis of transient laminar natural convection inside spheres. By simultaneously solving the coupled momentum and energy equations, they calculated stream lines and temperatures profiles resulting from a step change in wall temperature. Their calculated stream lines agree qualitatively with the patterns observed by Jahn and Reineke (1974). They calculated local Nusselt Numbers as functions of time and angular position on the sphere. Their average Nusselt Numbers started at 10, rising to about 18 at 38 seconds and 40 at 125 seconds for air inside a one-foot diameter sphere, with a Rayleigh Number of about  $2 \times 10^7$ . Note that the  $t_1$  and  $t_2$  values for this case, based on the approach outlined by Ede (1967), are 3.3 and 8.4 seconds, respectively. The transient times for natural convection inside spheres, then, may be considerably greater than those for flat plates.

#### 2.4.4 Effects of Vibration

Vibration of the solid boundary can have a substantial effect on natural convection heat transfer. Ede (1967) reported work that indicated first a small drop in heat transfer, then an increase of up to 50%, with increasing vibrational frequency. Increases of up to 220% were found when the fluid (air) was set in motion by sound waves at about 200 Hz.

Baxi and Ramachandran (1969) reported natural convection heat transfer increases of up to a factor of 7 for frequencies of 2.5 to 15.5 Hz for copper spheres vibrating in air. They correlated their data in the following form:

$$\frac{Nu_v}{Nu_o} = 0.83 \left[ \frac{Re_v^{0.5} (a/D)^{0.1}}{Gr^{0.25}} \right]^{1.28} \quad (2-34)$$

with the "vibrational Reynolds Number,"  $Re_v$ , defined as:

$$Re_v = \frac{D \rho}{\mu} (\sqrt{2} \pi a f) \quad (2-35)$$

Gebhart (1963) presents a somewhat different analysis for natural convection under low gravity conditions. He assumes that there are random vibrations of amplitude,  $a$ , occurring at time intervals,  $t$ . His analysis then predicts a Nusselt Number, for the flat-plate situation, of:

$$Nu_n = 1 + \left( \frac{\rho C_p a^2}{k t} \right)^{0.5} \quad (2-36)$$

The observed increases in heat transfer with vibrations can be explained qualitatively. Initially, the heat transfer rate is high because the system is in the conduction phase where the heat transfer is substantially greater than under steady-state conditions, as described in Section 2.4.3. A vibration brings new fluid to the solid-fluid interface. This starts a new conduction phase all over again. The process is repeated over and over. The system never reaches the steady-state phase of smooth laminar convective heat transfer.

## 2.5 Combinations of Heat Transfer Processes

Several combining rules have been suggested for situations where conduction, natural and forced convection are all significant (Churchill, 1977). Most of them take the following form:

$$Nu^n = \sum_{i=1}^m Nu_i^n \quad (2-37)$$

When the exponent is equal to 1.0, of course, this is a simple linear combination of effects. Churchill's recommendation, based on plots of data from over fifty sources, is a slightly modified form of Equation 2-37, with the exponent equal to 3.0:

$$(Nu - Nu_c)^3 = Nu_f^3 + Nu_n^3 \quad (2-38)$$

## 2.6 A Priori Estimate of Heat Transfer Coefficient

An a priori estimate of the Nusselt Number for calculating steady-state heat transfer coefficients for the orbiting ORS experiment was made prior to taking experimental data into account. Equation 2-38 was used to combine mechanisms. Conduction is based on Equation 2-15, forced convection on Equation 2-22, and natural convection on Equation 2-24 with a constant of 0.59. The entire correlation is given as:

$$Nu = 10 + (0.0417 Re^{1.5} + 0.205 Ra^{0.75})^{1/3} \quad (2-39)$$

Figure 2-3 shows curves of Nu as a function of Ra for various values of Re for this correlation.

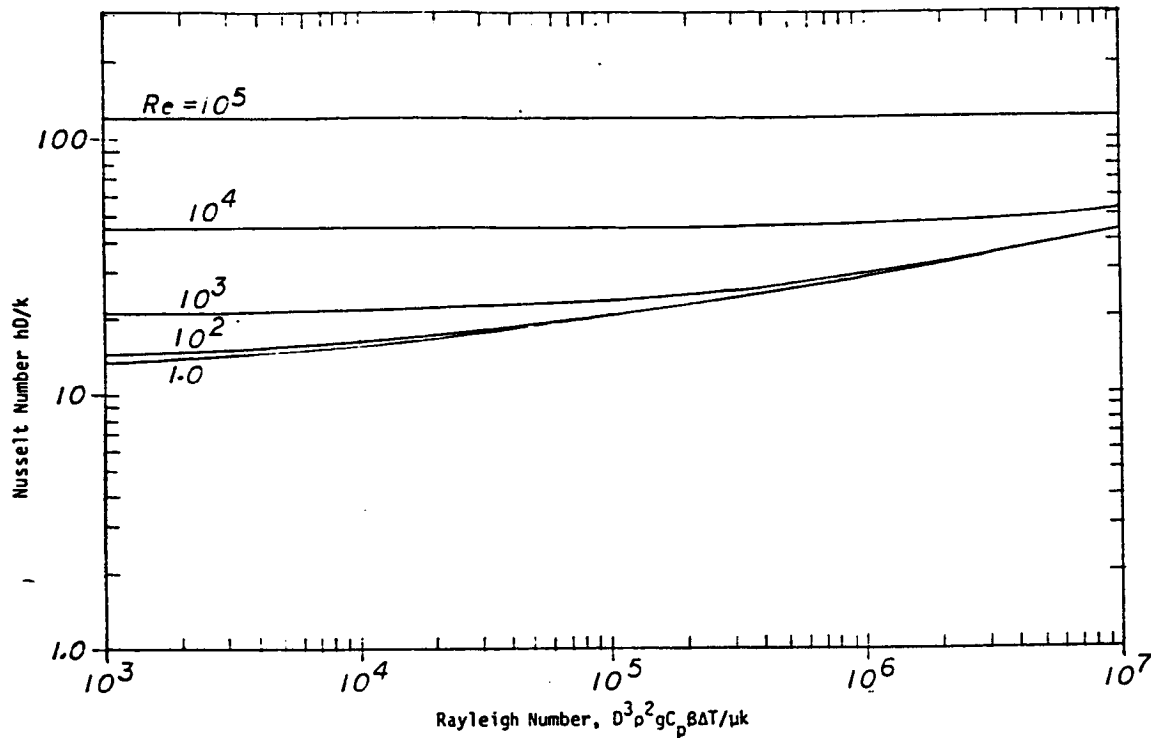


Figure 2-3. A-Priori Estimate of Nusselt Number

### 3.0 ORS DATA

#### 3.1 System Description

The Orbital Refueling System (ORS) was an experiment flown on the Space Shuttle STS 41-G mission in October, 1984. The ORS was designed to transfer liquid hydrazine back and forth from one tank to another using pressurized nitrogen as the driving force. Figure 3-1 is a photograph of the ORS experiment package in the payload bay of the Orbiter Challenger prior to launch. It was mounted on the MPESS (Mission Peculiar Equipment Support Structure) along with the Large Format Camera near the aft end of the bay. The propellant distribution system was contained in the primary housing (approximately 3 ft x 3 ft x 5 ft). The  $GN_2$  pressurization system was contained in the circular-faced protrusion seen in the photograph, adjacent to the astronaut work station on the front of the main housing. The avionic system was contained in the smaller box on the side of the main housing.

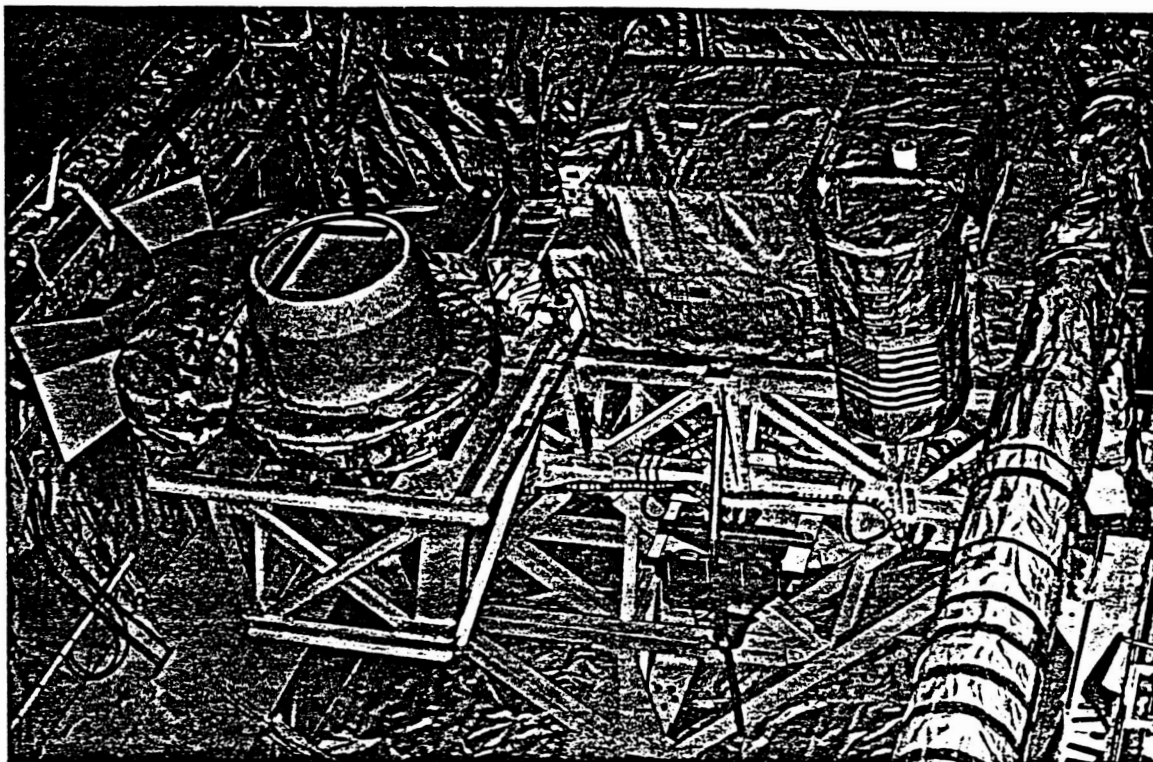


Figure 3-1. ORS Experiment Package in Orbiter Payload Bay

Figure 3-2 is a schematic diagram of the system. The two propellant tanks were 28-inch diameter titanium bladder tanks. The entire system - tanks, piping valves, etc., - was contained in an insulated box with an internal thermal control system designed to maintain an ambient temperature of 70°F. For most hydrazine transfer operations, the "by-pass" line was used. The "mod-kit" line was installed by the astronauts as part of the experiment, and one hydrazine transfer was made through this line. Detailed descriptions of the equipment design and calibration and the experiment procedures are available from other sources (e.g., Boyd, 1984, and other NASA reports.)

A time table of the ORS experiment conducted during STS 41-G is given in Table 3-1. Thirty discrete "events" were selected for possible analysis: coast periods, fuel transfers, tank ventings and tank pressurizations. Data

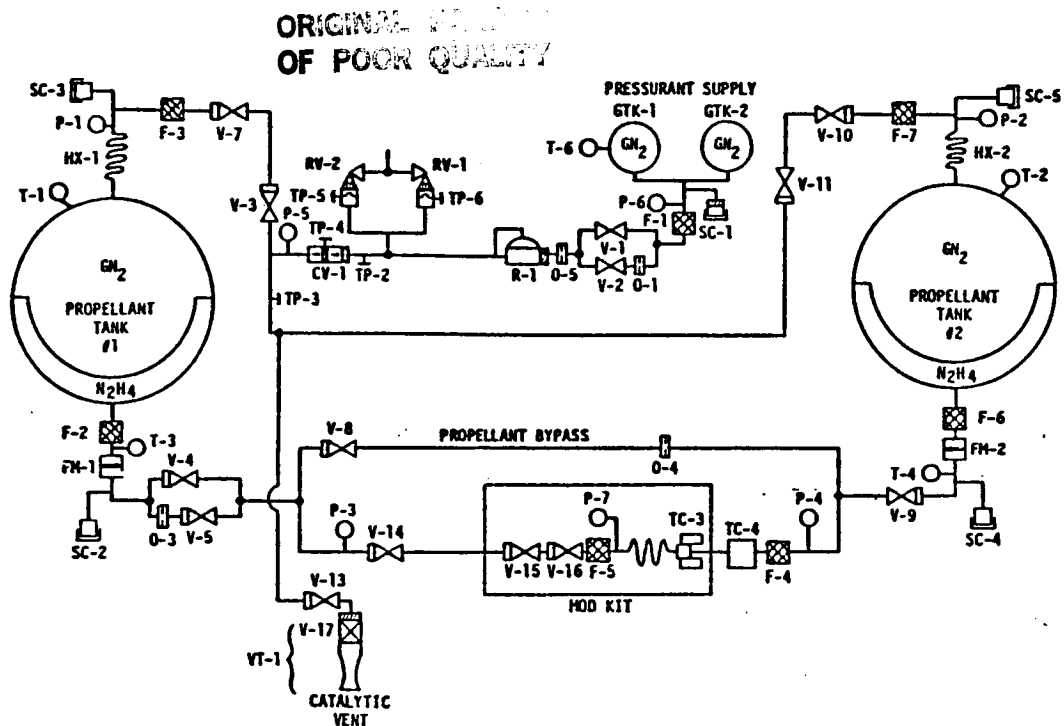


Figure 3-2. Schematic - ORS Fluid System

from 23 of these events were transcribed from the flight data records and put in a computer file for convenient use. For some events, especially coast periods, the data in the computer file cover only a portion of the total event time. Thus the "total duration" may exceed the "data duration." The "dead time" column represents time from the end of the event listed until the start of the next event. There often were additional actions taking place during this dead time, such as tank venting and pressurization. The "No data" entry means simply that the flight data were not transcribed and placed in the computer file; original flight data are available for the duration of the entire flight.



Table 3-1  
Schedule of ORS Events

Event No.	Event	Transfer Quantity (lbm)	Total Duration (min)	Data Duration (min)	Dead Time (min)
1	Transfer #1, Tk #1 to Tk #2	68.2	25	25	9
2	Vent Tk #1		26	26	0
3	Coast		1180	120	0
4	Pressurize Tk #2		5	5	60
5	Transfer #2a, Tk #2 to Tk #1	133.4	33	32	0
6	Coast		170	170	0
7	Pressurize Tk #2		5	No data	7
8	Transfer #2b, Tk #2 to Tk #1	55.9	16	15	6
9	Vent Tk #2		21	20	0
10	Coast		125	120	0
11	Pressurize Tk #1		2	2	1038
12	Transfer #3a, Tk #1 to Tk #2	135.0	37	37	0
13	Coast		201	170	0
14	Pressurize Tk #1		5	No data	7
15	Transfer #3b, Tk #1 to Tk #2	54.4	20	20	0
16	Vent Tk #1		20	No data	0
17	Coast		985	No data	0
18	Pressurize Tk #2		5	No data	7
19	Transfer #4a, Tk #2 to Tk #1	132.7	33	2	0
20	Coast		255	120	0
21	Pressurize Tk #2		5	No data	7
22	Transfer #4b, Tk #2 to Tk #1	56.2	16	16	16
23	Vent Tk #2		22	20	0
24	Coast		3957	130	0
25	Pressurize Tk #1		5	No data	7
26	Transfer #5, Tk #1 to Tk #2	140.0	52	52	5
27	Vent Tk #1		12	12	0
28	Coast		63	60	0
29	Transfer #6, Tk #2 to Tk #1	141.2	53	52	6
30	Vent Tk #2		16	16	-

The data recorded on the flight and transcribed for the computer file include the following parameters:

t <sub>elp</sub>	elapsed time from start of event (sec)
P-1	pressure in tank #1 (psia)
P-2	pressure in tank #2 (psia)
P-3	line pressure downstream of tank #1 isolation valves (psia)
P-4	line pressure downstream of tank #2 isolation valves (psia)
P-5	pressurization system check valve outlet pressure (psia)
P-6	nitrogen supply tank pressure (psia)
P-7	"mod kit" line pressure (psia)
T-1	tank #1 upper skin temperature (°F)
T-2	tank #2 upper skin temperature (°F)
M-1	quantity of liquid hydrazine in tank #1 (lbm)
M-2	quantity of liquid hydrazine in tank #2 (lbm)

Note that the system design had no means for direct measurement of gas temperatures. They had to be calculated from pressure, volume and mass data. Note, too, that the placement of P-1 and P-2 provided direct readings of ullage gas pressure only when there was no significant nitrogen flow in the supply lines. When nitrogen was flowing, ullage pressure had to be determined from the P-1 or P-2 data and a calculated pressure drop through the heat exchanger.

### 3.2 Approximate Energy Flows

The analysis on ullage gas temperature and pressure represents, to some degree, a search for small, significant differences among large quantities. To get a feel for the amount of energy involved in the various processes, consider Transfer #2a, in which 133 lbm (2.1 cubic feet) of hydrazine were transferred from Tank 2 to Tank 1. Tank 1 was originally at 70°F and 80 psia and contained 2.60 lbm of nitrogen. If the compression process were perfectly adiabatic, the nitrogen would end up at about 158°F and 137 psia. The total thermal energy increase of the nitrogen would be 41 Btu. The tank itself has a thermal capacity of about 22 Btu/°F, and the 133 lbm of hydrazine has a

thermal capacity of 98 Btu/°F. The total heat energy added to the nitrogen is sufficient to heat up the tank and its contents only about 0.3°F.

Return for a moment to one of the basic reasons for this study: the possibility of hydrazine on the ullage side of the bladder. If some liquid hydrazine has leaked into the ullage chamber, a small amount of it will vaporize. Will this vaporization process absorb a significant amount of the compressive thermal energy? Consider an ullage compartment originally at 70°F and 100 psia. At 70°F the vapor pressure of hydrazine is only 0.22 psia, so its mole-fraction in the gas is only 0.0022. Suppose that the gas is compressed to 200 psia adiabatically. Its temperature reaches 186°F, where the vapor pressure of hydrazine is 5.2 psia, permitting a hydrazine mole fraction of 0.026. If the ullage tank were the same size as those used in the ORS experiment, 0.010 lbm of hydrazine would vaporize, absorbing 6.2 Btu. The total thermal energy added to the gas by the compression would be 50 Btu. So, at most, the vaporization of the hydrazine would absorb only 12% of the energy.

### 3.3 ORSCOMP Program

The ORSCOMP computer program was developed by Mr. William C. Boyd, NASA JSC, to simulate the operation of the ORS equipment both on the ground and in orbit. It is a very detailed model, incorporating unsteady-state fluid flow and heat transfer calculations for every component of the system. Actual ground test data were used to determine many of the flow resistance terms. Ground-based experimental heat transfer data could not be directly applied to on-orbit conditions.

The ORSCOMP program has been used in many different ways. First, it was used in conjunction with ground tests to verify system performance and to obtain a great deal of calibration data. A version of ORSCOMP was used on-board the spacecraft to predict the behavior of the ORS system prior to the start of each fuel transfer. It has been used extensively in the analysis of the flight data, both for this present study and for other analyses.

### 3.4 Fixed Nusselt Number Correlations

The first approach used to analyze the ORS flight data was a fairly simple one: assume the ullage gas is perfectly mixed, and find a single Nusselt Number for each event which will fit the data. This method provided a simple means for comparing heat transfer rates for various events throughout the test series without introducing too many variables.

Preliminary analysis had shown that the amount of heat transfer observed was considerably greater than that which could be accounted for by conduction alone. There was clearly some mixing in the ullage gas. The ORSCOMP program includes options for both perfectly mixed (uniform temperature) and perfectly stratified (conduction heat transfer only) ullage gas. The "uniform temperature" option was used. Instead of calculating a heat transfer coefficient from flow rates and gas property data, single values for the Nusselt Number for heat transfer from the gas to the tank wall and bladder were entered. The program was then run, and the calculated pressures were compared with the pressure measurements from the flight data. The error criterion was defined as the sum of the squares of the differences between the calculated and measured pressure values. The Nusselt Number was varied until the error criteria was minimized. This was done for both tanks for each of the 23 events for which there were data in the computer file. Plots of pressure, mass of hydrazine transferred and temperature for Transfer #4a are given in Figures 3-3, 3-4 and 3-5. The data are matched quite closely.

Reynolds Numbers, Rayleigh Numbers and heat transfer coefficients were calculated for the best-fit Nusselt Numbers. The choices of the length and velocity terms for the Reynolds numbers are somewhat arbitrary. For cases where there was nitrogen flowing from the supply tank to the ullage space, the velocity used was the velocity in the feed line, and the length term was the feed line diameter. Similarly for tank venting, the velocity and length were based on the outlet tube conditions. For cases in which the ullage gas was simply compressed or expanded, the velocity used was that of the tank bladder (obviously a very low velocity), and the length term was the tank diameter. Resulting Reynolds Numbers were in the range of 6000 to 51000 for the cases in which nitrogen gas was flowing into or out of the tank, and 6 to 20 for the

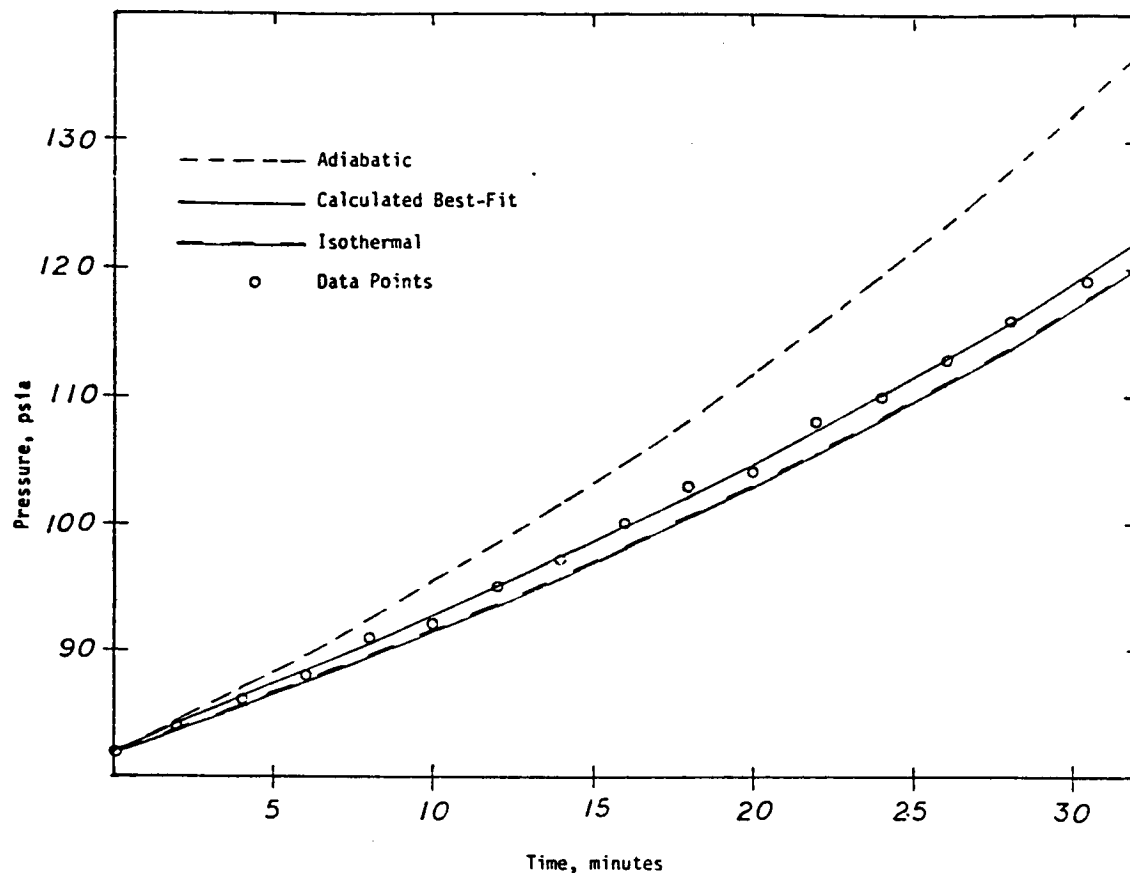


Figure 3-3. Pressure Profiles for Transfer #4a

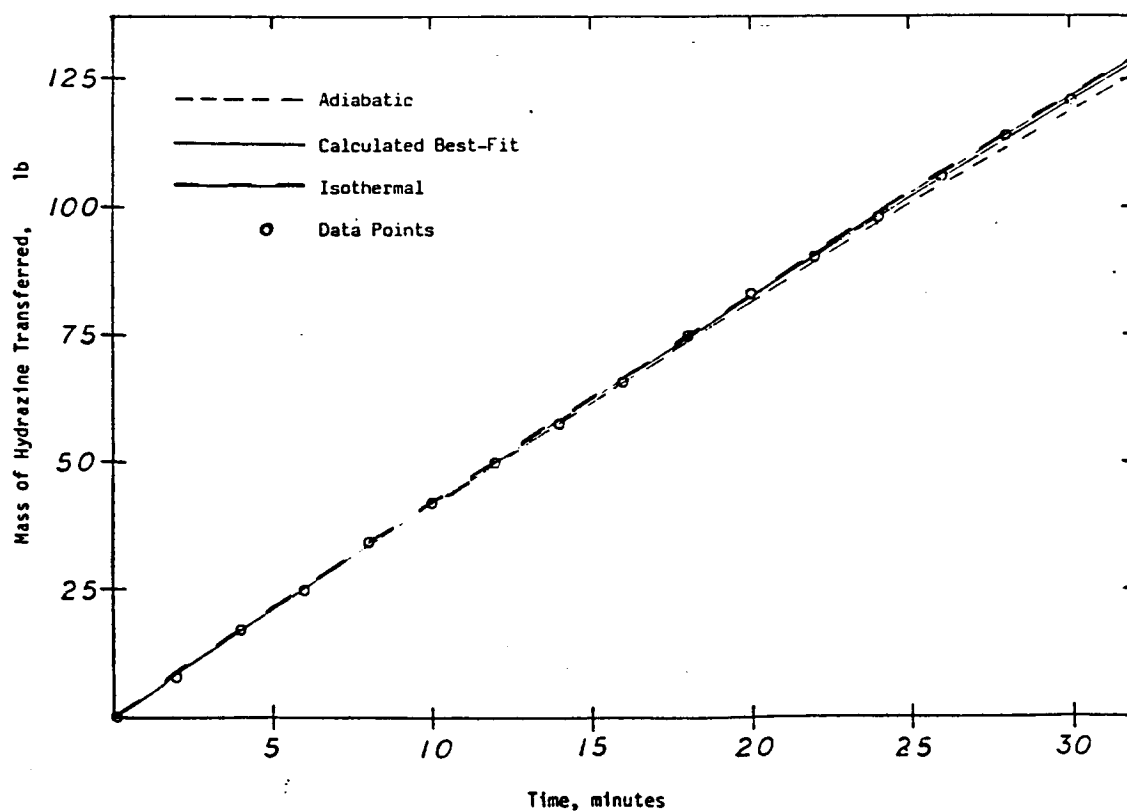


Figure 3-4. Hydrazine Mass Profiles for Transfer #4a

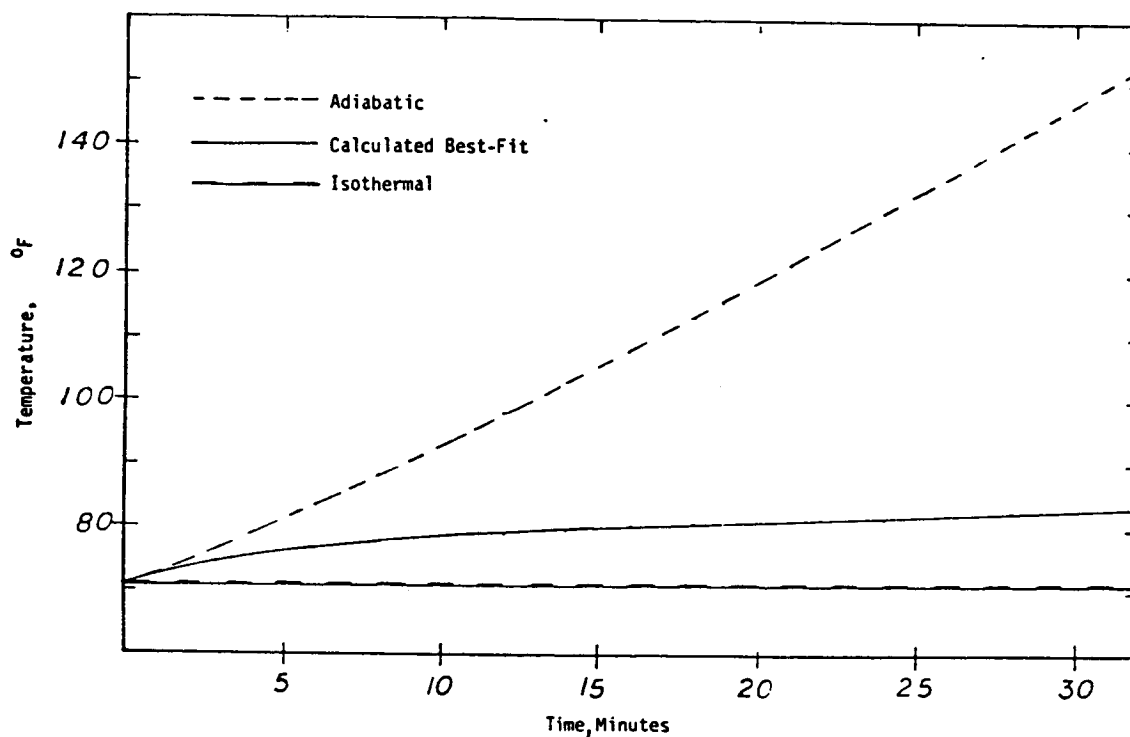


Figure 3-5. Temperature Profiles for Transfer #4a

gas compression or expansion cases. Rayleigh Numbers were calculated using the tank diameter as the length term and  $10^{-5}$  g as the acceleration term. The acceleration choice is obviously somewhat arbitrary. The calculated Rayleigh Numbers ranged from 25,000 to 1,680,000.

Results of these constant Nusselt Number correlations are given in Table 3-2. Only those events for which there was a calculated temperature change of 5°F or more are included; smaller temperature changes lead to extremely wide ranges of Nusselt Numbers which fit the flight data equally well. The "estimated precision" column is based on the range of Nusselt Numbers for which the error criterion is essentially constant. The same data are plotted in Figures 3-6 and 3-7, along with curves based on Equation 2-39.

Table 3-2  
Fixed Nusselt Number Correlations

Event No.	Event	Tank No. * & Action	Re	Calculated Average Ra	Nu	h **	Est. % Precision
(Low Reynolds Number Events)							
1	Trans #1	1 B	20	378,000	78	0.48	10
1	Trans #1	2 F	17	209,000	50	0.31	9
2	Vent Tk #1	2 C	0	70,000	64	0.39	22
3	Coast	1 C	0	76,000	24	0.15	21
5	Trans #2a	1 F	13	55,000	74	0.46	9
6	Coast	1 C	0	25,000	40	0.25	44
8	Trans #2b	1 F	20	106,000	86	0.53	9
9	Vent Tk #2	1 C	0	47,000	41	0.25	16
10	Coast	2 C	0	142,000	29	0.18	9
12	Trans #3a	2 F	15	201,000	38	0.23	5
13	Coast	2 C	0	195,000	8	0.05	9
15	Trans #3b	2 F	19	382,000	34	0.21	6
19	Trans #4a	1 F	13	74,000	64	0.39	8
20	Coast	1 C	0	25,000	55	0.34	90
22	Trans #4b	1 F	20	184,000	52	0.32	8
24	Coast	2 C	0	118,000	40	0.25	14
26	Trans #5	2 F	12	118,000	53	0.33	11
28	Coast	1 C	0	332,000	33	0.20	12
28	Coast	2 C	0	121,000	8	0.05	35
29	Trans #6	1 F	6	142,000	32	0.19	13
29	Trans #6	2 B	12	81,000	79	0.49	19
(High Reynolds Number Events)							
2	Vent Tk #1	1 V	19,100	786,000	44	0.27	11
4	Pres Tk #2	2 P	18,100	867,000	100	0.62	10
5	Trans #2a	2 E	9,700	158,000	90	0.56	44
9	Vent Tk #2	2 V	22,800	1,677,000	3	0.02	200
11	Pres Tk #1	1 P	51,000	401,000	345	2.13	12
12	Trans #3a	1 E	8,200	152,000	130	0.80	50
19	Trans #4a	2 E	9,500	85,000	360	2.22	56
23	Vent Tk #2	2 V	23,100	1,600,000	5	0.03	40
26	Trans #5	1 E	6,300	125,000	105	0.65	200
27	Vent Tk #1	1 V	28,000	1,030,000	6	0.04	40
30	Vent Tk #2	2 V	10,800	106,000	66	0.41	9

\* B - Tank Blowdown, C - Coasting, E - Tank Emptying, F - Tank Filling,  
P - Tank Pressurization, V - Tank Venting

\*\* Units for the heat transfer coefficient are BTU/ft<sup>2</sup>hr°F

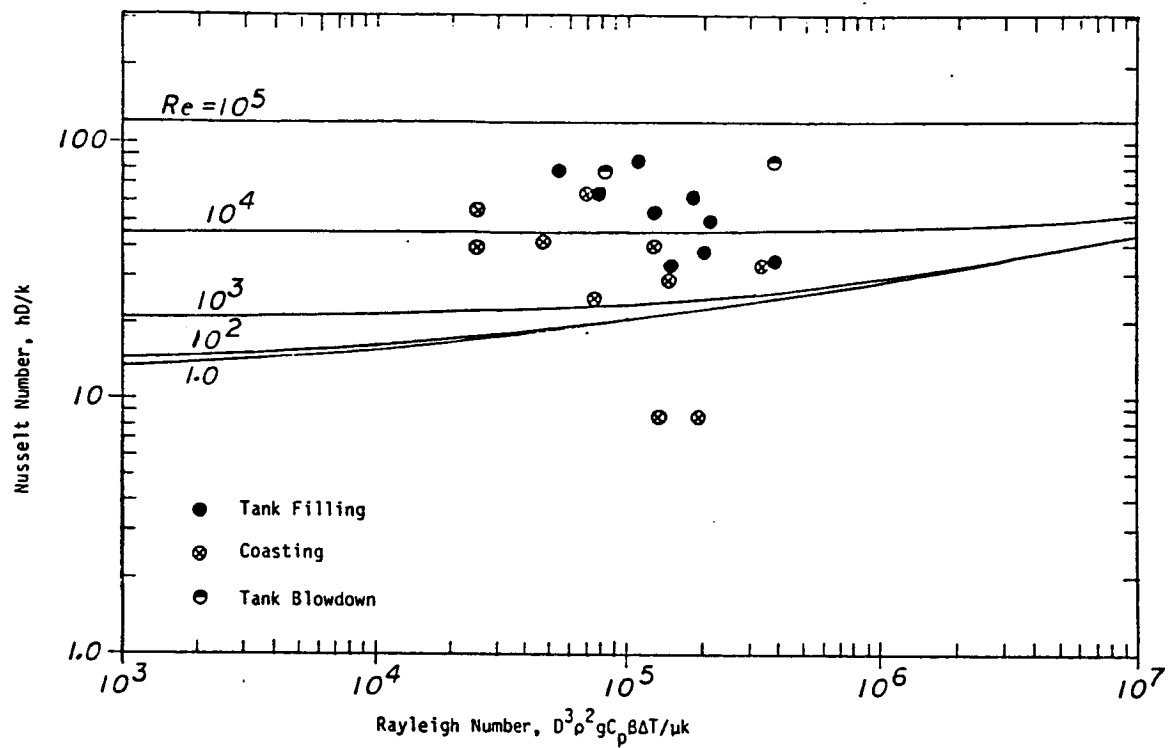


Figure 3-6. Fixed Nusselt Number Correlations for Low-Re Events

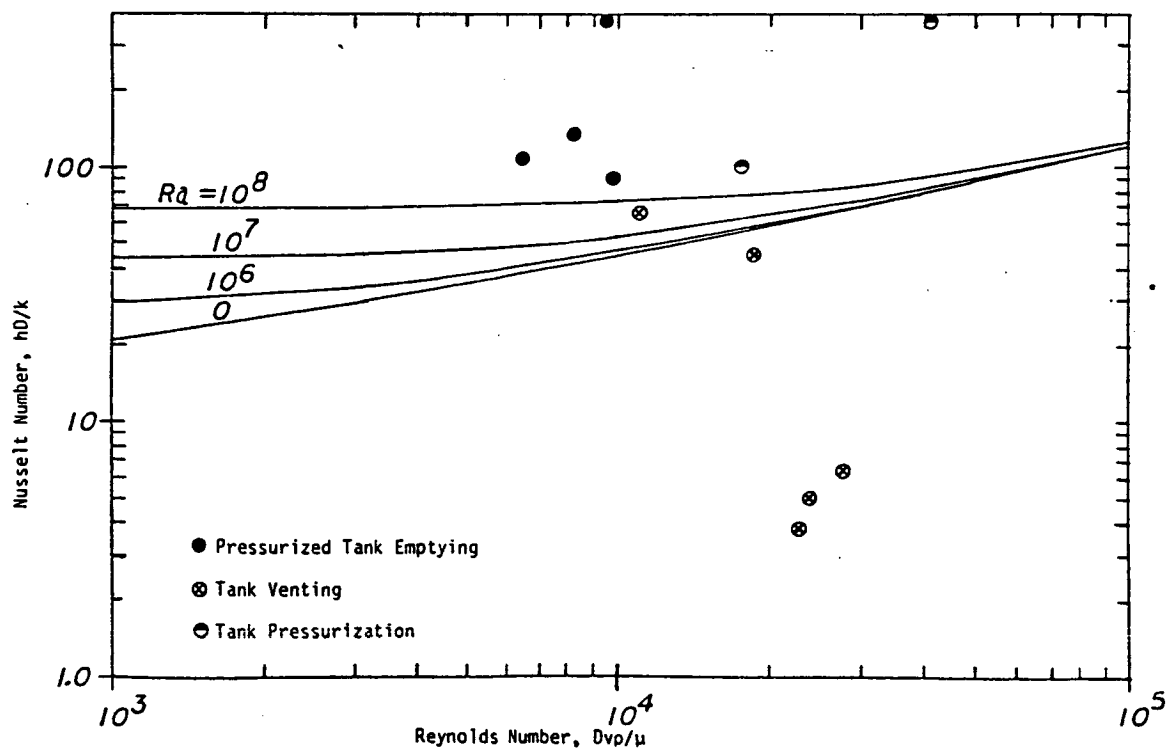


Figure 3-7. Fixed Nusselt Number Correlations for High-Re Events



### 3.5 Variable Nusselt Number Correlations

The next analysis of the ORS flight data was somewhat more sophisticated. It attempted to account for all the expected variations in Nusselt Number due to fluid properties and flow conditions. Nusselt Numbers were calculated using Equation 2-39. These Nusselt Numbers were then multiplied by an arbitrary factor,  $F$ , in order to match the data. As before, the sum of the squares of the differences in the calculated and measured pressures was used as the error criterion.  $F$  was varied until this criterion was minimized.

For this analysis, the Reynolds Numbers were defined just as before. The length term in the Rayleigh Number, however, was changed from the tank diameter to one-fourth of the tank circumference. It was felt that this latter value was more representative of the path length of any natural convection flow field that could develop. The values of the Rayleigh Numbers, therefore, are somewhat lower than in the previous analysis.

Results of this analysis are given in Table 3-3 and in Figures 3-8 and 3-9. In Table 3-3, the "calculated" Nusselt Number is the one found directly from Equation 2-39. The "data" Nusselt Number is the calculated value multiplied by  $F$ , the fixed correction factor for each case.

### 3.6 Thruster Acceleration Data

The Rayleigh Number is directly proportional to the local acceleration. For the variable-Nusselt-Number analysis, a constant acceleration of  $10^{-5}$  g was assumed. To see whether this assumption was reasonable, and to see whether accelerations might account for the apparent increased heat transfer by changing the Rayleigh Number, an estimate was made of the acceleration at the ORS experiment location during several key events. Vernier thruster data from the flight records were used to calculate accelerations for seven five-minute time periods during six transfer events, taking into account vehicle mass, attitude, ORS location, etc.

Table 3-3  
Variable Nusselt Number Correlations

Event No.	Event	Tank No. * & Action	Calculated Re	Average Ra	Nu	Data Nu	h **	Est. % Precision
(Low Reynolds Number Events)								
1	Trans #1	1 B	19	191,000	22	74	0.46	6
1	Trans #1	2 F	16	104,000	20	47	0.30	9
2	Vent Tk #1	2 C	0	38,000	18	51	0.33	24
3	Coast	1 C	0	37,000	18	21	0.13	9
5	Trans #2a	1 F	13	28,000	18	68	0.44	10
6	Coast	1 C	0	9,000	16	33	0.21	27
8	Trans #2b	1 F	19	52,000	19	83	0.53	8
9	Vent Tk #2	1 C	0	23,000	17	39	0.25	17
10	Coast	2 C	0	69,000	19	25	0.16	11
12	Trans #3a	2 F	15	94,000	20	38	0.24	4
13	Coast	2 C	0	97,000	20	5	0.03	18
15	Trans #3b	2 F	19	181,000	22	57	0.22	4
19	Trans #4a	1 F	13	33,000	18	61	0.41	11
20	Coast	1 C	0	10,000	16	72	0.46	66
22	Trans #4b	1 F	19	87,000	20	52	0.33	10
24	Coast	2 C	0	50,000	18	34	0.21	19
26	Trans #5	2 F	11	48,000	18	59	0.38	11
28	Coast	1 C	0	165,000	21	29	0.18	6
28	Coast	2 C	0	57,000	19	8	0.06	30
29	Trans #6	1 F	6	56,000	18	37	0.23	14
29	Trans #6	2 B	11	13,000	16	240	1.52	67
(High Reynolds Number Events)								
2	Vent Tk #1	1 V	18,000	317,000	56	57	0.35	7
4	Press Tk #2	2 P	15,700	308,000	50	135	0.86	15
5	Trans #2a	2 E	9,400	30,000	44	287	1.82	25
9	Vent Tk #2	2 V	21,000	764,000	59	8	0.05	35
11	Press Tk #1	1 P	42,800	654,000	88	48	0.31	20
12	Trans #3a	1 E	8,100	87,000	42	104	0.67	60
19	Trans #4a	2 E	9,100	84,000	44	118	0.76	20
23	Vent Tk #2	2 V	21,000	726,000	59	9	0.06	25
26	Trans #5	1 E	6,200	57,000	37	112	0.72	100
27	Vent Tk #1	1 V	25,800	472,000	67	59	0.36	5
30	Vent Tk #2	2 V	9,800	23,000	13	177	1.10	40

\* B - Tank Blowdown, C - Coasting, E - Tank Emptying, F - Tank Filling  
P - Tank Pressurization, V - Tank Venting

\*\* Units for the heat transfer coefficient are BTU/ft<sup>2</sup>hr°F

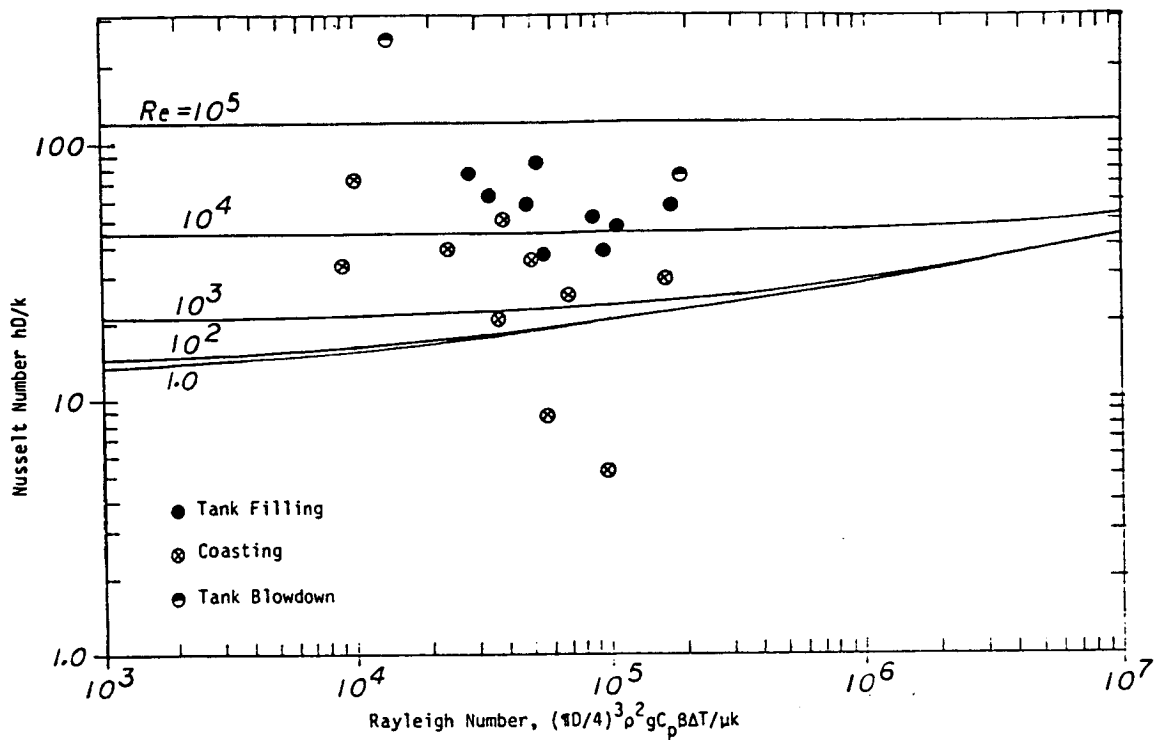


Figure 3-8. Variable Nusselt Number Correlations for Low-Re Events

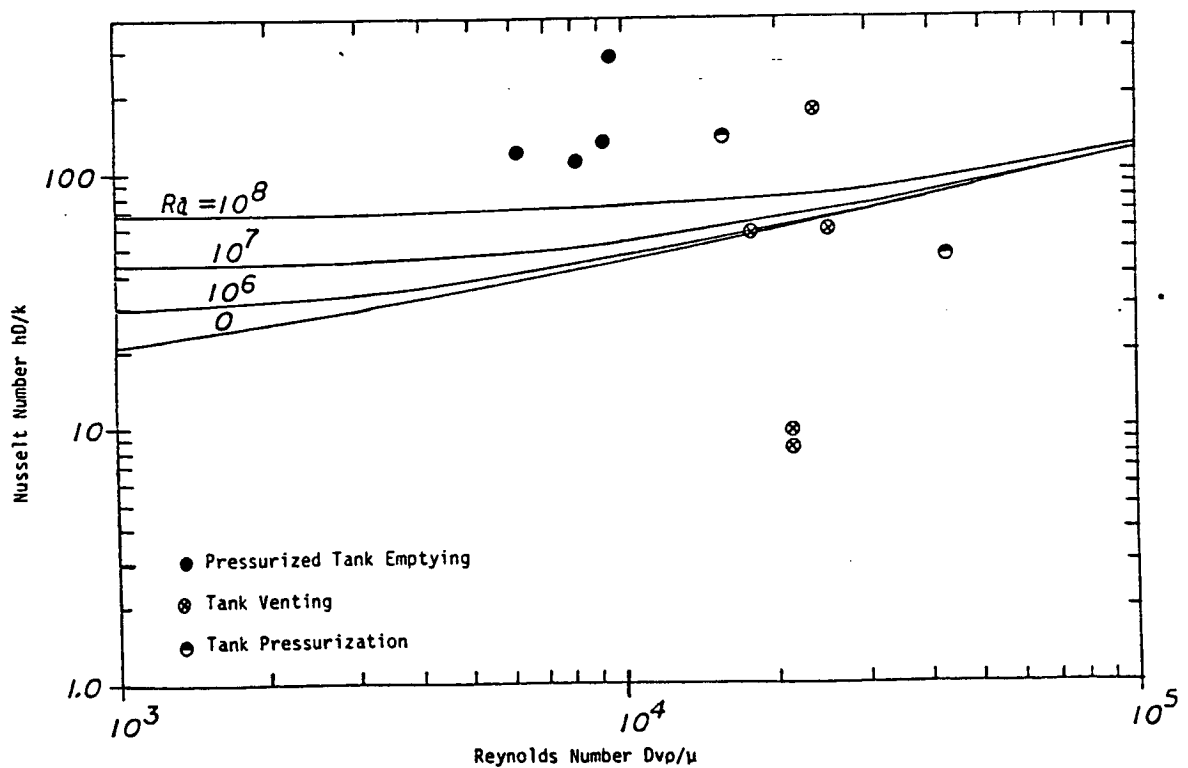


Figure 3-9. Variable Nusselt Number Correlations for High-Re Events

Results of the acceleration calculations are given in Table 3-4. The "Applied Acceleration" term gives the vehicle acceleration while the thrusters are firing. The "Mean Acceleration" term is the time-weighted-average of the "Applied Acceleration," taking into account the periods of time in which the thrusters were not firing. During the periods selected, only the vernier thrusters were in use. (These calculations were performed by Mr. Eric Hurlbert, NASA JSC.)

Table 3-4  
Accelerations on ORS from Vernier Thrusters

Event No.	Event	Impulses per Minute	Average Firing Duration (sec.)	Applied Acceleration (g's)	Mean Acceleration (g's)
5	Trans #2a	6.2	0.31	$1.5 \times 10^{-4}$	$5.5 \times 10^{-6}$
8	Trans #2b	3.6	0.56	$1.2 \times 10^{-4}$	$5.7 \times 10^{-6}$
12	Trans #3a	36.7	1.63	$2.1 \times 10^{-4}$	$130 \times 10^{-6}$
12	Trans #3a	23.2	0.11	$1.2 \times 10^{-4}$	$6.6 \times 10^{-6}$
15	Trans #3b	1.7	0.07	$1.0 \times 10^{-4}$	$0.23 \times 10^{-6}$
19	Trans #4a	5.0	0.13	$1.2 \times 10^{-4}$	$1.7 \times 10^{-6}$
29	Trans #6	4.5	0.12	$1.2 \times 10^{-4}$	$1.5 \times 10^{-6}$

#### 4.0 ORS ANALYSIS

##### 4.1 Analysis of Low-Re Events

Three types of events had very low, or even zero, Reynolds Numbers: tank fillings, coasts, and blowdown tank emptyings. Data from the 21 events in this group are summarized in Tables 3-2 and 3-3 and in Figures 3-6 and 3-8. For all of these cases, the Reynolds Number is so small that its contribution to the overall Nusselt Number, based on Equation 2-39, is essentially zero. The Nusselt Number is therefore expected to be of the form:

$$Nu = Nu_c + C Ra^n \quad (4-1)$$

Several analyses of the data were carried out. First, the two sets of correlations were compared. There was no significant improvement in fitting the experimental data with the variable Nusselt Number analysis, as compared to the fixed Nusselt Number analysis. In fact, the calculated values were significantly different only for the blowdown tank emptying in event 29. Both approaches gave unrealistically low heat transfer coefficients for two coast events, numbers 13 and 28, both for Tank 2. The apparent heat transfer coefficient due to conduction alone is about  $0.06 \text{ Btu/ft}^2\text{hr}^\circ\text{F}$ .

A statistical analysis of the Nusselt Numbers and Rayleigh Numbers for the tank filling events, using the values from the variable Nusselt Number analysis, gave the following results. Allowing both constants in Equation 4-1 to vary, but maintaining the conduction Nusselt Number at 10 yields:

$$Nu = 10 + 145 Ra^{-0.082} \quad (4-2)$$

Fixing the exponent at 0.25 yields:

$$Nu = 60 + 0.0096 Ra^{0.25} \quad (4-3)$$

An additional analysis was made to determine a linear regression line for the experimental Nusselt Number as a function of the one calculated from Equation 2-39. This yielded:

$$Nu = 65.0 - 0.246 Nu_0 \quad (4-4)$$

In none of these correlations, however, was the degree of correlation significant. From a statistical viewpoint, it is more justifiable to state simply that, within the scatter of the data, the heat transfer coefficient for fill events was  $0.34 \text{ Btu/ft}^2\text{hr}^\circ\text{F}$ , with an uncertainty of  $\pm 30\%$ ; or that the Nusselt Number was  $60 \pm 14$  (or  $\pm 24\%$ ).

For coast events, the results were similar. The three correlations corresponding to Equations 4-2, 4-3 and 4-4, are:

$$Nu = 10 + 3840 Ra^{-0.47} \quad (4-5)$$

$$Nu = 30 + 0.14 Ra^{0.25} \quad (4-6)$$

$$Nu = 159 - 7.0 Nu_0 \quad (4-7)$$

Again, however, none of these are significant correlations. The scatter in the data is somewhat greater than that for tank fills. The best that can be justified statistically is an average heat transfer coefficient of  $0.22 \text{ Btu/ft}^2\text{hr}^\circ\text{F}$ , with an uncertainty of  $\pm 68\%$ , or a Nusselt Number of  $32 \pm 20$ . The coast operation, however, is a less critical one in terms of safety than the tank filling operation; so obtaining a better correlation here is of secondary importance.

In order to assess whether vehicle acceleration changes could account for the increases and variations in heat transfer coefficients, the thruster data summarized in Table 3-4 were examined. There was no significant correlation between acceleration and heat transfer. One would expect the heat transfer coefficients to increase as the one-fourth power of the acceleration, in line with Equation 4-1. The observed heat transfer, however, was fairly low for both the highest and lowest accelerations, transfers #3a and #3b.

The correlation used by Jahn and Reineke (1974) included the Dammkohler Number. In the ORS experiments it had a value of about 1000 for tank filling events and a value of zero for coast events. The mean Nusselt Numbers for the coast events are indeed lower than those for the tank filling events, but not enough lower to fit Equation 2-30 using exponents in the range they reported.

The time needed to reach steady-state was examined using the approach outlined by Ede (1967). Evaluating Equations 2-31 and 2-32 using a 5°F temperature difference and  $10^{-5}$  g acceleration,  $t_1$  has a value of 2100 seconds and  $t_2$  has a value of 5300 seconds. These times are indeed long compared to the total event times. It would appear likely that this unsteady-state factor is playing an important role, but it is a very difficult one to quantify for any geometry except vertical flat plates. Equation 2-33, integrated over a finite period of time, would lead one to conclude that the time-average heat transfer coefficient should vary inversely with the square root of the time. A correlation of the form:

$$Nu = Nu_c + C/\sqrt{t} \quad (4-8)$$

was tried. For tank fills, it gave:

$$Nu = 43 + 690/\sqrt{t} \quad (4-9)$$

and for coast events:

$$Nu = 19 + 770/\sqrt{t} \quad (4-10)$$

The correlation was positive, but not statistically significant.

The vibration effect on Nusselt Number proposed by Gebhart (1963) was examined, applying the vernier thruster firing frequency Equation 2-36. There was no significant correlation.

## 4.2 Analysis of High-Re Events

Three types of events were characterized by having large Reynolds Numbers: pressurized tank emptying, tank venting and tank pressurization. Data for 11 events of this sort having temperature changes of 5°F or more are given in Tables 3-2 and 3-3 and in Figures 3-7 and 3-9. In all of these cases, the Reynolds Number contribution to the overall Nusselt Number was much larger than that of the Rayleigh Number contribution, based on Equation 2-39. The expected form of the Nusselt Number correlation is then:

$$Nu = Nu_c + C Re^n \quad (4-11)$$

Again there was no significant improvement in fit to the data from using the variable Nusselt Number approach rather than the fixed Nusselt Number approach. For the high Reynolds Number events, there were many more cases of significant differences between the two approaches, but the differences seemed to be random. For Transfer #2a, the tank-emptying Nusselt Number was much higher for the variable approach. For Transfer #4a, the reverse held true. Tank vents gave highly variable results. Some of the variability in these events can be attributed to uncertainty in the initial conditions for the event. Small uncertainties in the calculated amount of nitrogen originally present in the tank can lead to large uncertainties in the heat transfer rates.

A least-squares fit of the data for the high Reynolds Number events gave the following correlation, keeping the exponent fixed at one-half:

$$Nu = 104 - 0.098 Re^{0.5} \quad (4-12)$$

The correlation coefficient is almost zero, however, so it is of no real significance.

The four tank-emptying events give an average heat transfer coefficient of  $0.99 \pm 0.55$  Btu/ft<sup>2</sup>hr°F, or an average Nusselt Number of  $155 \pm 87$ .



### 4.3 System Uncertainty Analysis

The expected uncertainty in the experimental determination of some quantity can be estimated from the uncertainties of each of the known or measured parameters which are involved, by the equation:

$$[E(y)]^2 = \sum_{i=1}^n \left[ \left( \frac{\delta y}{\delta x_i} \right) E(x_i) \right]^2 \quad (4-13)$$

$E(y)$  is the expected uncertainty, similar to the standard deviation, in the dependent variable,  $y$ , for a single experiment. This approach assumes that the uncertainties in the independent variables,  $x_i$ , are all normally distributed. This is rarely the case, but the approach is still useful in analyzing an experiment to see which variables are most important.

Consider a tank-filling event with conditons similar to those of Transfer #2a. The dependent variable is the heat transfer coefficient. The time-dependent energy balance is written as:

$$\frac{\delta(C_v NT)}{\delta t} = -P \frac{\delta V}{\delta t} - h A(T - T_w) \quad (4-14)$$

This can be combined with the ideal gas law and rearranged to solve for the heat transfer coefficient explicitly in terms of known or measured quantities:

$$h = \frac{NRP\dot{V} + NC_v P\dot{V} + NC_v V\dot{P}}{NRAT_w - APV} \quad (4-15)$$

$E(h)$  is now calculated from Equation 4-13. For all practical purposes,  $A$ ,  $C_v$ , and  $R$  are known exactly. The other six parameters on the right-hand-side of

Equation 4-15 form the set of independent variables. Their values and an estimate of the uncertainties in their values are as follows:

<u>Parameter</u>	<u>Value</u>	<u>Estimated Uncertainty</u>
P	90 psia	0.75 psia
V	6.0 ft <sup>3</sup> of N <sub>2</sub>	0.01 ft <sup>3</sup> of N <sub>2</sub>
$\dot{V}$	-3.88 ft <sup>3</sup> /hr	0.02 ft <sup>3</sup> /hr
$\dot{P}$	60 psi/hr	6 psi/hr
N	0.0928 moles	0.0009 moles
T <sub>w</sub>	71°F	0.75°F

The uncertainty estimates are based on examination of the scatter in the orbital test data.

After evaluating all the derivatives and plugging in the appropriate numerical values, the uncertainty in the heat transfer coefficient is estimated to be 0.206 Btu/ft<sup>2</sup>hr°F. The actual value of the coefficient calculated from these parameters is 0.309 Btu/ft<sup>2</sup>hr°F. The uncertainty, then, is 67% of the actual value. In other words, from the data used in the example, one would have about 95% confidence from one experiment that the coefficient was in the range of 0.103 to 0.515 Btu/ft<sup>2</sup>hr°F.

Of the 67% uncertainty in the value of the heat transfer coefficient, 46% is attributable to uncertainties in pressure and the pressure/time derivative, and 47% is attributable to uncertainties in the amount of gas originally present, N. (N was, of course, calculated from initial pressure and temperature data. The uncertainty estimate for N was made in the same way as the overall uncertainty estimate.) About 9% of the uncertainty is attributable to volume and volume rate uncertainties, and 7% is attributable to wall temperature uncertainty. The high influence of N and pressure uncertainties is partly due to the fact that they are used to calculate gas temperature, for which there are no measured values.

The analysis so far is for a single experiment. When multiple experiments are done, the expected uncertainty can be reduced:

$$E_n(y) = \frac{E(y)}{\sqrt{n - m}} \quad (4-16)$$

Here,  $n$  is the number of experiments and  $m$  is the number of unknown parameters to be fixed by the experiment for any appropriate correlation. If there are nine experiments, the nine tank filling events, the expected uncertainty is reduced from 67% to 22% for determining a single, average heat transfer coefficient. This is not out of line with the observed results from the nine ORS tank filling events, which had a standard deviation of 24%. If the nine events were used to fit a two-parameter model, the expected uncertainty would be about 25%.

Overall, the observed scatter in data is not unexpected considering the design of the experiment, the number of tests carried out and the uncertainties in the various measured parameters. The observed data are not inconsistent with the assumption of a single Nusselt Number for tank filling events. The data scatter, and the fact that it is reasonably consistent with the expected uncertainty, precludes making any other statistically significant correlation. This does not mean that such a correlation does not exist, it simply means that it can't be proved with the available data.

In order to obtain  $\pm 10\%$  uncertainty in results using the present ORS experimental system, the value of  $(n - m)$  would have to be about 45. Alternatively, the individual experiment uncertainty might be reduced by using more precise instrumentation and by careful filtering of data. In particular, better means of determining the amount of nitrogen initially present and in determining pressure/time derivatives would be useful.

#### 4.4 ORS Limitations

There were several inherent limitations in using ORS data to develop heat transfer correlations for ullage gas in space operation. Some are inherent

limitations due to safety and operational factors. Others are limitations that might be removed in any similar tests in the future. Citing them here is not meant to imply criticism; it is more the result of hindsight.

The most significant limitations appear to be in the basic understanding of convective heat transfer in closed containers with internal heat generation at low Rayleigh Numbers under transient conditions subject to outside disturbances. There is no suitable, proven model to use for such a problem, even for ground-based experiments. These limitations are addressed further in Sections 5 and 6 of this report.

The most significant drawback in the equipment itself was the lack of any means to obtain gas temperatures directly. Such data would have been extremely valuable. Alternatively, data on the density of the nitrogen inside the tanks could have provided an indirect measurement of temperature. There was also a lack of good, precise vehicle acceleration data. From the limited amount of thruster data analyzed, acceleration does not appear to be very significant, but it would have been useful to search for correlations during coasts and other events as well as during short periods of several tank fillings. Of somewhat less importance, the pressure data provided were measured on the opposite side of the nitrogen heat exchangers from the tanks. In some cases there was a significant pressure difference between the tank and the measuring point due to the flow of nitrogen. The reliability of the data would have been enhanced had the pressure transducers been closer to the tanks themselves.

There were two basic limitations imposed from an operational standpoint. First, much of the uncertainty on the amount of nitrogen originally present in each tank was due to pressurizing the tank to be emptied just prior to the fuel flow events. The entire system was not at a steady-state when the transfers began. Second, the transfers were essentially all duplications of the same experimental conditions, with the exceptions of using the "mod-kit" for one transfer and using blowdown procedures for two. Temperatures, flow rates, pressures, etc. were all very similar. As a proof-of-feasibility concept, this was fine. As an engineering experiment, it left large regions of possible operating conditions unexplored.

## 5.0 SUMMARY OF CURRENT KNOWLEDGE

### 5.1 Conductive Heat Transfer - The Conservative Approach

Pure conduction represents a very conservative lower bound on the heat transfer which takes place between ullage gas and tank walls. So long as there is any gas at all present, conduction will take place. Any convective heat transfer will simply increase the overall heat transfer rate. It would be appropriate to use conductive heat transfer alone for calculations related to safety and worst-case conditions.

#### 5.1.1 Modelling Considerations

For a sphere with internal heat generation  $q_i$ , an energy balance at the wall gives:

$$hA(\bar{T} - T_o) = -kA \left. \frac{\delta T}{\delta r} \right|_{r_o} \quad (5-1)$$

It can be easily shown that the apparent Nusselt Number will have a value of 10, or:

$$h = 10 k/D \quad (5-2)$$

For a long cylinder, in which end effects are neglected, the comparable value is 8:

$$h = 8 k/D \quad (5-3)$$

For the space between infinite parallel plates, the comparable value is 4:

$$h = 4 k/H \quad (5-4)$$

For a spherical bladder tank, it would be appropriate to use:

$$h = \max \left\{ \frac{10k}{D}, \frac{4k}{H} \right\} \quad (5-5)$$

where H is the maximum distance from the center of the bladder to the opposite tank center, through the ullage gas (See Figure 5-1). In this way, the spherical tank result is used until the tank is about 60% full, then the flat plate result is used as the gas space flattens and decreases in volume.

The above results are based on average gas temperatures. It is also necessary to determine the maximum gas temperature. For a sphere, it is given by:

$$T_{\max} - T_w = \frac{q_i D^2}{24k} \quad (5-6)$$

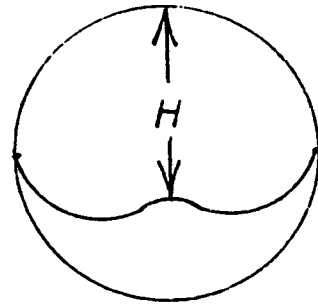
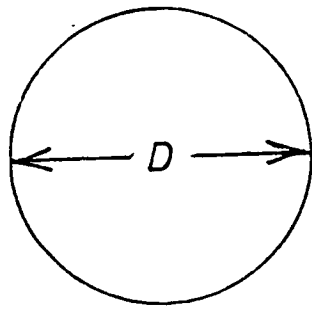
For a flat plate it is:

$$T_{\max} - T_w = \frac{q_i H^2}{8k} \quad (5-7)$$

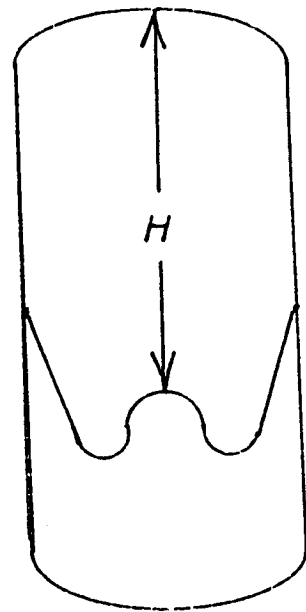
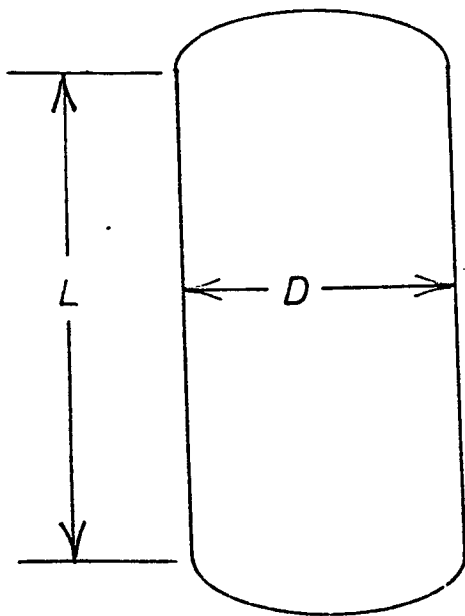
The appropriate conduction-only calculation for the maximum temperature, then, is:

$$T_{\max} - T_w = \min \left\{ \frac{q_i D^2}{24k}, \frac{q_i H^2}{8k} \right\} \quad (5-8)$$

This correlation shifts from the spherical result to the flat plate result at  $H = 0.577 D$ .



a. Spherical



b. Cylindrical

Figure 5-1. Spherical and Cylindrical Tank Geometries

Similar equations can be developed for cylindrical tanks, neglecting heat transfer through the ends:

$$h = \max \left\{ \frac{8k}{D}, \frac{4k}{H} \right\} \quad (5-9)$$

$$T_{\max} - T_w = \min \left\{ \frac{q_i D^2}{16k}, \frac{q_i H^2}{8k} \right\} \quad (5-10)$$

The crossovers from cylindrical to flat-plate geometry occur at  $H = 0.5 D$  for the heat transfer coefficient, and at  $H = 0.707 D$  for the maximum temperature.

### 5.1.2 Scale-Up Considerations

Some interesting implications arise regarding scale-up to larger tanks sizes. The heat generation term,  $q_i$ , is proportional to the fuel fill rate. For both spherical and cylindrical tanks, the maximum temperature rise is proportional to the fill rate and the absolute ullage gas pressure. For spheres, it is inversely proportional to the diameter for a fixed fuel flow rate; for cylinders, inversely proportional to the length.

It is most likely, however, that with larger tanks, faster flow rates would be desired. If the percentage filled per unit time remains constant, the maximum temperature rise is proportional to the square of the diameter for both geometries. Higher fill rates and higher fill volumes, which result in high ullage pressures, both lead to increases in the temperature rise.

If spherical and cylindrical tanks of equal volumes are compared, cylindrical tanks will have lower temperature rises. For a cylindrical tank with a length/diameter ratio of 5, for instance, the maximum temperature rise, assuming only conductive heat transfer, is only 39% as great as it would be for a spherical tank of equal volume.



## 5.2 Combined Heat Transfer - The Realistic Approach

Conduction-only heat transfer calculations will give conservatively low heat transfer rates. In order to estimate realistic rates, both convection and conduction must be considered.

Estimates of the on-orbit heat transfer for the ORS experiments, based on Equation 2-39, lead to Nusselt Numbers ranging from 16 to 67, of which conduction accounts for 10. Analysis of the test data, however, leads to values ranging from 5.1 to 287, with 80% of the values falling between 21 and 135. For the majority of the cases, including all nine tank fill events, the observed Nusselt Number was about 2 to 3 times larger than the estimated one.

### 5.2.1 Modelling Considerations

From the information available at this time, the following Nusselt Numbers are suggested for use in modelling ullage gas heat transfer:

Tank fills:             $Nu = 60$

Coasts:                 $Nu = 32$

High Re-events:     $Nu = 90$

Note that this value for the high-Reynolds Number events is somewhat below the observed mean value of 155. This lower recommendation is based primarily on the very wide spread in the observed data.

For tank fill events, the maximum gas temperature is estimated to be:

$$T_{\max} - T_w = 1.2 (\bar{T} - T_w) \quad (5-11)$$

These correlations have a large amount of uncertainty in them, but they should be reasonable accurate for making estimates of what will actually occur.

An alternate modelling approach which would be valid is the multi-layer conduction model, but with an effective thermal conductivity used to account for mixing among the gas layers. For tank fills,  $k_{eff}$  should be 6 times the intrinsic molecular thermal conductivity. For coast periods and high-Reynolds Number events, factors of 3 and 9 are recommended, respectively. This method, of course, calculates the maximum temperature directly.

### 5.2.2 Scale-Up Considerations

When convective heat transfer is significant, the scale-up impact is somewhat different. At constant fill rates, the maximum temperature rise is now proportional to the absolute pressure and the fill rate, as before; but it is inversely proportional to the square of the diameter for spheres and to the diameter-length product for cylinders. For constant percentage fill rates, the temperature increase is proportional to the diameter to the first power for both spheres and cylinders. The convective effect, then, whether it occurs naturally or is induced by direct action, can have a substantial impact on the maximum temperature.

## 5.3 Gaps in Current Knowledge

### 5.3.1 Natural Convection Inside Spheres

The only experimental data found for natural convection inside spheres was that of Chow and Akins (1975). As shown in Section 2.4.2, there is a great deal of scatter in their data, and it covers only a limited range of Rayleigh Numbers.

### 5.3.2 Natural Convection with Internal Heat Generation

Very little data is available on natural convection inside closed containers with internal heat generation. Jahn and Reineke (1974) give data for two geometries which are not directly applicable to the ullage gas heat transfer problem.

### 5.3.3 Transient Natural Convection

Transient effects in natural convection have been studied theoretically and experimentally for vertical flat plates (Ede, 1967), but not for many other geometries. In light of the very large values of  $t_1$  and  $t_2$  estimated for the ORS experiments, this effect should be considered in more detail.

### 5.3.4 Natural Convection with Vibrations

Vibration influences on natural convection are known for only a limited range of conditions (Baxi and Ramachandran, 1969; Gebhart, 1963). It is not now possible to predict the effects of the low-energy, somewhat random vibrations experienced on spacecraft.

### 5.3.5 Combined Effects on Natural Convection

The ullage gas heat transfer problem involves, to some extent at least, natural convection or mixing with internal heat generation, at conditions far from steady-state, and subject to low level external vibrations. At this time, there is no satisfactory way to take all these effects into account, or even to determine conclusively which ones are important.

### 5.3.6 Mixed Forced and Natural Convection under Low Gravity Conditions

When pressurization gas is flowing into or out of the ullage space, both natural and forced convection effects may be important. The correlation by Churchill (1977), Equation 2-38, fits a large amount of data reasonably well, meaning most experimental Nusselt Numbers fit within a factor of 2 or 3. Whether it is appropriate for the case at hand is not known. Furthermore, as mentioned in Section 3.4, it is not totally clear what terms are most appropriate for use in the Reynolds and Rayleigh Numbers.

### 5.3.7 On-Orbit Acceleration Environment

Data are apparently not readily available for determining specific and typical acceleration profiles for Shuttle missions. Such data would appear to be useful for a variety of purposes, not just for analyzing ullage gas heat transfer. Ideally, one would like to have data to permit easy calculation of accelerations at any specified location on any specified mission. In addition, one would like to have a set of "typical" data, perhaps in the form of averages and frequency profiles.

## 6.0 SUGGESTED EXPERIMENTS

This Section outlines two possible experimental approaches to provide design and operations data for on-orbit ullage heat transfer analysis. The experiments and equipment discussed are limited to spherical geometry for simplicity and ease of understanding. Other geometries could be included in the experimental program very easily. The equipment and procedures presented here are typical of what would be needed; they do not represent definitive designs. Any experimental program should start with a thorough definition of the problem and an examination of alternate ways for obtaining the data.

### 6.1 Fundamental Approach

In this approach, experiments are carried out to obtain basic engineering data and correlations for the various phenomena involved. Initially, these phenomena must be carefully defined. Then data are obtained using small, laboratory-scale equipment covering as wide a range as feasible, being sure to include the full range of expected on-orbit conditions. Very wide ranges can be obtained in this situation by varying gas pressures, mole weights, temperature differences, etc. Simple experiments are carried out first, then various combinations of effects are tested until the entire problem is simulated. Then larger scale ground and orbital tests are carried out to validate the work and/or fill in regions of data that can not be reached in small laboratory-scale equipment on the ground.

All laboratory experiments would involve convective heat transfer inside spheres. Additional effects would be added based on the following schedule:

<u>Test Series</u>	<u>Internal Heat Generation</u>	<u>Start-up Transients</u>	<u>Vibration</u>
1	No	No	No
2	Yes	No	No
3	No	Yes	No
4	No	No	Yes
5	Yes	Yes	No
6	Yes	No	Yes
7	No	Yes	Yes
8	Yes	Yes	Yes

#### 6.1.1 Natural Convection Inside Spheres

The first essential step is to obtain natural convection heat transfer data inside spherical containers. An apparatus which could be used for this purpose is sketched in Figure 6-1.

The test vessel is a metal sphere about 6 inches in diameter fitted with a fill port. It is instrumented with a pressure transducer (a simple solid-state strain-gauge type which screws in flush with the vessel wall would be satisfactory). A radiation source on one side and a detector on the opposite side would serve to give a measure of average gas density independent of the pressure and temperature measurements. Thermocouples would be mounted on the inside and outside of the vessel wall and on fine support wires within the vessel. (Such internal support wires and thermocouples might possibly interfere significantly with the natural convection flow pattern. The easiest way to tell whether this is the case is to run tests with several different mounting geometries and compare the results). The vessel is mounted in an insulated, stirred tank equipped with heating and cooling coils.

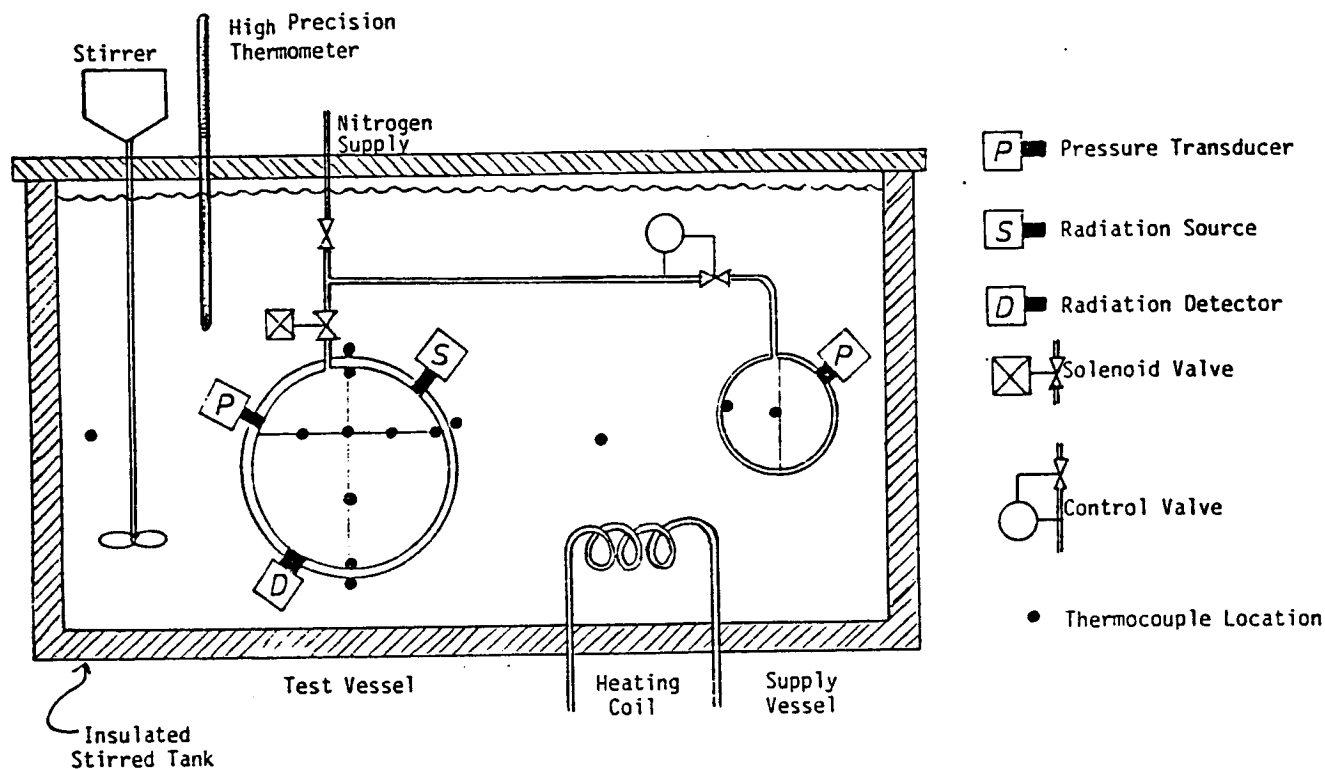


FIGURE 6-1. Typical Laboratory Apparatus Design

The system is operated by bringing everything to thermal equilibrium at the start. Then the water is heated at a controlled rate. After an initial start-up period, the temperature difference should remain fairly constant even though the absolute temperature of the system is rising. Temperatures inside and outside the vessel are recorded as functions of time. The heating rate can be calculated and then correlated with the bath temperature to obtain heat transfer coefficients. Careful analysis of the equipment and procedures would be necessary to insure obtaining meaningful data since, as in the ORS experiment, the total heat flows will not be large. Proper choice of gas composition, heating rates, and initial temperatures and pressures should allow data to be taken over a very wide range of Rayleigh Numbers.

### 6.1.2 Natural Convection Inside Spheres with Internal Heat Generation

Internal heat generation, with a constant external temperature, can be studied in the same apparatus with the addition of a pressurization system. In order to make energy balance calculations easier, it would be best to include the pressurization supply within the insulated tank, although this is not entirely necessary. A simple solenoid valve would open to start the sequence. Gas inlet flow rate would be controlled. Temperature, pressure and density data would again be recorded as functions of time to obtain the heat transfer coefficients. The internal temperature profiles would be extremely useful in this situation to assess the degree of mixing which takes place.

Other heat generation methods should be considered in addition to pressurization. Possibilities include heat generation by chemical reaction, by radioactive isotope decay, and by microwave or diathermic heating. These methods all present additional experimental problems, but they offer the potential of better control of the heat generation rate.

### 6.1.3 Transient Effects in Natural Convection Inside Spheres

The start-up transient problem can be addressed using the same apparatus. Operating conditions must be adjusted to obtain reasonably large values of  $t$  in order to obtain meaningful data. This is discussed further in Section 6.4.5.

### 6.1.4 Vibration Effects in Natural Convection Inside Spheres

For this series of tests, some sort of external vibration system is required. The whole apparatus might possibly be mounted on a shake table, or mechanical vibrations might be imparted to the test vessel alone using rigid supports through the lid of the insulated tank. The product of the frequency and amplitude should be on the order of 0.1 ft/sec. For a 0.01 foot amplitude, a frequency of about 10 Hz would be needed.



#### 6.1.5 Combined Effects

Following the test of individual effects, various combinations would be tested together, as outlined above for test series 5, 6, 7 and 8. In addition, tests would be run which combine flow and natural convection, both filling and emptying the vessel.

#### 6.1.6 Ground Proof Tests

Following all the lab-scale tests, the next step would be to build a total system suitable for both ground and orbital testing. It would be intermediate in size between the laboratory scale and a full-size operational system. Tank diameters of 2.5 feet seem about right. It would have some features very similar to the ORS design, but it would be designed and instrumented more as an experiment than as a demonstration. The system would serve two purposes. First, it would be used to validate scale-up procedures based on the earlier data. Second, it would be used to fill in gaps in the lab data. Section 6.4 outlines regions which might not be accessible using small equipment. Obtaining similar Reynolds Numbers may be one of the most important of these effects.

#### 6.1.7 Orbital Proof Tests

The last series of validation tests would be carried out on orbit using equipment essentially the same as in the ground tests. It would serve the same purposes as the ground tests: verification of design and scale-up and fill-in of gaps in the data.

### 6.2 Engineering Simulation Approach

The engineering simulation approach follows a somewhat different experimental philosophy. A preliminary design is made for the final system: a full-size orbital refueling system. Then that design is scaled down to a convenient size, or sizes, for smaller scale laboratory test work. Tests are run at conditions matching those expected for the full-scale system. The data range is extended when feasible, so long as doing so does not compromise the

basic test program or the equipment. This approach essentially assumes that the process is too complex to understand from simple principles; it is better to study the total process from the start and simply scale-up the results. The size of equipment needed for this approach would most likely be at the intermediate size used for the ground and orbital proof testing in the previous approach. Smaller equipment might be cheaper, permitting several units to be run in parallel; but the scale-up would be less certain.

#### 6.2.1 Pressurization Heat Transfer

Actual tests would start with the combination of heat generation by pressurization and natural convection heat transfer inside the vessel. The tests should be run with a spherical vessel first, then in the same or similar vessel with an internal bladder. Instrumentation needed would be similar to that shown in Figure 6-1. The start-up transient tests could be run in the same equipment.

#### 6.2.2 Pressurization Heat Transfer with Vibration

Tests with vibration would be run in a separate series since they tend to make the equipment and instrumentation more complex.

#### 6.2.3 Ground Test Simulation

This series of tests would simulate on-orbit operations to the extent possible. As with the previous approach, it would be largely to verify earlier test results and to fill in gaps in the data.

#### 6.2.4 Orbital Test Simulation

The orbital test would be similar to that mentioned in Section 6.1.7.

### 6.3 Comparison of Approaches

Each of the approaches outlined above has some advantages and some disadvantages. The fundamental approach would provide a better understanding of the basic processes involved. It would cover a wider range of the pertinent variables. It would be easier to apply its results to other system designs and different applications. It would be more likely to discover any unsuspected phenomena that might have an influence on the problem.

The engineering simulation approach would be faster in terms of providing data for a particular class of designs. Its biggest drawback is that the initial preliminary design on which it is based may be a poor one. It could provide a great deal of information, but for the wrong problem.

In the chemical process industries, with which I am more familiar, a great deal of design work for full-scale plants is done from fundamental data and correlations. This is the case for heat exchangers, distillation columns, etc. Pilot-plant testing -- the engineering simulation approach -- is used in situations where there are a great many interacting variables and where the fundamentals are not as well understood. This is done, for instance, in the design of catalytic chemical reactors.

The situation for ullage gas heat transfer is somewhat analogous to the latter case; there are many interacting variables, several of which are not well understood. If there is any time constraint to obtaining answers, the engineering simulation approach would be preferable. It could lead to equipment ready for the orbital tests in two to three years. Working strictly through the fundamental approach would probably add another one to two years to the total program. If there are time constraints, it would still be worthwhile to do some of the fundamental work in parallel with simulation, but the program schedule should not be constrained to it.

### 6.4 Ranges of Interest for Variables

The variables of interest in the ullage gas heat transfer problem can be expressed in terms of four common dimensionless groups and the time to reach

steady-state. The sections below make estimates of the extreme ranges in these terms likely to be encountered in both operational systems and test systems. Four basic systems are considered: a large operational orbital system (designated LO) with a tank diameter of about ten feet; an orbital test system (designated OT) with a tank diameter of about 2.5 feet; a ground test system (designated GT) of similar size; and a laboratory test system (designated Lab) with a tank diameter of about 0.5 feet. Note that values given below are estimates of extreme ranges of operating conditions; they are not intended to be normal design or operating conditions.

#### 6.4.1 Rayleigh Number

As seen in Section 2.1, the Rayleigh number can be expressed as:

$$Ra = L^3 \rho^2 g C_p \beta \Delta T / \mu k \quad (2-5)$$

Both minimum and maximum values for the Rayleigh Number are of interest. Table 6-1 gives the maximum and minimum values achievable with the four systems. As is evident from the values in the table, it may be necessary to use fairly small lab equipment to match the Rayleigh Numbers expected on orbit with the test or operational equipment.

Table 6-1  
Ranges for the Rayleigh Number

System	Diam. (ft)	Pres. (psia)	Temp. (°F)	g/g <sub>0</sub>	ΔT (°F)	Ra
LO (min)	10	10	70	10 <sup>-6</sup>	5	1.5x10 <sup>4</sup>
LO (max)	10	500	70	10 <sup>-4</sup>	100	8 x10 <sup>10</sup>
OT (min)	2.5	10	70	10 <sup>-6</sup>	5	230
OT (max)	2.5	500	70	10 <sup>-4</sup>	50	1.5x10 <sup>8</sup>
GT (min)	2.5	10	70	1	2	1 x10 <sup>8</sup>
GT (max)	2.5	500	70	1	50	8 x10 <sup>12</sup>
Lab (min)	0.5	5	200	1	1	5 x10 <sup>4</sup>
Lab (max)	0.5	1000	32	1	20	1 x10 <sup>11</sup>

#### 6.4.2 Reynolds Number

$$Re = Dv\rho/\mu \quad (2-2)$$

The Reynolds Number based on fill-pipe diameter and velocity very likely plays an important part in high-Reynolds Number heat transfer correlations. Table 6-2 gives the maximum feasible Reynolds Numbers for the four systems. In this case, they scale approximately with the size of the system. Exact similarity may be very difficult to obtain. It may be feasible to extend the range of the Reynolds Number for the lab and ground-test cases by using gases other than nitrogen, thus increasing the gas density without changing the pressure and temperature.

Table 6-2

Ranges for the Reynolds Number

<u>System</u>	<u>Time to Fill (minutes)</u>	<u>Diam. (in)</u>	<u>Velocity (ft/sec)</u>	<u>Press. (psia)</u>	<u>Density (lb/cu.ft)</u>	<u>Re</u>
L0	10	2	40	500	2.5	$1.4 \times 10^6$
OT	5	0.5	20	500	2.5	$1.7 \times 10^5$
GT	5	0.5	20	500	2.5	$1.7 \times 10^5$
Lab	1.0	0.1	20	1000	5.0	$7.0 \times 10^4$

#### 6.4.3 Vibrational Reynolds Number

$$Re_v = \frac{D\rho}{\mu} (\sqrt{2} \pi a f) \quad (2-35)$$

Again, the maximum values are of primary importance. It is simple to match conditions for low values of the Vibrational Reynolds Number, as shown in Table 6-3.

Table 6-3

Ranges for the Vibrational Reynolds Number

System	Diam. (ft)	Density (lb/cu.ft)	ampl. (ft)	freq. (1/sec)	Re <sub>v</sub>
L0	10	2.5	0.02	1	2x10 <sup>5</sup>
OT	2.5	2.5	0.01	1	2x10 <sup>5</sup>
GT	2.5	2.5	0.05	1	1x10 <sup>5</sup>
Lab	0.5	5	0.01	10	9x10 <sup>4</sup>

#### 6.4.4 Dammkohler Number

$$Da = q_i D^2 / k \Delta T \quad (2-29)$$

With the Dammkohler Number we are interested only in maximum values; it is always possible to get lower values by decreasing the heating rate. The maximum Dammkohler Number is given in Table 6-4 for the four systems. Ground systems appear able to match orbital systems very easily for this parameter.

Table 6-4

Ranges for the Dammkohler Number

System	Diam. (ft)	Time to Fill (minutes)	Press. (psia)	$\Delta T$ (°F)	Da
L0	10	10	500	10	4.0x10 <sup>4</sup>
OT	2.5	5	500	20	1.2x10 <sup>4</sup>
GT	2.5	5	500	20	1.2x10 <sup>4</sup>
Lab	0.5	1	1000	20	5.0x10 <sup>4</sup>

#### 6.4.5 Time to Reach Steady-State

$$t_2 = 5.24 (0.952 + Pr)^{0.5} \left( \frac{x}{g \beta \Delta T} \right)^{0.5} \quad (2-32)$$

The time estimated to reach steady-state varies considerably from ground to orbital conditions. It will be necessary to run experiments for about twice the value of  $t_2$  to be assured of reaching steady-state. The time values shown in Table 6-5 indicate that it may not be feasible to do so with large systems on orbit.

Table 6-5

Ranges for the Time to Reach Steady-State

System	Diam. (ft)	$\Delta T$ (°F)	$g/g_0$	$2 \times t_2$ (sec) (min)	
L0 (max)	10	$10^{-6}$	10	55000	9200
L0 (min)	10	$10^{-4}$	10	5500	920
OT (max)	2.5	5	$10^{-6}$	39000	6500
OT (min)	2.5	5	$10^{-4}$	3900	650
GT	2.5	2	1	62	1
Lab	0.5	1	1	39	0.7

## 7.0 CONCLUSIONS AND RECOMMENDATIONS

### 7.1 Conclusions

The following principal conclusions have been reached as a result of this study:

- (a) Existing published correlations are insufficient for estimating the natural convection or combined natural and forced convection heat transfer coefficients inside spherical containers with internal heat generation, with or without external vibrations, at steady-state or during transient start-up periods.
- (b) The best model that can be postulated for on-orbit ullage gas heat transfer strictly from theory and literature sources is a variation of the correlation proposed by Churchill (1977):

$$Nu = 10 + (0.0417 Re^{1.5} + 0.205 Ra^{0.75})^{1/3} \quad (2-39)$$

- (c) The ORS experiment data for each individual event can be fit using a well-mixed ullage gas model with a fixed Nusselt Number or with a Nusselt Number varying in accord with Equation 2-39. There is no significant difference between the two.
- (d) There is no significant correlation between the observed Nusselt Numbers (heat transfer coefficients) from the ORS experiment with Rayleigh Numbers, Reynolds Numbers or known vehicle accelerations.
- (e) For all tank-fill events, the mean Nusselt Number for the ORS experiment is  $60 \pm 14$ . For coast periods, it is  $32 \pm 20$ . For high-Reynolds Number events, such as tank ventings and pressurizations, the mean Nusselt Number is  $155 \pm 95$ .



- (f) Based on an analysis of the equipment and the data, the uncertainty, or expected standard deviation, in calculating a heat transfer coefficient or Nusselt Number from a single ORS experiment is  $\pm 67\%$ . For the nine separate events, the expected uncertainty is  $\pm 22\%$ , assuming that there indeed is just one single "correct" Nusselt Number. The standard deviation actually observed was  $\pm 24\%$ .
- (g) Proper scale-up of pressurized fluid transfer processes to larger tanks and higher flow rates can be highly dependent on ullage heat transfer characteristics. Pure conduction heat transfer leads to temperature rises proportional to the square of the tank diameter, while convective heat transfer temperature increases are proportional to the tank diameter to the first power for equivalent fill times.

## 7.2 Recommendations

The following recommendations are made based on the conclusions reached in this study:

- (a) Until additional data are available, calculations based on conductive heat transfer only should be used to determine conservative lower bounds on gas-phase heat transfer in orbit.

For spheres:

$$h = \max \left\{ \frac{10k}{D}, \frac{4k}{H} \right\} \quad (5-5)$$

$$T_{\max} - T_w = \min \left\{ \frac{q_i D^2}{24k}, \frac{q_i H^2}{8k} \right\} \quad (5-8)$$

For cylinders:

$$h = \max \left\{ \frac{8k}{D}, \frac{4k}{H} \right\} \quad (5-9)$$

$$T_{\max} - T_w = \min \left\{ \frac{q_i D^2}{16k}, \frac{q_i H^2}{8k} \right\} \quad (5-10)$$

- (b) Until additional data are available, calculations based on fixed Nusselt Numbers should be used for estimates of actual heat transfer from ullage gas on orbit. For tank fills, use a Nusselt Number of 60; for coast periods, use 32; for vents and pressurizations, use 90.
- (c) Additional experiments, primarily ground-based with orbital verification, should be carried out, using one of the approaches outlined in Section 6.

## NOMENCLATURE

### Roman Letters

A	Area, $\text{ft}^2$
a	Amplitude of vibration, ft
C	Constant in Nusselt Number correlation, dimensionless
$C_p$	Constant-pressure heat capacity, $\text{Btu/lb}^\circ\text{F}$
$C_v$	Constant-volume heat capacity, $\text{Btu/lb}^\circ\text{F}$
D	Diameter of sphere or cylinder, ft
dp	Pipe diameter, ft
Da	Dammkohler Number, $q_i L^2 / k \Delta T$ , dimensionless
E	Expected uncertainty operator
F	Multiplying factor for Nusselt Number, dimensionless
f	Frequency, 1/sec
g	Gravitational acceleration, $\text{ft/sec}^2$
$g_0$	Gravitational acceleration at earth's surface, $\text{ft/sec}^2$
Gr	Grashof Number, $L^3 g \beta \Delta T / \mu^2$ , dimensionless
H	Distance from bladder to tank wall, ft
h	Local heat transfer coefficient, $\text{Btu/ft}^2 \text{hr}^\circ\text{F}$ or $\text{Btu/ft}^2 \text{sec}^\circ\text{F}$
$h_1$	Local heat transfer coefficient, based on average fluid temperature, $\text{Btu/ft}^2 \text{hr}^\circ\text{F}$ or $\text{Btu/ft}^2 \text{sec}^\circ\text{F}$
$h_2$	Local heat transfer coefficient, based on maximum fluid temperature, $\text{Btu/ft}^2 \text{hr}^\circ\text{F}$ or $\text{Btu/ft}^2 \text{sec}^\circ\text{F}$
k	Thermal conductivity, $\text{Btu/ft-sec}^\circ\text{F}$
$k_{\text{eff}}$	Effective thermal conductivity, $\text{Btu/ft-sec}^\circ\text{F}$
L	Length, ft
m	Number of constants in correlation
N	Amount of ullage gas, lb-moles
n	Constant in Nusselt Number correlation, or number of data points, dimensionless
Nu	Nusselt Number, $hL/k$ , dimensionless
$Nu_c$	Nusselt Number based on conduction only, dimensionless
$Nu_f$	Nusselt Number for forced convection, dimensionless
$Nu_n$	Nusselt Number for natural convection, dimensionless

## NOMENCLATURE (cont)

### Roman Letters (cont)

$Nu_o$	Nusselt Number in the absence of vibration, or estimated Nusselt Number, as compared to experimental one, dimensionless
$Nu_v$	Nusselt Number in the presence of vibration, dimensionless
$P$	Pressure, psia
$\dot{P}$	Rate of change of pressure, psia/hr
$Pr$	Prandtl Number, $C_p\mu/k$ , dimensionless
$Q$	Heat transfer rate, Btu/ft <sup>2</sup> hr, or Btu/ft <sup>2</sup> sec
$q_i$	Internal heat generation rate, Btu/ft <sup>2</sup> sec
$R$	Gas constant, psi-ft <sup>3</sup> /lb-mole°R, or Btu/lb-mole R
$r$	Radial position in sphere or cylinder, ft
$r_o$	Radius of sphere or cylinder, ft
$Ra$	Rayleigh Number, $L^3\rho^2gC_p\beta\Delta T/\mu k$ , dimensionless
$Re$	Reynolds Number, $Lvp/\mu$ , dimensionless
$Re_v$	Reynolds Number for vibration, dimensionless
$T$	Temperature, °F
$\bar{T}$	Average temperature, °F
$T_{max}$	Maximum temperature, °F
$T_o$	Wall or external temperature, °F
$T_s$	Surroundings temperature, °F
$\Delta T$	Temperature difference, °F
$t$	Time, sec
$t_1$	Time for conduction/transition change, sec
$t_2$	Time for transition/steady-state change, sec
$V$	Volume of ullage gas, ft <sup>3</sup>
$\dot{V}$	Rate of change of volume of ullage gas, ft <sup>3</sup> /hr
$v$	Velocity, ft/sec
$x$	Distance along flat plate, ft, or arbitrary independent variable
$y$	Arbitrary dependent variable

## NOMENCLATURE (cont)

### Greek Letters

$\beta$	Thermal expansion coefficient, $1/^{\circ}\text{F}$
$\gamma$	Ratio of specific heats, dimensionless
$\delta$	Boundary layer thickness, ft
$\mu$	Viscosity, lb/ft-sec
$\rho$	Density, lb/ft

## REFERENCES

1. Baxi, C. B., and Ramachandran, A., "Effect of Vibration on Heat Transfer from Spheres," J.Heat Trans., Vol.91, pp.337-343, (1969).
2. Bergholz, R. F., "Natural Convection of a Heat Generating Fluid in a Closed Cavity," J.Heat Trans., Vol.102, pp.242-247, (1980).
3. Boyd, W. C., Orbital Refueling System, STS 41-G, Quick-Look Data Report, NASA JSC, Internal Report (1984).
4. Burmeister, L. C., Convective Heat Transfer, John Wiley & Sons, (1983).
5. Chow, M. Y., and Akins, R. G., "Pseudosteady-State Natural Convection Inside Spheres," J.Heat Trans., Vol.97, pp.54-59, (1975).
6. Churchill, S. W., "A Comprehensive Correlating Equation for Laminar, Assisting, Forced and Free Convection," A.I.Ch.E.J., Vol.23, pp.10-16, (1977).
7. Eckert, E. R. G., "Heat Transfer Review, 1954," Ind.Engrg.Chem., Vol.46, p.932 (1954)
8. Ede, A. J., "Advances in Free Convection," Adv.Heat Trans., Vol.4, pp.1-64, (1967).
9. Gebhart, B., "Random Convection under Conditions of Weightlessness," AIAA J., Vol.1, pp.380-383, (1963).
10. Griffin, J. W., Orbital Refueling System (ORS) Overview, NASA JSC, Flight Projects Engineering Office, Internal Briefing Report, (1985).
11. Jahn, M., and Reineke, H. H., "Free Convection Heat Transfer with Internal Heat Sources, Calculations and Measurements," Trans.5th Intl. Heat Trans.Conf., Vol.3, pp.74-78, (1974).
12. Kullas, M. C., Handbook on Astronaut Crew Motion Disturbances for Control System Design, NASA-RP-1025, (1979).
13. Martin, H., "Heat and Mass Transfer between Impinging Gas Jets and Solid Surfaces," Adv.Heat Trans., Vol.13, pp.1-60 (1977).
14. NASA (National Aeronautics and Space Administration), Orbital Refueling Demonstration System Description, NASA JSC Program Development Office, Internal Report (1983).
15. Olsen, R. E., and Mockovciak, J., Jr., "Operational Factors Affecting Microgravity Levels in Orbit," J.Spacecraft, Vol.18, pp.141-144, (1981).

#### REFERENCES (cont)

16. Siegel, R., "Effects of Reduced Gravity on Heat Transfer," Adv.Heat Trans., Vol.4, pp.143-228, (1967).
17. Sparrow, E. M., and Lovell, B. J., "Heat Transfer Characteristics of an Obliquely Impinging Circular Jet," J.Heat Trans., Vol.102, pp.202-209, (1980).
18. Whitley, H.G.,III, and Vachon, R.I., "Transient Laminar Free Convection in Closed Spherical Containers," J.Heat Trans., Vol.94, pp.360-366, (1972).

**N86 - 31 425**

D<sub>16</sub>

ENGINEERING GRAPHICS DATA ENTRY FOR SPACE STATION DATA BASE

13P

R. C. Lacovara, E. E.  
Affiliate Instructor  
Department of Electrical Engineering  
Stevens Institute of Technology  
Hoboken, New Jersey

18827

Abstract

Issues related to the entry of graphical engineering data into the Space Station Data Base were examined. These issues were: representation of graphics objects; representation of connectivity data; graphics capture hardware; graphics display hardware; site-wide distribution of graphics; and consolidation of tools and hardware. A fundamental assumption was that existing equipment such as IBM based graphics capture software and VAX networked facilities would be exploited.

Defensible conclusions reached after study and simulations of use of these systems at the engineering level are:

1. Existing IBM based graphics capture software is an adequate and economical means of entry of schematic and block diagram data for present and anticipated electronic systems for Space Station.
2. Connectivity data from the aforementioned system may be incorporated into the envisioned Space Station Data Base with modest effort.
3. Graphics and connectivity data captured on the IBM based system may be exported to the VAX network in a simple and direct fashion.
4. Graphics data may be displayed site-wide on VT-125 terminals and lookalikes.
5. Graphics hard-copy may be produced site-wide on various dot-matrix printers.
6. The system may provide integrated engineering services at both the engineering and engineering management level.

NASA Colleague: O. L. Schmidt/EE7/X6301



## Introduction

The engineering of the Space Station is a task comparable to the largest engineering works ever undertaken. Engineering tools which facilitate tasks of this magnitude are desirable. This report is the result of an investigation of one such tool.

Engineering tools applicable to large works are usually systems of smaller utilities grouped together. In particular, this system of utilities is a group of programs on the DEC VAX(1) and on the IBM PC(2) which together perform the following functions:

- 1) Engineering graphics data (schematics, block diagrams, and component attributes) may be entered at IBM PC work stations.
- 2) Connectivity data may be extracted from the engineering graphics by programs on the IBM PC.
- 3) The graphics and connectivity data may be sent to the VAX for archival storage; distributed to interested parties on the site-wide network; and incorporated into the Space Station Data Base (SSDB(3)).
- 4) Hardcopy output of the graphics and database information may be obtained on the IBM and DEC systems. Softcopy (video terminal) output may be obtained as well.

Some of these programs are commercial products and others have been developed in proof of concept here at JSC.

This system is of further interest since it is of use to a large vertical section of engineering staff: design engineers, systems engineers, and engineering managers.

Design engineers use the IBM PC work stations to enter schematic information into the system. Besides machine generated schematic diagrams, the design engineer receives machine generated wire lists, lists of materials, and may with optional software perform electronic modeling and simulations.

Systems engineers may access the connectivity information transferred to the database resident on the VAX for interface analysis and similar tasks. Simulation and modeling may be performed against component parameter data stored with the connectivity data.

Engineering managers may create and review block diagrams of the actual electronic systems and obtain connectivity data, and pertinent statistical information (weight, volume, power) at the same time. The block diagrams so obtained exist in a well defined relationship to the schematic diagrams created by design engineers.

## Theory

The system is divided somewhat arbitrarily into two parts at the interface between the programs and data resident on the IBM PC's and the second set of programs and data resident on the DEC VAX. Simply stated, the IBM half of the system performs data entry and processing functions. The DEC half of the system stores the data in a regular structure (a database), provides for site-wide distribution, and "read-only" services such as softcopy display and hardcopy output.

### IBM PC Services

A set of programs and hardware purchased commercially from FutureNet Corporation (4) are added to an IBM PC, XT or AT. The FutureNet programs are designed specifically for schematic capture. Specifically, the designer uses a mouse or trackball in conjunction with symbol libraries to create electrical schematic diagrams. Graphics capability is secondary to the processing which is then available for the schematics: connectivity data is extracted automatically from the graphics. The connectivity data is essentially a data file listing all of the symbols found in the schematic, all of the connections between symbols, and other information related to the textual fields found in the schematic. .

Typically, the only further use of the graphics file after the extraction of connectivity is hardcopy documentation. The connectivity file is used to create wire lists and enter materials data into a database. The FutureNet hardware/software package uses the IBM PC in a non-exclusive manner, so that the computer is available for other uses when not in use for schematic capture.

## DEC VAX Services

Two problems associated with the use of IBM PC's are the relatively small amount of online storage available compared to the need to access possibly thousands of detailed drawings, and the distributed nature of backup and maintenance of small computers. These disadvantages are offset by the nature of the programs usually run on an IBM PC in so far that the programs are relatively small. Also, the machines are inexpensive enough that it is feasible to run them as single user units. Indeed, one of the reasons that the IBM PC is useful for graphics capture (a computationally heavy task) is that it is a single user system.

The task at hand, however, will involve thousands of drawings at diverse sites. No reasonable number of small winchester drives as found on IBM PC's will suffice to store even a small subsystem of a major system such as Communications and Tracking. Further, individual users are not all reliable when backups of data are required. (IBM PC's are small enough to be occasionally dropped to the floor. Such an event usually has an "impact" on data integrity.)

A reasonable solution is to use equipment at hand, the network of DEC VAX's on site, to provide several solutions. The data generated on the various IBM PC's may be collected on the VAX online storage devices. Not only will enough space be found there, but the routine nature of backups performed on the VAX systems will provide for archival storage of the engineering data.

A further advantage of the VAX storage is that distribution of the information to interested parties site-wide is trivial: VAX terminals are found throughout the engineering offices at JSC.

## Results

### Graphics Considerations

A bridge is necessary between the structures on the IBM systems and the VAX systems. The programs which provide the bridge and the mechanisms which they supply are described here.

There are only two types of files on the IBM PC which need to be transferred. One of these is a binary file of graphics information, called a DWG file, which contains all of the information entered into the system when a drawing is created. The second is an ascii file, called a PIN file, which is a list of all the objects such as text and symbols found in the DWG file. The PIN file is generated from the DWG file by a program supplied by FutureNet. The PIN file may be thought of as a drawing or schematic less graphics information.

Sets of DWG files represent complete schematics of equipment, or block diagrams of complete systems. The corresponding PIN files, generated one for one from DWG files, may be combined to form a single file, called a NET file. The NET file contains all of the connectivity and material information found in an entire set of drawings. DWG files are used to reproduce hardcopy and softcopy of the graphics. NET files are used to prepare wire lists, lists of material, and enter data into databases.

The NET file is generated by a FutureNet program. However, there is no reason that this task might not be better performed on the VAX. The advantage of combining PIN files into a single NET file on the VAX is operational: paired DWG

and PIN files are moved IBM to VAX; PIN files are then combined into a global NET file. If files were spread across tens or hundreds of IBM PC's there would be no simple method of combining the many PIN files. Networks of IBM PC's have not been considered in this study, as they are not commonly available. Networks of DEC VAX's exist on-site.

Transmission of the files between the IBM PC's and DEC VAX is trivial. As long as an RS-232 link to the VAX is available from the IBM PC, a commercially available terminal emulator such as VTERM (7) may be used to transfer files. VTERM, as an example of such software, provides a sliding window error checked protocol for transfer of ascii and binary files. This ensures error free transfer of files between systems.

Once sets of DWG and PIN files are resident on the VAX, they may be considered archivally stored. Further, they are available to authorized users on the VAX network. Two programs were developed during this study to demonstrate the utility of VAX central storage.

One Pascal program set displays drawings on VT125 or VT240/1 terminals using REGIS. Various portions of drawings may be viewed on the terminal screen. The largest section of a drawing which may be viewed at the full resolution of the original file is about 9.6 by 6.0 inches. The normal resolution referenced to a pixel at that scale is 0.0125 inches. If an overview of a drawing is desired, an entire size A, B or larger drawing may be displayed on the screen. At those resolutions, however, text is not visible, but blocks and larger features may be seen. It might be noted that the original drawing is created on the IBM PC under similar softcopy constraints. Currently, the Pascal program

and PIN files are moved IBM to VAX; PIN files are then combined into a global NET file. If files were spread across tens or hundreds of IBM PC's there would be no simple method of combining the many PIN files. Networks of IBM PC's have not been considered in this study, as they are not commonly available. Networks of DEC VAX's exist on-site.

Transmission of the files between the IBM PC's and DEC VAX is trivial. As long as an RS-232 link to the VAX is available from the IBM PC, a commercially available terminal emulator such as VTERM (7) may be used to transfer files. VTERM, as an example of such software, provides a sliding window error checked protocol for transfer of ascii and binary files. This ensures error free transfer of files between systems.

Once sets of DWG and PIN files are resident on the VAX, they may be considered archivally stored. Further, they are available to authorized users on the VAX network. Two programs were developed during this study to demonstrate the utility of VAX central storage.

One Pascal program set displays drawings on VT125 or VT240/1 terminals using REGIS. Various portions of drawings may be viewed on the terminal screen. The largest section of a drawing which may be viewed at the full resolution of the original file is about 9.6 by 6.0 inches. The normal resolution referenced to a pixel at that scale is 0.0125 inches. If an overview of a drawing is desired, an entire size A, B or larger drawing may be displayed on the screen. At those resolutions, however, text is not visible, but blocks and larger features may be seen. It might be noted that the original drawing is created on the IBM PC under similar softcopy constraints. Currently, the Pascal program

does not implement all of the FutureNet drawing commands, such as curves and arcs. This is not due to any limitations of the IBM or DEC equipment, but time constraints during the study. The existing program demonstrates acceptable transfer of the drawings from the originating system to the VAX.

Hardcopy at full resolution may be obtained from the IBM PC using a dot matrix printer, or one of several plotters. Another Pascal program was written during the study to demonstrate the transfer of the DWG file to a dot matrix printer connected to the VT240. The particular printer was an LA210, but any 132 column dot matrix printer using sixel format graphics will be suitable with minor changes to the program. Again, the full graphics capabilities of the FutureNet format are not implemented by reason of time constraints during the study.

Transfer of the DWG file to plotter format on the VAX was investigated. Although a program was not written for demonstration purposes, no problems in principle were found. It is expected that transfer programs for individual plotters can be written in 80 to 100 man-hours, including documentation.

A great virtue of DWG and PIN file storage on the VAX is the demonstrated ability to produce softcopy and hardcopy anywhere on site that has a REGIS compatible terminal device and a VAX network connection.



## Database Considerations

The ability to generate schematics and build libraries of symbols for schematics is shared by several commercial systems. The ability of the FutureNet system to extract connectivity and component parameters from the graphics files separates it from most graphics systems in common use. It is this separated information which is desired in the Space Station Database. Since the connectivity and parametric information is obtained "for free" from the input schematics, considerable amounts of error-prone data entry are entered with no further operator effort.

A set of drawings for a device gives rise to a matching set of PIN files for the device. The combination of the PIN files into a single NET file is performed by a FutureNet program. As indicated above, if the number of PIN files is very large, the PIN files might be combined on the VAX by a program as yet unwritten. As only simple sorting is involved in the PIN to NET conversion, there is a no priori difficulty associated with the creation of a suitable program on the VAX.

The NET file is composed of three types of information. The first set of records describes the files which were combined to form the NET file. The second set type describes the individual symbols found in the drawing set. These records contain descriptive text, parametric information, and information related to simulation models. The third set of records contain the connectivity information; that is, the list of all nodes in the drawing which are connected in common.

This file is an ascii file. Investigation of the import requirements for database programs RIM(4) and DATATRIEVE(5) indicate that only modest amounts of processing of the NET file is required to add the data found in the NET file to a database.

## Conclusions

Almost all of the required hardware and most of the required software is available at JSC to implement an engineering tool of considerable scope and power. The graphics/database system offers services to design engineers, systems engineers, and engineering management. The system will capture electrical graphics and parametric data. The data will be available wherever terminals on the VAX network exist on the JSC site.

This study has produced two programs to demonstrate proof of concept transfer of data from IBM PC work stations to DEC VAX networked host computers. The data has been transferred in a useful format for both graphics display and automatic database entry.

Further work is required to fully implement the FutureNet drawing standards, and systematize the operations involved in the transfer. Work is required to port the data to a data base, but work on Space Station Database is proceeding in parallel. Some unresolved operational questions remain which are related to the database schema.

Further information pertaining to the programs and test drawings used in proof of concept may be found by consulting the author's on-site JSC colleague (6).

## References

- (1) DEC VAX            Registered trademarks of Digital Equipment Corporation, Maynard, Mass.
- (2) IBM PC            Registered trademarks of International Business Machine Corporation
- (3) SSDB              Space Station Database: Pilot RIM-based engineering database. Author: Eric Barnhart, LEMSCO
- (4) RIM                A database product of Boeing Corporation
- (5) DATATRIEVE        A database product of Digital Equipment Corporation
- (6)                    Oron L. Schmidt/EE7/Johnson Space Center
- (7) VTERM             Trademark of Coefficient Systems, Incorporated

**N86 - 31 426**

D17

**ANALYSIS OF NYSTAGMUS RESPONSE TO PSEUDORANDOM VELOCITY INPUT**

1049.

Charles S. Lessard, Ph.D.  
Associate Professor of Biomedical Engineering  
Texas A & M University  
College Station, Texas

18 E 28

**ABSTRACT**

Space motion sickness was not reported during the first Apollo missions; however, since Apollo 8 through the current Shuttle and Skylab missions, approximately 50% of the crewmembers have experienced instances of space motion sickness. Space motion sickness, renamed space adaptation syndrome, occurs primarily during the initial period of a mission until habitation takes place. One of NASA's efforts to resolve the space adaptation syndrome is to model the individual's vestibular response for basis knowledge and as a possible predictor of an individual's susceptibility to the disorder.

This report describes a method to analyse the vestibular system when subjected to a pseudorandom angular velocity input. A sum of sinusoids (pseudorandom) input lends itself to analysis by linear frequency methods. Resultant horizontal ocular movements were digitized, filtered and transformed into the frequency domain.

Programs were developed and evaluated to obtain the (1) auto spectra of input stimulus and resultant ocular response, (2) cross spectra, (3) the estimated vestibular-ocular system transfer function gain and phase, and (4) coherence function between stimulus and response functions.

---

NASA Colleague: Millard F. Reschke, Ph.D. SB X2381

## INTRODUCTION

An important part in NASA's biomedical research program is the problem of space motion sickness, a disorder whose adverse effects on the well-being and safety of space crewmembers justifies high priority efforts to resolve (J. M. Talbot, 1983). According to Dr. J. L. Homick, the challenge includes "research on the causes, prediction, prevention, and treatment of space motion sickness (Homick, 1979). One of NASA's in-house efforts to examine the etiological factors in space motion sickness is "The Middeck Rotator Vestibular Function Tests" (Reschke, 1984). Functional objectives four (FO-4) and seven (FO-7) support the overall aim for a better understanding of the vestibular system dynamics, its role in space motion sickness, and its possible use in prediction of an individual's susceptibility to space motion sickness.

Functional objective four (FO-4) specifies the input stimulus as a pseudorandom signal that will contain the sum of six sinusoids of frequencies between 0.1 and 1.0 hertz (Hz) as given in Table 1. The vestibular-ocular system response is obtained by electro-ocular gram (EOG) measurements.

The specific objective of this study is to develop those software programs necessary to evaluate the vestibularocular response to pseudorandom angular velocity input stimulus. The analytical programs for this study are limited to linear frequency analysis. The program development is constrained to harmonic analysis via Fast Fourier Transformation (FFT) for spectral, transfer, and coherence functions.

## METHOD

An engineer's approach to the analysis of a system is to observe the system response to a predetermined deterministic excitation in order to determine the system's transfer function. Knowledge of the system's transfer function permits prediction of the system response to other deterministic excitations. Although, linear systems analysis is the most popular and useful analytical method to evaluate explicit mathematical models, i.e., transfer function of a biological system, the method applies only to systems that are linear.

The most commonly used excitation signals in system analysis are single frequency sinusoid, step, and impulse functions. The use of other than deterministic input signals did not fully develop until computers with large number handling capacity became available (Lee and Schetzen, 1965). The Wiener method of nonlinear system identification by observation of a system's response to zero-mean, Gaussian white noise enables one to predict the response (linear and nonlinear) of the system to any input, but not without major problems (Victor and Shapley 1980).

A pseudorandom input stimulus lies between the simple single frequency sinusoid and the complex random Gaussian white noise, but according to Victor and Shapley can produce results similar to the Wiener method. An excellent description of the sum of sinusoids method capability for both linear and nonlinear analysis in the frequency domain is presented by Victor and Shapley, 1980. The crux of the method is the use of a modulation signal that is a sum-of-sine waves and the measurement of nonlinear response of the system as cross-talk between the input frequencies

(Victor and Shapley, 1980). Thus the sum-of-sinusoids method uses a deterministic rather than random Gaussian noise input stimulus, is not restricted to a small signal regime like the harmonic input method (Bedrosian and Rice, 1971), and is different from the use of a single sinusoid method because the response to a sum-of-sinusoids stimulus contains the nonlinear interaction terms, i.e., sum and difference frequency terms ( $f_h \pm f_g$ ) which are intermodulation of cross-talk frequencies (Victor and Shapley, 1980).

The sum-of-sine waves can be made periodic if the time varying function is of the form

$$x(t) = \sum_{n=1}^{\infty} X_n \sin(2\pi f t + \theta_n) \quad [1]$$

where the ratio ( $f_n/f_m$ ) is a rational number. If the ratio of two frequencies in the sum is not equal to a rational number the resulting wave form will have an almost-periodic character (Bendat and Piersol, 1971). Then the sum-of-sinusoids (also referred to as complex periodic data) can be defined mathematically by a time varying function that repeats itself at some finite period (T). Most complex periodic signals can be transformed into the frequency domain by a Fourier series or transform (Bendat and Piersol, 1971). Complex periodic waveforms can be characterized by discrete frequency spectra. In contrast, nonperiodic transient data can not be represented by a discrete frequency spectra.



## ANALYTICAL PROGRAM

The analytical program developed for determining the transfer function (magnitude and phase) of the vestibularocular system follow the methods well described in most signal processing books (Bendat and Piersol 1966, 1971, 1980; McGillem and Cooper, 1974; Oppenheim and Schafer, 1975).

Figure 1 shows the signal flow process from input signal to output results.

In general, the data is obtained from digital files and filtered. The response signal is differentiated to obtain ocular velocity since the input stimulus is angular velocity. The time sequences of input and output signals are transformed to coefficients of complex frequencies and the various spectra are obtained in order to calculate the magnitude, phase and coherence functions.

### Program Structure

The structure of the program was dictated by three factors; the frequency of the vestibular response, the amount of computer memory available, and the desire for operator interaction. The vestibular system frequency response is between 0.01 and 5.0 Hz. In order to obtain good spectral resolution to 0.01 Hz, the amount of data to be analyzed must exceed 100 seconds. By the Nyquist sampling criteria, the sampling frequency (SF) must be twice the highest frequency of interest or SF must equal 10 samples per second. Hence, the smallest array must contain 1000 sample values. Since the standard Cooley-Tukey fast fourier transform (FFT) requires the number of elements in the array to be a power of two ( $N = 2^m$ ), the smallest array size is 1024. The arrays for both input stimulus and output response signals are complexed for transformation thereby increasing each array size

by two. Also real numbers require 2-byte words whereas complex numbers require 4-bytes.

The first factor sets program requirements but the second factor determines programming method. The computer memory available to a user on the LSI-11 system is 32K. This may be extended to 64K on some machines. The program and the system lab library occupied so much memory the program could not be linked or run. Programming techniques to overcome this problem include the use of virtual arrays, the use of overlays, or the combination of both virtual arrays and overlays. The use of overlays forces the program into a sequential mode of calling subroutines and returning to main program. Minimizing the number of arrays by common or equivalence can not be used with virtual. Hence, these restraints dictated serial processing of subroutines and the use of a temporary array. The limitation is that data written over in the temporary array cannot be retrieved. The program is unsympathetic to "Oophs! I forgot I wanted to view or save that data."

The last factor stems from the research nature and the desire to view and validate the process at each step. The program was structured to view graphs, reset scale ranges, redraw a new graph, make a hard copy and save. (store) the intermediate results on a diskette. This highly interactive program required the lab library which takes up a large space in the memory. User decisions slows the process and forces a serial sequence.

## MAIN PROGRAM

As seen in figure 1, the main elements of the program are the main program, XYPSE, which initializes the parameters, calls the subroutines and interacts with the operator. The major subroutines are GETDAT, WIN, FFT, CRSPEC, PLT, AND SAVDAT. Flow diagram and listing are given in Appendix A.

GETDAT is a subroutine to obtain the digitized data from any analog signal channel to the buffer and into the proper array. The digitized data stream is converted from A/D bit counts to physical units of degrees.

The subroutine is called twice by the main program after the operator has designated the channels that carry the stimulus input signal and the output response signal respectively. After each call, the program will ask if the operator would like to see a plot of the raw data.

The subroutine WIN consists of four successive subprograms. The first subprogram removes any D.C. or offset by computing the mean of the array and subtracting the mean value from each element in the array. Both signals are processed at the same time. The second subprogram is a 15 point finite impulse response linear phase digital filter (FIR) that was designed with a separate program called EQFIR (IEEE 1975, 1979). This FIR design package uses the REMEZ exchange algorithm. The FIR coefficients obtained from the EQFIR program are convolved with the input and response signals. The filter characteristics are; a flat band-pass from 0.0 to 1.5 Hz with a maximum deviation of 0.019 or 0.17 db and a stop-band from 3.0 to 5.0 Hz with a 0.0039 deviation or -47.99 db. The filtering is applied to both signals in order to reduce the effects of aliasing. Filter coefficients and results of filtering are given in Appendix C.

The next subprogram is a differentiator. The difference expression for the first derivative was obtained by the Taylor series expansion method to obtain the sixth order central difference formula which is given by the following expression.

$$d x_i = (x_{i+3} - 9x_{i+2} + 45x_{i+1} - 45x_{i-1} + 9x_{i-2} - x_{i-3}) / 60h \quad [2]$$

where h is the interval between samples (Ketter and Prawel, 1969). The error in computing the derivative is given as:

$$\mathcal{E}_r = -\frac{1}{140} h^6 x_o^{vii} \quad [3]$$

where h in the program is ISTEP/120.

(For the particular runs in the results, ISTEP = 12; h = 0.10 seconds.) Expanded results of the differentiation subprogram are given in Appnendix D.

The response signal is filtered again with the same 15-term FIR filter after differentiation. In order to align the two signals after the response has undergone its preprocessing, the input stimulus is delayed. The final subprogram in this subroutine performs a modified cosine taper from 0-10% and 90-100% of the window interval (Bendat and Piersol, 1971) on both input and response signals. The main program will ask the operator if he desires to view either signal after processing through the WIN sub-routine.

The next subroutine called is a fast fourier transform program called "FFT". This subroutine is based on Cooley's FFT program which uses decimation in the time algorithm. In the subroutine, X is an  $N = 2^m$  point complex array that initially contains the input stimulus array, and on output from the transformation contains the complex fourier coefficients. The subroutine can be used to compute the forward and inverse fourier

transform (IEEE, 1979). Both signals are transformed and stored in the complex virtual arrays, XRAY and YRAY. At this point, the input and output signals are in frequency domain representation,  $X(f)$  and  $Y(f)$ , respectively.

The next subroutine called by the main program is CRSPEC. This subroutine calculates the raw estimate of the cross spectral density function.

where

$$\tilde{G}_{xy}(f) = \frac{2h}{N} (\text{CONJUGATE } X(f))(Y(f)) \quad [4]$$

The cross spectrum,  $G_{xy}(f)$ , is a complex array which may be represented with real and imaginary components.

$$\tilde{G}_{xy}(f) = \tilde{C}_{xy}(f) - j \tilde{Q}_{xy}(f) \quad [5]$$

or in polar form as

$$\tilde{G}_{xy}(f) = |\tilde{G}_{xy}(f)| e^{-j\theta_{xy}(f)} \quad [6]$$

where

$$|\tilde{G}_{xy}(f)| = (\tilde{C}_{xy}^2(f) + \tilde{Q}_{xy}^2(f))^{\frac{1}{2}} \quad [7]$$

and

$$\theta_{xy}(f) = \text{TAN}^{-1} \left[ \frac{Q_{xy}(f)}{C_{xy}(f)} \right] \quad [8]$$

The real component,  $C_{xy}(f)$ , is called the coincident spectral density function (or cospectrum) and the imaginary component,  $Q_{xy}(f)$  is called the quadrature spectral density function (or quadspectrum) (Bendat and Piersol 1971, 1980).

Smoothed estimates of the cospectrum,  $\hat{C}_k$ , and quad spectrum,  $\hat{Q}_k$ , components are calculated by using the Hanning method.

$$\hat{C}_0 = 0.5 \tilde{C}_0 + 0.5 \tilde{C}_1 \quad [9]$$

$$\hat{C}_k = 0.25 \tilde{C}_{k-1} + 0.5 \tilde{C}_k + 0.25 \tilde{C}_{k+1} \quad [10]$$

$$\text{for } k = 1, 2, \dots, m-1$$

and

$$\hat{C}_m = 0.5 \tilde{C}_{m-1} + 0.5 \tilde{C}_m \quad [11]$$

The notation " $\sim$ " denotes raw spectrum and " $\wedge$ " means the smoothed spectrum. The subscript  $k$  is the harmonic number. The Hanning frequency smoothing serves to reduce leakage by broadening the main lobe of the power spectral density function while decreasing the negative effects of the side lobes.

This subroutine also calculates the raw power spectral density functions (may also be called the autospectral density function or autospectrum) of the stimulus input  $\tilde{G}_{xx}(f)$ , and of the output response,  $\tilde{G}_{yy}(f)$ , (Bendat and Piersol, 1971) by the following equations.

$$\tilde{G}_{xx}(f) = \frac{2}{T} |X(f, T)|^2 \quad [12]$$

or

$$\tilde{G}_k = \tilde{G}_{xx}(f_k) = \frac{2}{Nh} |X(f, T)|^2 = \frac{2h}{N} |X_k|^2 \quad [13]$$

where

$$f_k = \frac{k}{T} = \frac{k}{Nh} \quad \text{for } k = 0, 1, 2, \dots, N-1 \quad [14]$$

The smoothed estimates of the input and output power spectra are obtained by using the Hanning method.

The output arrays from the subroutine are the smoothed estimates of the cross spectrum ( $\hat{G}_{xy}$ ), the input autospectrum ( $\hat{G}_{xx}$ ), the input autospectrum ( $\hat{G}_{yy}$ ), the cospectrum ( $\hat{C}_{xy}$ ), and the quadspectrum ( $\hat{Q}_{xy}$ ). All estimates are adjusted by the scale factor  $G_k/0.875$  due to the modified cosine tapering in subroutine WIN (Bendat and Piersol, 1971).

Upon return to the main program from the subroutine CRSPEC, the operator is asked sequentially if he would like to graph, copy, and save the cross spectrum, the autospectrum of the input, and the autospectrum of the output, respectively.

The main program then calculates the system transfer function magnitude  $|\hat{H}_{xy}(f)|$ , stores results in the temporary real array TPYRAY. The system transfer magnitude function or the optimum frequency response estimate is given by the expression.

$$\hat{H}_{xy}(f) = \frac{|\hat{G}_{xy}(f)|}{G_{xx}(f)} \quad [15]$$

(Bendat and Piersol 1971, 1980). The frequency response function,  $\hat{H}_{xy}(f)$ , is a complex variable which may be denoted in complex polar rotation as

$$\hat{H}_{xy}(f) = |\hat{H}_{xy}(f)| e^{-j\phi(f)} \quad [16]$$

where

$$\phi(f) = \theta_{xy}(f) \quad [17]$$

is the phase function. Again, the operator is queried, "Graph? Copy? Save?"

The next process is to convert the transfer function magnitude into decibels, DB's, by taking  $10 \log H_{xy}(f)$ . The factor of 10 is used instead of 20 because the spectra is already in units of power, i.e.,  $G = |X|^2$ . Results of the calculation are stored in the temporary array, TPYRAY. At this point it is not possible for the operator to go back and ask for the transfer function magnitude not in decibels. The operator is asked if he wishes to graph, copy, and save the frequency response magnitude in decibels.

The next step is calculation of the smoothed frequency response phase function in degree. The smoothed phase function,  $\hat{\phi}_{xy}(f)$  is calculated by taking the arc tangent of the ratio of the quadspectrum and the cospectrum (see equation 8).

$$\hat{\phi}_{xy}(f) = \hat{\theta}_{xy}(f) = \text{TAN}^{-1} \left[ \frac{\hat{Q}_{xy}(f)}{\hat{C}_{xy}(f)} \right] \quad [18]$$

The operator is then asked, "Graph? Copy? Save?", respectively.

The final calculation is very important since it provides a measure of whether or not two variables are interrelated. In an engineering context, the correlation coefficient is a measure of interrelationships between some controlled excitation and the observed response of a physical system. In analysis of random data, the coherence function,  $\gamma_{xy}^2(f)$ , is analogous to the squared correlation coefficient function. The coherence function is calculated by the expression

$$\gamma_{xy}^2(f) = \frac{|G_{xy}(f)|^2}{G_{xx}(f) G_{yy}(f)} \quad [19]$$

for

$$0 \leq \gamma_{xy}^2(f) \leq 1$$



For linear systems, the fractional portion of the output response mean square value which may be related to the input at a particular frequency is the coherence function value,  $\delta_{xy}^2(f)$ , at the particular frequency,  $f_k$ . The portion not accounted for by the input at the particular frequency is one minus the coherence function at the frequency, i.e.,  $[1 - \delta_{xy}^2(f)]$  for coherence values less than one but greater than zero, the unrelated portion may be due to noise in the measurement, interrelationships with other inputs, or the system is not linear (Bendat and Piersol, 1971, 1980). The coherence function is stored in the temporary array, TPYRAY, and the operator is asked if he would like to graph, copy and save the resulting function before the program terminates.

The two most called upon subroutines are PLT and SAVDAT. The PLT subroutine plots a variable versus time or frequency on to a Tektronix 4014 graphics terminal. The program is interactive with a menu for labeling the graph. This subroutine requires the support of a system library called, "LAB.LIB" which was developed by Technology Incorporated for the NASA Johnson Space Center Neuroscience Research Laboratory (Cosier and Bueker, 1983). The LAB.LIB contains subroutines CHRISZ - character size, ERASE, GRID - for drawing grid lines, ANOTAT - for calculating and annotating axes, and XYPLOT - to graph two scaled variables. These LAB.LIB subroutines are called by PLT.

The subroutine SAVDAT is called when the programmer wishes to store intermediate results onto a diskette during the analyses process. The subroutine will prompt the operator for the file name under which the data is to be stored. The operator must enter disk drive number, abbreviated subject identification (e.g., initials), data identification, and run number;

for example, DY0:MDJXCS.001. The colon and the period in the filename are necessary. Once data is stored on the disk without error, the program will type on screen that the action is completed and will continue to the next instruction.

#### AVERAGING PROGRAM

A second program was written to average results stored from the analysis program XYPSE. The averaging program called RDATA uses two subroutines, SAVDATA and PLT, and the LAB.LIB. The main program can compute the averaged function of any of the functions saved on diskette. The program is designed to average whether the first file read is in a single record or the results from previous averaging of several records.

The program will ask the operator to enter the number of records previously averaged and name of the file to be read from the diskette which contains the processed data. The file name indicates which disk drive to read, type of data-summed average or subject, which variable, and the run number or number of runs averaged. As an example, "DY0:MDJXCS.001" is interpreted as disk drive 0, subject initials MDC, variable cross spectral density function from run number one. The file "DY1:SUMCOH.5X1" is read as disk drive one, the averaged summary of five coherence function data files obtained from responses to one times sixteen (X1). Sixteen degrees per second is the peak value of the sine terms in the stimulus input signal.

The operator may view and save (store onto diskette) the results of averaging as each file is entered. In other words, if the operator wanted to average ten files but wishes to view the averaging as each file is added he may do so. This results in a very flexible program where the operator

may stop at any time view and save the average of several files and begin averaging with the results a week later. The program prompts the operator by means of questions.

Flow diagram and listing of the averaging program are given in appendix B.

## RESULTS AND DISCUSSION

This section is divided into two parts. The first part will present results from the analysis program, XYPSE and the second will present results from the averaging program RDAT.

Figures 1 and 2 show the raw and filtered input stimulus signals. Figure 3 is the raw horizontal EOG response measurement viewed after return from the subroutine GETDAT. Figure 4 is the filtered and differentiated EOG response after the subroutine WIN. Figure 5 is the smoothed cross spectral density function,  $\hat{G}_{xy}(f)$ . Note that the peaks of the cross spectrum correspond to the frequency peaks of the autospectrum of the input stimulus which consists of six sum-of-sinusoids (Figure 6). Figure 7 presents the autospectral density function of the differentiated EOG response shown in figure 4. Figure 8 is the magnitude or transfer function gain. Figure 9 is the most important since it presents the magnitude function in dbs. It is readily noticable that the minimas of the function between 0.1 and 1.0 Hz correspond to the frequencies of the input stimulus frequencies. These points trace an ascending line approximately 10 db per decade. Figure 10 presents the phase function and Figure 11 is the coherence function. These two functions are difficult to interpret since for the linear response we are only interested in the values at those points

which correspond to the input stimulus frequencies. In Figure 11, the corresponding coherence values at the frequencies of interest lie above 0.8.

The only results from the averaging program which are of interest in the analysis of the vestibular ocular system are the transfer function magnitude in dbs, the phase function and the coherence function at the frequencies of interest. Figure 12 is the resultant transfer function in dbs. As in figure 9, the minimas between 0.0 and 1.0 Hz correspond to the frequencies of interest. Figure 13 and 14 present the results after averaging the phase function and the coherence function respectively. The RDATA program printed these values to facilitate ease of reading the value at the frequencies of interest. Table 1 summarizes the results of averaging seven runs.

In all cases the coherence function was above 0.78 but below 1.0 indicating noise in the response measurement or nonlinearities in the system. To analyze the nonlinear characteristics of the system, programs must be written to follow the method developed by Victor and Shapley.

As stated earlier the coherence function is an important calculation not only because it provides a measure of interrelationships between input to output, but because coherence is used to determine the random error of the estimate for a single input/output model as given by the following calculations (Bendat and Piersol 1980).

$$E_r [\hat{G}_{xx}(f), \hat{G}_{yy}(f)] = \frac{1}{\sqrt{n_d}} \quad [20]$$

$$E_r [\hat{G}_{xy}(f)] = \frac{1}{|\gamma_{xy}(f)| \sqrt{n_d}} \quad [21]$$

$$E_r [\hat{H}_{xy}(f)] = \frac{[1 - \gamma_{xy}^2(f)]^{1/2}}{|\gamma_{xy}(f)| \sqrt{2 n_d}} \quad [22]$$

$$E_r [\hat{\gamma}_{xy}^2(f)] = \frac{\sqrt{2} [1 - \gamma_{xy}^2(f)]}{|\gamma_{xy}(f)| \sqrt{n_d}} \quad [23]$$

$$E_r [\Delta \hat{\phi}_{xy}(f)] \approx \frac{[1 - \gamma_{xy}(f)]^{1/2}}{|\gamma_{xy}(f)| \sqrt{2 n_d}} \quad [24]$$

Calculation of the random error serves two purposes. First, it may be used after  $n_r$  number of runs to determine the error knowing the average coherence value. Secondly, if the assumption is made that the coherence will remain constant, the number of runs necessary to obtain a predetermined value for the random error can be calculated. For example, if the averaged coherence value after 8 runs ( $n_r = 8$ ) is 0.8, the transfer function gain and phase errors are 0.125. If the random error is to be reduced by half (0.0625), then a total of 64 runs are required.

#### SUMMARY AND RECOMMENDATION

An analytical program and an averaging program were developed to analyze the vestibular ocular system response to pseudorandom velocity input. The linear transform function gain, phase, and coherence were obtained from seven subjects. Coherence results at the frequencies of interest were greater than 0.8 but less than 1.0. The values of coherence less than one could be attributed to noise in the output signal, another source of stimulation, or nonlinear characteristics of the system.

I recommend that the Space Biomedical Research Institute of the Space and Life Sciences Directorate, NASA, study the nonlinear response characteristics of the vestibular ocular system by extension of the sum-of-sinusoids method to the intermodulation of cross-talk frequencies. I would also recommend runs at frequencies a decade higher and a decade lower, if it is physically possible.

## REFERENCES

1. Bedrosian, E., and S. O. Rice, The Output Properties of Volterra Systems Driven by Harmonic and Gaussian Inputs. Proc. IEEE, 59: 1688-1707, 1971.
2. Bendat, J. S., and A. G. Piersol, Measurement and Analysis of Random Data, John Wiley & Sons, 1966.
3. Bendat, J. S., and A. G. Piersol, Random Data: Analysis and Measurement Procedures, John Wiley & Sons, 1971.
4. Bendat, J. S., and A. G. Piersol, Engineering Applications of Correlation and Spectral Analysis, John Wiley & Sons, 1980.
5. Crosier, W. G., and P. A. Bueker, Special Report: A General Purpose Data Acquisition and Analysis System for Nystagmus Related Data. Version 2.0, NASA Contract: NAS9-14880, August 1983.
6. Homick, J. L., Space Motion Sickness, Acta Astronautica, 6:1259-1272, 1979.
7. IEEE Ed., Selected Papers in Digital Signal Processing II, IEEE Press, 1975.
8. IEEE Ed., Program for Digital Signal Processing, IEEE Press, 1979.
9. Ketter, R. L., and S. P. Prawel, Jr., Modern Methods of Engineering Computation, McGraw-Hill, 1969.
10. Lee, Y. N., and M. Schetzen, Measurement of the Kernels of a Nonlinear System by Cross Correlation, Intern'l J. of Control, 2:237-254, 1965.
11. McGillem, C. D. and G. R. Cooper, Continuous and Discrete Signal and System Analysis, Holt, Rinehart and Winston, Inc., 1974.
12. Oppenheim, A. V. and R. W. Schaffer, Digital Signal Processing, Prentice-Hall, Inc., 1975.
13. Reschke, M. F., Middeck Rotator Vestibular Function Tests: Modification of Eye Movements, Visual-Vestibular Function Responses and Perception During Angular Rotation as a Function of Altered Otolith Input in Microgravity, NASA-Internal Research Proposal NASA-Johnson Space Center, June 1984.

14. Talbot, J. M., Ed, Research Opportunities in Space Motion Sickness: Final Report Phase II, NASA Contract NASW-3616, NASA Contractor Report-3708, July 1983.
15. Victor, J. D. and R. Shapley, A. Method of Nonlinear Analysis in the Frequency Domain, Biophys. J. 29: 459-484, 1980.
16. Victor, J. D. and B. W. Knight, Nonlinear Analysis with an Arbitrary Stimulus Ensemble, Quarterly of Applied Mathematics, XXXVII 2: 113-136, 1979.



TABLE 1  
PSEUDORANDOM STIMULUS PROFILE  
FUNDAMENTAL FREQUENCY 0.05 Hz

Harmonics		Magnitude = 16 Deg/Sec			
	Harmonic	Frequency	Phase	I	I=I <sub>n</sub> +1
1)	2	0.1	$-\pi$	11	11.24
2)	3	0.15	$\pi/2$	16	16.36
3)	5	0.25	$-\pi/2$	27	26.6
4)	7	0.35	$-\pi/2$	37	36.84
5)	11	0.55	$\pi$	57	57.32
6)	19	0.95	$\pi/2$	98	98.28

TABLE 2  
RESULTS OF AVERAGING PROGRAM  
TRANSFER FUNCTION

FREQ. Hz	MAG Dbs	PHASE 0 Degrees	COHERENCE
-0.1	-12.1	-60	.80
0.15	-10.2	- 3	.80
0.25	- 8.7	-90	.84
0.35	- 8.5	-35	.83
0.55	- 8.4	31	.78
0.95	- 4.7	-40	.94

FILENAME: DY0MDJH4AA08

INPUT STIMULUS VS TIME

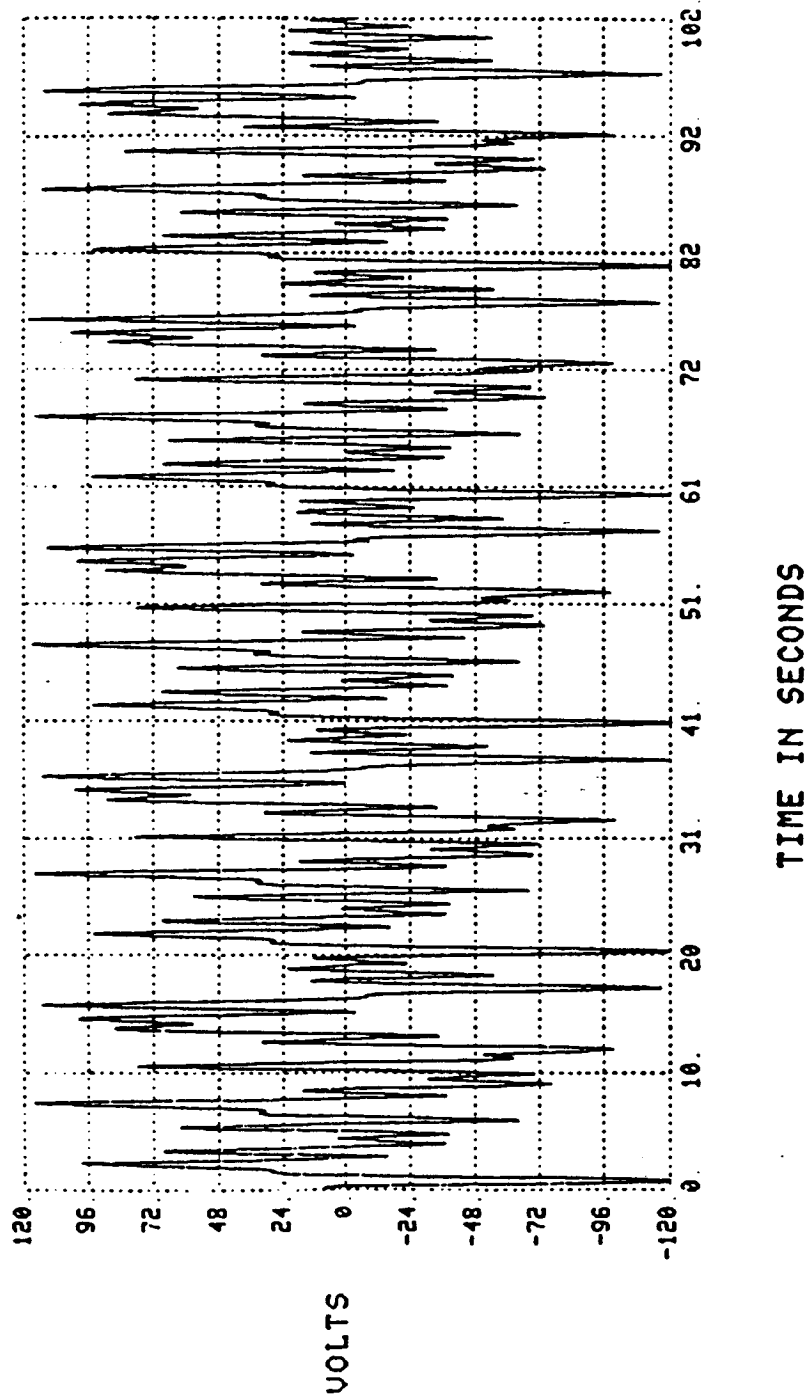


Fig. 1 - Raw Input Stimulus. Four cycles of the sum-of-(six) sinusoids input stimulus are shown in 102.4 second data window. The signal was obtained from a tachometer which measures the angular velocity of the rotating chair. This graph was made after the GEIDAT subroutine.

FILENAME: DYQMDJH4AA08

INPUT STIMULUS VS TIME

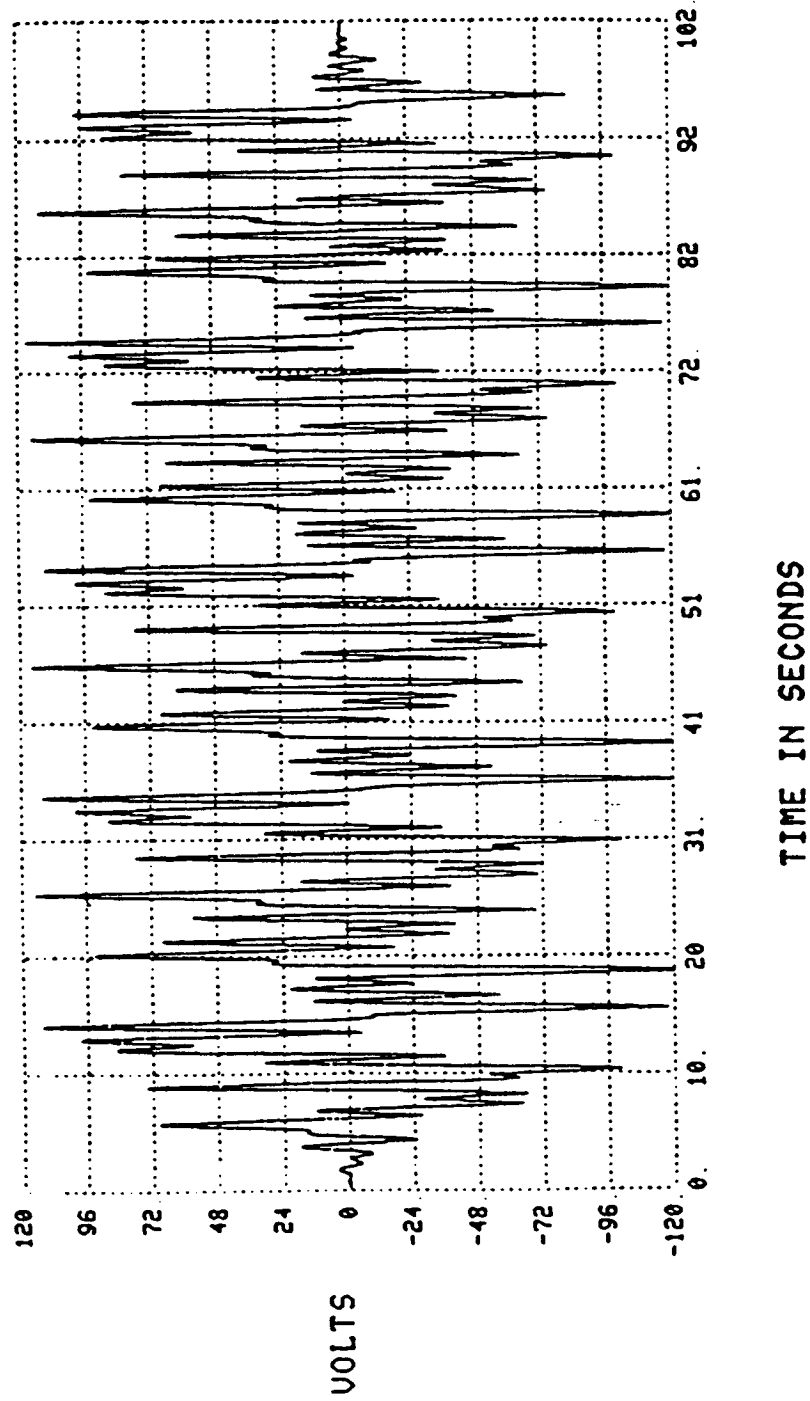


Fig. 2 - Filtered Input Stimulus. The effects of the 15-point FIR digital filter and the modified cosine tapered window are shown in the IQ2.4 second data window. This graph was made after the WIN subroutine.

FILENAME · DY0MDJH4AA08

HORIZONTAL EYE MOVEMENTS VS TIME

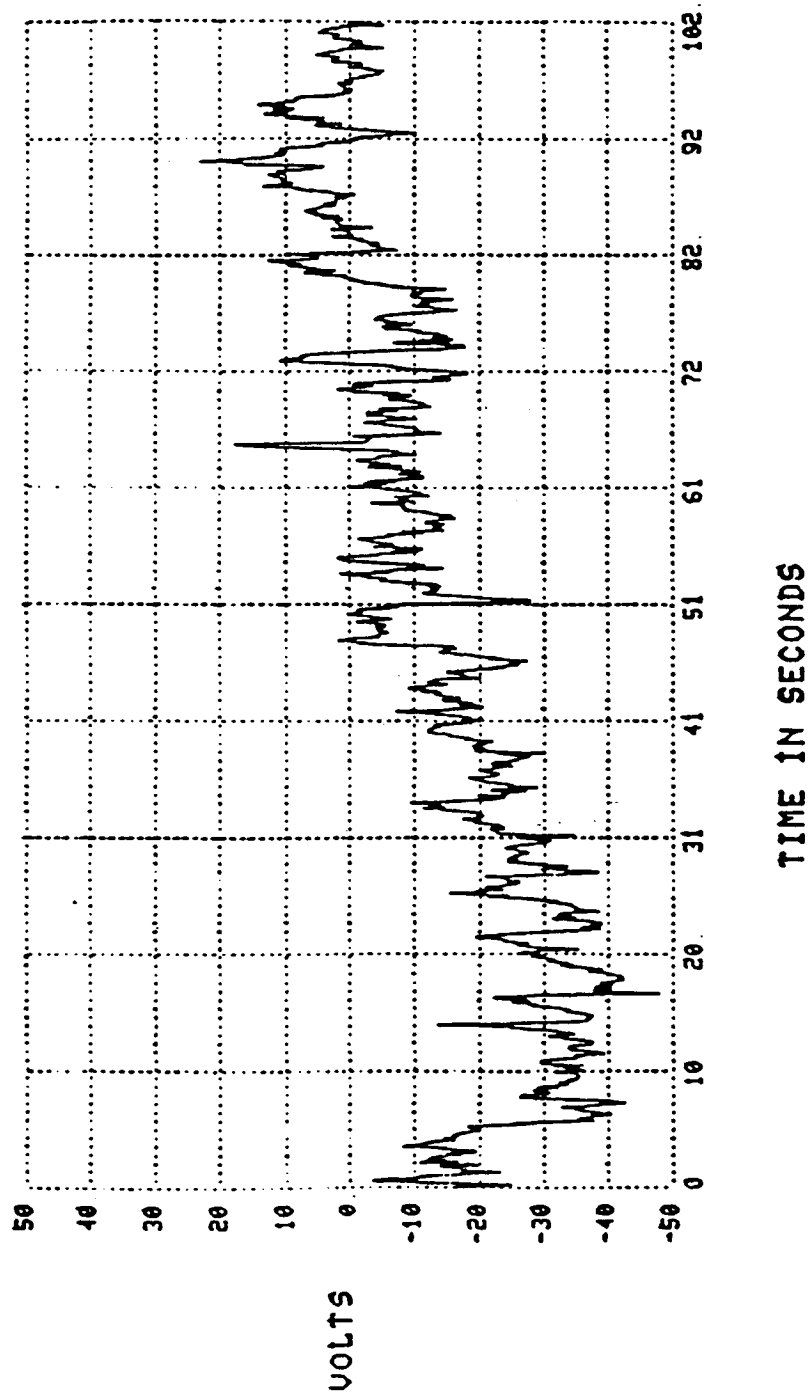


Fig. 3 - Raw Horizontal EOG Output Response. Left electro-oculogram (EOG) was obtained from subject stimulated by pseudorandom velocity shown in Fig. 1.

FILENAME: DY0MDJH4AA08

# HORIZONTAL EYE MOVEMENTS VS TIME

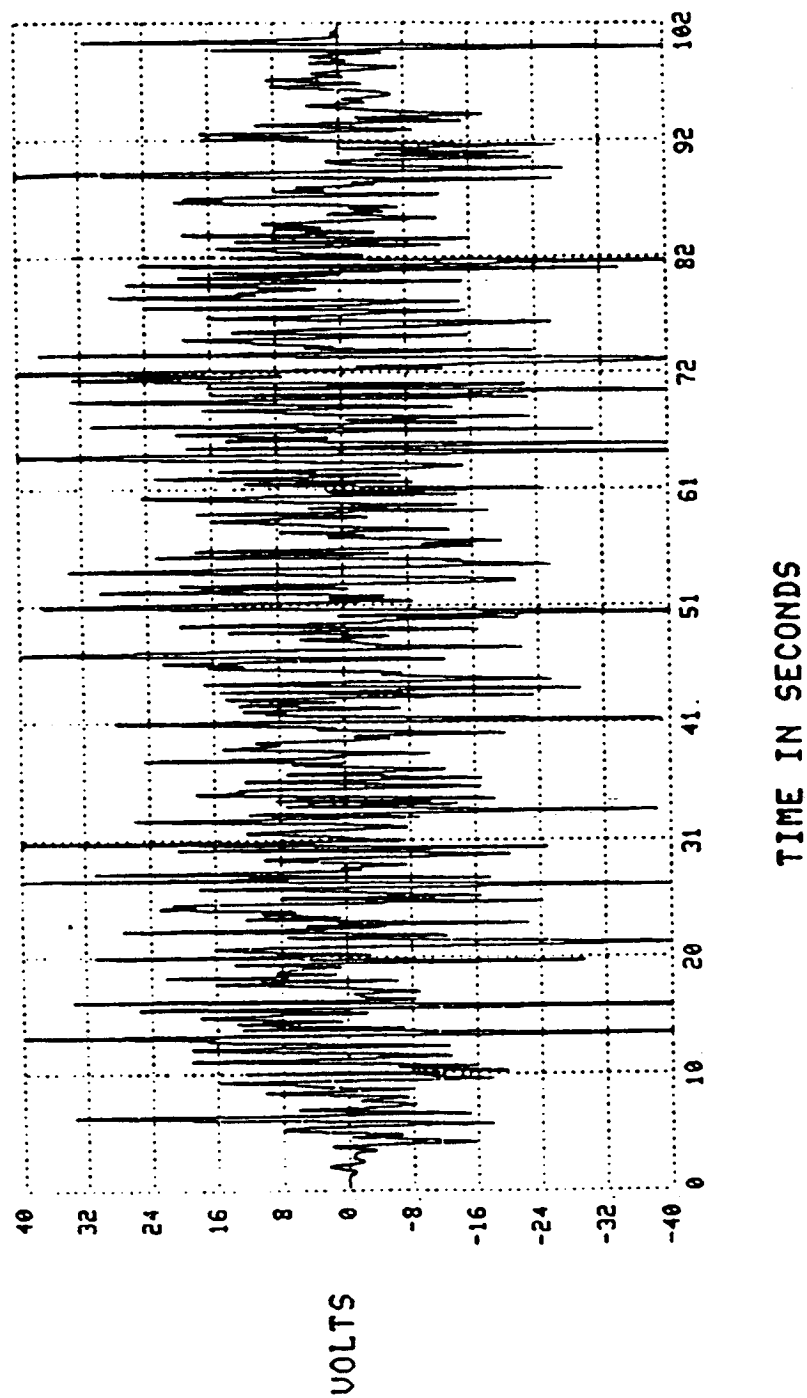


Fig. 4 - Filtered and Differentiated Response. The results of the WIN sub-routine on the raw EOG response signal of Fig. 3 are shown.

FILENAME: DY0MDJH4AA08

# CROSS-SPECTRA

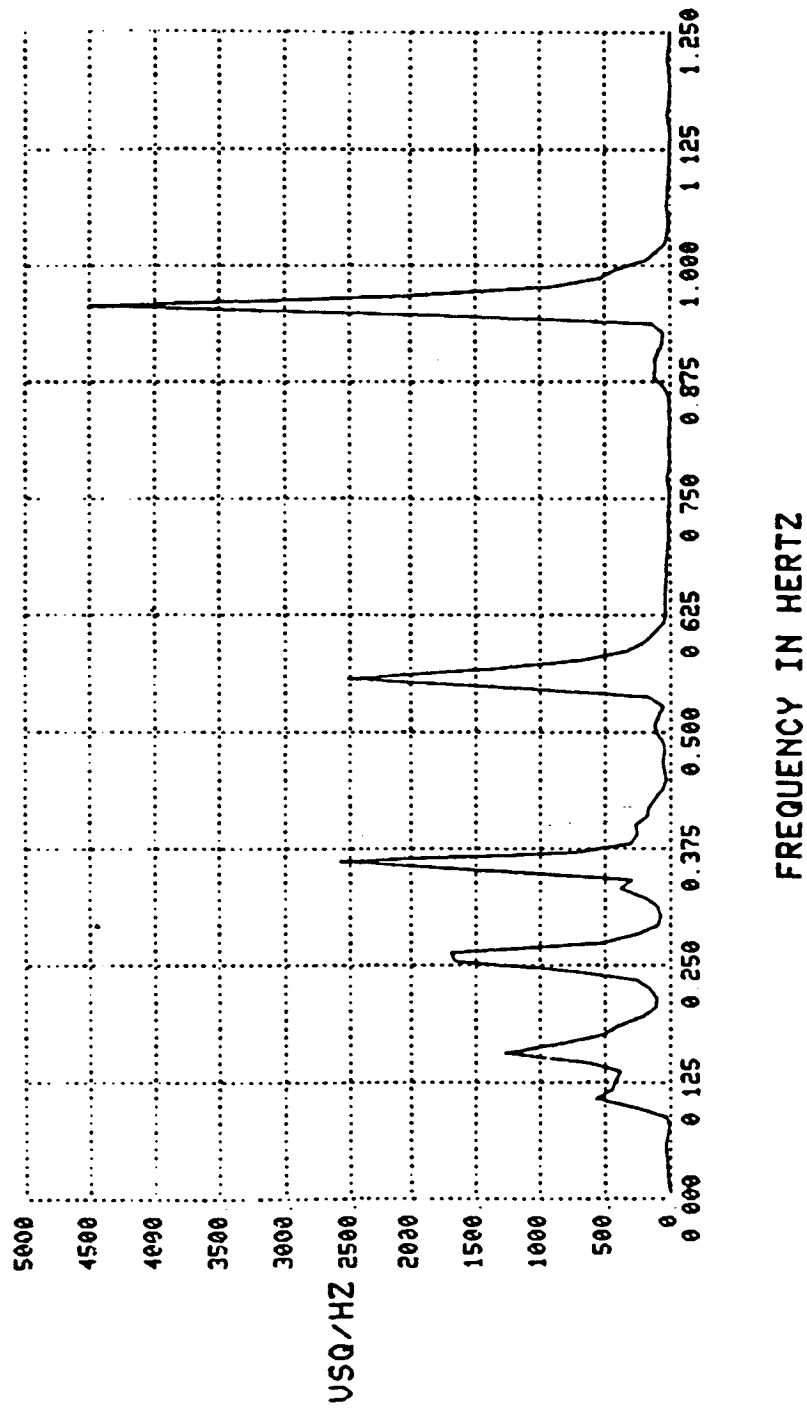


Fig. 5 - Smoothed Cross Spectral Density Function. The cross spectrum computed by CRSPEC subroutine and smoothed by a 3-point Hanning Smoothing is shown with the x-axis scale expanded to show one fourth of the total computed spectral band (0 to 5.0 Hz). The vertical axis is scaled in volts squared per hertz (VSQ/Hz).

FILENAME: DY0MDJH4AA08

# POWER SPECTRUM OF INPUT STIMULUS

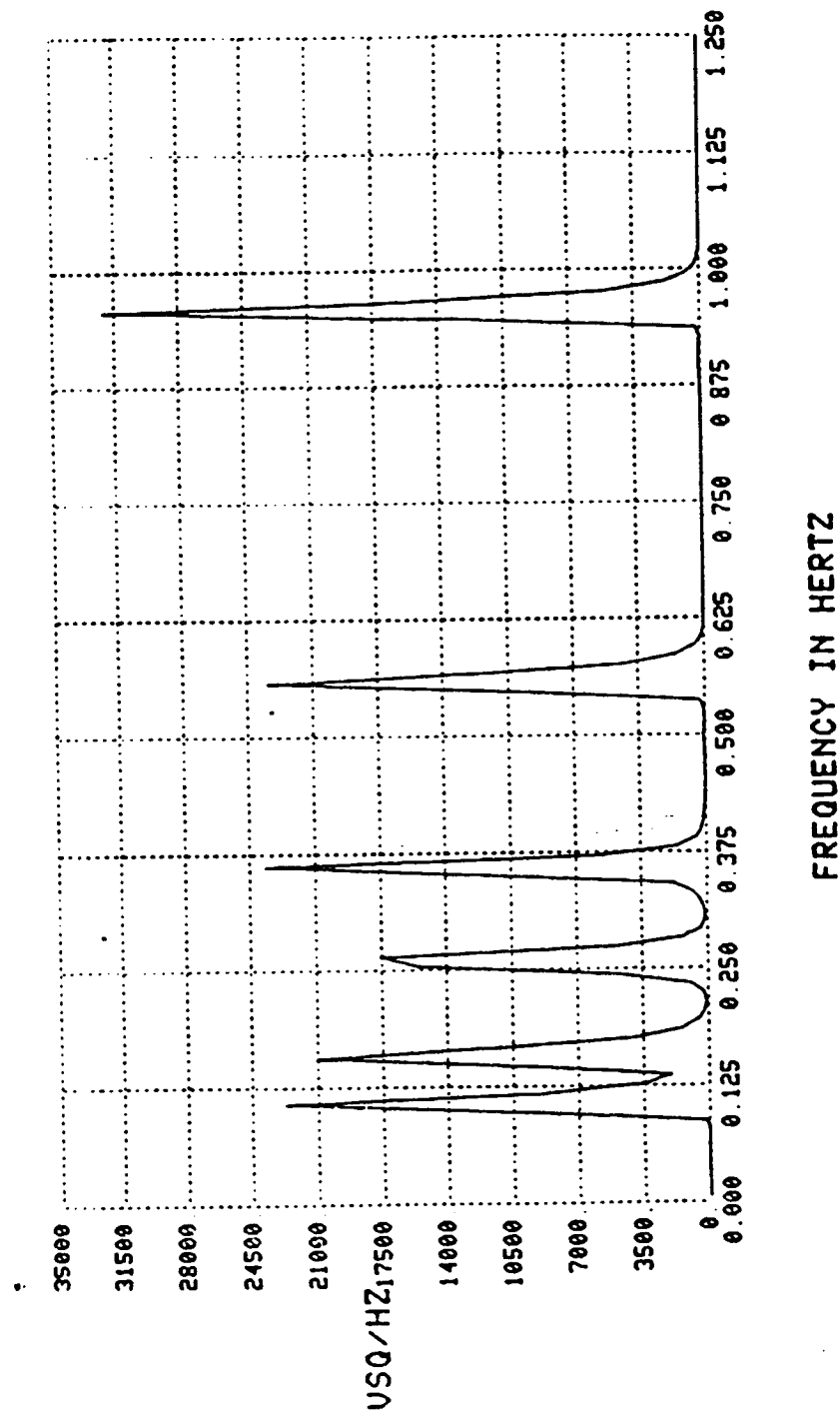


Fig. 6 - Smooth Spectral Density Function of Input Stimulus. This spectrum shows the six frequencies used to produce the pseudorandom stimulus. The lack of nonuniformity in magnitude may be the result of the chair and subject dynamics. Horizontal scale was expanded.



FILENAME: DY0MDJH4AA08

# POWER SPECTRUM OF OCULAR RESPONSE

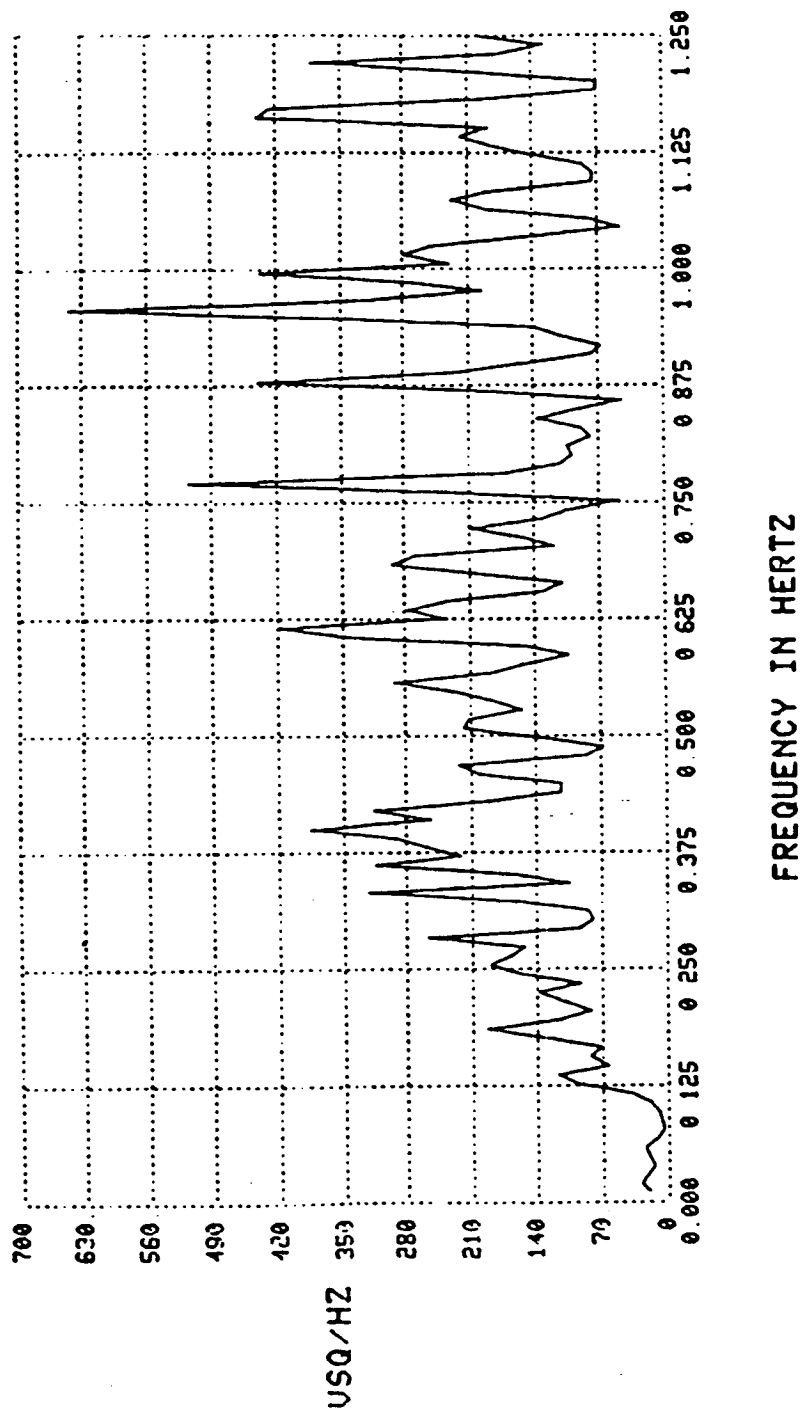


Fig. 7 - Smoothed Spectral Density Function of Differentiated EOG Response. Dominant peaks at other than the frequencies of stimulation may indicate nonlinearity of the system response or noise from fast phase nystagmus discontinuities. Horizontal scale expanded.

FILENAME: DY0MDJH4AA08

# TRANSFER FUNCTION GAIN

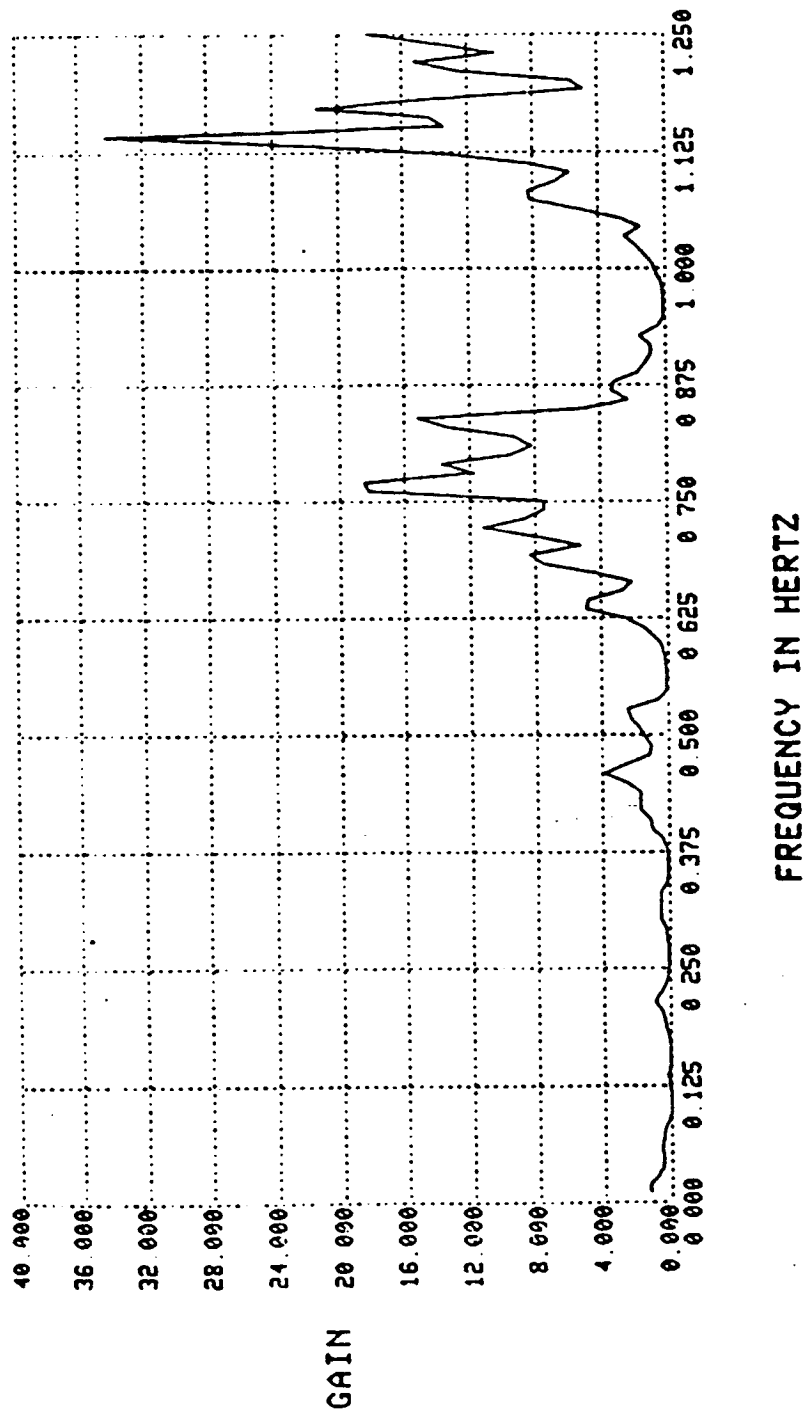


Fig. 8 - Transfer Function Gain. Transfer function gain, also called the magnitude function, is shown with expanded horizontal scale. Note that all values at the frequencies of interest are close to zero.

FILENAME: DY0MDJH4AA08

TRANSFER FUNCTION IN DBs

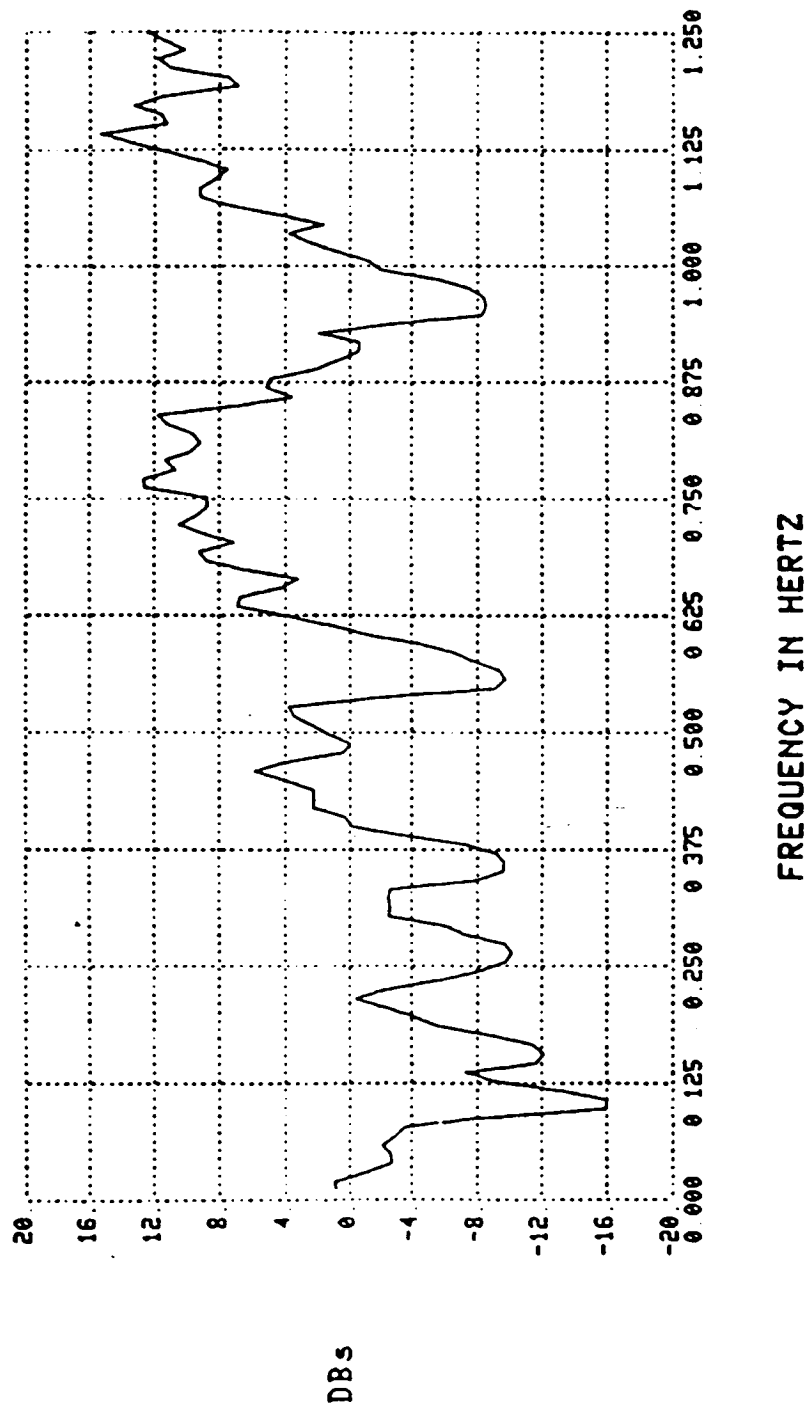


Fig. 9 - Magnitude Function in db's. The magnitude function of Fig. 8 is shown in decibel (db) units. The six largest minimas (troughs) correspond to the six frequencies of the input stimulus. Connecting the six minimas is the transfer function in the frequency domain. Frequency axis expanded.

FILENAME: DY0MDJH4AA08

PHASE FACTOR IN DEGREES

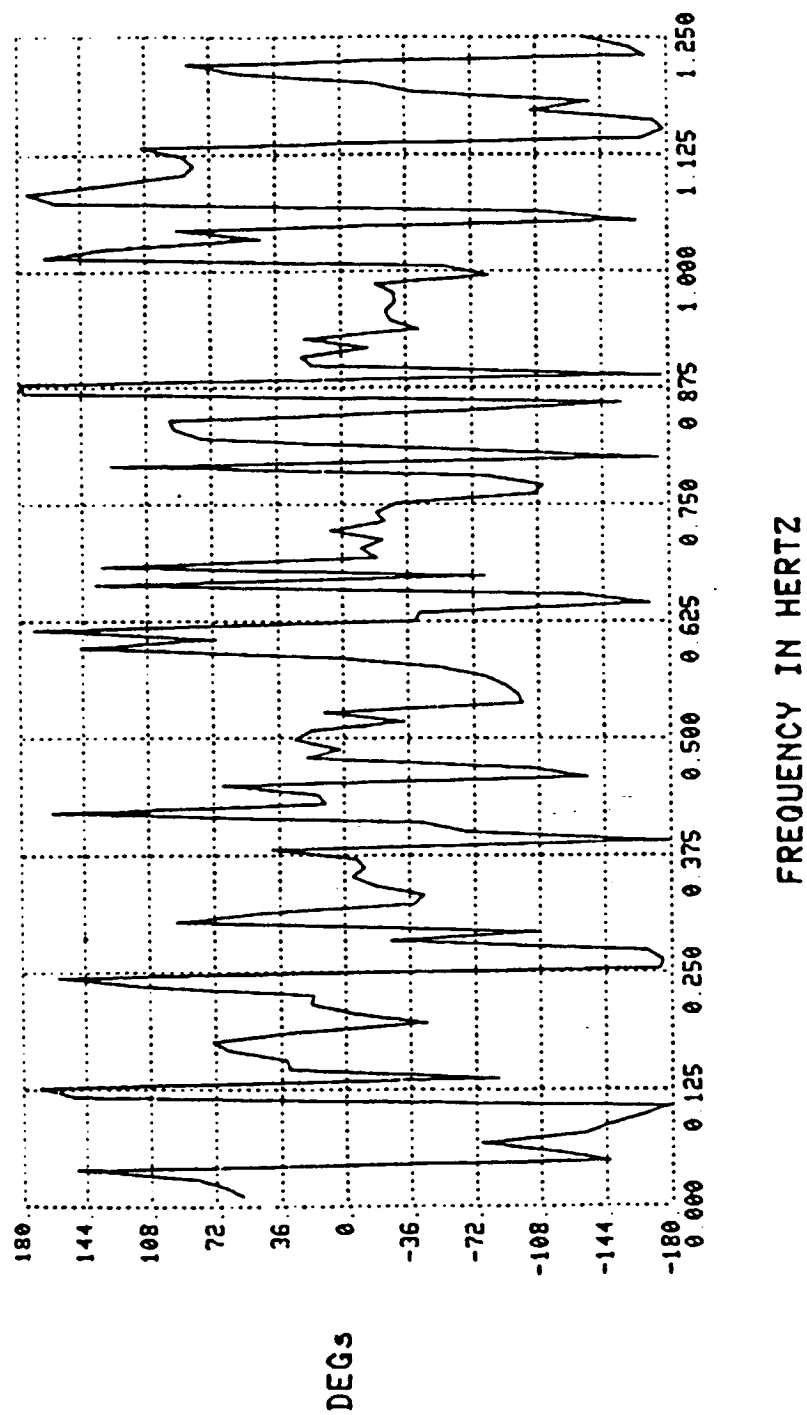


Fig. 10 - Phase Function. The transfer function phase angle is shown in degrees with an expanded horizontal axis.

FILENAME: DY0MDJH4AA08

# COHERENCE FUNCTION

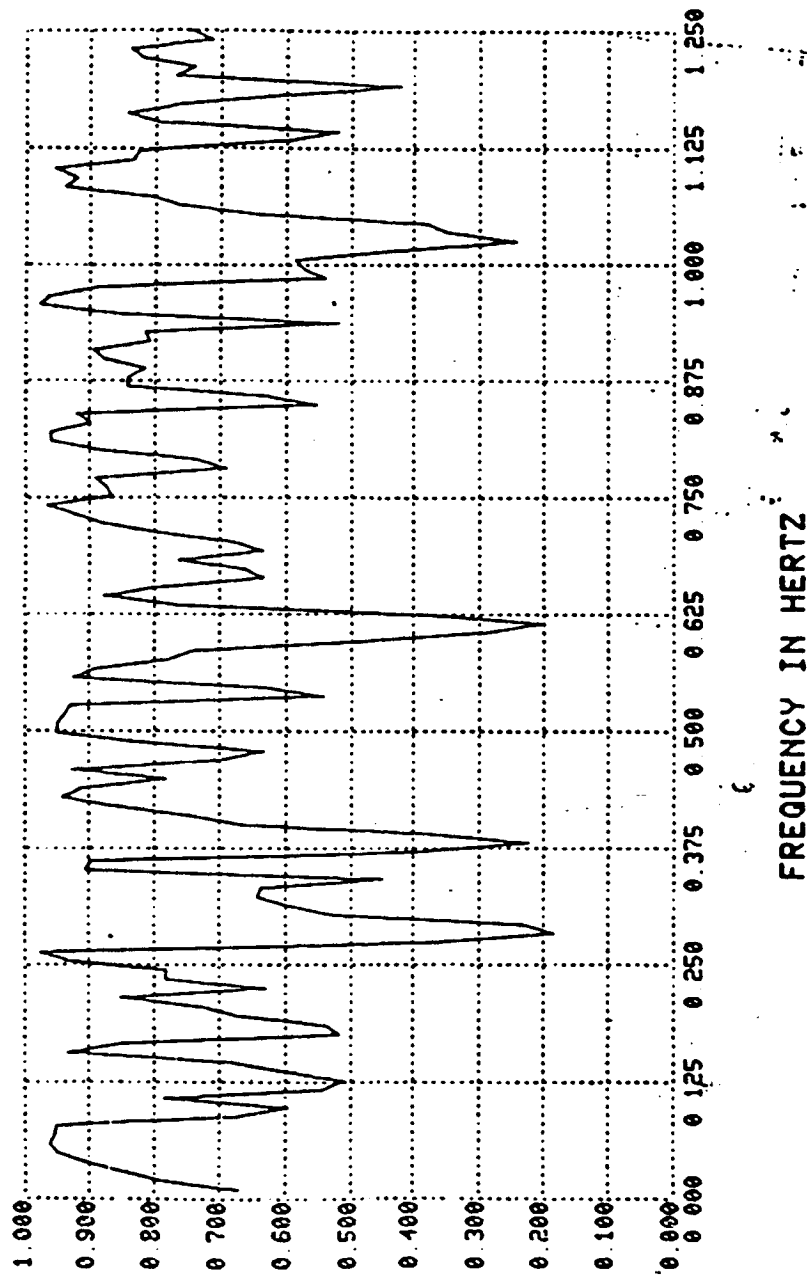


Fig. 11 - Coherence Function. The coherence function is shown with expanded horizontal axis.

FILENAME:AUGEDRESULTS

TRANSFER FUNCTION IN DBs

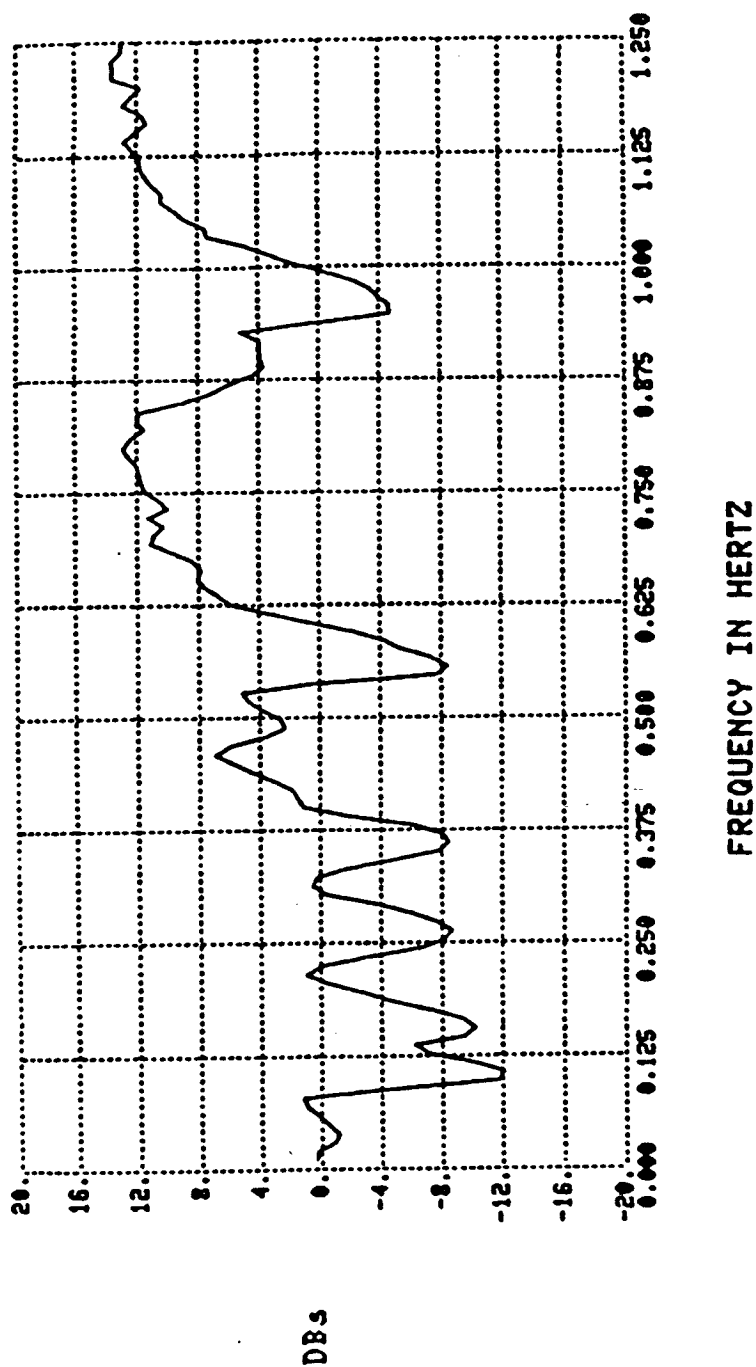
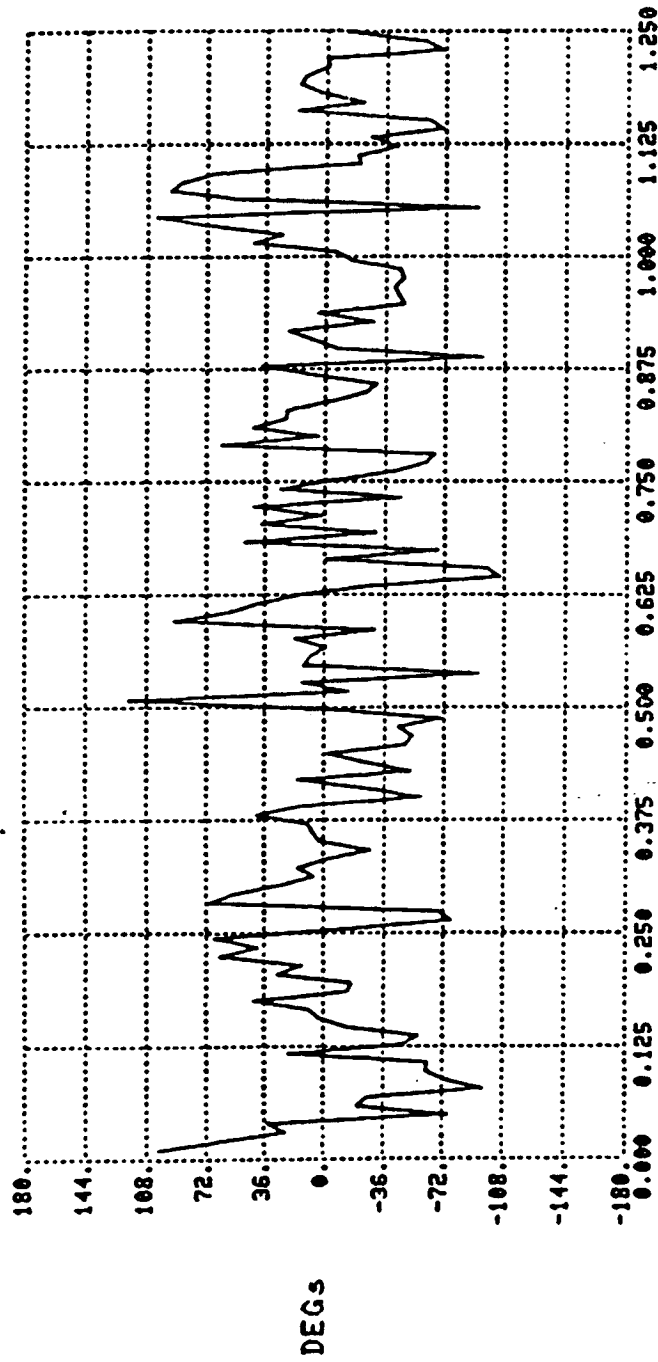


Fig. 12 - Averaged Magnitude Function in db's. The magnitude function resulting from the average of seven runs is shown with the horizontal axis expanded.

FILENAME: AUGEDRESULTS

PHASE FACTOR IN DEGREES



FREQUENCY IN HERTZ

Fig. 13 - Averaged Phase Function. The phase function resulting from the average of seven runs is shown with the horizontal axis expanded.

FILENAME:AUGEDRESULTS

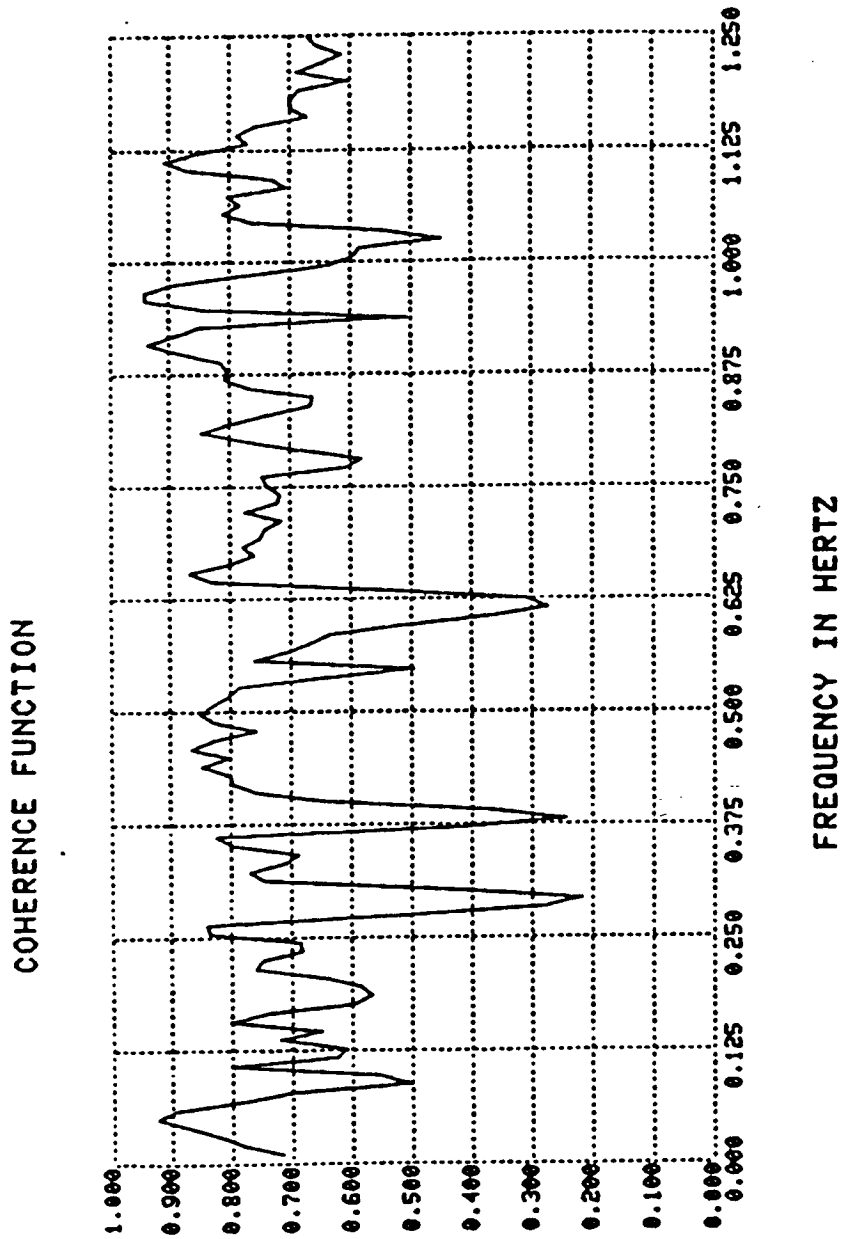


Fig. 14 - Averaged Coherence Function. The coherence function resulting from the average of seven runs is shown with the horizontal axis expanded.



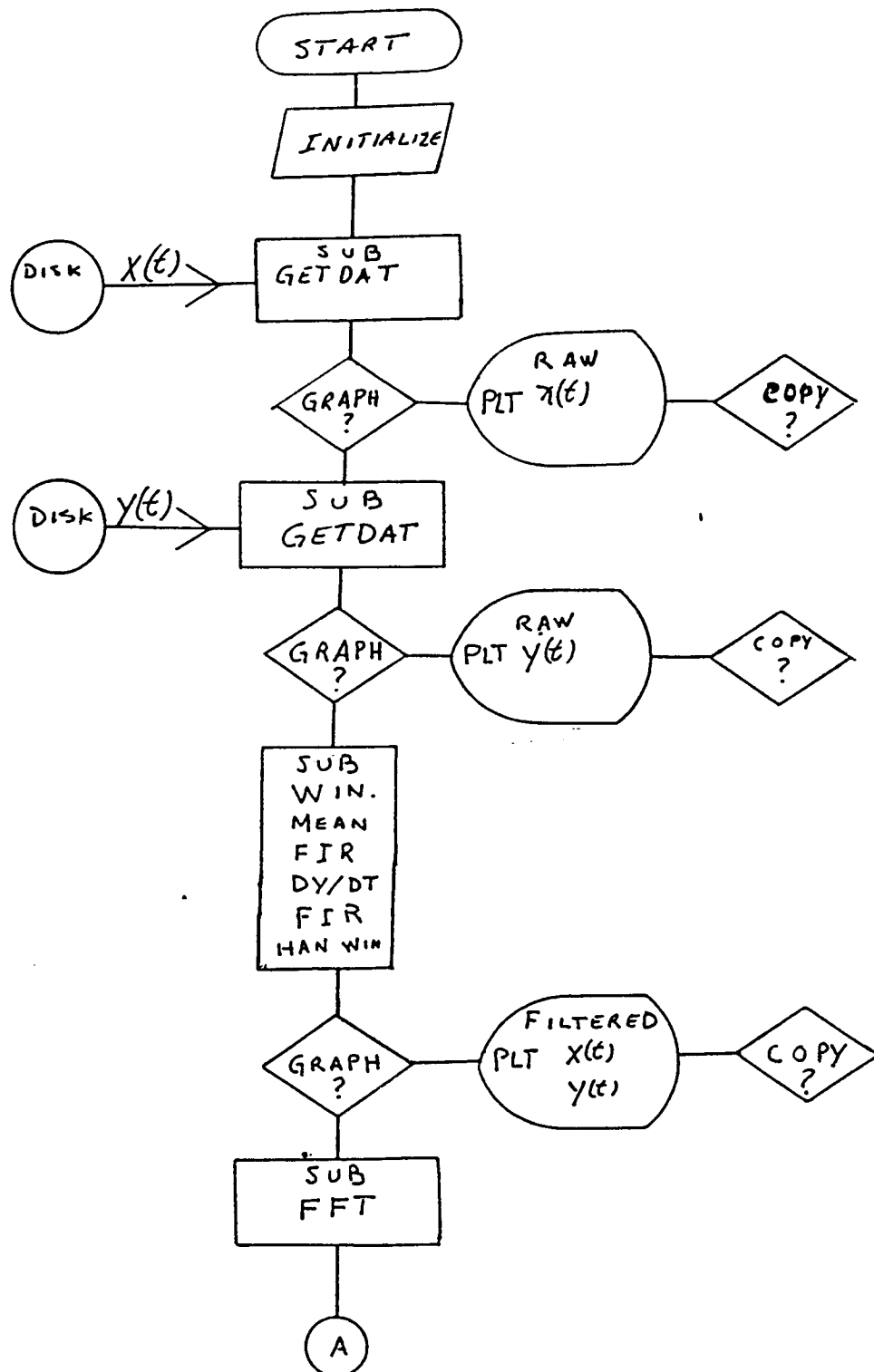
APPENDIX A

FLOW DIAGRAM AND PROGRAM LISTING

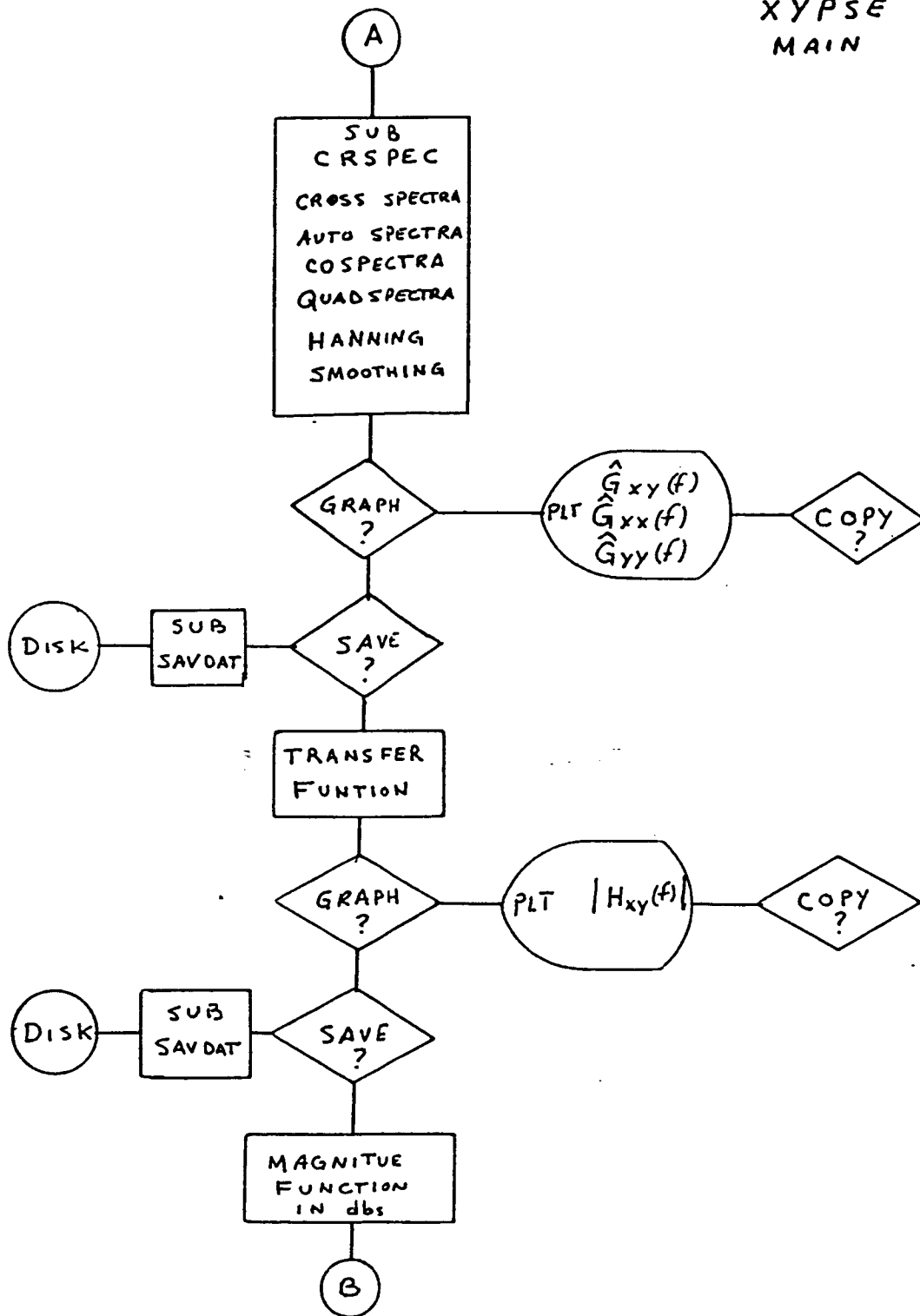
XYPSE

ANALYSIS PROGRAM

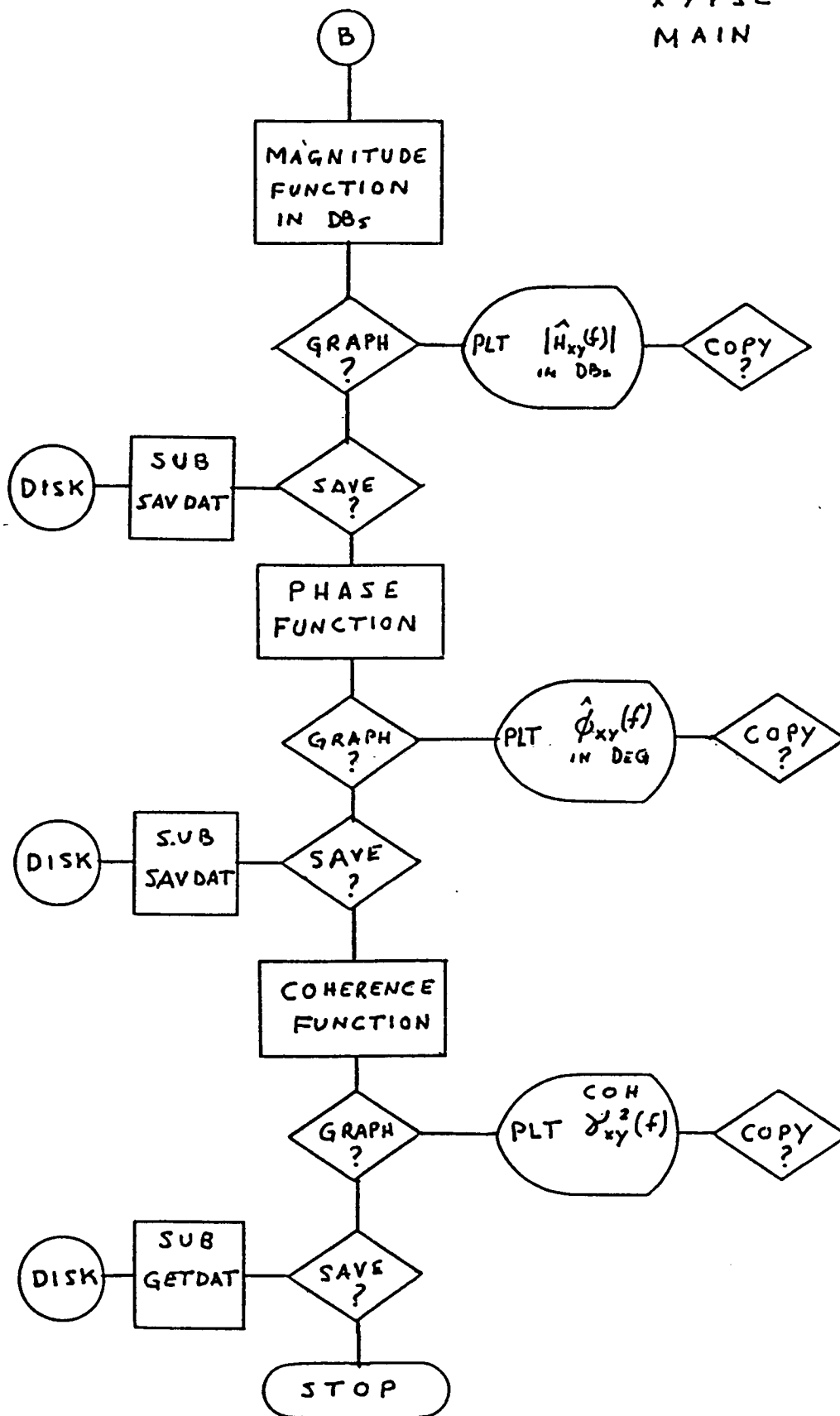
# PROGRAM XYPSE



XYPSE  
MAIN



XYPSE  
MAIN



```
0001      PROGRAM XYPSE
      C      LENGTH IS THE WINDOW LENGTH
      C
0002      INTEGER Z(512),DSKINC,NBLK,IPOSN(16),MAX(16),ICNUM(16),LENGT
0003      REAL AMPL, PERIOD, INTRAT, HEOG(1024), XT(1024), STIMIN(1024)
0004      VIRTUAL XRAY(1024), YRAY(1024), GXYRAY(512), YHEOG(1024)
0005      VIRTUAL YSTIM(1024)
0006      COMPLEX XRAY, YRAY, GXYRAY
0007      REAL TPYRAY(512), SGXY(512), COEF(17), YHEOG, YSTIM
0008      LOGICAL*1 IFILE(15)
      C
0009      EQUIVALENCE (AMPL,Z(150)),(PERIOD,Z(152)),(INTRAT,Z(159)),
      1 (DSKINC,Z(167)),(NBLK,Z(172)),(ICNUM,Z(177)),
      2 (IPOSN,Z(225)),(MAX,Z(241))
      C
0010      COEF(1) = .0037165603
0011      COEF(2) = .020235427
0012      COEF(3) = .013399956
0013      COEF(4) = -.040643737
0014      COEF(5) = -.066073574
0015      COEF(6) = .061152663
0016      COEF(7) = .30294424
0017      COEF(8) = .43047285
0018      DO 5 N = 1, 7
0019      COEF(16-N) = COEF(N)
0020      5 CONTINUE
      C
0021      INTEGER BUFR2(800), IERR
0022      BYTE FILNAM(12)
0023      10 DO 20 K=1,12
0024      20 FILNAM(K)=0
0025      TYPE 30
0026      30 FORMAT (' ENTER COMPLETE FILENAME'/' FILENAME ?',%)
0027      ACCEPT 40,FILNAM
0028      40 FORMAT (12A1)
      C
0029      CALL DISKIO(FILNAM,-3,Z,256,0,NDUMMY,IERR)
0030      IF (IERR .NE. 0) TYPE *, ' ERROR CODE',IERR, ' DURING READING'
      C
0032      TYPE *, ' ENTER CHANNEL NUMBERS IN ORDER:'
0033      TYPE *, ' ENTER INPUT STIMULUS CHANNEL: '
0034      ACCEPT *,K1
0035      TYPE *, ' ENTER OUTPUT RESPONSE CHANNEL: '
0036      ACCEPT *,K2
      C
0037      45 TYPE *, ' ENTER THE NUMBER OF DATA POINTS FOR EOG FFT LENGTH'
0038      ACCEPT *,LENGTH
0039      TYPE *, ' DO YOU WANT TO PLOT EVERY POINT? ENTER STEP SIZE!'
0040      ACCEPT *,ISTEP
0041      TYPE *, ' DO YOU WANT FILES LEFT OPEN? (1=YES)'
0042      ACCEPT *,LOPEN
      C
0043      H = FLOAT(ISTEP)/120.
0044      SF = 120./FLOAT(ISTEP)
```

```
0045      LH = LENGTH/2
0046      CFAC = (2.*H)/(0.875*FLOAT(LENGTH))
0047      RTF = 1./SF
0048      RF = SF/FLOAT(LENGTH)
0049      K = K1

      C
0050      NWRDS = DSKINC* 256
0051      IBLK = 2
0052      IX = 1
0053      ITEMP = 0
0054      NPTS = (MAX(K)-IPOSN(K)+1)/ISTEP
0055      TYPE 50, NBLK, NWRDS, IBLK, DSKINC
0056 50    FORMAT (' NBLK=',I5,' NWRDS=',I5,' IBLK=',I5,' DSKINC=',I5)
0057      TYPE 51, MAX(K), IPOSN(K)
0058 51    FORMAT (' MAX(K) = ',I5,' IPOSN(K) = ',I5)
      C
0059 60    CALL GETDAT(FILNAM, LOPEN, NWRDS, IBLK, K, ISTEP, DSKINC, LENGTH,
1       ITEMP, NPTS, STIMIN, IPOSN, Z)
      C
0060      TYPE *, ' DO YOU WANT TO PLOT RAW INPUT STIMULUS DATA? (YES=1)'
0061      ACCEPT *, IYES
0062      IF (IYES .NE. 1) GO TO 65
0064      CALL PLT(STIMIN, XT, LENGTH, RTF, FILNAM)
0065 65    K = K2
      C
0066      NWRDS = DSKINC* 256
0067      IBLK = 2
0068      IX = 1
0069      ITEMP = 0
0070      NPTS = (MAX(K)-IPOSN(K)+1)/ISTEP
0071      TYPE 66, NBLK, NWRDS, IBLK, DSKINC
0072 66    FORMAT (' NBLK=',I5,' NWRDS=',I5,' IBLK=',I5,' DSKINC=',I5)
0073      TYPE 68, MAX(K), IPOSN(K)
0074 68    FORMAT (' MAX(K) = ',I5,' IPOSN(K) = ',I5)
      C
0075 70    CALL GETDAT(FILNAM, LOPEN, NWRDS, IBLK, K, ISTEP, DSKINC, LENGTH,
1       ITEMP, NPTS, HEOG, IPOSN, Z)
      C
0076      TYPE *, ' DO YOU WANT TO PLOT RAW OUTPUT RESPONSE DATA? (YES=1)'
0077      ACCEPT *, IYES
0078      IF (IYES .NE. 1) GO TO 80
0080      CALL PLT(HEOG, XT, LENGTH, RTF, FILNAM)
      C
0081 80    CALL WIN( STIMIN, YSTIM, HEOG, YHEOG, COEF, LENGTH, H)
      C
0082      TYPE *, ' DO YOU WANT TO PLOT FILTERED STIMULUS INPUT? (YES=1)'
0083      ACCEPT *, IYES
0084      IF (IYES .NE. 1) GO TO 83
0086      CALL PLT(STIMIN, XT, LENGTH, RTF, FILNAM)
      C
0087 83    TYPE *, ' DO YOU WANT TO PLOT FILTERED OUTPUT RESPONSE? (YES=1)'
0088      ACCEPT *, IYES
0089      IF (IYES .NE. 1) GO TO 85
0091      CALL PLT(HEOG, XT, LENGTH, RTF, FILNAM)
```

```
      C
0092  85    DO 90 I = 1, LENGTH
0093        XRAY(I) = CMPLX(STIMIN(I), 0.0)
0094        YRAY(I) = CMPLX(HEOG(I), 0.0)
0095  90    CONTINUE
      C
0096  100   CALL FFT (XRAY, LENGTH, 0)
      C
0097        CALL FFT (YRAY, LENGTH, 0)
      C
0098        CALL CRSPEC(XRAY,YRAY,TPYRAY,STIMIN,HEOG,GXYRAY,SGXY,YSTIM,YHE
1 LH,CFAC)
      C
0099        TYPE *, ' DO YOU WANT THE CROSS-SPECTRA PLOT? (YES=1)'
0100        ACCEPT *, IES
0101        IF (IES .NE. 1) GO TO 110
0103        CALL PLT(TPYRAY, XT, LH, RF, FILNAM)
      C
0104        CALL SAVDAT(TPYRAY, LH, IFILE)
      C
      C
0105  110   TYPE *, ' PLOT AUTO-SPECTRA OF INPUT STIMULUS? (YES=1)'
0106        ACCEPT *, IES
0107        IF ( IES .NE. 1) GO TO 120
0109        LH = LENGTH/2
0110        CALL PLT(STIMIN, XT, LH, RF, FILNAM)
      C
0111        CALL SAVDAT(STIMIN, LH, IFILE)
      C
0112  120   TYPE *, ' PLOT AUTO-SPECTRA OF OUTPUT RESPONSE? (YES=1)'
0113        ACCEPT *, IES
0114        IF (IES .NE. 1) GO TO 130
0116        LH = LENGTH/2
0117        CALL PLT(HEOG, XT, LH, RF, FILNAM)
      C
0118        CALL SAVDAT(HEOG, LH, IFILE)
      C
0119  130   TYPE *, ' PLOT TRANSFER FUNTION GAIN ? (YES=1) '
0120        ACCEPT *, IES
0121        IF ( IES .NE. 1) GO TO 150
0123        LH = LENGTH/2
0124        DO 132 I = 1, LH
0125        TPYRAY(I) = TPYRAY(I)/STIMIN(I)
0126  132   CONTINUE
0127        CALL PLT(TPYRAY, XT, LH, RF, FILNAM)
      C
0128        CALL SAVDAT(TPYRAY, LH, IFILE)
      C
0129  135   TYPE *, ' PLOT TRANSFER FUNCTION IN DBs ? (YES=1)'
0130        ACCEPT *, IES
0131        IF (IES .NE. 1) GO TO 142
0133        LH = LENGTH/2
0134        DO 138 I = 1, LH
0135        T = ALOG10(TPYRAY(I))
```

```
0136      TPYRAY(I) = 10.*T
0137 138      CONTINUE
0138      CALL PLT(TPYRAY, XT, LH, RF, FILNAM)
      C
0139      CALL SAVDAT(TPYRAY, LH, IFILE)
      C
0140      LH = LENGTH/2
0141      DO 140 I = 1, LH
0142      TPYRAY(I) = 0.0
0143 140      CONTINUE
      C
0144 142      TYPE *, 'PLOT THE PHASE FACTOR ? (YES=1)'
0145      ACCEPT *, IYES
0146      IF (IYES .NE. 1) GO TO 150
0148      RTD = 180./3.14159265
0149      DO 144 I = 1, LH
0150      TPYRAY(I) = ATAN2(AIMAG(GXYRAY(I)), REAL(GXYRAY(I)))
0151      TPYRAY(I) = RTD*TPYRAY(I)
0152 144      CONTINUE
0153      CALL PLT(TPYRAY, XT, LH, RF, FILNAM)
      C
0154      CALL SAVDAT(TPYRAY, LH, IFILE)
      C
0155      LH = LENGTH/2
0156      DO 145 I = 1, LH
0157      TPYRAY(I) = 0.0
0158 145      CONTINUE
      C
0159 150      TYPE *, ' PLOT THE COHERENCE FUNCTION ? (YES=1)'
0160      ACCEPT *, IES
0161      IF ( IES .NE. 1) GO TO 200
0163      DO 155 I = 1, LH
0164      TPYRAY(I) = (SGXY(I) * SGXY(I))/(STIMIN(I) * HEOG(I))
0165 155      CONTINUE
0166      CALL PLT(TPYRAY, XT, LH, RF, FILNAM)
      C
0167      CALL SAVDAT(TPYRAY, LH, IFILE)
      C
0168 200      STOP
0169      END
```



# FORTTRAN IV

## Storage Map for Program Unit XYPSE

Local Variables, .PSECT \$DATA, Size = 045442 ( 9617. words)

Name	Type	Offset		Name	Type	Offset	Name	Type	Offset	
AMPL	R*4	000454	Eqv	CFAC	R*4	045332	DSKINC	I*2	000516	Eqv
H	R*4	045320		I	I*2	045362	IBLK	I*2	045350	
IERR	I*2	045300		IES	I*2	045364	INTRAT	R*4	000476	Eqv
ISTEP	I*2	045314		ITEMP	I*2	045354	IX	I*2	045352	
IYES	I*2	045360		K	I*2	045304	K1	I*2	045310	
K2	I*2	045312		LENGTH	I*2	045276	LH	I*2	045330	
LOPEN	I*2	045316		N	I*2	045302	NBLK	I*2	000530	Eqv
NDUMMY	I*2	045306		NPTS	I*2	045356	NWRDS	I*2	045346	
PERIOD	R*4	000460	Eqv	RF	R*4	045342	RTD	R*4	045372	
RTF	R*4	045336		SF	R*4	045324	T	R*4	045366	

Local and COMMON Arrays:

Name	Type	Section	Offset	-----Size-----	Dimensions
BUFR2	I*2	\$DATA	042126	003100 ( 800.)	(800)
COEF	R*4	\$DATA	042002	000104 ( 34.)	(17)
FLINAM	L*1	\$DATA	045226	000014 ( 6.)	(12)
HEOG	R*4	\$DATA	002002	010000 ( 2048.)	(1024)
ICHNUM	I*2	\$DATA	000542	000040 ( 16.)	(16)
IFILE	L*1	\$DATA	042106	000017 ( 8.)	(15)
IPOSN	I*2	\$DATA	000702	000040 ( 16.)	(16)
MAX	I*2	\$DATA	000742	000040 ( 16.)	(16)
SGXY	R*4	\$DATA	036002	004000 ( 1024.)	(512)
STIMIN	R*4	\$DATA	022002	010000 ( 2048.)	(1024)
TFYRAY	R*4	\$DATA	032002	004000 ( 1024.)	(512)
XT	R*4	\$DATA	012002	010000 ( 2048.)	(1024)
Z	I*2	\$DATA	000002	002000 ( 512.)	(512)

VIRTUAL Arrays, Total Size = 00070000 ( 14336. words)

Name	Type	Offset	-----Size-----	Dimensions
GXYRAY	C*8	00040000	00010000 ( 2048.)	(512)
XRAY	C*8	00000000	00020000 ( 4096.)	(1024)
YHEOG	R*4	00050000	00010000 ( 2048.)	(1024)
YRAY	C*8	00020000	00020000 ( 4096.)	(1024)
YSTIM	R*4	00060000	00010000 ( 2048.)	(1024)

Subroutines, Functions, Statement and Processor-Defined Functions:

Name	Type	Name	Type	Name	Type	Name	Type	Name	Type
AIMAG	R*4	ALOG10	R*4	ATAN2	R*4	CMPLX	C*8	CRSPEC	R*4
DISKIO	R*4	FFT	R*4	FLOAT	R*4	GETDAT	R*4	FLT	R*4
REAL	R*4	SAVDAT	R*4	WIN	R*4				

```
0001      SUBROUTINE GETDAT(FILNAM,LOPEN,NWRDS,IBLK,K,ISTEP,DSKINC,  
1  LENGTH,ITEMP,NPTS,HEOG,IPOSN,Z)  
      C  
0002      DIMENSION HEOG(1)  
0003      BYTE FILNAM(12)  
0004      INTEGER BUFR2(800), Z(512), IPOSN(16),DSKINC  
      C  
0005      IF (K .NE. 4) GO TO 5  
0007      SCL = 1000./4096.  
0008      GO TO 10  
      C  
0009      5  TYPE *, ' ENTER SCALE FACTOR FOR OUTPUT! '  
0010      ACCEPT *,SCL  
      C  
0011      10  IRMODE=3  
0012      IF (LOPEN .EQ. 1) IRMODE = -3  
0014      TYPE *, ' NOW READING FROM DISK '  
0015      20  CALL DISKIO(FILNAM,IRMODE,BUFR2,NWRDS,IBLK,NDUMMY,IERR)  
0016      IF (IERR .NE. 0) TYPE *, ' ERROR CODE ',IERR, ' DURING READ '  
      C  
0018      DO 40 L = 1,NPTS  
0019      HEOG(L+ITEMP) = BUFR2(IPOSN(K)+L*ISTEP)  
      C  
0020      40  CONTINUE  
      C  
0021      IBLK = IBLK + DSKINC  
0022      ITEMF = ITEMF + NPTS  
0023      IF (ITEMF .LT. LENGTH) GO TO 20  
      C  
0025      DO 45 I = 1, LENGTH  
0026      HEOG(I) = SCL*HEOG(I)  
0027      45  CONTINUE  
      C  
0028      50  RETURN  
0029      END
```

FORTRAN IV

Storage Map for Program Unit GETDAT

Local Variables, .FSECT \$DATA, Size = 003152 ( 821. words)

Name	Type	Offset	Name	Type	Offset	Name	Type	Offset
DSKINC	I*2 @	000014	I	I*2	003150	IRLK	I*2 @	000006
IERR	I*2	003144	IRMODE	I*2	003140	ISTEP	I*2 @	000012
ITEMP	I*2 @	000020	K	I*2 @	000010	L	I*2	003146
LENGTH	I*2 @	000016	LOPEN	I*2 @	000002	NDUMMY	I*2	003142
NPTS	I*2 @	000022	NWRDS	I*2 @	000004	SCL	R*4	003134

Local and COMMON Arrays:

Name	Type	Section	Offset	-----Size-----	Dimensions
HUFR2	I*2	\$DATA	000032	003100 ( 800.)	(800)
FILNAM	L*1	@ \$DATA	000000	000014 ( 6.)	(12)
HEOG	R*4	@ \$DATA	000024	000004 ( 2.)	(1)
IPOSN	I*2	@ \$DATA	000026	000040 ( 16.)	(16)
Z	I*2	@ \$DATA	000030	002000 ( 512.)	(512)

Subroutines, Functions, Statement and Processor-Defined Functions:

Name	Type	Name	Type	Name	Type	Name	Type	Name	Type
DISKIO	R*4								

```

0001      SUBROUTINE GETDAT(FILNAM,LOPEN,NWRDS,IBLK,K,ISTEP,DSKINC,
1  LENGTH,ITEMP,NPTS,HEOG,IPOSN,Z)
      C
0002      DIMENSION HEOG(1)
0003      BYTE FILNAM(12)
0004      INTEGER BUFR2(800), Z(512), IPOSN(16),DSKINC
      C
      C
0005      IRMODE=3
0006      IF (LOPEN .EQ. 1) IRMODE = -3
0008      TYPE *, '    NOW READING FROM DISK'
0009  20    CALL DISKIO(FILNAM,IRMODE,BUFR2,NWRDS,IBLK,NDUMMY,IERR)
0010      IF (IERR .NE. 0) TYPE *, ' ERROR CODE',IERR,' DURING READ'
      C
0012      DO 40 L = 1,NPTS
0013      HEOG(L+ITEMP) = BUFR2(IPOSN(K)+L*ISTEP)
      C
0014  40    CONTINUE
      C
0015      IBLK = IBLK + DSKINC
0016      ITEMp = ITEMp + NPTS
0017      IF (ITEMP .LT. LENGTH) GO TO 20
      C
0019  50    RETURN
0020      END

```

FORTTRAN IV                      Storage Map for Program Unit GETDAT

Local Variables, .PSECT \$DATA, Size = 003142 ( 817. words)

Name	Type	Offset	Name	Type	Offset	Name	Type	Offset
DSKINC	I*2 @	000014	IBLK	I*2 @	000006	IERR	I*2	003136
IRMODE	I*2	003132	ISTEP	I*2 @	000012	ITEMP	I*2 @	000020
K	I*2 @	000010	L	I*2	003140	LENGTH	I*2 @	000016
LOPEN	I*2 @	000002	NDUMMY	I*2	003134	NPTS	I*2 @	000022
NWRDS	I*2 @	000004						

Local and COMMON Arrays:

Name	Type	Section	Offset	-----Size-----	Dimensions
BUFR2	I*2	\$DATA	000032	003100 ( 800.)	(800)
FILNAM	L*1	@ \$DATA	000000	000014 ( 6.)	(12)
HEOG	R*4	@ \$DATA	000024	000004 ( 2.)	(1)
IPSN	I*2	@ \$DATA	000026	000040 ( 16.)	(16)
Z	I*2	@ \$DATA	000030	002000 ( 512.)	(512)

Subroutines, Functions, Statement and Processor-Defined Functions:

Name	Type	Name	Type	Name	Type	Name	Type	Name	Type
DISKIO	R*4								

```
0001      SUBROUTINE WIN( STIMIN, YSTIM, HEOG, YHEOG, COEF, LENGTH, H)
      C
0002      DIMENSION HEOG(1), STIMIN(1), COEF(1)
0003      VIRTUAL YHEOG(1024), YSTIM(1024)
0004      REAL YHEOG, YSTIM
      C
0005      L = LENGTH
      C
      C      COMPUTE THE MEAN OF THE DATA
      C
0006      XSUM = 0.0
0007      YSUM = 0.0
0008      FTL = FLOAT(LENGTH)
0009      DO 10 I = 1, LENGTH
0010      XSUM = XSUM + STIMIN(I)
0011      YSUM = YSUM + HEOG(I)
0012 10      CONTINUE
0013      XMEAN = XSUM/FTL
0014      YMEAN = YSUM/FTL
0015      DO 20 I = 1, LENGTH
0016      STIMIN(I) = STIMIN(I) - XMEAN
0017      HEOG(I) = HEOG(I) - YMEAN
0018 20      CONTINUE
      C
0019      TYPE *, ' FILTER DATA : 15 POINT FIR FILTER '
      C
0020      NCO = 15
0021      DO 24 I = 2, L+NCO
0022      XSM = 0.0
0023      YSM = 0.0
0024      DO 22 J = 1, NCO
0025      IF (J .GE. I) GO TO 22
0027      IF (I-J .GT. L) GO TO 22
0029      HX = COEF(J) * STIMIN(I-J)
0030      XSM = XSM + HX
0031      HY = COEF(J) * HEOG(I-J)
0032      YSM = YSM + HY
0033 22      CONTINUE
0034      YSTIM(I-1) = XSM
0035      YHEOG(I-1) = YSM
0036 24      CONTINUE
0037      J2 = 14
0038      DO 26 J = 15, L+J2
0039      YSTIM(J-J2) = YSTIM(J)
0040      YHEOG(J-J2) = YHEOG(J)
0041 26      CONTINUE
      C
      C      TYPE DIFFERENTIATOR : 6TH ORDER CENTRAL DIFFERENCE '
      C
0042      DO 30 I = 4, L-3
0043      HEOG(I) = (((YHEOG(I+3)-YHEOG(I-3)))+(9.*(YHEOG(I-2)-YHEOG(I+2))))
1 + (45.*(YHEOG(I+1)-YHEOG(I-1))))/(H*60.)
0044 30      CONTINUE
0045      HEOG(1) = HEOG(4)
```

```

0046      HEOG(2) = HEOG(4)
0047      HEOG(3) = HEOG(4)
0048      HEOG(L) = HEOG(L-3)
0049      HEOG(L-1) = HEOG(L-3)
0050      HEOG(L-2) = HEOG(L-3)
      C
      C      FILTER DATA : 15 POINT FIR FILTER
      C
0051      NCO = 15
0052      DO 44 I = 2, LENGTH+NCO
0053      BYSUM = 0.0
0054      DO 42 J = 1, NCO
0055      IF (J .GE. I) GO TO 42
0057      IF (I-J .GT. LENGTH) GO TO 42
0059      HYF = COEF(J) * HEOG(I-J)
0060      BYSUM = BYSUM + HYF
0061 42      CONTINUE
0062      YHEOG(I-1) = BYSUM
0063 44      CONTINUE
0064      DO 46 M = 15, L+J2
0065      YHEOG(M-J2) = YHEOG(M)
0066 46      CONTINUE
      C
0067      DO 48 I = 18, LENGTH
0068      STIMIN(I-17) = STIMIN(I)
0069 48      CONTINUE
0070      DO 49 I = 1, 17
0071      STIMIN(L+I) = STIMIN(L)/FLOAT(I)
0072 49      CONTINUE
      C
      C      HANNING WINDOW (COSINE TAPER)
      C
0073      TPI = 31.4159265
0074      ITPCL = LENGTH/10
0075      NPCL = (LENGTH*9)/10
0076      DO 50 I = 1, ITPCL
0077      STIMIN(I) = STIMIN(I)*(.5 - .5*COS((TPI*(I-1))/(LENGTH-1)))
0078      HEOG(I) = YHEOG(I)*(.5 - .5*COS((TPI*(I-1))/(LENGTH-1)))
0079 50      CONTINUE
      C
0080      DO 60 I = NPCL, LENGTH
0081      STIMIN(I) = STIMIN(I)*(.5-.5*COS((TPI*I)/LENGTH))
0082      HEOG(I) = YHEOG(I)*(.5-.5*COS((TPI*I)/LENGTH))
0083 60      CONTINUE
      C
0084 70      RETURN
0085      END

```

FORTTRAN IV                      Storage Map for Program Unit WIN

Local Variables, .PSECT \$DATA, Size = 000220 (    72. words)

Name	Type	Offset	Name	Type	Offset	Name	Type	Offset
BYSUM	R*4	000126	FTL	R*4	000062	H	R*4 @	000014
HX	R*4	000114	HY	R*4	000120	HYF	R*4	000132
I	I*2	000066	ITPCL	I*2	000144	J	I*2	000112
J2	I*2	000124	L	I*2	000050	LENGTH	I*2 @	000012
M	I*2	000136	NCO	I*2	000100	NPCL	I*2	000146
TPI	R*4	000140	XMEAN	R*4	000070	XSM	R*4	000102
XSUM	R*4	000052	YMEAN	R*4	000074	YSM	R*4	000106
YSUM	R*4	000056						

Local and COMMON Arrays:

Name	Type	Section	Offset	-----Size-----	Dimensions
COEF	R*4	@ \$DATA	000010	000004 (    2.)	(1)
HEOG	R*4	@ \$DATA	000004	000004 (    2.)	(1)
STIMIN	R*4	@ \$DATA	000000	000004 (    2.)	(1)

VIRTUAL Arrays, Total Size = 00000000 (        0. words)

Name	Type	Offset	-----Size-----	Dimensions
YHEOG	R*4	@    000006	00010000 (    2048.)	(1024)
YSTIM	R*4	@    000002	00010000 (    2048.)	(1024)

Subroutines, Functions, Statement and Processor-Defined Functions:

Name	Type	Name	Type	Name	Type	Name	Type	Name	Type
COS	R*4	FLOAT	R*4						



```
0001      SUBROUTINE FFT(X, N, INV)
0002      VIRTUAL X(1024)
0003      COMPLEX X, U, W, T, CMPLX
      C
      C      X = COMPLEX ARRAY OF SIZE N--ON INPUT X CONTAINS
      C      THE SEQUENCE TO BE TRANSFORMED
      C      ON OUTPUT X CONTAINS THE DFT OF THE INPUT
      C      N = SIZE OF FFT TO BE COMPUTED--N=2**M FOR 1.LE.M.LE.15
      C      INV = PARAMETER TO DETERMINE WHETHER TO DO A DIRECT TRANSFORM (IN
      C      OR AN INVERSE TRANSFORM (INV=1)
      C
0004      M = ALOG(FLOAT(N))/ALOG(2.) + .1
0005      NV2 = N/2
0006      NM1 = N - 1
0007      J = 1
0008      DO 40 I=1,NM1
0009      IF (I.GE.J) GO TO 10
0011      T = X(J)
0012      X(J) = X(I)
0013      X(I) = T
0014      10    K = NV2
0015      20    IF (K.GE.J) GO TO 30
0017      J = J - K
0018      K = K/2
0019      GO TO 20
0020      30    J = J + K
0021      40    CONTINUE
0022      PI = 4.*ATAN(1.0)
0023      DO 70 L=1,M
0024      LE = 2**L
0025      LE1 = LE/2
0026      U = (1.0,0.0)
0027      W = CMPLX(COS(PI/FLOAT(LE1)), -SIN(PI/FLOAT(LE1)))
0028      IF (INV.NE.0) W = CONJG(W)
0030      DO 60 J=1,LE1
0031      DO 50 I=J,N,LE
0032      IP = I + LE1
0033      T = X(IP)*U
0034      X(IP) = X(I) - T
0035      X(I) = X(I) + T
0036      50    CONTINUE
0037      U = U*W
0038      60    CONTINUE
0039      70    CONTINUE
0040      IF (INV.EQ.0) RETURN
0042      DO 80 I=1,N
0043      X(I) = X(I)/CMPLX(FLOAT(N),0.)
0044      80    CONTINUE
0045      RETURN
0046      END
```

FORTRAN IV            Storage Map for Program Unit FFT

Local Variables, .PSECT \$DATA, Size = 000130 (    44. words)

Name	Type	Offset	Name	Type	Offset	Name	Type	Offset
I	I*2	000046	INV	I*2 @	000004	IF	I*2	000064
J	I*2	000044	K	I*2	000050	L	I*2	000056
LE	I*2	000060	LE1	I*2	000062	M	I*2	000036
N	I*2 @	000002	NM1	I*2	000042	NV2	I*2	000040
PI	R*4	000052	T	C*8	000026	U	C*8	000006
W	C*8	000016						

VIRTUAL Arrays, Total Size = 00000000 (            0. words)

Name	Type	Offset	-----Size-----	Dimensions
XRAY	C*8	@ 000000	00020000 ( 4096.)	(1024)

Subroutines, Functions, Statement and Processor-Defined Functions:

Name	Type	Name	Type	Name	Type	Name	Type	Name	Type
ALOG	R*4	ATAN	R*4	CMPLX	C*8	CONJG	C*8	COS	R*4
FLOAT	R*4	SIN	R*4						

```

0001      SUBROUTINE CRSPEC(XRAY,YRAY,TPYRAY,STIMIN,HEOG,GXYRAY,
1 SGXY,YSTIM,YHEOG,LH,CFAC)
      C
0002      DIMENSION HEOG(1), STIMIN(1), TPYRAY(1), SGXY(1)
      C
0003      VIRTUAL XRAY(1024), YRAY(1024), GXYRAY(512)
0004      VIRTUAL YSTIM(1024), YHEOG(1024)
0005      COMPLEX XRAY, YRAY, GXYRAY
      C
0006      DO 10 I = 1, LH
0007      GXYRAY(I) = (CONJG(XRAY(I)))*(YRAY(I))
0008      STIMIN(I) = REAL(GXYRAY(I))
0009      HEOG(I) = AIMAG(GXYRAY(I))
0010      TPYRAY(I) = CFAC*(CABS(GXYRAY(I)))
0011      10 CONTINUE
      C
      C      HANNING SMOOTHING
      C
0012      YSTIM(1) = 0.5*(STIMIN(1) + STIMIN(2))
0013      YHEOG(1) = 0.5*(HEOG(1) + HEOG(2))
0014      DO 20 I = 2, LH-1
0015      YSTIM(I) = 0.25*(STIMIN(I-1) + STIMIN(I+1)) + 0.5*STIMIN(I)
0016      YHEOG(I) = 0.25*(HEOG(I-1) + HEOG(I+1)) + 0.5*HEOG(I)
0017      20 CONTINUE
0018      YSTIM(LH) = 0.5*(STIMIN(LH-1) + STIMIN(LH))
0019      YHEOG(LH) = 0.5*(HEOG(LH-1) + HEOG(LH))
      C
0020      DO 30 I = 1, LH
0021      GXYRAY(I) = CMPLX( YSTIM(I), YHEOG(I))
0022      30 CONTINUE
      C
0023      DO 40 I = 1, LH
0024      STIMIN(I) = CFAC*((CABS(XRAY(I)))*2.)
0025      HEOG(I) = CFAC*((CABS(YRAY(I)))*2.)
0026      40 CONTINUE
      C
      C      HANNING SMOOTHING OF AUTO SPECTRA
0027      SGXY(1) = 0.5*(TPYRAY(1) + TPYRAY(2))
0028      SGXY(LH) = 0.5*(TPYRAY(LH-1) + TPYRAY(LH))
      C
0029      YSTIM(1) = 0.5*(STIMIN(1) + STIMIN(2))
0030      YSTIM(LH) = 0.5*(STIMIN(LH-1) + STIMIN(LH))
      C
0031      YHEOG(1) = 0.5*(HEOG(1) + HEOG(2))
0032      YHEOG(LH) = 0.5*(HEOG(LH-1) + HEOG(LH))
      C
0033      DO 50 I = 2, LH-1
0034      SGXY(I) = 0.25*(TPYRAY(I-1) + TPYRAY(I+1)) + 0.5*TPYRAY(I)
0035      YSTIM(I) = 0.25*(STIMIN(I-1) + STIMIN(I+1)) + 0.5*STIMIN(I)
0036      YHEOG(I) = 0.25*(HEOG(I-1) + HEOG(I+1)) + 0.5*HEOG(I)
0037      50 CONTINUE
      C
0038      DO 60 I = 1, LH
0039      TPYRAY(I) = SGXY(I)

```

```
0040      STIMIN(I) = YSTIM(I)
0041      HEOG(I) = YHEOG(I)
0042 60    CONTINUE
      C
0043      RETURN
0044      END
```

# FORTTRAN IV            Storage Map for Program Unit CRSPEC

Local Variables, .PSECT \$DATA, Size = 000226 (    75. words)

Name	Type	Offset	Name	Type	Offset	Name	Type	Offset
CFAC	R*4	@ 000024	HL	R*4	000112	I	I*2	000110
LH	I*2	@ 000022						

Local and COMMON Arrays:

Name	Type	Section	Offset	-----Size-----	Dimensions
HEUG	R*4	@ \$DATA	000010	000004 (    2.)	(1)
SGXY	R*4	@ \$DATA	000014	000004 (    2.)	(1)
STIMIN	R*4	@ \$DATA	000006	000004 (    2.)	(1)
TPYRAY	R*4	@ \$DATA	000004	000004 (    2.)	(1)

VIRTUAL Arrays, Total Size = 00000000 (    0. words)

Name	Type	Offset	-----Size-----	Dimensions
GXYRAY	C*8	@ 000012	00010000 (   2048.)	(512)
XRAY	C*8	@ 000000	00020000 (   4096.)	(1024)
YHEOG	R*4	@ 000020	00010000 (   2048.)	(1024)
YRAY	C*8	@ 000002	00020000 (   4096.)	(1024)
YSTIM	R*4	@ 000016	00010000 (   2048.)	(1024)

Subroutines, Functions, Statement and Processor-Defined Functions:

Name	Type	Name	Type	Name	Type	Name	Type	Name	Type
AIMAG	R*4	CABS	R*4	CMPLX	C*8	CONJG	C*8	REAL	R*4

```
0001      SUBROUTINE FLT(Y,XT,LGTH,XSF,FILNAM)
0002      DIMENSION Y(1), XT(1)
0003      BYTE FILNAM(12)
0004      LTEMP = LGTH
C
0005      TYPE *, '      SELECT THE TYPE OF GRAPH!'
0006      TYPE *, ' |-----| '
0007      TYPE *, ' | 1 ..TIME FUNCTION OF INPUT | '
0008      TYPE *, ' | 2 ..TIME FUNCTION OF RESPONSE | '
0009      TYPE *, ' | 3 ..CROSS SPECTRA | '
0010      TYPE *, ' | 4 ..AUTO SPECTRA OF INPUT | '
0011      TYPE *, ' | 5 ..AUTO SPECTRA OF RESPONSE | '
0012      TYPE *, ' | 6 ..TRANSFER FUNTION : GAIN | '
0013      TYPE *, ' | 7 ..TRANSFER FUNCTION IN DBs | '
0014      TYPE *, ' | 8 ..PHASE FUNTION IN DEGREES | '
0015      TYPE *, ' | 9 ..COHERENCE FUNTION | '
0016      TYPE *, ' |-----| '
0017      TYPE *, '      ENTER THE CORRESPONDING NUMBER:'
0018      ACCEPT *, NUM
C
C
0019      3 TYPE *, ' SET YMIN = ?'
0020      ACCEPT *, YMIN
0021      TYPE *, ' YMIN= ', YMIN
0022      TYPE *, ' SET YMAX = ?'
0023      ACCEPT *, YMAX
0024      TYPE *, ' DO YOU WANT TO EXPAND THE FREQUENCY SCALE? (YES=1)'
0025      ACCEPT *, ISCAL
0026      IF (ISCAL .NE. 1) GO TO 6
0028      TYPE *, ' TYPE IN DESIRED SCALE FACTOR. '
0029      ACCEPT *, IXSCF
0030      LGTH = LGTH/IXSCF
C
0031      6 DO 10 J = 1, LGTH
0032      XT(J) = XSF*FLOAT(J)
0033      10 CONTINUE
C
0034      XLGT = XSF*FLOAT(LGTH)
C
0035      ILFT = 600
0036      IRIT = 3500
0037      IBOT = 1000
0038      ITOP = 2500
0039      XMIN = 0.
0040      XMAX = XLGT
C
0041      CALL TSXCHK
0042      CALL GRINIT(4014,4631,1)
0043      CALL CHRISZ(3)
0044      CALL ERASE
0045      CALL GRID(10,10,ILFT,IRIT,IBOT,ITOP,97)
C
0046      CALL ANOTAT(10,10,ILFT,IRIT,IBOT,ITOP,XMIN,XMAX,YMIN,YMAX)
C
```

```
0047      CALL XYPLOT(XT,Y,LGTH,ILFT,IRIT,IBOT,ITOP,XMIN,XMAX,  
1 YMIN,YMAX,1,0)  
      C  
0048      CALL CHR Siz(2)  
      C  
0049      CALL MPLOT(ILFT-500, ITOP+500, -1)  
0050      TYPE 14, FILNAM  
0051      14  FORMAT ('+FILENAME:',14A1)  
      C  
0052      GO TO (20,30,40,50,60,70,80,90,100),NUM  
      C  
0053      20  CALL MPLOT(ILFT+500, ITOP+200, -1)  
0054      TYPE 22  
0055      22  FORMAT ('+INPUT STIMULUS VS TIME '  
0056      CALL MPLOT(ILFT-500, IBOT+750, -1)  
0057      TYPE 24  
0058      24  FORMAT ('+VOLTS')  
0059      CALL MPLOT(ILFT+800, IBOT-300, -1)  
0060      TYPE 26  
0061      26  FORMAT ('+TIME IN SECONDS '  
0062      CALL MPLOT( 0, IBOT-600, -1)  
0063      GO TO 150  
      C  
0064      30  CALL MPLOT(ILFT+500, ITOP+200, -1)  
0065      TYPE 32  
0066      32  FORMAT ('+HORIZONTAL EYE MOVEMENTS VS TIME '  
0067      CALL MPLOT(ILFT-500, IBOT+750, -1)  
0068      TYPE 34  
0069      34  FORMAT ('+VOLTS')  
0070      CALL MPLOT(ILFT+800, IBOT-300, -1)  
0071      TYPE 36  
0072      36  FORMAT ('+TIME IN SECONDS '  
0073      CALL MPLOT( 0, IBOT-600, -1)  
0074      GO TO 150  
      C  
0075      40  CALL MPLOT(ILFT+500, ITOP+200, -1)  
0076      TYPE 42  
0077      42  FORMAT ('+CROSS-SPECTRA '  
0078      CALL MPLOT(ILFT-500, IBOT+750, -1)  
0079      TYPE 44  
0080      44  FORMAT ('+VSQ/HZ')  
0081      CALL MPLOT(ILFT+800, IBOT-300, -1)  
0082      TYPE 46  
0083      46  FORMAT ('+FREQUENCY IN HERTZ '  
0084      CALL MPLOT( 0, IBOT-600, -1)  
0085      GO TO 150  
      C  
0086      50  CALL MPLOT(ILFT+500, ITOP+200, -1)  
0087      TYPE 52  
0088      52  FORMAT ('+POWER SPECTRUM OF INPUT STIMULUS '  
0089      CALL MPLOT(ILFT-500, IBOT+750, -1)  
0090      TYPE 54  
0091      54  FORMAT ('+VSQ/HZ')  
0092      CALL MPLOT(ILFT+800, IBOT-300, -1)
```

```
0093      TYPE 56
0094 56    FORMAT ('+FREQUENCY IN HERTZ')
        C
0095      CALL MPLLOT( 0, IBOT-600, -1)
0096      GO TO 150
        C
0097 60    CALL MPLLOT(ILFT+500, ITOP+200, -1)
0098      TYPE 62
0099 62    FORMAT ('+POWER SPECTRUM OF OCULAR RESPONSE')
0100      CALL MPLLOT(ILFT-500, IBOT+750, -1)
0101      TYPE 64
0102 64    FORMAT ('+VSQ/HZ')
0103      CALL MPLLOT(ILFT+800, IBOT-300, -1)
0104      TYPE 66
0105 66    FORMAT ('+FREQUENCY IN HERTZ')
0106      CALL MPLLOT( 0, IBOT-600, -1)
0107      GO TO 150
        C
0108 70    CALL MPLLOT(ILFT+500, ITOP+200, -1)
0109      TYPE 72
0110 72    FORMAT ('+TRANSFER FUNCTION GAIN')
0111      CALL MPLLOT(ILFT-500, IBOT+750, -1)
0112      TYPE 74
0113 74    FORMAT ('+GAIN')
0114      CALL MPLLOT(ILFT+800, IBOT-300, -1)
0115      TYPE 76
0116 76    FORMAT ('+FREQUENCY IN HERTZ')
0117      CALL MPLLOT( 0, IBOT-600, -1)
0118      GO TO 150
        C
0119 80    CALL MPLLOT(ILFT+500, ITOP+200, -1)
0120      TYPE 82
0121 82    FORMAT ('+TRANSFER FUNCTION IN DBs')
0122      CALL MPLLOT(ILFT-500, IBOT+750, -1)
0123      TYPE 84
0124 84    FORMAT ('+DBs')
0125      CALL MPLLOT(ILFT+800, IBOT-300, -1)
0126      TYPE 86
0127 86    FORMAT ('+FREQUENCY IN HERTZ')
0128      CALL MPLLOT( 0, IBOT-600, -1)
0129      GO TO 150
        C
0130 90    CALL MPLLOT(ILFT+500, ITOP+200, -1)
0131      TYPE 92
0132 92    FORMAT ('+PHASE FACTOR IN DEGREES ')
0133      CALL MPLLOT(ILFT-500, IBOT+750, -1)
0134      TYPE 94
0135 94    FORMAT ('+DEGs')
0136      CALL MPLLOT(ILFT+800, IBOT-300, -1)
0137      TYPE 96
0138 96    FORMAT ('+FREQUENCY IN HERTZ')
0139      CALL MPLLOT( 0, IBOT-600, -1)
0140      GO TO 150
        C
```



```
0141 100  CALL MPLOT(ILFT+500, ITOP+200, -1)
0142      TYPE 102
0143 102  FORMAT ('+COHERENCE FUNCTION ')
0144      CALL MPLOT(ILFT+800, IBOT-300, -1)
0145      TYPE 106
0146 106  FORMAT ('+FREQUENCY IN HERTZ')
0147      CALL MPLOT( 0, IBOT-600, -1)
      C
0148 150  CALL CHRISZ(3)
0149      TYPE *, ' DO YOU WANT A HARD COPY? (YES=1)'
0150      ACCEPT *, HCPY
0151      IF (HCPY .NE. 1) GO TO 160
      C
0153      CALL COPY(0)
      C
0154 160  TYPE *, ' DO YOU WANT ANOTHER PLOT? (YES=1)'
0155      ACCEPT *, IYS
0156      IF (IYS .NE. 1) GO TO 200
0158      TYPE 165,LTEMP
0159 165  FORMAT (' LTEMP = ',I4)
0160      LGTH = LTEMP
0161 170  GO TO 3
      C
0162 200  RETURN
0163      END
```

# FORTRAN IV

## Storage Map for Program Unit FLT

Local Variables, .FSECT \$DATA, Size = 000266 ( 91. words)

Name	Type	Offset	Name	Type	Offset	Name	Type	Offset
HCFY	R*4	000062	IBOT	I*2	000046	ILFT	I*2	000042
IRIT	I*2	000044	ISCAL	I*2	000030	ITOP	I*2	000050
IXSCF	I*2	000032	IYS	I*2	000066	J	I*2	000034
LGTH	I*2 @	000004	LTEMP	I*2	000014	NUM	I*2	000016
XLGT	R*4	000036	XMAX	R*4	000056	XMIN	R*4	000052
XSF	R*4 @	000006	YMAX	R*4	000024	YMIN	R*4	000020

### Local and COMMON Arrays:

Name	Type	Section	Offset	-----Size-----	Dimensions
FILNAM	L*1	@ \$DATA	000010	000014 ( 6.)	(12)
XT	R*4	@ \$DATA	000002	000004 ( 2.)	(1)
Y	R*4	@ \$DATA	000000	000004 ( 2.)	(1)

### Subroutines, Functions, Statement and Processor-Defined Functions:

Name	Type	Name	Type	Name	Type	Name	Type	Name	Type
ANOTAT	R*4	CHRSIZ	R*4	COPY	R*4	ERASE	R*4	FLOAT	R*4
GRID	R*4	GRINIT	R*4	MFLOT	I*2	TSXCHK	R*4	XYPLOT	R*4

```
0001      SUBROUTINE SAVDAT(X, LT, IFILE)
0002      DIMENSION X(1)
0003      LOGICAL*1 IFILE(15)
0004      C
0004      5      TYPE *, ' SAVE DATA ON DISK? (YES=1)'
0005      ACCEPT *, ISK
0006      IF (ISK .NE. 1) GO TO 100
0007      C
0008      10     TYPE 20
0009      20     FORMAT ('+ENTER NAME OF DATA FILE: ', $)
0010      ACCEPT 30, IFILE
0011      30     FORMAT(15A1)
0012      IFILE(15) = 0
0013      C
0013      OPEN (UNIT=2, NAME=IFILE, ERR=40)
0014      WRITE (2,*) LT, (X(I), I=1, LT)
0015      TYPE *, '+DATA SAVED ON DISKETTE '
0016      CLOSE (UNIT=2)
0017      GO TO 100
0018      C
0018      40     TYPE 50
0019      50     FORMAT ('+ERROR: DATA WAS NOT SAVED! TRY AGAIN? (YES=1)')
0020      ACCEPT *, IS
0021      IF (IS .NE. 1) GO TO 100
0022      GO TO 10
0023      10     RETURN
0024      100    RETURN
0025      END
```

FORTRAN IV          Storage Map for Program Unit SAVDAT

Local Variables, .FSECT \$DATA, Size = 000016 (      7. words)

Name	Type	Offset	Name	Type	Offset	Name	Type	Offset
I	I*2	000012	IS	I*2	000014	ISK	I*2	000010
LT	I*2 @	000002						

Local and COMMON Arrays:

Name	Type	Section	Offset	-----Size-----	Dimensions
IFILE	L*1	@ \$DATA	000004	000017 (      8.)	(15)
X	R*4	@ \$DATA	000000	000004 (      2.)	(1)

```
R LINK
XYPSE,XYPSE = XYPSE,SY:LABLIB,SY:FFU/P:300.//
GETDAT/0:1
WIN/0:1
FFT/0:1
CRSPEC/0:1
PLT/0:1
SAVDAT/0:1
//
```

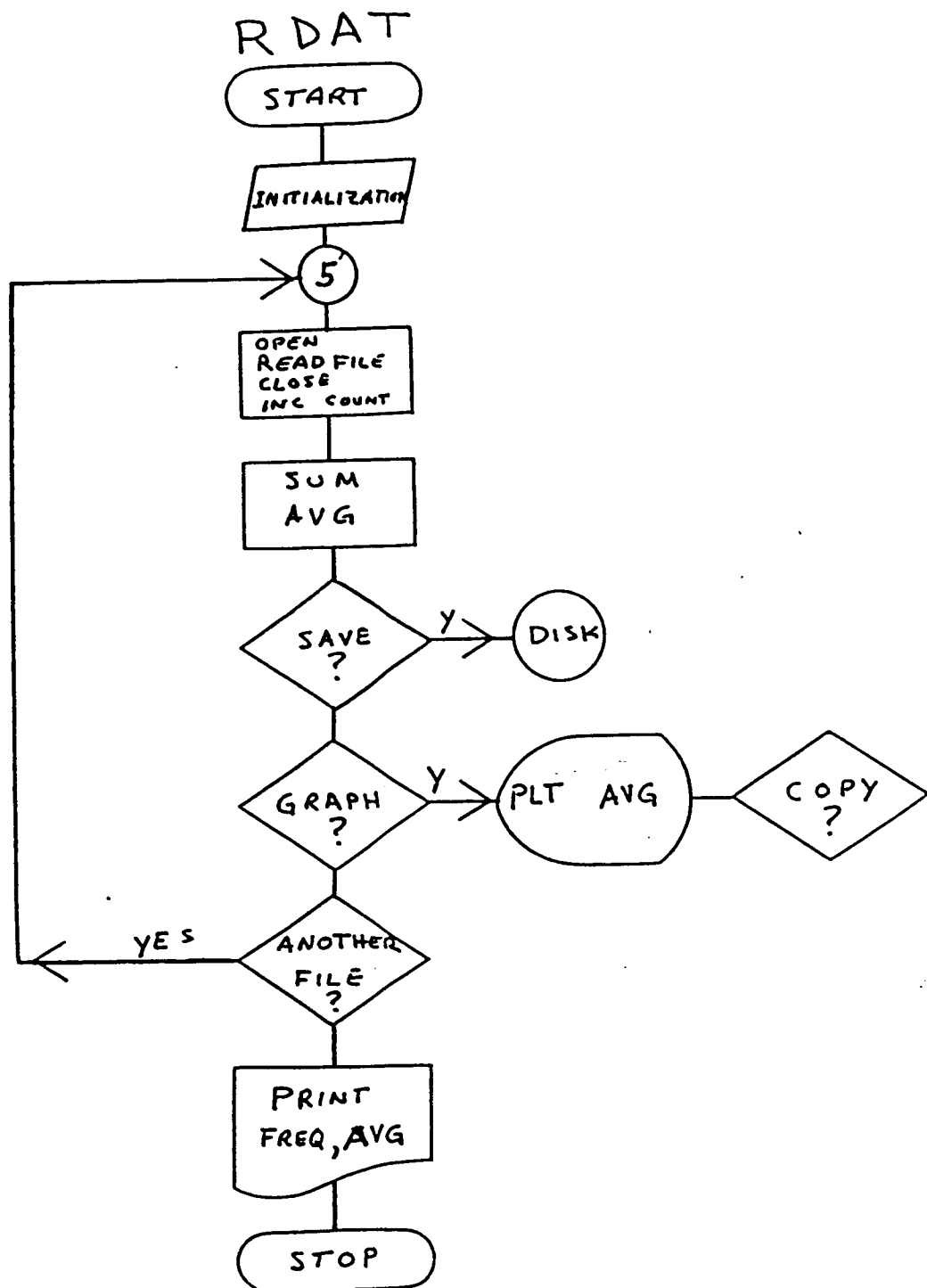
APPENDIX B

FLOW DIAGRAM AND PROGRAM LISTING

RDAT

AVERAGING PROGRAM

# AVERAGING PROGRAM



```
0001      PROGRAM RDAT
0002      DIMENSION RST(512), SUM(512), FREQ(6), TR(6), XT(512)
0003      LOGICAL*1 IFILE(15)
0004      BYTE FILNAM(12)

      C
0005      TYPE *, ' ENTER NUMBER OF RECORDS PREVIOUSLY AVERAGED!'
0006      ACCEPT *, RNOF

      C
0007      FREQ(1) = 0.1
0008      FREQ(2) = 0.15
0009      FREQ(3) = 0.25
0010      FREQ(4) = 0.35
0011      FREQ(5) = 0.55
0012      FREQ(6) = 0.95

      C
0013      LTR = 6
0014      RF = 10./1024.
0015      FILNAM(1) = 'A'
0016      FILNAM(2) = 'V'
0017      FILNAM(3) = 'G'
0018      FILNAM(4) = 'E'
0019      FILNAM(5) = 'D'
0020      FILNAM(6) = 'R'
0021      FILNAM(7) = 'E'
0022      FILNAM(8) = 'S'
0023      FILNAM(9) = 'U'
0024      FILNAM(10) = 'L'
0025      FILNAM(11) = 'T'
0026      FILNAM(12) = 'S'

      C
0027      DO 2 I = 1, 512
0028      SUM(I) = 0.0
0029      2 CONTINUE

      C
0030      5 DO 10 I = 1, 7
0031      10 IFILE(K) = 0
0032      TYPE 20
0033      20 FORMAT ( ' ENTER FILENAME'// ' IFILE? ', $)
0034      ACCEPT 30, IFILE
0035      30 FORMAT (15A1)
0036      IFILE(15) = 0

      C
0037      OPEN (UNIT=2, NAME=IFILE, TYPE='OLD', ERR=50)
0038      READ (2,*) LH, (RST(I), I=1, LH)
0039      TYPE *, ' DATA WAS READ FROM DISK FILE '
0040      CLOSE (UNIT=2)

      C
0041      DO 40 I = 1, LH
0042      SUM(I) = RNOF*SUM(I)
0043      40 CONTINUE
0044      TYPE *, ' WAS 1ST FILE PREVIOUSLY AVGD & STORED? (YES=1)'
0045      ACCEPT *, JES
0046      IF (JES .NE. 1) GO TO 47
0048      DO 45 I = 1, LH
```



```
0049      SUM(I) = RST(I)
0050 45     CONTINUE
0051      GO TO 5
      C
0052 47     RNOF = RNOF + 1.
0053      GO TO 60
      C
0054 50     TYPE 55
0055 55     FORMAT (' ERROR IN LOCATING FILE; TRY AGAIN? (YES=1)')
0056      ACCEPT *,IES
0057      IF (IES .NE.1) GO TO 100
0059      GO TO 5
      C
0060 60     DO 65 I = 1, LH
0061      SUM(I) = (SUM(I) + RST(I))/RNOF
0062 65     CONTINUE
      C
0063      CALL SAVDAT(SUM, LH, IFILE)
      C
0064      TYPE *, ' DO YOU WANT A PLOT OF THE AVERAGED RESULTS? (YES=1)'
0065      ACCEPT *,IYES
0066      IF (IYES .NE. 1) GO TO 67
0068      CALL PLT(SUM, XT, LH, RF, FILNAM)
      C
0069 67     TYPE *, ' READ IN ANOTHER DATA FILE? (YES=1)'
0070      ACCEPT *, ISH
0071      IF (ISH .EQ. 1) GO TO 5
      C
0073 68     TR(1) = SUM(11)
0074      TR(2) = SUM(16)
0075      TR(3) = SUM(27)
0076      TR(4) = SUM(37)
0077      TR(5) = SUM(57)
0078      TR(6) = SUM(98)
      C
0079      PRINT 61,LH,RNOF
0080 61     FORMAT (' LH= ',I4,5X,' NO. FILES AVGD = ',F5.1)
0081      PRINT 70, FREQ(1), SUM(11)
0082      PRINT 70, FREQ(2), SUM(16)
0083      PRINT 70, FREQ(3), SUM(27)
0084      PRINT 70, FREQ(4), SUM(37)
0085      PRINT 70, FREQ(5), SUM(57)
0086      PRINT 70, FREQ(6), SUM(98)
0087 70     FORMAT (' FREQ = ',F6.4,5X,' AVG RESULTS = ',F10.5)
      C
0088 100    STOP
0089      END
```

FORTTRAN IV

Storage Map for Program Unit RDATA

Local Variables, .PSECT \$DATA, Size = 014162 ( 3129. words)

Name	Type	Offset	Name	Type	Offset	Name	Type	Offset
I	I*2	014144	IES	I*2	014154	ISH	I*2	014160
IYES	I*2	014156	JES	I*2	014152	K	I*2	014146
LH	I*2	014150	LTR	I*2	014136	RF	R*4	014140
RNOF	R*4	014132						

Local and COMMON Arrays:

Name	Type	Section	Offset	-----Size-----	Dimensions
FILNAM	L*1	\$DATA	014077	000014 ( 6.)	(12)
FREQ	R*4	\$DATA	010000	000030 ( 12.)	(6)
IFILE	L*1	\$DATA	014060	000017 ( 8.)	(15)
RST	R*4	\$DATA	000000	004000 ( 1024.)	(512)
SUM	R*4	\$DATA	004000	004000 ( 1024.)	(512)
TR	R*4	\$DATA	010030	000030 ( 12.)	(6)
XT	R*4	\$DATA	010060	004000 ( 1024.)	(512)

Subroutines, Functions, Statement and Processor-Defined Functions:

Name	Type	Name	Type	Name	Type	Name	Type	Name	Type
FLT	R*4	SAVDAT	R*4						

```
0001      SUBROUTINE SAVDAT(X, LT, IFILE)
0002      DIMENSION X(1)
0003      LOGICAL*1 IFILE(15)

      C
0004      5      TYPE *, ' SAVE DATA ON DISK? (YES=1) '
0005      ACCEPT *, ISK
0006      IF (ISK .NE. 1) GO TO 100

      C
0008      10     TYPE 20
0009      20     FORMAT ('+ENTER NAME OF DATA FILE: ', $)
0010      ACCEPT 30, IFILE
0011      30     FORMAT(15A1)
0012      IFILE(15) = 0

      C
0013      OPEN (UNIT=2, NAME=IFILE, ERR=40)
0014      WRITE (2,*) LT, (X(I), I=1, LT)
0015      TYPE *, '+DATA SAVED ON DISKETTE '
0016      CLOSE (UNIT=2)
0017      GO TO 100

      C
0018      40     TYPE 50
0019      50     FORMAT ('+ERROR: DATA WAS NOT SAVED! TRY AGAIN? (YES=1) ')
0020      ACCEPT *, IS
0021      IF (IS .NE. 1) GO TO 100
0023      GO TO 10
0024      100    RETURN
0025      END
```

FORTRAN IV      Storage Map for Program Unit SAVDAT

Local Variables, .PSECT \$DATA, Size = 000016 (    7. words)

Name	Type	Offset	Name	Type	Offset	Name	Type	Offset
I	I*2	000012	IS	I*2	000014	ISK	I*2	000010
LT	I*2 @	000002						

Local and COMMON Arrays:

Name	Type	Section	Offset	-----Size-----	Dimensions
IFILE	L*1	@ \$DATA	000004	000017 (    8.)	(15)
X	R*4	@ \$DATA	000000	000004 (    2.)	(1)

```

0001      SUBROUTINE FLT(Y,XT,LGTH,XSF,FILNAM)
0002      DIMENSION Y(1), XT(1)
0003      BYTE FILNAM(12)
0004      LTEMP = LGTH
C
0005      TYPE *, '      SELECT THE TYPE OF GRAPH!'
0006      TYPE *, ' |-----| '
0007      TYPE *, ' | 1 ..TIME FUNCTION OF INPUT | '
0008      TYPE *, ' | 2 ..TIME FUNCTION OF RESPONSE | '
0009      TYPE *, ' | 3 ..CROSS SPECTRA | '
0010      TYPE *, ' | 4 ..AUTO SPECTRA OF INPUT | '
0011      TYPE *, ' | 5 ..AUTO SPECTRA OF RESPONSE | '
0012      TYPE *, ' | 6 ..TRANSFER FUNTION : GAIN | '
0013      TYPE *, ' | 7 ..TRANSFER FUNCTION IN DBs | '
0014      TYPE *, ' | 8 ..PHASE FUNTION IN DEGREES | '
0015      TYPE *, ' | 9 ..COHERENCE FUNTION | '
0016      TYPE *, ' |-----| '
0017      TYPE *, '      ENTER THE CORRESPONDING NUMBER:'
0018      ACCEPT *, NUM
C
C
0019      3 TYPE *, ' SET YMIN = ?'
0020      ACCEPT *, YMIN
0021      TYPE *, ' YMIN= ', YMIN
0022      TYPE *, ' SET YMAX = ?'
0023      ACCEPT *, YMAX
0024      TYPE *, ' DO YOU WANT TO EXPAND THE FREQUENCY SCALE? (YES=1)'
0025      ACCEPT *, ISCAL
0026      IF (ISCAL .NE. 1) GO TO 6
0028      TYPE *, ' TYPE IN DESIRED SCALE FACTOR. '
0029      ACCEPT *, IXSCF
0030      LGTH = LGTH/IXSCF
C
0031      6 DO 10 J = 1, LGTH
0032      XT(J) = XSF*FLOAT(J)
0033      10 CONTINUE
C
0034      XLGT = XSF*FLOAT(LGTH)
C
0035      ILFT = 600
0036      IRIT = 3500
0037      IBOT = 1000
0038      ITOP = 2500
0039      XMIN = 0.
0040      XMAX = XLGT
C
0041      CALL TSXCHK
0042      CALL GRINIT(4014,4631,1)
0043      CALL CHRISZ(3)
0044      CALL ERASE
0045      CALL GRID(10,10,ILFT,IRIT,IBOT,ITOP,97)
C
0046      CALL ANOTAT(10,10,ILFT,IRIT,IBOT,ITOP,XMIN,XMAX,YMIN,YMAX)
C

```

```
0047      CALL XYPLOT(XT,Y,LGTH,ILFT,IRIT,IBOT,ITOP,XMIN,XMAX,  
1 YMIN,YMAX,1,0)  
      C  
0048      CALL CHRSTZ(2)  
      C  
0049      CALL MPLOT(ILFT-500, ITOP+500, -1)  
0050      TYPE 14, FILNAM  
0051  14    FORMAT ('+FILENAME:',14A1)  
      C  
0052      GO TO (20,30,40,50,60,70,80,90,100),NUM  
      C  
0053  20    CALL MPLOT(ILFT+500, ITOP+200, -1)  
0054      TYPE 22  
0055  22    FORMAT ('+INPUT STIMULUS VS TIME '  
0056      CALL MPLOT(ILFT-500, IBOT+750, -1)  
0057      TYPE 24  
0058  24    FORMAT ('+VOLTS')  
0059      CALL MPLOT(ILFT+800, IBOT-300, -1)  
0060      TYPE 26  
0061  26    FORMAT ('+TIME IN SECONDS '  
0062      CALL MPLOT( 0, IBOT-600, -1)  
0063      GO TO 150  
      C  
0064  30    CALL MPLOT(ILFT+500, ITOP+200, -1)  
0065      TYPE 32  
0066  32    FORMAT ('+HORIZONTAL EYE MOVEMENTS VS TIME '  
0067      CALL MPLOT(ILFT-500, IBOT+750, -1)  
0068      TYPE 34  
0069  34    FORMAT ('+VOLTS')  
0070      CALL MPLOT(ILFT+800, IBOT-300, -1)  
0071      TYPE 36  
0072  36    FORMAT ('+TIME IN SECONDS '  
0073      CALL MPLOT( 0, IBOT-600, -1)  
0074      GO TO 150  
      C  
0075  40    CALL MPLOT(ILFT+500, ITOP+200, -1)  
0076      TYPE 42  
0077  42    FORMAT ('+CROSS-SPECTRA '  
0078      CALL MPLOT(ILFT-500, IBOT+750, -1)  
0079      TYPE 44  
0080  44    FORMAT ('+VSQ/HZ')  
0081      CALL MPLOT(ILFT+800, IBOT-300, -1)  
0082      TYPE 46  
0083  46    FORMAT ('+FREQUENCY IN HERTZ '  
0084      CALL MPLOT( 0, IBOT-600, -1)  
0085      GO TO 150  
      C  
0086  50    CALL MPLOT(ILFT+500, ITOP+200, -1)  
0087      TYPE 52  
0088  52    FORMAT ('+POWER SPECTRUM OF INPUT STIMULUS '  
0089      CALL MPLOT(ILFT-500, IBOT+750, -1)  
0090      TYPE 54  
0091  54    FORMAT ('+VSQ/HZ')  
0092      CALL MPLOT(ILFT+800, IBOT-300, -1)
```

```
0093      TYPE 56
0094  56    FORMAT ('+FREQUENCY IN HERTZ')
        C
0095      CALL MPLOT( 0, IBOT-600, -1)
0096      GO TO 150
        C
0097  60    CALL MPLOT(ILFT+500, ITOP+200, -1)
0098      TYPE 62
0099  62    FORMAT ('+POWER SPECTRUM OF OCULAR RESPONSE')
0100      CALL MPLOT(ILFT-500, IBOT+750, -1)
0101      TYPE 64
0102  64    FORMAT ('+VSQ/HZ')
0103      CALL MPLOT(ILFT+800, IBOT-300, -1)
0104      TYPE 66
0105  66    FORMAT ('+FREQUENCY IN HERTZ')
0106      CALL MPLOT( 0, IBOT-600, -1)
0107      GO TO 150
        C
0108  70    CALL MPLOT(ILFT+500, ITOP+200, -1)
0109      TYPE 72
0110  72    FORMAT ('+TRANSFER FUNCTION GAIN')
0111      CALL MPLOT(ILFT-500, IBOT+750, -1)
0112      TYPE 74
0113  74    FORMAT ('+GAIN')
0114      CALL MPLOT(ILFT+800, IBOT-300, -1)
0115      TYPE 76
0116  76    FORMAT ('+FREQUENCY IN HERTZ')
0117      CALL MPLOT( 0, IBOT-600, -1)
0118      GO TO 150
        C
0119  80    CALL MPLOT(ILFT+500, ITOP+200, -1)
0120      TYPE 82
0121  82    FORMAT ('+TRANSFER FUNCTION IN DBs')
0122      CALL MPLOT(ILFT-500, IBOT+750, -1)
0123      TYPE 84
0124  84    FORMAT ('+DBs')
0125      CALL MPLOT(ILFT+800, IBOT-300, -1)
0126      TYPE 86
0127  86    FORMAT ('+FREQUENCY IN HERTZ')
0128      CALL MPLOT( 0, IBOT-600, -1)
0129      GO TO 150
        C
0130  90    CALL MPLOT(ILFT+500, ITOP+200, -1)
0131      TYPE 92
0132  92    FORMAT ('+PHASE FACTOR IN DEGREES ')
0133      CALL MPLOT(ILFT-500, IBOT+750, -1)
0134      TYPE 94
0135  94    FORMAT ('+DEGs')
0136      CALL MPLOT(ILFT+800, IBOT-300, -1)
0137      TYPE 96
0138  96    FORMAT ('+FREQUENCY IN HERTZ')
0139      CALL MPLOT( 0, IBOT-600, -1)
0140      GO TO 150
        C
```

```
0141 100  CALL MPLOT(ILFT+500, ITOP+200, -1)
0142      TYPE 102
0143 102  FORMAT ('+COHERENCE FUNCTION ')
0144      CALL MPLOT(ILFT+800, IBOT-300, -1)
0145      TYPE 106
0146 106  FORMAT ('+FREQUENCY IN HERTZ')
0147      CALL MPLOT( 0, IBOT-600, -1)
      C
0148 150  CALL CHRISZ(3)
0149      TYPE *, ' DO YOU WANT A HARD COPY? (YES=1)'
0150      ACCEPT *, HCPY
0151      IF (HCPY .NE. 1) GO TO 160
      C
0153      CALL COPY(0)
      C
0154 160  TYPE *, ' DO YOU WANT ANOTHER PLOT? (YES=1)'
0155      ACCEPT *, IYS
0156      IF (IYS .NE. 1) GO TO 200
0158      TYPE 165,LTEMP
0159 165  FORMAT (' LTEMP = ',I4)
0160      LGTH = LTEMP
0161 170  GO TO 3
      C
0162 200  RETURN
0163      END
```



# FORTTRAN IV

## Storage Map for Program Unit FLT

Local Variables, .FSECT \$DATA, Size = 000266 ( 91. words)

Name	Type	Offset	Name	Type	Offset	Name	Type	Offset
HCFY	R*4	000062	IBOT	I*2	000046	ILFT	I*2	000042
IRIT	I*2	000044	ISCAL	I*2	000030	ITOP	I*2	000050
IXSCF	I*2	000032	IYS	I*2	000066	J	I*2	000034
LGTH	I*2 @	000004	LTEMP	I*2	000014	NUM	I*2	000016
XLGT	R*4	000036	XMAX	R*4	000056	XMIN	R*4	000052
XSF	R*4 @	000006	YMAX	R*4	000024	YMIN	R*4	000020

Local and COMMON Arrays:

Name	Type	Section	Offset	-----Size-----	Dimensions
FILNAM	L*1	@ \$DATA	000010	000014 ( 6.)	(12)
XT	R*4	@ \$DATA	000002	000004 ( 2.)	(1)
Y	R*4	@ \$DATA	000000	000004 ( 2.)	(1)

Subroutines, Functions, Statement and Processor-Defined Functions:

Name	Type	Name	Type	Name	Type	Name	Type	Name	Type
ANOTAT	R*4	CHRSIZ	R*4	COPY	R*4	ERASE	R*4	FLOAT	R*4
GRID	R*4	GRINIT	R*4	MFLOT	I*2	TSXCHK	R*4	XYPLOT	R*4

## APPENDIX C

### FIR RESULTS

#### FINITE IMPULSE RESPONSE

#### DIGITAL FILTER COEFFICIENTS

#### AND TEST PROGRAM.

\*\*\*\*\*

FINITE IMPULSE RESPONSE (FIR)  
LINEAR PHASE DIGITAL FILTER DESIGN  
REMEZ EXCHANGE ALGORITHM

BANDPASS FILTER

FILTER LENGTH = 15

\*\*\*\*\* IMPULSE RESPONSE \*\*\*\*\*

H( 1) = 0.37165603E-02 = H( 15)  
H( 2) = 0.20235427E-01 = H( 14)  
H( 3) = 0.13399956E-01 = H( 13)  
H( 4) = -0.40643737E-01 = H( 12)  
H( 5) = -0.66073574E-01 = H( 11)  
H( 6) = 0.61152663E-01 = H( 10)  
H( 7) = 0.30294424E+00 = H( 9)  
H( 8) = 0.43047285E+00 = H( 8)

	BAND 1	BAND 2
LOWER BAND EDGE	0.0000000	0.3000000
UPPER BAND EDGE	0.1500000	0.5000000
DESIRED VALUE	1.0000000	0.0000000
WEIGHTING	10.0000000	50.0000000
DEVIATION	0.0199359	0.0039872
DEVIATION IN DB	0.1714583	-47.9866638

EXTREMAL FREQUENCIES--MAXIMA OF THE ERROR CURVE

0.0000000	0.0664062	0.1250000	0.1500000	0.3000000
0.3195313	0.3664063	0.4289063	0.5000000	

\*\*\*\*\*

# RAW DATA

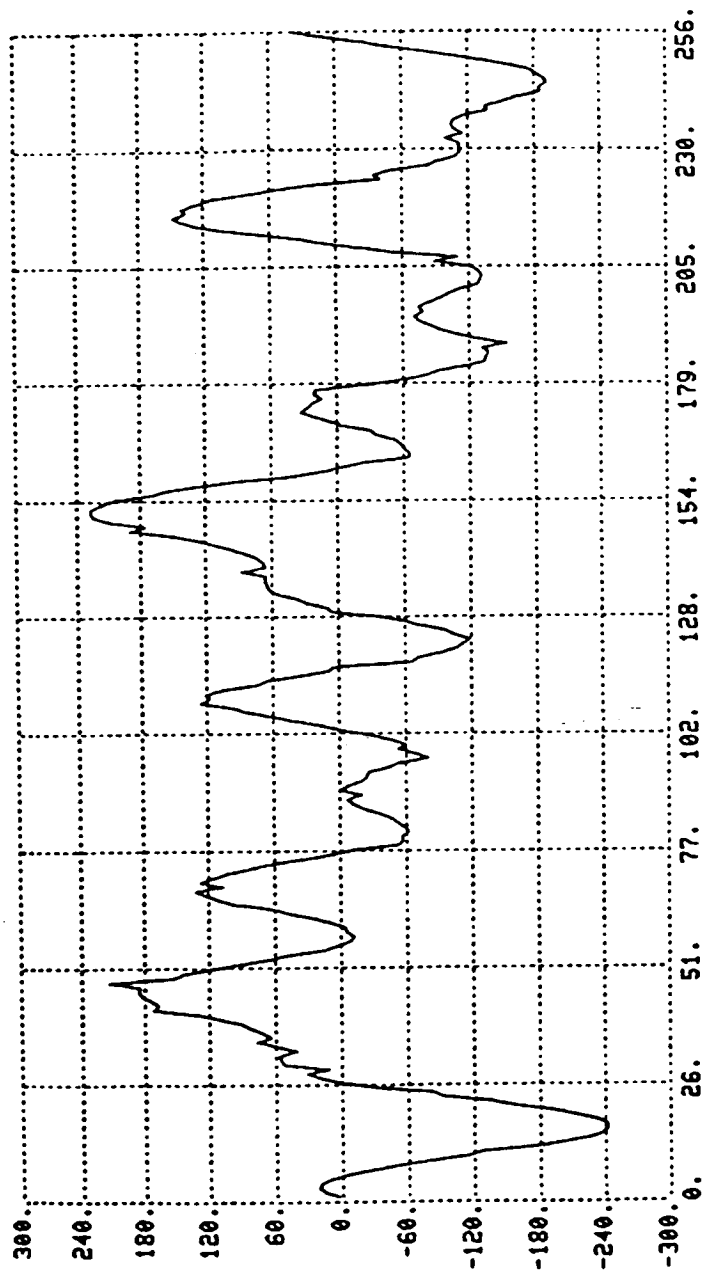


Fig C-1 Unfiltered Input Stimulus. Raw input data is shown with the x-axis expanded to show the first 256 data points of a 1024-point array.

# FILTERED DATA

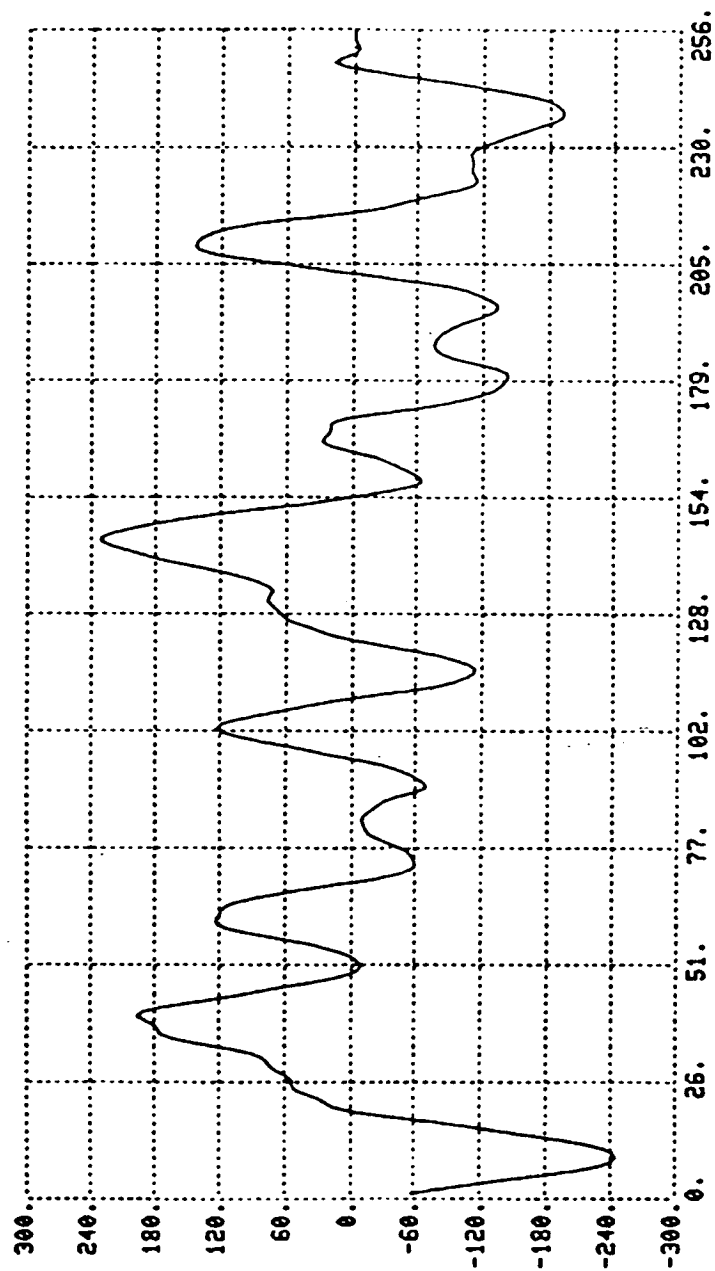


Fig C-2 Filtered Input Stimulus. Input data of Fig C-1 is shown after passing through the 15-point Finite Impulse Response (FIR) digital filter.

RAW DATA

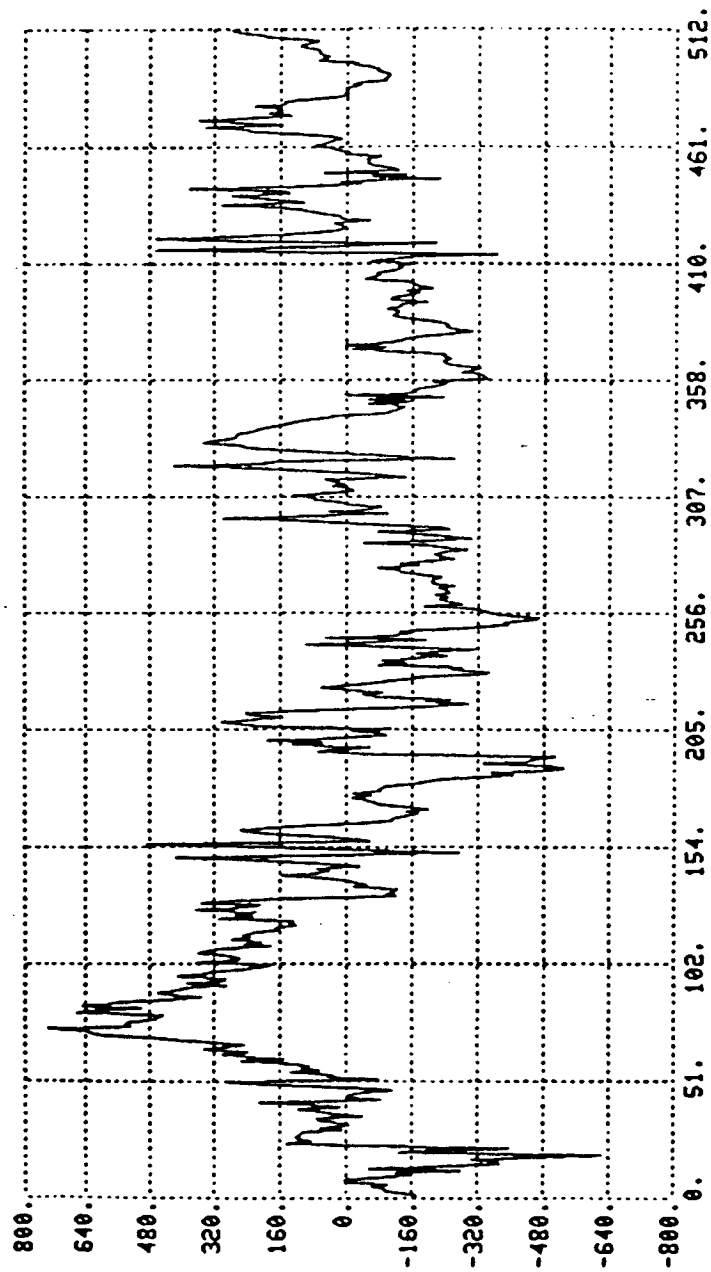


Fig C-3 Unfiltered ECG Response. Unfiltered response is shown with x-axis expanded by 2.

# FILTERED DATA

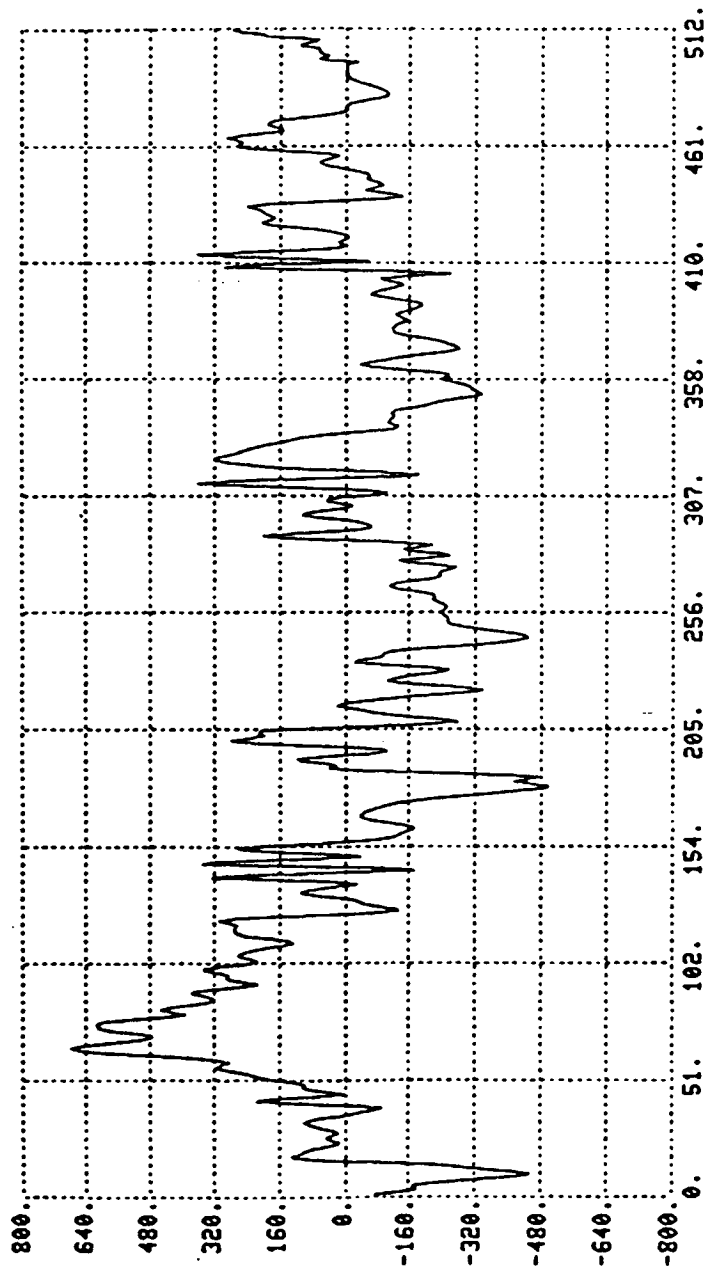


Fig C-4 Filtered EOG Response. EOG response of Fig C-3 is shown after passing through the 15-point Finite Impulse Response (FIR) digital filter.

```
0001      PROGRAM TSTFIR
C
0002      INTEGER Z(512),DSKINC,NBLK,IPOSN(16),MAX(16),ICHNUM(16),LENGTH
0003      REAL AMPL, PERIOD, INTRAT, HEOG(1040), XT(1024), COEF(25),
1 DIFCO(25), YHEOG(1050)
C
0004      EQUIVALENCE (AMPL,Z(150)),(PERIOD,Z(152)),(INTRAT,Z(159)),
1 (DSKINC,Z(167)),(NBLK,Z(172)),(ICHNUM,Z(177)),
2 (IPOSN,Z(225)),(MAX,Z(241))
C
0005      INTEGER BUFR2(1024), IERR
0006      BYTE FILNAM(12)
0007  10    DO 20 K=1,12
0008  20    FILNAM(K)=0
0009      TYPE 30
0010  30    FORMAT (' ENTER COMPLETE FILENAME'/' FILENAME ?',%)
0011      ACCEPT 40,FILNAM
0012  40    FORMAT (12A1)
C
0013      CALL DISKIO(FILNAM,-3,Z,256,0,NDUMMY,IERR)
0014      IF (IERR.NE. 0) TYPE *, ' ERROR CODE',IERR, ' DURING READING'
C
0016  42    TYPE *, ' CHAN NO.'
0017      ACCEPT *,K
0018  45    TYPE *, ' ENTER THE NUMBER OF DATA POINTS FOR EOG'
0019      ACCEPT *,LENGTH
0020      TYPE *, ' DO YOU WANT FILES LEFT OPEN? (1=YES)'
0021      ACCEPT *,LOPEN
C
0022      NWRDS = DSKINC* 256
0023      IBLK = 2
0024      ITEMP = 0
0025      TYPE 50, NBLK, NWRDS, IBLK,DSKINC
0026  50    FORMAT (' NBLK=',I5,' NWRDS=',I5,' IBLK=',I5,'DSKINC=',I5)
0027      TYPE 51,MAX(K),IPOSN(K)
0028  51    FORMAT (' MAX(K) = ',I5,' IPOSN(K) = ',I5)
C
0029      TYPE *, ' DO YOU WANT TO PLOT EVERY POINT? ENTER STEP SIZE!'
0030      ACCEPT *,ISTEP
C
0031      IRMODE=3
0032      IF (LOPEN.EQ. 1) IRMODE = -3
0033      TYPE *, ' NOW READING FROM DISK'
0035  52    CALL DISKIO(FILNAM,IRMODE,BUFR2,NWRDS,IBLK,NDUMMY,IERR)
0036      IF (IERR.NE. 0) TYPE *, ' ERROR CODE',IERR, ' DURING READ'
C
0038      NPTS = (MAX(K)-IPOSN(K)+1)/ISTEP
0039      DO 57 L = 1,NPTS
0040      HEOG(L+ITEMP) = BUFR2(IPOSN(K) + L*ISTEP)
0041  57    CONTINUE
C
0042      IBLK = IBLK + DSKINC
0043      ITEMP = ITEMP + NPTS
C
```



```

0044      IF (ITEMP .LT. LENGTH) GO TO 52
0046      XLGT = FLOAT(LENGTH)
      C
0047      DO 60 J = 1,LENGTH
0048      XT(J) = FLOAT(J)
0049  60    CONTINUE
0050      TYPE *, ' SET YMIN!'
0051      ACCEPT *,YMIN
0052      TYPE *, ' SET YMAX!'
0053      ACCEPT *,YMAX
      C
0054      ILFT = 600
0055      IRIT = 3500
0056      IBOT = 1000
0057      ITOP = 2500
0058      XMIN = 0.
0059      XMAX = XLGT
0060      CALL TSXCHK
0061      CALL GRINIT(4014,4631,1)
0062      CALL CHRISZ(3)
0063      CALL ERASE
0064      CALL GRID(10,10,ILFT,IRIT,IBOT,ITOP,97)
0065      CALL ANOTAT(10,10,ILFT,IRIT,IBOT,ITOP,XMIN,XMAX,YMIN,YMAX)
0066      CALL XYPLOT(XT,HEOG,LENGTH,ILFT,IRIT,IBOT,ITOP,XMIN,XMAX,
1 YMIN,YMAX,1,0)
      C
0067      CALL MPLOT(ILFT+500,ITOP+300,-1)
0068      TYPE 61
0069  61    FORMAT(' +RAW DATA ')
      C
0070      TYPE *, ' DO YOU WANT A HARD COPY? (YES=1)'
0071      ACCEPT *,IS
0072      IF (IS .NE. 1) GO TO 62
      C
0074      CALL COPY(0)
      C
0075  62    TYPE *, ' ENTER NUMBER OF FIR COEFFICIENTS: '
0076      ACCEPT *,NCO
0077      NE = NCO+1
0078      NEH = NE/2
0079      DO 65 N = 1, NEH
0080      TYPE *, ' ENTER FIR COEF VALUE FOR N= ',N
0081      ACCEPT *, COEF(N)
0082      COEF(NE-N) = COEF(N)
0083  65    CONTINUE
      C
0084      DO 80 I = 2, LENGTH+NCO
0085      SUM = 0.0
0086      DO 70 J = 1,NCO
0087      L = J
0088      IF (J .GE. I) GO TO 70
0090      IF (I-J .GT. LENGTH) GO TO 70
0092      H = COEF(J) * HEOG(I-J)
0093      SUM = SUM + H

```

```
0094 70    CONTINUE
0095      YHEOG(I-1) = SUM
0096 80    CONTINUE
      C
0097      J2 = NE-1
0098      DO 81 J = NE, LENGTH+J2
0099      YHEOG(J-J2) = YHEOG(J)
0100 81    CONTINUE
      C
0101      CALL TSXCHK
0102      CALL GRINIT(4014,4631,1)
0103      CALL CHRISZ(3)
0104      CALL ERASE
0105      CALL GRID(10,10,ILFT,IRIT,IBOT,ITOP,97)
0106      CALL ANOTAT(10,10,ILFT,IRIT,IBOT,ITOP,XMIN,XMAX,YMIN,YMAX)
0107      CALL XYPLOT(XT,YHEOG,LENGTH,ILFT,IRIT,IBOT,ITOP,XMIN,XMAX,
1 YMIN,YMAX,1,0)
      C
0108      CALL MPLOT(ILFT+500,ITOP+300,-1)
0109      TYPE 82
0110 82    FORMAT ('+FILTERED DATA')
0111      TYPE *, ' DO YOU WANT A HARD COPY? (YES=1)'
0112      ACCEPT *, IS
0113      IF (IS .NE. 1) GO TO 83
      C
0115      CALL COPY(0)
      C
0116      TYPE *, ' TRY ANOTHER FILTER? (YES=1)'
0117      ACCEPT *, JYES
0118      IF (JYES .EQ. 1) GO TO 62
      C
0120 83    TYPE *, ' ENTER NUMBER OF DIFFERENTIATOR COEFFICIENTS: '
0121      ACCEPT *, NDCO
0122      ND = NDCO+1
0123      NDEH = NDCO/2
0124      DO 85 N = 1, NDEH
0125      TYPE *, ' ENTER FIR COEF VALUE FOR N= ', N
0126      ACCEPT *, DIFCO(N)
0127      DIFCO(ND-N) = DIFCO(N)
0128 85    CONTINUE
      C
0129      DO 100 I = 2, LENGTH+NDCO
0130      DSUM = 0.0
0131      DO 90 J = 1, NDCO
0132      IF (J .GE. I) GO TO 90
0133      IF (I-J .GT. LENGTH) GO TO 90
0134      DH = DIFCO(J) * YHEOG(I-J)
0135      DSUM = DSUM + DH
0136 90    CONTINUE
0137      HEOG(I-1) = DSUM
0138 100   CONTINUE
      C
0141      JD = ND - 1
0142      LN = LENGTH + NDCO
```

```
0143      DO 101 M = ND, LN
0144      HEOG(M-JD) = HEOG(M)
0145 101   CONTINUE
      C
0146      CALL TSXCHK
0147      CALL GRINIT(4014,4631,1)
0148      CALL CHRSTZ(3)
0149      CALL ERASE
0150      CALL GRID(10,10,ILFT,IRIT,IBOT,ITOP,97)
0151      CALL ANOTAT(10,10,ILFT,IRIT,IBOT,ITOP,XMIN,XMAX,YMIN,YMAX)
0152      CALL XYPLT(XT,HEOG,LENGTH,ILFT,IRIT,IBOT,ITOP,XMIN,XMAX,
      1 YMIN,YMAX,1,0)
      C
0153      CALL MPLOT(ILFT+500,ITOP+300,-1)
0154      TYPE 110
0155 110   FORMAT ('+DIFFERENTIATED DATA')
      C
0156      CALL COPY(0)
      C
0157      TYPE *, ' TRY ANOTHER DIFFERENTIATOR? (YES=1)'
0158      ACCEPT *, IES
0159      IF (IES .EQ. 1) GO TO 83
      C
0161      TYPE *, ' ANOTHER CHANNEL OF DATA? (YES=1)'
0162      ACCEPT *, JES
0163      IF (JES .EQ. 1) GO TO 42
      C
0165      TYPE *, ' TRY ANOTHER FILE? (I=YES) ? '
0166      ACCEPT *, MORE
0167      IF (MORE .EQ. 1) GO TO 10
      C
0169      STOP
0170      END
```

Local Variables, .PSECT \$DATA, Size = 037014 ( 7942. words)

Name	Type	Offset		Name	Type	Offset	Name	Type	Offset	
AMPL	R*4	000454	Eqv	DM	R*4	036746	DSKINC	I*2	000516	Eqv
DSUM	R*4	036742		H	R*4	036724	I	I*2	036716	
IBLK	I*2	036632		IBOT	I*2	036670	IERR	I*2	036620	
IES	I*2	036760		ILFT	I*2	036664	INTRAT	R*4	000476	Eqv
IRIT	I*2	036666		IRMODE	I*2	036640	IS	I*2	036704	
ISTEP	I*2	036636		ITEMP	I*2	036634	ITOP	I*2	036672	
J	I*2	036652		JD	I*2	036752	JES	I*2	036762	
JYES	I*2	036732		J2	I*2	036730	K	I*2	036622	
L	I*2	036644		LENGTH	I*2	036616	LN	I*2	036754	
LOPEN	I*2	036626		M	I*2	036756	MORE	I*2	036764	
N	I*2	036714		NBLK	I*2	000530	Eqv	NCO	I*2	036706
ND	I*2	036736		NDCO	I*2	036734	NDEH	I*2	036740	
NDUMMY	I*2	036624		NE	I*2	036710	NEH	I*2	036712	
NPTS	I*2	036642		NWRDS	I*2	036630	PERIOD	R*4	000460	Eqv
SUM	R*4	036720		XLGT	R*4	036646	XMAX	R*4	036700	
XMIN	R*4	036674		YMAX	R*4	036660	YMIN	R*4	036654	

Local and COMMON Arrays:

Name	Type	Section	Offset	-----Size-----	Dimensions
BUFR2	I*2	\$DATA	032562	004000 ( 1024.)	(1024)
COEF	R*4	\$DATA	022102	000144 ( 50.)	(25)
DIFCO	R*4	\$DATA	022246	000144 ( 50.)	(25)
FILNAM	L*1	\$DATA	036562	000014 ( 6.)	(12)
HEOG	R*4	\$DATA	002002	010100 ( 2080.)	(1040)
ICHNUM	I*2	\$DATA	000542	000040 ( 16.)	(16)
JPOSN	I*2	\$DATA	000702	000040 ( 16.)	(16)
MAX	I*2	\$DATA	000742	000040 ( 16.)	(16)
XT	R*4	\$DATA	012102	010000 ( 2048.)	(1024)
YHEOG	R*4	\$DATA	022412	010150 ( 2100.)	(1050)
Z	I*2	\$DATA	000002	002000 ( 512.)	(512)

Subroutines, Functions, Statement and Processor-Defined Functions:

Name	Type	Name	Type	Name	Type	Name	Type	Name	Type
ANDTAT	R*4	CHRSIZ	R*4	COPY	R*4	DISKIO	R*4	ERASE	R*4
FLOAT	R*4	GRID	R*4	GRINIT	R*4	MPLOT	I*2	TSXCHK	R*4
XYFLOT	R*4								

APPENDIX D

DIFFERENTIATION RESULTS

TEST PROGRAM FOR EVALUATING

THE DIFFERENTIATION SUBPROGRAM

# RAW DATA

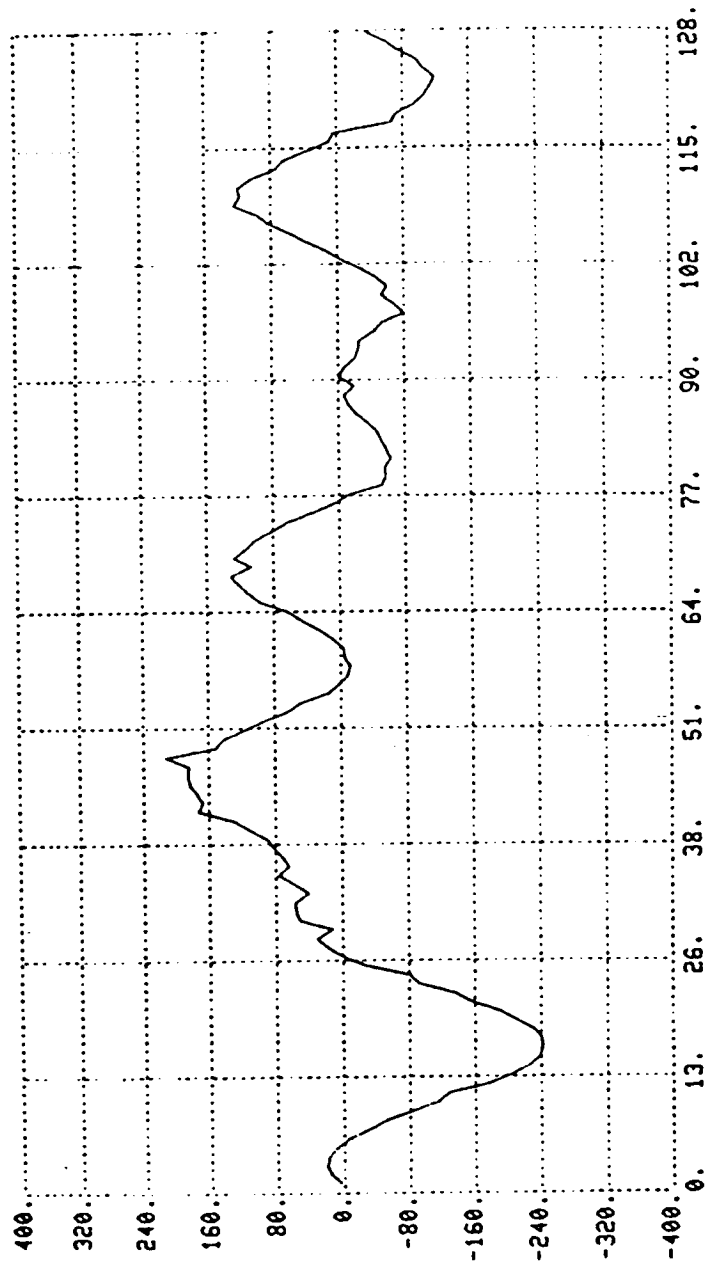


Fig D-1 Raw Input. Unfiltered input stimulus is shown with the x-axis expanded to show the first 128 data points of a 1024-point array.

# FILTERED DATA

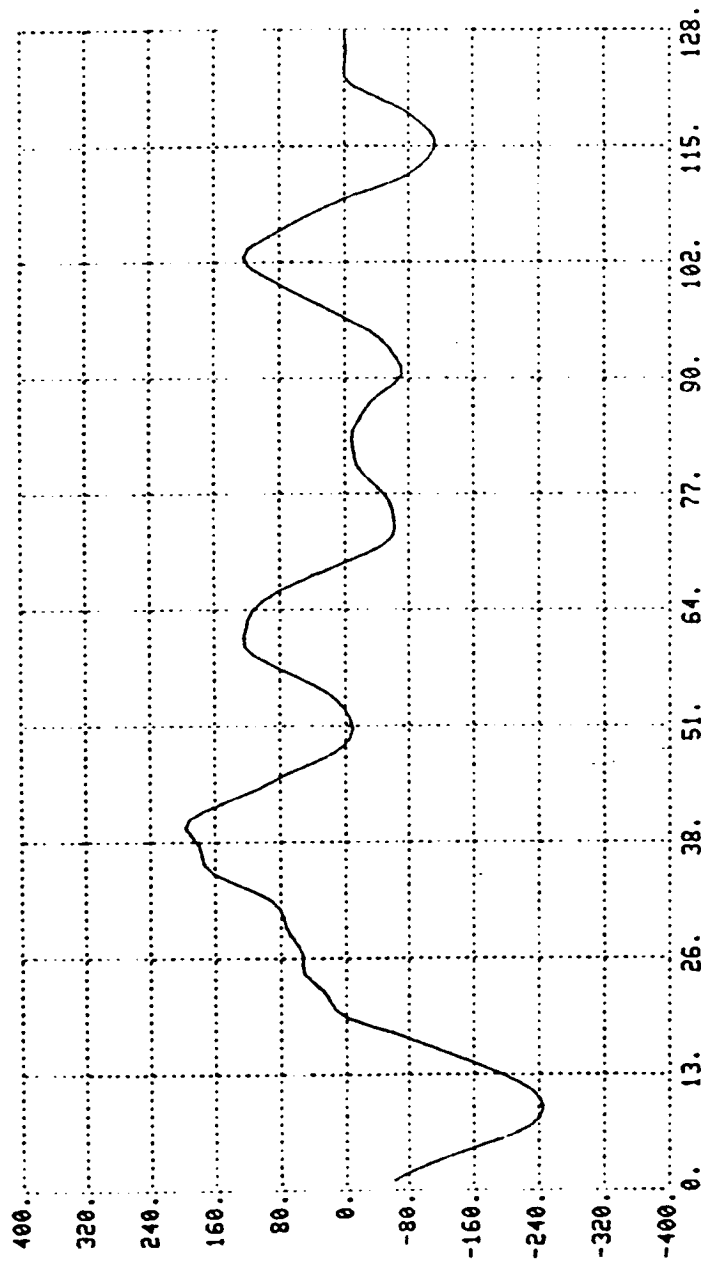


Fig D-2 Filtered Input. Input data of Fig D-1 is shown after passing through the 15-point Finite Impulse Response (FIR) digital filter.

# DIFFERENTIATED DATA

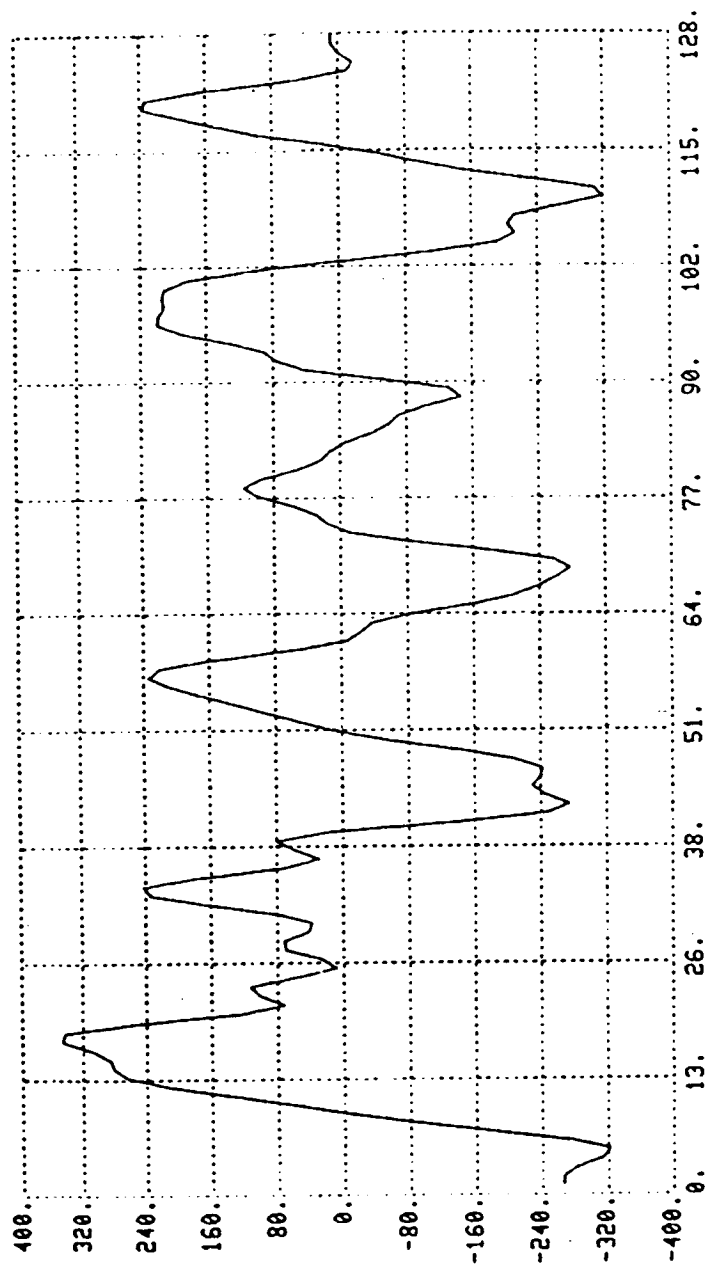


Fig D-3 Differentiated Input-2. Filtered input data of Fig D-2 is shown after passing through a 2nd order differentiator.



# DIFFERENTIATED DATA

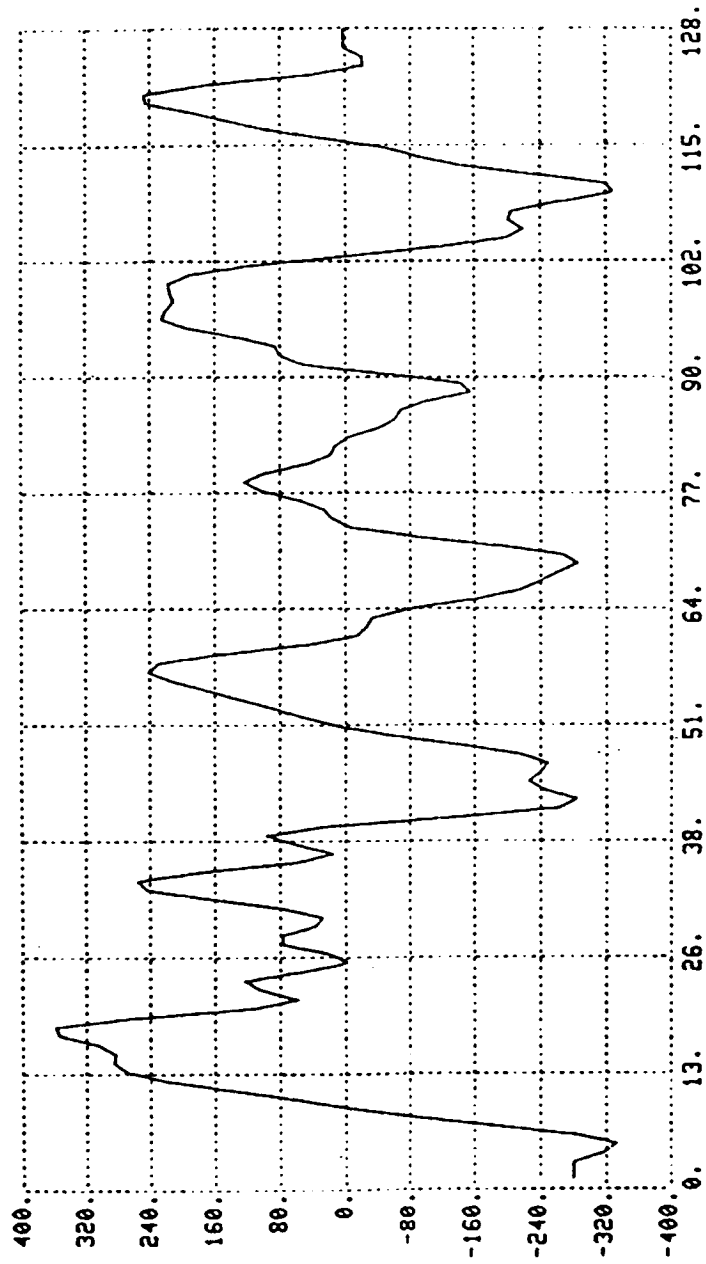


Fig D-4 Differentiated Input-4. Filtered input data of Fig D-2 is shown after passing through 4th order differentiator.

# DIFFERENTIATED DATA

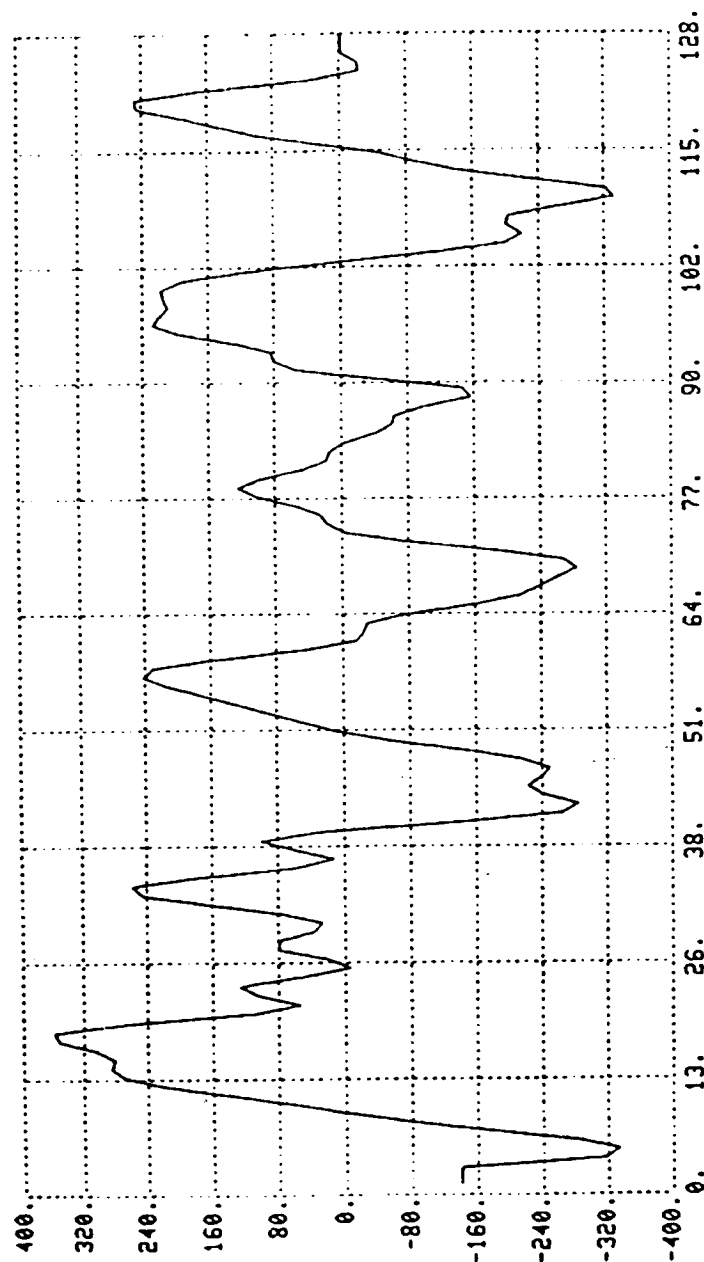


Fig D-5 Differentiated Input-6. Filtered input data of Fig D-2 is shown after passing through a 6th order differentiator.

# FIL+DIF+FILTERED DATA

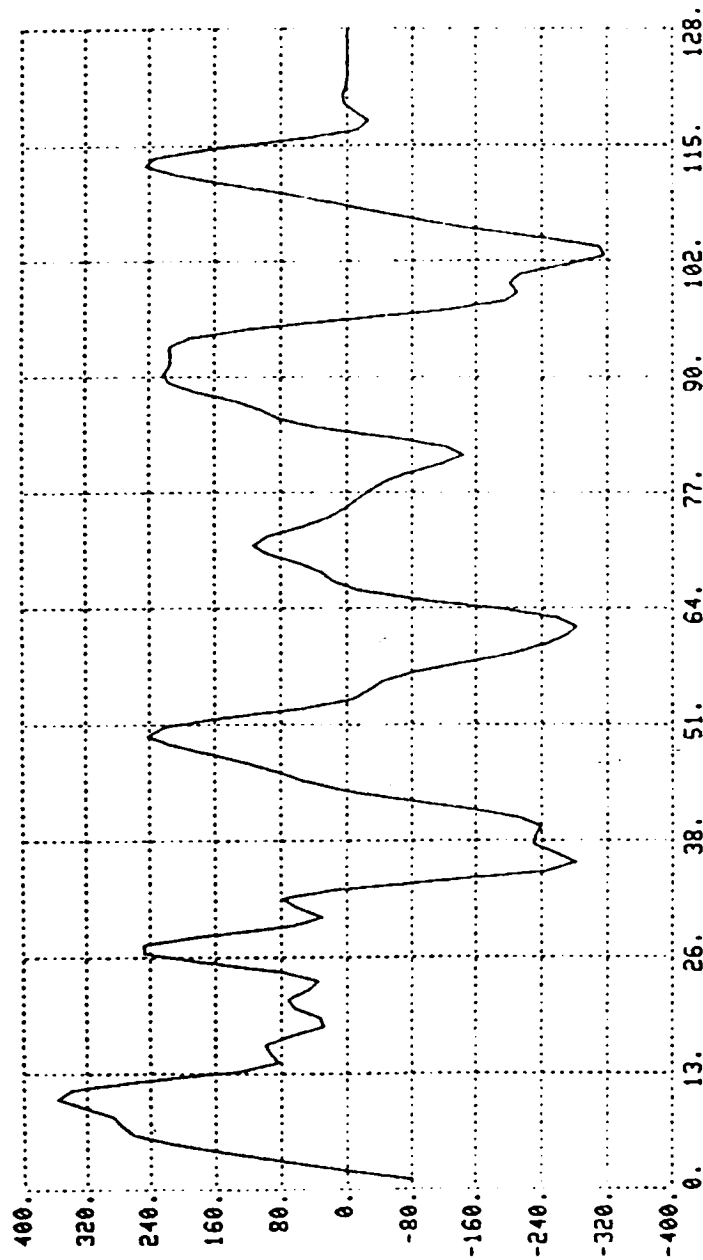


Fig D-6 Refiltered Input. Differentiated input data of Fig D-5 is shown after passing through a second 15-point Finite Impulse Response (FIR) digital filter.

# RAW DATA

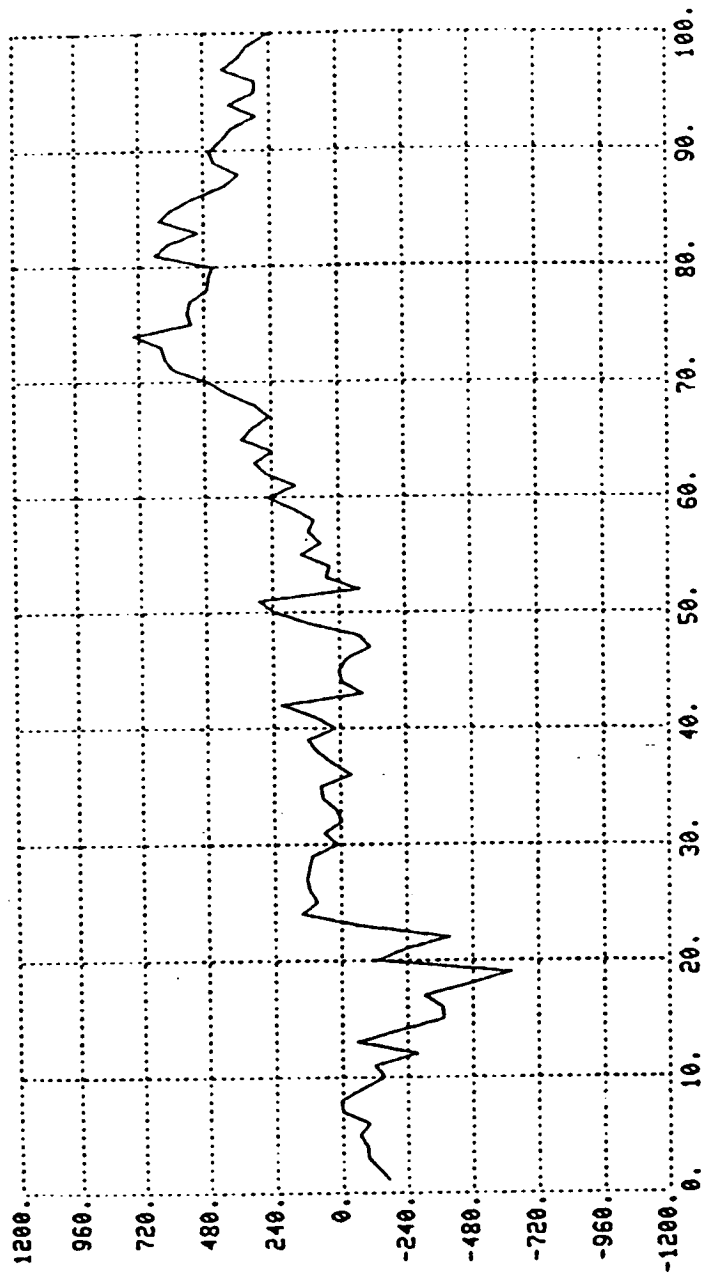


Fig D-7 Raw EOG Response. Unfiltered raw EOG response is shown with the x-axis expanded to show the first 100 data points of a 1024-point array.

# FILTERED DATA

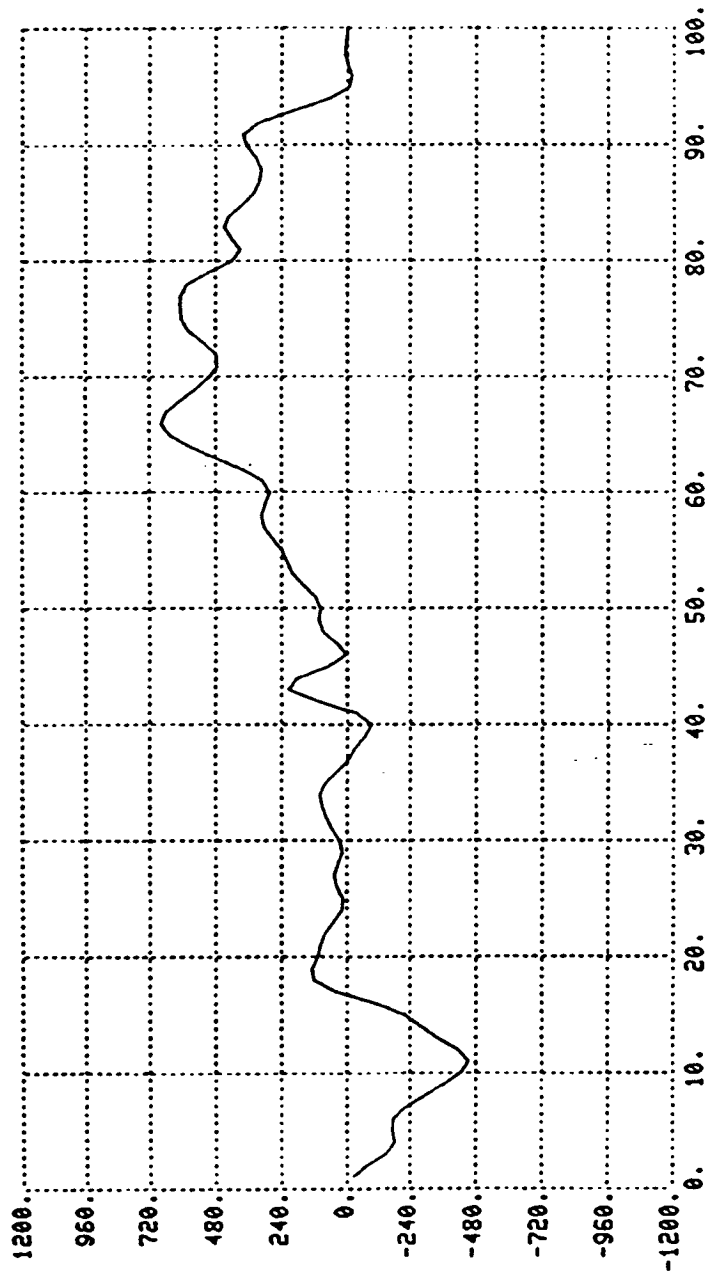


Fig D-8 Filtered EOG Response. EOG response of Fig D-7 is shown after passing through the 15-point Finite Impulse Response (FIR) digital filter.

# DIFFERENTIATED DATA

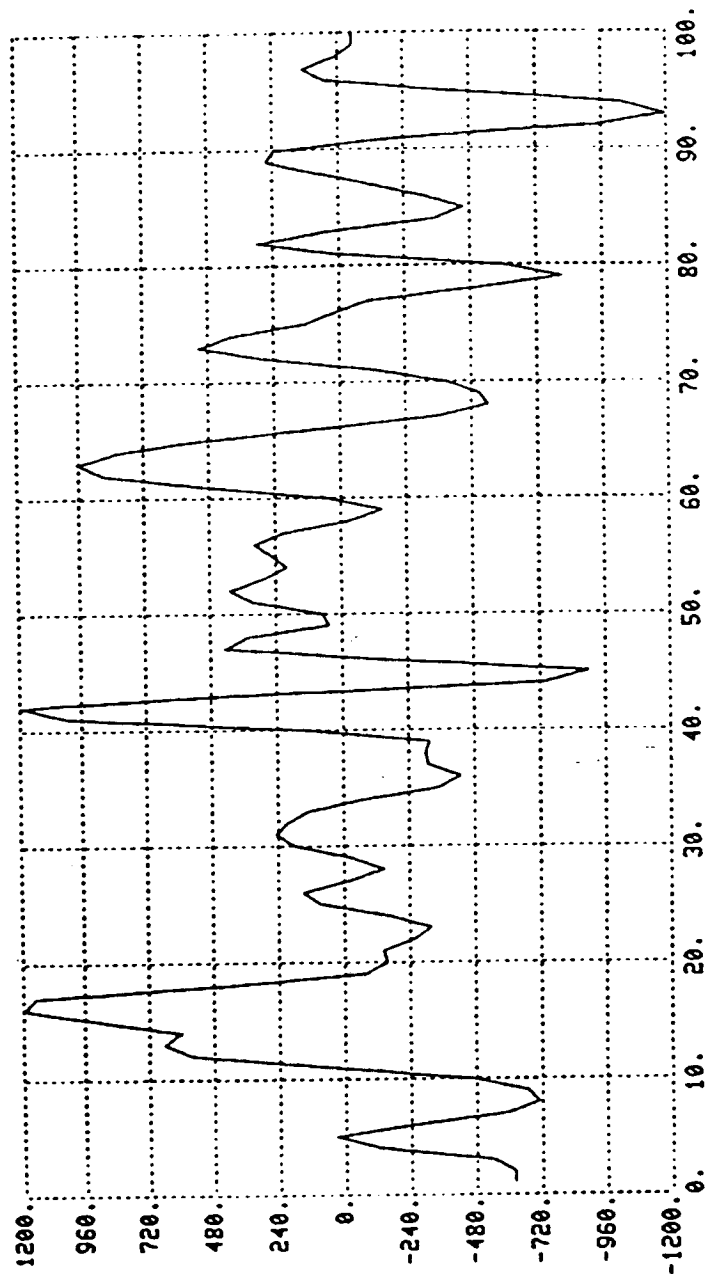


Fig D-9 Differentiated EOG Response-2. Filtered EOG response of Fig D-8 is shown after passing through a 2nd order differentiator.

# DIFFERENTIATED DATA

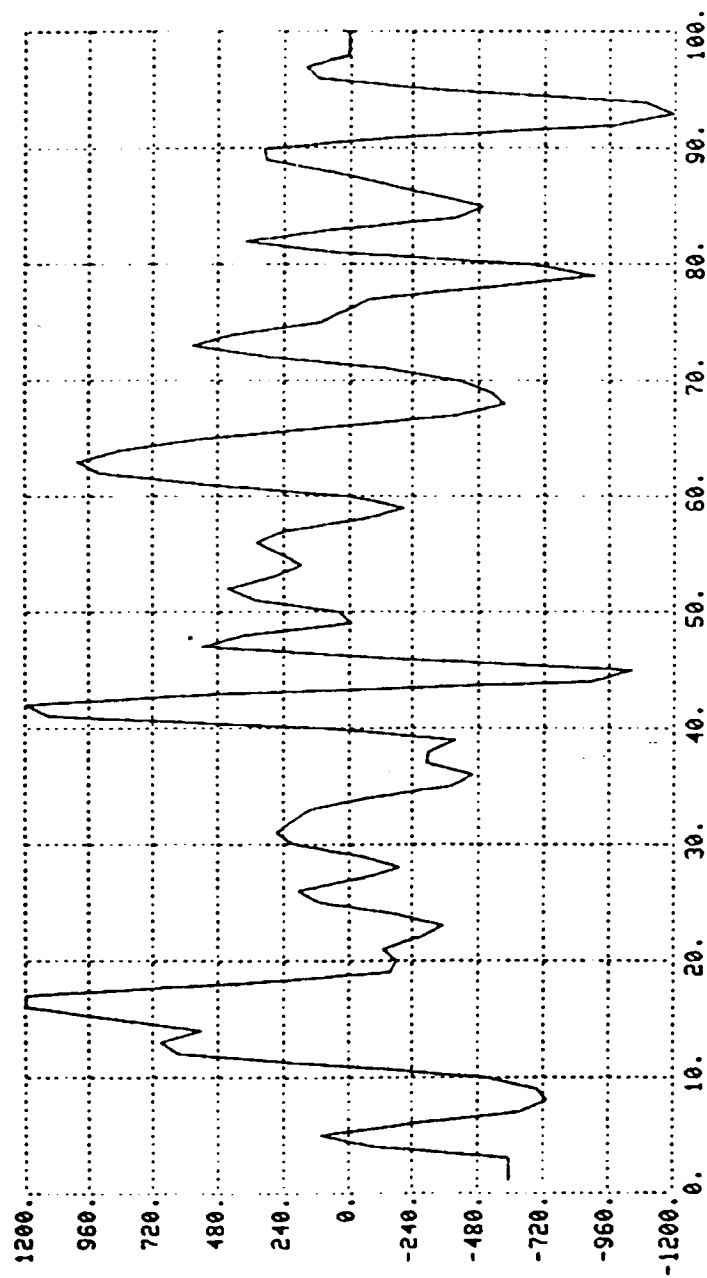


Fig D-10 Differentiated EOG Response-4. Filtered EOG response of Fig D-8 is shown after passing through a 4th order differentiator.

# DIFFERENTIATED DATA

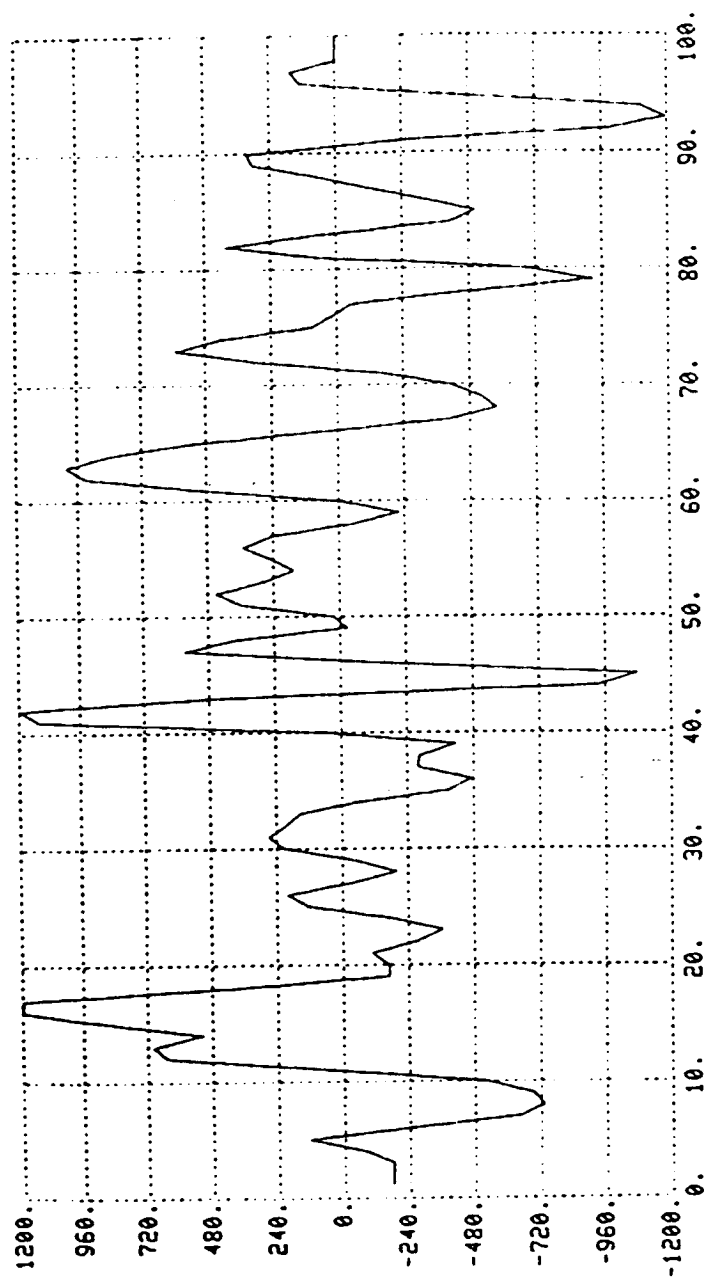


Fig D-11 Differentiated EOG Response-6. Filtered EOG response of Fig D-8 is shown after passing through a 6th order differentiator.



# FIL+DIF+FILTERED DATA

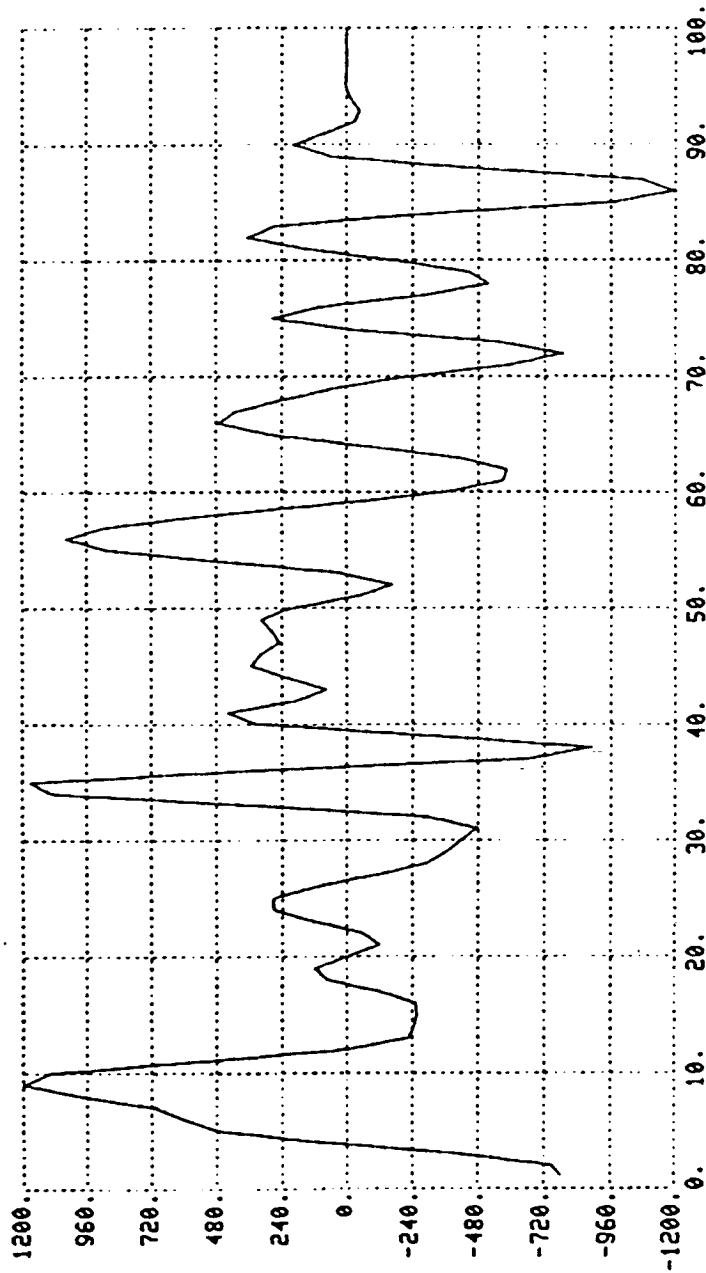


Fig D-12 Refiltered EOG Response. Differentiated EOG response of Fig D-11 is shown after passing through a second 15-point Finite Impulse Response (FIR) digital filter.

```

0001      PROGRAM DFIR
C
0002      INTEGER Z(512),DSKINC,NBLK,IPOSN(16),MAX(16),ICHNUM(16),LENGTH
0003      REAL AMPL, PERIOD, INTRAT, HEOG(1040), XT(1024), COEF(25),
1 YHEOG(1050)
C
0004      EQUIVALENCE (AMPL,Z(150)),(PERIOD,Z(152)),(INTRAT,Z(159)),
1 (DSKINC,Z(167)),(NBLK,Z(172)),(ICHNUM,Z(177)),
2 (IPOSN,Z(225)),(MAX,Z(241))
C
0005      COEF(1) = .0037165603
0006      COEF(2) = .020235427
0007      COEF(3) = .013399956
0008      COEF(4) = -.040643737
0009      COEF(5) = -.066073574
0010      COEF(6) = .061152663
0011      COEF(7) = .30294424
0012      COEF(8) = .43047285
0013      NEH = 8
0014      DO 5 N = 1, 7
0015      COEF(16-N) = COEF(N)
0016      5 CONTINUE
C
0017      INTEGER BUFR2(1024), IERR
0018      BYTE FILNAM(12)
0019      10 DO 20 K=1,12
0020      20 FILNAM(K)=0
0021      TYPE 30
0022      30 FORMAT (' ENTER COMPLETE FILENAME'// ' FILENAME ?',%)
0023      ACCEPT 40,FILNAM
0024      40 FORMAT (12A1)
C
0025      CALL DISKIO(FILNAM,-3,Z,256,0,NDUMMY,IERR)
0026      IF (IERR .NE. 0) TYPE *, ' ERROR CODE',IERR, ' DURING READING'
C
0028      42 TYPE *, ' CHAN NO.'
0029      ACCEPT *,K
0030      45 TYPE *, ' ENTER THE NUMBER OF DATA POINTS FOR EOG'
0031      ACCEPT *,LENGTH
0032      TYPE *, ' DO YOU WANT FILES LEFT OPEN? (1=YES)'
0033      ACCEPT *,LOPEN
C
0034      NWRDS = DSKINC* 256
0035      IBLK = 2
0036      ITEMF = 0
0037      TYPE 50, NBLK, NWRDS, IBLK,DSKINC
0038      50 FORMAT (' NBLK=',I5,' NWRDS=',I5,' IBLK=',I5,' DSKINC=',I5)
0039      TYPE 51,MAX(K),IPOSN(K)
0040      51 FORMAT (' MAX(K) = ',I5,' IPOSN(K) = ',I5)
C
0041      TYPE *, ' DO YOU WANT TO PLOT EVERY POINT? ENTER STEP SIZE!'
0042      ACCEPT *,ISTEP
C
0043      IRMODE=3

```

```
0044      IF (LOPEN .EQ. 1) IRMODE = -3
0046      TYPE *, '    NOW READING FROM DISK'
0047  52    CALL DISKIO(FILNAM,IRMODE,BUFR2,NWRDS,IBLK,NDUMMY,IERR)
0048      IF (IERR .NE. 0) TYPE *, ' ERROR CODE',IERR,' DURING READ'
      C
0050      NPTS = (MAX(K)-IPOSN(K)+1)/ISTEP
0051      DO 57 L = 1,NPTS
0052      HEOG(L+ITEMP) = BUFR2(IPOSN(K) + L*ISTEP)
0053  57    CONTINUE
      C
0054      IBLK = IBLK + DSKINC
0055      ITEMP = ITEMP + NPTS
      C
0056      IF (ITEMP .LT. LENGTH) GO TO 52
0058      XLGT = FLOAT(LENGTH)
      C
0059      DO 60 J = 1,LENGTH
0060      XT(J) = FLOAT(J)
0061  60    CONTINUE
0062      TYPE *, ' SET YMIN!'
0063      ACCEPT *,YMIN
0064      TYPE *, ' SET YMAX!'
0065      ACCEPT *,YMAX
      C
0066      ILFT = 600
0067      IRIT = 3500
0068      IBOT = 1000
0069      ITOP = 2500
0070      XMIN = 0.
0071      XMAX = XLGT
0072      CALL TSXCHK
0073      CALL GRINIT(4014,4631,1)
0074      CALL CHRISZ(3)
0075      CALL ERASE
0076      CALL GRID(10,10,ILFT,IRIT,IBOT,ITOP,97)
0077      CALL ANOTAT(10,10,ILFT,IRIT,IBOT,ITOP,XMIN,XMAX,YMIN,YMAX)
0078      CALL XYPLOT(XT,HEOG,LENGTH,ILFT,IRIT,IBOT,ITOP,XMIN,XMAX,
1 YMIN,YMAX,1,0)
      C
0079      CALL MPLOT(ILFT+500,ITOP+300,-1)
0080      TYPE 61
0081  61    FORMAT(' +RAW DATA ')
      C
0082      TYPE *, ' DO YOU WANT A HARD COPY? (YES=1)'
0083      ACCEPT *,IS
0084      IF (IS .NE. 1) GO TO 62
      C
0086      CALL COPY(0)
      C
0087  62    -NCO = 15
0088      DO 80 I = 2, LENGTH+NCO
0089      SUM = 0.0
0090      DO 70 J = 1,NCO
```

```

0092      IF (J .GE. I) GO TO 70
0094      IF (I-J .GT. LENGTH) GO TO 70
0096      H = COEF(J) * HEOG(I-J)
0097      SUM = SUM + H
0098  70    CONTINUE
0099      YHEOG(I-1) = SUM
0100  80    CONTINUE
        C
0101      J2 = 14
0102      DO 81 J = 15, LENGTH+J2
0103      YHEOG(J-J2) = YHEOG(J)
0104  81    CONTINUE
        C
0105      CALL TSXCHK
0106      CALL GRINIT(4014,4631,1)
0107      CALL CHRSTZ(3)
0108      CALL ERASE
0109      CALL GRID(10,10,ILFT,IRIT,IBOT,ITOP,97)
0110      CALL ANOTAT(10,10,ILFT,IRIT,IBOT,ITOP,XMIN,XMAX,YMIN,YMAX)
0111      CALL XYPLT(XT,YHEOG,LENGTH,ILFT,IRIT,IBOT,ITOP,XMIN,XMAX,
1 YMIN,YMAX,1,0)
        C
0112      CALL MPLT(ILFT+500,ITOP+300,-1)
0113      TYPE 82
0114  82    FORMAT ('+ FILTERED DATA')
0115      TYPE *, ' DO YOU WANT A HARD COPY? (YES=1)'
0116      ACCEPT *,IS
0117      IF (IS .NE. 1) GO TO 83
        C
0119      CALL COPY(0)
        C
0120  83    H = FLOAT(ISTEP)/120.
0121      L = LENGTH
0122      TYPE *, ' SET DESIRED HALF ORDER OF DIFFERENTIATOR:'
0123      ACCEPT *,NDIF
0124      GO TO (84,86,88),NDIF
        C
0125  84    DO 85 I = 2, LENGTH
0126      HEOG(I) = (YHEOG(I+1) - YHEOG(I-1))/(H * 2.)
0127  85    CONTINUE
0128      HEOG(1) = HEOG(2)
0129      HEOG(L) = HEOG(L-1)
0130      GO TO 90
        C
0131  86    DO 87 I = 3, L-2
0132      HEOG(I) = ((YHEOG(I-2) - YHEOG(I+2)) + (8.*(YHEOG(I+1) -
1 YHEOG(I-1))))/(H*12.)
0133  87    CONTINUE
0134      HEOG(1) = HEOG(3)
0135      HEOG(2) = HEOG(3)
0136      HEOG(L) = HEOG(L-2)
0137      HEOG(L-1) = HEOG(L-2)
0138      GO TO 90
        C

```

D18  
N86 - 31427 , 628

MATERIALS CONSIDERATIONS IN THE DESIGN OF A METAL-HYDRIDE HEAT PUMP  
FOR AN ADVANCED EXTRAVEHICULAR MOBILITY UNIT

Bruce E. Liebert  
Associate Professor of Mechanical Engineering  
University of Hawaii  
Honolulu, Hawaii 96822

18829

ABSTRACT

A metal-hydride heat pump (HHP) has been proposed to provide an advanced regenerable nonventing thermal sink for the liquid-cooled garment worn during an extravehicular activity (EVA). The conceptual design indicates that there is a potential for significant advantages over the one presently being used by shuttle crew personnel as well as those that have been proposed for future use with the space station.

Compared to other heat pump designs, a HHP offers the potential for extended use with no electrical power requirements during the EVA. In addition, a reliable, compact design is possible due to the absence of moving parts other than high-reliability check valves.

A review of the relevant physical properties of metal hydrides is presented for heat pump applications. Particular attention is given to the influence of nonidealities of hydrides on the performance of the HHP as well as to the differences in requirements between conventional heat pump applications and those for a space station based extravehicular mobility unit. Thermodynamic cyclic efficiency, comminution, degradation, and heat capacity are all of secondary importance compared to the performance of the HHP during the EVA.

The rare-earth hydrides have shown particular promise for this application since they have a high hydrogen-to-metal ratio, are capable of rapidly and reversibly absorbing and desorbing hydrogen over a range of temperatures with very little overpressure, and their properties can be varied almost at will by proper alloy design.

Because there are many subtleties in the properties of metal hydrides for heat pump applications, it is essential that a prototype hydride heat pump be constructed with the selected materials before a commitment is made for the final design. Particular care must be given to the evaporator heat exchanger worn by the astronaut since the performance of hydride heat pumps is generally heat transfer limited.

---

NASA Colleague: Chin H. Lin, Ph.D. EC2 X4941

Water decomposed into its primitive elements, and decomposed doubtless by electricity, which will then have become a powerful and manageable force... Yes, my friends, I believe that water will one day be employed as fuel, that hydrogen and oxygen, which constitute it, used singly or together, will furnish an inexhaustible source of heat\* and light of an intensity, of which coal is not capable -Jules Verne, The Mysterious Island.  
\* or cooling!

## INTRODUCTION

A metal hydride chemical heat pump (hereafter referred to as the hydride heat pump or HHP) has been proposed as a device to maintain the comfort of crewmembers during an Extravehicular Activity (EVA) for the space station missions [Lin, 1985a]. Presently, water is sublimated in the Portable Life Support System, or PLSS, (see Fig. 1) to maintain an acceptable Liquid Cooling and Ventilating Garment (LCVG) temperature for shuttle crewmembers during an EVA. Fig. 2 shows a schematic of the thermal control section of the PLSS.

For space station missions, however, this solution is unacceptable for at least two reasons. First, water is too valuable a commodity to use since both the expected duration of an EVA (8 hours) and frequency necessary for assembly and maintenance of the space station would result in the loss of unacceptably large amounts of nonrecoverable water over a period of several months. Second, even if sufficient water was transported to the space station, many experiments planned for the space station need as pristine an environment as possible; therefore, contaminants due to sublimating water, for example, are unacceptable.

A brief discussion of conventional and hydride heat pumps is presented and the differences between HHPs for earth- and space-bound applications are described. The physical properties of metal hydrides that are relevant to this application numbers in parenthesis refer to notes in Section 5.3

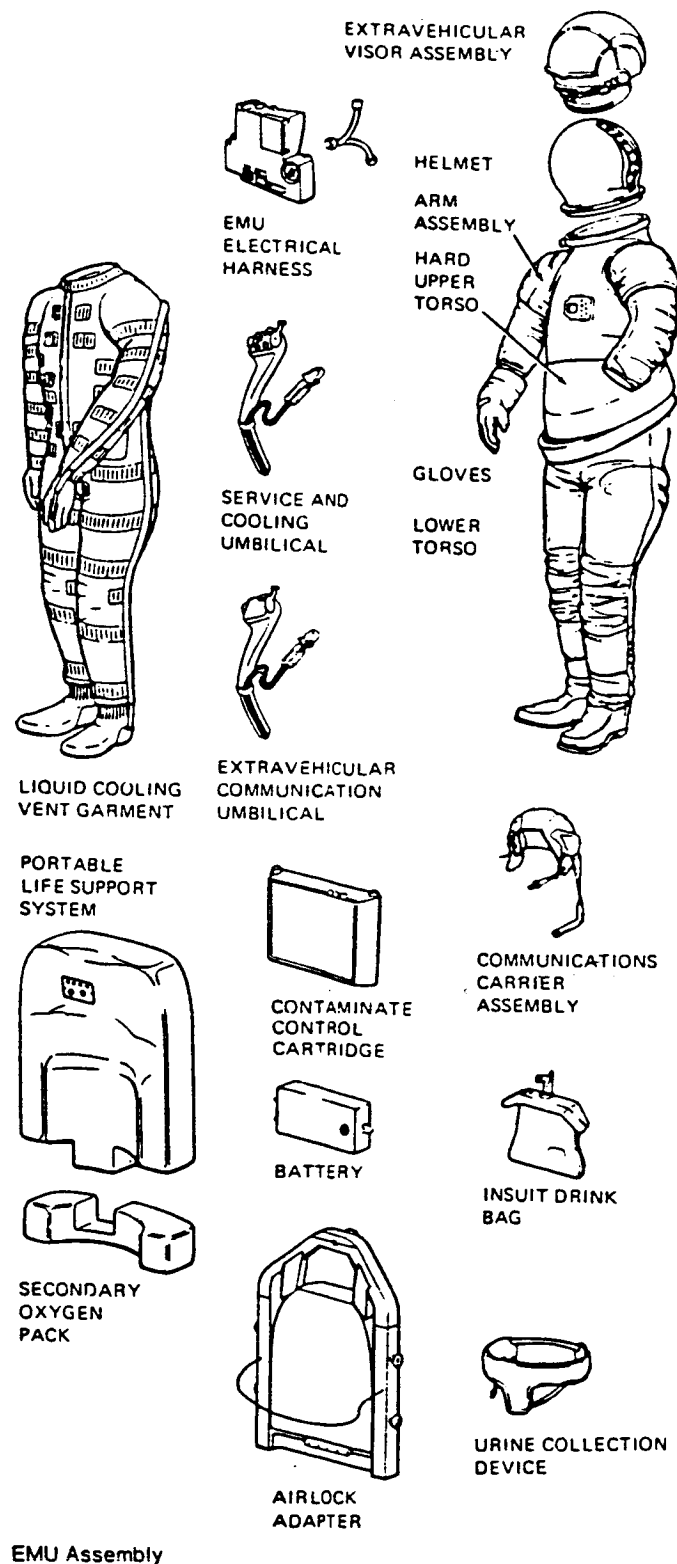


Fig. 1. The components of the Extravehicular Mobility Unit (EMU). The Portable Life Support System (PLSS) presently contains water that is sublimated to absorb the waste heat from the Liquid Cooling and Ventilating Garment (LCVG). The proposed hydride heat pump would be contained within the PLSS and radiate the waste heat to a backpack-mounted space radiator [NASA Facts].

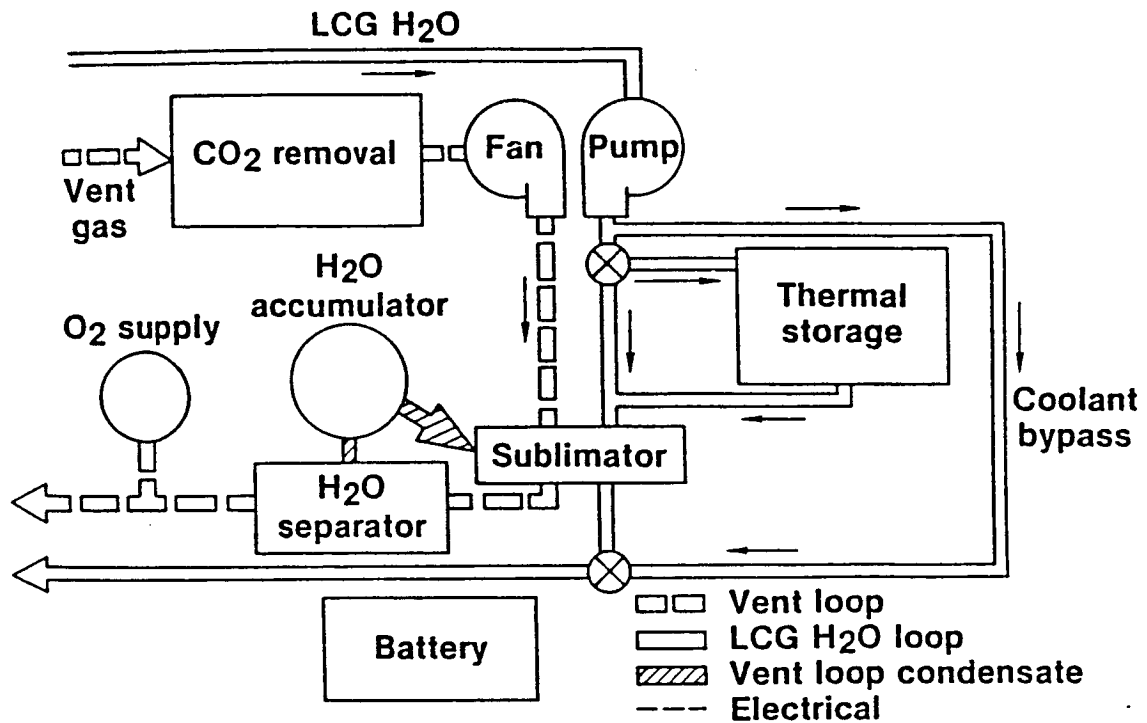


Fig. 2. A schematic of the present shuttle EVA Regenerable Nonventing Thermal Sink (RNTS). The thermal requirements of the proposed space station RNTS preclude the use of ice as a thermal storage medium. Therefore, a more advanced design, such as a hydride heat pump, is required [Hodgson and Dresser, 1982].

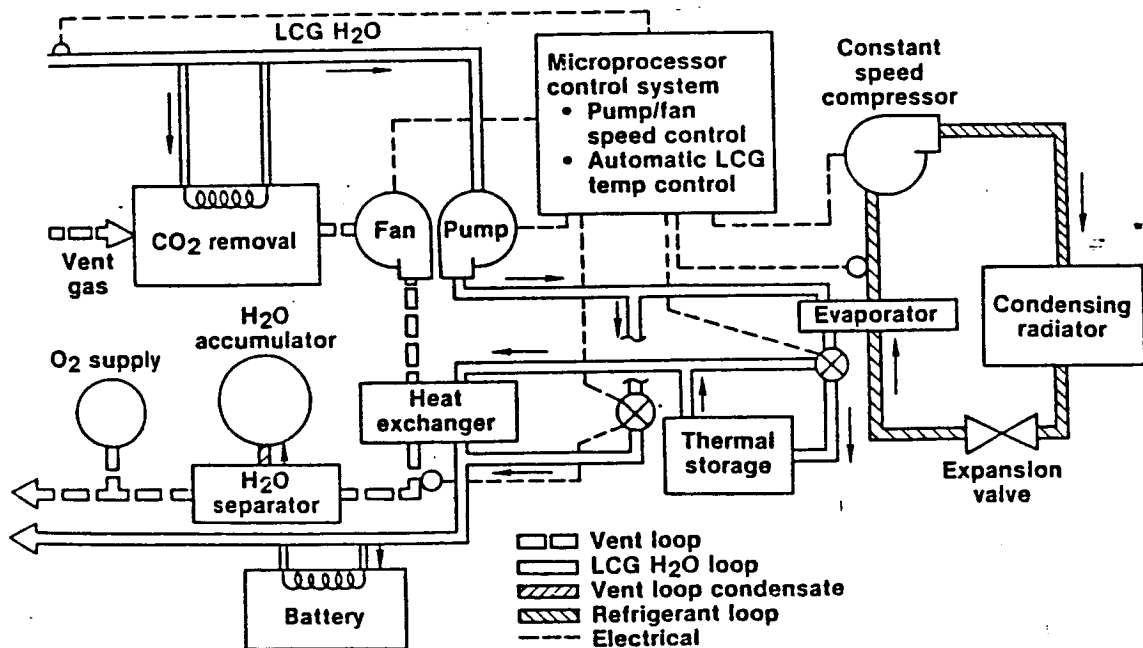


Fig. 3. A proposed alternate RNTS schematic to provide sufficient cooling for the space-station mission. Cooling is provided by compressing a working fluid and radiating the waste heat to space via a backpack-mounted space radiator [Hodgson and Dresser, 1982]. There is some question as to the ability of the batteries to supply sufficient energy during an eight-hour EVA [Lin, 1985a].



are reviewed, with special emphasis on the nonidealities of hydrides that can affect the performance during an EVA. A comparison of heat-pump cycles is made for a number of hydride pairs and recommendations are suggested that will assist in the evaluation of materials with unique properties.

### 1.1 Conventional Heat Pumps

Other systems employing mechanical and thermoelectric heat pumps have been proposed for LCV6 cooling [Hodgson and Dresser, 1982]. As can be seen in Fig. 3, these designs are rather complex and involve numerous components with moving parts (e.g., a compressor) that require substantial amounts of electrical energy during the EVA. It is not clear that present state-of-the-art batteries are capable of supplying sufficient electrical energy to meet the mission goals.

A heat pump based on metal hydrides offers the potential for considerable simplicity, over other design, due to the absence of moving parts coupled with the ability to operate without electrical energy during the EVA.

### 1.2 Hydride Heat Pumps

Heat pumps for temperature upgrading using the thermodynamic properties of metal hydrides were first proposed by Terry in 1972. There have been a number of papers (e.g. Sheft et al., 1980) describing the use of hydrides as chemical heat pumps for such applications as heating and cooling residential and industrial buildings since that time; however, all of these have considered cyclic efficiency, rate, and cost to be of primary importance.

The use of hydrides to provide cooling during an EVA has considerably different constraints from conventional applications; thus many HHP criteria described in

the literature are not particularly applicable for this purpose. For example, the thermodynamic efficiency during the EVA is of primary concern; post-EVA recharging can accept considerable inefficiencies due to the excess energy available on a space station compared to what can be carried on an extravehicular mobility unit. Therefore, the coefficient of performance (COP) of the HHP is only of secondary importance.

The operation of the HHP is conceptually quite simple. As shown in Fig. 4a, 72°F water from the liquid-cooled ventilating garment is circulated through a high-pressure hydride (#1) evaporator resulting in hydrogen desorption and absorption of heat [1]. Hydrogen flows through a hydride filter, an on/off valve, a pressure-regulating one-way check valve [2], and into a low-pressure hydride (#2) condenser where it is absorbed. The exothermic heat of formation is discharged to open space via a backpack-mounted radiator at a temperature above 100°F, which is the minimum temperature that can be radiated to space using the 10.5 ft<sup>2</sup> available on the backpack.

When all the useful capacity of hydride #1 has been exhausted, the valve is closed and the EVA must terminate to avoid excessive LCVG water temperatures.

To recharge the HHP after the EVA, heat from some source (electrical or solar) is applied to hydride #2 to desorb the hydrogen previously absorbed during the EVA. As shown in Fig. 4b, the valve is opened allowing the hydrogen to be absorbed by hydride #1, which is maintained at 80°F by the space station's thermal management system.

When all of the hydrogen in hydride #2 has been desorbed, the valve is closed and the HHP is available for another EVA [3].

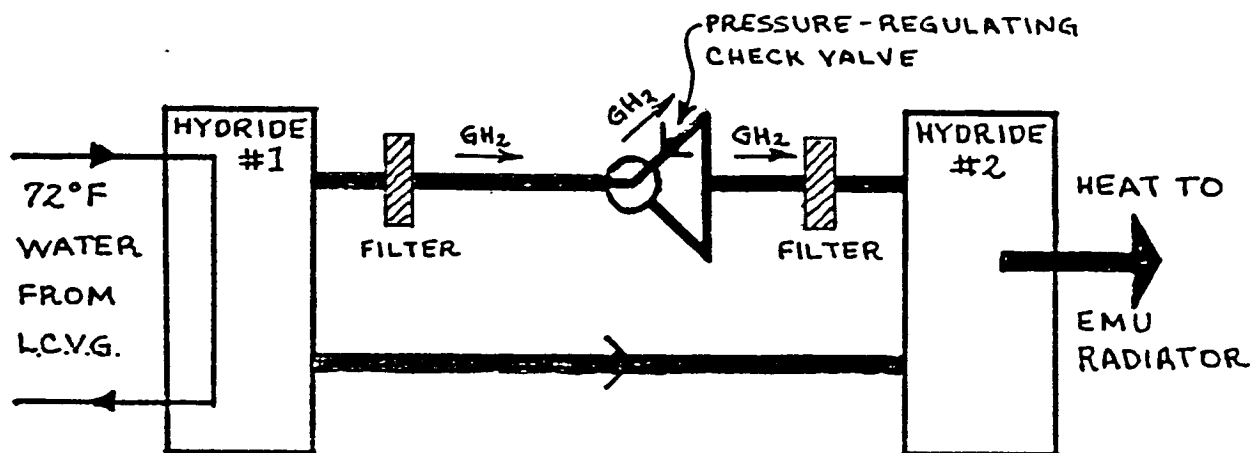


Fig. 4a. Conceptual design of a chemical hydride heat pump operating during an EVA. When the valve is opened, heat from the LCVG water desorbs hydrogen in the evaporator resulting in the absorption of heat. Subsequent absorption of hydrogen releases heat to the space radiator.

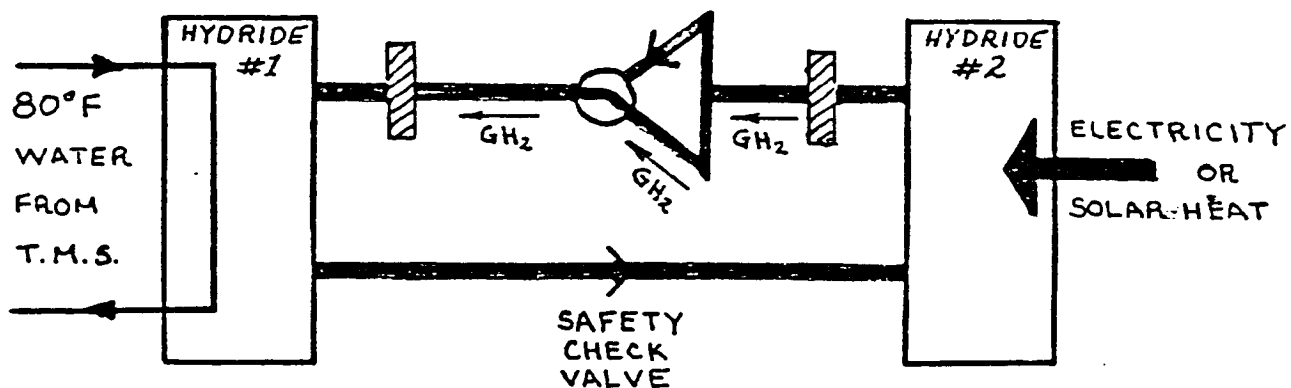


Fig. 4b. Chemical hydride heat pump being recharged post EVA. The valve is opened and heat is applied to the evaporator desorbing hydrogen into the condenser, which is connected to the space station's thermal management system.

## THEORY

### 2.1 Physical Properties of the Metal Hydrides

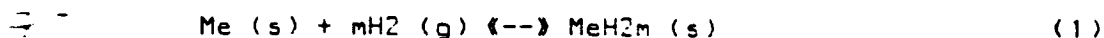
#### 2.1.1 Hydrogen Storage Capacity

Perhaps the most unusual property of the metallic hydrides is their ability to absorb remarkably large quantities of hydrogen per unit volume. In fact, many of these hydrides can contain more hydrogen than an equivalent volume of either liquid or solid hydrogen. Table 1 shows the hydrogen storage capacity and energy density of a number of hydrides as well as for liquid and gaseous hydrogen. All of the metal hydrides have a higher hydrogen-storage capacity than an equal volume of liquid or gaseous (at 100 atm.) hydrogen. It has also been found that the capacity is affected by subtle metallurgical factors during alloy preparation [Sandrock and Huston, 1981].

Although the metal hydrides do not have a particularly high storage density in terms of weight, heavy-walled pressure vessels are not required to contain the hydrogen, thus eliminating the container as a major component in terms of weight.

#### 2.1.2 van't Hoff Constants

If all hydrides can be considered as pseudo-binary systems in the presence of hydrogen, then for two-phase equilibria the well-known van't Hoff equation [e.g., Huston and Sandrock, 1980] describes the variation in the equilibrium hydrogen pressure ( $P_{H_2}$ ) for the reaction:



where Me is the alloy to be hydrided. The van't Hoff equation can be written

TABLE 1

## Comparison of Hydrogen Storage Media

Medium	Maximum Effective H Storage Capacity		Energy Density Heat of Combustion <sup>a</sup> (higher)	
	by wt %	by vol, g/ml	cal/g	cal/ml of vol
MgH <sub>2</sub> <sup>b</sup>	7.0	0.101	2373	3423
Mg <sub>2</sub> NiH <sub>4</sub>	3.16	0.081	1071	2745
VH <sub>2</sub>	2.07		701	
FeTiH <sub>1.95</sub>	1.75	0.096	593	3245
TiFe <sub>.7</sub> Mn <sub>.2</sub> H <sub>1.9</sub>	1.72	~0.09	583	~3050
LaNi <sub>5</sub> H <sub>7.0</sub>	1.37	0.089	464	3051
R.E.Ni <sub>5</sub> H <sub>6.5</sub> <sup>c</sup>	1.35	~0.09	458	~3050
Liquid H <sub>2</sub>	100	0.07	33900	2373
Gaseous H <sub>2</sub> (100 atm. press)	100	0.007	33900	244
N-Octane			11400	8020

<sup>a</sup> Refers to H only in metal hydrides.

<sup>b</sup> Starting alloy 94% Mg 6% Ni.

<sup>c</sup> R. E. refers to mischmetal, a commercial rare earth alloy.

taken from Reilly, 1978b

$$\ln(PH_2) = - dS^*/mR + dH^*/mRT \quad (2)$$

where  $dS^*$  and  $dH^*$  are the standard entropy and enthalpy of formation and  $R$  and  $T$  have their usual meanings. The change in entropy is almost completely determined by the transition of hydrogen from the gaseous to the solid phase and therefore is nearly the same for all hydrides--about  $-30 \pm 6$  cal/mol. Thus  $dH^*$  primarily determines the plateau pressure. An absorption enthalpy of  $-9$  kcal/mol results in a 1 atm plateau pressure at room temperature [Cohen and Wernick, 1981].

The chemical potential of hydrogen, represented here by the two-phase equilibrium (or plateau) pressure, must be the same in both phases; therefore, Eqn. (2) gives the temperature variation of the two-phase plateau pressure.

It has been shown that, for the case of a conventional heat-pump cycle that operates at three temperature levels (low, medium, and high), the lowest temperature (for fixed medium and high temperatures) is attained if  $dS^*(\text{hydride \#1}) = dS^*(\text{hydride \#2})$  and the least effective heat pump operation occurs when  $dH^*(\text{hydride \#1}) = dH^*(\text{hydride \#2})$ ; however, the difference between the best and worst cases is only of the order of 10 percent [Gruen et al., 1978].

Since the proposed thermal cycle for this application involves four temperature levels:

	<u>Hydride #1</u>	<u>Hydride #2</u>
T <sub>low</sub> :	about 40°F (LCVG)	radiator temperature >100°F
T <sub>high</sub> :	about 80°F (TMS)	recharging temperature

the three-temperature-level criteria are not necessarily applicable. (40°F is a good design temperature to keep the water from the LCVG sufficiently cool and above the freezing point and 80°F is available from the space-station's thermal management system. The radiator's temperature must be above 100°F to keep the area of the backpack radiator less than 10.5 ft<sup>2</sup> and the recharging temperature should be kept as low as possible to avoid safety and power problems from excessively high temperatures [Lin, 1985b].)

Eqn. 2 can be simplified to:

$$\ln(PH_2) = A/T + B \quad (3)$$

where A and B are temperature-independent constants [Huston and Sandrock, 1980]. Table 2 gives these constants for a number of commercially available hydrides and Fig. 5 shows the corresponding van't Hoff plots. It is clear from Fig. 5 that hydrides with larger slopes (enthalpies of formation) have lower plateau pressures.

These "constants" have been determined for desorption conditions as close to equilibrium as possible. It has been reported that the "apparent reaction enthalpy" measured during dynamic tests is lower for absorption and higher for desorption compared to results obtained under static conditions. This was attributed to strain and interfacial energies [Goodell et al., 1980]. These differences, of course, can affect the selection of hydrides for specific operating pressures and temperatures.

TABLE 2

van't Hoff and Hysteresis Constants for Selected Hydrides

HY-STOR alloy	Nominal composition	$\Delta H$ (kcal (mol H <sub>2</sub> ) <sup>-1</sup> )	A (K)	B	$P_d^a$ (atm)	$P_a^a$ (atm)	$P_a/P_d$	$\ln(P_a/P_d)$
101	FeTi	-6.7	-3383	12.76	5.3 <sup>b</sup>	10.0	1.89	0.64
102	Fe <sub>0.9</sub> Mn <sub>0.1</sub> Ti	-7.0	-3545	12.87	4.7 <sup>c</sup>	8.7	1.85	0.62
103	Fe <sub>0.8</sub> Ni <sub>0.2</sub> Ti	-9.8	-4952	14.29	0.87 <sup>d</sup>	0.91	1.05	0.05
201	CaNi <sub>5</sub>	-7.6	-3838	12.17	0.47	0.55	1.17	0.16
202	Ca <sub>0.7</sub> Mo <sub>0.3</sub> Ni <sub>5</sub>	-6.4	-3204	12.08	3.8	4.2	1.11	0.10
203	Ca <sub>0.2</sub> Mo <sub>0.8</sub> Ni <sub>5</sub>	-5.8	-2923	13.08	25.0	37.0	1.48	0.39
204	MNi <sub>5</sub> <sup>a</sup>	-5.0	-2539	11.64	23.0	~120	5.2	1.65
205	LaNi <sub>5</sub>	-7.4	-3712	12.96	1.65	2.0	1.21	0.19
207	LaNi <sub>4.7</sub> Al <sub>0.3</sub>	-8.1	-4090	12.84	0.42	0.44	1.05	0.05
208	MNi <sub>4.5</sub> Al <sub>0.5</sub>	-6.7	-3366	12.61	3.8	4.25	1.12	0.11
209	MNi <sub>4.15</sub> Fe <sub>0.85</sub>	-6.0	-3041	12.60	11.0	13.0	1.18	0.17
301 <sup>e</sup>	Mg <sub>2</sub> Ni	-15.4	-7736	14.71	-	-	-	-
302	Mg <sub>2</sub> Cu	-17.4	-8771	17.12	-	-	-	-
-	Mg	-18.5	-9314	16.63	-	-	-	-

<sup>a</sup>These data were obtained using a hydrogen-to-metal ratio (H/M) of 0.5 at 25 °C.<sup>b</sup>These data were obtained using H/M = 0.5 at 30 °C.<sup>c</sup>These data were obtained using H/M = 0.5 at 40 °C.<sup>d</sup>These data were obtained using H/M = 0.3 at 70 °C.<sup>e</sup>HY-STOR 301 is a two-phase mixture of Mg<sub>2</sub>Ni and magnesium. The actual composition is Mg<sub>2.4</sub>Ni.

taken from Huston and Sandrock, 1980



ORIGINAL PAGE IS  
OF POOR QUALITY

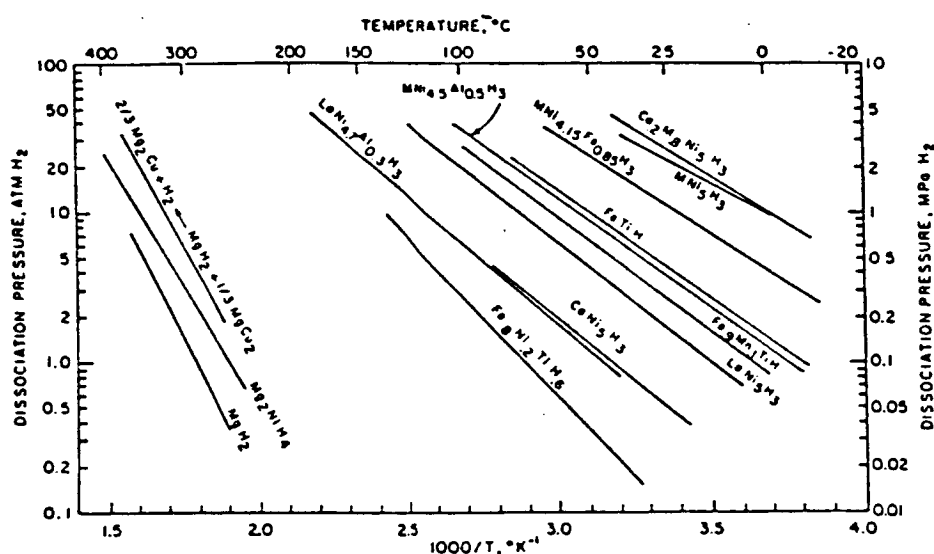


Fig. 5. van't Hoff desorption plots for selected hydrides. The corresponding absorption plots would be displaced upwards. In addition, since the slope of the pressure-composition isotherm is nonzero, these lines have a finite width that varies with each alloy as well as with temperature [Huston and Sandrock, 1980]

### 2.1.3 Chemical Diffusivity

The reaction between hydrogen and the metal hydride occurs at the surface and the resulting concentration gradient changes the composition in one (or both) of two ways. Hydrogen may diffuse into a solid solution (in which the composition of the material changes continuously with depth) or a new phase may nucleate and grow. Most commercially available hydrides form new phases, which results in a relatively constant equilibrium hydrogen pressure over a considerable hydrogen-to-metal (H/M) compositional range.

The reaction rate may be limited by interfacial and/or diffusion reactions, in addition to heat transfer. In the case of LaNi<sub>5</sub>-based devices where heat transfer limitations have been eliminated by careful design, it has been found that the hydriding rate is under the mixed control of a surface and a bulk process. The bulk process, attributed to diffusion, tends to become rate limiting at low temperatures and at high pressures. Dehydriding appears to be rate limited by a surface process [Goodell and Rudman, 1983].

For hydrides in which hydrogen sorption is limited by diffusion, rather than by interfacial reactions or heat transfer, the chemical diffusion coefficient,  $D$ , determines the rate of hydrogen sorption. The diffusion coefficient follows the well-known Arrhenius Rate Law:

$$D = D_0 \cdot \exp(-Q/RT) \quad (4)$$

where  $D_0$  is a constant and  $Q$  is the activation enthalpy for diffusion. It is, therefore, advantageous to operate these materials at a sufficiently high temperature to ensure that the diffusion coefficient does not seriously limit the rate of hydrogen sorption.

Fig. 6 shows the temperature dependence of the (tracer) diffusion coefficient of hydrogen in LaNi<sub>5</sub> and FeTi, as well as for a number of elemental metals. The diffusion coefficient of hydrogen in LaNi<sub>5</sub> is about two orders of magnitude greater than in FeTi. The chemical diffusion coefficient, which determines the rate of chemical equilibrium, may be considerably larger than the intrinsic or tracer diffusion coefficient due to the thermodynamic factor [Weppner and Huggins, 1978].

In most cases, the diffusion coefficient is not the rate-determining step. The particle size of the hydrides after a number of cycles is very small (of the order of 1  $\mu$ m [Jones and Golben, 1985]) due to a large (10 to 25 percent) volume increase upon hydrogen absorption. Therefore, not only are diffusion distances extremely short, the rate of chemical equilibration is very fast since the time for chemical equilibrium is roughly proportional to the square of the diffusion distance.

In any case, quantitative information regarding the kinetics of hydrogen equilibration in most of these materials is either not available in the open literature or the measurements have been made with such a wide variety of methods that it is difficult to rank one material with another [Goodell and Rudman, 1983]. Because the kinetics are very sensitive to material preparation, gas purity, system design, etc., it is questionable whether any of the reported measures of kinetics are reliable [Rudman, 1983].

Nuclear magnetic resonance, decomposition kinetics, inelastic neutron scattering, magnetic after-effects, etc. have all been used to obtain an estimate of the diffusion coefficient. Unfortunately, in many cases measurements of the diffusion coefficient on the same alloy are in substantial

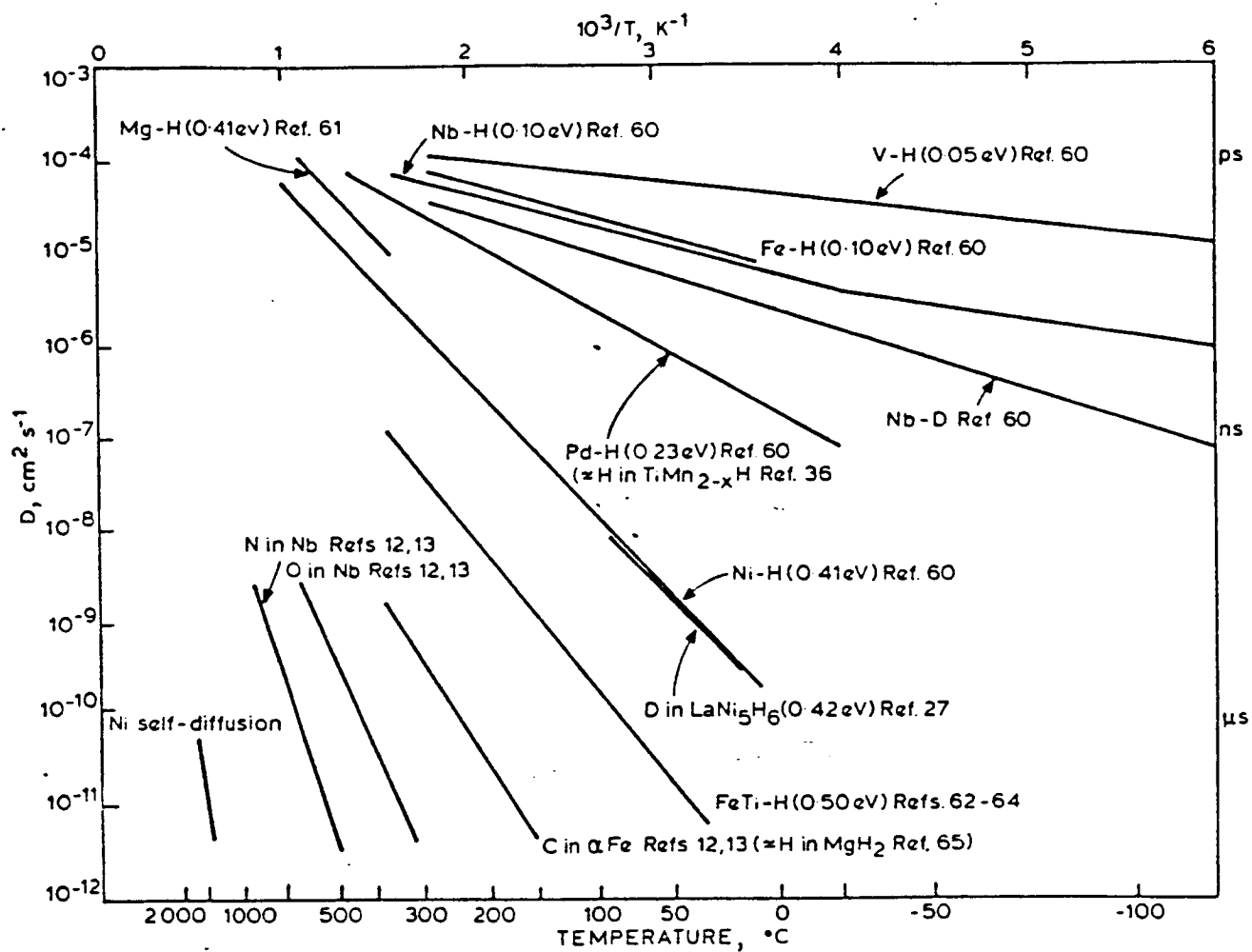


Fig. 6. Tracer diffusion coefficients of hydrogen as a function of temperature for  $\text{LaNi}_5$  and  $\text{FeTi}$  hydrides as well as for a number of elemental metals. The slopes of each line are related to the activation enthalpy for diffusion [Wenzl, 1982].

disagreement. For example, the diffusion coefficient of hydrogen in  $\text{LaNi}_5$  at 300 K was reported to be  $1.4 \text{ E-}8$  and  $4.0 \text{ E-}18 \text{ cm}^2/\text{sec}$ , a difference of more than 10 orders of magnitude [Buschow et al., 1982]. Clearly, there is a need for reliable data on diffusion or transformation rates for these materials.

#### 2.1.4 Thermal Conductivity

In most cases, heat transfer limits the rate of hydrogen sorption in hydrides for hydride containers greater than a few inches in diameter due to the low thermal conductivity for the powdered hydride. However, by proper design of the container, it is possible to make the chemical kinetics, rather than heat transfer, the rate-determining step [Rosso, 1985b].

Although the constituent metals that comprise the alloy generally have excellent thermal conductivities ( $10\text{-}100 \text{ W/m/K}$ ), the bulk thermal conductivity of a hydrided powder is quite low (about  $1 \text{ W/m/K}$ ) [Wenzl, 1982]. The effective thermal conductivity depends on particle size, packing, void space, etc.; therefore, it is essential to design the container to optimize heat transfer.

In the past, heat transfer has been improved by incorporating the hydrided powder in an expanded metal foam such as Duocell [Gorman and Moritz, 1979]. Roughly 95 percent of the foam volume is empty allowing easy access to hydrogen gas but still permitting the high thermal conductivity aluminum (for example) foam to be in direct thermal contact with a substantial fraction of the hydride powder. This could be particularly important for this application since the zero-g environment will tend to result in less packing and thus less thermal contact with the heat exchanger.

Another method used to improve the thermal conductivity of the hydride bed has been to mix the hydride with hydrogen-inert metals, such as copper and aluminum powders [Tuscher and Weinzierl, 1983]. Clearly, any heat pump must be designed to optimize the rate of heat transfer between the heat exchanger and the hydride.

#### 2.1.5 Heat Capacity

The heat capacity of some selected hydrides is given in Table 3. Unlike conventional heat pumps where the HHP's heat capacity must be minimized to permit rapid recycling, the heat capacity of the system for this application is only of secondary importance. A high heat capacity would require more thermal input to raise the sensible heat of system; thus, ideally the overall heat capacity should be minimized.

### 2.2 Nonidealities of Hydrides

#### 2.2.1 Solid Solutions vs. Multi-phases

For simple hydrogen storage applications it may be irrelevant whether a single phase solid solution is formed during hydriding or whether a new phase nucleates and grows. As shown in Fig. 7, if the temperature is greater than  $T_c$ , a solid solution is formed; the hydrogen pressure increases with hydrogen content. Below  $T_c$ , however, a two-phase mixture (indicated by a constant hydrogen pressure) is stable over a range of composition that depends on temperature.

For heat pump applications, however, since a flat plateau pressure is a desirable property, two (or more) phase alloys are required. Many hydride isotherms have an appreciable slope indicating that there is either an extensive range of solid solubility or there are too few phases for the number

TABLE 3

Plateau Slopes, Usable Capacity, and Heat Capacity for Selected Hydrides

HY-STOR alloy	Plateau slope <sup>a</sup> $d(\ln P_d)/d(H/M)$	Usable capacity <sup>b</sup>		Heat capacity (cal g <sup>-1</sup> °C <sup>-1</sup> )
		$\Delta(H/M)$	(wt.%)	
101	0.00 <sup>c</sup>	0.90 <sup>c</sup>	1.75	0.13
102	0.65 <sup>d</sup>	0.92 <sup>d</sup>	1.79	0.13
103	0.36 <sup>e</sup>	0.62 <sup>e</sup>	1.21	0.12
201	0.19	0.71	1.39	0.13
202	3.27	0.96	1.60	0.12
203	0.98	0.74	1.08	0.105
204	0.54	1.01	1.41	0.10
205	0.09	1.02	1.43	0.10
206 <sup>h</sup>	0.32	0.91	1.27	0.095
207	0.48	0.95	1.36	0.10
208	0.36	0.83	1.20	0.10
209	0.43	0.82	1.15	—
301 <sup>f</sup>	0.02 <sup>f</sup>	1.31 <sup>f</sup>	3.84	0.18
302	0.17 <sup>g</sup>	0.75 <sup>g</sup>	2.04	0.18

<sup>a</sup>The data refer to the principal plateau at 25 °C.<sup>b</sup>The capacity between 0.1P<sub>d</sub> and 10P<sub>d</sub>.<sup>c</sup>The measurement was obtained at 30 °C.<sup>d</sup>The measurement was obtained at 40 °C.<sup>e</sup>The measurement was obtained at 70 °C.<sup>f</sup>The measurement was obtained at 298 °C for Mg<sub>2.4</sub>Ni.<sup>g</sup>The measurement was obtained at 324 °C.<sup>h</sup>206 is MNi<sub>5</sub> where M is cerium-free mischmetal.

taken from Huston and Sandrock, 1980.

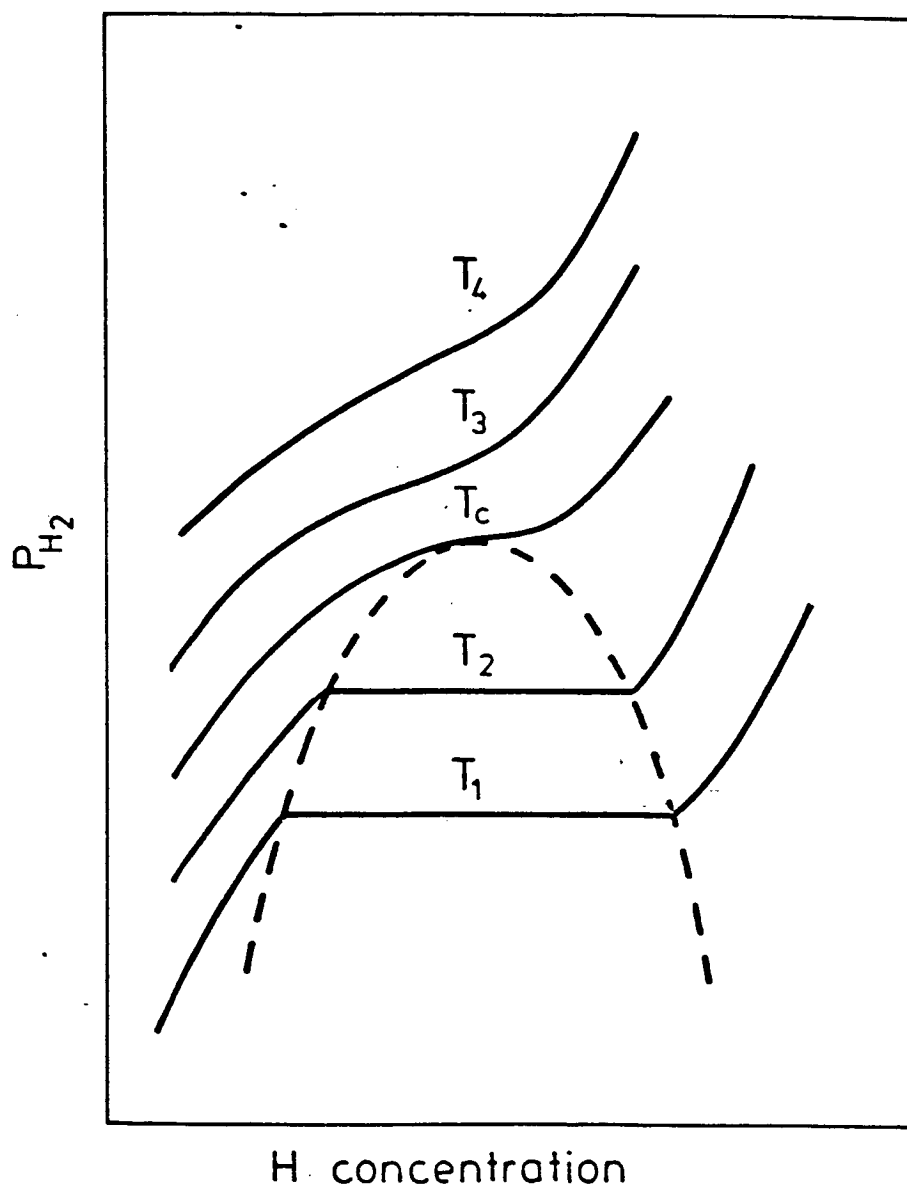


Fig. 7. Schematic representation of pressure-composition isotherms of metal-hydrogen systems. At temperatures below a critical temperature  $T_c$ , two phases are stable over a range of composition that varies with temperature. For temperatures above  $T_c$ , a solid solution is formed over the entire compositional range shown [Buschow and Miedema, 1978].



of components to maintain a constant pressure at the given temperature. Since hysteresis is absent in pure solid solutions, materials with sloping isotherms may be expected to have minimal hysteresis. This has been shown to be the case in the TiFe-Mn system [Reilly, 1976].

The plateau slope for the desorbing high-pressure hydride as well as for the absorbing low-pressure hydride should be minimized for this application. It is only of secondary importance that hysteresis effects be minimized. Therefore, solid-solution hydrides are not desirable for this application.

### 2.2.2 Hysteresis

For most hydrides, the absorption and desorption plateau pressures are different, in some cases by more than 100 atm. [Snape and Lynch, 1980]. The hysteresis effect is given by

$$(P_{des}/P_{abs})_c$$

where  $P_{des}$  and  $P_{abs}$  are the "equilibrium" plateau pressures for dehydriding (desorption) and hydriding (absorption) at a given concentration,  $c$ . The magnitude of the hysteresis of a number of hydrides is given in Table 2.

The hysteresis effect of hydrogen in FeTi is shown in Fig. 8. A considerably greater equilibrium pressure is found for absorption than for desorption. In the two-phase region, the equilibrium desorption pressure is about 7.5 atm, whereas the equilibrium absorption pressure is about twice as high.

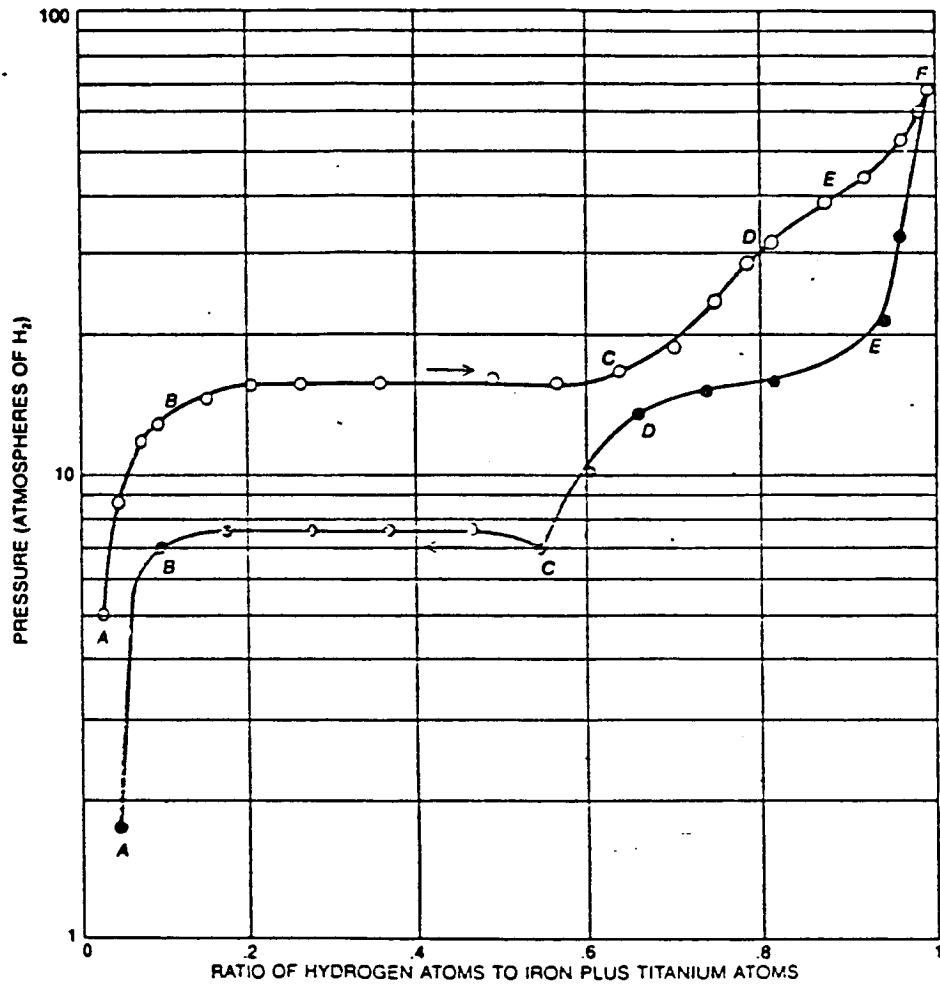


Fig. 8. The hysteresis effect in the FeTi-Hydrogen system. When hydrogen is added to FeTi at a constant temperature, the upper curve is followed. When hydrogen is desorbed at the same temperature, the lower curve results. This is believed to be due to lattice strains and results in thermodynamic inefficiencies [Reilly and Sandrock, 1980].

Hysteresis has been reported to both increase [Gruen et al., 1978] and decrease [Lynch et al., 1984] with increasing temperature. This has been attributed to internal stresses associated with large volume changes during hydriding and dehydriding. Dislocation densities of the order of  $10^{12}$  per  $\text{cm}^3$  are introduced as  $\alpha\text{-LaNi}_5\text{x}$  transforms to  $\beta\text{-LaNi}_5\text{Hy}$  at increasing H/M ratios [Flanagan et al., 1980]. In addition, the magnitude of the hysteresis can be a function of sorption rate [Tuscher and Weinzierl, 1983] and composition, as for the case of  $\text{Ca}_{0.2}\text{M}_{0.8}\text{Ni}_5$  at room temperature, which has a sloping desorption isotherm but a relatively flat absorption isotherm [Huston and Sandrock, 1980].

Hysteresis, therefore, results in a reduction in the overall thermodynamic efficiency of the HHP. Since excess power will be available on the space station, the loss in efficiency during recharging is insignificant--it is only the loss in efficiency (half the total loss) during the EVA that is of consequence.

### 2.2.3 Plateau Slope

According to Gibbs Phase Rule, for a binary (two component system) with two-phase equilibria, the pressure must be constant at any given temperature and independent of the amount of each phase that is present. Since the pressure of most plateaus is not independent of hydrogen concentration (percentage of phases), equilibrium is not established. This is believed to be due to inhomogeneities in the overall chemical composition as well as lattice strains generated during sorption. The plateau slope is defined by

$$\ln(P_{0C1}/P_{0C2})/(C1-C2)$$

where  $P_{0C1}$  and  $P_{0C2}$  are the equilibrium hydrogen pressures at concentration  $C1$

and  $\text{CO}_2$ , respectively. Table 3 lists the plateau slopes for a number of hydride materials.

Fig. 9 shows the effect on the plateau slope of aluminum additions to a mischmetal-nickel hydride. At low concentrations of aluminum, the slope is very low; however, as nickel is replaced by more and more aluminum, the slope increases significantly.

The effect of an isotherm that exhibits a pressure variation with hydrogen concentration is a reduction in the overall thermodynamic efficiency proportional to the magnitude of the slope; however, the slope can be reduced considerably by suitable heat treatment of the as-prepared alloy [Huston and Sandrock, 1980; Wenzl, 1982]. It is important to note that the desorption slope may be different from the one for absorption; the absorption slope is larger than for desorption in some alloys [Lynch et al., 1984].

For this specific application, it is the desorption slope of the high-pressure hydride and the absorption slope of the low-pressure hydride that is of greatest importance since those respective slopes affect the efficiency during the EVA. Recharging a HHP (after the EVA) that contains hydrides with large plateau slopes would require higher evaporator temperatures but would not otherwise effect the performance.

#### 2.2.4 Pressure Requirements for Finite Reaction Rates

Since almost all pressure-composition-temperature (PCT) plots are published for equilibrium or pseudo-equilibrium conditions [4], all materials must be supplied with a hydrogen pressure either above the absorption or below the desorption isotherm to achieve a finite rate of reaction. Clearly, the faster

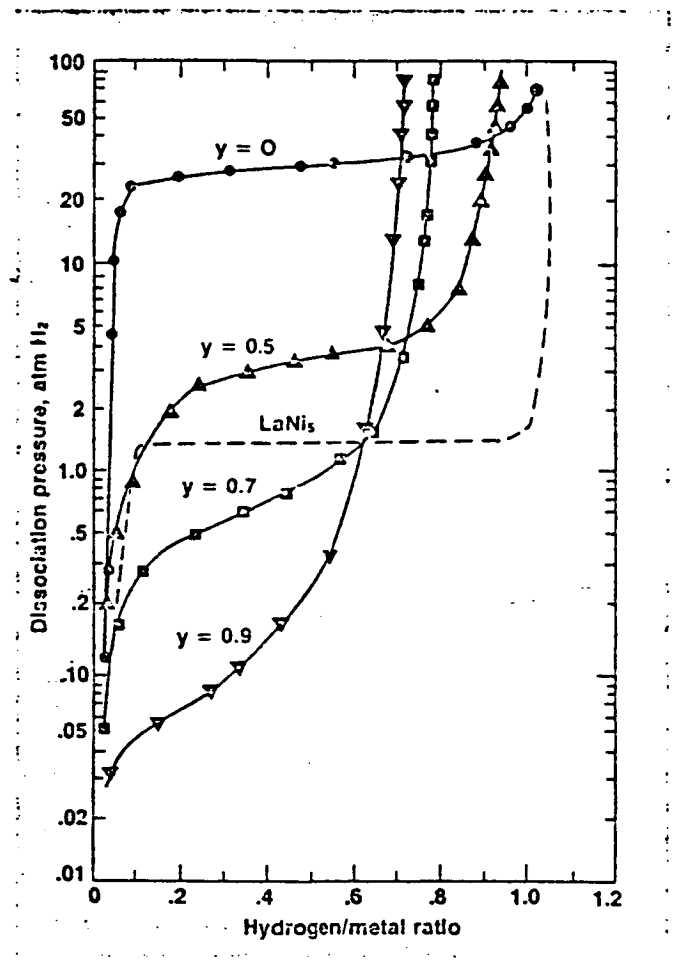


Fig. 9. The effect of aluminum substitution for nickel on the plateau slope for a mischmetal-nickel alloy. At sufficiently high aluminum concentrations, the plateau slope would be too large to use the hydride in a heat pump [Sandrock and Huston, 1981].

the desired rate the greater the difference from the equilibrium plateau pressure required. For example, according to Goodell et al., 1980, the absorption plateau of  $\text{LaNi}_5$  increased by 15 percent for a continuous charging rate of 0.02 H/M atoms per minute [5]; however, the differences between static and dynamic results did not change even at rates estimated to be days in duration.

The magnitude of the overpressure required for absorption and the underpressure for desorption may be of the order of 10 percent for the  $\text{LaNi}_5$  alloys in order to achieve fast enough kinetics for most applications [Rosso, 1985b]. A considerably greater difference is to be expected for the  $\text{FeTi}$  alloys [Reilly, 1985]. The differences between these two materials is clearly shown in Fig. 10. The difference between the static and dynamic behavior becomes less at higher temperatures, approaching zero at temperatures near 100°C [Anevi et al., 1984]. They suggested that "Particular caution is advisable in using enthalpy and entropy data from equilibrium experiments to predict the performance of essentially dynamic devices such as hydride heat pumps."

Another effect has been reported that shows the difference between dynamic and static behavior; a slightly higher pressure is associated with the start of the two-phase absorption reaction and has been referred to as the "onset overpressure" due, perhaps, to the presence of a surface film or nucleation difficulties [Goodell et al., 1980]. Fig. 11 shows the presence of an onset overpressure at intermediate reaction rates; at low or high rates of charging, the effect is absent. The onset overpressure is analogous to the familiar undercooling phenomena at the onset of solidification.

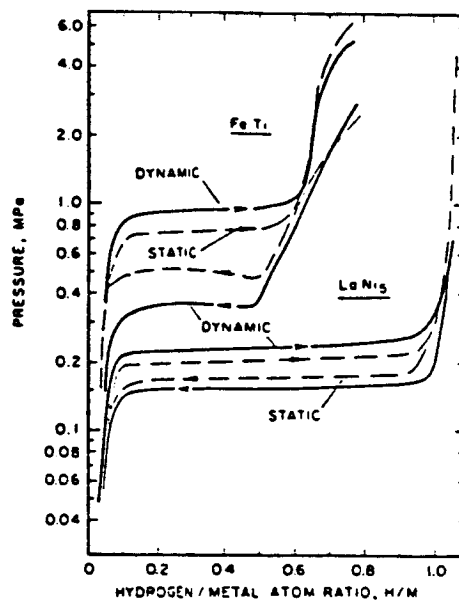


Fig. 10. Comparison of static and dynamic pressure-composition isotherms for LaNi<sub>5</sub> and FeTi at 25°C. The differences are greatest for FeTi and may preclude its use in a heat pump for this application [Goodell et al., 1990].

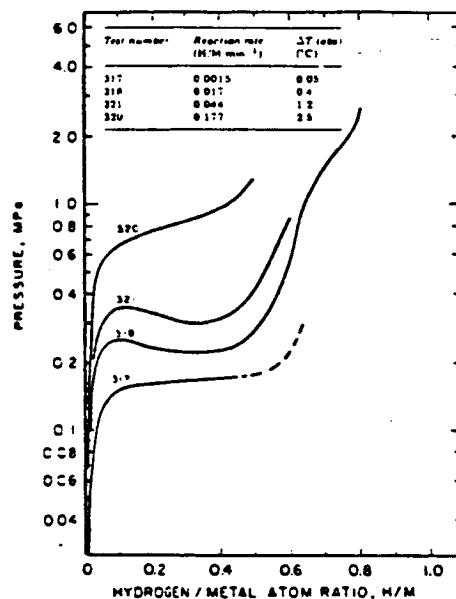


Fig. 11. Dynamic pressure-composition isotherms at -18°C for FeTi showing the onset overpressure at intermediate test rates. No onset overpressure effects are seen at either high or low rates [Goodell et al., 1980].

Again, all of these nonequilibrium effects lower the thermodynamic efficiency of the heat pump. In addition to the intrinsic nonequilibrium nature of the hydrides, an improperly designed hydride container can have significant pressure drops along its length. Fortunately, the anticipated sorption rates required for this application should be sufficiently low that it may be possible to neglect these effects; however, this can only be established with certainty after a prototype HHP is constructed.

#### 2.2.5 Useable Capacity vs. Temperature

As shown in Fig. 12, the hydrogen capacity of hydrides tends to decrease with increasing temperature, analogous to evaporation/condensation in a single-component liquid-gas system [Gruen et al., 1978; Abelson and Horowitz, 1980]. This variation has not been reported for most alloys. Therefore, sufficient material must be available at higher temperatures to contain the amount of hydrogen absorbed at lower temperatures in order to prevent excess pressure build up during recharging.

#### 2.2.6 Degradation

Degradation can be classified as intrinsic or extrinsic. Intrinsic degradation refers to the tendency of the alloy to disproportionate into its components whereas extrinsic degradation refers to the susceptibility to poisoning by impurities, such as oxygen or water vapor.

Binary hydrides have shown a tendency to disproportionate after many (thousand) cycles at elevated temperatures due to diffusion of the metal atoms. For example,  $\text{LaNi}_5$  has been found to decompose to the more stable  $\text{LaH}_2$ , which is nonreversible at room temperatures. Adding small amounts of Al makes the alloy resistant to disproportionation up to  $200^\circ\text{C}$  [Jones and Golben, 1985].



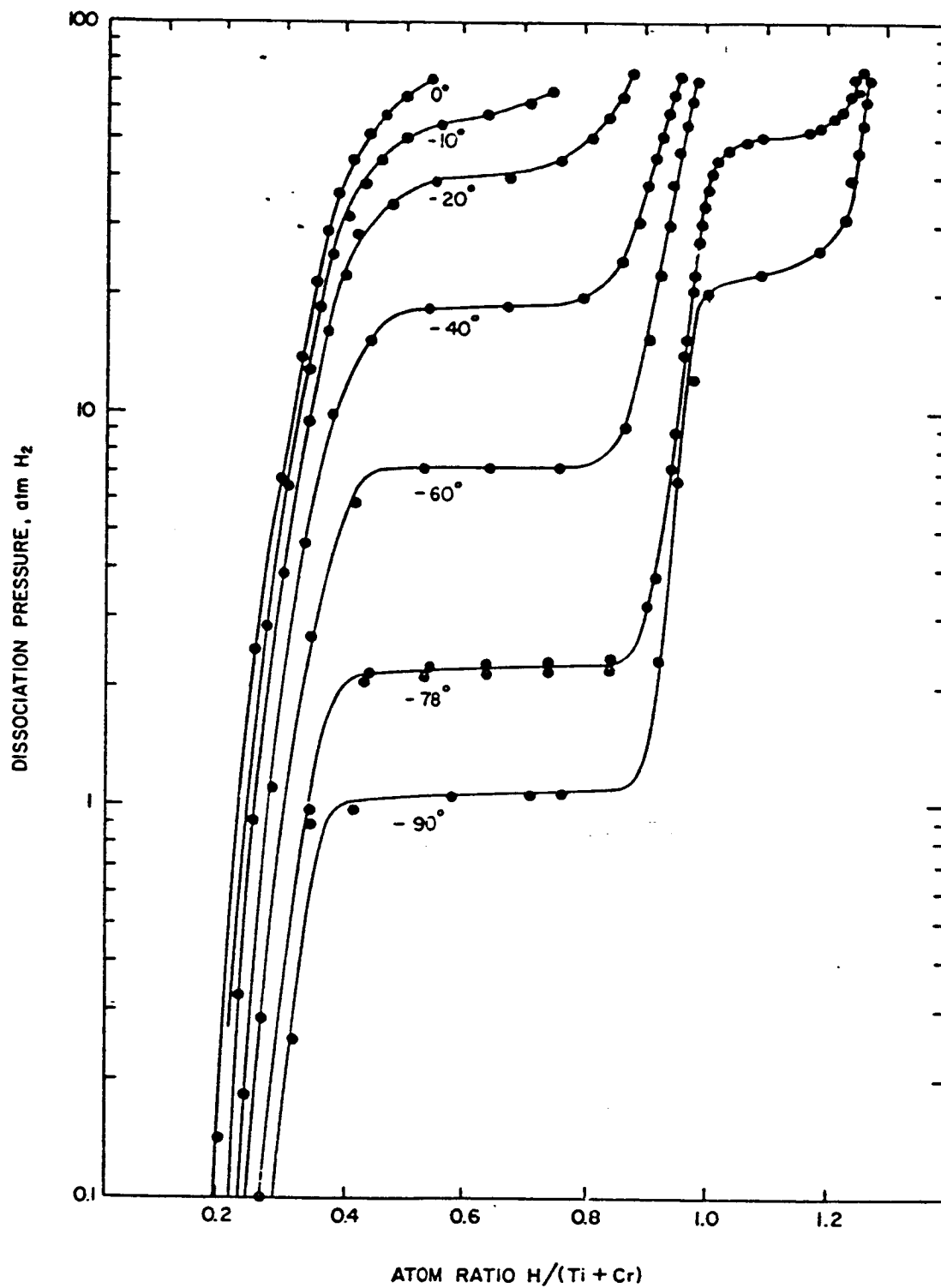


Fig. 12. The variation in the hydrogen capacity of TiCr<sub>1.8</sub> as a function of temperature. The trend follows that shown schematically in Fig. 7. Sufficient hydride material must be available for the intended amount of heat transfer at the highest operating temperatures or excessive pressures may result during recharging [Reilly, 1978a].

Because of the relatively small number of cycles proposed for this application (500) and the low temperatures involved (less than 100°C), intrinsic degradation should not be considered a serious problem even for LaNi<sub>5</sub> [Cohen and Wernick, 1981]. LaNi<sub>5</sub> and LaNi<sub>5-x</sub>Al<sub>x</sub> alloys have been cycled below 100°C for over 35,000 cycles with no detectable disproportionation [Golben, 1983]. However, because long-term cyclic tests are not available for many of the rare-earth nickel-based alloys, it is not clear that they will be sufficiently stable for this application; therefore, degradation studies should be performed to demonstrate the stability of any custom alloy.

Extrinsic degradation is a far more serious problem for those systems that continually expose the hydride to a different atmosphere, as in the case of hydrogen purification. Fig. 13 shows schematically the loss of capacity of a hydride exposed to impure hydrogen after numerous cycles. The loss would be different, of course, for different hydrides.

Due to the closed nature of the proposed HHP, impurity contamination should not be a concern. Neither nitrogen nor helium, even in substantial amounts, should result in the degradation of any hydride that may be selected [Sandrock and Goodell, 1984; Rosso, 1985b]. The only possible effect of these gasses, and only if they were present in significant concentrations, would be to provide a physical barrier around the hydride that could shield it from access to hydrogen during absorption. Since it is unlikely these inert gasses would be present in a closed system in any other than trace amounts, they should not be considered a problem in the long-term performance of the HHP.

#### 2.2.7 Comminution

The large lattice strains associated with hydriding result in a very small

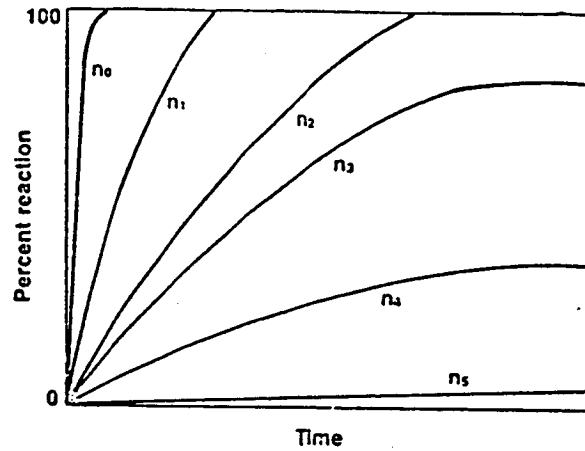


Fig. 13. Schematic reaction curves showing loss of kinetics and capacity as a result of cycling with impure hydrogen [Sandrock and Huston, 1981].

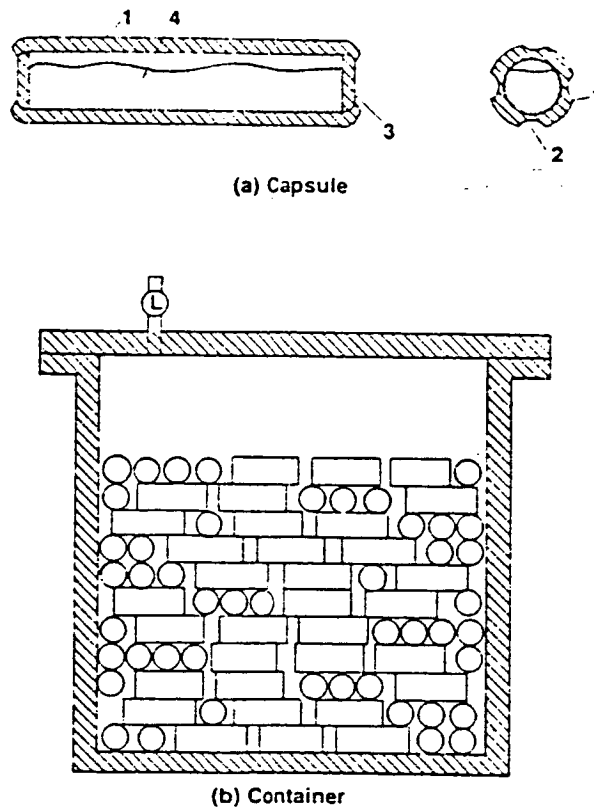


Fig. 14. Encapsulation of hydride to prevent expansion and packing problems. As a side benefit, the effective contact between the hydride and hydrogen gas is enhanced. 1=aluminum capsule, 2=flute, 3=porous filter, 4=hydride [Sandrock and Huston, 1981].

particle size after a number of cycles and, as mentioned before, lead to enhanced diffusion and degraded thermal conductivity. In addition, the fine particle size results in the tendency of the hydride powder to "pack" together under the influence of gravity. This results in two problems; namely, slower chemical kinetics due to the exclusion of hydrogen from the surface and the possibility of rupturing of the container after many cycles [Cohen and Wernick, 1981]. Because of the requirement of gravity for hydride packing, comminution should not be a problem for this application.

Since the resulting particle size is so small, 0.5 to 2.0  $\mu\text{m}$  filters (sintered stainless steel, fiberglass, etc.) must be employed to prevent the migration of the powders from the evaporator to the condenser. These filters will not clog if hydrogen is permitted to flow both ways through the filter [Jones and Golben, 1985].

These filters may introduce significant pressure drops (about 10 psi) between the two ends of the HHP at high flow rates but only small drops (about  $\frac{1}{2}$  psi) are found at normal flow rates [Rosso, 1985b]. Since it is anticipated that the flow rates for this application will be low, the pressure drop due to filters can be treated as a second-order effect.

Design of the container is particularly important because of comminution. Encapsulation designs, such as the one shown in Fig. 14, have been used with success. Rupture of the container wall can be prevented if small quantities of the hydride are enclosed in separate compartments. Encapsulation also increases the effective contact area between the hydride and the hydrogen working fluid [Sheft et al., 1980].

### 2.2.8 Activation

The intermetallic hydrides do not absorb hydrogen without undergoing an "activation" process, which involves cycling the material through a number of charge-discharge cycles [Cohen and Wernick, 1981]. Both the kinetics and hydrogen capacity greatly increase during this process. One reason for the increased kinetics from the activation process is due, of course, to a greatly increased surface area of the bulk sample resulting from the large volume change associated with hydriding.

LaNi<sub>5</sub> can be easily activated at room temperature and a few atmospheres of hydrogen; however, FeTi requires much higher temperatures (300-450°C) followed by 2-10 days' exposure to high pressure hydrogen (>30 atm) at room temperature [Sandrock and Huston, 1981].

If FeTi is exposed to air, it must be reactivated, unlike LaNi<sub>5</sub>. Therefore reactivation of a FeTi HHP would be considerably less straightforward compared to a LaNi<sub>5</sub> HHP due to the higher pressures and temperatures required.

## 2.3 Properties of Selected Hydrides

It is instructive to review the general properties in each of several classes of hydrides for this HHP application. Iron-titanium, the rare-earths, calcium-nickel, magnesium, and newly-discovered alloys will each be discussed separately.

### 2.3.1 Iron-Titanium Alloys

The FeTi alloys have excellent properties for use as hydrogen storage media. They are inexpensive and the raw material is abundant. The plateau pressures are sufficiently high at ordinary temperatures for them to be considered for

many diverse applications. If exposed to air, they become deactivated allowing them to be handled in air without decomposition and then subsequently reactivated, as described in Section 2.2.8 [Reilly, 1979].

In spite of many advantages of FeTi, the amount of overpressure required for hydrogen sorption, as shown in Fig. 10, is considerably larger than for the rare-earth alloys [Reilly, 1985]. Because of this disadvantage, the iron-titanium alloys have not been used extensively for heat pump applications.

Iron can be partially replaced by other transition metals to improve the properties of FeTi. As shown in Fig. 15, for example, small additions of manganese reduce the amount of hysteresis but the plateau slope increases substantially; however, activation can proceed at room temperature [Reilly, 1979]. Additions of nickel result in an alloy with a very small amount of hysteresis [Huston and Sandrock, 1980].

### 2.3.2 Rare-Earth Alloys

The most widely studied of the rare-earth alloys is LaNi<sub>5</sub>, which reacts rapidly and reversibly with hydrogen (even in the bulk) at room temperature with a high dissociation pressure. Alloys based on this system show relatively small hysteresis and have a compositional range greater than 1 H/M atom ratio.

Of particular importance for this HHP application is the capability of varying the properties of the rare-earth alloys almost at will by substituting in whole or in part other metals for lanthanum and nickel [Reilly, 1979]. For example mischmetal (Mm) can be substituted for lanthanum and aluminum for nickel. Both substitutions have dramatic effects on the thermodynamic properties.

Unfortunately, the storage capacity, plateau slope, and kinetics are degraded

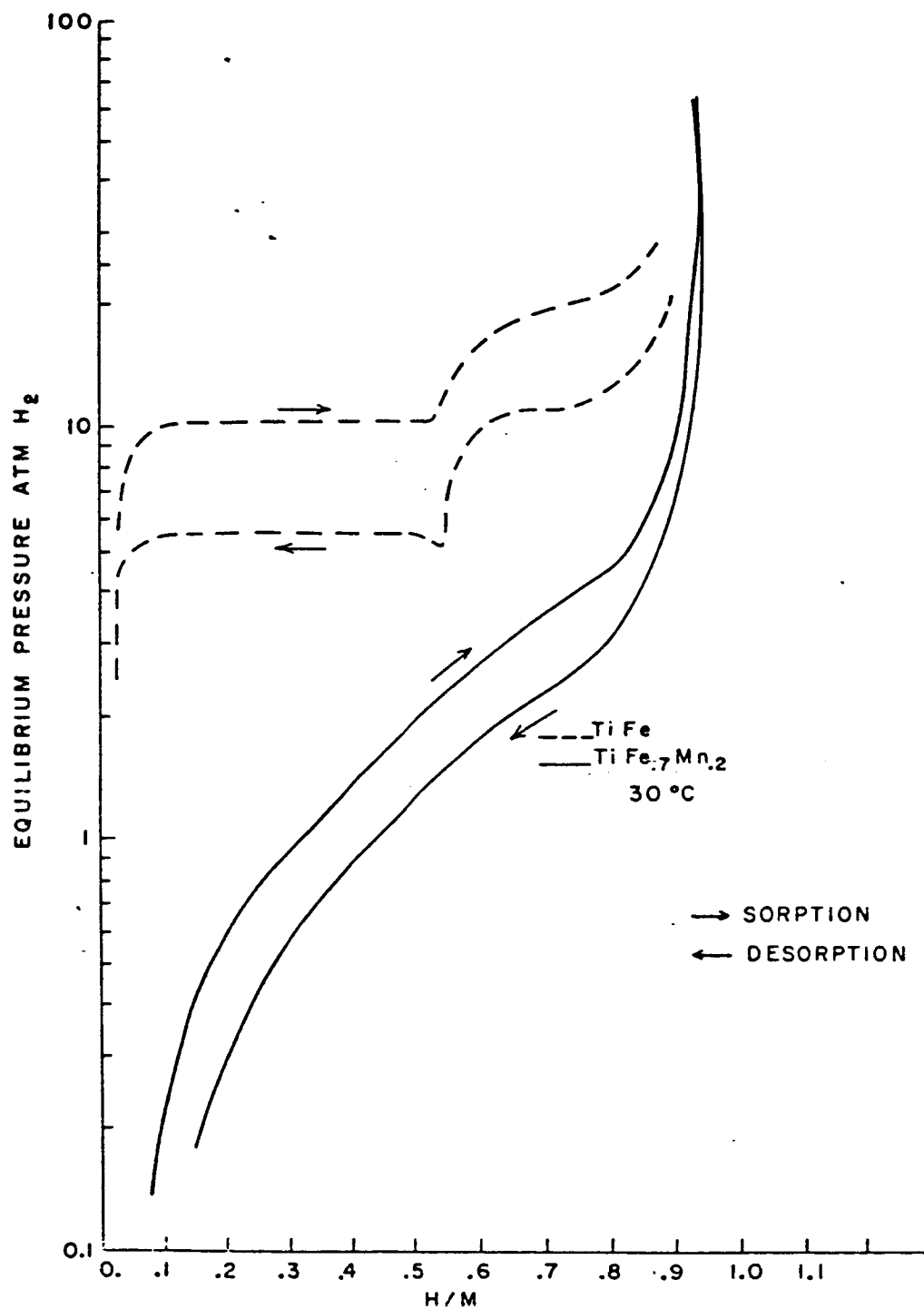


Fig. 15. The effect of manganese substitution for iron in the FeTi alloy. The addition of manganese results in an alloy that may be activated at room temperature and the degree of hysteresis is reduced; however, the equilibrium pressures are reduced and the slope of the isotherms is greatly increased [Reilly, 1978a].

compared to  $\text{LaNi}_5$ , although in most cases not significantly.

The substitution of aluminum for nickel significantly lowers the plateau pressure at any given temperature [Diaz et al., 1979]; however, both the hydrogen capacity and diffusion coefficient are also reduced [Rosso, 1985b]. The diffusion coefficient is more than two orders of magnitude lower near room temperature (compared to undoped  $\text{LaNi}_5$ ) due to an increase in the activation energy [Bowman et al., 1980]. Addition of aluminum has been found to be beneficial in reducing the tendency of  $\text{LaNi}_5$  to disproportionate [Jones and Golben, 1985].

In practice, hydrides can be designed for nearly any heat pump application [Sheft et al., 1978, Rosso, 1985b]. For example, plateau pressures from 0.1 to 50 atm. at room temperature can be obtained by mixing various combinations of rare earths and other elements with nickel. Thus, the materials engineer is not limited to those alloys published in the literature. However, it should be noted that much of hydride alloy design is proprietary, or patented, as well as any heat treatment used to minimize the plateau slope.

### 2.3.3 Calcium-Nickel Alloys

The substitution of calcium for lanthanum, forming  $\text{CaNi}_5$ , results in a much less expensive hydride that can still be activated easily at room temperature; however, the plateau slope is more than doubled [Huston and Sandrock, 1980] and the alloy is especially susceptible to degradation [Sheft et al., 1980].

$\text{CaNi}_5$  and  $\text{MnNi}_5$  form a continuous solid solution so that a complete range of van't Hoff lines between  $\text{CaNi}_5$  and  $\text{MnNi}_5$  can be achieved [Sandrock and Huston, 1981]. Replacing 30 percent of the calcium with mischmetal increases the



plateau pressure by a factor of 8 at room temperature, slightly lowers the hysteresis, increases the capacity by 25 percent, but increases the plateau slope by a factor of 17 [Huston and Sandrock, 1980]. Although this alloy may be suitable for some HHP applications, because of the greatly increased plateau slope, it is not suitable for this one.

#### 2.3.4 Magnesium Alloys

Generally, the magnesium-based alloys possess a very good H/M weight ratio compared to the other metallic hydrides; however, they are rather stable, decomposing at relatively high temperatures, as shown in Fig. 5. In addition, the chemical kinetics of hydrogen sorption are considerably slower compared to the other hydrides due, perhaps, to the presence of a gas-proof hydride layer initially formed at the surface [Belkhir et al., 1981].

The alloy  $Mg_2Ni$  readily reacts with hydrogen even at room temperature; however, its energy density is only half that of magnesium hydride. Alloys containing copper have been found to disproportionate [Reilly, 1979]. Because of these limitations, these alloys do not hold much promise for this HHP application.

#### 2.3.5 Other Alloys

Hydrides based on other materials have been and will be continued to be discovered. Among the more promising series of alloys are  $TiMn_{1.5}$  and the multicomponent zirconium-based alloys  $Zr_{0.8}Ti_{0.2}MnCr_{1.25}$ ,  $ZrMnFeTx$ ,  $ZrCrFe_{1+x}$ , and  $Zr_{1-x}TxMnyFez$ , where T is Ti, Mn, or Fe [Suda et al., 1981a; Sinha and Wallace, 1985; Sinha et al., 1985]. Some of these alloys have large hydrogen capacities and favorable dissociation pressures, and all have fast kinetics. They appear to have particular promise for heat pump applications. It appears, however, that the plateau slopes are much larger for these materials than for

LaNi<sub>5</sub>. Further studies are needed to determine their long-term stability; therefore, these alloys cannot be recommended for this application at the present time.

## RESULTS AND DISCUSSION

There are numerous subtleties in the properties of metal hydrides that may impact the final design of the HHP for this application. These include the following:

- different enthalpies for absorption and desorption
- hydrogen sorption limited by heat transfer, diffusion, or interfacial reactions
- different absorption and desorption plateau pressures (hysteresis)
- changes in hysteresis with temperature, sorption rate, and composition
- changes in plateau slope with temperature, sorption rate, and composition
- higher (or different) absorption than desorption slopes
- changes in plateau pressures, enthalpies, and entropies with sorption rate
- higher pressures required to start hydriding ("onset overpressure")
- pressure drops due to filters, piping, valves, heat exchangers, and improperly designed hydride beds
- changes in hydrogen capacity with temperature
- changes in hydrogen capacity with time (degradation)
- changes in pressure drops with time due to comminution

Before the nonidealities of the hydrides are considered, however, it is instructive to consider two hydrides, ignoring all nonideal effects. Nonidealities will be treated separately in later sections.

### 3.1 A Case Study of Two Hydrides

The following examples consider two hydrides:  $\text{MmNi}_{4.5}\text{Al}_{0.5}$  as the high-pressure hydride and  $\text{LaNi}_{4.7}\text{Al}_{0.3}$  as the low-pressure hydride. Their properties have been obtained from Huston and Sandrock, 1981.

#### 3.1.1 Ideal Behavior

The following conditions have been assumed for this (and some following) examples:

- a. The evaporator temperature of 40°F is determined by a pressure regulator (check valve) between the two heat exchangers.
- b. The condenser temperature is determined by the surface area and absorption/emission properties of a space radiator [6]. The area must be selected to maintain the pressure equal to, or below, the evaporator.
- c. The A and B constants in Eqn. (3) are -3366 K and 12.61 for hydride #1 and -4090 K and 12.84 for hydride #2. Both hydrides are considered to be in sufficient quantity to achieve the necessary amount of heat transfer, assumed to be 11,680 Btu, with a metabolic rate vs. time as shown in Fig. 16 [Hodgson and Dresser, 1982].
- d. Pressure drops and other nonidealities are insignificant.

Fig. 17 shows the path taken by hydrogen in the HHP during the EVA as well as during post-EVA (recharging).

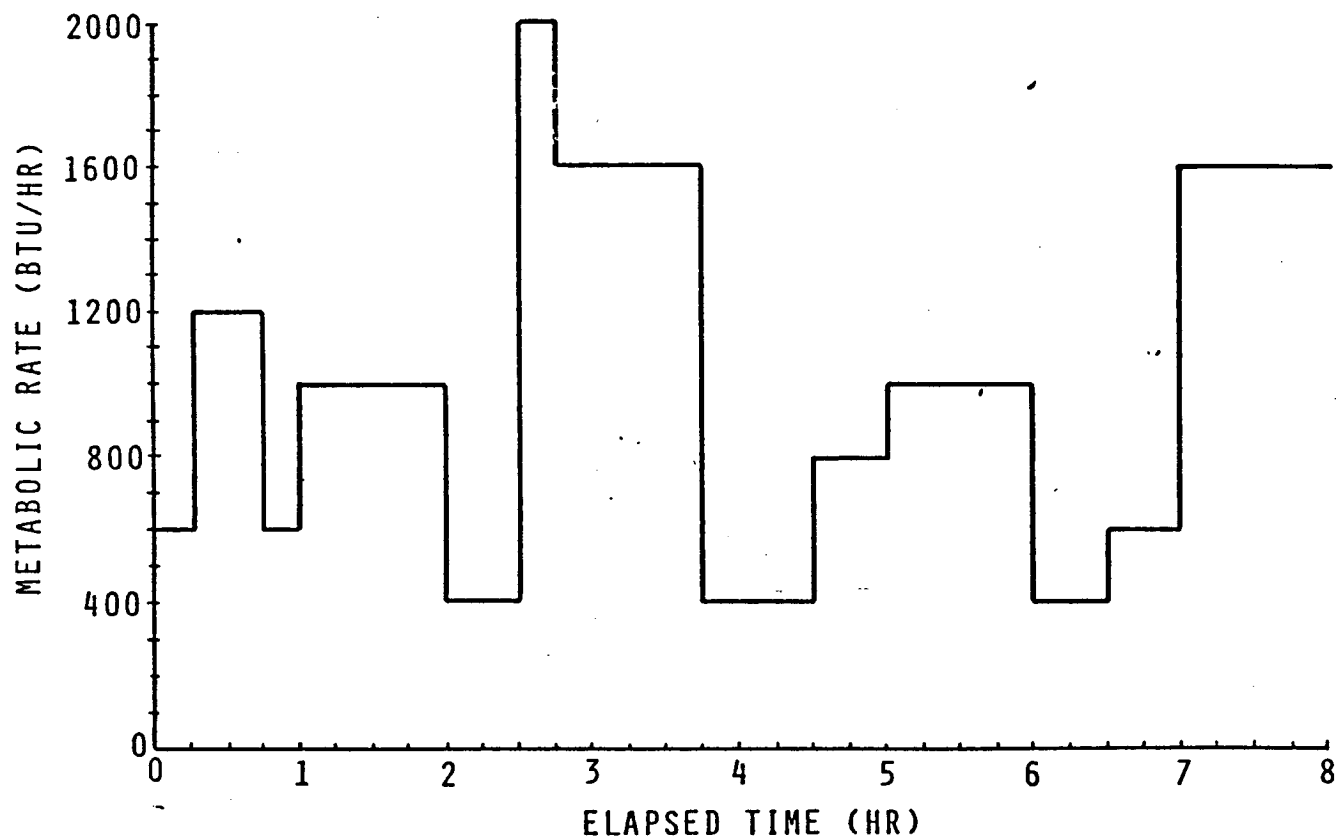


Fig. 16. The proposed metabolic rate load of a crewmember on the space station mission. The total thermal demand is 11,680 Btu, with a peak of 2,000 Btu/hr [Howard and Dresser, 1982].

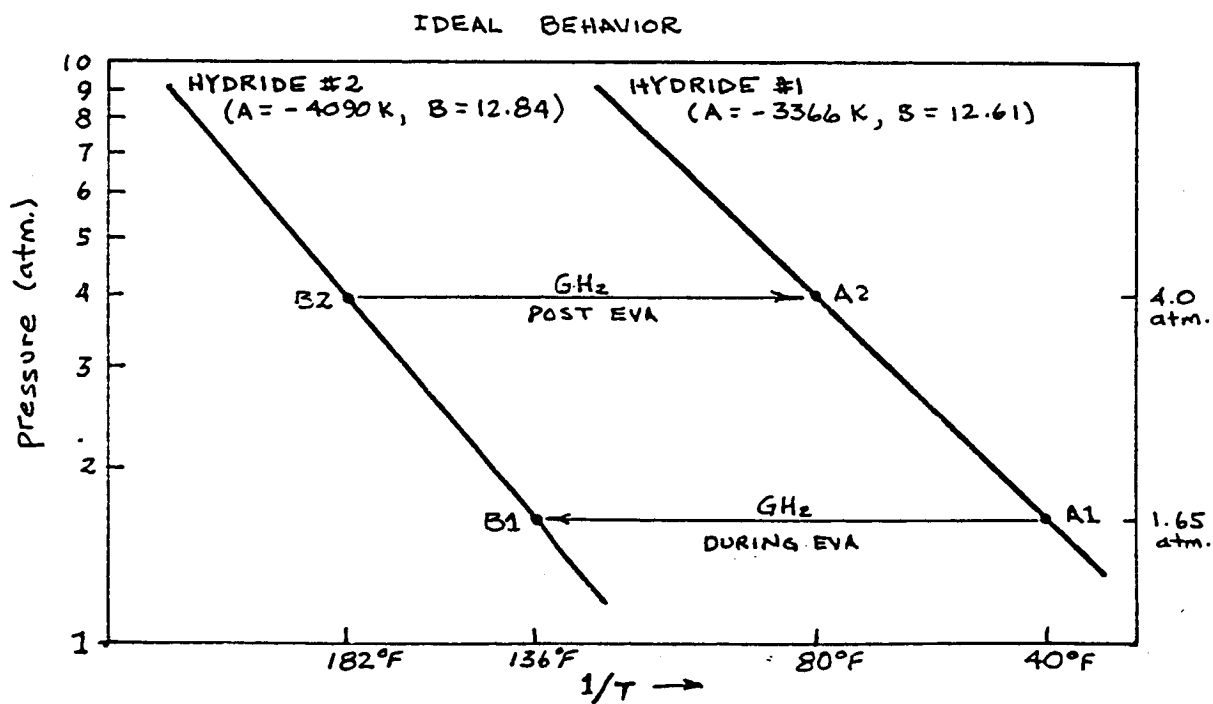


Fig. 17. van't Hoff plots of the ideal behavior of two hydrides based on  $\text{MnNi}_{14.5}\text{Al}_{10.5}$  and  $\text{LaNi}_{4.7}\text{Al}_{0.3}$ . The hydride heat pump initially desorbs hydrogen at A1 and absorbs at B1. The HHP is recharged by desorbing hydrogen at B2 and absorbing at A2.

A. Thermal equilibrium with the space station

Hydride #1: 80°F and 4.0 atm.

Hydride #2: 80°F and 0.45 atm.

Initially, both hydride #1 and #2 are assumed to be in thermal equilibrium with the interior of the space station (assumed to be 80°F).

B. LCVG water circulates and the connecting valve is opened

Hydride #1: 80°F → 40°F and 4.0 atm. → 1.65 atm.

Hydride #2: 80°F → 136°F and 0.45 atm → 1.65 atm.

When water from the LCVG is circulated through hydride #1 and the valve between the hydrides is opened, hydrogen begins to desorb from hydride #1 lowering its temperature to point A1, which is determined by the pressure-regulating check valve set to 1.65 atm. The hydrogen is absorbed by hydride #2, raising its temperature to 136°F. Since hydride #2 is in thermal contact with a space radiator, the heat of formation is rejected to space.

The temperature of hydride #2 is, in fact, determined not by the pressure of hydride #1, rather it is determined solely by the physical characteristics of the space radiator, such as the absorptivity, emissivity, and area. Based on the  $T^4/\text{area}$  relationship, a 8.2 ft<sup>2</sup> radiator is the minimum area required. If the area is smaller than 8.2 ft<sup>2</sup>, the temperature of the radiator could not be maintained at 136°F or below; therefore, the pressure in hydride #2 would exceed that in #1 and no hydrogen would be desorbed from hydride #1. If the area is greater than 8.2 ft<sup>2</sup>, the actual temperature of hydride #2 would be less than 136°F, which would result in a lower condenser pressure. Since it has been assumed in this example that no pressure drops exist, the extra area of the radiator would be wasted.

C. During the EVA

Hydride #1: 40°F and 1.65 atm.

Hydride #2: 136°F and 1.65 atm.

During this time, hydride #1 is being depleted in hydrogen, with the waste heat from the LCVG supplying the thermal energy for the endothermic heat of desorption. Assuming there is an excess of hydride #2, the cooling effect will cease when all of the hydrogen has desorbed from hydride #1. If hydride #1 is in excess, the EVA must terminate when the capacity of hydride #2 has been reached since the pressure would rise abruptly at that point and no further hydrogen transfer could occur.

D. End of the EVA and return to the space station

Hydride #1: 80°F and 4.0 atm.

Hydride #2: 80°F and 0.45 atm.

It is assumed that the HHP has come to thermal equilibrium with the space station once again.

E. Recharging

Hydride #1: 80°F and 4.0 atm.

Hydride #2: 182°F and 4.0 atm.

Hydride #1 is connected to the space-station's thermal management system, which is assumed to be at 80°F. Therefore, in order to recharge hydride #1, the temperature of hydride #2 must be raised to at least 182°F in order to achieve a pressure of 4.0 atm. The temperature of hydride #2 can be raised by solar or electrical energy. Since the HHP is now onboard the space station, it is assumed that there is sufficient energy available for this purpose.

After recharging has ended (either by an abrupt rise in temperature of hydride #1 or the exhaustion of hydrogen in hydride #2), the HHP can be returned to the PLSS for reuse. During that time, it will, of course, come to thermal equilibrium with the space station once again.

The amount of material needed to transfer 11,680 Btu may be calculated if the following assumptions are made:

hydride #1: 0.83 H/M capacity,  $\Delta H^\circ = -6.7 \text{ kcal/mol-H}_2$ , 6 M-atoms/mol, 433 g/mol

hydride #2: 0.95 H/M capacity,  $\Delta H^\circ = -8.1 \text{ kcal/mol-H}_2$ , 6 M-atoms/mol, 423 g/mol

For hydride #1,  $6 \times 0.83 = 4.98$  moles of H are contained in one mole of hydride #1. At  $6.7 \text{ kcal/mol-H}_2$ , for 11,680 Btu (2940 kcal) of heat transfer,  $2,940/6.7 = 438.8$  moles of  $\text{H}_2$  or 877.6 moles of H are required. Finally,  $877.6/4.98 = 176.2$  moles of hydride #1 at 423 g/mol results in 76,295 g or 168 lbs of hydride. If the effective hydride density is  $4 \text{ g/cm}^3$ , this corresponds to a volume of  $19,074 \text{ cm}^3$  or a cube 10.5 in. on a side.

The corresponding results for hydride #2 are 53,882 g = 119 lbs for a volume of  $13,471 \text{ cm}^3$  or a cube 9.4 in. on a side. The same effective density has been used for this calculation.  $4 \text{ g/cm}^3$  is a reasonable value for the effective density if the crystal density is similar to that for  $\text{LaNi}_5$  ( $6.4 \text{ g/cm}^3$ ) and some volume is allowed for expansion.

### 3.1.2 Effect of Hysteresis

The absorption/desorption pressure ratio (a measure of the hysteresis) is taken to be 1.12 and 1.05 for hydride #1 and #2, respectively. Isotherms show hysteresis during absorption and desorption, which are assumed to be the same.



Fig. 18 shows the path taken by hydrogen in the HHP during the EVA as well as during post-EVA (recharging). The narrow lines represent the static behavior and the heavy lines the dynamic behavior. The absorption isotherms will be above and the desorption isotherms below the static isotherms.

Hydride #1 begins at point A1 (40°F and 1.5 atm) and hydride #2 at B1 (131°F and 1.5 atm). Clearly, since the condenser temperature has been reduced from 136 to 131°F, a greater radiator area is required compared to the ideal case. Recharging hydride #2 requires a temperature increase from 182 to 188°F, only a minor change from the ideal case.

### 3.1.3 Effect of Plateau Slope

Isotherms do not have a constant pressure; rather, they depend on composition, temperature, and alloy preparation. The plateau slope,  $(d \ln P)/(dH/M)$ , is taken to be 0.36 and 0.48 for hydrides #1 and #2, respectively (equivalent to 0.16 and 0.21 for a base-10 logarithmic plot). If excess hydride material is used in the HHP, the hydride can be operated over a flatter range of the plateau pressure, thus increasing the efficiency during the EVA as well as the overall efficiency.

Fig. 19 shows the path taken by hydrogen in the HHP during the EVA as well as during post-EVA (recharging).

Hydride #1 begins at point A1 (32°F and 1.6 atm) and hydride #2 at B1 (125°F and 1.0 atm.). Because of the sloping isotherm, as hydrogen is removed from hydride #1, the temperature increases to point A2 (48°F and 1.6 atm.). It is not possible to maintain the temperature of hydride #1 at 40°F if the pressure is held constant at 1.6 atm. Since a temperature lower than the ice point is

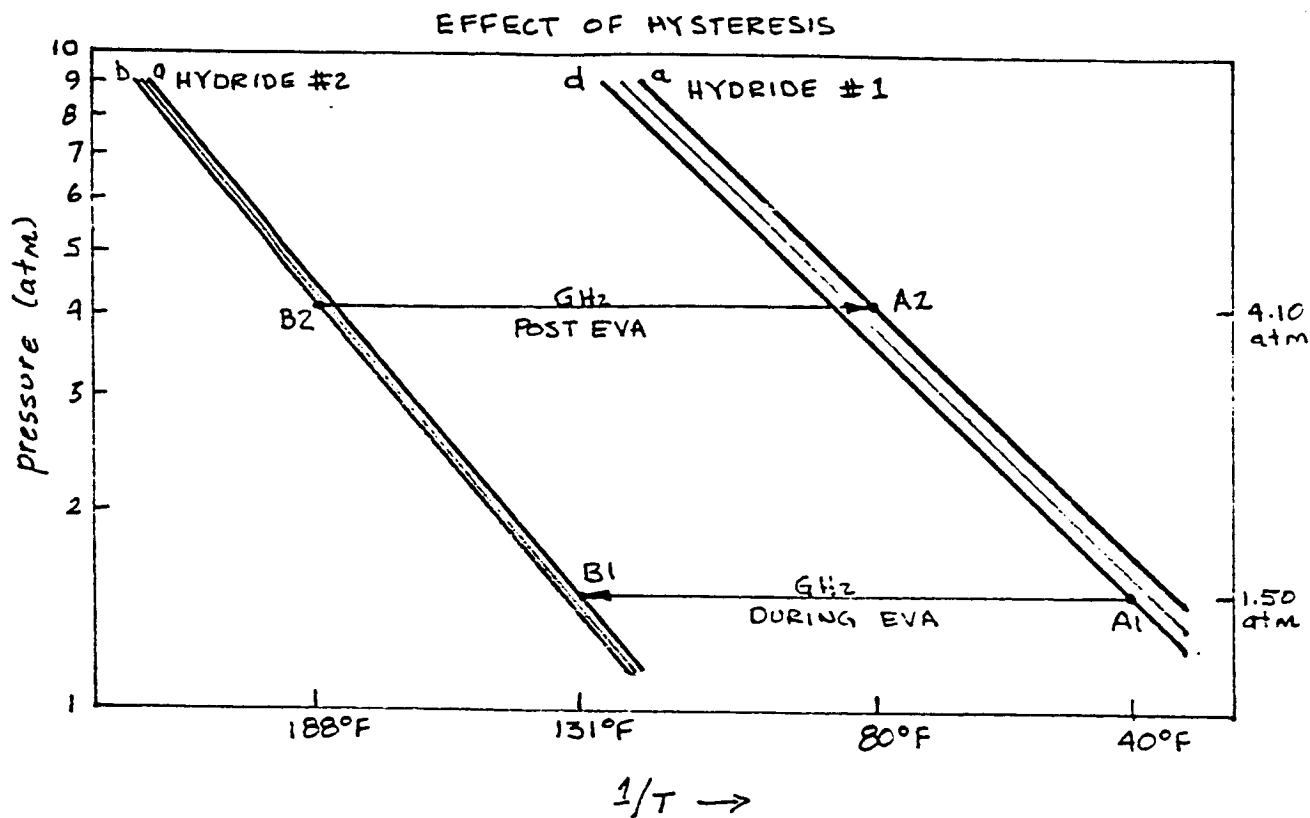


Fig. 18. van't Hoff plots showing only the effect of hysteresis on the pair of hydrides. Hydride #1 has a larger hysteresis than hydride #2. The radiator temperature must decrease from 136 to 131°F.

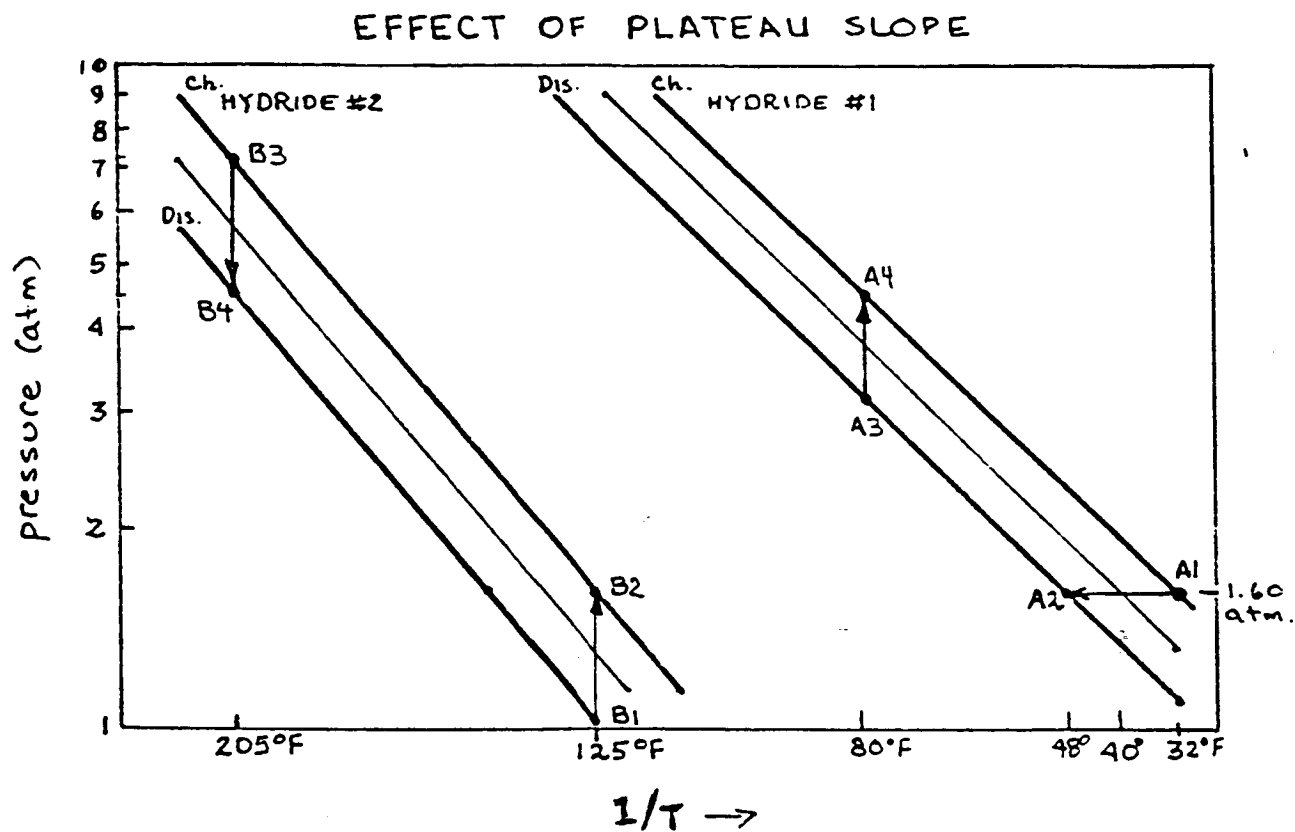


Fig. 19 van't Hoff plots showing only the effect of a nonzero plateau slope on the pair of hydrides. As hydrogen desorbs from hydride #1 at a constant pressure, the temperature rises from 32 to 48°F while the pressure in hydride #2 rises from 1 to 1.6 atm.

not desirable, the temperature of hydride #1 at the end of the EVA will be 48°F.

As hydrogen is transferred to hydride #2, the pressure rises from 1 to 1.6 atm if the temperature is maintained constant at 125°F by the space radiator. The EVA must terminate when either hydride #1 is depleted of hydrogen or if the hydrogen pressure of hydride #2 exceeds 1.6 atm.

Recharging involves heating hydride #2 to point B3 (205°F and 7.2 atm) where desorption will result in a pressure drop to point B4 (205°F and 4.6 atm). Hydride #1 will be initially at point A3 (80°F and 3.2 atm) but will increase in pressure to point A4 (80°F and 4.6 atm) as hydrogen is absorbed.

Not only is a larger radiator required, compared to the ideal case, the cooling effect may be somewhat reduced since the temperature of hydride #1 at the end of the EVA will be at 48, not 40°F, although it will be at 32°F at the start.

#### 3.1.4 Effect of Finite Hydrogen Sorption Rates

If the maximum rate is 2,000 Btu/hr, as illustrated in Fig. 15, this corresponds to 8.4 kcal/min. For hydride #1,  $8.4/6.7 = 1.25$  moles H<sub>2</sub>/min. Since 76.3 kg of hydride is required, and 1 H/M per min. is about 6.94 mol H<sub>2</sub> per kg of hydride per min. [5], this corresponds to a discharge rate of  $0.0164/6.94$ , or 0.0024 H/M per min.

It is instructive to compare this rate with that reported by Goodell, et al. in 1980 for LaNi<sub>5</sub>. They found that the absorption plateau of LaNi<sub>5</sub> increased by 15 percent for a continuous charging rate of 0.02 H/M atoms per min. The

that value; therefore, no more than a 15 percent increase in absorption or decrease in desorption pressures are expected. As mentioned in Section 2.2.4, even discharge rates as low as those anticipated for this application should still result in significant deviations from static results.

Assuming a 15 percent increase in absorption and 15 percent decrease in desorption pressures, the effect on the performance of the HHP can be illustrated in Fig. 20.

Hydride #1 begins at point A1 (40°F and 1.4 atm) and hydride #2 at point B1 (123°F and 1.4 atm). Again, since the condenser temperature has been reduced from 136 to 123°F, a corresponding increase in radiator area is required.

Recharging hydride #2 requires a temperature increase from 182 to 198°F; however, this is not expected to be a problem.

### 3.1.5 Combined Nonideal Effects

In addition to the effects of hysteresis, plateau slopes, and finite sorption rates, there will be pressure drops due to piping, valves, filters, etc. that must be included in any discussion of nonidealities. Since pressure drops are very design dependent, a reasonable 2 psi drop will be assumed.

Fig. 21 shows the effect of hysteresis, plateau slopes, a sorption rate that changes the isotherms by 15 percent, and a 2 psi pressure drop (there is a built-in 1 psi pressure drop for each heavy line).

Hydride #1 starts at point A1 (32°F and 1.4 atm) and desorbs hydrogen at a constant pressure until point A2 is reached (51°F and 1.4 atm). Hydride #2

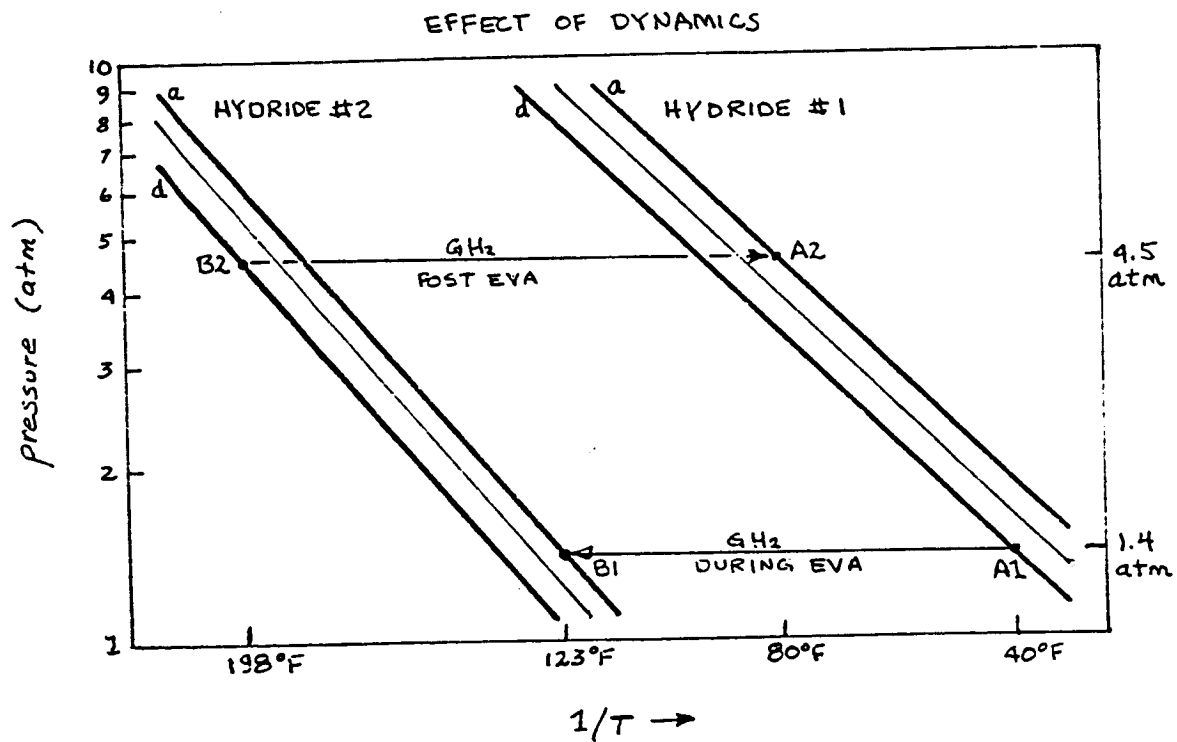


Fig. 20. van't Hoff plots showing only the effect of a finite hydrogen sorption rate on the pair of hydrides. The temperature of the radiator must be lowered from 136 to 123°F for proper operation.

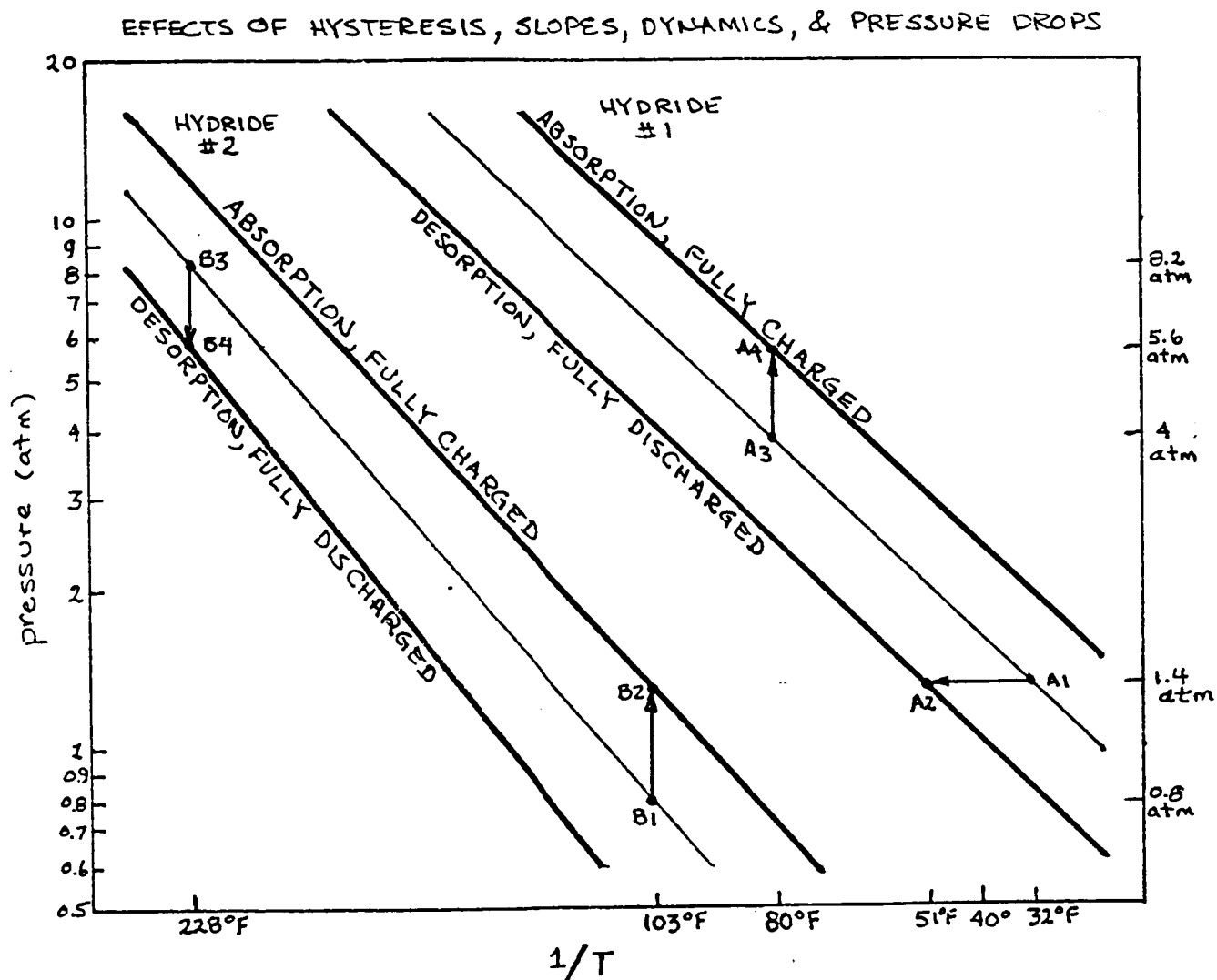


Fig. 21. van' Hoff plots showing the approximate combined effects of hysteresis, nonzero plateau slopes, finite charging rates, and a 2 psi pressure drop on the pair of hydrides. Hydride #1 desorbs from 32 to 51°F and the radiator temperature is only 103°F. Furthermore, recharging hydride #2 must be done at 228°F.

starts at point B1 (103°F and 0.8 atm) and absorbs hydrogen at a constant temperature until point B2 is reached (103°F and 1.4 atm).

Recharging hydride #2 requires a temperature of 228°F to ensure an adequate pressure drop to hydride #2 at 80°F. Hydride #2 desorbs hydrogen at point B3 (228°F and 8.2 atm) until point B4 (228°F and 5.6 atm) is reached. Hydride #1 absorbs hydrogen at point A3 (80°F and 4 atm) until point A4 (80°F and 5.6 atm) is reached.

Clearly, the inclusion of these four nonidealities significantly reduces the efficiency of the HHP. The consequences for the EVA include

- a temperature sink for the LCVG that varies from 32 to 51°F
- a radiator area increase from 8.2 to 10.3 ft<sup>2</sup>

After the EVA, the only penalty of any consequence is increasing the temperature of hydride #2 from 182 to 228°F, which should be easily achieved. None of these nonideal effects should seriously limit this particular combination of hydrides for this HHP application.

### 3.2 LaNi5 and CaNi5

The paper by Gruen et al., 1978 incorrectly reports absorption and desorption pressure-temperature variations for LaNi5. Although the enthalpy reported is close, both absorption and desorption pressures are too high. See Huston and Sandrock, 1980 for correct data.

It is easy to show that when the actual properties of this pair of hydrides are considered, along with any nonideal effects, it would be impossible to use them for this application.



### 3.3 Other Hydride Pairs

A considerable number of other hydride pairs would, most likely, be suitable for this application since it is possible to design the rare-earth-based hydrides for a given set of van't Hoff constants. The properties of most of these custom alloys, and the thermal heat treatments needed to minimize plateau slope, etc., have not been published. Even for those hydrides that are well characterized, unforeseen characteristics may result in considerably different behavior from that expected. It will be essential to build a prototype of a HHP for this application using the hydride pairs that have been selected based on their assumed properties.

## SUMMARY

### 4.1 Additional Physical Property Data Required

The issue of hydride cost has not been addressed in this paper. Clearly, if a few hundred pounds of relatively expensive hydride material is required for each PLSS, the cost will not be negligible; however, this design should still be cost competitive with alternative designs.

It must be established what limits the reaction rate: heat transfer, hydrogen diffusion, interfacial reactions, pressure drops, etc. and steps taken to reduce the limiting step. However, since the rates of reaction for this application are expected to be low, compared to conventional hydride heat pump applications, the rate of reaction may not be a critical design parameter.

If custom (unpublished) alloys are used in the design, it is essential that all of the properties mentioned above be known. In particular, the following

nonidealities are listed in order of importance:

- a minimum plateau slope during desorption of the high-pressure hydride
- a minimum plateau slope during absorption of the low-pressure hydride
- a minimum underpressure during desorption of the high-pressure hydride
- a minimum overpressure during absorption of the low-pressure hydride
- a minimum hysteresis for both hydrides

Other nonidealities can be considered as secondary for this application.

#### 4.2 Recommendations

An almost unlimited number of alloy compositions are available that will result in any combination of properties desired for a particular application.

However, the properties of even relatively simple alloys, such as  $\text{LaNi}_5$ , may show considerable variation depending on the sample preparation, purity, design of the testing apparatus, etc. Therefore, it is clear that a prototype of the HHP for this purpose must be constructed before the final design is chosen.

Because of the exponential dependence of pressure with temperature, it will be essential to establish maximum operating and storage temperatures for the particular hydrides selected for the HHP. Failure to maintain the temperature below this limit may result in catastrophic rupture of the container or venting of hydrogen into a potentially explosive atmosphere. The HHP could be designed with a one-way check valve from the high-pressure to the low-pressure hydride that would open only if the pressure exceeded a preset limit. This would avoid any loss of hydrogen to the environment.

The rare-earth based metal hydrides have been shown to possess a combination of properties that make them desirable for heat pump applications; namely, they absorb and reversibly desorb relatively large amounts of hydrogen with

excellent kinetics with a small degree of overpressure. In addition, their composition can be varied almost at will to achieve a given set of properties.

In addition to the conventional two-hydrate heat pump concept, the unique conditions of the space station can be used to advantage. It has been proposed [Rosso, 1985c] that the same cooling effect could be achieved with only a single hydrate and evaporator, which would eliminate not only the second hydrate and condenser, but also the backpack radiator and associated heating and cooling connections. This concept is similar to that proposed by Jones and Golben in 1985 for spacecraft cooling to 20 K. The disadvantage to this concept would be the requirement of a connection to a waste hydrogen vent from the fuel tanks and the introduction of hydrogen into the space station environment as a possible contaminant.

## REFERENCES

### 5.1 Primary References

- Abelson, H.; Horowitz, J.S., "A Thermodynamic Analysis of a Metal Hydride Heat Pump," Proc. 15th Intersociety Energy Conversion Engineering Conference, Orlando, FL, Aug. 21-26, 1980, Vol. 4, pp. 1746-1753.
- Anevi, G.; Jansson, L.; Lewis, D., "Dynamics of Hydride Heat Pumps," J. Less-Common Metals, Vol. 104, pp. 341-348, 1984.
- Belkbir, L.; Joly, E.; Gerard, N., "Comparative Study of the Formation-Decomposition Mechanisms and Kinetics in LaNi<sub>5</sub> and Magnesium Reversible Hydrides," Int. J. Hydrogen Energy, Vol. 6, pp. 285-294, 1981.
- Bowman, R.C.; Craft, B.D.; Attalla, A., "Role of Aluminum Substitution on Hydrogen Diffusion in beta-LaNi<sub>5</sub>-yAl<sub>x</sub>H<sub>x</sub>," J. Less-Common Metals, Vol. 73, pp. 227-232, 1980.
- Buschow, K.H.J.; Miedema, A.R., "Hydrogen Absorption in Rare Earth Intermetallic Compounds," Hydrides for Energy Storage, Proc. Intl. Symp. Geilo, Norway, 14-19 Aug. 1977, pp. 235-249, Pergamon Press, 1978.
- Buschow, K.H.J.; Bouten, P.C.P.; Miedema, A.R., "Hydrides Formed from Intermetallic Compounds of Two Transition Metals: A Special Class of Ternary Alloys," Rep. Prog. Phys., Vol. 45, pp. 937-1039, 1982.
- Cohen, R.L. and Wernick, J.H., "Hydrogen Storage Materials: Properties and Possibilities," Science, Vol. 214, No. 4525, pp. 1081-1087, Dec., 1981.
- Diaz, H.; Percheron-Guegan, A.; Achard, J.C.; Chatillon, C.; Mathieu, J.C., "Thermodynamic and Structural Properties of LaNi<sub>5</sub>-yAl<sub>x</sub> Compounds and Their Related Hydrides," Int. J. Hydrogen Energy, Vol. 4, pp. 445-454, 1979.
- Flanagan, Ted B.; Bowerman, B.S.; Biehl, G.E., "Hysteresis in Metal/Hydrogen Systems," Scripta Metall., Vol. 14, pp. 443-447, 1980.
- Golben, P.M., "Multi-Stage Hydride-Hydrogen Compressor," Proc. 18th Intersociety Energy Conversion Engineering Conference, pp. 1746-1753, 1983.
- Goodell, P.G.; Sandrock, G.D.; Huston, E.L., "Kinetic and Dynamic Aspects of Rechargeable Metal Hydrides," J. Less-Common Metals, Vol. 73, pp. 135-142, 1980.
- Goodell, P.D.; Rudman, P.S., "Hydriding and Dehydriding Rates of the LaNi<sub>5</sub>-H System," J. Less-Common Metals, Vol. 89, pp. 117-125, 1983.
- Gorman, R.; Moritz, P.S., "Design Study and Cost-Effectiveness of the Metal Hydride Solar Heat Pump and Power System (HYCSOS)," Proc. 14th Intersociety Energy Conversion Engineering Conference, pp. 109-113, 1979.
- Gruen, D.M.; Mendelsohn, M.H.; Sheft, I., "Metal Hydrides as Chemical Heat Pumps," Solar Energy, Vol. 21, pp. 153-156, 1978.

- Hodgson, E.W.; Dresser, K.J., "Subsystem Conceptual Study Report for the Regenerable Non-Venting Thermal Sink (RNTS)," Contract No. NAS9-16609, United Technologies, Hamilton Standard, December 1982.
- Huston, E.L.; Sandrock, G.D., "Engineering Properties of Metal Hydrides," J. Less Common Metals, Vol. 74, pp. 435-443, 1980.
- Jones, J.A.; Golben, P.M., "Design, Life Testing, and Future Designs of Cryogenic Hydride Refrigeration Systems," Cryogenics, Vol. 25, pp. 212-219, April 1985.
- Lin, C., "Statement of Work for A Metal Hydride Chemical Heat Pump for Advanced Extravehicular Mobility Unit," NASA-JSC Internal Document, pp. 1-15, May 1985a.
- Lin, C., NASA-JSC, Code EC2, personal communication, June 1985b.
- Lynch, J.F.; Libowitz, G.G.; Maeland, A.J., "Hysteresis in the Nb-V-H System," J. Less-Common Metals, Vol. 103, pp. 117-122, 1984.
- NASA Facts, "A Wardrobe for Space," JSC-09378 (Rev. A), pp. 1-8.
- Reilly, J.J.; Johnson, J.R., "Titanium Alloy Hydrides; Their Properties and Applications," Proc. 1st World Hydrogen Energy Conference, Miami Beach, Florida, pp. 8B.3-8B.26, March, 1976.
- Reilly, J.J., "Synthesis and Properties of Useful Metal Hydrides: A Review of Recent Work at Brookhaven National Laboratory," Hydrides for Energy Storage, Proc. Intl. Symp. Geilo, Norway, 14-19 Aug. 1977, pp. 301-322, Pergamon Press, 1978a.
- Reilly, J.J., "Metal Hydride Technology," Zeit. Phys. Chem. N.F., Vol. 117, pp. 155-184, 1979.
- Reilly, J.J.; Sandrock, G.D., "Hydrogen Storage in Metal Hydrides," Scientific American, pp. 118-129, Feb., 1980.
- Reilly, J.J., Dept. Applied Science, Brookhaven National Laboratory, Upton, Long Island, NY 11973, personal communication, July 9, 1985.
- Rosso, M.J., Ergenics Corp., 681 Lawlins Rd., Wykoff, NJ 07481, (201) 891-9103, personal communication, July 9, 1985b.
- Rosso, M.J., *ibid.*, July 18, 1985c.
- Rudman, P.S., "Hydriding and Dehydriding Kinetics," J. Less-Common Metals, Vol. 89, pp. 93-110, 1983.
- Sandrock, G.D.; Huston, E.L., "How Metals Store Hydrogen," Chemtech, Vol. 11, pp. 754-762, 1981.
- Sandrock, G.D.; Goodell, P.D., "Cyclic Life of Metal Hydrides with Impure Hydrogen: Overview and Engineering Considerations," J. Less-Common Metals, Vol. 104, pp. 159-173, 1984.

- Sheft, I.; Gruen, D.M.; Lamich, G.J.; Carlson, L.W.; Knox, A.E.; Nixon, J.M.; Mendelsohn, M.H., "HYCOS: A System for Evaluation of Hydrides as Chemical Heat Pumps," *Hydrides for Energy Storage; Proc. Intl. Symp., Geilo, Norway, Aug. 14-19, 1977, Pergamon Press, Ltd., 1978, pp. 551-567.*
- Sheft, I.; Gruen, D.M.; Lamich, G.J., "Current Status and Performance of the Argonne HYCOS Chemical Heat Pump System," *J. Less-Common Metals, Vol. 74, pp. 401-409, 1980.*
- Sinha, V.K.; Wallace, W.E., "Hydrides of ZrMn<sub>2</sub>-Based Alloys Substoichiometric in Zirconium for Engineering Applications," *J. Less-Common Metals, Vol. 106, 199-210, 1985.*
- Sinha, V.K.; Yu, G.Y.; Wallace, W.E., "Hydrogen Storage in Some Ternary and Quaternary Zirconium-Based Alloys with the C14 Structure," *J. Less-Common Metals, Vol. 106, pp. 67-77, 1985.*
- Snape, E.; Lynch, F.E., "Metal Hydrides Make Hydrogen Accessible-I," *Chemtech, Vol. 10, pp. 578-583, 1980.*
- Suda, S.; Komazaki, Y.; Kobayashi, N., "Mixing Effects of Metal Hydrides on Equilibrium Behavior and Reaction Kinetics," *Int. J. Hydrogen Energy, Vol. 6, pp. 275-284, 1981a.*
- Terry, L.E., "Hydrogen-Hydride Absorption Systems and Methods for Refrigeration and Heat Pump Cycles," *U.S. Patent 4,055,962, Nov. 1, 1972.*
- Tuscher, E.; Weinzierl, P.; Eder, O.J., "Dynamic Characteristics of Single- and Dual-Hydride Bed Devices," *J. Less-Common Metals, Vol. 95, pp. 171-179, 1983.*
- Wenzl, H., "Properties and Applications of Metal Hydrides in Energy Conversion Systems," *Int. Metals Rev., Vol. 27, pp. 140-168, 1982.*
- Weppner, W.; Huggins, R.A., "Electrochemical Methods for Determining Kinetic Properties of Solids," *Ann. Rev. Materials Science, Vol. 12, R.A. Huggins, Ed., Annual Reviews, Inc., Palo Alto, CA, p. 271, 1978.*

## 5.2 Secondary References

- Andresen, A.F.; Maeland, A.J., Eds., "Hydrides for Energy Storage," *Proceedings of an International Symposium held in Geilo, Norway, 14-19 August 1977, Pergamon Press, 1978.*
- Argabright, T.A., "Metal Hydride/Chemical Heat-Pump Development Project," *Phase I, Final Report, Brookhaven National Laboratory, Contract No. DE-AC02-76CH00016, U.S.D.O.E., pp. 1-199, Feb. 1982.*
- Argabright, T.A., "Heat/Mass Flow Enhancement Design for a Metal Hydride Assembly," *Phase II, Final Report, Brookhaven National Laboratory, Contract No. DE-AC02-76CH00016, U.S.D.O.E., pp. 1-60, Sept. 1983.*

- Belkbir, L.; Gérard, N.; Percheron-Guégan, A.; Achard, J.C., "Kinetics of Hydrogen Absorption and Desorption by Ternary  $\text{LaNi}_5$ -type Intermetallic Compounds," *Int. J. Hydrogen Energy*, Vol. 4, pp. 541-557, 1979.
- Bittner, H.F.; Badcock, C.C., "Electrochemical Utilization of Metal Hydrides," *J. Electrochem. Soc.*, Vol. 130, pp. 193C-198C, 1983.
- Busch, G.; Schlapbach, L.; von Waldkirch, T., "Hydrides of Rare Earth-Nickel Compounds: Structure and Formation Enthalpies," *Hydrides for Energy Storage*, Proc. Intl. Symp. Geilo, Norway, 14-19 Aug. 1977, pp. 287-299, Pergamon Press, 1978.
- Butera, R.A.; Peterman, D.J.; Franciosi, A.; Peterson, D.T., "Hydrogen Diffusion and Hydride Formation at the Metal-Hydride Interface," *J. Chem. Phys.*, Vol. 79, pp. 2395-2399, 1983.
- Cox, K.E.; Williamson, K.D., Eds., "Hydrogen: Its Technology and Implications," CRC Press, Inc., Cleveland, OH, 1977.
- de Pous, O.; Lutz, H.M., "Use of Binary Titanium Alloys for Hydrogen Storage," *Hydrogen Energy System*, Proc. 2nd World Hydrogen Energy Conference, Zurich, Switzerland, 21-24 Aug. 1978, T.N. Veziroglu and W. Seifritz, Eds., pp. 1525-1541, Pergamon Press, 1979a.
- de Pous, O.; Lutz, H.M., "Effect of the Interstitial Hole Size and Electron Concentration on Complex Metal Hydride Formation," *ibid.*, pp. 1597-1611, 1979b.
- Golben, P.M.; Huston, E.L., "A Technique for Analyzing Reversible Metal Hydride System Performance," *J. Less-Common Metals*, Vol. 89, pp. 333-340, 1983.
- Gorman, R.; Moritz, P.S., "Metal Hydride Solar Heat Pump and Power System (HYCSOS)," *AIAA/ASERC Conference on Solar Energy: Technology Status*, pp. 1-5, Nov. 1978.
- Griessen, R.; Driessen, A.; De Groot, D.G., "Search for New Metal-Hydrogen Systems for Energy Storage," *J. Less-Common Metals*, Vol. 103, pp. 235-244, 1984.
- Heckes, A.A.; Hinkebein, T.E.; Northrup, C.J.M., "Hydride Engines," *Proc. 14th Intersociety Energy Conversion Engineering Conference*, pp. 743-746, 1979.
- Huston, E.L.; Sheridan, J.J., "Industrial Applications of Rare Earth Elements," *ACS Symposium Series*, No. 164, *Industrial Applications of Rare Earth Elements*, Karl A. Gschneider, Jr. Ed., pp. 223-250, Las Vegas, Nevada, August 25-26, 1980b.
- Isa, B., "Characterization of  $\text{LaNi}_{4.7}\text{Al}_{0.3}$  Hydride for Hydrogen Storage," M.E. 499 Senior Project, Dept. Mechanical Engineering University of Hawaii, pp. 1-26, Dec. 1983.
- Ivey, D.G.; Northwood, D.O., "Storing Energy in Metal Hydrides: A Review of the Physical Metallurgy," *J. Mater. Sci.*, Vol. 18, pp. 321-347, 1983.

- Karlicek, R.F., "Hydrogen Diffusion in beta-LaNi<sub>5</sub> Hydride," *J. Less-Common Metals*, Vol 73, pp. 219-225, 1980.
- Libowitz, G.G., "Metal Hydrides for Thermal Energy Storage," *Proc. 9th Intersociety Energy Conversion Engineering Conference*, pp. 322-325, 1974.
- Maeland, A.J., "Survey of the Different Types of Hydrides," *Hydrides for Energy Storage*, *Proc. Intl. Symp. Geilo, Norway, 14-19 Aug. 1977*, A.F. Andresen and A.J. Maeland, Eds., pp. 19-31, Pergamon Press, 1978.
- Maeland, A.J., "Investigation of Some New Hydride Systems," *J. Less-Common Metals*, Vol 89, pp. 173-182, 1983.
- Miyamoto, M.; Yamaji, K.; Nakata, Y., "Reaction Kinetics of LaNi<sub>5</sub>," *J. Less-Common Metals*, Vol 89, pp. 111-116, 1983.
- Nagel, M.; Komazaki, Y.; Uchida, Y.; Sud; Matsubara, Y., "Operating Characteristics of a Metal Hydride Heat Pump for Generating Cooled Air," *Int. Symp. Properties and Applications of Metal Hydrides, Eliat, Israel, April 9-13, 1984*; *J. Less-Common Metals*, Vol. 104, pp. 307-318, 1984.
- Nishizaki, T.; Miyamoto, K.; Yoshida, K., "Coefficients of Performance of Hydride Heat Pumps," *J. Less-Common Metals*, Vol. 89, pp. 559-566, 1983.
- Nomura, K.; Akiba, E.; Ono, S., "Kinetics of the Reaction between Mg<sub>2</sub>Ni and Hydrogen," *Int. J. Hydrogen Energy*, Vol. 6, pp. 295-303, 1981.
- Ohlendorf, D.; Flotow, H.E., "Experimental Heat Capacities of LaNi<sub>5</sub>, alpha-LaNi<sub>5</sub>H<sub>0.36</sub>, and beta-LaNi<sub>5</sub>H<sub>6.39</sub> from 5 to 300 K. Thermodynamic Properties of the LaNi<sub>5</sub>-H<sub>2</sub> System," *J. Chem. Phys.*, Vol. 73, pp. 2937-2948, 1980.
- Okamoto, M; Hagiwara, Z, "Kinetic Study on Sorption of Hydrogen with Metals," *Journal Japan Institute of Metals*, Vol. 44, pp. 1111-1121 (1980) [abstract]
- Reilly, J.J., "Applications of Metal Hydrides," *Hydrides for Energy Storage*, *Proc. Intl. Symp. Geilo, Norway, 14-19 Aug. 1977*, pp. 527-550, 1978b.
- Reilly, J.J.; Johnson, J.R.; Lynch, J.F.; Reidinger, F., "Irreversible Effects in the FeTi-H System," *J. Less-Common Metals*, Vol. 89, pp. 505-512, 1983.
- Reilly, J.J.; Johnson, J.R., "The Kinetics of the Absorption of Hydrogen by LaNi<sub>5</sub>H<sub>x</sub>-n-Undecane Suspensions," *J. Less-Common Metals*, Vol. 104, pp. 175-190, 1984.
- Rhoy, D.A.; Angabright, T.A.; Wade, G.W., "Metal Hydride Heat Pump." *Proc. 17th Intersociety Energy Conversion Engineering Conference, Los Angeles, CA, Aug. 8-12, 1982*, pp. 1160-1165 [abstract].
- Ron, M., "A Hydrogen Heat Pump as a Bus Air Conditioner," *J. Less-Common Metals*, Vol. 104, pp. 259-278, 1984.
- Rosso, M.J., Ergenics Corp., 681 Lawlins Rd., Wykoff, NJ 07481, (201) 891-9103, personal communication, June 5, 1985a.



- Rudman, P.S., "Hydrogen-Diffusion-Rate-Limited Hydriding and Dehydriding Kinetics," *J. Appl. Phys.*, Vol. 50, pp. 7195-7199, 1979.
- Sandrock, G.D., "The Metallurgy and Production of Rechargeable Hydrides," *Hydrides for Energy Storage*, Proc. Symposium, Geilo, Norway, pp. 353-393, Aug. 1977.
- Suda, S.; Kobayashi, N., "Reaction Kinetics of Metal Hydrides and Their Mixtures," *J. Less-Common Metals*, Vol. 73, pp. 119-126, 1980.
- Suda, S.; Kobayashi, N.; Yoshida, K., "Thermal Conductivity in Metal Hydride Beds," *Int. J. Hydrogen Energy*, Vol. 6, pp. 521-528, 1981.
- Suda, S., "Recent Development of Hydride Energy Systems in Japan," *Proc. 5th World Hydrogen Energy Conference*, Toronto, July 1984a.
- Suda, S., "Experimental Evaluation of Heat Pump Performance in Connection with Metal Hydride Properties," *Proc. Int. Symp. Properties and Applications of Metal Hydrides*, Eliat, Israel, April 9-13, 1984; *J. Less-Common Metals*, Vol. 104, pp. 211-222, 1984b.
- Suzuki, R.; Ohno, J.; Gondoh, H., "Effect of Sulphur Addition on the Properties of Fe-Ti Alloy for Hydrogen Storage," *J. Less-Common Metals*, Vol. 104, pp. 199-206, 1984.
- Tanaka, S.; Flanagan, T.B., "Hydrogen in LaNi<sub>5</sub> Intermetallic Compound," *Hydrogen in Metals: Proc. 2nd Intl. Symp.*, Minakami, Gumma, Japan, Nov. 26-29, 1979. [abstract]
- van Mal, H.H., "The Activation of a Lanthanum-Nickel-Five Hydrogen Absorbent (Research Film)," *Hydrogen Energy*, Vol. A, Proc. Hydrogen Economy Miami Energy (THEME) Conference, Miami Beach, Florida, March 18-20, 1974, T.N. Veziroglu, Ed., pp. 605-610, Plenum Press, 1975.
- van Rijswijk, M.H.J., "Metal Hydride Electrodes for Electrochemical Energy Storage," *Hydrides for Energy Storage*, pp. 261-271, 1978.
- Veziroglu, T.N., Ed., *Proceedings of the 1st World Hydrogen Energy Conference*, 1-3 March 1976, Miami Beach, Florida, University of Miami Press, 1976.
- Veziroglu, T.N.; Seifritz, W., Eds., "Hydrogen Energy System," *Proceedings of the 2nd World Hydrogen Energy Conference*, Zurich, Switzerland, 21-24 August 1978.
- Yonezu, I.; Nasako, K.; Honda, N.; Sakai, T., "Development of Thermal Energy Storage Technology using Metal Hydrides," *J. Less-Common Metals*, Vol. 89, pp. 351-358, 1983.
- Yvon, K., "Structural Aspects of Ternary Metal Hydrides: A Critical Review," *J. Less-Common Metals*, Vol. 103, pp. 53-70, 1984.

### 5.3 Notes

1. Oxygen is also circulated through the crewmember's suit and the waste heat is transferred to the same evaporator as the water using a three-phase heat exchanger.
2. The pressure is regulated to maintain the temperature of the LaNi<sub>5</sub> evaporator at 40°F. These one-way check valves can be designed to open whenever the pressure on the input side is greater (by  $\frac{1}{2}$  psi) than the output side and close if the pressure is greater on the output side than on the input. Due to their simple operation, these valves are extremely reliable and maintenance free [Golben, 1983].
3. One major advantage of this system is that no thermal insulation is required (or desired) for storage. This is, of course, unlike phase-change methods used for cooling, such as the water sublimator. The system is available on demand simply by opening valve #1.
4. Most PCT plots are reported for desorption, rather than absorption, since this is thought to more closely represent the intrinsic characteristics of the material.
5. 1 H/M per minute corresponds to 6.94 mol H<sub>2</sub> per kg of LaNi<sub>5</sub> per min. [Golben and Huston, 1983].
6. Assuming the space radiator is constructed of silver-backed teflon that provides an alpha-solar of 0.08 and an IR emissivity (epsilon) of 0.78 (alpha/epsilon = 0.1), 10.5 ft<sup>2</sup> is required to provide a thermal sink at about 100°F [Hodgson and Dresser, 1982]. Since the back surface of the backpack is only 6 ft<sup>2</sup>, a higher temperature would be required to radiate enough heat from the smaller area. The area-temperature relationship is approximately  $A = 9.8E10/T^4$ . Therefore, 184°F would need 6 ft<sup>2</sup>.
7. If another EVA is planned immediately following the recharging process, the CaNi<sub>5</sub> evaporator at 161°F could be connected to the thermal management system to reduce its temperature to 80°F, recovering the sensible heat. Otherwise, the system should come to thermal equilibrium with the environment in a few hours since the system is not insulated.

### 5.4 Acknowledgments

The author wishes to acknowledge the following individuals and organizations for assistance in the completion of this document. Chin H. Lin, NASA-JSC, Houston, TX for initially proposing the problem; Matthew J. Rosso, Jr., Ergenics Corporation, Wyckoff, NJ; Jim J. Reilly, Brookhaven National Laboratory, Upton, Long Island, NY; and Jack A. Jones, Jet Propulsion Laboratory, Pasadena, CA for helpful discussions and documentation on the properties of hydrides and heat pumps; and finally, The NASA/ASEE Summer Faculty Research Fellowship Program; and The Hawaii Natural Energy Institute, University of Hawaii at Manoa, Honolulu, HI, Project No. 2757-20 for financial and material support.

N86 - 31428

D9  
7P.

FLOW CYTOMETRY ANALYSIS OF HORMONE RECEPTORS ON HUMAN  
PERIPHERAL BLOOD MONONUCLEAR CELLS TO IDENTIFY  
STRESS-INDUCED NEUROENDOCRINE EFFECTS

18830

Richard T. Meehan, M.D.  
Assistant Professor  
Department of Internal Medicine  
University of Texas Medical Branch  
Galveston, Texas

Understanding the role of circulating peptide hormones in the pathogenesis of space-flight induced disorders (space adaptation syndrome, musculo-skeletal atrophy, and immune dysfunction) would be greatly facilitated by a method which allows monitoring chronic levels of hormones and their effects upon in vivo cell physiology. Single and simultaneous multi-parameter flow cytometry analysis was employed to identify subpopulations of mononuclear cells bearing receptors for ACTH, Endorphin, and Somatomedin-C using monoclonal antibodies and monospecific antisera with indirect immunofluorescence.

Blood samples were obtained from normal donors and subjects participating in decompression chamber studies (acute stress), medical student academic examination (chronic stress), and a drug study (Dexamethasone). Preliminary results indicate most ACTH and Endorphin receptor positive cells are monocytes and B-cells, exhibit little diurnal variation but the relative percentages of receptor positive cells are influenced by exposure to various stressors and ACTH inhibition.

This study demonstrates the capability of flow cytometry analysis to study cell surface hormone receptor regulation which should allow insight into neuroendocrine modulation of the immune and other cellular systems during exposure to stress or microgravity.

---

NASA Colleague: Jim Waligora SD3 X5281

C-7

## INTRODUCTION

Prior studies document elevated levels of various hormones during space flight but their role in the pathogenesis of musculoskeletal atrophy, space adaptation syndrome (SAS) or immune depression is unclear (1,2). The relationship of neuropeptides to SAS is intriguing since; ACTH release may correlate with susceptibility to motion sickness in humans (3), the pituitary adrenal axis modulates blood brain barrier permeability in rats (4) and dexamethasone therapy appears to reduce symptoms of motion sickness (5).

A regulatory circuit between the immune and CNS systems involve common peptides and receptors modulated by feedback mechanisms (6, 7). Hormone receptor physiology has greatly expanded our understanding of hormone action at the cellular level in humans (8). Therefore, in vivo neuropeptide receptor expression on circulating immune cells may represent a novel method to; monitor chronic hormone levels or identify neuroendocrine modulation of the immune system or other organs at the cellular level during exposure to stress or microgravity.

## THEORY/OBJECTIVES

This study utilized flow cytometry analysis to:

1. Identify and characterize peripheral blood lymphocyte and monocyte populations bearing ACTH, endorphin, and somatomedin-C hormone receptors using indirect immunofluorescence with anti-receptor monospecific antisera or monoclonal antibodies.
2. Determine if neuropeptide receptor regulation is influenced by exposure to different stressors or changes in circulating hormone (ligand) levels.

## METHODS

Peripheral blood mononuclear cells were isolated by boyant density sedimentation as previously described (2). Cells were washed in PBS and incubated for 30 minutes in PBS containing sodium azide with the appropriate monoclonal antibody or monospecific antisera against neuropeptide receptors (9,10). Following two subsequent washes, a second incubation was performed using goat anti-rabbit conjugated with FITC or phycoerythrin conjugated to  $T_4$  (helper),  $T_8$  (suppressor),  $M_3$  (monocytes), Dr (Monocytes and B cells) monoclonal antibodies. After additional washes cells were fixed in 1% paraformaldehyde. Flow cytometry analysis was performed on  $12 - 20 \times 10^3$  cells using logarithmic integral green or red fluorescence after gating on forward angle light scatter. The receptor or surface phenotype positive cells were identified by subtracting the control sample histograms from those containing antibodies.

## RESULTS

There was no diurnal variation in the frequency of ACTHr or ENDORPHINr cells in the peripheral blood from five donors at 8:00 a.m. and 3:00 p.m. daily for five days ( $13 \pm 1\%$  vs.  $12 \pm 2\%$  for ACTHr and  $17 \pm 1\%$  vs.  $17 \pm 1\%$  for ENDORPHINr cells). Simultaneous two parameter subset analysis from 7 subjects demonstrated that most ACTHr and ENDORPHINr cells are monocytes but neuropeptide receptors are also identified on some of  $T_8$  and  $T_4$  positive cells. Similar results were obtained with somatomedin-C receptor positive cells.

	<u>All Cells</u>	<u>Dr<sup>+</sup></u>	<u>M<sub>3</sub><sup>+</sup></u>	<u>T<sub>4</sub><sup>+</sup></u>	<u>T<sub>8</sub><sup>+</sup></u>
ACTHr	11 $\pm$ 1%	41 $\pm$ 9%	69 $\pm$ 8%	8 $\pm$ 1%	23 $\pm$ 6%
ENDORPHINr	18 $\pm$ 3%	52 $\pm$ 7%	84 $\pm$ 2%	10 $\pm$ 1%	32 $\pm$ 7%
Somatomedinr	9 $\pm$ 1%	33%	57%	7%	51%

We did not detect a difference in the percentage of ACTHr positive cells from 17 subjects tested twice within 24 hours, when samples were obtained before and immediately after a decompression chamber study simulating six hours of EVA ( $17 \pm 2\%$  pre vs.  $17 \pm 2\%$  post). Preliminary data from eight subjects taking dexamethasone 9 mg per day did strongly suggest that drug treatment which blocks ACTH release increases the number of cells bearing ACTH and ENDORPHIN receptors.

	<u>Dexamethasone</u>		
	<u>Off Drug</u>	<u>Three Days</u>	<u>Seven Days</u>
ACTHr	$6 \pm 3\%$	$25 \pm 5\%$	$16 \pm 2\%$
ENDORPHINr	$11 \pm 3\%$	$25 \pm 3\%$	$23 \pm 4\%$

Data from 10 UTMB medical students on the day of a major academic examination (chronic stress) was remarkable since 5 of 10 subjects had ENDORPHINr/ACTHr cell ratios less than 1 (range 0.4 to 0.9). This was observed in only three of 78 other individuals under a variety of different conditions to date which may represent an objective marker of chronic stress. These 10 subjects demonstrated  $18 \pm 3\%$  ACTHr cells vs.  $18 \pm 3\%$  ENDORPHINr cells and will be compared with data obtained during a "nonstress" control interval.

#### CONCLUSIONS

1. Simultaneous multiparameter flow cytometry analysis represents an excellent method to identify hormone receptor positive cells in vivo and determine which subpopulation of cells express specific receptors and surface phenotype markers.
2. Our data indicate ACTH and ENDORPHIN receptor positive cells have minimal diurnal variation and are primarily expressed on monocytes but also on some T helper and T suppressor cells.

3. Preliminary results to date indicate:

- a. The number of ACTH receptor positive cells are unaltered within 24 hours following exposure to acute stress (decompression study simulating EVA activity).
- b. An ENDORPHIN:ACTH receptor positive cell ratio less than 1 was seen in 50% of medical students during academic examination which may represent an objective marker of perceived chronic stress.
- c. Dexamethasone appears to increase ACTH receptor positive cells which may represent "up regulation" in response to suppression of circulating ACTH levels.

#### APPLICATIONS

Flow cytometry analysis of human leukocyte hormone receptor regulation may identify an objective marker of perceived stress and provide a method for determining chronically elevated or depressed levels of circulating neuropeptides or hormones. This technique could be employed for in-flight monitoring of crew members and studying neuroendocrine or microgravity-induced influences at the cellular level.

#### Acknowledgment

The study could not have been completed without the expert technical assistance from Lori Neal (Northrop), Gerald Taylor, Ph.D. (NASA), Ulric Duncan (UTMB) and the development and use of antibodies from Drs. Bost, Blalock and Stuart (UTMB faculty).

## References

1. Leech, C.S., Branbaut, P.C., "Biochemical responses of the skylab crewman: An Overview," Biomedical Results from Skylab, NASA SP 377, pp. 204-215, 1977.
2. Dardano, J., Taylor, G.R., "Human cellular immune responses following space flight," Aviation Space Environmental Medicine, 54:555, 1983.
3. Kohl, R.L., "Endocrine correlates of susceptibility to motion sickness" in press: Aviation Space Environmental Medicine.
4. Long, J.B., Holiday, J.W., "Blood brain barrier endogenous modulation by adrenal cortical function," Science, 227:1580-1582, 1985.
5. Kohl R. (1955) Pharmacology and Endocrinology: Perspectives on the Problem of Space Adaption Syndrome. In Proceedings of the Space Adaptation Syndrome Drug Workshop. July, 1983 (R.L. Kohl, ed.) p. 21-22. Space Biomedical Research Institute. USRA Division of Space Biomedicine, Houston.
6. Blalock, J.E., Harbour-McMenzmin, D., Smith, E. Peptide hormones shared by the neuroendocrine and immunologic systems. J. Immunol. 135:858s-961s, 1985.
7. Blalock, J.E., Smith, "A Complete Regulatory Loop Between the Immune and the Neuroendocrine Systems", Federation Proceedings, 44:108-111, 1985.



8. Pollet, R.J., Levey, G.S., "Principles of membrane receptor physiology and their application to clinical medicine", *Annals Int. Med.* 92:663-680, 1980.
9. Maron, R., Jackson, R.A., Jacobs, S., Eisenbarth, G., Kahn, C.R., "Analysis of the insulin receptor by anti-receptor antibodies and flow cytometry:", *Prop. Natl. Acad. Sci.* 81:7446-7450, 1984.
10. Bost, K.L., Smith, E.M., Blalock, J.E., "Similarity between the corticotropin (ACTH) receptor and a peptide encoded by an RNA that is complementary to ACTH MRNA", *Proc. Natl. Acad. Sci.* 82:1372-1375, 1985.

N86 - 31429 D20

178.

18831

AUTOMATION OF REVIEW/APPROVAL CYCLE OF MCAUTO CAD/CAM GENERATED

DRAWINGS AND DOCUMENTS

HOWARD S. MINN SC.D.

PROFESSOR OF ELECTRICAL ENGINEERING

MCNEESE STATE UNIVERSITY

LAKE CHARLES, LOUISIANA

NASA - ASEE Summer Fellow

Johnson Space Center

Man - Systems Division

NASA Colleague: Don Young/SP2

August 1985

## ABSTRACT

At the present the review/approval of MCAUTO/UNIGRAPHICS CAD/CAM generated drawings and documents are done through routing of hard copies of drawings and memos via mail. This process is rather time consuming and expensive due to physical routine of documents and the need for repeated reproduction of hard copies.

This author proposes a set of procedures and the required software tools by which transmission, revision, and signing-off of such documents will be accomplished via electronic data transfer while maintaining a sufficient degrees of data integrity and individual security. A main resistance to such technique will be due to the limited size of the display screen (19 inch class) and infrequent layer switching with the attendant time delay during the process of reviewing the drawing. However such opposition should diminish as the users become familiar with both the hardwares and its operation.

The author suggests that the user profiles are set so that the protection class list of the originator of the drawing includes at least one common class with each of the individuals who will be involved in the Revision/Approval cycle. In this way the originator will be able to transfer a file for their review and also be able to copy back the file to make the necessary permanent changes.

The integrity of the file is maintained by layer copying, layer blanking, display color change, and restricted owner access privilege. The individual security is maintained by restricted access to signature files and by restricting the list of individuals who will be authorized to signoff. This is accomplished through two softwares: LAYCOPY and SIGN.

The author feels that this proposed procedures and

techniques will adequately maintain both the file integrity and individual security during Review/Approval Cycle of MCAUTO generated drawings without the need for hardcopy routing.

---

NASA Colleague: Don Young, SP2, X4161

## CHAPTER I. INTRODUCTION

At present the review/approval of MCAUTO/UNIGRAPHIC CAD/CAM generated drawings and documents are accomplished through routing of hard copies via mail. This process is rather slow and expensive due to the need for physical routing of the hard copies and the need for repeated reproduction of the hard copies.

This author purposes a set of procedures through which the above stated task may be accomplished through electronic transfer of files and memos while the integrity of the part file and the security of individuals who are involved in the cycle are adequately protected. This will eliminate the need for physical routing of hard copies. This report also includes a set of softwares which simplifies the above stated task.

The author expects some objections initially from the personnel who will be involved in the review/approval cycle since this is something different from the past practices. As I see it, maybe the most apparent shortcomings are the limited size of the display screen and some time lags during layer switching. However as the users become familiar with both the hardware itself and its operation, this limitations should become of less significance.

This report presents the sequential steps through which creation, review, and correction of a design would normally follow. Therefore by following the suggested sequence of steps, a given user can complete the given portion of the task, and the job would be ready for the next person in the cycle. This procedure is set up so that the originator who should be reasonably familiar with the UGII file management techniques would do most of the file manipulations while the rest of the user in the cycling would make simple use of UGII only.

## CHAPTER II

### CREATION AND PREPARATION OF A PART FILE

The original designer of the part file will be referred as the originator, and he will be responsible for designing the part and for setting up the proper environment for cycling of the file; i.e. the originator is responsible for maintaining the part integrity and individual security by controlling the file access. Before a file can be put in the Review/Approval cycle the following steps need to be completed:

- a. All original design should lie in layers 1 through 100.
- b. Layer 1 shall contain the signature block and the layer listing.
- c. The signature of each person who needs to sign shall be filed in archives format in each individual directory with his initials (first, middle, last name) as the file name.

Furthermore the signature (would be convenient to use digitpad to generate) should be located in layer one left justified at the WCS origin with proper scaling.

- d. The initials of those who will be involved in the review cycle will be inserted properly in GRIP source program "SIGN.GRS" via editing, then the program should be compiled and linked to generate "SIGN.GRX" file for later use.
- e. Have the system manager configure the protection class list of the originator so that this list will contain at least one common protection class with each person who will be in the review cycle.
- f. When each of the above steps has been completed and the proper part file has been designed and is placed in the current file, follow the steps below:
  1. Set registers A=1, B=100, and C = 100 through calculator mode.
  2. Run GRIP program "LACOPY.GRX". This will copy layers 1 through 100 to layers 101 through 200 (this process might take a while depending on the complexity of the file, so be patient!)
  3. Change the entity display color to that which has not been used so far in the existing part. This will enable the originator to readily detect any changes that have been made by the latest reviewer when the file has been returned.
  4. File the part in checkpoint format. Now this part is

ready to be transferred for revision. If it needed, proceed to Chapter III.

## CHAPTER III

### TRANSFER OUT AND REVISION OF A FILE

This chapter will explain the steps required for transferring out a file to a sendee's directory and the subsequent revision by the receiver:

a. Move the affect part file from the originaotr to the sendee by file management executive command "MOVE" as:

MOVE ALWAYS VERIFY (part name.PRT) to (Sendee's Directory).

Also move "SIGN.GRX" (this file needs to be moved only once to a given individual for a given project) as:

MOVE ALWAYS VERIFY SIGN.GRX TO (Sendee's Directory).

b. Modify the part file header so that the new owner is the sendee and the protection class is the one which is common to the originator and the sendee as:

MODIFY HEADER (Sendee's Directory: part name.PRT) to OWNER (Sendee) PCLASS (Common Protection Class).

Now the sendee will be able to retrieve and make changes on this part. Also modify the header of "SIGN.GRX" as:

MODIFY HEADER (Sendee's Directory): SIGN.GRX to PCLASS (a common PCLASS).

c. Now the file is ready for the sendee to use. Inform him by an electronic memo stating:

1. The part file name.
2. Confine the revision to layers 1 through 100.
3. Upon completion of revision, run GRIP "SIGN" to signoff entering his initials and indicating the sign position when the computer prompts.

d. To revise the part, follow the steps below:

1. Using UGII, retrieve the desired part file and make all necessary corrections on layers 1 through 100.
2. When completed, signoff by running GRIP "SIGN".



3. File the part in checkpoint format.
4. Inform the originator via electronic memo informing that you have completed the revision .

## CHAPTER IV.

### RETURN OF THE REVISED FILE AND PERMANENT CORRECTION

Upon receiving a message from the sendee that the file has been signed off, the originator will run through the following procedures to transfer in the part file and make all permanent corrections:

- A. Copy the part file back to the originator's directory using a file management executive command "COPY" as:

COPY (part file specs TO (part name.PRT).

The part name should be chosen so that it will be unique and also give some good indication to the progress of the file. One convenient way would be to assign a number as the last character of the part name which will increase as the file progresses through the revision cycle.

- B. Retrieve the copied file.
- C. Unblank layers 101 through 200.
- D. Change the entity display color to the original one.
- E. Make all permanent corrections on layers 101 through 200 in Reference to layer 1 through 100.
- F. Transfer the latest signature from layer 1 to layer 101.
- G. Set the registers: A=101, B=200, and C=100.
- H. Run GRIP "LACOPY" to copy layers 101 through 200 to layers 1 through 100.

Now return to step II.F.3 in order to proceed to the next step in the cycle.

## CHAPTER V CONCLUSION

It was stated in the introduction that there are some obvious shortcomings in this Revision/Approval procedures which I have proposed using the existing hardwares.

However the limited size of the display screen problem may be somewhat leviated by judicious use of the Zoom/Pan capability of UGII. As for the file integrity, the originator will always have a copy of the part file in his directory which should be the latest version. Also the blanked layers 101 through 200 in the transfered file is an original file which is protected from the user somewhat. Thus it should be possible to recover a valid file anytime during the Revision/Approval cycle.

The individual security is adequately protected because: (1) the individual signature resides in that particular individual's directory, (2) the protection class of this file can be made quite unique to that of the particular individual, and (3) the initials of an authorized person has to be placed in the GRIP Source Program "SIGN.GRS" in a proper sequence by the originator. Thus the originator has a rather strict control on who is authorized to sign and whose signature may be placed on the drawing.

The author feels that once the users become familiar with this proposed procedures and techniques and with both the UGII hardwares and softwares, the Revision/Approval cycle of CAD/CAM generated drawings and documents can be automated with minimal difficulties while maintaining an adequate integrity for the data file and a sufficient security for those who are involved in the process.

## REFERENCES

1. Part 8, Chapter 3 layer control, GRAF Operational Description, Volume 2, McDonnell Douglas Automaiton Company.
2. GRIP Programming Manual, McDonnell Douglas Automation Company.
3. Chapter 6 FMEXEC Commands, UGFM System Operation, McDonnell Douglas Automation Company.

## APPENDIX A

### A. GRIP PROGRAM "LACOPY"

This program copies a group of sequential layers to a another group of sequential layers where the group of layers and the off-set are determined by the contents of register A, B, and C. The sequence of tasks done by this program is:

1. Delete all entitles from the destination layers (A + C through B + C).
2. Copies all entitles from the source layers (A through B) to the respective destination layers.
3. Blank all entitles on the higher numbered duplicate layers.
4. Set layer 1 to work layer and the rest to inactive status (invisible and unselectable).

Prior to running this program, there should be a valid current file and, the registers A, B, and C are set for the desired values. While this program is running, the register L (12th) will show the layer number which is being copied currently.

The execution procedures are as follows:

1. Set the registers A, B, and C to the desired values in calculator mode (positive C for up coping and negative C for down coping).
2. With a valid current file, enter GRIP (option 13) in the Design Menu.
3. Enter run (option 4).
4. Type in "LACOPY" for prompted file specs and return.  
Depending on the complexity of the layer entitles and the load on the host computer, execution of this program might take a while, thus it will be advisable to run this program during the off-peak time.

# UNIGRAPHIC'S TEXT FILE LACOPY.GRS

```

10 $$ LAYER COPYING A THRU 8 TO A + C THRU B + C
20 $$ COPYING FROM ACTIVE TO WORK LAYER
30 $$ INITIALIZE
40 ENTITY/ENT (100)
50 NUMBER/MAT1(12)
60 $$ CLEANUP THE DETINATION LAYERS
70 NL = REGF(2)-REGF(1)+1
80 LD =REGF(1)+REGF(3)-1
90 DO/L10: ,M,1,NL
100 LW=LD+M
110 LAYER/WORK,LW,INACT,REST
120 DELETE/ALL
130 L10:
140 $$ SET THE LOOP A:LLIM, B:ULIM, C:DELTA
150 LL=REGF(1)
160 LU=REGF(2)
170 MAT1=MATRIX/TRANSL,0,0,0
180 $$ START LAYER CYCLE
190 DO/L4: ,I,LL,LU
200 J=I+REGF(3)
210 FLAG=0
220 $$ INITIALIZE SOURCE LAYER
230 LAYER/WORK,I,INACT,REST
240 INEXTE/ALL
250 L2:
260 LAYER/WORK,I,INACT,REST
270 $$ BEGIN 100 ENT SELECTION, IF END FLAG=1
280 DO/L5: ,K,1,100
290 ENT(K)=NEXTE/IFEND,L6:
300 L5:
310 N=K
320 JUMP/L7:
330 L6: FLAG=1
340 N=K-1
350 IF/N,L3:L3: ,L7:
360 L7:
370 $$ TRANSFER ENT
380 LAYER/WORK,J,INACT,REST
390 ENT(1..N)=TRANSF/MAT1,ENT(1..N)
400 IF/FLAG,L2:L2: ,L3:
410 $$ THIS LAYER FINISHED? NO NO YES
420 L3:
430 STORE/12,I
440 L4:
450 $$DECIDING UP COPING OR DOWN COPING
460 IF/REGF(3), , , L8:
470 X = REGF(1)
480 Y=REGF(2)
490 JUMP/L9:
500 L8:
510

```

520 X=REGF(1)+REGF(3)  
530 Y=REGF(2)+REGF(3)  
540 L9:  
550 \$\$BLANK UPPER COPY LAYERS  
560 LAYER/WORK,X,ACTIVE,X..Y,INACT,REST  
570 BLANK/ALL  
580 LAYER/WORK,1,INACT,REST  
590 HALT

## B. GRIP PROGRAM "SIGN.GRX"

This program enables a user to place his signature at a specific position on layer 1 of the current file. The individual signature must have been filed in archive format in that particular individual's directory with his three initials (first, middle, and last name) as its file name. Furthermore the signature should be properly scaled and is located left justified to the WCS origin on layer one.

The original GRIP source program "SIGN-GRS" needs to be customized for a given project. The three letter initials of those individuals who would be authorized to sign should be placed in the data statement (referred to a listing to follow), and the same sequence of initials should be placed in sign statements which follow L1 through L10. Upon entering these initials, the GRIP source program need to be compiled and linked to generate GRIP executable program (SIGN.GRX). This is the program which will be moved to each users in the cycle.

The execution procedures of GRIP program "SIGN" are as follows:

1. Enter GRIP (option 13) from desgin menu.
2. Enter run (option 4).
3. Type "SIGN" for requested file specs and hit return.
4. Type your three initials (First, middle, last) when prompted "YOUR INITIALS FML".
5. When a message "INDICATE SIGN POSITION" appears, pick the lower left corner position where the signature should appear with the cross hair indicator. If you have been authorized and your signature have been generated and filed properly, your signature should appear where you have indicated. If you have not been authorized, a message "YOU'RE NOT AUTHORIZED" would appear. If you signature has not been stored, a message "YOUR SIGN NOT FOUND" would appear. In either case by pressing "ENTRY COMP" key, you would exit the GRIP program execution mode.

The most convenient way to generate the signature file would be to use a DIGITPAD which might be acquired for this installation in the near future. For the time being the approximatity of the signature may be generated through spline creation routine in UGII.



# UNIGRAPHICS TEXT FILE SIGN.GRS

```

10 $$$SIGN MERGE PROG
20 $$EACH SIGNATURE IN THE OWNERS ARCHIVE FILE
30 $$WITH THEIR INITIALS(FIRST,MIDDLE,LAST)AS THE FILE NAME
40 $$THE POSITION OF SIGNATURE LEFT JUSTIFIED AT WCS ORIGIN
50 NUMBER/M1(12)
60 ENTITY/SIGN
70 STRING/INT(10,3),XYZ(3)
80 $$ TEN AUTHORIZED INITIALS FIRST MIDDLE LAST
90 DATA/INT,'AB1','AB2','AB3','AB4','AB5','AB6','AB7','AB8',
  'AB9','AB0'
100 L11:
110 LAYER/WORK,1,INACT,REST
120 TEXT/'YOUR INITIALS FML',XYZ,RSP
130 JUMP/L11:,L15:,,,RSP
140 $$ SEARCHING INITIALS, IF MATCHES, AUTHORIZED
150 DO/L13:,I,1,10
160 ANS=COMPSTR(XYZ,INT(I))
170 IF/ANS,,L14:,
180 L13:
190 MESSG/'YOU'R NOT AUTHORIZED'
200 JUMP/L15:
210 L14:
220 POS/'IND SIGN POS',X,Y,Z,RSP
230 JUMP/L14:,L15:,,,RSP
240 M1=MATRIX/TRANSL,X,Y,Z,
250 JUMP/L1:,L2:L3:,L4:L5:L6:L7:,L8:,L9,L10:,I
260 $$TEN INITIALS IN L1:-L10: CORRESPND
270 $$TO THOSE INITIALS IN DATA STATEMENT ABOVE.
280 $$$SEARCHING SIGNATURES IN ARCHIEV FILE
290 L1:
300 SIGN=RPATTG/'AB1',M1,IFERR,L22:
310 JUMP/L15:
320 L2:
330 SIGN=RPATTG/'HSM',M1, LAYER,IFERR,L22:
340 JUMP/L15:
350 L3:
360 SIGN=RPATTG/'AB3',M1,IFERR,L22:
370 JUMP/L15:
380 L4:
390 SIGN=RPATTG/'AB3'M1,IFERR,L22:
400 JUMP/L15:
410 L5:
420 SIGN=RPATTG/'AB5',M1,IFERR,L22:
430 JUMP/L15
440 L6:
450 SIGN=RPATTG/'AB6',M1,IFERR,L22:
460 JUMP/L15:
470 L7:
480 SIGN=RPATTG/'AB7',M1IFERR,L22:
490 JUMP/L15:
500 L8:
510 SIGN=RPATTG/'AB8',M1,IFERR,L22:

```

520 JUMP/L15:  
530 L9:  
540 SIGN=RPATTG/'AB9',M1,IFERR,L22:  
550 JUMP/L15  
560 L10:  
570 SIGN=RPATG/'AB0',1,IFERR,L22:  
580 JUMP/L15:  
590 L22:  
600 MESSG/'YOUR SIGN NOT FOUND'  
610 L15:  
620 HALT

THERMALLY REGENERATIVE HYDROGEN/OXYGEN  
FUEL CELL POWER CYCLES

Jeffrey H. Morehouse  
Associate Professor  
Mechanical Engineering Department  
University of South Carolina  
Columbia, South Carolina 29208

18832

ABSTRACT

Two innovative thermodynamic power cycles are analytically examined for future engineering feasibility. The power cycles use a hydrogen-oxygen fuel cell for electrical energy production and use the thermal dissociation of water for regeneration of the hydrogen and oxygen. The TDS (thermal dissociation system) uses a thermal energy input at over 2000°K to thermally dissociate the water. The other cycle, the HTE (high temperature electrolyzer) system, dissociates the water using an electrolyzer operating at high temperature (1300°K) which receives its electrical energy from the fuel cell. The primary advantages of these cycles is that they are basically a "no moving parts" system, thus having the potential for long life and high reliability, and they have the potential for high thermal efficiency.

Both cycles are shown to be classical heat engines with ideal efficiency close to Carnot cycle efficiency. The feasibility of constructing actual cycles is investigated by examining process irreversibilities and device efficiencies for the two types of cycles. The results show that while the processes and devices of the 2000°K TDS exceed current technology limits, the high temperature electrolyzer system appears to be a state-of-the-art technology development. The requirements for very high electrolyzer and fuel cell efficiencies are seen as determining the feasibility of the HTE system, and these high efficiency devices are currently being developed. It is concluded that a proof-of-concept HTE system experiment can and should be conducted.

22-2A 987

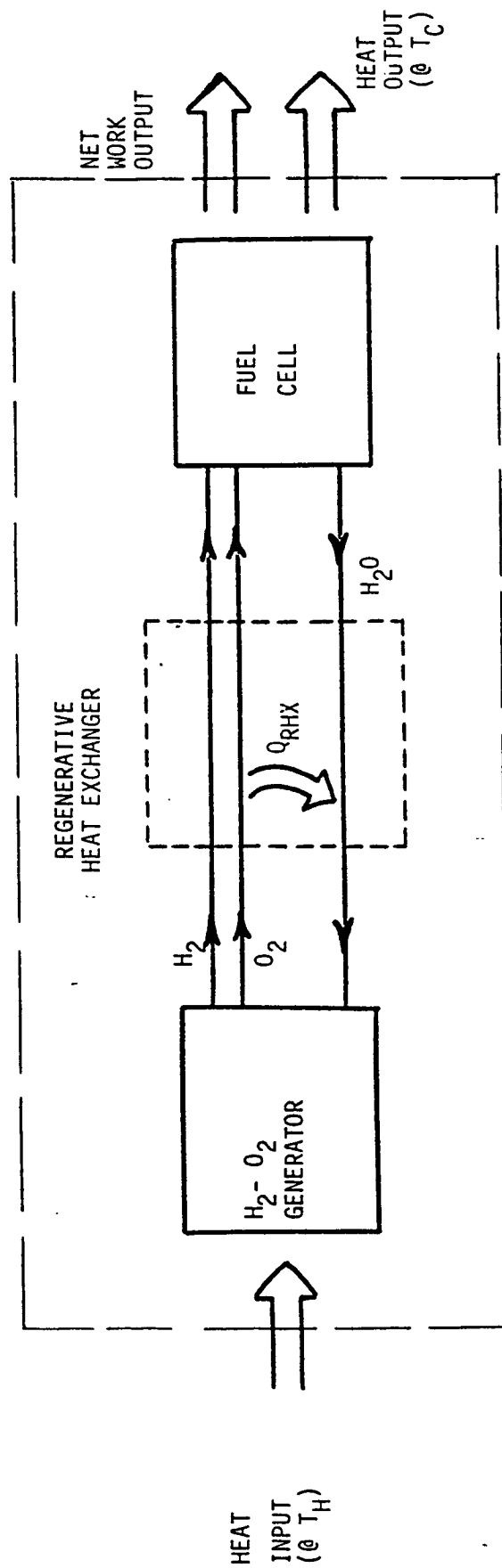


Figure 1. SCHEMATIC OF THERMALLY-DRIVEN REGENERATIVE FUEL CELL HEAT ENGINE

## INTRODUCTION

Conceptual power system designs for the proposed Space Station include both photovoltaic and thermal dynamic cycle (Rankine, Brayton, Stirling) options (Refs. G-1, 3,4). The photovoltaic system option includes an electrically-driven regenerative hydrogen-oxygen electrolyzer/fuel cell subsystem for storage and continuous operation during the orbital dark period.

The possibility of thermally-driving a fuel cell power system is attractive from several engineering aspects, as it combines some of the better features of both photovoltaic (PV) and dynamic systems. Like the PV system, a fuel cell power cycle can produce electricity without the rotating motor-generator mechanical components. Moreover, the fuel cell power cycle is capable of higher efficiencies than PV systems; much closer to the higher dynamic system thermal efficiencies. As the fuel cell cycle is thermally-driven, it can operate during a complete light-dark orbit using stored thermal energy, similar to the dynamic system operating concept. A hydrogen-oxygen fuel cell is proposed because of high efficiency and because using water as the working fluid with space missions has several inherent advantages, including crew compatibility (non-toxic, life supporting) and possible use as a reaction fuel.

The objective of this study is to examine the feasibility of methods for thermally-driving a hydrogen-oxygen fuel cell power cycle as a thermodynamic heat engine. The basic heat engine schematic is shown in Figure 1 with heat input at high temperature where water is dissociated into hydrogen and oxygen, a regenerative heat exchange between the water and hydrogen-oxygen, and a fuel cell producing electrical energy while rejecting heat. The feature of primary interest in the cycle is the method for thermally regenerating hydrogen and oxygen from the water leaving the fuel cell.

### Methods of H<sub>2</sub> - O<sub>2</sub> Generation

There are three basic methods for generating hydrogen and oxygen from water:

- o Thermal Dissociation - at high temperatures a fraction of water dissociates into H<sub>2</sub> and O<sub>2</sub> in an equilibrium reaction;
- o Thermochemical Decomposition - a series of reactions using water and other chemicals leads to H<sub>2</sub> and O<sub>2</sub>; and
- o Electrolysis - an electrical energy input causes dissociation of the water.

The thermochemical decomposition method is not examined in this study because of the comprehensive and many current and past researches in this field (Refs. A-3, 4, 5, 13; B-5, 7, 9, 12). Also, significant doubts concerning these thermochemical methods have been aired (Ref. E-17), primarily due to complexity and lack of perfect chemical recycling. Thus, this study will examine the thermal dissociation and electrolysis methods for inclusion in the fuel cell power cycle.

### IDEAL CYCLE THEORY

The thermal dissociation and electrolysis methods of generating hydrogen and oxygen have both been subjects of interest to researchers, but primarily as methods to produce hydrogen fuel, not as part of a heat engine. The development of the basic relations for the thermal dissociation and the electrolysis fuel cell systems is based on the water dissociation energy reaction.

### Hydrogen-Oxygen-Water Energies

The water reaction and equilibrium equation is



The dissociation energy or energy of reaction ( $\Delta H_f$ ) is a mild function of reaction temperature, as seen in Figure 2. For an isothermal reaction, this  $\Delta H_f$  can be thought of as "ideally" consisting of two parts or types of energy input (or output, depending on the direction of reaction):

$$\Delta H_f = \Delta G_f + T \cdot \Delta S_f \quad (2)$$

where,

$\Delta G_f$  is the Gibb's free energy, the available work (ideal work)

$T \cdot \Delta S_f$  is the isothermal heat transfer (ideal heat transfer)

As is seen in Figure 2, the ideal heat and work in the water reaction are strong functions of the reaction temperature. This property of the water reaction is what permits operation of a thermally regenerative fuel cell cycle. At high temperatures a small amount of work is needed to cause the water dissociation reaction, while at low temperature a greater amount of work is available from the hydrogen-oxygen association reaction.

#### Thermal Dissociation System

The Thermal Dissociation System (TDS) is conceptually the simplest; heating water to a high temperature will cause a portion to "naturally" dissociate into  $H_2$  and  $O_2$  in the equilibrium reaction (Eq. 1), and then the  $H_2$  and  $O_2$  is used to drive a fuel cell. However, very high temperatures are needed to cause an appreciable percentage dissociation (see Figure 3). Also, the separation of  $H_2$  and  $O_2$  from the equilibrium mixture must somehow be accomplished, and the gases will be separated only at their very low partial pressures and must be compressed back to mixture pressure to operate cyclically.

Several concepts for separation of the  $H_2$  and  $O_2$  have been proposed and examined, including various membranes (Refs. A-1, 10, 14, 21; C3), using the diffusion/effusion effect (Refs. A-7, 14, 18, 21; D-15), and quenching means

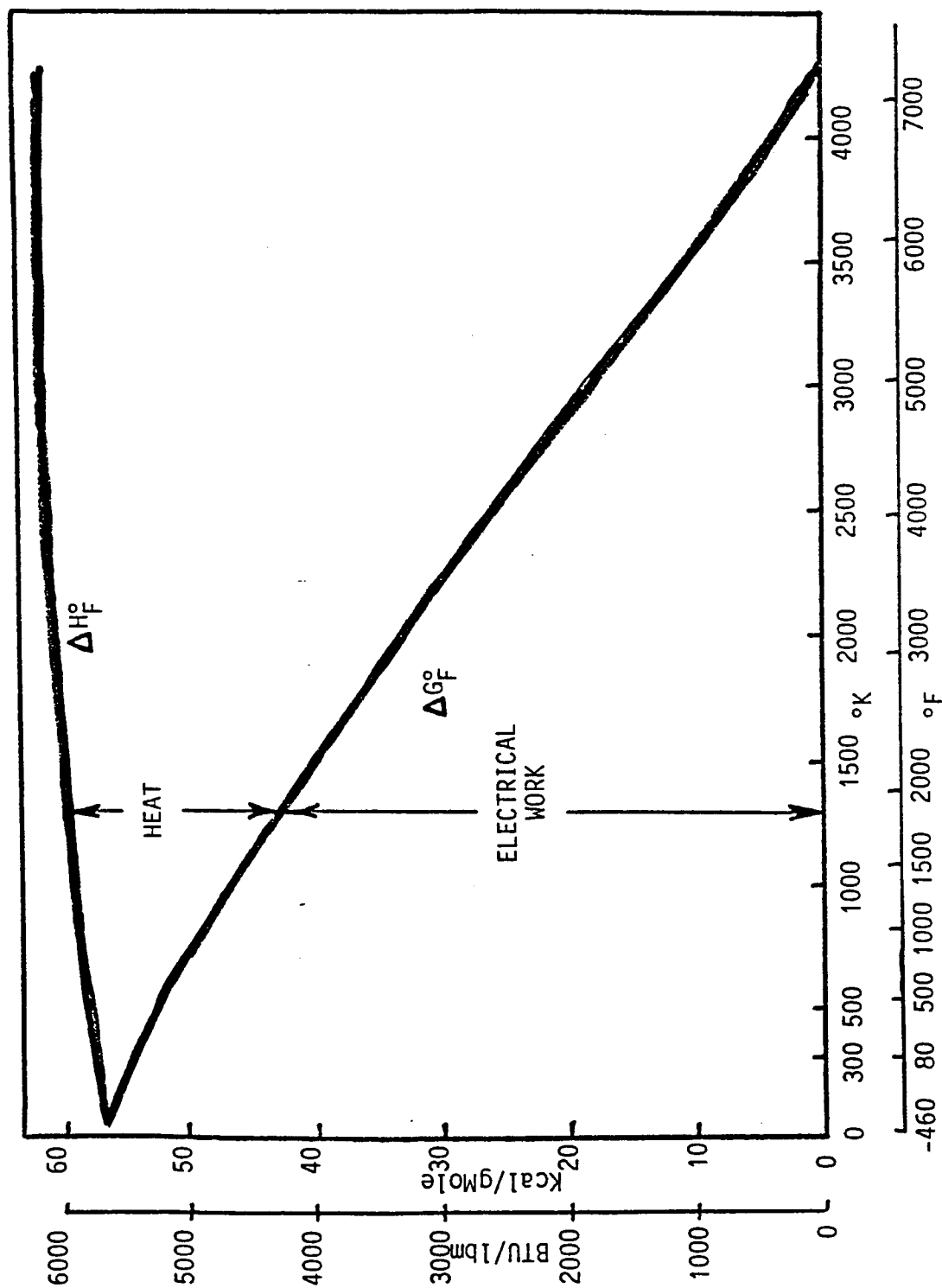


Figure 2. DISSOCIATION ENERGY ( $\Delta H_F^0$ ) AND GIBBS FREE ( $\Delta G_F^0$ ) ENERGY AS A FUNCTION OF TEMPERATURE FOR WATER



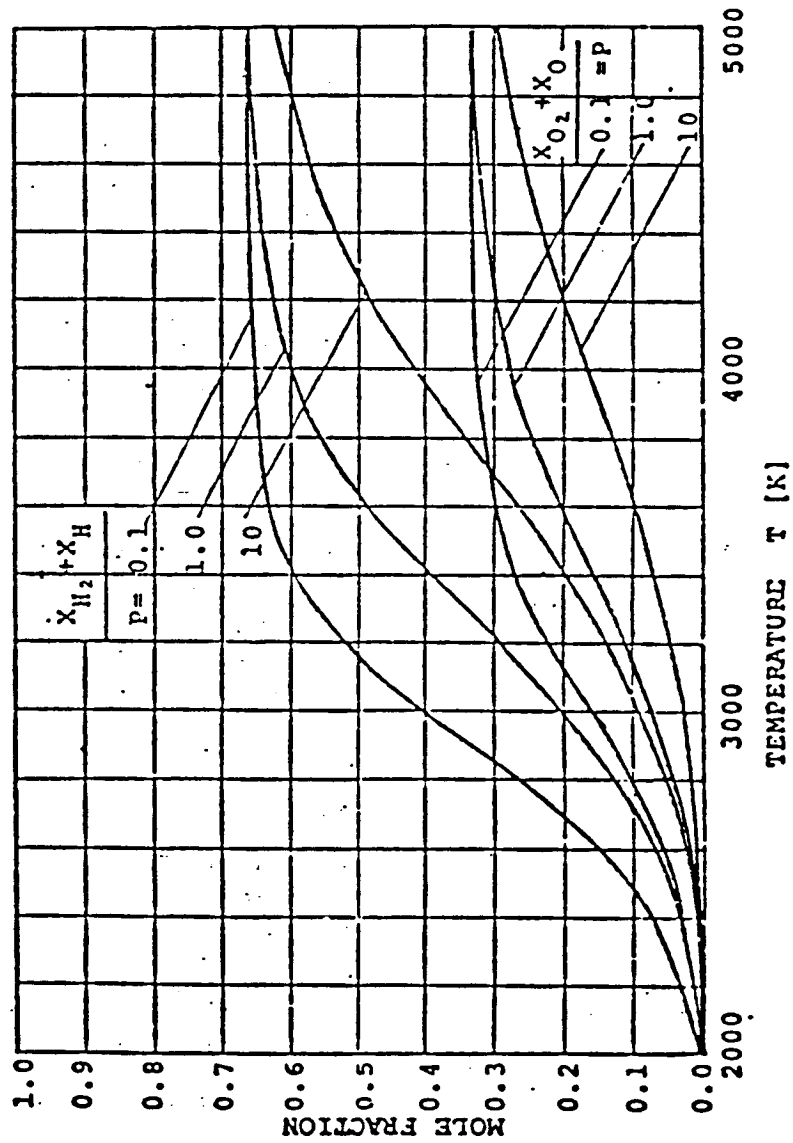


Figure 3. Mole fraction of hydrogen and oxygen in dissociated water vapor. (Ref. A-7)

(Ref. A-11, 14, 24). While none of the methods has been demonstrated as having engineering feasibility to date, it does appear that a 'static' reactor which effuses  $H_2$  and  $O_2$  without reactor recirculation is the most promising approach (Refs. C-3 ; D-18).

Writing the expression for the thermal efficiency of a TDS with the  $H_2/O_2$  regenerator at a high temperature,  $T_H$ , and the fuel cell at a lower temperature,  $T_C$ ,

$$\eta_{\text{Ideal TDS Thermal}} = (W_{FC} - W_{\text{comp}})/Q_{\text{HOT}} \quad (3)$$

where,  $W_{FC}$  is the ideal fuel cell work ( $=\Delta G_{T_C}$ ),

$Q_{\text{HOT}}$  is the ideal heat input ( $=\Delta H_{T_H}$ ); and

$W_{\text{comp}}$  is the ideal work to compress the  $H_2$  and  $O_2$  back to mixture pressure,

$$\text{and, } W_{\text{comp}} = n(T_C) \ln (P/P_{\text{mix}})$$

$$= n(T_C/T_H) (T_H) \ln (P/P_{\text{mix}})$$

$$W_{\text{comp}} = (T_C/T_H) \cdot \Delta G_{T_H} \quad (4)$$

Substituting the definitions and Eq. 4 into Eq. 3, the ideal thermal efficiency is given by:

$$\eta_{\text{Ideal TDS Thermal}} = [\Delta G_{T_C} - (T_C/T_H)\Delta G_{T_H}]/\Delta H_{T_H} \quad (5)$$

The variation in TDS ideal thermal efficiency is plotted in Figure 4 as a function of  $T_H$  and  $T_C$ . It should be also noted that the efficiency is slightly less than Carnot due to differing specific heats of  $H_2$ ,  $O_2$  and water.

#### High Temperature Electrolyzer System

The High Temperature Electrolysis (HTE) system consists of an electrolyzer operating at high temperature,  $T_H$ , a regenerative heat exchanger, and a fuel

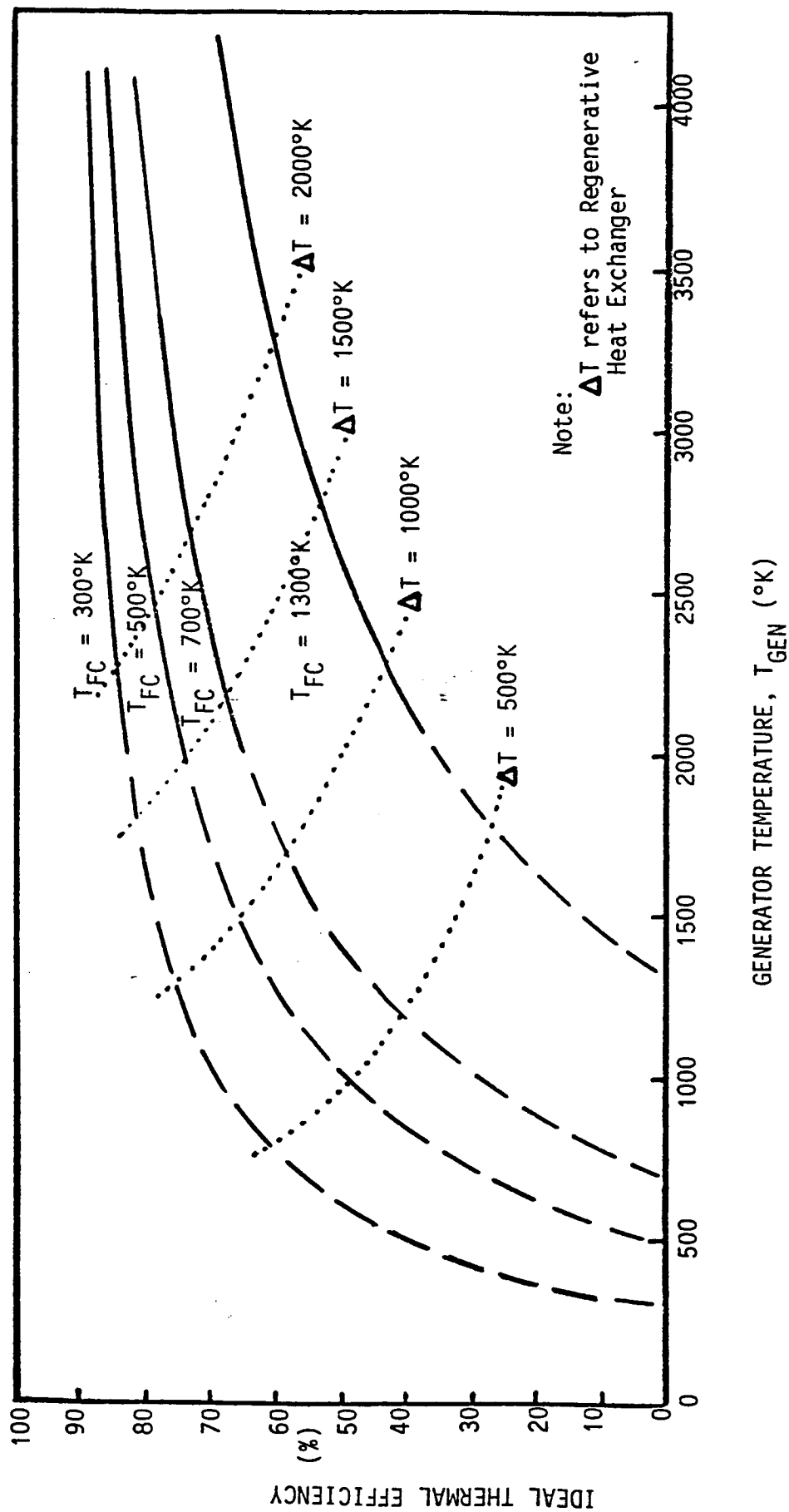


Figure 4. IDEAL TDS CYCLE THERMAL EFFICIENCY

cell operating at low temperature,  $T_C$ . The electrolyzer is run from the electrical output of the fuel cell, plus a high temperature heat input. The cyclic net work output consists of the fuel cell's electrical work which exceeds the electrolyzer requirements; this net work is graphically illustrated as the difference between  $\Delta G$ 's at two temperatures on Figure 2.

The separation of the  $H_2$  and  $O_2$  is done by the electrolyzer without loss in pressure. Thus, compressors are not needed in this cycle, nor are special separation techniques. The thermal efficiency of the ideal HTE system is written:

$$\eta_{\text{Ideal HTE Thermal}} = (W_{FC} - W_{EU})/Q_{HOT} \quad (6)$$

where,  $W_{FC}$  is the ideal fuel cell work ( $= \Delta G_{T_C}$ ),

$W_{EU}$  is the ideal electrolyzer work ( $= \Delta G_{T_H}$ ); and

$Q_{HOT}$  is the ideal heat input into the electrolyzer ( $= \Delta H_{T_H} - \Delta G_{T_H}$ ).

so,

$$\eta_{\text{Ideal HTE Thermal}} = \frac{\Delta G_{T_C} - \Delta G_{T_H}}{\Delta H_{T_H} - \Delta G_{T_H}} \quad (7)$$

and this relationship is presented as a function of temperature in Figure 5. Again, this cycle differs from Carnot efficiency only by the small difference in  $H_2$ ,  $O_2$  and water specific heat capacities.

#### PRELIMINARY FEASIBILITY ANALYSIS

The preceding information indicates that both the TDS and HTE system are conceptually sound. In order to initially judge the engineering feasibility of these cycles, the effects of real processes with irreversibilities and device efficiencies are examined by performing a basic parametric sensitivity analysis.

##### The "Real" Thermal Dissociation System

The ideal dissociation and subsequent separation process involved no

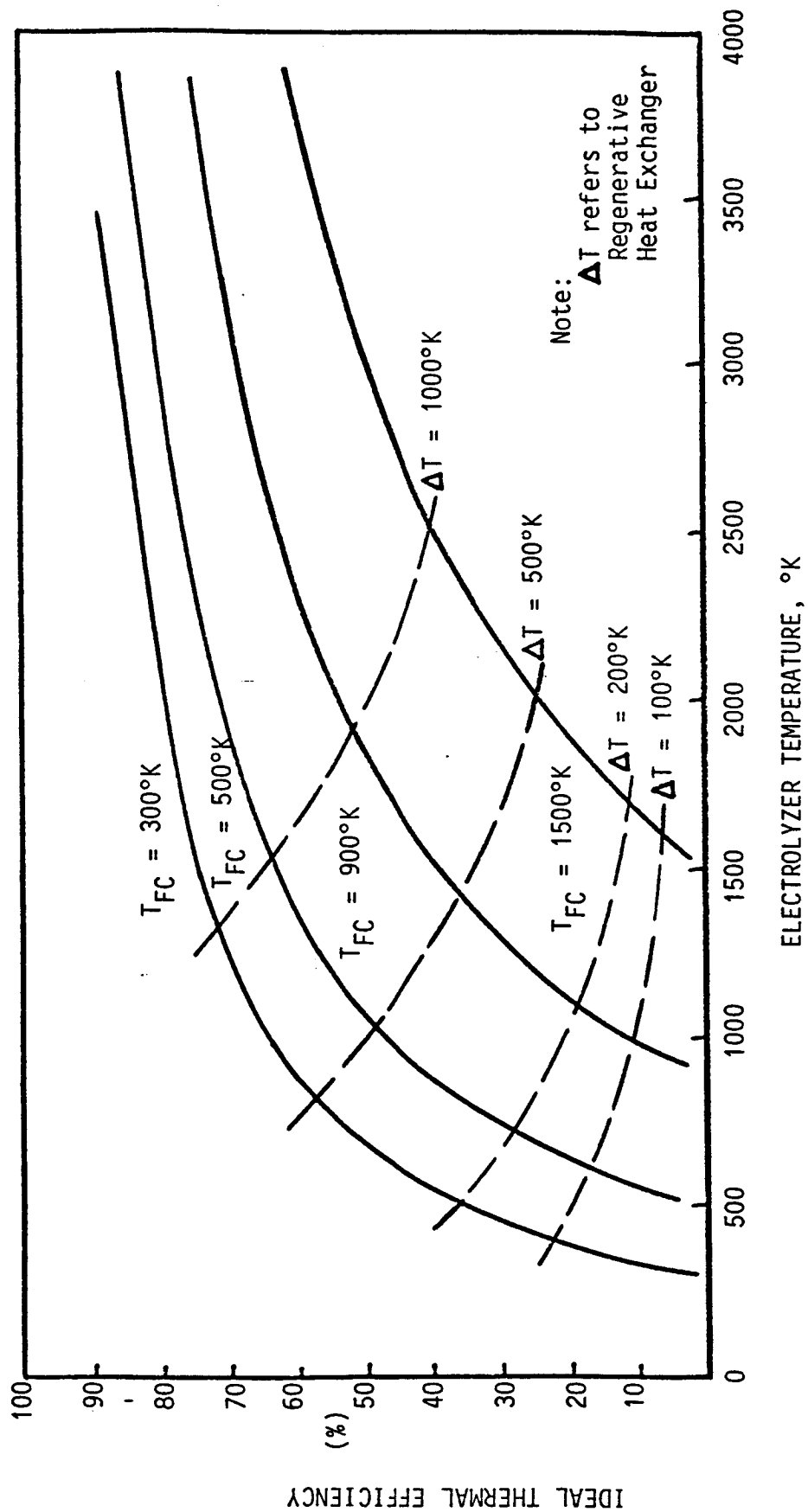


Figure 5. IDEAL HTE CYCLE THERMAL EFFICIENCY

'driving pressure drop' across the  $H_2$  and  $O_2$  separation membranes. An actual TDS must have a pressure difference across the separation membrane to induce transport. Thus, the compressors will have to do more work than previously calculated to restore the gases to the dissociation pressure. This compression work is minimized in an isothermal process which can be written:

$$W_{\text{comp}}^{\text{isoth. } T_C} = (T_C/T_H) \Delta G_{T_H} + RT_C (\ln E_{HY} + 1/2 \ln E_{OX}) \quad (8)$$

where,  $E_{HY} = P_{hy}/P_{hy}^{\text{dissoc.}}$  and  $E_{OX} = P_{ox}/P_{ox}^{\text{dissoc.}}$

The first term in the work expression of Eq. 7 is due to the ideal dissociation partial pressures, while the second term is due to the membrane pressure drop. With pressure ratio drops of 10 ( $E=0.1$ ), the increased compressor work reduces the ideal efficiency by 3-5%.

The TDS thermal efficiency sensitivity to real device and process efficiency is found by defining the following:

$$\eta_{\text{GEN}} = \frac{Q_{\text{GEN}} + Q_{\text{RHX}}}{Q_{\text{HOT}}}, \text{ the ratio of the heat needed in the dissociation generator and the deficit in the regenerative heat exchanger to the actual heat added to the system (90\% } \pm \text{ 5\%);}$$

$$\eta_{\text{COMP}} = \frac{W_{\text{comp}}^{\text{isotherm}}}{W_{\text{comp}}}, \text{ The ratio of the compressor isothermal work to the actual work (75\% } \pm \text{ 15\%);}$$

$$\eta_{\text{FC}} = \frac{W_{\text{FC}}}{\Delta G_{\text{FC}}}, \text{ the actual fuel cell work divided by the reaction Gibbs's free energy (80\% } \pm \text{ 10\%);}$$

$$1 - \eta_{\text{RHX}} = \frac{Q_{\text{RHX}}}{C_p(T_H - T_C)}, \text{ the ratio of the reheat needed to the ideal heat transfer in the regenerative heat exchanger } (\eta_{\text{RHX}} = 90\% \pm 5\%).$$

The percent values represent the expected ranges for the various efficiencies.

The definitions were substituted into Eq. 3 to give:

$$\eta_{\text{TDS}} = \frac{\eta_{\text{FC}} \cdot \Delta G_{T_C} - (W_{\text{comp}}/\eta_{\text{comp}}^{\text{isoth.}})}{[\Delta H_{T_H} + (1 - \eta_{\text{RHX}}) C_p (T_H - T_C)]/\eta_{\text{GEN}}} \quad (9)$$

and with the ranges listed for  $T_C = 300^{\circ}\text{K}$  and  $T_H = 2100^{\circ}\text{K}$ , it is seen that:

$$\eta_{\text{TDS}} = 54\% \pm 9\%$$

with the fuel cell and generator efficiencies having 1:0.8 and 1:0.6 parametric effect on thermal efficiency percentage. The parametric sensitivities for each parameter are presented in Table 1.

### The "Real High Temperature Electrolyzer System"

The thermal efficiency expression for the "real" HTE system is developed using the same efficiency definitions for fuel cell and regenerative heat exchanger efficiencies as used with the TDS. Additionally,

$$\eta_{\text{EU}} = \frac{\Delta G_{\text{H}}}{W_{\text{EU}}}, \text{ the ratio of Gibb's free energy change to the actual work;}$$

$$Q_{\text{EU}} = \text{heat transfer required by the electrolyzer unit } (= \Delta H_{\text{H}} - W_{\text{EU}}).$$

So, substituting these definitions into Eq. 6,

$$\eta_{\text{HTE}} = \frac{(\eta_{\text{FC}} \Delta G_{\text{T}_C} - \Delta G_{\text{T}_H} / \eta_{\text{EU}}) \eta_{\text{GEN}}}{\Delta H_{\text{T}_H} - \Delta G_{\text{T}_H} / \eta_{\text{EU}} + (1 - \eta_{\text{RHX}}) C_p (T_H - T_C)} \quad (10)$$

It is immediately noticed that fuel cell and electrolyzer efficiency dominate this expression, plus the range of fuel cell and electrolyzer efficiencies is limited by the numerator of Eq. 10 to:

$$\eta_{\text{FC}} \cdot \eta_{\text{EU}} > \Delta G_{\text{T}_H} / \Delta G_{\text{T}_C} \quad (11)$$

in order to have positive thermal efficiency values. Assuming the two device efficiencies are equal, then the minimum allowable device efficiency decreases from 95% at  $T_H = 800^{\circ}\text{K}$  to 80% at  $T_H = 1800^{\circ}\text{K}$ . The variation of HTE thermal efficiency with various device efficiencies is presented in Figure 6 as a function of  $T_H$ .

### TECHNOLOGY STATUS

A Thermal Dissociation System power cycle has not been constructed.

TABLE 1. TDS Parametric Sensitivity

a. TDS Efficiency Range (Max/Min):

- o Nominal:  $\eta_{TDS} = 53.8\%$
- o Maximum:  $\eta_{TDS} = 67.8\%$
- o Minimum:  $\eta_{TDS} = 34.8\%$

b. Parameter Versus System Sensitivity

$$d\eta_{TDS} = \frac{\partial \eta_{TDS}}{\partial X_i} \cdot dX_i, \text{ where } X_i = \text{parameter}$$

1.  $d\eta_{FC} = \pm 10\%$  yields  $d\eta_{TDS} = \pm 7.9\%$
2.  $d\eta_{GEN} = \pm 5\%$  yields  $d\eta_{TDS} = \pm 3.0\%$
3.  $d\eta_{COMP} = \pm 15\%$  yields  $d\eta_{TDS} = \pm 1.9\%$
4.  $d\eta_{RHX} = \pm 5\%$  yields  $d\eta_{TDS} = \pm 0.7\%$

and the "SUM OF SQUARES" Variation:

$$d\eta_{TDS} = \pm \left[ \sum \left( \frac{\partial \eta_{TDS}}{\partial X_i} \cdot dX_i \right)^2 \right]^{1/2}$$

$$\therefore = \pm 9.2\%$$



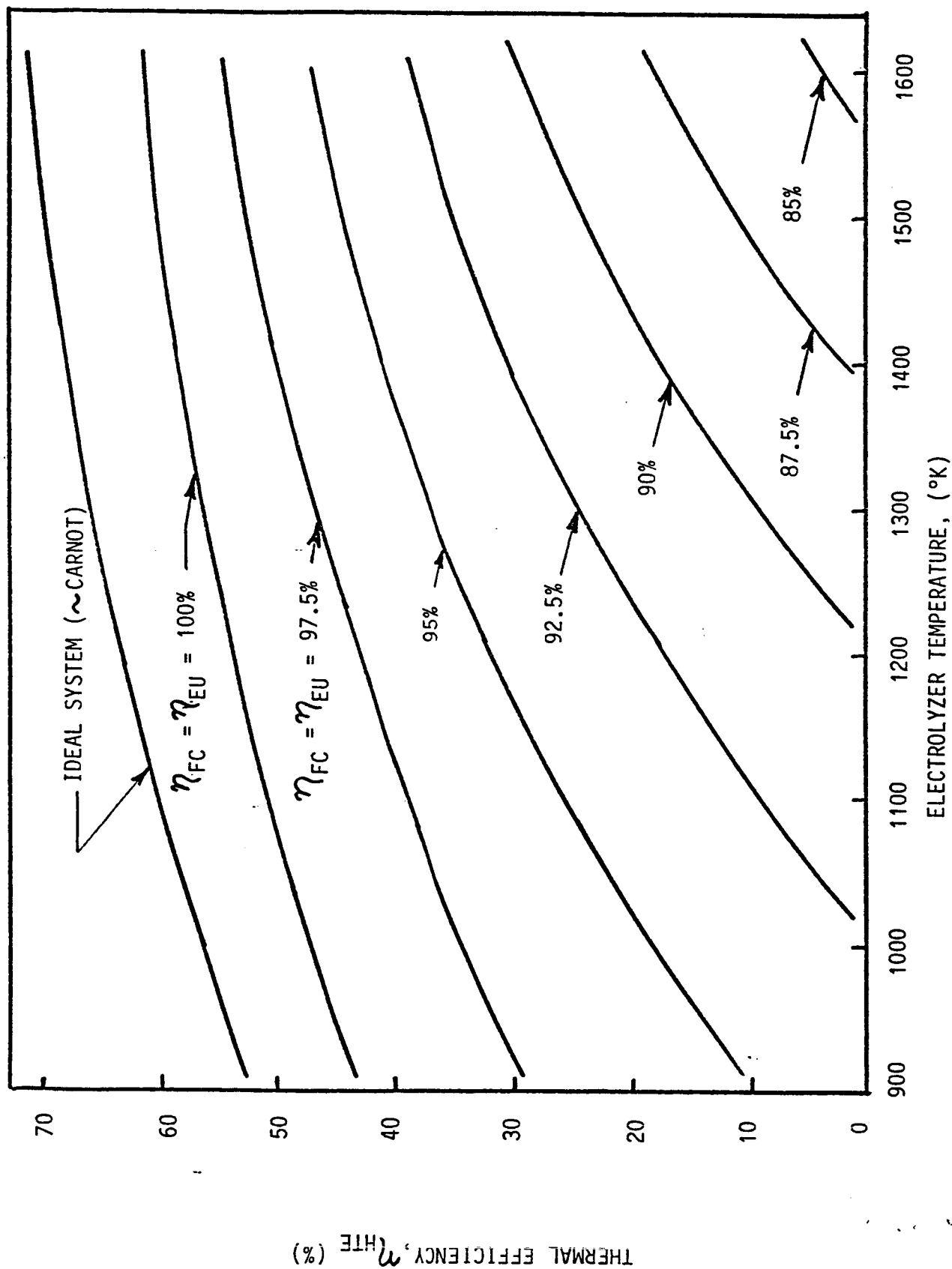


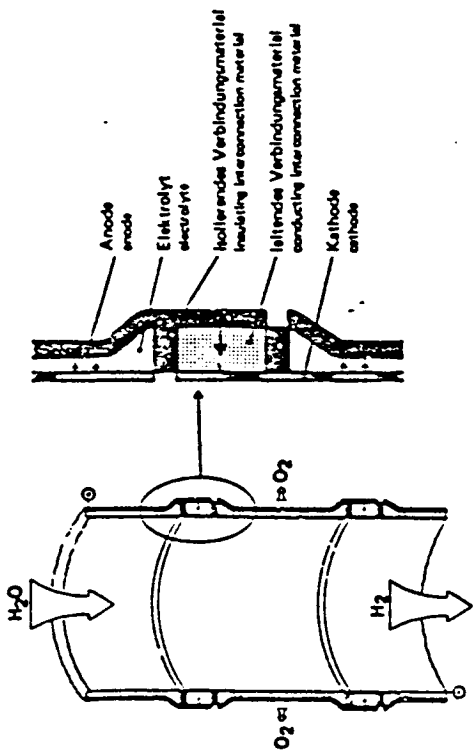
Figure 6. HTE "REAL" SYSTEM THERMAL EFFICIENCY VARIATION AS A FUNCTION OF FUEL CELL AND ELECTROLYZER UNIT EFFICIENCIES ( $\eta_{FC}, \eta_{EU}$ ) with  $T_{FC} = 400^\circ$ K

However, there have been thermal dissociation experiments run to test the operative dissociation composition (Refs. A-11, 15, 20, 21, 24; E-18). Researchers have tried several separation techniques and materials (Refs. A-1, 17, 21, 24), primarily using a solar concentrator/furnace to produce the 2000<sup>0</sup>K+ temperatures required (Refs. A-14, 20, 24; F-1). Research work continues on the identification of both appropriate separation techniques and specific materials (A-21, 24). Researchers in France appear to be doing the bulk of the experimental work (Ref. A-11), with limited work underway in the USA (A-21, 24). The primary aim of all current researchers is the production of hydrogen for use as a fuel, and not specifically as a portion of a power cycle.

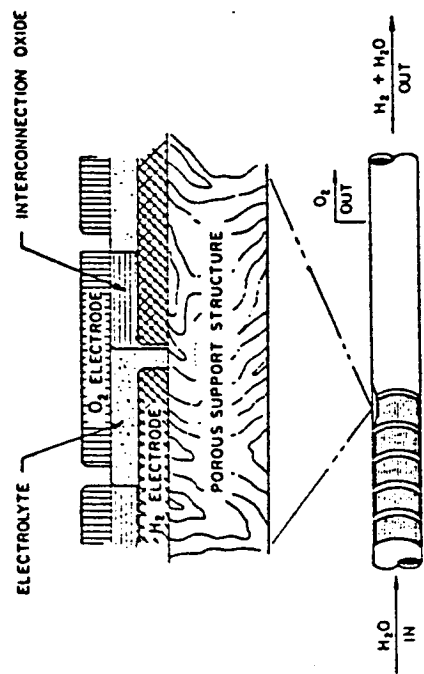
The high temperature electrolyzer system concept was proposed at least as early as 1959 (Refs. D-19, 20, 22). The possibility of building high temperature devices for producing hydrogen fuel was of interest and re-examined in the 1970's. Again, the use of the HTE system as a power cycle was not a concern.

The present approach to development of high temperature electrolyzers and fuel cells involves the use of a solid oxide electrolyte. In the USA, the Department of Energy with Brookhaven National Laboratory sponsors much of the solid oxide fuel cell development work, which is primarily conducted by Westinghouse (Refs. C-1, 4, 5, 11). The German emphasis is on a HTE nicknamed "Hot Elly" (Refs. C-2, 9 ) and is similar to the Westinghouse design.

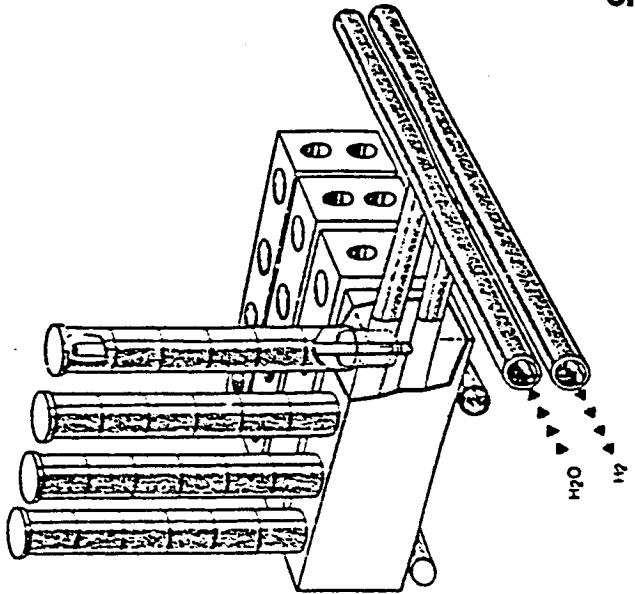
The solid oxide cell being developed has a 30-micron thick solid electrolyte consisting of a Yttria-stabilized Zirconia. Figure 7 illustrates the construction of both the German and Westinghouse cells in the proposed stacked-cell tube design and the proposed module concept. Currently the cell stacks are being tested in the 1300<sup>0</sup>K range. Single cells have been tested



A) GERMAN CELL DESIGN (Ref. C-2)



B) WESTINGHOUSE CELL DESIGN (Ref. C-5)



C) MODULE CONCEPT (Ref. C-2)

ORIGINAL PAGE IS  
OF POOR QUALITY

Figure 7. SOLID OXIDE CELL DESIGNS AND MODULE UNIT CONCEPT

for hundreds of hours without degradation and with near-theoretical open-circuit voltage. Figure 8 presents the cell voltage versus current density cell results, from which it can be seen that 90% efficiency is obtained below  $0.1 \text{ amps/cm}^2$  operation.

#### RESEARCH RECOMMENDATIONS

The high temperature electrolyzer system appears to be within the boundaries of advanced state-of-the-art technology. The separate components of the system are under active development, and the overall system concept appears both promising and feasible. The basic requirement is the development of very efficient (95%+) fuel cells and electrolyzers. Given this requirement is met, the HTE system will then be of practical engineering concern. It appears feasible now to begin designing a proof-of-concept level HTE system based on the solid oxide cell design. Development of high temperature cells (above  $1500^{\circ}\text{K}$ ) should also be examined, as HTE system size (see Figure 9) and system efficiency are strong functions of electrolyzer operating temperature.

The research associated with the thermal dissociation system should remain fairly basic. The examination and identification of separation techniques and materials is of primary importance. Experimental evidence is needed that separation can be performed at temperatures in excess of  $2000^{\circ}\text{K}$ .

In conclusion, Figure 10 illustrates the position occupied by the HTE and TDS cycles as compared to more conventional cycles. The ranges for the cycles are those discussed in this report and illuminate the fact that both cycle efficiencies appear within reasonable bounds of Carnot (50%-65%), similar to other cycles. The HTE system is seen to extend across currently attainable operating temperatures, but the TDS is alone at its operating temperatures.

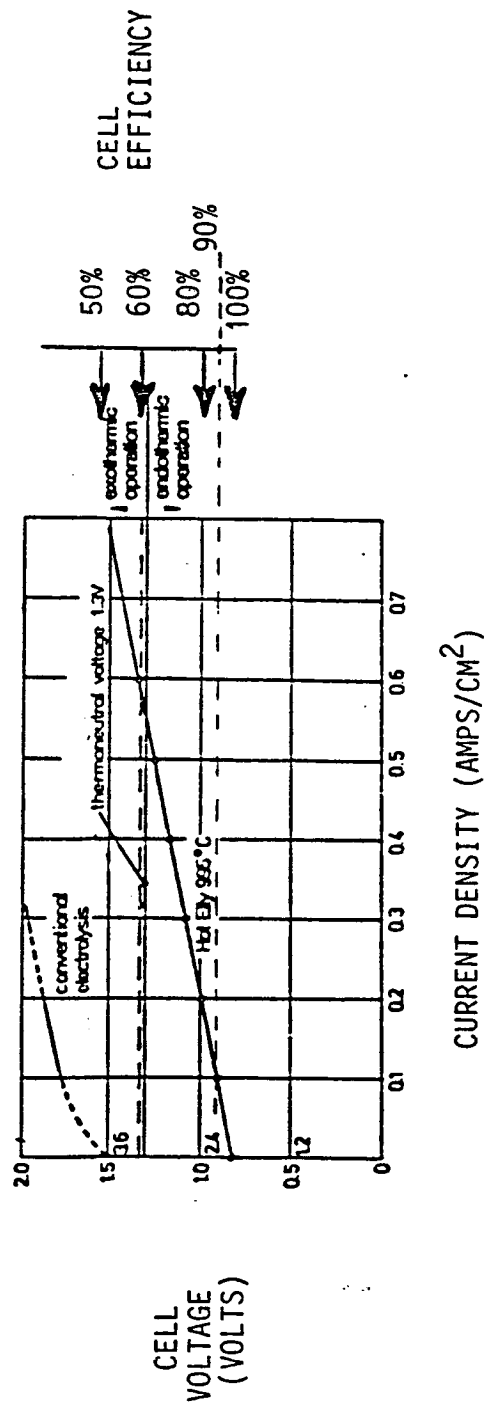


Figure 8. "HOT ELLY" CURRENT-VOLTAGE CHARACTERISTICS AND EFFICIENCY AT 1268°K (Ref. C-2)

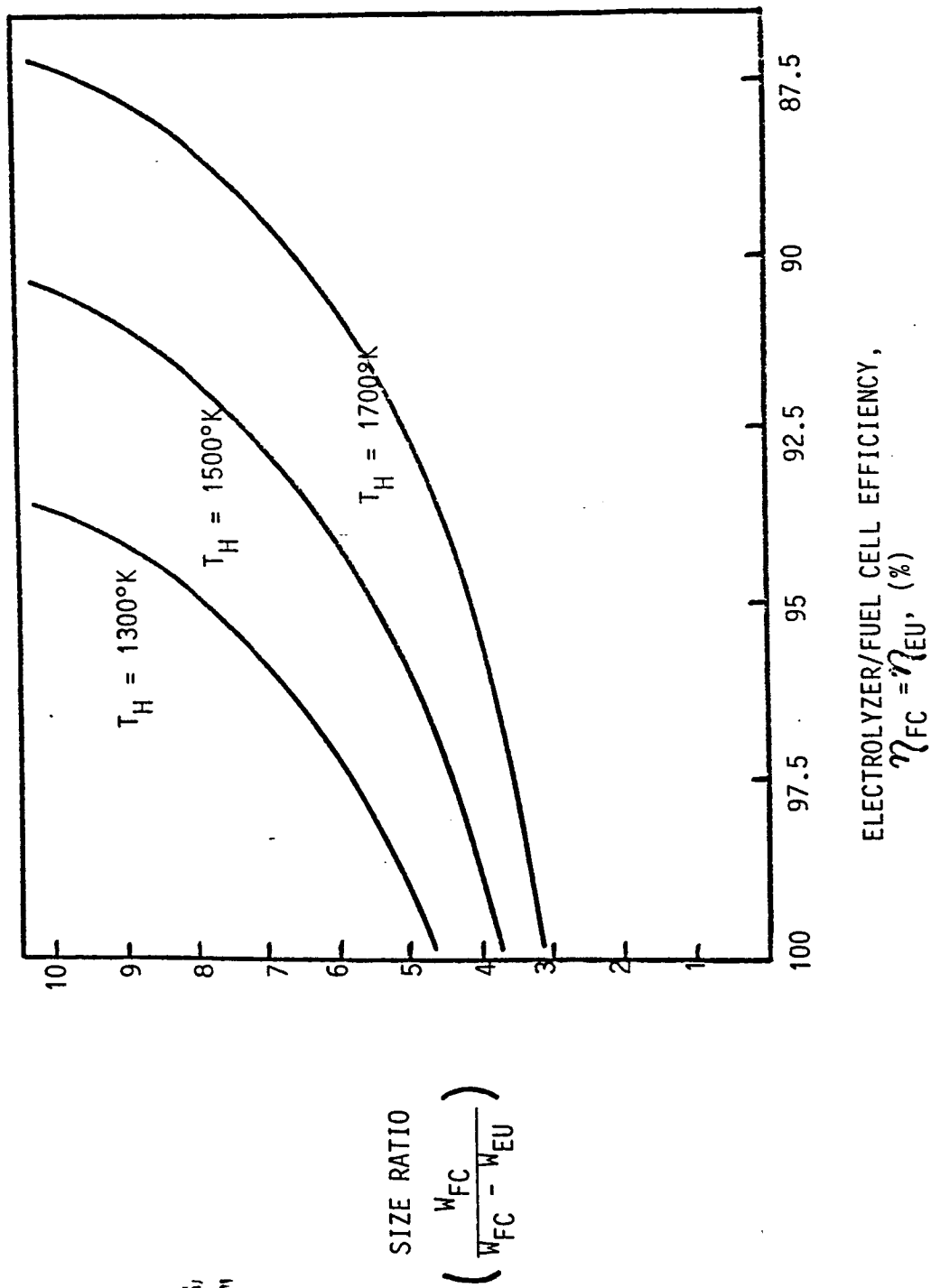


Figure 9. HTE SYSTEM SIZE RATIO VERSUS FUEL CELL/ELECTROLYZER EFFICIENCY FOR THREE ELECTROLYZER TEMPERATURES (with  $T_C = 400^\circ K$ )

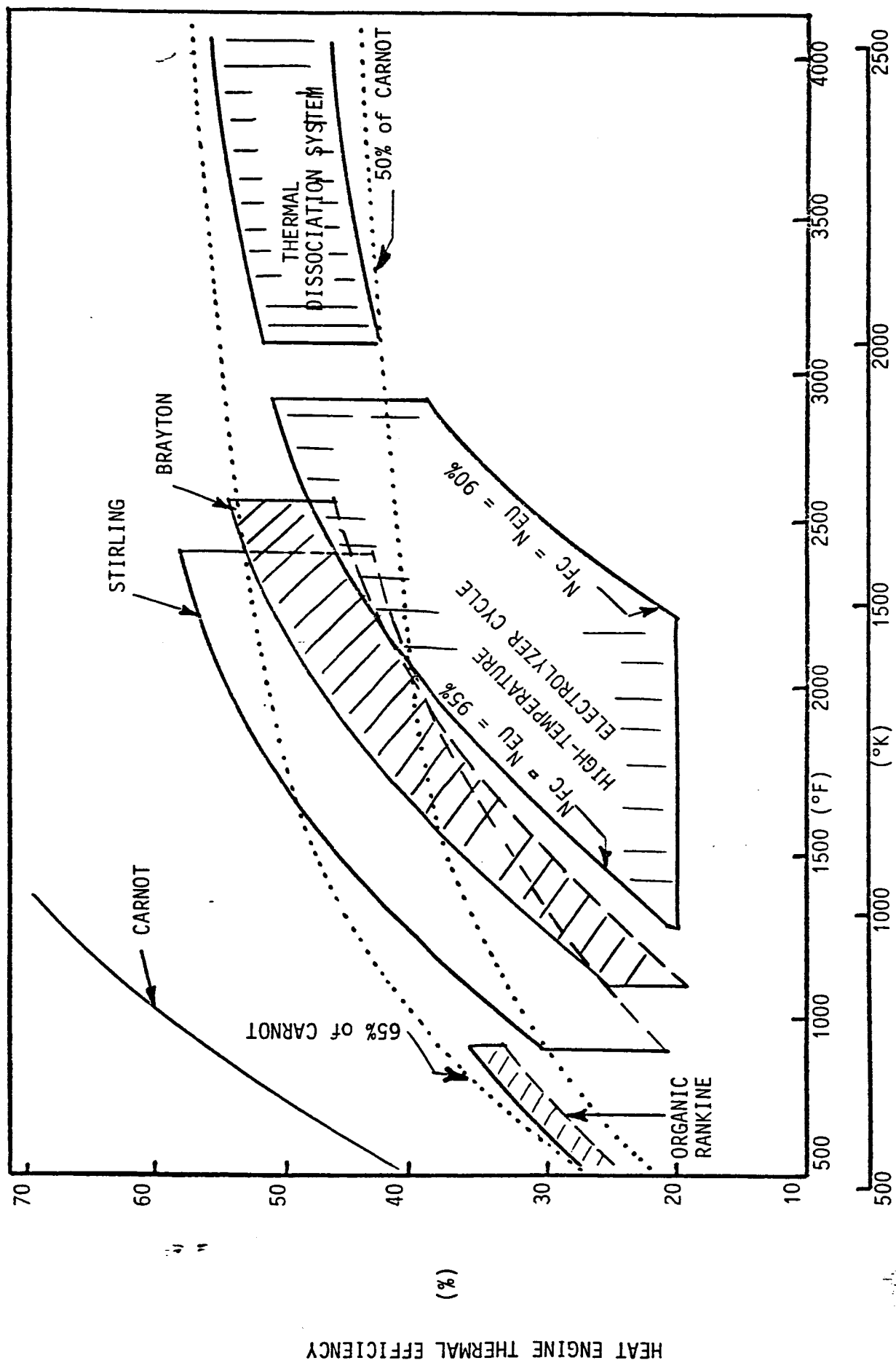


Figure 10. THERMODYNAMIC CYCLE COMPARISONS FOR VARIOUS OPERATING TEMPERATURES  
(FROM ROCKWELL INTERNATIONAL FIGURE)

## REFERENCES

### A. THERMAL DISSOCIATION

1. Jellinek, H. H. G., et. al., "Hydrogen Production from Thermal Decomposition of Water (By Solar Radiation)," Technical Report to Gas Research Institute, period 1 July 1980 - 31 July 1981, GRI Contract #GRI-5014-363-01 submitted Oct. 31, 1981.
2. Nakamura, T. "An Investigation of Hydrogen Production from Water at High Temperature," Proceedings of 1st World Hydrogen Energy Conference, Miami Beach Fla; Vol. 2, pp.5B-71 to 5B-96; March 1976.
3. Pangborn, J. B. and Greccorgy, D. P. "Nuclear Energy Requirements for Hydrogen Production from Water," Proceedings of the 9th IECEC, San Francisco, CA, pp. 400-404, 1974.
4. Funk, J. E. "The Generation of Hydrogen By the Thermal Decomposition of Water," Proceeding of the 9th IECEC, San Francisco, CA, pp. 394-399, 1974.
5. Funk, J. E. "Thermodynamics of Multi-Step Water Decomposition Processes," American Chemical Society; 163rd National Meeting, Symposium on Non-Fossil Chemical Fuels, Vol. 16, No. 4, April 1972.
6. Nakamura, T. "Hydrogen Production from Water Utilizing Solar Heat at High Temperatures," Solar Energy, Vol. 19, pp. 467-475, 1977.
7. Ihara, S. "Feasibility of Hydrogen Production by Direct Water Splitting at High Temperature" Proceedings of the 1st World Hydrogen Energy Conference, Vol. 2, pp.5B-55 to 5B-70, Miami Beach, Fl, March 1976.
8. (Same as C-3)
9. Gretz, J., "On the Potential of Solar Energy Conversion into Hydrogen and/or other Fuels," International Journal of Hydrogen Energy, Vol. 5, pp.269-280, 1980.
10. Ihara, S. "On the Study of Hydrogen Production from Water Using Solar Thermal Energy," International Journal of Hydrogen Energy, Vol. 5, pp.527-534, 1980.
11. Lede, J., Lopicque, F. and Villermux, J., "Production of Hydrogen by Direct Thermal Decomposition of Water," International Journal of Hydrogen Energy, Vol. 8, No. 9, pp. 675-679, 1983.
12. (Same as C-6),
13. Pangborn, J. B. and Sharer, J. C. "Analysis of Thermochemical Water-Splitting Cycles," Hydrogen Energy, Part A, Proceedings of Theme Conference, Miami, Fl, pp. 499-515, 1974.



14. Bilgen, E., "Solar Hydrogen Production by Direct Water Decomposition Process: A Preliminary Engineering Assessment," International Journal of Hydrogen Energy, Vol. 9 No. 1/2, pp.53-58, 1984.
15. Jellinek, H. H. G. and Kachi, H., "The Catalytic Thermal Decomposition of Water and The Production of Hydrogen" International Journal of Hydrogen Energy, Vol. 9, No. 8, pp. 667-688, 1984.
16. Biligen, E. "Solar Hydrogen Production at High Temperatures" International Symposium - Workshop on Solar Energy, Cairo, Egypt, p. 297-302, 1978.
17. Genequand, P. "Direct Thermal Water Splitting by Concentrated Solar Radiation for Hydrogen Production," Final report, Phase 0: Proof of Concept Experiment, NASA-CR-164137, Jet Propulsion Lab, 1980.
18. Fletcher, E. A. and Moen R. L., "Hydrogen and Oxygen from Water," Science, Vol. 197, pp.1050-1056, 1977.
19. Fletcher, E. A. and Ihara, S. "Comments on Feasibility of Hydrogen Production by Direct Water splitting at High Temperatures" International Journal of hydrogen Energy, vol. 4, pp.225-227, Technical Discussion, 1979.
20. Bilgen, E., et. al, " Use of Solar energy for Direct and Two-Step Water Decomposition Cycles," Internation Journal of Hydrogen Energy, Vo. 2, pp. 251-257, 1977.
21. Fletcher, E. A. and Yu, R. C., "Considerations Related to the Effusional Separation of Equilibrium Components of High Temperature Water - The Separation of Helium - Argon Mixtures," Energy, Vol. 4, pp. 373-381, 1979.
22. (Same as D-15)
23. (Same as D-16)
24. Diver, R. B. ET AL, "Hydrogen and Oxygen from Water - VI: Quenching the Effluent from a Solar Furnace," Energy, Vol. 8, No. 12, pp. 947-955, 1983.
25. (Same as D-18)

#### B. MULTI-STEP THERMOCHEMICAL DECOMPOSITION

1. (Same as A-2)
2. (Same as A-4)
3. (Same as A-5)
4. (Same as A-3)
5. Krakowski, R. A., et. al., "Synfuel (Hydrogen) Production from Fusion Power," Proceedings of the 14th IECEC, Boston, MA, pp. 1544-1548, 1979.

6. (Same as A-15)
7. England, C. "Thermodynamics of Water Decomposition Catalyzed by Zeolites" International Journal of Hydrogen Energy, Vol. 9, No. 4, pp. 315-317, 1984.
8. (Same as A-16)
9. Wentorf, R. H. and Hanneman, R. E., "Thermochemical Hydrogen Generation," Science, Vol. 185, No. 4148, pp. 311-314, 1974.
10. (Same as D-21)
11. (Same as D-22)
12. Chao, R. E., "Thermochemical Water Decomposition Processes," Industrial and Engineering Chemistry, Product Research and Development, Vol. 13, No. 2, pp. 94-101, 1974.

#### C. HIGH-TEMPERATURE FUEL CELLS/ELECTROLYZERS

1. Isenberg, A. O., "Cell Performance and Life Characteristics of Solid Oxide Electrolyte Fuel Cells," Proceedings of the Conference on High Temperature Solid Oxide Electrolytes Brookhaven National Lab; Vol. I, pp.5-15, Oct. 1983.
2. Doenitz, W., et. al, "High Temperature Electrolysis of Water Vapor - Status and Perspectives of the German Research and Development Activities," Proceedings of the Conference on High Temperature Solid Oxide Electrolytes, BrookHaven Nat. Lab. (BNL51728), pp. 67-80, 1983.
3. Fletcher, E. A., Diver, R. B. and Noring, J. E., "High Temperature Oxide Electrolytes for the Splitting of Water -- The ROC Process," Proceedings of the Conference on High Temperature Solid Oxide Electrolytes, Brookhaven Nat. Lab (BNL51728), pp. 89-102, 1983.
4. Maskalick, N. J., et. al. , "Hydrogen Production Employing High-Temperature Solid Oxide Cells," Proceedings of the 19th IECEC, San Francisco, CA, pp. 1415-1420, 1984.
5. Powell, J. R. and Fillo, J. "Advanced Synfuel Production with Fusion," Proceeding of the 14th IECEC, Boston, MA, pp. 1549-1552, 1979.
6. Dang, V. D., et. al., "Hydrogen Production From High Temperature Electrolysis and Fusion Reactor," Proceedings of the 13th IECEC, San Diego, CA, pp. 1142-1149, 1978.
7. Nagata, S., et. al., "Development of High Temperature Solid Oxide Electrolyte Fuel Cells," Proceedings of the 19th IECEC, San Francisco, CA, pp. 827-832, 1984.

15. Diver, R. B. and Fletcher, E. A., "Hydrogen and Oxygen from Water - II: Some Considerations in the Reduction the Idea to Practice," Energy, Vol. 4, pp. 1139-1150, 1979.
16. Diver, R. B. and Fletcher, E. A., "Hydrogen and Oxygen from Water - III: Evaluation of a Hybrid Process," Energy, Vol. 5, pp. 597-607, 1980.
17. Diver, R. B. and Fletcher, E. A., "Note: Hydrogen and Oxygen from Water - IV: Control of an Effusional Separator During a Solar Intensity Transient," Energy, Vol. 5, pp. 1261-1263, 1980.
18. Noring, J. E., Diver, R. B. and Fletcher, E. A., "Hydrogen and Oxygen from Water - V: The ROC System," Energy, Vol. 6, pp. 109-121, 1981.
19. Liebhafsky, H. A., "The Fuel Cell and The Carnot Cycle," Journal of the Electrochemical Society, Vol. 106, pp. 1068-1071, 1959.
20. de Bethune, A. J., "Fuel Cell Thermodynamics," Journal of the Electrochemical Society, Vol. 107, pp. 937-939, 1960.
21. Abraham, B. M. and Schreiner, F., "General Principles Underlying Chemical Cycles Which Thermally Decompose Water into the Elements," Industrial and Engineering Chemistry, Fundamentals, Vol. 13, No. 4, pp.305-310, 1974.
22. Funk, J. E. and Reinstrom, R. M., "Energy Requirements in the Production of Hydrogen from Water," Industrial and Engineering Chemistry, Process Design and Development, Vol. 5, No. 3, pp. 336-342, 1966.
23. Henderson, R. E., "Thermally Regenerative Fuel Cells," Proceedings of the 6th AGARD Combustion and Propulsion Colloquim, Cannes, France, March 1964.

#### E. GENERAL OVERVIEW/BASIC REFERENCES

1. Salzano, F. J., "Proceedings of the Conference on High Temperatures Solid Oxide Electrolytes," Brookhaven National Laboratory, Report BNL 51726, August 16-17, 1985.
2. Veziroglu, T. N. and Kakac, S., "Solar Hydrogen Energy System and Solar Hydrogen Production Methods," International Symposium-Workshop on Solar Energy, Cairo, Egypt, pp. 275-296, June 1978.
3. "Chemical Engineers Handbook," 5th Edition, Membrane Processes, pp. 17-34 to 17-58.
4. (Same as A-9)
5. Kelly, J. H. "Hydrogen Tomorrow: Demands and Technology Requirements," Report of the NASA Hydrogen Energy Systems Technology Study, Jet Propulsion Laboratory, 1975.

8. Bowman, R. M., et. al., "High Temperature Water Electrolysis for Hydrogen Production," Proceedings of the 15th IECEC, Seattle, WA, pp. 1725-1730, 1980.
9. Dietrich, G. and Schaffer, W. "Advances in the Development of Thin-Film Cells for High Temperature Electrolysis, International Journal of Hydrogen Energy, Vol. 9, No. 9, pp. 747-752, 1984.
10. Barbi G. B. and Mari, C. M. "A Parameter for Defining the Energetic Efficiency of the Cathodic Process at High Temperature, High Current Density Electrolysis of Steam," International Journal of Hydrogen Energy, Vol. 9, No. 11, pp. 895-899, 1984.
11. Fee, D. C., et. al., "Solid-Oxide Fuel Cell Performance," 2nd Solid Oxide Fuel Cell Workshop, Brookhaven National Lab, August 1983.
12. (Same as G-1)

#### D. REGENERATIVE CYCLES/THERMODYNAMICS

1. (Same as A-5)
2. (Same as A-4)
3. (Same as A-3)
4. (Same as A-6/A-2)
5. (Same as A-7)
6. (Same as C-3)
7. (Same as A-9)
8. (Same as C-5)
9. (Same as C-8)
10. (Same as E-6)
11. (Same as B-7)
12. (Same as B-9)
13. Hammond, R. H. and Risen, W. M. Jr., "An Electrochemical Heat Engine for Direct Solar Energy Conversion", Solar Energy, Vol. 23, pp. 443-449, 1979.
14. Bidard, R. and LaRoche, U., "Modern Technology Electrolysis for Power Application - I. Fundamentals of Efficient Thermolysis of Water", International Journal of Hydrogen Energy, Vol. 4, pp. 123-131, 1979.

6. Funk, J. E. and Prueitt, J. K., "Process Economics and the Second Law in Thermochemical Hydrogen Production: The Effect of Heat Transfer," Proceedings of the 15th IECEC, Seattle, WA, pp. 2000-2003, 1980.
7. Eisenstadt, M. M. and Cox, K. E., "Hydrogen Production from Solar Energy," Solar Energy, Vol. 17, pp. 59-65, 1975.
8. "A Hydrogen Energy Carrier," Report of NASA-ASEE Systems Design Institute, Johnson Space Center, 1973.
9. Zollars, G. F., "Hydrogen Production" Citations from The International Aerospace Abstracts Data Base 1977-July 1979, NTIS/PS-79/0773.
10. Williams, K. R. (Editor), "An Introduction to Fuel Cells," Elsevier Publishing Co., 1966.
11. Berger, C. (Editor), "Handbook of Fuel Cell Technology," Prentice-Hall, Inc. 1968.
12. Soo, S. L., "Direct Energy Conversion," Prentice-Hall Inc., 1968.
13. Margrave, J. L. (Editor), "The Characterization of High Temperature Vapors," John Wiley and Sons, Inc., 1967.
14. Venugopalan, M. and Jones, R. A., "Chemistry of Dissociated Water Vapor and Related Systems," Interscience Publishers, 1968.
15. Bockris, J. O'M and Srinivasan, S., "Fuel Cells: Their Electrochemistry," McGraw-Hill, Inc., 1969.
16. Bockris, J. O'M., "Energy: The Solar-Hydrogen Alternative," Halsted Press, 1976.
17. Bockris, J. O'M., "Energy Options," Australia and New Zealand Book Company, 1980.
18. Stull, D. R. and Prophet, H., "JANAF Thermochemical Tables," 2nd Edition, NSRDS-NBS37, 1971.

#### F. SOLAR CONCENTRATORS

1. Bilgen, E. and Galindo, "High Temperature Solar Reactors for Hydrogen Production," International Journal of Hydrogen Energy, Vol. 6, pp. 139-152, 1981.
2. (Same as A-14)
3. (Same as G-2)

## G. SPACE STATION

1. "Space Station Electrical Power System Configuration Impact Assessment," JSC-19994 Power System Branch, NASA/Johnson Space Center, August 1984.
2. Wagner, H. "Design of a Large Deployable Solar Concentrator," JSC-20373, Solar Power Section, Power Branch, NASA/Johnson Space Center, August 1984.
3. "Space Station Reference Configuration Description," JSC-19989, NASA/Johnson Space Center, August 1984.
4. "Conceptual Design and Evaluation of Selected Space Station Concepts," JSC-19521, NASA/Johnson Space Center, 1983.

N86 - 31431

D22  
99.

18833

CYTOGENETIC ANALYSES OF PERIPHERAL LYMPHOCYTES  
SUBJECTED TO SIMULATED SOLAR FLARE RADIATION

Howard M. Prichard, Ph.D.

Assistant Professor

Environmental Sciences

University of Texas School of Public Health

P. O. Box 20186

Houston, TX 77225



## ABSTRACT

Solar Flare protons share many radiological health characteristics of the inner Van Allen Belt protons, and both types of radiation pose serious constraints for a number of contemplated missions. It is therefore appropriate to evaluate crew dose determination procedures in terms of the type of radiation responsible for the major part of the projected dose, i.e., protons in the neighborhood of 100 MeV. Monitoring chromosome abnormalities in peripheral lymphocytes is one method to determine an individual's accumulated radiation exposure. Cell culture and harvest is a relatively simple procedure and is well within the capabilities of a station health facility, but the evaluation of prepared microscopic slides is time consuming and subjective procedure. This project is part of an effort to demonstrate the utility of automated image processing and evaluation procedures in expediting dose evaluation. The initial goal of this project is to produce a set of reference chromosome spreads produced from control lymphocytes and from lymphocytes exposed in whole blood to protons or gamma rays. The results of manual and automated aberration scoring will ultimately be compared to test for systematic differences between the two evaluation procedures and between the two radiation qualities. Proton irradiations are performed at the University of Texas Health Science Center at Houston Cyclotron Facility. Proton dosimetry is supplemented by TLD packets from and by assay of short-lived proton activation products in the irradiated blood samples.

---

NASA Colleague: Gerald Taylor, Ph.D. S.D. 3



## INTRODUCTION

Energetic protons are the primary constituents of the space radiation environment. In terms of flux, energy deposition, and presumed biological effect, protons are the single most important component of galactic cosmic rays, solar flare radiation, and Inner Van Allen belt radiation (Haffner, 1967). Electrons are the major constituents of the outer Van Allen belt, but even minimal hull thicknesses ( $0.5 \text{ g/cm}^2$  aluminum) provide extensive shielding against electrons of energies typical of that environment. While there is at present a great deal of interest in the biological effects of the high energy heavy nuclei found in the galactic cosmic ray flux, it appears at present that protons in the range of (approximately) 10 to 1000 MeV are the limiting form of radiation for most contemplated deep space and Low Earth Orbit (LEO) missions. Solar flare protons account for the bulk of the ca. 400 rem mission dose projected for a 3 year Mars mission, and the predominantly proton radiation associated with the South Atlantic Anomaly imposes potential constraints on the orbital parameters and structural requirements of the Space Station. The efficacy of protons of various energies in producing short term and long term biological damage in primates has been demonstrated in recently reported research (Yochmowitz, 1985).

Assessing the biological effects of proton radiation in the space environment is a complicated task. The flux of protons incident on the hull (or pressure suit) represents the summation of several continuous energy spectra. This complex summation spectrum will be further modified by passage through hull

material and intervening equipment, as well as through less sensitive tissues overlying the more radiosensitive organs. Both the incident proton spectrum and the effective shielding due to the spacecraft will be markedly anisotropic and the proton spectrum inside the craft will vary temporally with spacecraft attitude. Individual dose histories will be further complicated by differences in bodily position and attitude throughout the mission.

Chromosome aberration studies have long been used to determine the extent of radiation exposure in cases in which conventional dosimetry systems were either not in place or not appropriate for the mode of irradiation (e.g. Collins 1980, Brewen 1982, Evans 1979, Lloyd 1979). Relatively few studies of the effectiveness of protons have been reported in the open literature, but some work has been done in this area (e.g., Bettega 1981). Lymphocytes obtained from peripheral blood samples are cultured and arrested at metaphase, then treated to yield observable chromosome spreads for microscopic evaluation. The culture and treatment procedures are not particularly difficult, and numerous options exist, but experience has shown that consistency throughout is vital for reproducible dose-response relationships. At present, the most labor-intensive and potentially subjective aspect of the procedure is the manual evaluation of chromosome spreads. For a one Gray (100 rad) dose, the expected yield of dicentric and acentric aberrations is on the order of 1 per 20 cells, while the "spontaneous" background rate is about one per hundred cells (Lloyd 1980). Therefore, many cells must be examined to obtain reliable statistics on sub-lethal radiation exposures, the exact number being dependent on the dose and the degree of precision required, among other things. This represents a significant investment in skilled time compared to other cytogenetic investigations, such as testing for inherited defects. While this approach has

been shown to be practical in many ground-based applications, it is clear that some degree of simplification and automation will be required if cytogenetics is to play a part in routine or emergency radiation dosimetry during extended missions. The goal of this project has been to lay the groundwork for evaluating the utility of processing digitized microscopic images of chromosome spreads from blood subjected in vitro to a simulated space radiation environment.

## MATERIALS AND METHODS

### General

At the time of this project's inception, it was anticipated that hardware and software for autokaryotyping would be in place at the Cell Image Analysis Laboratory at JSC in time for use during the summer of 1985. Difficulties beyond the control of JSC delayed delivery of the software, and it was eventually decided that new hardware and proven compatible software would be obtained for use in 1986. The goal of the Summer 1985 project was accordingly redefined to be the preparation of microscopic slides to be evaluated both by manual observation and by the new equipment at the time that it comes on line. The automated technique could then be compared directly to manual readings on slides obtained from blood exposed to various radiation environments.

## Radiation Exposures

All blood samples were subjected to one of three radiation treatments: 1). Control - no radiation, 2). Gamma - 0.662 MeV gamma rays from a Cs-137 irradiator, and 3). Proton - 40 MeV protons from the University of Texas Health Science Center at Houston Cyclotron Facility. Venous blood was drawn into a heparinized 15 ml vacutainer tube, which was then shaken and placed into a 35 to 37 degree transfer case until treatment and/or culture. Aliquots were given the appropriate radiation treatment and returned to the sample case. Another aliquot was cultured for a predetermined interval, irradiated, then returned to the incubator.

Gamma exposures were readily performed and judged to be accurate within a factor of 10%. Gamma irradiations were used as a rough check on the influence of the chosen culture protocol on radiation induced aberration yield. Proton exposures required considerably more preparation and coordination than the gamma exposures. Appropriate sample holders that would fit into the cyclotron target delivery system had to be devised. (Without beam port modifications beyond the scope of this project, the volume that could be effectively irradiated was a disc 30 millimeters in diameter and 10 millimeters in depth.) Provision had to be made for dosimetry, as the Faraday cup and electrometer in the cyclotron beam path could give only an approximate exposure measurement at the relatively low beam currents required for a ca. 100 rad exposure. Two forms of supplemental dosimetry were found to be practical: TLD dosimetry and activation analysis. TLD chips were found to be small enough to be placed on the beam-side surface of the sample holder without serious perturbation of the

radiation field inside. A second indication of actual proton dose is provided by the proton - alpha reaction by which Oxygen-16 is converted to Nitrogen-13. The resulting 0.511 MeV gamma radiation is produced in sufficient quantities to be readily quantified with a NaI-Tl scintillation counting system.

#### Culture, Harvest, and Mapping

The cell culturing techniques used in this project were closely based on those used by the Cellular Genetics Laboratory of the M. D. Anderson Hospital in Houston. (It is recognized, however, that any set of techniques proposed for use in space must be adapted to the microgravity environment and the probable requirement of obtaining results more quickly than would be possible with the incubation times described below.) Briefly, 0.5 ml of whole blood was placed in a culture tube along with 4.5 ml of culture medium (see Appendix A for solution compositions) and stimulated with the mitogen PHA. The culture tubes were placed in a 37 C incubator for the desired incubation period (72 hours or 48 hours, depending on circumstances). One hour before harvest, Colcemide (final conc. = 0.1 ug/ml) was added to arrest dividing cells at metaphase. The contents of two identically treated culture tubes were then transferred to a 15 ml centrifuge tube and spun down to separate the cellular mass from the supernatant plasma. All but the lower half centimeter of plasma was pipetted off and replaced by hypotonic KCl to bring the solution to 10 ml, after which the solution was thoroughly mixed and allowed to stand for 30 minutes. Three ml of fixative solution was then added, the solution mixed, and spun down. The supernatant was discarded and the cellular pellet resuspended in 10 ml of fixative, then spun down again. The wash in fixative was repeated at least three times, after which the cellular mass was resuspended in 5 ml of fixative,

either for immediate slide preparation or for storage at 4 C for up to several days. Chromosome spreads for microscopic examination were prepared by allowing several drops of the fixative containing suspended cells to fall ca. one meter onto a clean slide still wet from storage in 4 C distilled water. The slides were then air dried, stained with Giemsa, and coverslipped after a zero point disk had been placed in the center to facilitate mapping. The slides were then scanned at low power with a Zonax micro-computer driven microscope and the locations of chromosome spreads were stored on a floppy disk to permit rapid examination under high power objectives.

#### RESULTS AND CONCLUSIONS

This project has successfully demonstrated the feasibility of conducting proton irradiations of whole blood samples at a facility proximate to the Johnson Spaceflight Center and obtaining readable chromosome spreads from irradiated samples with the use of simple laboratory procedures. Sets of slides representing control, gamma, and proton irradiations have been prepared, mapped, and stored for future automated karyotyping when the appropriate equipment becomes available next year. In addition, aliquots of many of the preparations from which slide sets were made have been frozen for cross analysis by a DNA restriction technique under development at the University of Texas Health Science Center-Houston. While equipment difficulties beyond the control of this project have precluded the reporting of quantitative results at this point, a good beginning has been made towards the ultimate testing of the utility of chromosome analysis by autokaryotyping techniques in an extended space mission environment.

## REFERENCES

- Bettega 1981 - "Chromosome Aberrations Induced by Protons up to 31 MeV in Cultured Human Cells", D. Bettega, S. Dubini, A. M. F. Conti, T. Pelucchi, and L. T. Lombardi, *Radiat. Environ. Biophys.* 19, 91-100, 1981
- Brewen 1982 - "Chromosome Aberrations in Mammals as Genetic Parameters in Determining Mutagenic Potential and Assessing Genetic Risk." *Progress in Mutation Research*, Vol. 3, ed. by K. C. Bora, G. R. Douglas, and E. R. Nestman, Elsevier Biomedical Press, Amsterdam, Oxford, New York.
- Collins 1980 - "A Case of Child Abuse by Radiation Exposure", V. P. Collins and M. E. Gaulden, in *The Medical Basis for Radiation Accident Preparedness*, ed by K. F. Hubner and S. A. Fry., Elsevier North Holland Inc. 1980.
- Evans 1979 - "Radiation Induced Chromosome Aberrations in Nuclear Dockyard Workers", H. J. Evans, K. E. Buckton, G. E. Hamilton, and A. Carothers. *Nature* 277, 531-534, 1979
- Haffner 1967 - "Radiation and Shielding in Space", James W. Haffner, Academic Press, New York, 1967
- Lloyd 1979 - "Radiation Exposure and Chromosome Damage", D. C. Lloyd, *Occupational Health*, Nov. 1979, pp 504-509.
- Lloyd 1980 - "The Incidence of Unstable Chromosome Aberrations in Peripheral Blood Lymphocytes from Unirradiated and Occupationally Exposed People", D. C. Lloyd, R. J. Purrott, and E. J. Reeder, *Mutation Research* 72, 523-532, 1980.
- Yochmowitz 1985 - "Seventeen-Year Mortality Experience of Proton Radiation in Macaca Mulatta", M. G. Yochmowitz, D. H. Wood, and Y. L. Salmon, *Radiation Research* 102, 13-34, 1985.

## APPENDIX A

### Solutions Used

- Culture Medium - 1000 ml RPMI Commercial Medium  
                  2 g  $\text{NaHCO}_3$   
                  10 ml Pen/Strep anti-mycotic solution  
                  10 ml (0.29 g) L-glutamine  
                  1 ml Heparin
- Hypotonic - 0.073 M KCl in distilled water
- Fixative - (3:1 v/v) Methanol and Glacial Acetic Acid

N86 - 31432

D 23  
479.

Integration of an Expert System into a User Interface  
Language Demonstration

18834

Daniel C. St. Clair, Ph. D.  
Professor of Computer Science  
University of Missouri  
St. Louis, Missouri

ACKNOWLEDGEMENTS

The authors would like to gratefully acknowledge the willing and capable assistance received from personnel at Johnson Space Center as well as Lockheed Engineering and Management Services Company, Inc (LEMSCO) personnel. A special thanks to Mr. Jim Duron and Mr. Greg Blackburn of Johnson Space Center and Mr. Bill Bennett, Mr. Brad Wells, and Mr. Dick Herold of LEMSCO for their invaluable assistance in developing the FORTRAN interface routines.

A special note of thanks goes to the people at JSC and Texas A & M University who supported and administered the NASA-ASEE Summer Faculty Fellowship Program.

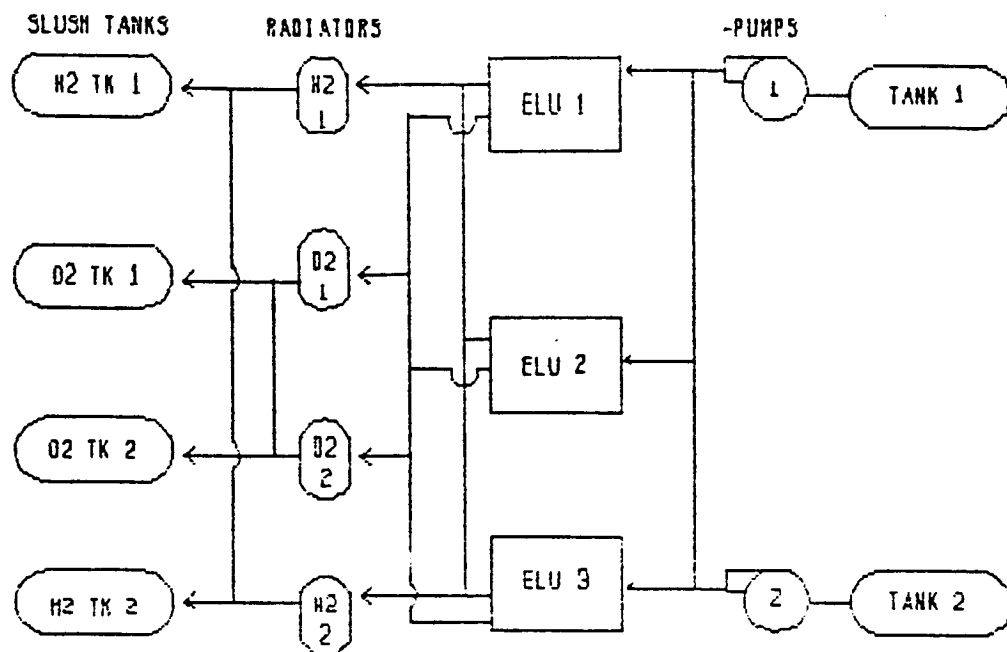


## THE UIL LANGUAGE DEMONSTRATION

The need for a User Interface Language (UIL) has been recognized by the Space Station Program Office as a necessary tool to aid in minimizing the cost of software generation by multiple users. Previous history in the Space Shuttle Program has shown that many different areas of software generation, such as operations, integration, testing, etc., have each used a different user command languages although the types of operations being performed were similar in many respects. Since the Space Station represents a much more complex software task, a common user command language--a user interface language--is required to support the large spectrum of space station software developers and users. To assist in the selection of an appropriate set of definitions for a UIL, EF2 was asked to generate a series of demonstration programs with which to test UIL concepts against specific Space Station scenarios using operators from the astronaut and scientific community. Because of the importance of expert systems in the space station, it was decided that an expert system should be embedded in the UIL. This would not only provide insight into the UIL components required but would

indicate the effectiveness with which an expert system could function in such an environment.

An expert system called the UIL-Expert System for Propulsion Subsystem Analysis and Diagnosis (UIL-ESP-AD) was designed and integrated into the UIL operating system. The propulsion subsystem chosen for expert system analysis and diagnosis produces and stores  $H_2/O_2$  using water as the raw material. This  $H_2/O_2$  Production Subsystem is shown in Figure 1. In the UIL language demonstration, UIL-ESP-AD reads the values of the parameters in this system, performs analysis on any parameters which are not nominal, and instructs the  $H_2/O_2$  Production Subsystem to replace defective units. Because of the data driven nature of the problem, UIL-ESP-AD was designed as a knowledge based expert system which uses a forward reasoning inference engine. It varies from earlier process control systems in that analyses and diagnoses are performed in priority order, much the same way as would a human expert. Those conditions which point to specific units as having failed are analyzed first. Having diagnosed the "obvious" failures, UIL-ESP-AD proceeds to analyze the less obvious failures. Again, much like the human expert, UIL-ESP-AD considers those units which are most likely to fail. Having completed that analysis, the system moves to the unit which is the next most likely to fail. This process, which can detect multiple failures, continues until all units have been analyzed.



H2/O2 PRODUCTION SUBSYSTEM

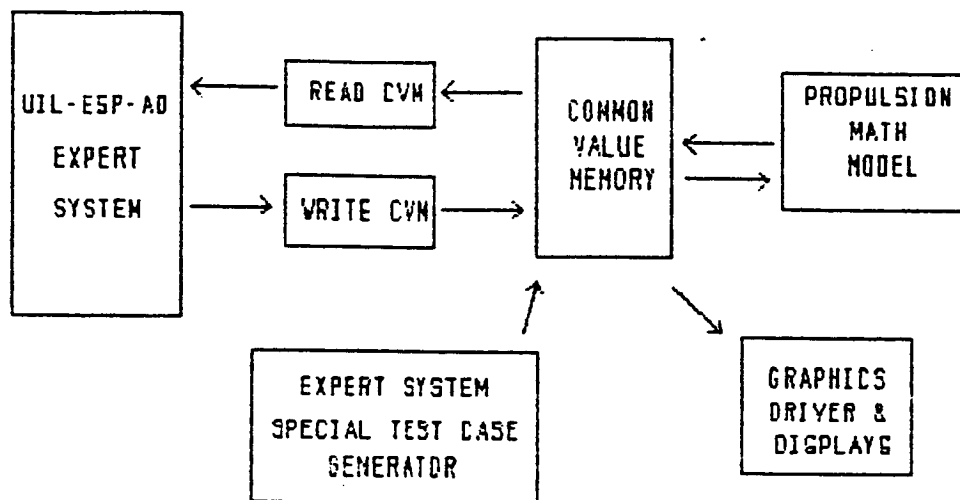
The complexity of system faults, the speed by which system diagnoses must occur, and the commonality of this problem to others on the space station provide an excellent problem for studying expert systems embedded in a UIL application. The subsystem math model was written in FORTRAN.

The expert system language chosen for implementing the expert system was OPS5. This language, developed by Carnegie-Mellon University, provides a forward reasoning inference engine and the knowledge base representation structures necessary for implementation of UIL-ESP-AD. UIL-ESP-AD system was developed on a VAX 11/780 where it was integrated to the Propulsion Math Model. This provides a truly interactive system where changes in the math model are detected and analyzed by the expert system. A stand-alone version of UIL-ESP-AD provides a facility for performing user designed tests.

## II. UIL-ESP-AD SYSTEM ENVIRONMENT

Figure 2 shows the UIL-ESP-AD system configuration. The key components in this diagram are UIL-ESP-AD, Current Value Memory (CVM), and the Propulsion Math Model. UIL-ESP-AD is the expert system component of the environment which will be discussed in the next section. The Propulsion Math Model is the model for the  $H_2/O_2$  Production Subsystem. The Expert System Special Test Case Generator is used to allow users to input special  $H_2/O_2$  Production Subsystem test cases which the Propulsion Math Model is currently not capable of generating. (These limitations are due to the Propulsion Math Model and not the  $H_2/O_2$  Production Subsystem itself.) The Graphics Driver & Displays component is used to graphically display current system conditions as well as the corresponding expert system and math model responses. CVM is the dataarray which serves as the common data access point for all UIL Language Demonstration functions.

In the normal operating mode, the FORTRAN Propulsion Math Model writes the current status of each system unit to CVM. When this has been completed, UIL-ESP-AD calls a FORTRAN subroutine to read the desired parameter values from CVM, perform the necessary formatting required by the expert system, and then transfer these values to UIL-ESP-AD. UIL-ESP-AD then performs the appropriate analyses and diagnoses of the system status, informs the user of what it has found and what system reconfigurations have been requested, and updates



## UIL-ESP-AD EMBEDDED SYSTEM

CVM. Updates to CVM are done by a FORTRAN subprogram called from the OPSS expert system. CVM updates consist of instructions to take certain units off-line and put certain units on-line. No other CVM values are set. Following this update procedure, the Propulsion Math Model reads CVM and performs its modeling calculations. The next section describes UIL-ESP-AD and these associated subroutines.

In the special test case mode, specific test cases can be chosen which illustrate aspects of UIL-ESP-AD. In most cases, the fault scenarios presented by the test cases are different than those which the math model is currently capable of generating. The Expert System Special Test Case Generator then sets the appropriate values in CVM and signals the expert system to begin analysis. Upon completion, the expert system signals the special test case generator that it has completed execution. The expert system then halts and waits for further instructions from the special test case generator.

The Graphics Driver & Displays component reads CVM and performs the corresponding graphical interpretation of the information that it finds. To enhance this capability, UIL-ESP-AD contains a subroutine which can be used to provide tracking of the expert system functions. In this way, graphics can show which components the expert system is analyzing. This routine will be described in the next section.

It should be noted that, in general, the functioning of UIL-ESP-AD is independent of the other system functions. When invoked, UIL-ESP-AD simply reads CVM, performs its analyses and diagnoses, and then writes information back to CVM. Hence, alterations to other

components in the system do not require alterations to the logic in the UIL-ESP-AD component. Accordingly, descriptions of the Expert System Special Test Case Generator and the Graphics Driver & Displays components are not included in this document.



### III. UIL-ESP-AD ARCHITECTURE

The UIL-ESP-AD architecture consists of the OPS5 expert system program itself and the several FORTRAN subroutines which it calls. This section provides both a functional description and a data description for each of these modules.

#### A. ESFOR.OPS

The heart of the UIL-ESP-AD expert system is the OPS5 program ESFOR.OPS. ESFOR.OPS, as any expert system program, contains two key components, a knowledge base and an inference engine.

The knowledge base component contains data about the various units in the system; i.e., tanks, pumps, ELUs, H<sub>2</sub>/O<sub>2</sub> radiators, and H<sub>2</sub>/O<sub>2</sub> slush tanks. The following example shows how tank data is defined and stored in the system.

```
tank
  ^no
  ^pci
  ^ena
  ^oper
  ^stdby
  ^quan
  ^rate
  ^temp
  ^pres
```

In this example, tank represents the unit name. The items preceded by ^ denote the various tank attributes. A list of components and their attributes can be found in the section of ESFOR.OPS code labeled "Define classes and attributes." This list is reproduced in Appendix A.

The knowledge base also contains a set of if-then rules of the form:

```
(p rule-name
  (a)
  (b)
  :
  :
-->
  (action 1)
  (action 2)
  :
  :
  (action n)
)
```

These rules describe the various actions to be performed when certain criteria are met. All decisions made as to the condition of specific units are expressed in productions of this form. The conditional expressions (a), (b), ... denote the hypothesis (if) part of the rule. The actions denote the conclusion (then) portion of the rule.

The inference engine used by OPSS is data driven (forward reasoning). OPSS maintains an area of storage called working memory (WM). The data items describing the various system units--pumps, tanks, etc.--are stored in WM. Whenever WM contains the components listed in the hypothesis portion of a rule, OPSS marks that rule for firing. At any point in time, multiple rules may be marked for firing. OPSS notes those rules marked for firing and executes them one at a time beginning with those which have the most complicated hypotheses. Whenever a rule is fired, the right hand side actions (shown as action 1, action 2, etc.) are performed. One of the types of actions which may be performed is that of adding working memory elements (WMEs). In this way, the execution of one rule can lead to the creation of WMEs which cause additional rules to be executed, etc.

The rules in UIL-ESP-AD are broken into several classes which have been called service levels. Each service level performs a given set of functions. The service levels, listed in the priority order of processing, are:

START

Classifies unit faults according to Problem Cause Indicators (PCIs). Replacement requests are initiated for units which are definitely bad; i.e., PCI = 1. The status of all on-line units is printed.

PCI-1

Performs replacement of all units which were labled PCI=1 by the START service level.

ELU

Productions which analyze and diagnose faulty electrolysis units.

O2-RAD

Productions which analyze and diagnose faulty oxygen radiators.

H2-RAD

Productions which analyze and diagnose faulty hydrogen radiators.

PUMP

Productions which analyze and diagnose faulty water pumps.

TANK

Productions which analyze and diagnose faulty water tanks.

O2-SLUSH

Productions which analyze and diagnose faulty oxygen slush tanks.

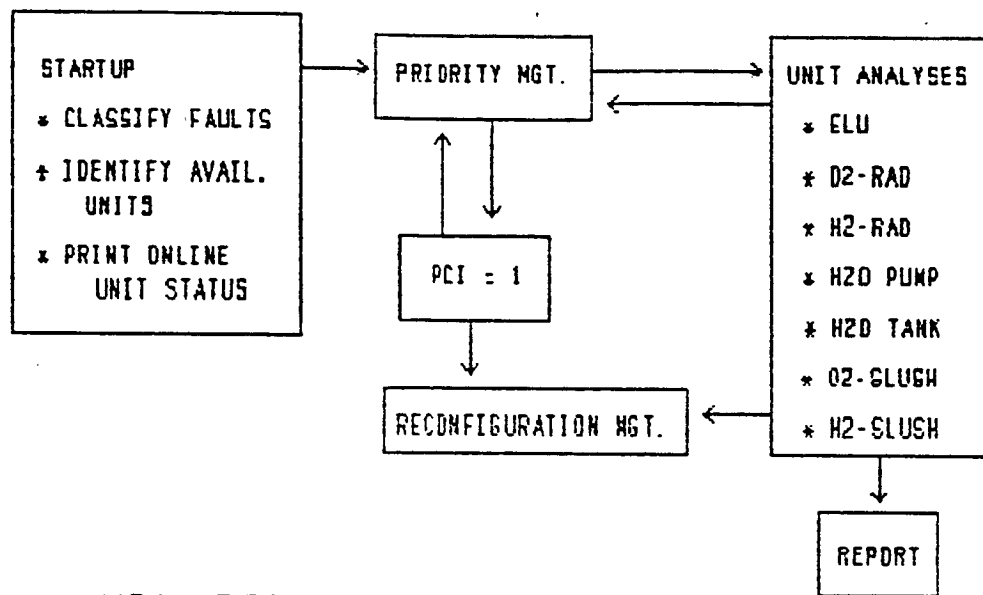
H2-SLUSH

Productions which analyze and diagnose faulty hydrogen slush tanks.

FINISHED

Productions which conclude expert system analysis, call the routine to write information to CVM, and prepare the expert system for the next set of data.

Figure 3 shows the top level flow through these procedures.



## UIL-ESP-AD PROCEDURE

Following initialization, those productions in each level which are applicable are fired beginning with the START service level. When no productions remain to be fired at this level, productions in the Priority Management level are fired to reduce the service level to PCI = 1 or to the ELU service level. If productions in the START level fail to identify on-line units which need to be replaced, processing skips the PCI-1 service level and proceeds directly to the ELU service level. Units which are marked for replacement by the PCI-1 service level receive additional analyses in the succeeding service levels. From the PCI = 1 service level, productions in the Reconfiguration Management level are enabled for firing so that the appropriate unit replacements may be made.

After moving to Unit Analysis, the expert system analyzes productions for each of the service levels shown. Whenever unit replacement is noted, the appropriate productions in the Reconfiguration Management level are enabled for firing. As these units are being reconfigured, the expert system continues to execute productions in Unit Analysis. Service levels for which no productions apply are automatically skipped by the inference engine. The expert system provides complete information to the user at each step of the analyses and diagnoses process by informing him of the productions applied and the corresponding results.

The order of production testing is controlled by a WME called

priority-list. Initially, priority-list contains the following:

```
priority-list
^a finished
^b h2-slush
^c o2-slush
^d tank
^e pump
^f h2-rad
^g o2-rad
^h elu
^i pci-1
^j start
```

The order of processing is determined by the order of the items in this list. To change the order of processing, change the order of the elements in this list. The only exceptions to this rule are that the finished and start items cannot be moved! The length of this list is controlled by a WME called: (number of priority levels 11). The program documentation contained in the ESFOR.OPS program listing shows how to change priority level information.

The priority levels were arranged in the order shown because experience indicates that this is the order in which the different units are expected to fail. Additional code could be added to the model which would monitor the history of unit failures and dynamically change this priority list as the expert system gains more information about unit failures!

Appendix B contains instructions for:

1. Changing PCI indicator settings in the START service level.
2. Adding and/or changing rules related to unit analyses and diagnoses.

## B. ESINIT.FOR

ESINIT.FOR is a FORTRAN subroutine called during initialization of ESFOR.OPS. ESINIT.FOR reads the values of desired CVM elements, converts them for use by the expert system, and calls special OPS5 functions which in turn create the WMEs needed by ESFOR.FT. The conversion process is required because the expert system expects to receive the relative measurements high (H), low (L), or normal (N) for such unit parameters as temperature, voltage, etc. (See Appendix A) ESINIT.FOR reads numerical values from CVM and, where appropriate, converts them into the corresponding relative measurements. These changes are completely controllable from within ESINIT.FOR without requiring any changes in the logic of the expert system itself. Special care should be taken in modifying any code in this program which creates WMEs since the order in which attributes are placed in a given WME is different than the order defined in Appendix A. This order was chosen to match the order in which OPS5 automatically arranges the WME attributes within each unit type.

## C. ESRECON.FOR

The expert system calls the FORTRAN subroutine ESRECON.FOR when it has completed analyzing and diagnosing the current state of CVM. The list of arguments passed to this subroutine depend on the type of information being reported.

When the expert system has found units which need to be replaced the form of the parameter list it passes to ESRECON.FOR is:

(RECON unit bad-unit-no good-unit-no unit bad-unit-no ...)

Bad-unit-no refers to the number of the unit being replaced while good-unit-no is the number of the unit which is to replace it. The length of the list depends on the number of units which are to be replaced. ESRECON.FOR translates this information into the appropriate CVM memory values and then updates CVM.

When the expert system analysis determines that no units need to be replaced, the parameter list passed to ESRECON.FOR takes the form:

(RECON DONE)

ESRECON.FOR interprets this parameter list to mean that the expert system has completed its analyses and that no unit replacements are required.

In addition to reporting unit replacement information, any call to ESRECON.FOR implies that the expert system analysis of the current state of the model has been completed. Hence, in the analysis of any given state of the model, the expert system makes only one call to this subroutine. ESINIT.FOR and ESRECON.FOR contain additional logic for starting and terminating cycles of ESFOR.OPS operation. Timing between expert system analyses and math model actions is controlled by using switches in CVM.



#### D. ESLEVEL.FOR

The FORTRAN subroutine ESLEVEL.FOR reports the service level on which the expert system is currently working. This subroutine provides information which can be used by external routines for such functions as graphics, etc. Its use is not necessary for the proper operation of the expert system. It is called by ESFOR.OPS whenever there is a change in service level.

The calling argument passed to ESLEVEL.FOR by ESFOR.OPS takes the form:

(LEVEL diag-level on-line unit unit-no unit unit-no ...)

where:

diag-level = FCI-1, PUMP, TANK, ELU, O2-RAD, H2-RAD,  
O2-SLU, or H2-SLU.

unit = name of system unit

unit-no = number corresponding to system unit.

Unit and unit-no pairs are repeated until every on-line unit is included. Hence, the length of this list is determined by the number of units currently on-line in the system.

## E. ES.OPS

ES.OPS is an alternative version of ESFOR.OPS. ES.OPS is a stand-alone version of the expert system which does not interface with CVM. This version requests that the user enter the number of a test case stored on disk. The test case is loaded and the corresponding analyses and diagnoses are performed. All output comes to the screen. The only subroutine called is ESEXIT.FOR which simply terminates execution of the program.

Additional test cases may be developed by following the instructions provided in Appendix C.

## UIL-ESP-AD EXAMPLES

The output shown in this section demonstrates the type of results produced by UIL-ESP-AD. It was produced by the ES.OPS version of UIL-ESP-AD. Appendix C describes the technique for generating test case data for ES.OPS. Note that all parameter values except no, ena, oper, and stdby are assigned one of three values, low, high, or normal. ESFOR.OPS generates the same output but takes input from Current Value Memory (CVM) and writes unit replacement instructions to common memory.

The first example, shown in Figure 4, is fairly simple. Pump 2 is not enabled meaning that it is out of service and can not be used. Pump 1 has a high temp and ELU 1 has a high H<sub>2</sub>-temp. UIL-ESP-AD first checks for units that are off-line, i.e. not

enabled. The unit may simply not be there, may be awaiting repairs, or is turned off. With pump 2 not enabled, it is not available for reconfiguration and the expert system tags it as such. Next, the expert system checks units which are definitely bad. Such a condition would call for immediate reconfiguration. No such failure types were found in this case. (In designing the expert system, the expert identified the parameters that indicate, with a high probability, the unit has failed.) At the same time UIL-ESP-AD is looking for these types of failures, it is also noting other types of failures. After this first pass, those parameters that are out of tolerance are analyzed to determine the source and/or location of the failure.

```

*****
*
*           Welcome to
*
*           UIL-ESP-AD
*
*           UIL Expert System for Propulsion Subsystem
*           Analysis & Diagnosis
*
*           Developed by
*
*           Daniel C. St. Clair, PhD
*           University of MO -- Rolla
*           Graduate Engineering Center
*           St. Louis, MO
*
*****

```

Input name of test data file (tc0..tc8,exit): tc1

Thank you.

\*-----  
Test Data File TC1  
Status of initial on-line units (H = high, L = low, N = normal):

NOTE \*\*\*\*\* PUMP 2 is not enabled!

TANK 1							
Quan	=	N	Rate	=	N	Temp	= N
PUMP 1							
Volt	=	N	Cur	=	N	Rate	= H
Pres	=	N				Temp	
H2-SLUSH 1							
Volt	=	N	Cur	=	N	Rate	= N
Pres	=	N	Quan	=	N	Temp	= N
O2-SLUSH 2							
Volt	=	N	Cur	=	N	Rate	= N
Pres	=	N	Quan	=	N	Temp	= N
ELU 1							
Volt	=	N	Cur	=	N	H2O-S1	= N
H-O-S2	=	N	H-O-S3	=	N	O-H-s3	= N
H2-temp	=	H	O2-pres	=	N	O2-temp	= N

Figure 4. Test Case 1

ELU 2							
Volt	=	N	Cur	=	N	H2O-S1	= N Dry = N
H-O-S2	=	N	H-O-S3	=	N	O-H-s3	= N H2-pres = N
H2-temp	=	N	O2-pres	=	N	O2-temp	= N

H2-RAD 1							
Pres-in	=	N	Pres-out	=	N	Temp-in	= N Temp-out = N
Stemp 1	=	N	Stemp 2	=	N	Stemp 3	= N Stemp 4 = N
Stemp 5	=	N	Stemp 6	=	N		

O2-RAD 2							
Pres-in	=	N	Pres-out	=	N	Temp-in	= N Temp-out = N
Stemp 1	=	N	Stemp 2	=	N	Stemp 3	= N

```

*****
Unit parameters were found which are out of tolerance,
however no bad units have been identified. UIL-ESP-AD
will now perform additional analyses to determine which
units need to be replaced.
*****

```

```

*****
Analyzing & Diagnosing ELU units
*****

```

ELU 1 hydrogen output temperature is H .  
 ELU 1 replacement has been requested.

--> ELU 1 has been replaced with ELU 3 since ELU 1  
 is no longer operational.

```

*****
Analyzing & Diagnosing O2-RAD -units
*****

```

```

*****
Analyzing & Diagnosing H2-RAD units
*****

```

Figure 4. Test Case 1 (contd.)

```

*****
Analyzing & Diagnosing PUMP units
*****

```

```

PUMP 1 temperature is H.
TANK 1 temperature is N.
Pump 1 - tank 1 replacements have been requested.

```

```

PUMP 1 needs to be replaced.
No standby pumps are available.
UIL-ESP-ADE is unable to reconfigure the system.

```

```

*****
Analyzing & Diagnosing TANK units
*****

```

```

*****
Analyzing & Diagnosing O2-SLUSH units
*****

```

```

*****
Analyzing & Diagnosing H2-SLUSH units
*****

```

```

*-----*-----*-----*-----*-----*
          UIL-ESP-AD
          EXPERT SYSTEM
    ANALYSIS & DIAGNOSIS OF THE PROPULSION SYSTEM:

```

```

--> The following units have been reconfigured:

```

```

** ELU 1 has been replaced with ELU 3
Reason(s) for this action are (H = high, L = low, N = normal):
    Hydrogen output temperature is H .

```

```

--> The following units could not be replaced due to lack
    of available standby units.

```

```

    PUMP unit # 1
    Reason(s) this replacement was requested:
    (H = high, L = low, N = normal):
        PUMP 1 temperature is H but TANK temperature is N.

```

Figure 4. Test Case 1 (contd.)

--> The following units are in standby and are available for immediate use:

O2-SLUSH unit # 1  
H2-SLUSH unit # 2  
O2-RAD unit # 1  
H2-RAD unit # 2  
TANK unit # 2

--> NOTE the following additional system information:

PUMP 2 is not enabled.

UIL-ESP-AD expert system analysis of the current state of the electrolysis system has been completed.

\*-----\*-----\*-----\*-----\*-----\*

Figure 4. Test Case 1 (contd.)

This example is straightforward; ELU 1 has a high output temp and is replaced with ELU 3. Pump 1 also has a high temp but pump 2 is off-line; therefore, it cannot be replaced. A warning is issued and a summary of the analysis and diagnosis is given at the end of the second pass. It should be noted that UIL-ESP-AD analyzes each unit in the order that the expert feels is most probable to fail or is most critical in the process path.

The second example is shown in Figure 2. The second example differs from the first. At first analysis, pump 2 and ELU 3 have been replaced because they were immediately identified as faulty. However, upon further analysis, it was noted that the H<sub>2</sub>O sieve sensor #1 should be checked. In fact, the particular parameter--H<sub>2</sub>O sieve--probably should not cause the unit to be replaced. The conclusion of UIL-ESP-AD is that the sensor is bad and the unit could perform normally. At this point, the user might prefer to override the expert system's decision. It should be noted, however, that UIL-ESP-AD will leave a unit on-line if there is not backup unit on standby. This prevents one bad system configuration from replacing another bad system configuration.

The third test case is a demonstration of the type of analysis that can keep a good unit on-line despite suspected failures. The O2-RAD 2 pres-out indicated high and was noted in the analysis. However, the O2-SLUSH pres was low and the output rate was low. The system noted this data and correlated the readings from the separate units. The correct analysis is that there may be a blockage in the connecting line or there may be a sensor failure. Additionally,



\*-----  
 Test Data File TCB  
 Status of initial on-line units (H = high, L = low, N = normal):

TANK 2							
Quan	=	N	Rate	=	N	Temp	= N
PUMP 2							
Volt	=	N	Cur	=	L	Rate	= N
Pres	=	N				Temp	= N
H2-SLUSH 2							
Volt	=	N	Cur	=	N	Rate	= N
Pres	=	N	Quan	=	N	Temp	= N
O2-SLUSH 2							
Volt	=	N	Cur	=	N	Rate	= N
Pres	=	N	Quan	=	N	Temp	= N
ELU 2							
Volt	=	N	Cur	=	N	H2O-S1	= N
H-O-S2	=	N	H-O-S3	=	N	O-H-s3	= N
H2-temp	=	N	O2-pres	=	N	O2-temp	= N
ELU 3							
Volt	=	N	Cur	=	N	H2O-S1	= H
H-O-S2	=	N	H-O-S3	=	N	O-H-s3	= N
H2-temp	=	N	O2-pres	=	N	O2-temp	= N
H2-RAD 2							
Pres-in	=	N	Pres-out	=	N	Temp-in	= N
Stemp 1	=	N	Stemp 2	=	N	Stemp 3	= N
Stemp 5	=	N	Stemp 6	=	N	Stemp 4	= N
O2-RAD 2							
Pres-in	=	N	Pres-out	=	N	Temp-in	= N
Stemp 1	=	N	Stemp 2	=	N	Stemp 3	= N

\*\*\*\*\*  
 UIL-ESP-AD has identified units which need to be replaced  
 and has requested the appropriate replacements.  
 These requests are shown below.  
 UIL-ESP-AD will now perform additional analyses on these  
 units as well as the other online units in the system.  
 \*\*\*\*\*

--> PUMP 2 has been replaced with PUMP 1 since PUMP 2  
 is no longer operational.  
 --> TANK 2 has also been replaced with TANK 1  
 --> ELU 3 has been replaced with ELU 1 since ELU 3  
 is no longer operational.

Figure 5. Test Case 2

```

*****
Analyzing & diagnosing ELU units
*****

```

ELU 3 H2O sieve 1 % value is H.  
The corresponding H/O sieve 2 and H/O sieve 3 % values are N.  
H2O sieve sensor #1 should be checked.  
ELU 3 replacement has been requested.

ELU 3 H2O sieve 1 % value is H.  
The corresponding H/O sieve 2 and O/H sieve 3 % values are N.  
H2O sieve sensor #1 should be checked.  
ELU 3 replacement has been requested.

```

*****
Analyzing & Diagnosing O2-RAD units
*****

```

```

*****
Analyzing & Diagnosing H2-RAD units
*****

```

```

*****
Analyzing & Diagnosing PUMP units
*****

```

```

*****
Analyzing & Diagnosing TANK units
*****

```

```

*****
Analyzing & Diagnosing O2-SLUSH units
*****

```

```

*****
Analyzing & Diagnosing H2-SLUSH units
*****

```

Figure 5. Test Case 2 (contd.)

```

*-----*
      UIL-ESP-AD
      EXPERT SYSTEM
      ANALYSIS & DIAGNOSIS OF THE PROPULSION SYSTEM:

--> The following units have been reconfigured:

** ELU 3 has been replaced with ELU 1
Reason(s) for this action are (H = high, L = low, N = normal):
    H2O-S1 is H while HO-S2 and OH-S3 are N.
    H2O-S1 is H while HO-S2 and HO-S3 values are N.
    H2O-SIEVE 1 value is H .

** PUMP 2 has been replaced with PUMP 1
Reason(s) for this action are (H = high, L = low, N = normal):
    PUMP current is L .

** TANK 2 has been replaced with TANK 1
Reason(s) for this action are (H = high, L = low, N = normal):
    PUMP 2 replacement was requested.

--> The following units are in standby and are available for
    immediate use:

        O2-SLUSH unit # 1
        H2-SLUSH unit # 1
        O2-RAD unit # 1
        H2-RAD unit # 1

UIL-ESP-AD expert system analysis of the current state of the
electrolysis system has been completed.

*-----*

```

Figure 5. Test Case 2 (contd.)

\*-----  
 Test Data File TC4  
 Status of initial on-line units (H = high, L = low, N = normal):

NOTE \*\*\*\*\* O2-SLUSH 2 is not enabled!

TANK 1							
Quan	=	N	Rate	=	N	Temp	= N
PUMP 1							
Volt	=	N	Cur	=	N	Rate	= N
Pres	=	N				Temp	= N
H2-SLUSH 1							
Volt	=	N	Cur	=	N	Rate	= N
Pres	=	N	Quan	=	N	Temp	= N
O2-SLUSH 1							
Volt	=	N	Cur	=	N	Rate	= N
Pres	=	L	Quan	=	N	Temp	= N
ELU 1							
Volt	=	N	Cur	=	N	H2O-S1	= N
H-O-S2	=	N	H-O-S3	=	N	O-H-s3	= N
H2-temp	=	N	O2-pres	=	N	O2-temp	= N
ELU 2							
Volt	=	N	Cur	=	N	H2O-S1	= N
H-O-S2	=	N	H-O-S3	=	N	O-H-s3	= N
H2-temp	=	N	O2-pres	=	N	O2-temp	= N
H2-RAD 2							
Pres-in	=	N	Pres-out	=	N	Temp-in	= N
Stemp 1	=	N	Stemp 2	=	N	Stemp 3	= N
Stemp 5	=	N	Stemp 6	=	N	Temp-out	= N
O2-RAD 2							
Pres-in	=	N	Pres-out	=	H	Temp-in	= N
Stemp 1	=	N	Stemp 2	=	N	Stemp 3	= N

\*\*\*\*\*  
 Unit parameters were found which are out of tolerance,  
 however no bad units have been identified. UIL-ESP-AD  
 will now perform additional analyses to determine which  
 units need to be replaced.  
 \*\*\*\*\*

\*\*\*\*\*  
 Analyzing & Diagnosing ELU units  
 \*\*\*\*\*

Figure 6. Test Case 3

\*\*\*\*\*  
Ananalyzing & Diagnosing O2-RAD units  
\*\*\*\*\*

\*\*\*\*\*  
Ananalyzing & Diagnosing H2-RAD units  
\*\*\*\*\*

\*\*\*\*\*  
Ananalyzing & Diagnosing PUMP units  
\*\*\*\*\*

\*\*\*\*\*  
Ananalyzing & Diagnosing TANK units  
\*\*\*\*\*

\*\*\*\*\*  
Ananalyzing & Diagnosing O2-SLUSH units  
\*\*\*\*\*

O2-SLUSH tank 1 pressure is L .  
O2-RADIATOR 2 output pressure is H.  
There may be a block in the line between O2-RADIATOR 2  
and O2-SLUSH tank 1 .

O2-SLUSH tank 1 flow rate is L .  
O2-SLUSH tank 1 rate sensor may need repair or there may  
be a failure down-line from the O2-slush tank.

\*\*\*\*\*  
Ananalyzing & Diagnosing H2-SLUSH units  
\*\*\*\*\*

Figure 6. Test Case 3 (contd.)

\*-----\*

UIL-ESP-AD  
EXPERT SYSTEM  
ANALYSIS & DIAGNOSIS OF THE PROPULSION SYSTEM:

--> The following units are in standby and are available for immediate use:

H2-SLUSH unit # 2  
O2-RAD unit # 1  
H2-RAD unit # 1  
ELU unit # 3  
PUMP unit # 2  
TANK unit # 2

--> NOTE the following additional system information:

O2-SLUSH 1 flow rate is L .  
O2-SLUSH 1 pressure is L , O2-RAD output pressure is H.  
O2-SLUSH 2 is not enabled.

No online units need to be replaced at this time.

UIL-ESP-AD expert system analysis of the current state of the electrolysis system has been completed.

\*-----\*

Figure 6. Test Case 3 (contd.)

since the flow rate was low from the slush tank, it is possible that there is also a sensor problem or a blocked line downstream from the slush tank. The important part of this analysis is that an operational unit was not taken off-line. Additional programming of UIL-ESP-AD would allow tanks to be switched, data from the new configuration read and compared to the previous configuration, and this additional information then used to determine if a sensor had failed or if there indeed was a blockage in the O<sub>2</sub> lines.

These examples demonstrate the essence of UIL-ESP-AD: catch the obvious problem first and reconfigure (if possible), diagnose and analyze multiple failures on a priority basis, and distinguish between unit and other failures (sensor or line blockage) by comparing data from all of the relevant units (prevents good units from being taken off-line). Other examples were constructed which were variations of the above.

C-8

## V. REMARKS

The entire system was developed to reflect a way the human expert would approach the problem. As such, it looks for obvious faults first and performs the required actions. Next, it analyzes units in the same order as would a human expert. For this type of problem, and the numerous other space station expert system applications like it, the OPS5 language and this design approach worked extremely well. The rules and facts known by the human expert were easily represented in OPS5. The forward reasoning inference engine was a natural for taking input data from the system units and applying rules to determine the set of conclusions which described the system's behavior.

In addition, the system design provides for easy insertion of new rules and/or the alteration of existing rules. These types of modifications can be made by a person with only a basic knowledge of the system structure. The priority in which unit analyses are performed can also be altered. The system design would allow for the easy addition of code so that it could modify the priority order.

Programming in a logic based language is quite different from programming in an algorithmic language such as FORTRAN. Not only are the mechanisms for establishing control schemes different but multiple processes can occur simultaneously. These features played a vital role in designing UIL-ESP-AD.



The OPS5 for a VAX/VMS development environment was cumbersome compared to the development environments for KEE, ART, etc. The OPS5 development environment provided only a full screen editor and a debugger but none of the graphics capabilities which aid in constructing logic and control flows which are available with other systems. However the OPS5 language itself was powerful enough to adequately perform the expert system requirements.

From the standpoint of the User Interface Language, much effort is needed in the area of defining the requirements for Logical Programming Languages (LPL). An LPL needs to be more "user friendly" than OPS5, but needs to be fast and compact like OPS5. The goal of UIL is for a nonprogrammer to be able to sit down and produce effective programs in a short period of time with little formal training.

The usefulness of UIL-ESF-AD is very apparent, especially when thinking in terms of a very large and complex system such as the Space Station. One of the key features of UIL-ESF-AD that should be incorporated into space station expert system applications of this type include the LPL's supporting the design of expert systems which perform systems analyses and diagnoses functions in much the same way as does the human expert. Further, actions of the expert system must be visible to and understandable by the user in order to promote confidence in the system's decisions. The LPL should support the recording of a history of actions taken so that the program can modify its courses of action based on these historical results.

## REFERENCES

The following references were used in the design and development of UIL-ESP-AD.

B.G. Buchanan and E.H. Shortliffe, RULE-BASED EXPERT SYSTEMS: THE MYCIN EXPERIMENTS OF THE STANFORD HEURISTIC PROGRAMMING PROJECT, Addison Wesley, Reading, Mass, 1984.

R. Davis and D.B. Lenat, KNOWLEDGE-BASED SYSTEMS IN ARTIFICIAL INTELLIGENCE, McGraw-Hill, New York, 1982.

K.A. Frenkel, "Toward Automating the Software-Development Cycle," COMMUNICATIONS OF THE ACM, Vol. 28, No. 6, June 1985, pp 578-589.

D.L. Kaiser, "Use of a Man Machine Interface in the Development of Two Expert Systems for Space Station Applications," Proceedings of ROBEXS '85: The First Annual Workshop on Robotics and Expert Systems, NASA/Johnson Space Center, June 1985, pp 149-152.

F. Harmon and D. King, EXPERT SYSTEMS: ARTIFICIAL INTELLIGENCE IN BUSINESS, John Wiley & Sons, Inc., New York, 1985.

J.T. Malin, N. Lance, "An Expert System for Fault Management and Automatic Shutdown Avoidance in a Regenerative Life Support System," Proceedings of ROBEXS '85: The First Annual Workshop on Robotics and Expert Systems, NASA/Johnson Space Center, June 1985, pp 185-193.

OPSS FOR VAX USER'S GUIDE AA-BH99A-TE, Digital Equipment Corporation, March 1984.

OPSS USER'S MANUAL AA-BH00A-TE, Digital Equipment Corporation, March 1984.

E. Rich, ARTIFICIAL INTELLIGENCE, McGraw-Hill Book Company, New York, 1983.

# APPENDIX A

## ESFOR.OPS COMPONENTS

(literalize tank

```

        no      ;tank number
        pci      ;=99 unit disabled, =98 unit enabled but
oper=stdby=0,
               ;=nil initial, 0= ok,
               ;= 1 reconfig, =2!3!4 determine action
        ena      ;=1 unit enabled, =0 unit disabled
        oper      ;=1 unit online, =0 unit offline
        stdby     ;=1 unit on standby, =0 unit not on standby
        quan      ;h,1,n
        rate      ;h,1,n
        temp      ;h,1,n
        pres      ;h,1,n
    )

```

(literalize pump

```

        no      ;pump number
        pci      ;=99 unit disabled, =98 unit enabled but
               ; oper=stdby=0,
               ;=nil initial, 0= ok,
               ;= 1 reconfig, =2!3!4 determine action
        ena      ;=1 unit enabled, =0 unit disabled
        oper      ;=1 unit online, =0 unit offline
        stdby     ;=1 unit on standby, =0 unit not on standby
        volt      ;h,1,n
        cur      ;h,1,n
        rate      ;h,1,n
        temp      ;h,1,n
        pres      ;h,1,n
    )

```

(literalize elu

```
no      ;elu number
pci     ;=99 unit disabled, =98 unit enabled but
        ; oper=stdby=0,
        ;=nil initial, 0= ok,
        ;= 1 reconfig, =2!3!4 determine action
ena     ;=1 unit enabled, =0 unit disabled
oper    ;=1 unit online, =0 unit offline
stdby   ;=1 unit on standby, =0 unit not on standby
volt    ;h,1,n
cur      ;current: h,1,n
h2o-s1  ;H2O in sieve 1: h,1,n
dry      ;Outline humidity: h,1,n
  h-o-s2 ;% H2 in O2 sieve 2: h,1,n
h-o-s3  ;% H2 in O2 sieve 3: h,1,n
o-h-s3  ;% O2 in H2 sieve 3: h,1,n
h2-pres ;H2 output pressure: h,1,n
h2-temp ;H2 output temperature: h,1,n
o2-pres ;O2 output pressure: h,1,n
o2-temp ;O2 output temperature: h,1,n
```

(literalize h2-rad

```
no      ;h2-rad number
pci     ;=99 unit disabled, =98 unit enabled but
        ; oper=stdby=0,
        ;=nil initial, 0= ok,
        ;= 1 Dureconfig, =2!3!4 determine action
ena     ;=1 unit enabled, =0 unit disabled
oper    ;=1 unit online, =0 unit offline
stdby   ;=1 unit on standby, =0 unit not on standby
pres-in ;Input pressure: h,1,n
pres-out ;Output pressure: h,1,n
temp-in ;Input temperature: h,1,n
temp-out ;Output temperature: h,1,n
stemp-1 ;Sensor 1 surface temperature: h,1,n
stemp-2 ;Sensor 2 surface temperature: h,1,n
stemp-3 ;Sensor 3 surface temperature: h,1,n
stemp-4 ;Sensor 4 surface temperature: h,1,n
stemp-5 ;Sensor 5 surface temperature: h,1,n
stemp-6 ;Sensor 6 surface temperature: h,1,n
```

)

(literalize o2-rad

```
no      ;o2-rad number
pci     ;=99 unit disabled, =98 unit enabled but
        ; oper=stdby=0,
        ;=nil initial, 0= ok,
        ;= 1 reconfig, =2!3!4 determine action
ena     ;=1 unit enabled, =0 unit disabled
oper    ;=1 unit online, =0 unit offline
stdby   ;=1 unit on standby, =0 unit not on standby
pres-in ;Input pressure: h,1,n
pres-out ;Output pressure: h,1,n
temp-in ;Input temperature: h,1,n
temp-out ;Output temperature: h,1,n
stemp-1 ;Sensor 1 surface temperature: h,1,n;
stemp-2 ;Sensor 2 surface temperature: h,1,n;
stemp-3 ;Sensor 3 surface temperature: h,1,n
```

)

(literalize h2-slush

```
no      ;h2-slush tank number
pci     ;=99 unit disabled, =98 unit enabled but
        ; oper=stdby=0,
        ;=nil initial, 0= ok,
        ;= 1 reconfig, =2|3|4 determine action
ena     ;=1 unit enabled, =0 unit disabled
oper    ;=1 unit online, =0 unit offline
stdby   ;=1 unit on standby, =0 unit not on standby
pres    ;pressure: h,1,n
temp    ;temperature: h,1,n
volt    ;voltage: h,1,n
cur     ;current: h,1,n
quan    ;quantity: h,1,n
bite    ;test indicator: h,1      <-- Not used in analysis
rate    ;flow rate: h,1,n
```

)

(literalize o2-slush

```
no      ;o2-slush tank number
pci     ;=99 unit disabled, =98 unit enabled but
        ; oper=stdby=0,
        ;=nil initial, 0= ok,
        ;= 1 reconfig, =2|3|4 determine action
ena     ;=1 unit enabled, =0 unit disabled
oper    ;=1 unit online, =0 unit offline
stdby   ;=1 unit on standby, =0 unit not on standby
pres    ;pressure: h,1,n
temp    ;temperature: h,1,n
volt    ;voltage: h,1,n
cur     ;current: h,1,n
quan    ;quantity: h,1,n
bite    ;test indicator: h,1      <-- Not used in analysis
rate    ;flow rate: h,1,n
```

)

APPENDIX B  
FORMAT OF UIL-ESP-AD RULES

RULES FOR SETTING PCI VALUES

Problem Cause Indicators (PCIs) are set in Step 1 of the START service level productions (See Appendix A). The general format for these rules is shown in the following example.

```
(p bad-elu-cur-pci
  (service level start)
  {<m> (elu ^no <x> ^pci << nil 4 >> ^cur { <q> <> n } )}
-->
  (make check elu <x> config)
  (modify <m> ^pci 1)
  (make summary configure elu <x> !Current is! <q> !.!)
)
```

This rule can be executed provided the program is in the START service level and there is an ELU available whose PCI value is nil or 4 and whose current value is not n (normal). When executed, this rule makes the WME:

(CHECK ELU <x> CONFIG)

where <x> will be replaced by the corresponding ELU number as it was determined when the hypothesis part of the rule was instantiated.

The modify statement changes the corresponding ELU unit pci value to 1 (i.e., this indicates a unit which must be replaced). The next statement produces the WME:

(SUMMARY CONFIGURE ELU <x> Current is <q>.)

This statement is used by productions in the FINISHED service level in reporting the reason unit reconfiguration was requested. In order to change the PCI value from 1 to 4, the 1 should be changed to a 4 in the modify statement and the (make check ELU <x> config) and the (make summary configure ....) actions should be removed.

The next example shows a case for which the PCI value is set to 4, indicating that the unit contains suspect readings but that further analysis is necessary to determine whether or not it needs to be replaced.

```
(p bad-elu-h2-pres-pci
  (service level start)
  {<m> ( elu ^no <x> ^pci nil ^h2-pres {<z> <> n )}}
-->
  (modify <m> ^pci 4)
)
```

Again, the rule will be executed only if the expert system is in the START service level and there is an ELU whose PCI is nil and whose h2-pres is not normal. In this case only the PCI value in the ELU WME instantiated in the hypothesis of this rule will be set to 4. Note that only those ELU units whose PCI values are nil will be candidates for instantiation by this rule. If this rule is changed so that the PCI is set to 1 instead of 4, the rule must be changed so that its format resembles that of the bad-ELU-cur-pci rule discussed earlier.

One further word of warning. Tanks and pumps occur in pairs. Hence, rules involving the setting of PCI values for tanks often involve statements which mention pump units. See the examples in the QPSS code.



## RULES FOR UNIT ANALYSES AND DIAGNOSES

The rules found in service levels such as ELU, PUMP, etc. are used in the detailed analysis of faulty units. Consider the following rule which is found in the list of rules in the O2-SLUSH service level.

```
(p o2radout-hpres-o2slush-hpres
  (service level o2-slush)
  (o2-rad <y> ^oper 1 ^pres-out h)
  (o2-slush <x> ^oper 1 ^pres h)
-->
  (write (crlf)
    !O2-SLUSH tank ! <x> ! input pressure is H.! (crlf)
    !O2-RADIATOR ! <y> ! output pressure is H.! (crlf)
    !O2-SLUSH tank ! <x> ! may need repair or there may!
    (crlf)
    !be a failure down-line from the O2-slush tank.!
    (crlf)(crlf))
  (make summary information o2-slush <y> !pressure is H
    and O2-RAD output pressure is H.)
)
```

In this case, the expert system is processing productions in the O2-SLUSH service level. If executed, the expert system will be processing rules in the O2-SLUSH service level and will have identified an operational O2-radiator whose pres-out value is h (high) and an operational O2-slush tank whose pressure is h. At this point, a message will be written to the screen telling the user what has occurred. The WME:

```
(SUMMARY INFORMATION O2-SLUSH <y> pressure is H and O2-RAD
  output pressure is H.)
```

will also be created. Again, this is used by the summary section of the expert system. Note that this rule provides only a warning message. It does not request that any units be replaced. Rules such as o2slush-hquan show what is necessary to request that a unit be removed from the system and replaced by an available unit.

The service level (TANK, PUMP, ELU, H2-RAD, O2-RAD, H2-SLUSH, or O2-SLUSH) in which a rule is to be placed is somewhat arbitrary. In general, it is desirable to place the rule in the service level which most closely matches the conclusion derived by the rule. The position of a rule within a given service level is immaterial since OPS5 executes only those rules whose hypotheses are satisfied by working memory. If several rules are candidates for execution (firing) at the same time, OPS5 will execute the one with the most number of conditional expressions in its hypothesis.

The replacement/addition of any rule should be done with extreme care. Errors may cause the model to produce incorrect results or may lead to abnormal termination of the expert system leaving the user in the OPS5 environment.

## APPENDIX C

### CREATION OF ES.OPS TEST CASES

Test cases for the ES.OPS version of UIL-ESP-AD can be created as shown in the following example.

```
$
```

```
$ copy tc0.ops tc9.ops
```

```
$ edt tc9.ops
```

Perform edit functions to set desired faults for the test case being developed.

```
*exit
```

```
DUA1:[UIL.OPS5]TC9.OPS;2 104 lines
```

```
$ run tcbld
```

```
OPS5>(@ tc9.ops)          <-- This loads tc9.ops into OPS5.
```

```
OPS5>(savestate tc9.)      <-- This saves test case 9 in the  
                           special file TC9. which can now be  
                           read by ES.OPS
```

```
OPS5>exit
```

```
$ dir tc9.*
```

```
Directory DUA1:[UIL.OPS5]
```

```
TC9.;1          TC9.OPS;2          TC9.OPS;1
```

```
Total of 3 files.
```

The test case TC9 is now ready for use by ES.OPS

The following shows the contents of the template test case file TC0.OPS.

```
$ type tc0.ops
```

```
(make tank
    ^no      1    ^ena    1    ^oper 0    ^stdby 1
    ^quan    n    ^rate   n
    ^temp    n    ^pres   n
)

(make tank
    ^no      2    ^ena    1    ^oper 1    ^stdby 0
    ^quan    n    ^rate   n
    ^temp    n    ^pres   n
)

(make pump
    ^no      1    ^ena    1    ^oper 0    ^stdby 1
    ^volt    n    ^cur     n
    ^rate    n    ^temp   n    ^pres   n
)

(make pump
    ^no      2    ^ena    1    ^oper 1    ^stdby 0
    ^volt    n    ^cur     n
    ^rate    n    ^temp   n    ^pres   n
)

(make elu
    ^no      1    ^ena    1    ^oper    0    ^stdby 1
    ^volt    n    ^cur     n
    ^h2o-s1  n    ^dry     n
    ^h-o-s2  n    ^h-o-s3  n    ^o-h-s3  n
    ^h2-pres n    ^h2-temp n    ^o2-pres n    ^o2-temp n
)

(make elu
    ^no      2    ^ena    1    ^oper    1    ^stdby 0
    ^volt    n    ^cur     n
    ^h2o-s1  n    ^dry     n
    ^h-o-s2  n    ^h-o-s3  n    ^o-h-s3  n
    ^h2-pres n    ^h2-temp n    ^o2-pres n    ^o2-temp n
)
```

```

(make elu
  ^no      3  ^ena      1  ^oper      1  ^stdby     0
  ^volt     n  ^cur      n
  ^h2o-s1   n  ^dry      n
  ^h-o-s2   n  ^h-o-s3   n  ^o-h-s3   n
  ^h2-pres  n  ^h2-temp  n  ^o2-pres  n  ^o2-temp  n
)

(make h2-rad
  ^no      1  ^ena      1  ^oper      0  ^stdby     1
  ^pres-in  n  ^pres-out n  ^temp-in   n  ^temp-out  n
  ^stemp-1  n  ^stemp-2  n  ^stemp-3   n  ^stemp-4   n
  ^stemp-5  n  ^stemp-6  n
)

(make h2-rad
  ^no      2  ^ena      1  ^oper      1  ^stdby     0
  ^pres-in  n  ^pres-out n  ^temp-in   n  ^temp-out  n
  ^stemp-1  n  ^stemp-2  n  ^stemp-3   n  ^stemp-4   n
  ^stemp-5  n  ^stemp-6  n
)

(make o2-rad
  ^no      1  ^ena      1  ^oper      0  ^stdby     1
  ^pres-in  n  ^pres-out n  ^temp-in   n  ^temp-out  n
  ^stemp-1  n  ^stemp-2  n  ^stemp-3   n
)

(make o2-rad
  ^no      2  ^ena      1  ^oper      1  ^stdby     0
  ^pres-in  n  ^pres-out n  ^temp-in   n  ^temp-out  n
  ^stemp-1  n  ^stemp-2  n  ^stemp-3   n
)

(make h2-slush
  ^no      1  ^ena      1  ^oper      0  ^stdby     1
  ^temp     n  ^volt     n  ^cur      n
  ^pres     n  ^quan     n
  ^bite     1
  ^rate     n
)

(make h2-slush
  ^no      2  ^ena      1  ^oper      1  ^stdby     0
  ^temp     n  ^volt     n  ^cur      n
  ^pres     n  ^quan     n
  ^bite     1
  ^rate     n
)

```

```

(make o2-slush
  ^no      1  ^ena      1  ^oper      0  ^stdby      1
  ^temp    n  ^volt    n  ^cur       n
  ^pres    n  ^quan    n  ^bite      1  ^rate      n
)

(make o2-slush
  ^no      2  ^ena      1  ^oper      1  ^stdby      0
  ^temp    n  ^volt    n  ^cur       n
  ^pres    n  ^quan    n  ^bite      1  ^rate      n
)

```

N86 - 31433

D24  
6P.

IN VITRO CYTOGENETIC STUDIES OF ORGANIC CHEMICALS FOUND  
AS CONTAMINANTS IN SPACECRAFT CABIN ATMOSPHERES

18835

Joseph Torres, Ph.D.  
Assistant Professor  
Department of Biological Sciences  
Southeastern Louisiana University  
Hammond, Louisiana

ABSTRACT

Astronauts can be exposed during spaceflight to organic chemical contaminants in the spacecraft cabin atmosphere. Toxic exposures may cause lesions in the cellular DNA which are subsequently expressed as sister-chromatid exchanges (SCE). Analysis of SCE is a sensitive short-term assay technique to detect and quantitate exposures to DNA-damaging (mutagenic) substances. The increase in SCE incidence over baseline (control) levels is generally proportional to the concentration of the mutagen and to the duration of exposure.

Dichloromethane (methylene chloride) was chosen for this study since it occurred as an atmospheric contaminant in ten of the first 12 STS flights, and has been reported to have toxic and mutagenic effects in various test systems. Glutaraldehyde was chosen because relatively few data are available on the toxicity or mutagenicity of this common biological fixative, which is carried on STS flights for use in biological experiments. The BHK-21 baby hamster kidney cell line was the in vitro test system used in this study. Neither dichloromethane (10 ppm to 500 ppm) nor glutaraldehyde (1 ppm to 10 ppm) increased SCE levels following 20-hour exposure of BHK-21 cells to the test chemicals.

---

NASA Colleague: Martin Coleman, Ph.D. SD4 X4086

## INTRODUCTION

Control of potentially toxic exposures to organic chemical contaminants in spacecraft cabin atmospheres is a vital concern to astronauts, who are exposed during spaceflight to a recirculating atmosphere containing trace amounts of numerous organic chemicals. Dichloromethane (methylene chloride) was selected from a list of more than 70 volatile organics detected during STS flights since it occurred as a contaminant in 10 of the first 12 STS flights, and has been reported to have toxic or mutagenic effects in various test systems. Glutaraldehyde was chosen because relatively few data are available on the toxicity and mutagenicity of this common biological fixative, which is carried on STS flights for use in biological experiments. This study proposed to test the mutagenic effects of glutaraldehyde and dichloromethane -- their ability to alter or damage DNA or chromosomes. Discovery of significant genetic toxicity of an organic compound would be an important factor in determining its spacecraft maximum allowable concentration (SMAC) limit.

Analysis of sister chromatid exchanges (SCE) is a sensitive short-term assay technique to detect and quantitate exposures to mutagenic substances (Perry & Evans, 1975; Latt & Schreck, 1980). The increase in SCE over baseline (control) levels is generally proportional to the concentration of the mutagen and to the duration of exposure.

BHK-21, an established cell line derived from baby hamster kidney cells, was chosen as the in vitro test system. BHK-21 cells are readily maintained in culture, are well-known in the biological literature, and are highly sensitive to toxic or mutagenic substances present in their growth media.



## MATERIALS AND METHODS

BHK-21 baby hamster kidney cells were obtained from the Biochemistry Department of the M.D. Anderson Hospital. Cells were cultured in RPMI-1640 medium supplemented with 10% fetal calf serum and maintained in a 37°C incubator in a humidified atmosphere of 5% carbon dioxide and 95% air.

Cell population doubling times were calculated from cell counts done on a Coulter model D2N electronic particle counter. Similar counting techniques were used to measure the dose-response of BHK-21 cells to glutaraldehyde and dichloromethane. Test chemicals were added to the growth media and cell counts done after 24 hours of exposure to either glutaraldehyde (1 ppm to 100 ppm) or dichloromethane (10 ppm to 1000 ppm). Controls had complete RPMI medium without test organics.

SCE staining was done by the "fluorescence-plus-Giemsa" (FPG) techniques currently used to resolve SCE for light microscopy (Kato, 1974; Perry & Wolff, 1974). Cells are exposed to bromodeoxyuridine (BrdU) for approximately two cell cycles, followed by metaphase arrest of mitotic cells with colcemid. Exposure to BrdU for two S-phases results in metaphase chromosomes in which one sister chromatid contains DNA with BrdU bifilarly substituted for thymidine, the other unifilarly substituted. This condition is the basis for differential FPG staining reactions in which one chromatid is darkly stained (unifilar BrdU substitution) and the other lightly stained (bifilar BrdU). SCE are scored by counting the number of times the polarity of light- vs. dark-staining segments is reversed, each marking the symmetrical interchange of material between sister chromatids. The number of SCE in 30 well-differentiated spreads is counted, averaged, and expressed as the number of SCE per cell ( $\pm$  s.d.).

## RESULTS

Control BHK-21 cells grew rapidly in culture, with population doubling times of about 12 hours. Dose-response curves to the test chemicals (Figure 1) yielded  $ID_{50}$  values of approximately 10 ppm for glutaraldehyde and 1000 ppm for dichloromethane. (The  $ID_{50}$  value represents the concentration of test chemical at which the population of treated cultures is half that of controls).

BHK-21 metaphase spreads showed a modal number of 44 chromosomes, with complements of submetacentric and acrocentric chromosomes, and a single large metacentric X chromosome, consistent with published karyotypes of the BHK-21 cell line.

Analysis of control SCE experiments showed that 20 hours was the optimum time for BrdU treatment. SCE experiments with the test chemicals were carried out with simultaneous exposure to BrdU and either glutaraldehyde or dichloromethane. SCE analysis showed no significant differences between BHK-21 controls and those treated with glutaraldehyde or dichloromethane.

### SISTER CHROMATID EXCHANGES IN BHK-21 CELLS (MEAN $\pm$ S.D.)

<u>Controls</u>	<u>Glutaraldehyde</u>		<u>Dichloromethane</u>	
6.67 $\pm$ 2.15	1 ppm	6.90 $\pm$ 1.90	10 ppm	6.25 $\pm$ 1.28
6.73 $\pm$ 1.80	2 ppm	6.20 $\pm$ 1.65	50 ppm	6.25 $\pm$ 0.96
7.33 $\pm$ 1.83	5 ppm	6.63 $\pm$ 1.92	100 ppm	6.17 $\pm$ 1.72
6.02 $\pm$ 1.78	10 ppm	6.77 $\pm$ 1.85	500 ppm	6.57 $\pm$ 1.38

## CONCLUSIONS

The BHK-21 baby hamster kidney cell line is a useful in vitro model system for use in genetic toxicology research.

Neither glutaraldehyde nor dichloromethane induced sister-chromatid exchanges during 20-hour exposures to concentrations that did not significantly inhibit cell growth.

No modifications of SMAC limits for glutaraldehyde or dichloromethane are suggested by these preliminary results.

## REFERENCES

- Kato, H. (1974). Spontaneous sister chromatid exchange detected by a BUdR-labelling method. Nature, 251, 70-72.
- Latt, S.A. & Schreck, R.R. (1980). Sister chromatid exchange analysis. Annual Review of Human Genetics, 32, 297-313.
- Perry, P. & Evans, H.J. (1975). Cytological detection of mutagen-carcinogen exposure by sister chromatid exchanges. Nature, 258, 121-125.
- Perry, P. & Wolff, S. (1974). New Giemsa method for differential staining of sister chromatids. Nature, 251, 156-158.

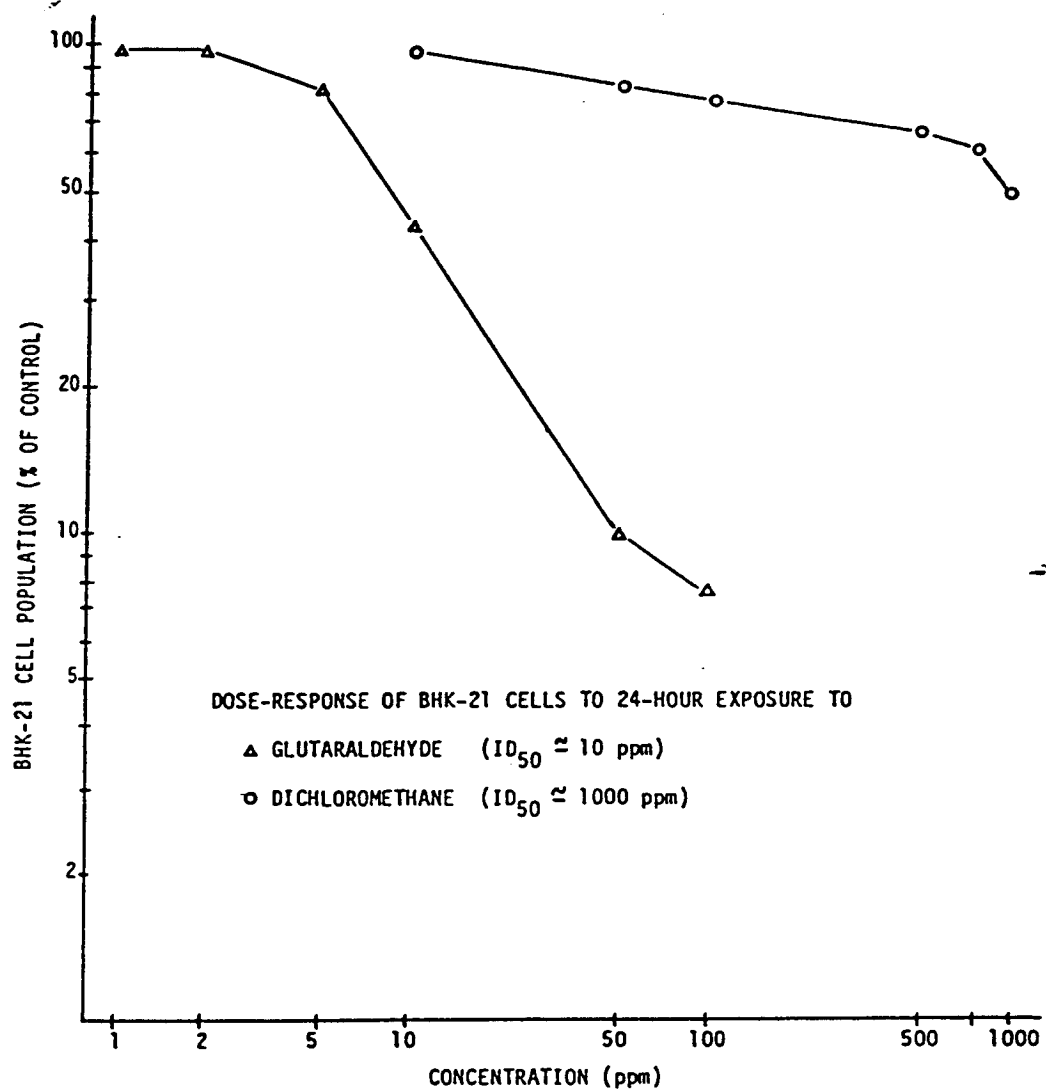


Figure 1. Dose-response of BHK-21 cells to 24-hour exposure to glutaraldehyde or dichloromethane.

## CSTAR STAR CATALOGUE DEVELOPMENT

Jo A. Uhde-Lacovara

18836

Assistant Professor  
Electrical Engineering Department  
Stevens Institute of Technology  
Hoboken, New Jersey

## ABSTRACT

The Continuous Stellar Tracking Attitude Reference (CSTAR) system is an in-house project for Space Station to provide high accuracy, drift free attitude and angular rate information for the GN&C system. Constraints exist on the star catalogue incorporated in the system. These constraints include the following: mass memory allocated for catalogue storage, star tracker imaging sensitivity, the minimum resolvable separation angle between stars, the width of the field of view of the star tracker, and the desired number of stars to be tracked in a field of view.

The Smithsonian Astrophysical Observatory (SAO) catalogue is the basis catalogue for this study. As it stands, the SAO does not meet the requirements of any of the above constraints. Star selection algorithms have been devised for catalogue optimization. Star distribution statistics have been obtained to aid in the development of these rules. VAX based software has been developed to implement the star selection algorithms. The software is modular and provides a design tool to tailor the catalogue to available star tracker technology. The SAO catalogue has been optimized for the requirements of the present CSTAR system.

## INTRODUCTION

The Orbiter uses rate gyroscopes and accelerometers as sensing devices to provide data for position and attitude control. These instruments need to be periodically updated by inertial reference information from star trackers, because their accuracy drifts with time. An alternative to this traditional system is being developed for Space Station as an in-house project of the Avionics Systems Division at Johnson Space Center. This project is called CSTAR for Continuous Stellar Tracking Attitude Reference. Drift free, high accuracy attitude and angular rate information is supplied by using solid state star trackers to continuously track stars.

The CSTAR system requires multiple fields-of-view (f.o.v.) to provide 3-axis information with minimal possibility of obscuration. A large star catalogue must be stored to ensure that there are always recognizable stars in the f.o.v. The Smithsonian Astrophysical Observatory (SAO) star catalogue is the basis for the development of the CSTAR catalogue. The SAO catalogue contains the positions and proper motions of approximately 259,000 stars. These are tabulated for the epoch and equinox of 1950. It is a compendium of several other catalogues and is by no means a complete enumeration of all stellar objects. It contains only those stars whose position and proper motion are precisely known. Knowledge of the proper motions of the stars is required so that the catalogue may be projected to the future. The SAO catalogue does not satisfy the CSTAR system constraints. Selection rules are needed to optimize the SAO catalogue for existing and potential CSTAR systems.

## THEORY

In order to develop algorithms to derive a CSTAR catalogue from the SAO catalogue, some knowledge of the magnitude and the two-dimensional spatial density distributions of the stars is required. The introduction to the SAO catalogue [SAO, 1966] contains a histogram of the magnitude distribution of the catalogue stars. This is presented in ranges of one order of magnitude. The literature on statistical astronomy indicates that stars recorded on a photographic plate would be expected to have a Poisson distribution [Trumpler and Weaver, 1962].

The catalogue derived from the SAO catalogue must conform to the constraints of the CSTAR system. These constraints include the following parameters: mass memory allocated for catalogue storage, star tracker imaging sensitivity, the minimum resolvable separation angle between stars, the width of the star tracker f.o.v., and the desired number of stars tracked in a f.o.v. Based on these constraints, the following star selection algorithms were developed. At each step, a new catalogue is formed; several iterations of the procedure produce a catalogue which meets the constraints of the system. These algorithms involve criteria which depend on both star retention and star removal.

Star selection algorithms:

- 1) Remove all stars having magnitudes greater than the dimmest star the star tracker can track. Dimmer stars have larger magnitudes.

2) Remove all stars with a separation angle to another star less than the minimum resolvable separation angle of the star tracker. This removal procedure may be modified in the case of bright binary stars. Such bright pairs may be retained if more sophisticated methods are devised for the estimation of position by the star tracker.

3) Find stars which are in sparse areas. Each star is considered, in turn, as the center of a circle having the same area as the tracker f.o.v. If there are less than the desired number of stars to be tracked in a field, the center star and the stars surrounding it in that field are marked as "backbone" stars. Backbone stars form the bedrock of the catalogue and cannot be removed by subsequent procedures. The unmarked stars are "temporary" stars and may be deleted from the catalogue by later steps.

4) Add bright temporary stars to the backbone. If a star can be seen by the naked eye (sixth order magnitude or less), it is marked to be retained. It is desirable that a crew person be able to look up a star seen with the unaided eye.

5) Iteratively process the catalogue to remove the dimmer stars in dense areas. Thresholds for magnitude ranges and maximum number of stars per field are set. Temporary stars which fall within the magnitude limits are considered, in turn, for removal. The number of stars in the surrounding field is found. The star is culled from the catalogue if this number is above the threshold. A culled star is no longer considered in the count of the number of stars in a field surrounding a neighboring star.



6) Form the backbone of the culled catalogue. The catalogue which is formed in Step 5) above is now examined for sparse areas. The backbone stars are found and marked as per Step 3) above.

Steps 5) and 6) are iterated until the desired catalogue is obtained. This may occur in one of two ways:

a) Stars are removed until the desired catalogue size is reached. The final catalogue then consists of both backbone and temporary stars.

b) The number of stars in the backbone approaches the desired number of stars in the catalogue. The final catalogue contains only backbone stars.

## RESULTS

### Star catalogue statistics:

Plots of the relative frequency versus stored magnitude for the various types of stars, resolvable, unresolvable, backbone or temporary, are shown in Figure 1. These plots are for a catalogue containing stars of 8.9 magnitude or brighter. These graphs show that the distributions are the same for the different types of stars. For stars in this magnitude range, the magnitude distribution is found to be independent of the spatial density. This distribution is of the form

$$f_m(m) = \begin{cases} K_1 e^{K_2 m} & -1.45 \leq m \leq 8.9 \\ 0 & \text{elsewhere} \end{cases}$$

where  $m$  represents the magnitude and  $f_m(m)$  is the probability density function. From statistics provided by the SAO magnitude histogram, the constant  $K_2$  is approximately equal to 1.25. The integral of the probability density function over the range -1.45 to 8.9 must be equal to unity. From this, the constant  $K_1$  is found to be equal to  $1.84 \times 10^{-5}$ .

The magnitude values of the catalogue itself were not used for the following reason: when the SAO catalogue was transferred to the local computer, the magnitude was stored in integer form; this was done incorrectly. The data has

periodic, 0.1 order magnitude ambiguities. This is not a serious factor for the star selection algorithms, but does make it inappropriate to use this data to derive the above constants. The plotted magnitudes have been smoothed to avoid these periodic discontinuities.

The spatial distribution was found to have the same shape for fields chosen at random and for fields chosen with each star as the center of the f.o.v. This distribution is not the expected Poisson distribution, but has a log-normal form [Hahn and Shapiro, 1967]; [Soong, 1981]. Let  $N_S$  be the number of stars with  $S$  other stars surrounding it as the center of a f.o.v. Let  $X = \ln(S)$ . Figure 2. is a plot of  $N_X$  versus  $X$ . It has the shape of a normal distribution. For the 8.9 magnitude or brighter, resolvable catalogue, the mean and standard deviation are as follows:

$$\mu_x = 2.73$$

$$\sigma_x = 0.518$$

These values agree well with the data.

Star selection algorithms:

The current specifications for the CSTAR system are the following:

1) Mass memory storage - 3 Megabytes; this allows approximately 100,000 stars to be stored in a triply redundant fashion.

2) Star tracker imaging sensitivity - 8.9 visual magnitude

3) Minimum resolvable separation angle - 0.05 degrees; this is based on a defocused star image covering a 6x6 array of star tracker pixels.

4) Width of tracker f.o.v. - 2 degrees x 2 degrees

5) Number of stars tracked in a f.o.v. - 10 stars

Table 1 summarizes the number of stars in the resulting catalogue after applying the star selection algorithms outlined in the theory section. The original SAO catalogue contains 258,997 stars. The 99,401 star, final catalogue is made up of only backbone stars. The spatial distribution of these stars has a mean of 10.0 stars per f.o.v. and a standard deviation of 3.38 stars. This distribution is plotted in Figure 3.

## CONCLUSIONS

The star selection algorithms have been implemented in a series of modular FORTRAN 77 programs for the ASD VAX/VMS computer. Programs have also been developed to produce catalogue statistics. The algorithms and the programs form an engineering tool to produce CSTAR star catalogues for a variety of hardware specifications. The catalogue statistics produced will aid in other areas of the CSTAR project such as centroiding algorithms, pattern recognition algorithms, and star tracker hardware requirements. An interesting modification to the culling algorithm (Step 5) is to locate the stars to be culled in a random fashion. The present program steps through the stars sequentially.

## REFERENCES

1. Smithsonian Astrophysical Observatory, Star Catalogue, Smithsonian Institution, Washington, D.C., Introduction, 1966
2. Trumpler, R. J., and Weaver, H. F., Statistical Astronomy, Dover, N. Y., Chapter 1, 1962
3. Hahn, G. J., and Shapiro, S. S., Statistical Models in Engineering, Wiley, N. Y., Chapter 3, 1967
4. Soong, T. T., Probabilistic Modeling and Analysis in Science and Engineering, Wiley, N. Y., Chapter 7, 1981

TABLE 1

STEP	DESCRIPTION	NUMBER OF STARS
1	Remove stars which are dimmer than 8.9 magnitude	155,765
2	Remove stars with separation angles below 0.05 degrees	150,774
3	Form the backbone based on 10 stars per f.o.v.	47,544 Backbone 103,230 Temporary
4	Include in the backbone all stars brighter than 6.0 mag.	51,232 Backbone 99,542 Temporary
5 and 6	After five iterations arrive at a final catalogue	99,401 (all backbone)

# STAR MAGNITUDE DISTRIBUTION

8.9 RESOLVABLE CATALOGUE

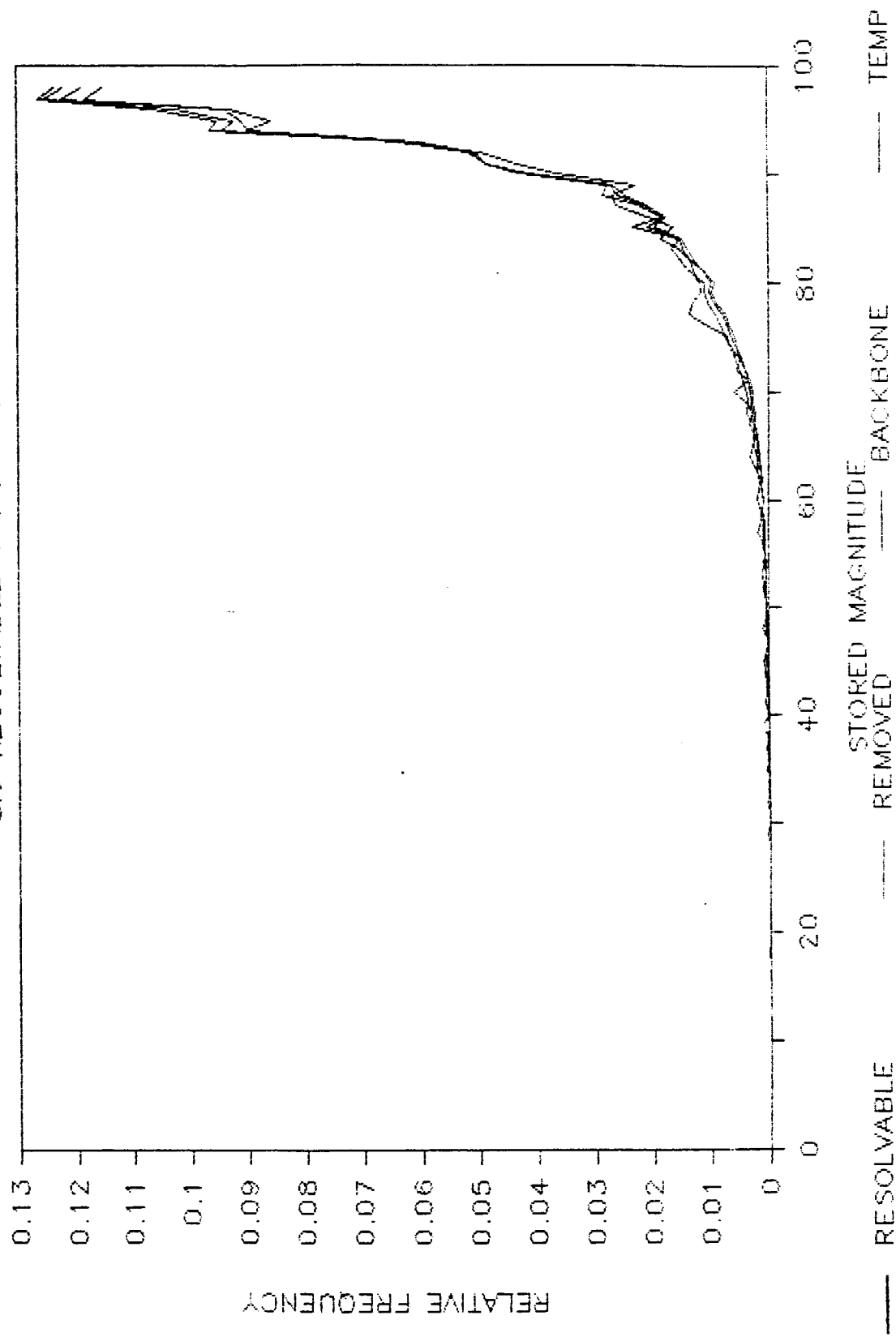


Figure 1



# SPATIAL DISTRIBUTION

8.9 MAG CATALOG - RESOLVABLE

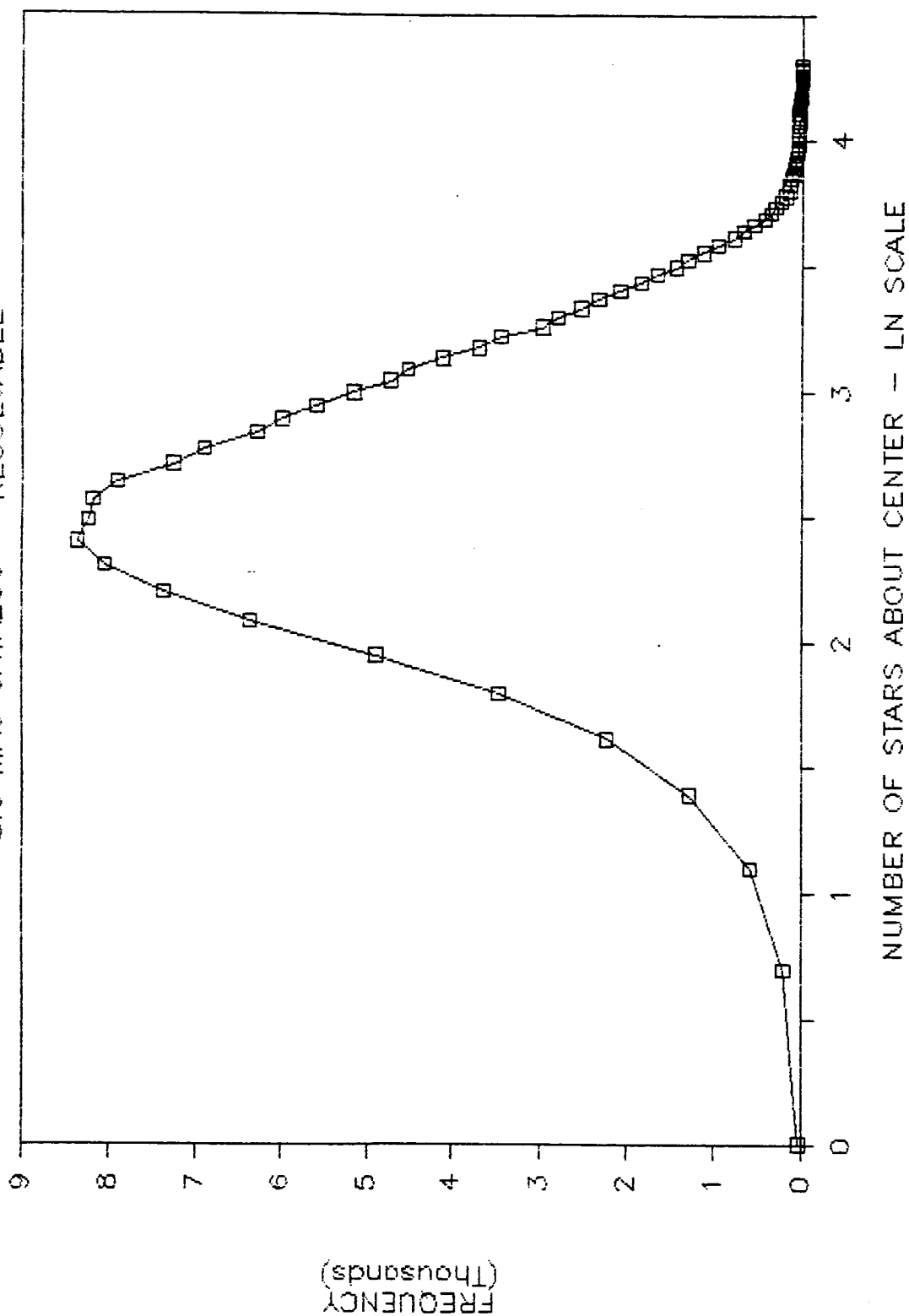


Figure 2

# SPATIAL DISTRIBUTION

99,401 STAR CATALOGUE

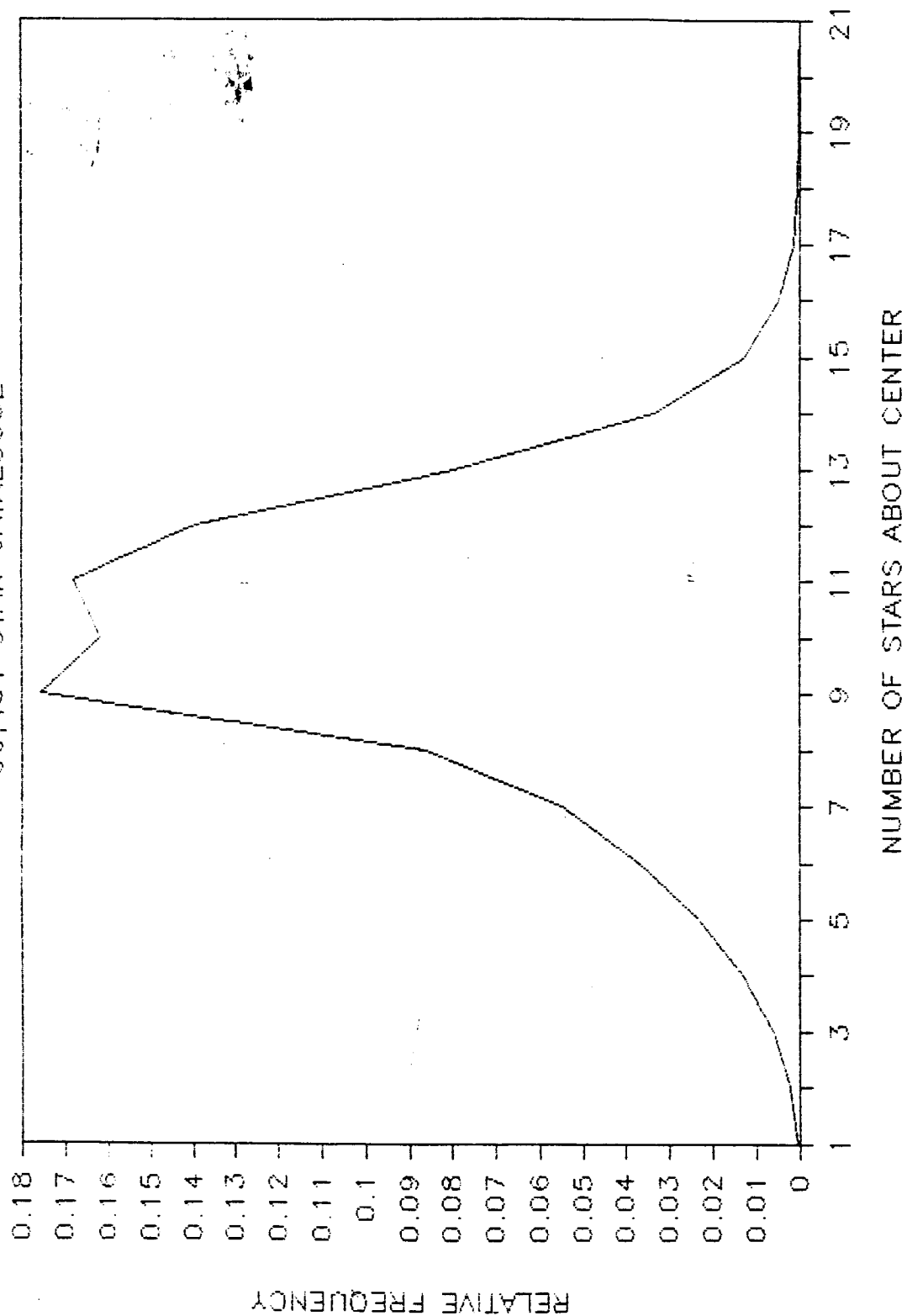


Figure 3

N86 - 31435

D26  
339

LASER TECHNIQUES FOR ARC JET PLASMA DIAGNOSTICS;

CONTINUATION OF A FEASIBILITY AND DESIGN STUDY

188 37

F. A. Wierum, Professor  
Mechanical Engineering and Materials Science Dept.  
Rice University - Houston, Texas

ABSTRACT

This study is concerned with the continuation of a feasibility and design study of laser-based diagnostic techniques for the non-intrusive measurement of species concentrations, temperatures, and velocity in the low density, high enthalpy flow through the arc-heated wind tunnel facility (ARMSEF) at NASA/JSC.

Last Summer several laser-induced radiation scattering methods were investigated and some preliminary measurements of the spectral distribution of radiation emitted by the arc-heated gas flow were made. Based upon those preliminary measurements and subsequent investigations, four laser-induced radiation scattering methods were selected for further detailed study, and preliminary design of a measurement system has been undertaken.

This Summer, further measurements of the spectral distribution of radiation emitted from the arc-heated free stream and shock layer flows, using a redesigned measurement system, have been made for one axial position in the flow for a range of tunnel operating power levels. Further study of the literature for physical property data, theoretical models of processes, and applications of the diagnostic methods has been also carried out.

## INTRODUCTION

One of the principal goals of the overall feasibility and design study, of which this Summer's work has been a part, is the identification of suitable laser-based diagnostic techniques for the measurement of species concentrations, temperatures, and velocity in the flow fields generated in the NASA/JSC low density, high enthalpy, arc-heated wind tunnel facility (ARMSEF).

Four techniques have been identified as suitable and viable for the arc jet facility. Three of these are concerned with temperature and number density determinations. All three can employ the same lasers and associated beam modifying components to supply the source beams. Further, all three can employ the same spectral detection components for acquiring, processing and storing the measurement signals. These are Spontaneous Raman Spectroscopy (SRS), Coherent Anti-stokes Raman Scattering (CARS), and Laser-Induced Fluorescence (LIF). The fourth technique is Laser Doppler Transit-time Anemometry (LTA), which provides velocity determination; it uses a different laser system and a different detection and data processing system, but it may be married to one of the other techniques in some instances. Further detailed study of these techniques is ongoing.

A part of this Summer's effort has been directed to surveying the literature for:

- (a) physical property data, such as transition probabilities, etc.;
- (b) suitable theoretical models necessary for reduction of measured data for temperature and number density determinations.

The literature in this area is extensive, recent, and growing rapidly. Most of it reports on measurements made in high pressure and/or temperature flow. Very few reports have been concerned with the combined very low pressure, low static temperature, high stagnation temperature flows involved in arc-heated tunnels such as ARMSEF. Most of the literature is concerned with atmospheric (or higher) pressure flows in aerodynamic type wind tunnels or with high temperature flame or combustion studies.

In Appendix A is a listing of some of the surveyed literature which is pertinent to and useful for developing appropriate design criteria and theoretical models for the laser-based diagnostic systems considered in this study. These references also contain some of the needed physical property data for the normal gaseous components of air. Additional search of the literature will be required to properly complete the data compilation for arc tunnel flows, with particular attention directed at the more recent literature.

Additional effort this Summer has been devoted to another important part of the overall feasibility and design study: the determination, over a range of arc tunnel operating conditions, of the background radiation and spectral description of the arc jet flow for use in designing and operating a laser-based diagnostic system. Knowledge of the spectral distribution and intensity of the radiation emitted from the arc jet flow, when analyzed on the basis of appropriate mathematical models of the physical processes involved, provides a means for determining local species concentrations and excitation temperatures of the constituents of the flow. Another function of this information, more pertinent to the purposes of this feasibility study, is that it provides the ability to identify those spectral regions in which the radiant emission from the arc jet flow, for a given set of tunnel operating conditions, might obscure or not the primary spectral signal, generated in the flow by an input laser beam, to be used as the diagnostic signal of interest.

Spectral measurements made during the Summer of 1984 were unable to provide information about the arc jet free stream flow. This inability to obtain adequate measurement data apparently arose from a combination of difficulties. Each of these difficulties has been analyzed and a redesign of the spectrographic measurement system has been carried out. A preliminary sequence of measurements, utilizing the redesigned measurement system, to obtain spectral scans of the radiation emitted from one axial location in the arc jet for a range of tunnel power levels has been carried out.

The results of these measurements verify that the redesigned system can indeed provide the desired spectral description of the arc jet flow. Further, though the survey is incomplete, the results of these preliminary measurements do provide means for identifying those spectral regions in which the specific design of the laser-based diagnostic techniques proposed might require special attention.

During the test sequence, however, it became obvious that a computer/data acquisition system capable of acquiring, storing, and transmitting larger quantities of data more rapidly than that used will be required in order to complete the desired spectral description of the arc jet flow without an inordinate expenditure of tunnel operating time.

#### Spectrographic Measurement System Redesign

In order to obtain the desired spectral distribution of the radiation emitted by the arc jet flow, the existing spectrographic measurement system had to be redesigned. A schematic diagram of the (redesigned) spectrographic measurement system employed is shown in Figure 1.1. The existing McPherson Model 216.5 spectrometer is employed as the dispersing element. This is an  $f/8.7$  effective aperture plane grating spectrometer using a Czerny-Turner mounting. The  $1/2$  meter focal length concave collimating and focusing mirrors are, respectively, 3 and 6 inches in diameter. The flat exit focal plane is 4 inches wide by 2 inches high. A 1200 groove/mm, 50 mm x 50 mm plane grating, blazed at 5000 Å is employed to provide a spectral range of 1050 Å to 10000 Å with a reciprocal linear dispersion of 16.6 Å/mm. First order resolution, using  $10 \mu\text{m} \times 4 \text{ mm}$  slits, is 0.4 Å. The bilateral entrance and exit slits are variable width, 10 - 2000  $\mu\text{m}$ , and height, 0-20 mm. Scan rate is variable from 0.5 to 2000 Å/min in a 1,2,5 sequence.

Optical access to the tunnel is through a  $1/2$  inch thick, 4 inch (free) diameter fused silica ( $n=1.4584$ ) window mounted in the tunnel access door. The center of the window is level with and 1.395 m from the centerline of the nozzle. Calculations were performed to enable various lens sizes, combinations, and positions to be used to provide collection

and transport of the maximum possible light from a chosen "sample point" in the free stream flow into the spectrometer with the requisite "filling" of the spectrometer for adequate spectral detection. The optical train used in the preliminary survey measurements is shown in Figure 1.2(a). A precision collimating telescope and tripod assembly were employed to establish accurate optical path alignment.

The spectral detection circuitry was redesigned to provide an adequate output electrical signal from the very low level light input expected from the arc jet free stream flows. An existing RCA 4832 Photomultiplier tube was employed. However, an RCA PF1042 solid state power supply with integral socket and voltage divider network was employed in place of the existing socket with external voltage divider and power supply. In addition, an Analog Devices Model 52 K low noise, low drift, precision FET operational amplifier was employed as a high gain, current-to-voltage converter in place of a load resistor for the photomultiplier. This op-amp and electronic circuit arrangement, shown in Figure 1.2(b), provides a significantly improved photomultiplier output voltage signal for very small light inputs with a minimum of background noise. This spectral detection circuit worked excellently in the preliminary measurement sequence and provided adequate signal relative to noise to be recorded directly, or with standard additional amplification means when desired.

#### PRELIMINARY MEASUREMENT SEQUENCE

Both analog and digital recording of the photomultiplier output signal is desired, for monitoring system operation and for numerical analysis of the data. The (analog) photomultiplier output obtained using the improved op-amp circuit was adequate for direct recording using a standard strip chart recorder. For this purpose an existing CEC Type 5-124 recording oscillograph, using a Type 7-363 high performance fluid damped galvanometer, was used.

To obtain a digital record of the output signal, it must be "sampled", that is, passed through an analog-to-digital converter, at a rate ade-

quate to preserve the information in the original signal. In sampling a continuous signal, such as that of the photomultiplier output, samples taken at more closely spaced intervals can be expected to describe the original signal more accurately than samples taken at larger intervals. The Nyquist sampling theorem provides a quantitative basis for the rate at which samples must be taken, based on the bandwidth of the signal. The theorem states that for a bandlimited dc signal, the sample rate must be at least twice the highest frequency component in the signal in order to avoid loss of information from the signal and to avoid spurious information from showing up. The critical sampling rate is called the Nyquist frequency. As a rule of thumb, a sampling rate of at least ten times the Nyquist frequency is desired and commonly employed.

With equal entrance and exit slit widths, the ideal spectrometer exit slit function is triangular. In such instance, the photomultiplier output signal corresponding to a single spectral line, as a function of time, is a triangular pulse of (temporal) width  $2w/r$ . Here  $w$  is the slit width, and  $r$  is the rate at which a spectral line "scans" (passes over) the exit slit. For such a triangular pulse of width  $2w/r$ , the Nyquist frequency is  $f_n = 2r/w$ . Consequently, the minimum sampling rate is  $S_{min} = 2w/r$ ; a desirable rate is 10 times this value. Using a spectrometer having a reciprocal linear dispersion  $D(\text{\AA}/\text{mm})$ , and employing a grating scan rate  $R(\text{\AA}/\text{min})$ , the corresponding spectral line scan rate  $r = R/60D$  (mm/sec). Then with (equal) spectrometer slit widths  $w(\text{mm})$ , the minimum sampling rate  $S_{min} = 2R/60Dw = R/30DW$  (samples/second).

For the preliminary sequence of measurements, the spectrometer slit widths were chosen to be  $w = 100 \mu\text{m}$  ( $= 0.10 \text{ mm}$ ) in order to provide adequate input radiation for a good photomultiplier output signal with acceptable resolution. The reciprocal linear dispersion of the spectrograph is  $D = 16.6 \text{ \AA}/\text{mm}$ . Hence, the minimum sample rate required is  $S_{min} = 0.02R$ . Using a grating scan rate  $R = 500 \text{ \AA}/\text{min}$ , requires  $S_{min} = 10$  samples/sec, and a desirable rate of at least 100 samples/sec. A grating scan rate  $R = 2000 \text{ \AA}/\text{min}$ , the fastest available, would require a minimum rate  $S_{min} = 40$  samples/sec, with a desirable of 400 samples/sec. Tunnel test time limitations suggest that the minimum scan rate be  $500 \text{ \AA}/\text{min}$ . To



scan the desired spectral range 2000 Å to 8500 Å at a rate of 500 Å/min would require a test time of 13 minutes, about the longest desired rate at higher power levels.

For the preliminary sequence of measurements, two different available computer/data acquisition systems were employed. These allowed evaluation of the requirements for analog-to-digital conversion and recording of the photomultiplier output signal. (See Figure 1.1) The photomultiplier output signal was fed directly to one channel of the Modcomp arc jet facility computer/data acquisition system and recorded on the system tape during each test run. This system provides a fixed A/D sampling rate of 10 samples/second, barely the minimum required rate for 500 Å/min scanning. This system accepts a maximum signal of 800 mv. During the measurement sequence it was found that the output signal frequently exceed 800 mv, so a voltage divider (approximately 0.45/1) was placed in the signal line to the Modcomp.

The photomultiplier output signal was also fed to an available Keithley Model 195A programmable multimeter for A/D conversion and then to an available HP 85B computer whose internal memory was expanded to provide adequate data storage capability for a given test run. The signal fed to this computer and the CEC oscillograph was first passed through a Neff type 119 amplifier which could provide signal amplification gain from 1 to 1000, in a 1,2,5 sequence, as desired or needed. This system was capable of sampling the analog input signal at a maximum rate of 20 sample/sec, somewhat greater than the required minimum rate for 500 Å/min scanning. Further, data storage limitations were such that a maximum of about 15000 data points could be stored. This provides a maximum data collection period of about 12 to 13 minutes. To collect data for a spectral scan from 2000 Å to 8500 Å, this requires a scan rate of 500 Å/minute or greater. Therefore, in order to provide for a (barely) adequate sampling rate and to not exceed data storage limitations or total test time duration, each test run in the preliminary measurement sequence consisted of the following steps.

Once the arc jet flow was stably established, a spectral scan was begun

at 2000 A and at a rate (upscale) of 500 A/min. The CEC oscillograph, the Modcomp computer, and the Keithley/HP85B system recorded data for 12 minutes, until the scan reached about 8000 A. At this time the Keithley/HP85B system terminated data collection; its storage limit was reached. The spectrometer was then changed to scan downscale at a rate of 2000 A/min. The CEC oscillograph and the Modcomp computer continued to record data for about 3 minutes, until the scan reached 2000 A, at which time the test was terminated. The total test time (continuous arc tunnel operation) was about 20-25 minutes for each run, during which about 15 minutes was devoted to taking data.

For this measurement sequence, air was the test gas in arc tunnel TP2. The arc heater was a "12-pack", and a conical nozzle with 2.25 in diameter throat and 15 in diameter exit was used. The spectrometer optical train was focused on a "sample point" located 10 in downstream of the nozzle exit plane and on the nozzle centerline. The primary goal of the test sequence was to record data for the arc jet free stream flow. However, several tests were run of the shock layer flow in front of a test article. In these runs, the test article was a 2 in diameter RCC flat puck placed in a 4 in diameter HRSI holder. The "sample point" location was the same as for free stream flows, but the test article was located with its front (flat) face 10.25 in downstream of the nozzle exit plane and its centerline on the nozzle centerline. The power level and mass flow rates used for this test sequence were chosen to coincide with those of a catalyticity test sequence to be run subsequently by NASA/JSC's Dr. Carl Scott; they corresponded to a set of runs made earlier in the SEADS program. The particular tests run are tabulated in Table 1.1.

The results of these measurements verify that the redesigned spectrographic measurement system can indeed provide the desired spectral description of the arc jet flow. Although the data reduction from these tests is as yet incomplete, the preliminary analysis indicates that the maximum available sampling rate of the two computer/data acquisition systems used is not adequate to provide the necessary information for a complete spectral survey of the arc jet flows without an inordinate expenditure of tunnel operating time and data transfer and analysis

time. It is recommended, therefore, that a new computer/data acquisition system be purchased and installed. A few basic requirements of such a system are discussed below.

TABLE 1.1

TEST RUNS - PRELIMINARY MEASUREMENT SEQUENCE

POWER LEVEL (MW)	MASS FLOW (#m/SEC)	SCAN RATE (UP/DOWN) (A/MIN)	DATA * RECORD ON (UP/DOWN)	NEFF GAIN	SLIT WIDTH ( $\mu$ m)	TEST TYPE
1.5	0.04	500/2000	MHC/MC	VARIABLE	100	SHOCK LAYER
1.5	0.08	2000/2000	MC/MC	1000	100	FREE STREAM
2.2	0.08	2000/2000	MHC/MC	1000	100	FREE STREAM
2.2	0.08	500/2000	MHC/MC	VARIABLE	100	SHOCK LAYER
2.2	0.08	2000/2000	MC/MC	1000	100	FREE STREAM
2.5	0.08	500/2000	MHC/MC	1000	75	FREE STREAM
2.5	0.08	500/2000	MHC/MC	1000	100	FREE STREAM
2.9	0.08	500/2000	MHC/MC	1000	100	FREE STREAM
2.9	0.08	500/2000	MHC/MC	VARIABLE	100	SHOCK LAYER
**3.3	0.08	500/2000	MHC/MC	500	100	FREE STREAM
3.3	0.08	500/500	M/M	1000	100	FREE STREAM
3.7	0.08	500/2000	MH/M	1000	100	FREE STREAM
4.1	0.11	500/2000	MHC/MC	1000	100	FREE STREAM

\* M = Modcomp Computer, H = Keithley/HP85B system, C = CEC oscillograph

\*\* A portion of CEC oscillograph trace for this run is shown in Figure 1.3.

Though the survey is incomplete, the results of these preliminary measurements show that the procedure does provide means for identifying those spectral regions in which specific design of the laser-based diag-

diagnostic techniques proposed might require special attention. In Figure 1.3 is shown a portion of the CEC oscillograph trace for one of the 3.3 MW runs. Marked on this trace are the locations of the 4880 Å and 5145 Å Argon ion laser principal lines to be used for initial Spontaneous Raman Spectroscopy studies. Also marked on this trace are the locations of the principal Stokes and anti-Stokes vibrational "lines" resulting from the Raman shift for  $O_2$ , NO, and  $N_2$ . For Spontaneous Raman Scattering, these are the primary locations where Laser excited Raman scattering signals will occur. Most of the spectral features in this trace are lines of atomic O and N; some have been identified. It is seen from the Figure, that in the immediate neighborhood of these spectral locations, there is not an appreciable background of other spectral features, at least at this power level. Consequently, provided the Raman scattered signal is strong enough, it is expected that SRS should provide the desired information for diagnostic purposes, and the present spectrographic measurement system should be able to discern the signal.

#### COMPUTER/DATA ACQUISITION SYSTEM

As discussed above, the existing computer/data acquisition systems do not furnish an adequate sampling rate to allow timely acquisition of the large amounts of data generated in a complete spectral survey of the arc jet flows for a range of tunnel operating conditions and "sample point" locations. Further, the data storage capability of the Keithley/HP85B system (having the highest sample rate) is inadequate for extended run times. Further yet, this particular system employs an electronic disk for storage. Once filled, the storage space must be cleared -- that is, the data transferred to another medium -- before another test can be run. As presently configured this transfer of data is a very slow process, taking up to 45 minutes to transfer one test run data set. Although alternate hardware can speed this up considerably, the problem lies inherently in the computer itself.

The computer/data acquisition system required to adequately allow completion of the spectral survey should be one which samples (that is, provides A/D conversion) at a minimum rate of 100 or more samples/sec-

ond, allows very rapid transfer of the sampled data into a memory, and provides a large memory to store the quantity of data generated. To provide versatility, the computer should also be able to handle data acquisition for more than a single channel simultaneously, and should be able to provide command control functions for remote scanning and positioning operations. Finally, it should be able to handle reasonably rapid data reduction and analysis capabilities when measurement runs are not being executed.

Such a computer data acquisition system will not only provide the need for the spectral survey, it will also provide the needs for the proposed LTA measurement system, and it will provide overall measurement system control. It is recommended that such a computer/data acquisition system be purchased and installed at the earliest opportunity.

#### APPENDIX A. - REFERENCES

In general, the references listed below fall into five categories:

- (1) Papers specifically concerned with arc-tunnel flows; these are references 2 - 5; they all relate to the Air Force Flight Dynamics Laboratory 50 MW Re-entry Nose Tip (RENT) Facility, which produces an atmospheric pressure, high enthalpy jet for a short (1-3 minutes) duration.
- (2) Papers which contain various physical property data, measured or calculated, for the normal components of air; these are References 1, 3, 4, 9-14, 20-23, 28-34, 38, 47, 48.
- (3) Papers which contain formulations of Theoretical Models, to various approximations, which can be utilized for interpreting measured data to obtain temperatures, number densities, and velocities in radiating flow fields; These are References 1, 3-6, 9-14, 20-26, 28-30, 35, 39, 40, 44, 47-50, 59.
- (4) Papers which report applications of the various laser-based diagnostic methods proposed herein to different flow fields

(mostly combustion and flames and aerodynamic wind tunnel flows); in these are reported some measured property data as well as some theoretical model formulations; these are References 1-6, 10-26, 35, 41-43, 45-46, 64-67.

- (5) Papers and books which provide general background theory and information about radiation and its measurement; These are References 7-9, 27-30, 36-37, 39-40, 47-48, 60-63.

From the References in category (3) it should be possible to develop a reasonably complete and accurate theoretical model for spectral emission from the arc jet flow, including the expected emissions induced by the laser input beams in the diagnostic methods proposed. Such a model can then be used as reliable basis for interpreting measured data for temperature, number density, and velocity determinations. Such a model may well serve also to substantiate existing physical property data or to add new data to the literature.

In particular, the line-by-line calculations of emission spectra formulated in References 20-26 should provide a sound basis to which can be added the laser Raman scattering, and laser induced fluorescence emissions which are formulated in References 1-3, 10-14, etc.

It is recommended that further effort be expended on completing the physical property data compilation, and on formulating the theoretical spectral emission model with an accompanying development of appropriate computer software to provide reliable models for measurement data reduction and analysis.

1. Lapp, M., and C. M. Penney, ed., Laser Raman Gas Diagnostics, Plenum Press, New York, 1974 (AD/A-001389)

This volume contains numerous papers on Laser Raman Scattering which are pertinent to and useful for the diagnostic methods proposal herein.

2. Boiarski, A.A., and F.L. Daum, Laser Raman Scattering - A Technique for Arc-Tunnel Flow Calibration, pp. 285 - 297 in Reference 1.
3. Boiarski, A.A., and F.L. Daum, An Application of Laser-Raman-Spectroscopy to Thermochemical Measurements in an Arc-Heated Wind Tunnel Flow, Aerospace Research Laboratories Report ARL 72-0126, December, 1972 (AD761500)
4. Lapp, M., C.M. Penney, and J.A. Asher, Application of Light - Scattering Techniques for Measurements of Density Temperature, and Velocity in Gasdynamics, Aerospace Research Laboratories Report ARL 73-0045, April, 1973 (AD759575).
5. Mastrup, F.N., Development of Spectroscopic and Optical Scattering Diagnostics for Non-Equilibrium Reacting Gas Flows, Air Force Flight Dynamics Laboratory Technical Report AFFDL TR-70-17, February, 1970 (AD867346).
6. Lederman, S., and S. Sacks, Laser Diagnostics for Flow fields, Combustion, and MHD Applications, AIAA Journal, Vol. 22, No. 2, February, 1984.
7. Demtroder, W., Laser Spectroscopy - Basic concepts and Instrumentation, Springer-Verlag, New York, 1981.
8. Freeman, M.P., Introduction to the Theory and Practice of Spectroscopic Diagnostics of High-Density Plasma Sources of Aerospace Interest and Chemical Synthetic Interest, pp. 255-322 in Progress in High Temperature Physics and Chemistry, Vol. 3, ed. by C. Rouse, Pergamon, Oxford, 1969.
9. Tien, C.L., Thermal Radiation Properties of Gases, pp. 253-324 in Advances in Heat Transfer, Vol. 5, ed. by T.F. Irvine, Jr. and J.P. Hartnett, Academic Press, New York, 1968.
10. Salzman, J.A., W.J. Masica, and T.A. Coney, Determination of Gas

Temperatures from Laser-Raman Scattering, NASA TND-6336, May 1971.

11. Coney, T.A., and J.A. Salzman, Determination of the Temperature of Gas Mixtures by Using Laser Raman Scattering, NASA TND-7126, January, 1973.
12. Measures, R.M., Analytical Use of Lasers in Remote Sensing, Chapter 6 (pp. 295-410) in Analytical Laser-Spectroscopy, ed. by N. Omenetto, John Wiley, New York, 1979.
13. Inaba, H., and T. Kobayasi, Laser-Raman Radar-Laser-Raman scattering methods for remote detection and analysis of atmospheric pollution, Opto-electronics, Vol. 4, pp. 101-123, 1972.
14. Hayden Smith, Wm., A new method for the detection of Raman scattering from atmospheric pollutants, Opto-electronics, Vol. 4, pp. 161-167, 1972.
15. Hanson, R.K., et.al, Advanced Diagnostics for Reacting Flows, High Temperature Gasdynamics Laboratory, Stanford University, Annual Report for AFOSR, Oct. 1, 1982 to Sept. 30, 1983.
16. Antcliff, R.R., CARS System for Turbulent Flame Measurements, AIAA-84-1537, AIAA 17th Fluid Dynamics, Plasma Dynamics, and Lasers conference, June 25-27, 1984, Snowmass, Colorado.
17. "New Light on Combustion Research", SANDIA Technology, SAND 84-0169, Vol. 8, No. 1, may 1984.
18. SANDIA Combustion Research Program, 1982-83 Annual Report.
  - (a) Rahn, L.A., R.L. Farrow, and R.L. Mattera, Nonlinear Raman Spectroscopy in Combustion Research.
  - (b) Dibble, R.N., and R.W. Schefer, Simultaneous Measurement of



Velocity and Scalars in a Turbulent Nonpremixed Flame.

- (c) Cattolica, R.J., and D.A. Stephenson, Two-Dimensional Imaging of Flame Temperature Using Laser Induced Fluorescence.
19. Gross, K.P., and R.L. McKenzie, Optical Measurements of Fluctuating Temperatures in a Supersonic Turbulent Flow Using One-and Two-Photon, Laser-Induced Fluorescence, AIAA 84-1536, AIAA 17th Fluid Dynamics, Plasma Dynamics, and Lasers Conference, July 25-27, 1984, Snowmass, Colorado.
  20. Arnold, J.O., E.E. Whiting, and G.C. Lyle, Line by Line Calculation of Spectra from Diatomic Molecules and Atoms Assuming a Voight Line Profile, J. Quant. Spectrosc. Radiat. Transfer, Vol. 9, pp. 775-798, 1969.
  21. E.E. Whiting, J.O. Arnold, and G.C. Lyle, A Computer Program for a Line-by-Line Calculation of Spectra from Diatomic Molecules and Atoms Assuming a Voight Line Profile, NASA TND-5088, March 1969.
  22. Park, C., Calculation of Nonequilibrium Radiation in the Flight Regimes of Aeroassisted Orbital Transfer Vehicles, AIAA 84-0306, AIAA 22nd Aerospace Sciences Meeting, Reno, Nevada, Jan. 9-12, 1984; Also in Progress in Astronautics and Aeronautics, Vol. 96: Thermal Design of Aeroassisted Orbital Transfer Vehicles, ed. by H.F. Nelson pp. 395-418, AIAA, New York, 1985.
  23. Park, C., Nonequilibrium Air Radiation (NEQAIR) Program; User's Manual, NASA TM 86707, July 1985.
  24. Park, C., Spectral Line Intensities in a Nonequilibrium Nitrogen Plasma, J. Quant. Spectrosc. Radiat. Transfer, Vol. 8, pp. 1633-1653, 1968.
  25. Park, C., Calculation of Radiative Properties of a Nonequilibrium

- Hydrogen Plasma, J., Quant. Spectrosc. Radiat. Transfer, Vol. 22, pp. 101-112, 1979.
26. Whiting, E.E., J.O. Arnold, and G.C. Lyle, Calculation of Molecular Band Spectra Assuming a Gaussian Line Profile, J. Quant. Spectrosc. Radiat. Transfer, Vol. 7, pp. 725-739, 1967.
27. Savitsky, A., and M.J.E. Golay, Smoothing and Differentiating of Data by Simplified Least Squares Procedures, Analytical Chemistry, Vol. 36, No. 8, pp. 1627-1639, July 1964.
28. Herzberg, G., Molecular Spectra and Molecular Structure, I. Spectra of Diatomic Molecules, 6th Edition, D. Van Nostrand, Princeton, N.J., 1950.
29. Long, D.A., Raman Spectroscopy, McGraw-Hill, New York, 1977.
30. Johnson, R.C., An introduction to Molecular Spectra, Methuen, London, 1949.
31. Allen, R.A., Air Radiation Tables: Spectral Distribution Functions for Molecular Band Systems, Research Report 236, AVCO-Everett Research Laboratory, April 1966.
32. Drellishak, K.S., Partition Function and Thermodynamic Properties of High Temperature Gases, AEDC-TDR-64-22, 1964.
33. Hansen, C.F., Rate Processes in Gas Phase, NASA RP 1090, May, 1983.
34. Pearse, R.W.B., and A.G. Gayden, The Identification of Molecular Spectra, 3rd Edition, John Wiley, New York, 1963.
35. Arnold, J.O., D.M. Cooper, C. Park, and S.G. Prakash, Line-by-Line Transport Calculations for Jupiter Entry Probes, in Progress in Astronautics and Aeronautics, Vol. 69: Entry Heating and Thermal Protection, ed. by W.B. Olstad, pp. 52-82, AIAA, New

York, 1980.

36. Grum, F. and R.J. Becherer, Optical Radiation Measurements Vol. 1, Radiometry, Academic Press, New York, 1979.
37. Nicodemus, F.E., Self-Study Manual on Optical Radiation Measurements, NBS Technical Notes 910-1 through 910-7, U. S. Department of Commerce/National Bureau of Standards.
38. Zaidel', A.N., et. al., Tables of Spectral Lines, IFI/Plenum, New York, 1970.
39. Guillory, W.A., Introduction to Molecular Structure and Spectroscopy, Allyn and Bacon, Boston, 1977.
40. Craig, D.P., and T. Thirunamachandran, Molecular Quantum Electrodynamics, An Introduction to Radiation-Molecule Interactions, Academic Press, New York, 1984.
41. Progress in Astronautics and Aeronautics, Vol. 95: Dynamics of Flames and Reactive Systems, ed. by J. R. Bowen, et.al., AIAA, new York, 1984.
  - (a) Dobbs, G.M., et.al., CARS Instrument for Practical Combustion Measurements, pp. 631-641.
  - (b) Michael-Saade, R., et.al., Flame Concentrations and Temperatures by Spontaneous Raman Spectroscopy, pp. 658-671.
  - (c) Yaney, P.P., et.al., The Application of Rotational Raman Spectroscopy to Dynamic Measurements in Gas Flowfields, pp. 672-699.
  - (d) Cattolica, R.J., and D.A. Stephenson, Two-Dimensional Imaging of Flame-Temperature Using Laser-Induced Fluorescence, pp. 714-721.

42. Progress in Astronautics and Aeronautics, Vol. 92: Combustion Diagnostics by Nonintrusive Means, ed. by T.D. McCay and J.A. Roux, AIAA, New York, 1984.

This volume is devoted to combustion diagnostics by nonintrusive spectroscopic methods. It includes five papers on CARS, three papers on Laser-Induced Fluorescence, three papers on particle diagnostics, and four papers on applications. Most of these papers are pertinent to and useful for the diagnostic methods proposed herein.

This volume is devoted to combustion diagnostics by nonintrusive spectroscopic methods. It includes five papers on CARS, three papers on Laser-Induced Fluorescence, three papers on particle diagnostics, and four papers on applications. Most of these papers are pertinent to and useful for the diagnostic methods proposed herein.

43. Crosley, D.R., Editor, Laser Probes for Combustion Chemistry, American Chemical Society Symposium Series 134, ACS, Washington, D.C., 1980.

This volume contains forty papers on Laser-based diagnostics of flames and combustion, including applications of LIF, SRS, CARS, etc., which are pertinent to and useful for the diagnostic methods proposed herein.

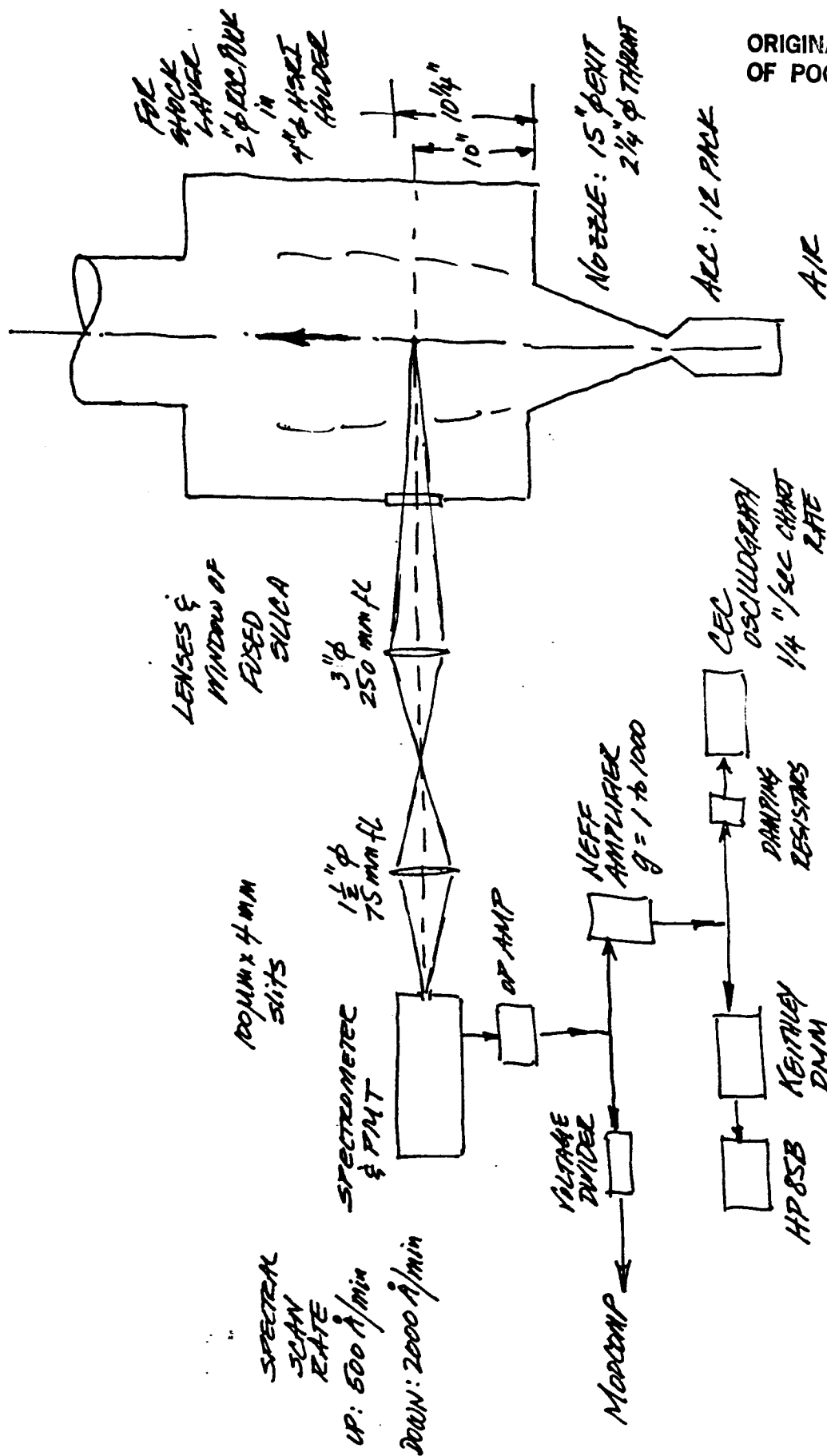
44. Williams, M.J., and C.E. Treanor, A Method for Calculating Diatomic Spectra Using a Digital Computer, Cornell Aeronautical Laboratory Report QM-1626-A-5, May, 1962(AD275746).
45. Goldsmith, J.E.M., and R.J.M. Anderson, Imaging of Atomic hydrogen in flames with two-step saturated fluorescence detection, Applied Optics, Vol. 24, No. 5, pp. 607-609, March 1, 1985.

46. Goldsmith, J.E.M., Two-step saturated fluorescence detection of atomic hydrogen in flames, Optics Letter, Vol. 10, No. 3, pp. 116-118, March, 1985.
47. Bond, J.W., Jr. K.M. Watson, and J.A. Welch, Jr., Atomic Theory of Gas Dynamics, Addison-Wesley, Reading, Mass., 1965.
48. Penner, S.S., Quantitative Molecular Spectroscopy and Gas Emmissivities, Addison-Wesley, Reading, Mass., 1959.
49. Vincenti, W.G., and C.H. Kruger, Introduction to Physical Gas Dynamics, John Wiley, New York, 1965.
50. Herzberg, G., Atomic Spectra and Atomic Structure, Dover, New York 1944.
51. Siegel, R., and J.R. Howell, Thermal Radiation heat Transfer, McGraw-Hill, New York, 1972.
52. Jenkins, F.A., and H.E. White, Fundamentals of Optics, 4th Edition, McGraw-Hill, New York, 1976.
53. Sawyer, R.A., Experimental Spectroscopy, 3rd Edition, Dover, New York, 1963.
54. Thorne, A.P., Spectrophysics, Halsted Press (John Wiley), New York, 1974.
55. Malmstadt, H.V., C.G. Enke, and S.R. Crouch, Electronics and Instrumentation for Scientists, Benjamin/Cummings, Reading, Mass., 1981.
56. Willey, R.J., The Identification of Excited Species in Arc Jet Flow, NASA/ASEE Summer faculty Fellows Program Report, September, 1984..

57. Wierum, F.A., Laser Techniques for Arc Jet Plasma Diagnostics: A Feasibility and Design Study, NASA/ASEE Summer Faculty Fellow Program Report, September, 1984.
58. Rochelle, N.C., et.al., Orbiter TPS Development and Certification Testing at the NASA/JSC 10MW Atmospheric Reentry Materials and Structures Evaluation Facility, AIAA 83-0147, AIAA 21st Aerospace Sciences Meeting, Jan. 10-13, 1983, Reno, Nevada.
59. Durst, F., A.Melling, and J.H. Whitelaw, Principles and Practice of Laser-Doppler Anemmetry, Academic Press, New York, 1976.
60. Diefenderfer, A.J., Principles of Electronic Instrumentation, 2nd Edition, W.B. Saunders, Philadelphia, 1979.
61. Wilemshurst, T.H., Signal Recovery From Noise in Electronic Instrumentation, Adam Hilger Ltd., Accord, Mass., 1985.
62. Magrab, E.B., and D.S. Blomquist, The Measurement of Time-Varying Phenomena, Wiley-Interscience, New York, 1971.
63. Brignell, J.E., and G.M. Rhodes, Laboratory On-Line Computing, John Wiley, New York, 1975.
64. International Work Shops on Laser Velocimetry (Project Squid):
  - (a) Purdue, 1972, W.H. Stevenson and H.D. Thompson, Ed.
  - (b) Purdue, 1974, W.H. Stevenson and H.D. Thompson, Ed.
  - (c) Minnesota, 1975, E.R.G. Eckert, Ed.
65. Yanta, W.J., The Use of Laser Doppler Velocimetry in Aerodynamics Facilities, AIAA 11th Aerodynamics Testing Conference, 1980.
66. Applications of Non-Intrusive Instrumentation in Fluid Flow

Research, AGARD CP-193.

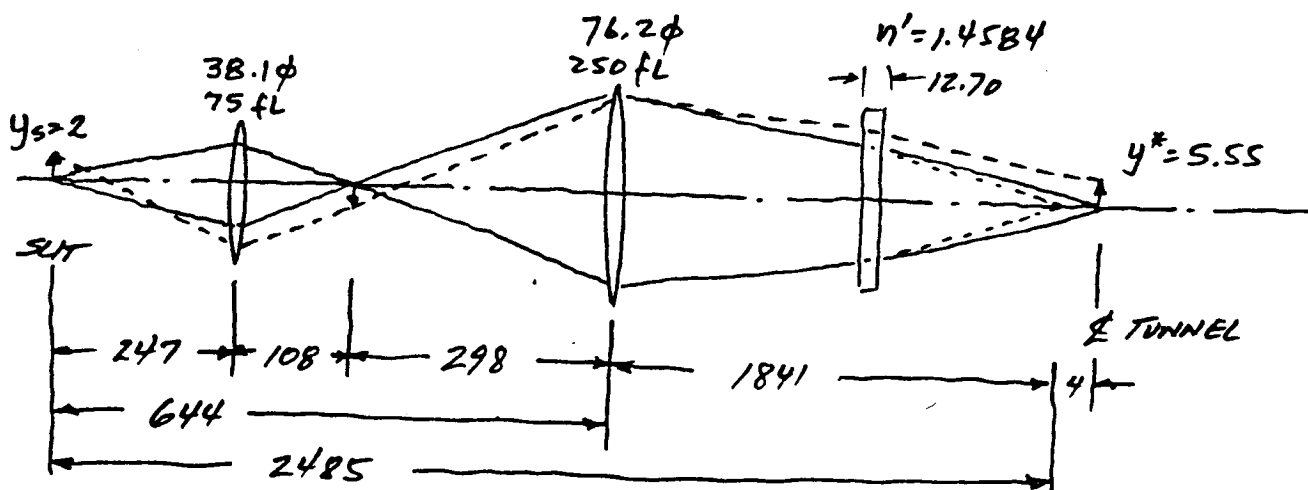
67. Durst, F., Studies of Particle Motion by Laser Doppler Techniques, Proc. of Dynamic Flow Conference, 1978.



ORIGINAL PAGE IS  
OF POOR QUALITY

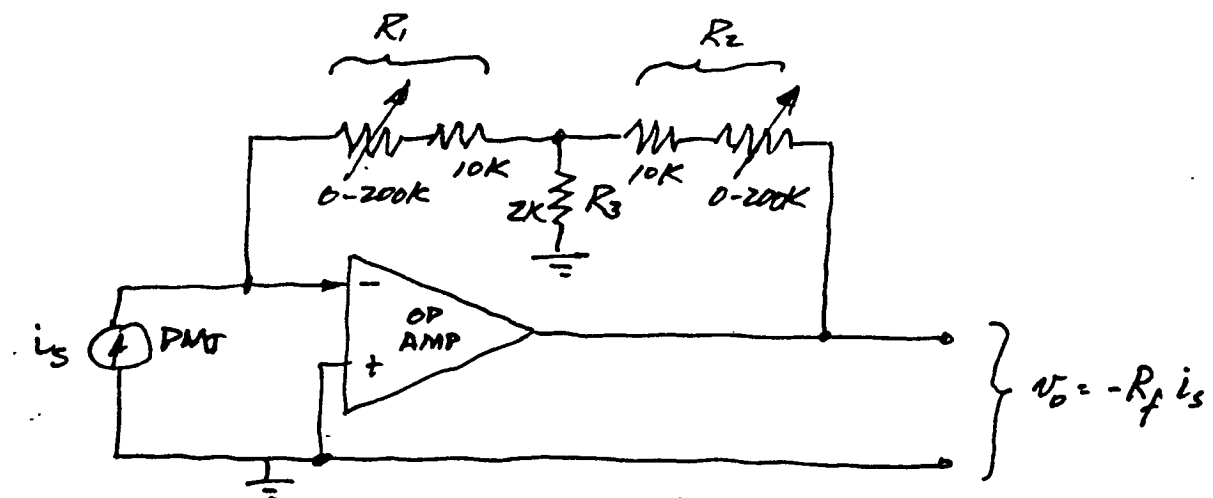
FIGURE 1.1 SPECTROGRAPHIC MEASUREMENT SYSTEM





ALL DIMENSIONS IN MILLIMETERS

## (A) OPTICAL TRAIN



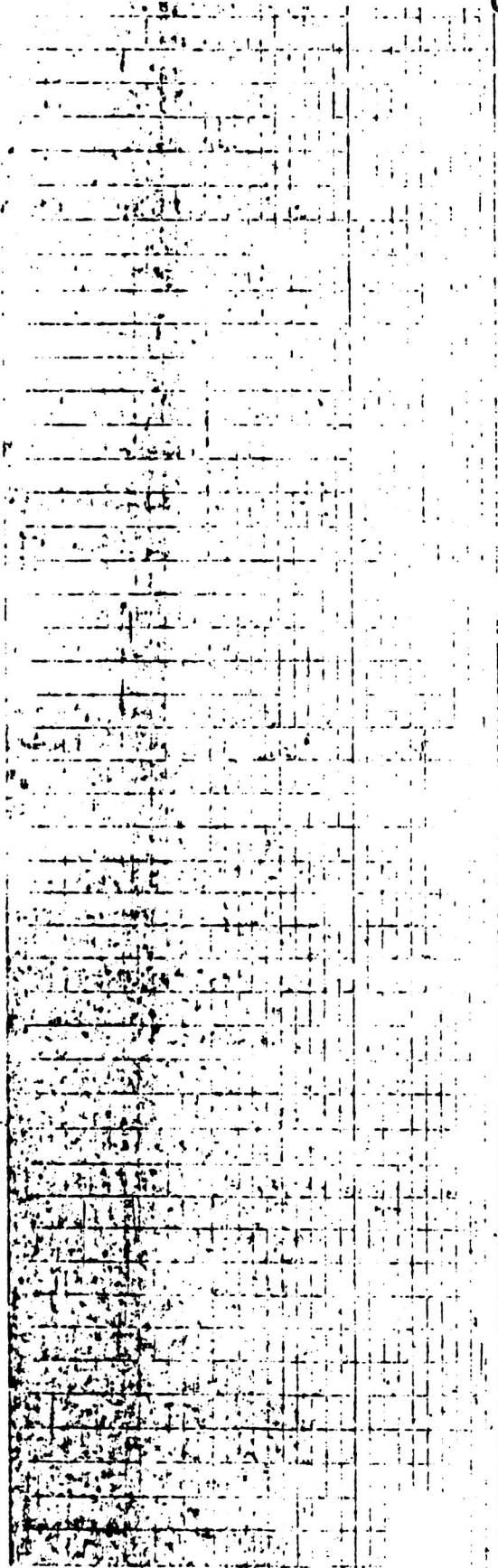
$$R_f = R_1 + R_2 + \frac{R_1 + R_2}{R_3} = 70 \text{ K to } 22.5 \text{ M } \Omega$$

Typical values of  $v_o$  = 0 to 10 mV in FREE STREAM  
0 to 1 V in SHOCK LAYER

## (B) PHOTOMULTIPLIER/OP-AMP CIRCUIT

FIGURE 1.2 OPTICAL & ELECTRONIC CIRCUITS

ORIGINAL PAGE 10  
OF POOR QUALITY



2585  
NOT  
0-3 2592

2468  
NOT  
0-2 2475

2560  
NOT  
0-1 2367

7 (A)

FIGURE 1.3 CEC OSCILLOGRAPH TRACE; FREE STREAM, 3.3 MW (a)

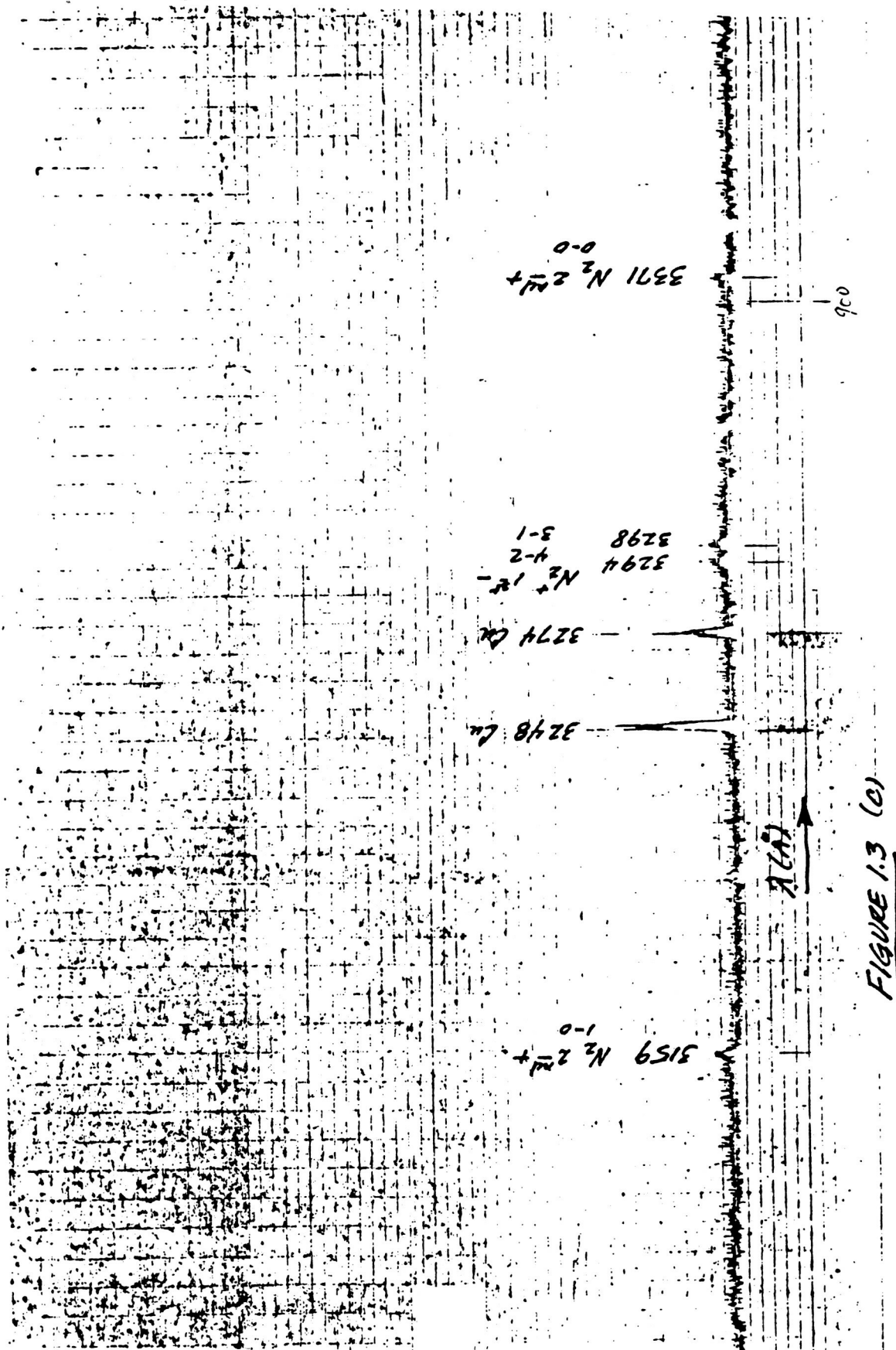
ORIGINAL PAGE IS  
OF POOR QUALITY

9-0 2972  
10N 1662

1-E 2962  
2-H 2952  
N 2942  
+ 2932

5-0 2982  
10N 2972

2 (A)  
FIGURE 1.3 (A)



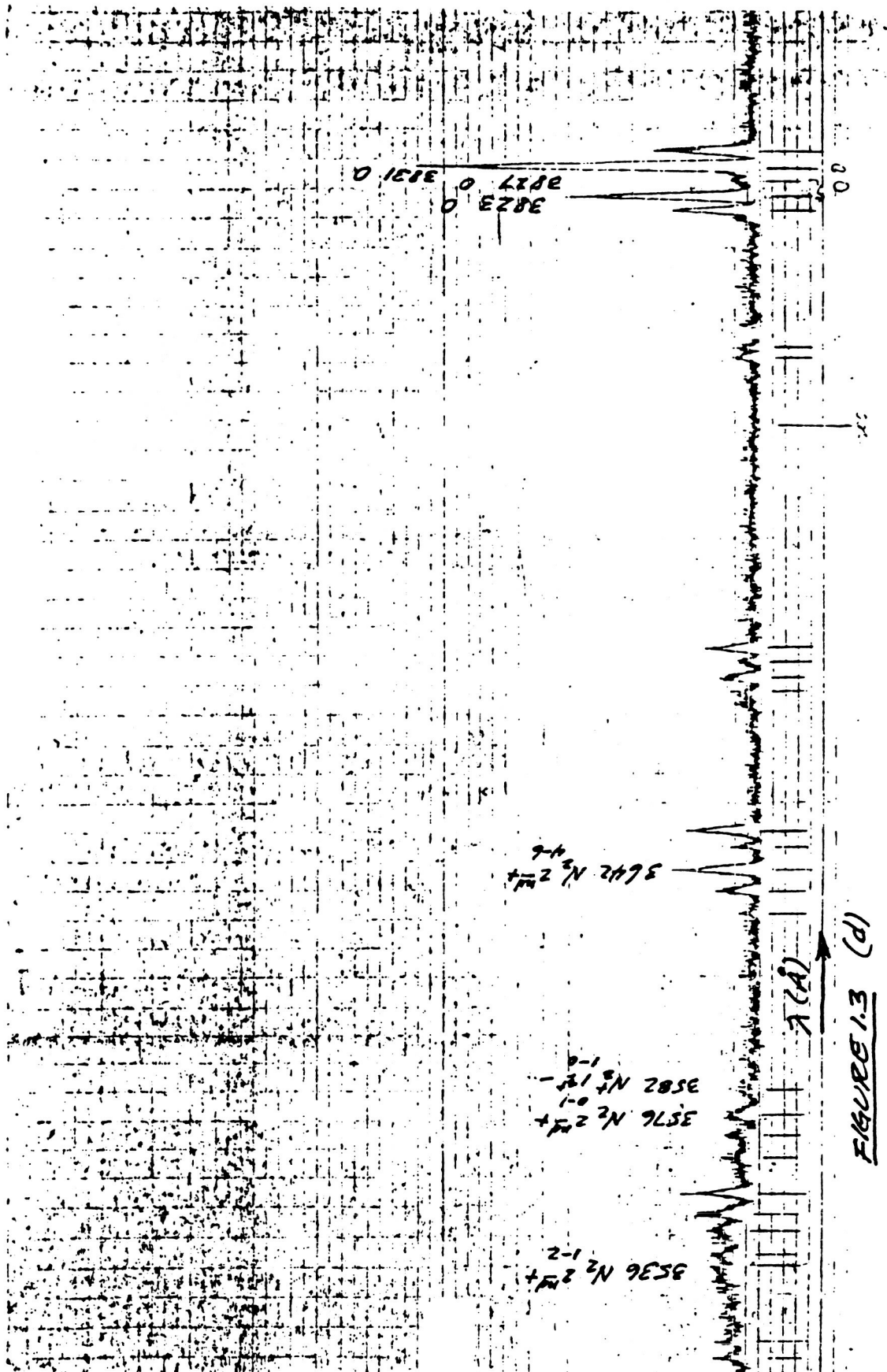


FIGURE 1.3 (d)

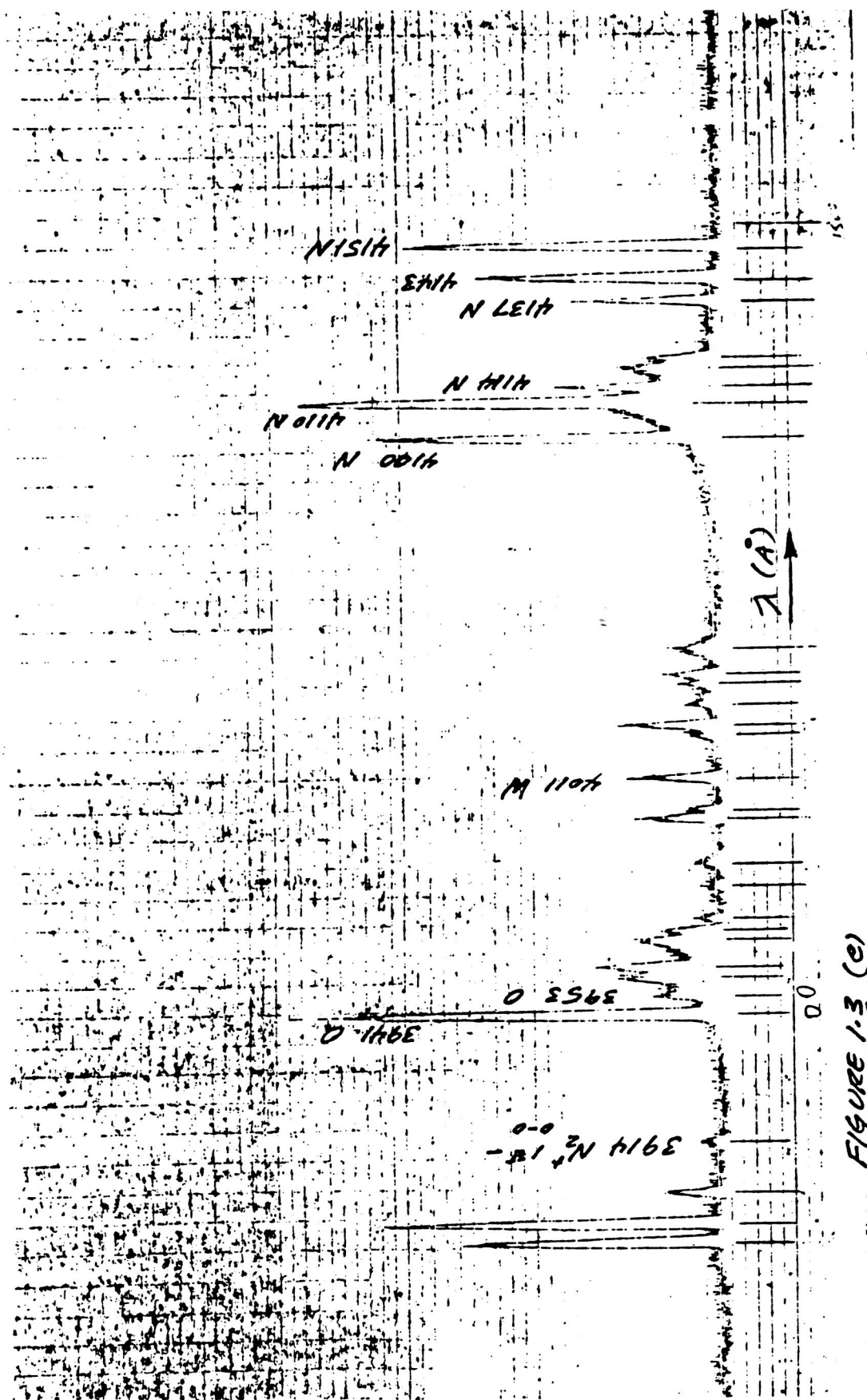
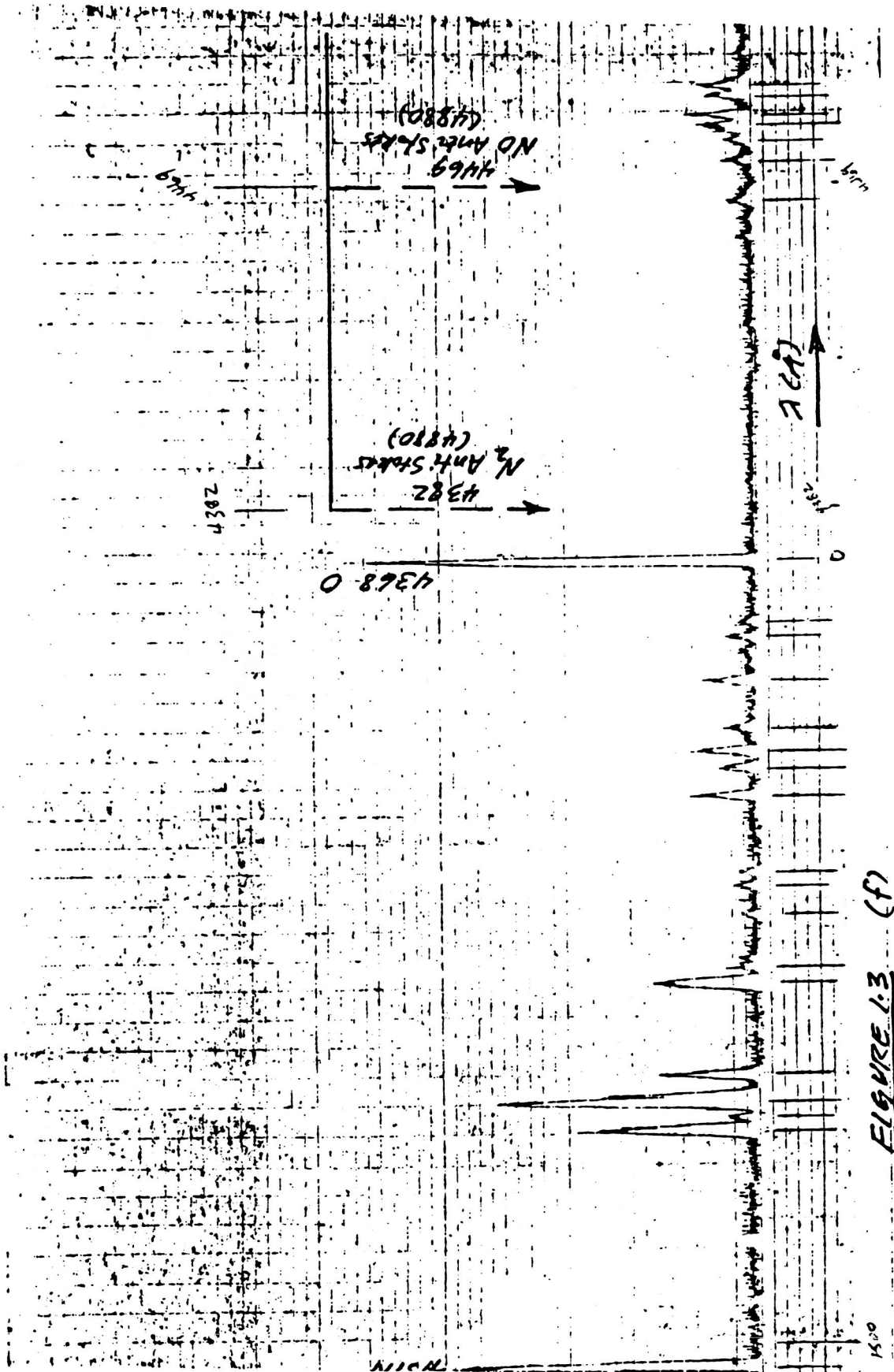
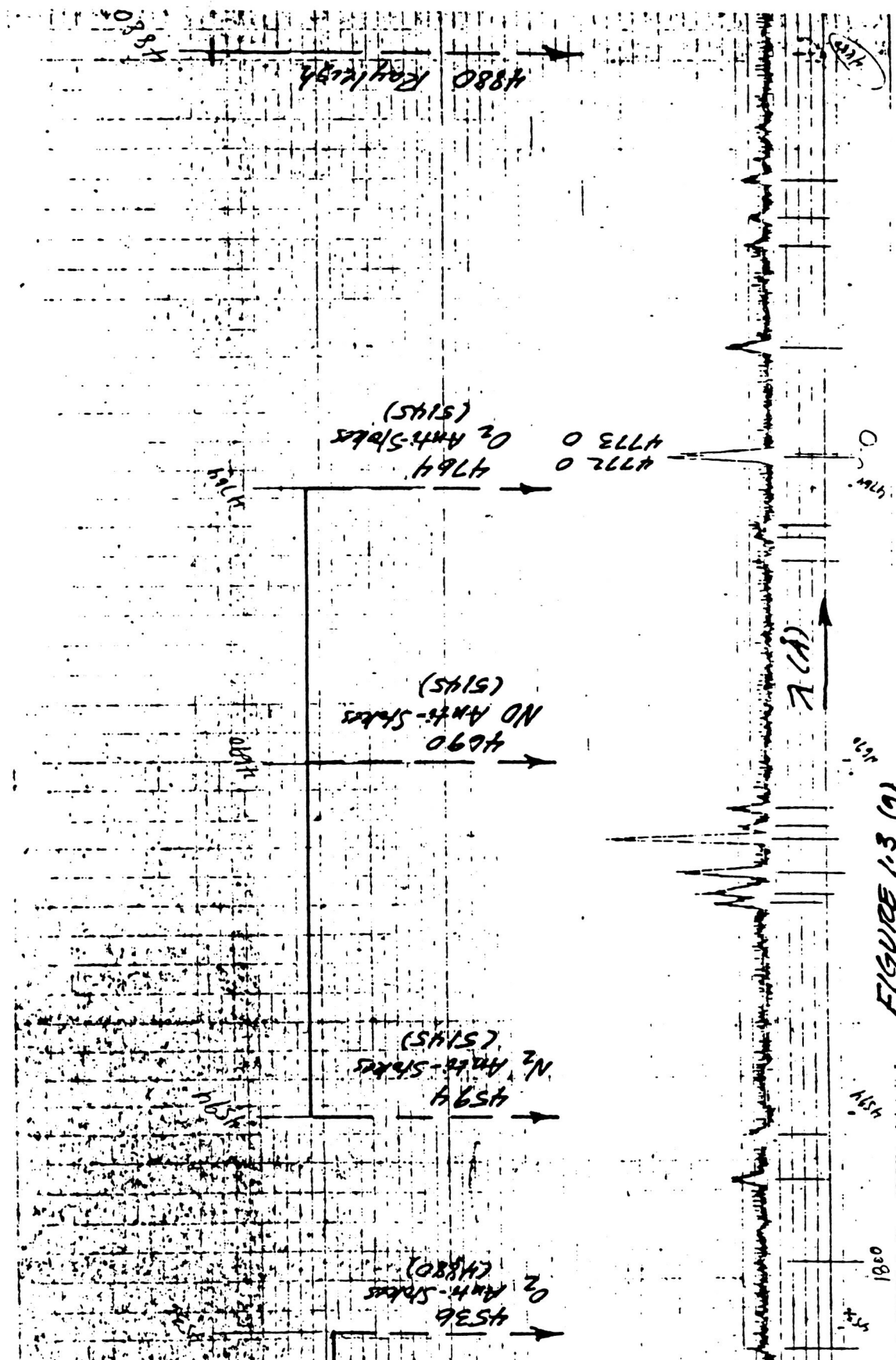


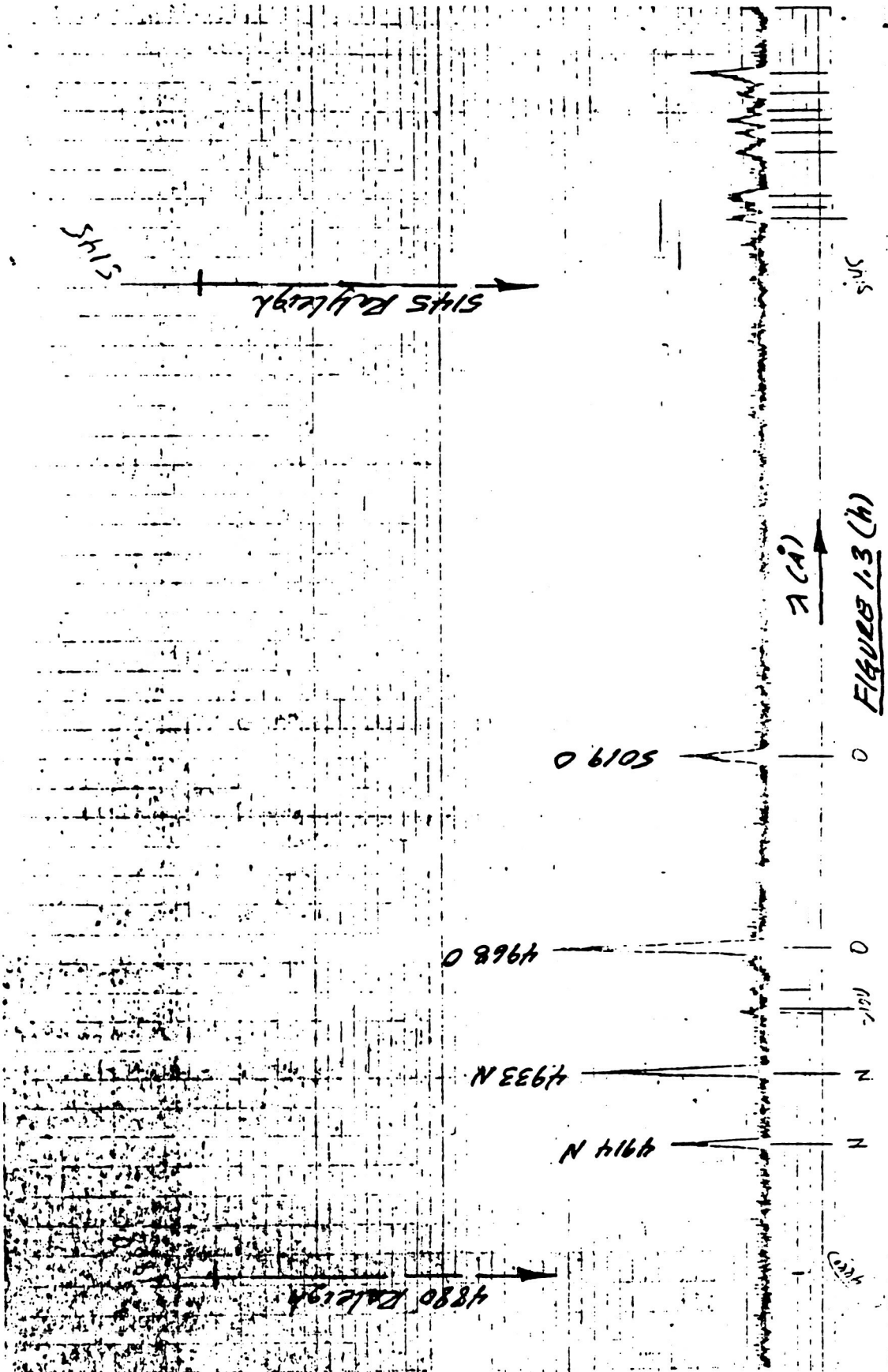
FIGURE 1.3 (c)

ORIGINAL PAGE IS  
OF POOR QUALITY

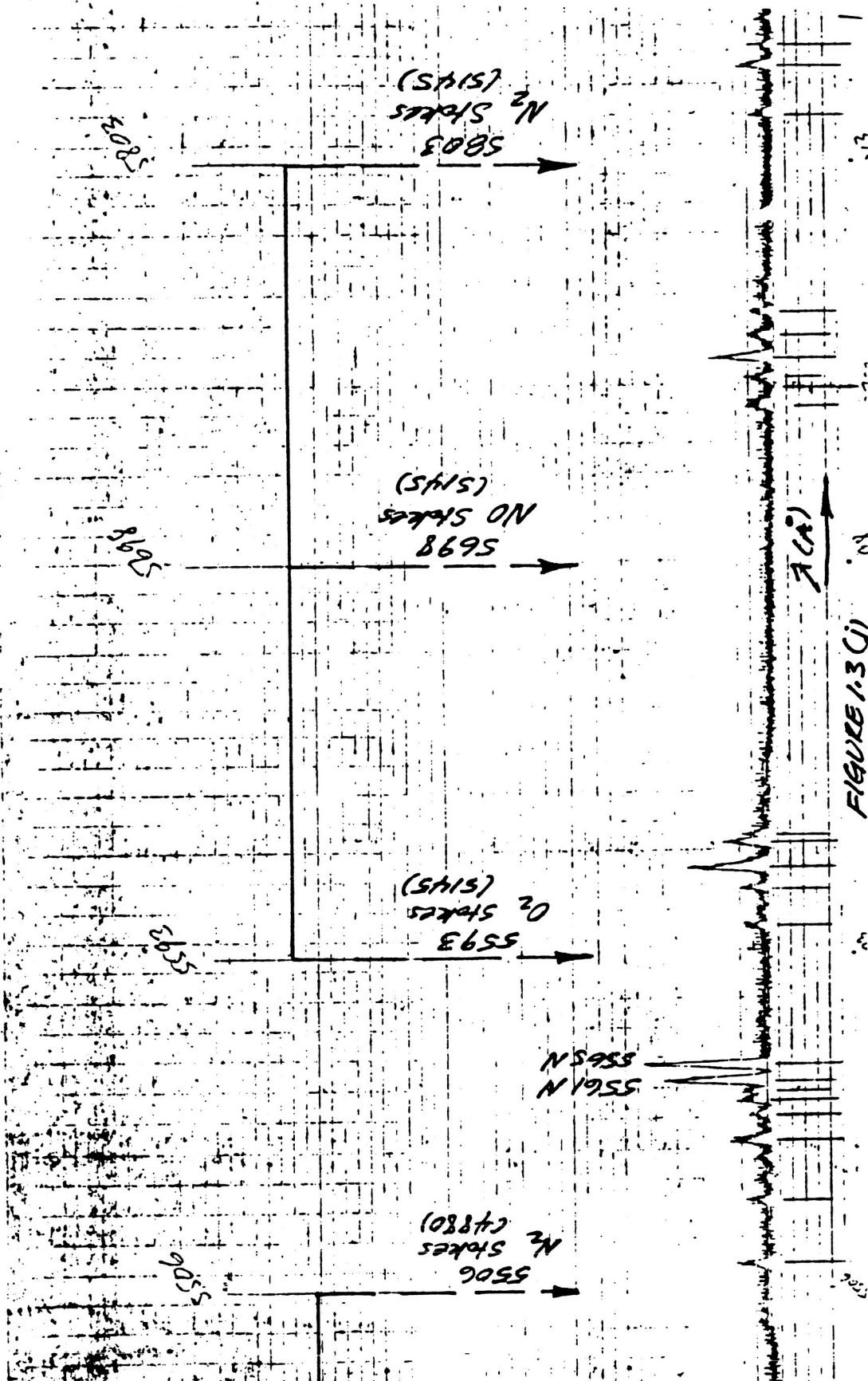












SELECTION OF AN APPROPRIATE ANIMAL MODEL  
FOR STUDY OF BONE LOSS IN WEIGHTLESSNESS

18838

Ira Wolinsky, Ph.D.  
Associate Prof. Nutrition  
Department of Human Development  
University of Houston, Houston, Texas 77004

ABSTRACT

Prolonged weightlessness in space flight results in a slow progressive demineralization of bone accompanied by an increased calcium output in the urine resulting in negative calcium balances. This possibly irreversible bone loss may constitute a serious limiting factor to long duration manned space flight. A number of preventative measures have been suggested viz: exercise during flight, dietary calcium supplements, use of specific prophylactic drugs. In order to facilitate research in these areas it is necessary to develop appropriate ground-based animal models that stimulate the human condition of osteoporosis. An appropriate animal model would enable bone density studies, calcium balance studies, biochemical analyses, ground-based simulation models of weightlessness (bed rest, restraint, immobilization) and the planning of in-flight experiments. Several animal models have been proposed in the biomedical research literature, but have inherent deficiencies. The purpose of this project was to evaluate models in the literature and determine which of these most closely simulates the phenomenon of bone loss in humans with regard to growth, bone remodeling, structural, chemical and mineralization similarities to human. This was accomplished by a comprehensive computer assisted literature search and report. Three animal models were examined closely for their relative suitability: the albino rat, monkey, and Beagle.

Loss of bone mineral is a predictable consequence of spaceflight.

Mechanical unloading during weightlessness is the most obvious factor which may play a role in this phenomenon since bone is dynamically responsive to the functional demand placed on it (Wolff's law). That is to say, the bone elements place or displace themselves in the direction of the functional forces to increase or decrease their mass to reflect, the amount of functional forces. Functional forces may include gravity, exercise and mechanical loading, or the lack thereof.

Two aberrations of calcium (Ca) metabolism occur during spaceflight: negative Ca balance and loss of bone mass. Data from the Skylab series of manned space flight showed that urinary Ca levels were about 100% greater than preflight values and persisted from about 30 days inflight to flight termination at 84 days. Fecal Ca increased linearly from about 10 days inflight on. Both urinary and fecal Ca excretions returned to near normal within about 10 days postflight. It has been calculated that a full year in flight might result in a loss of up to 25% of the total body Ca pool. Increases in urinary Ca presumably reflect skeletal losses. Bone mineral from the heel bone declined about 4-5% during 84 days inflight and available evidence indicates that this loss may be irreversible.

Although the derangements in Ca metabolism during spaceflight were not associated with detectable adverse health effects either inflight or postflight there is a risk that long duration, unchecked, losses of urinary calcium and bone loss may result in bone fracture, kidney stones or ectopic Ca deposition, thereby compromising the health of crewmembers and passengers and mission success.

In order to study the observed effects of hypogravity on Ca and bone metabolism, ground-based simulation models have been developed. In the human the best analog of weightlessness is uncomplicated bedrest studies. Bedrest, in which the subject lies recumbent for long periods and most compressive deformational

stresses are largely eliminated, most closely models the weightlessness state at least as far as the musculoskeletal system is concerned. Its validity as an analog for hypogravity has been confirmed by recent spaceflight experience. In bedrest, similar to that seen in spaceflight, there is a loss of os calcis mineral content, increased urinary Ca loss with ensuing negative Ca balances. Advantageous as this model may be, legal, ethical and practical constraints limit the extent to which human subjects can be used for research. The uncomplicated bedrest model is expensive and difficult to control; there are practical problems in conducting investigations over the human life span; intrusive experimentation (e.g. bone biopsy) is not possible. Hence, animal models must be sought for use as surrogates to human experimentation.

In evaluating ground-based animal models for simulated weightlessness research, practical and scientific considerations must be taken into account in order to determine their relevance and appropriateness. These include similarity of the animal's skeleton to that of man (both its architecture and remodeling characteristics) and comparability of the phenomenon under study to that in man (in this case comparability to human bedrest studies and spaceflight).

Three animal models were chosen for review: the albino rat because there have been inflight experiments using this animal as well as a voluminous literature using the rat as an experimental animal; the monkey and Beagle because their skeletal systems approximate that of man.

Tables 1-3 tentatively summarize the relative advantages and disadvantages of these three species for orthopedic research. The final results of our review will be prepared for publication in the literature.

### Selected Resources

Andersen, A.C., The Beagle as an Experimental Dog, Iowa State Univ. Press, Ames, 1970.

Federation of American Societies for Experimental Biology, Life Sciences Research Office, Research Opportunities in Bone Demineralization, Bethesda, MD, 1983.

National Research Council, Mammalian Models for Research on Aging, National Academy Press, Washington, D.C., 1981.

Nicogossian, A.E., Parker, J.F., Jr., Space Physiology and Medicine, NASA SP-447, 1982.

Recker, R.R. (ed.), Bone Histomorphometry: Techniques and Interpretation, CRC Press, Boca Raton, Fla., 1983.

Table 1.      RATS IN ORTHOPEDIC STUDIES

ADVANTAGES

- . Size, cost, inexpensive maintenance, docility
- . Commercially available from inbred, controlled colonies
- . Restraint models available for studies on specific types of bone loss
- . Most widely used experimental animal, therefore normative values for numerous systems available
- . Data available on bone studies performed during spaceflight

DISADVANTAGES

- . Skeletal growth is a continuous and lifelong process
- . Age-related bone loss-a mosaic response
- . Only excretes small amounts of calcium in the urine compared to man and other species
- . Adverse effects of restraint



Table 2.      MONKEYS IN ORTHOPEDIC RESEARCH

ADVANTAGES

- . Phylogenetic closeness to man
- . Near biped posture and humanoid torso
- . Bone remodeling system similar to man
- . Proven experimental models available on specific types of bone loss

DISADVANTAGES

- . Size limits use in spaceflight
- . Adverse effects of restraint
- . Cost and maintenance
- . Lack of inbred, controlled, commercial colonies

Table 3. BEAGLES IN ORTHOPEDIC RESEARCH

ADVANTAGES

- . Skeleton of adult man and Beagle nearly identical in composition and manner of remodeling
- . Well documented normative values for numerous systems available
- . Live long enough to provide skeletal biopsies for longitudinal studies
- . Proven experimental models available for studies on specific types of bone loss
- . Time required for intervention studies shorter than in man because of shorter life span and faster rate of bone turnover
- . Available commercially from inbred, controlled, colonies

DISADVANTAGES

- . Size limits use in spaceflight
- . Temperament, sometimes are not docile
- . Cost and maintenance
- . Apparent lack of menopause

1. Report No. NASA CR-171931		2. Government Accession No.		3. Recipient's Catalog No.	
4. Title and Subtitle  1985 NASA/ASEE Summer Faculty Fellowship Program				5. Report Date July 1986	
				6. Performing Organization Code	
7. Author(s)  Editors: Robert G. Chilton and Clarence E. Williams				8. Performing Organization Report No.	
9. Performing Organization Name and Address  Texas A&M University and The University of Houston - University Park				10. Work Unit No.	
				11. Contract or Grant No.  NGT-44-001-800	
12. Sponsoring Agency Name and Address  National Aeronautics and Space Administration Washington, D.C.				13. Type of Report and Period Covered  Contractor Report	
				14. Sponsoring Agency Code	
15. Supplementary Notes					
16. Abstract  <p>The 1985 JSC NASA/ASEE Summer Faculty Fellowship Research Program was conducted by Texas A&amp;M University and the Johnson Space Center. The ten week program was operated under the auspices of the American Society for Engineering Education (ASEE). The program at JSC, as well as those at other NASA Centers, was funded by the Office of University Affairs, NASA Headquarters, Washington, D.C. The basic objectives of the program, which began in 1965 at JSC and in 1964 nationally, are: (a) to further the professional knowledge of qualified engineering and science faculty members; (b) to stimulate an exchange of ideas between participants and NASA; (c) to enrich and refresh the research and teaching activities of participants' institutions; and (d) to contribute to the research objectives of the NASA Centers.</p> <p>The faculty fellows spent ten weeks at JSC engaged in a research project commensurate with their interests and background and worked in collaboration with a NASA/JSC Colleague. This document is a compilation of the final reports on their research during the summer of 1985. Texas A&amp;M Research Foundation Report No. 4194-85 is the Co-Directors report on the administrative operations of the Summer Faculty Fellowship Program.</p>					
17. Key Words (Suggested by Author(s))			18. Distribution Statement  Unclassified-Unlimited		
19. Security Classif. (of this report)  Unclassified		20. Security Classif. (of this page)  Unclassified		21. No. of Pages  730	
				22. Price*  NTIS	

\*For sale by the National Technical Information Service, Springfield, Virginia 22161